Geology of the Ashe Formation Between Fries and Galax, Virginia

by

Jonathan Lee Tso

Dissertation submitted to the Faculty of the

Virginia Polytechnic Institute and State University

in partial fulfillment of the requirements for the degree of

Doctor of Philosophy

in

Geological Sciences

APPROVED:

James R. Craig, Co-chairperson

M. Charles Gilbert, Co-chairperson

Lynn Glover, III

David A. Hewitt

J. Alexander Speer

August, 1987

Blacksburg, Virginia

Geology of the Ashe Formation Between Fries and Galax, Virginia

by

Jonathan Lee Tso

James R. Craig, Co-chairperson

M. Charles Gilbert, Co-chairperson

Geological Sciences

(ABSTRACT)

Field mapping, structural analysis, and mineral equilibria of rocks between Fries and Galax, Virginia provide information on the tectonic and metamorphic history of the Ashe Formation, a series of late Precambrian gneisses, pelitic schists and amphibolites, and the underlying Cranberry Gneiss. The dominant penetrative foliation of the rocks is composed of an early S_1 foliation that is crenulated and transposed by a later S_2 foliation which strikes N 50° E and dips SE. Metamorphic porphyroblast growth of biotite, garnet, staurolite, and kyanite followed penetrative foliation development, with metamorphic grade increaseing stratigraphically upward to form inverted isograds. Thrust faulting along the Fries Fault caused extensive mylonitization of the Cranberry Gneiss and offset of the metamorphic isograds. Textural evidence indicates that mylonitization is the greatest in rocks at the Fries Fault trace, and decreases upward through the Cranberry-Ashe contact. No textural evidence of an additional episode of faulting at the Ashe-Cranberry contact was observed, based on lack of an second episode of mylonite, relatively good preservation of sedimentary clasts in the Ashe, and similarity of metamorphic grade.

Mineral equilibria show systematic trends from chlorite-biotite grade to staurolite-kyanite grade. Muscovite compositions show an increase in paragonite component and decrease in celadonite component. Chlorite, biotite, garnet, and staurolite show a systematic increase in Mg/(Mg + Fe) toward higher grade. AFM topologies indicate that these compositional trends may be explained a series of continuous reactions (chl + mu = bi + q + V followed by chl + mu + q = gt + bi + V) and discontinuous reactions (gt + chl + mu = st + bi + V followed by st + chl + mu = ky + bi + V). Tem-

peratures inferred from garnet-biotite equilibria are approximately 550 to 600° C in the staurolite zone, with pressures estimated from various equilibria to be between 4.5-7 kb. The inversion of the isograds is interpreted as resulting from overthrusting of the Ashe metasediments during the Paleozoic.

The above information can also be applied to the deformation of the Gossan Lead massive sulfide. Structural data from the Bumbarger mine pit indicates that the massive sulfide underwent the same sequence of structural events as the surrounding rocks. During D_2, shearing of gneisses and schists in a matrix of ductile pyrrhotite caused isoclinal folding, fracture, and rotation of the metasediments while preserving the gross sedimentary layering. This information confirms synsedimentary models of the formation of the Gossan Lead.

Acknowledgements

The author would like to thank his committee members for their help and especially their patience. In particular, he appreciates the general guidance of Dr. M.C. Gilbert in the early stages of this project. Dr. J.A. Speer provided numerous insights and improvements to the petrology part of the dissertation. Dr. J.R. Craig provided "encouragement" toward the completion of the project and gave much assistance in the economic geology part of the study.

Many people generously gave their time and expertise. Dr. D.R. Gray provided his field expertise in the beginning stages of the study and helped transfrom me from an experimentalist to a field geologist. Todd Solberg taught me the ropes on the microprobe and never let me forget the first time I burned out a filament. Hal Pendrak provided his expertise in preparing and analyzing samples for the XRF. Doug and Kate Nedrich did a marvelous job in drafting the main geologic maps and various figures in the text, often working under extremely short deadlines. Brian Cooper served in the dual role as computing consultant and friend to commiserate with. Finally, the author thanks his family and friends, and the Radford University Geology staff for their support during the summers of field work, nights on the microprobe, and months of writing.

Table of Contents

PART I: GEOLOGY OF THE ASHE FORMATION BETWEEN FRIES AND GALAX, VIRGINIA 1

Introduction 2

Geologic Setting and Previous Works 5

Stratigraphy 13

The Fries Thrust Sheet 14

Cranberry Gneiss 14

Ashe Formation 15

Rocks of the Bowers Ferry Thrust Sheet 23

The Stone Mountain Thrust Sheet 26

Unicoi Formation 26

Structural Geology 27

Relationship of deformation to metamorphism 47

The Ashe-Cranberry Contact **51**

Comparison With Other Works **58**

Synthesis and Conclusions **62**

Late Precambrian history 62

Paleozoic history 64

Bibliography **67**

PART II: PETROLOGY OF THE ASHE FORMATION BETWEEN FRIES AND GALAX, VIRGINIA **72**

Introduction **73**

Geologic Setting and Previous Works **78**

Analytical Procedures **82**

Petrography **83**

General Statement 83

Unicoi Formation 85

Bowers Ferry Rocks 85

Cranberry Gneiss 88

Ashe Formation 89

Metasediments 89

Chlorite Zone 90

Biotite Zone 91

Garnet Zone 91
Staurolite-Paragonite Zone 92
Kyanite Zone 93
Amphibolite 94

Mineral Chemistry 100
Metasedimentary and Plutonic Rocks 100
Muscovite and Paragonite 100
Chlorite 101
Biotite 101
Garnet 104
Plagioclase 105
Staurolite 105
Amphibolites 108
Amphibole 108
Plagioclase 112
Chlorite 112
Other Minerals 112

Discussion 115
Evolution of Mineral Assemblages 115
Biotite 115
Garnet 116
Staurolite 117
Kyanite 120
Muscovite Compositional Changes With Metamorphic Grade 121
Paragonite 127
Garnet - Biotite Geothermometry 128

Interpretation of the Amphibolites 132

Geobarometry **138**

Regional Implications **142**

Conclusions **149**

Bibiliography **151**

PART III: DEVELOPMENTAL HISTORY OF THE GOSSAN LEAD MASSIVE SULFIDE **156**

Introduction **157**

Geologic Setting **159**

Local Geology **162**

Previous Works **164**

Description of the Gossan Lead at the Bumbarger Pit (Iron Ridge) **166**

General Statement 166

Stratigraphy 167

Foliated Ore (Zones A, B, C, G) 168

Massive Ore (Zones D and E) 168

Gneissic Ore (Zones A, B, C, and E) 174

Structural Geology **177**
General Statement 177
Structural Elements 177
Timing of Metamorphism With Respect to Structure 183
Synthesis of the Development of the Gossan Lead Structure 187
Discussion of Structure 188

Models for Ore Emplacement and Deformation **194**
Model 1: Ore emplacement is post-metamorphic and post-thrust faulting 194
Model 2: Ore emplacement is post-faulting and premetamorphic 197
Model 3: The ore is synsedimentary, but localized by later shearing 198
Model 4: Ore is synsedimentary 199

Discussion **201**

Summary and Conclusions **206**

Bibiliography **208**

Appendix A. Microprobe Analyses **212**
References 214

Appendix B. X-Ray Fluorescence Analyses **314**
Reference 314

Appendix C. Thin Section Mineralogy **317**

Appendix D. Biotite-Garnet Geothermometry **340**

List of Illustrations

Figure 1. Location map of study area 4
Figure 2. Regional geologic map 7
Figure 3. Photomicrographs of the Cranberry and Ashe Formations 18
Figure 4. Photomicrograph and outcrop photo of structure 30
Figure 5. Photomicrographs and photograph of the Cranberry mylonite 33
Figure 6. Photograph and photomicrograph of slip cleavage 36
Figure 7. Photomicrographs of Bowers Ferry rocks and 39
Figure 8. Stereonets - poles to bedding and foliation 42
Figure 9. Chart of mineral growth in relation to deformational events 48
Figure 10. Sketch map of Cranberry-Ashe contact, west side of New River. 52
Figure 11. Photomicrographs of the Cranberry-Ashe contact 54
Figure 12. Schematic diagram showing depositional environment of the Ashe 65
Figure 13. Location map 76
Figure 14. Tectonic map 77
Figure 15. Plutonic and metasedimentary sample and assemblage map 86
Figure 16. Mafic sample and assemblage map 87
Figure 17. Photomicrographs of typical lithologies 96
Figure 18. Muscovite compositions vs. distance 102
Figure 19. Fe/(Fe+Mg) vs. distance 103
Figure 20. Ca and Mn content of garnet vs. distance 106
Figure 21. Plagioclase (An) composition vs. distance in metasediments 107

Figure 22. Na/(Na + Ca) vs Al/(Al + Si) in zoned amphibole, sample A3-43B 109
Figure 23. Amphibole compositions vs. distance 110
Figure 24. Plagioclase (An) composition vs. distance in amphibolite 113
Figure 25. AFM plots of mineral compositions 118
Figure 26. Distance vs. X diagram 122
Figure 27. Na-Al-O system 124
Figure 28. Muscovite-paragonite compositions vs. temperature 126
Figure 29. Temperature vs. X(Ca + Mn) in garnet, sample A4-6A 131
Figure 30. Garnet-biotite temperatures vs. distance 133
Figure 31. Amphibole-plagioclase tie lines (after Spear, 1980) 135
Figure 32. ln(X(An)/X(Ab)) in plagioclase vs. ln(Ca(M4)/Na(M4)) in amphibole 137
Figure 33. P-T diagram 141
Figure 34. Map showing location of sulfide bodies in the Blue Ridge 160
Figure 35. Stratigraphic column of the ore horizons 169
Figure 36. General map and cross sections of mine (A-A′, B-B′,C-C′) 170
Figure 37. Photomicrographs and outcrop photographs of stratigraphy 175
Figure 38. Photographs of ore deformation 181
Figure 39. Series of stereonets 184
Figure 40. Schematic structural map showing trends of F(3) and F(4) folds 185
Figure 41. Block diagrams showing development of structure 189
Figure 42. Schematic diagram showing sedimentary-volcanic setting 204

List of Tables

Table 1. Structral data comparing other studies 59

Table 2. Table of structural history from Tso (1987) 84

Table 3. Representative results of biotite-garnet calculations 130

Table 4. Pressure estimates 140

Table 5. Structural elements 178

Part I: Geology of the Ashe Formation Between Fries and Galax, Virginia

Introduction

The Ashe Formation of the southwestern Virginia Blue Ridge has been the subject of debate for a number of years. Controversy has centered on such diverse topics as: the name of the formation, the nature of the protolith, the age of the formation and its correlation with other formations, the relationship between the Ashe and various plutonic and volcanic units in the region, the nature and timing of various deformational and metamorphic events, the origin of various massive-sulfide bodies within the formation, and most recently, the nature of the tectonic setting of deposition, the type of crust upon which it was deposited, and the type of contacts the Ashe has with its underlying formations. Complicating its interpretation is the fact that the Ashe Formation lacks a well defined stratigraphic sequence, and is complexly deformed and metamorphosed.

Reconaissance mapping (Stose and Stose, 1957, Espenshade and others, 1975) and geochemical studies (Gair and Slack, 1984) have been employed to help provide an overall stratigraphic and depositional framework. However, the details of the subsequent metamorphic and structural history are lacking, espcially in Virginia, primarily due to a dearth of detailed field mapping and structural data. Such studies would also provide information on the types of lithologies present in the Ashe, on their distribution, and on the timing between the various metamorphic and thrusting events.

This paper focuses on the Ashe Formation in southwest Virginia between the towns of Fries and Galax in an approximately 11 by 4 km area along the Carroll-Grayson County border (figure 1). This area was chosen because it:

1. includes typical Ashe stratigraphy as mapped by Stose and Stose (1957) and Espenshade and others (1975),

2. contains the basal Ashe section along with the underlying Cranberry Gneiss,

3. contains metamorphic isograds that range from chlorite zone in Fries to kyanite zone in Galax,

4. includes the Fries Fault, one of the major thrusts of the Blue Ridge,

5. hosts an economically important massive sulfide body, the Great Gossan Lead, and

6. has better than average exposure because of the presence of the New River, Chestnut Creek and various railroad cuts.

This study, by use of a field mapping, structural, and petrographic approach, concentrates on two major aspects of the Ashe Formation:

1. the description of the various litholgies of the Ashe Formation, their distribution in the field area, and a discussion of their implications towards the sedimentary models recently proposed, and

2. the analysis the structural geology of the area and its implications towards the relative timing between the metamorphism and deformation of the area, and the application of this data towards the problem of the nature the contact between the Ashe Formation and the underlying Cranberry Gneiss.

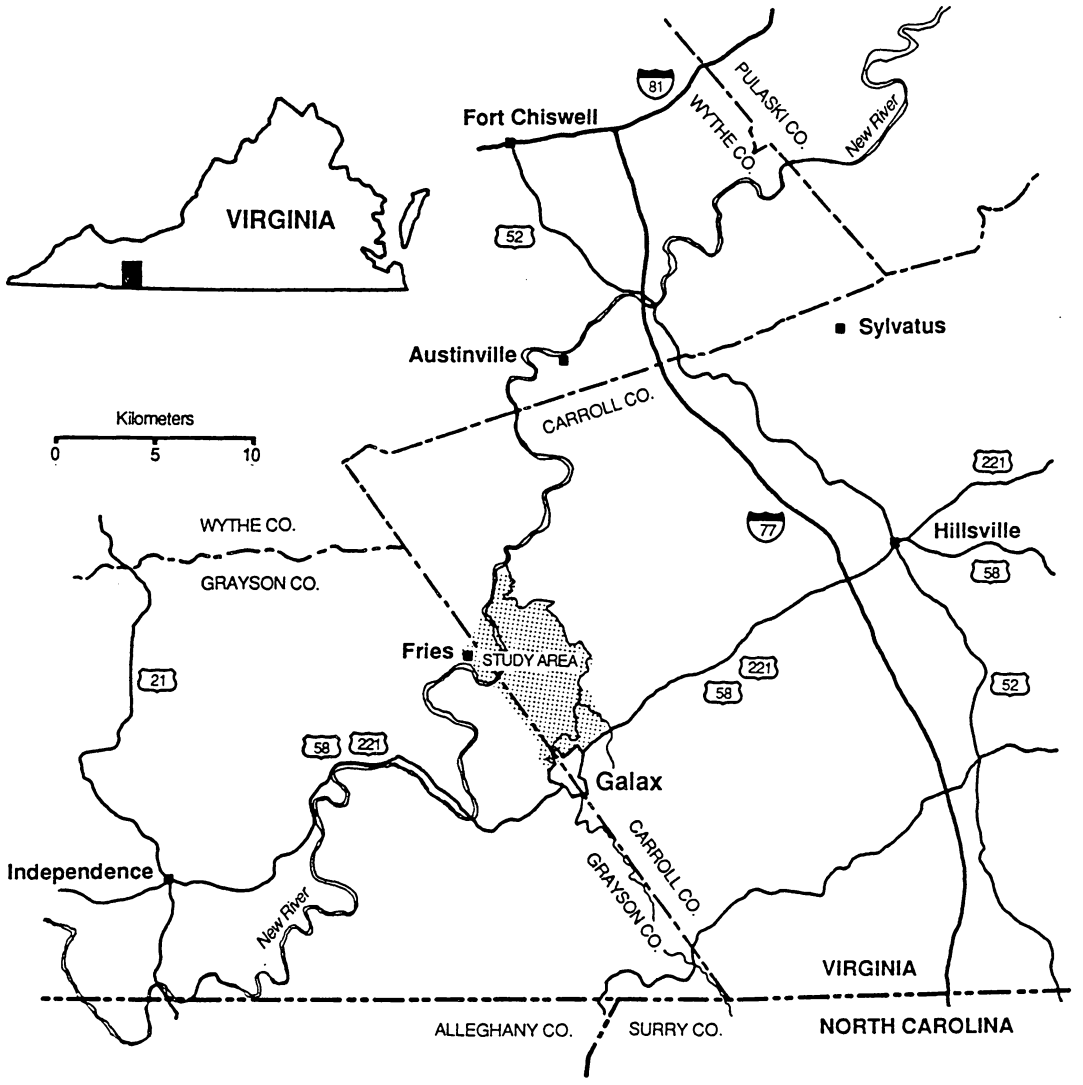


Figure 1. Location map of study area

Geologic Setting and Previous Works

Rankin (1970) applied the term "Ashe" to a broad belt of metasedimentary and metavolcanic schists, gneisses, and amphibolites from Ashe County, North Carolina as part of a reconaissance mapping project undertaken in 1965 to map the Winston-Salem 1:250,000 quadrangle (Rankin and others, 1972, Espenshade and others, 1975). He thus redefined formation names previously used, such as the Roan Gneiss (predominantly mafic) and the Carolina Gneiss (predominantly mica schists and gneisses) as used by Keith (1903, 1904, 1907) in North Carolina, and the Lynchburg Formation, as applied to the study area by Stose and Stose (1957). From the study area, this belt extends northeastward into central Virginia, where it is believed to be correlative with the Lynchburg Group (Rankin and others, 1973). To the southwest, the numerous correlative formations include: the Grandfather Mountain Formation of North Carolina (Rankin, 1970); the Mount Rogers Formation of southwestern Virginia (Rankin, 1970); the Ocoee Series of North Carolina-Georgia-Tennessee (Hadley, 1970); and the Tallulah Falls Formation of North Carolina-Georgia-Alabama (Hatcher and others 1980).

According to the stratigraphic framework established by Rankin and others (1973), the Ashe Formation rests nonconformably on the Cranberry Gneiss, which represents the approximately 1 billion year old Precambrian basement, and is conformably overlain by the Alligator Back Forma-

tion, a series of gneisses, metapelites, and amphibolites that is a bit more micaceous and calcic than the Ashe (figure 2).

Neither the Ashe nor the Alligator Back, however, are known to be in stratigraphic contact with any other formation of known age. Because of this, and the fact that metamorphism and deformation have masked the primary sedimentary structures and lithologies, the age of the Ashe - Alligator Back package is known only indirectly by its correlation with other formations that lie in approximately the stratigraphic position as the Ashe. The ages of these formations are known by the radiometric dating of various plutonic and volcanic units included within these formations. Unfortunately, the radiometric ages have yielded conflicting results. For example, Rankin and others (1969) analyzed zircon samples from a number of felsic-volcanic rocks in the Blue Ridge including the Grandfather Mountain Formation, the Mount Rogers Formation, and the Catoctin Formation of Pennsylvania, which in Virginia overlies the Lynchburg Group, and came to the conclusion that they collectively represent an age of 820 m.y. These rocks, together with felsic plutonic rocks such as the Striped Rock Granite, the Beech Granite and the rocks at Crossnore, N.C. define the "Crossnore Plutonic-Volcanic Group" of Rankin and others (1973), a bi-modal felsic-mafic suite. Odom and Fullagar (1982), however, challenged the 820 m.y. age, and using Rb/Sr whole rock analyses of the Crossnore Group, cited an age range of 690-570 m.y. The problems between the U/Pb data and the Rb/Sr data have been summarized by Odom and Fullagar (1971), Eckelman and Mose (1981) and Mose, Nagel and Tunsoy (1983). It is now generally believed that the Rb/Sr ages are more reliable.

Another major controversy is the nature and the site of deposition of the Ashe Formation. Since the work of Rankin (1975, 1976), the Ashe Formation has generally been considered to represent deposition in a fault-bounded trough during the rifting of the proto-Atlantic or Iapetus Ocean. Recent work supporting this idea was carried out by Wehr (1983) in a sedimentological study of the Lynchburg Group in central Virginia. He found that the Lower Lynchburg Group was deposited in a rapidly subsiding graben adjacent to glaciated granitic highlands. Schwab (1984) noted that the feldspar-rich litholgies, great formation thicknesses, and interbedded volcanics are similar

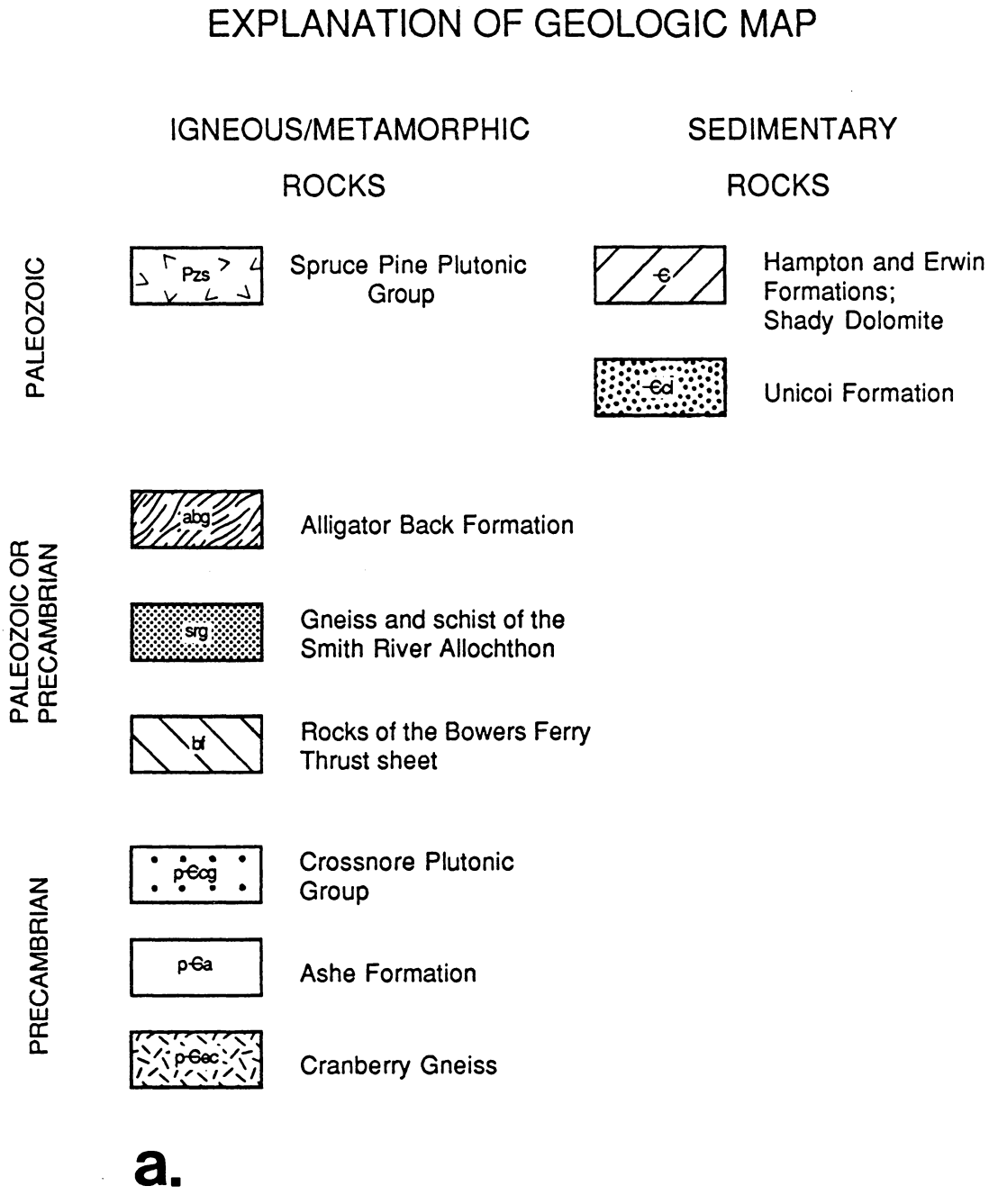
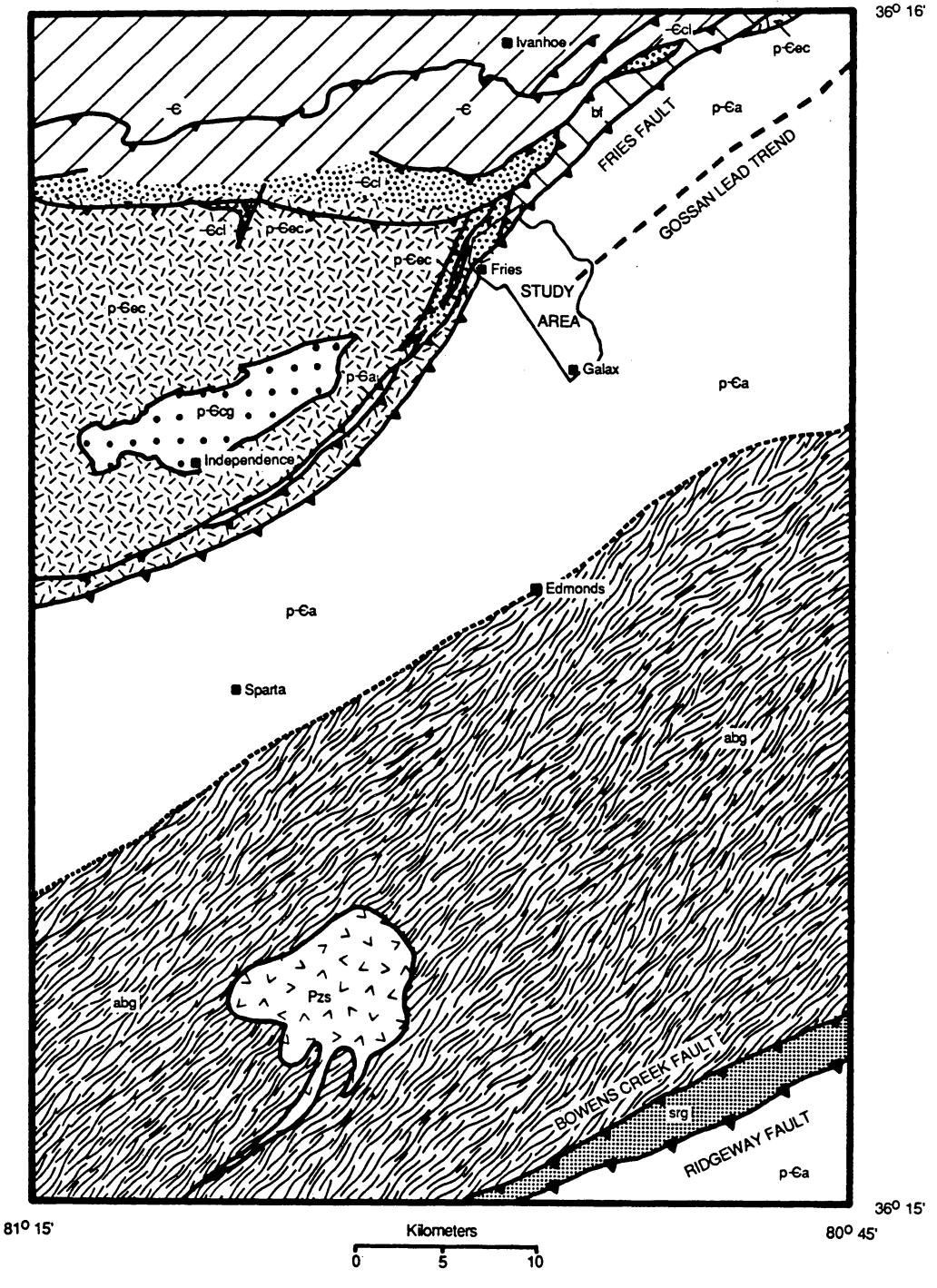


Figure 2. Regional geologic map: After Rankin and others (1972) and Espenshade and others (1975); a) explanation; b) geologic map



b.

Figure 2 (continued)

to modern rift settings such as the East African Rift. Gair and Slack (1984) have argued, on the basis of bulk rock chemistry, that the gneisses fall into ACF compositional fields that are typical of graywackes. In addition, study of the trace element chemistry of amphibolites from the study area (Slack and others, 1985) has suggested an affinity with mid-ocean ridge basalts, although one analysis suggested a within-plate continental basalt. Slack and others concluded that the metasedimentary and metavolcanic package was supportive of a rift setting during the initial opening of the Iapetus Ocean.

Unfortunately, there is a lack of geologic mapping between the central Virginia area, where sedimentary structures have been well described and paleocurrent data is available (Wehr, 1983), and the study area, a distance of some 200 km, where metamorphism has obliterated most primary structures. Despite the fact that most workers in the Blue Ridge agree with the proposed correlation between the Lynchburg and the Ashe, this lack of detailed mapping remains as one of the largest obstacles preventing the deciphering the Precambrian history of the southwest Virginia Blue Ridge.

In addition, there has also been much controversy over the nature of the contact between the Ashe and the underlying Cranberry Gneiss. The idea that the Ashe/Lynchburg nonconformably overlies continental basement is supported by Wehr and Glover (1985), who mapped part of the Lynchburg Group in central Virginia, and proposed that the Lynchburg rests on transitional continental crust in a fault-bounded trough seaward of a hinge zone. Unfortunately, exposures of the Ashe - Cranberry contact are rare. However, Rankin (1971) and Bartholomew and others (1983), both mapping in North Carolina, have reported localities where they believed the contact to be a nonconformity. However, Abbott and Raymond (1984), in a petrologic study of the Ashe Formation in North Carolina, believed the contact to be thrust faulted on the grounds that the Ashe Formation preserves higher metamorphic conditions than the underlying Cranberry Gneiss. They proposed that the Ashe Formation was deposited on oceanic crust, and was later thrusted into its present position over the granitic Cranberry Gneiss. This idea is consistent with the proposal of Hatcher (1978), that the Fries Fault along with the Hayesville Fault of North Carolina represents

a major boundary that divides the Blue Ridge into eastern and western sectors. The western Blue Ridge is thought to represent shallow depositional settings on continental crust, while the eastern Blue Ridge represents a much deeper water facies deposited on oceanic crust with the Fries Fault acting as a large Paleozoic thrust fault moving the generally higher grade metamorphic rocks of the east over the generally lower grade rocks of the west. The idea that the eastern Blue Ridge was deposited on oceanic crust may also explain why mafic rocks in general are more abundant in the east, and why small ophiolite bodies that may represent mantle material are present in this area.

However, recent mapping in North Carolina by Bartholomew and Lewis (1984) has provided an alternate view. They have divided the Blue Ridge into a series of thrust fault-bounded "massifs" on which late Precambrian and lower Paleozoic cover rocks nonconformably overlie continental Grenville basement. In the study area, for example, Bartholomew and Lewis propose that the Ashe Formation overlies the Grenville Basement as represented by the Cranberry Gneiss on the "Elk River Massif". In addition, Bartholomew and Lewis believe that as the Hayesville Fault is pre-or-synmetamorphic and the Fries Fault is post-metamorphic, the two faults are not really part of the same system. The issue of the origin of the ophiolite bodies remains unresolved.

In a sense, the study area serves as a microcosm of the larger debate over the Ashe-Cranberry contact. Stose and Stose (1957) have mapped the contact as a thrust fault (their "Gossan Lead Fault"), thus making the Cranberry Gneiss a thin, fault-bounded sliver less than 1/2 km wide. Espenshade and others (1975), tracing the Cranberry from more widespread exposures in North Carolina (Rankin and others, 1972), have mapped the contact as a nonconformity. Unfortunately, the contact is not exposed in the study area, and the rocks adjacent to the contact are all within the Fries Fault mylonitic zone. However, determination of the type of contact may be surmised from indirect observations such as: differences in metamorphic grade from on side of the contact to the other, differences in structural style from one side to the other, and in the truncation of stratigraphic units as observed from geologic mapping. Field mapping, petrography, and structural analysis of the rocks surrounding the contact from this study provide insights into the the complexities involved with either interpretation.

Subsequent to deposition, the Ashe Formation experienced a long and complicated period of Paleozic metamorphism and deformation as reflected by radiometric data on the Ashe and correlative formations. Butler (1972) summarized the then current literature, and placed the minimum age at 430 m.y. Dallmeyer (1975), studying rocks of the Ocoee sequence, used an Ar-40/Ar-39 incremental age technique on hornblendes and biotites, and estimated that kyanite grade conditions were reached at about 480 m.y. ago at a depth of 25.6 km.

Fortunately, the Ashe and the overlying Alligator Back Formations are intruded by numerous felsic bodies of the Spruce Pine Plutonic Group (Rankin and others, 1973) in North Carolina which appear to post-date the development of the main regional foliation, thus providing an upper limit on the age of metamorphism. A number of radiometric dates have been published on these bodies (summarized in Lesure, 1968), with ages ranging from 420 m.y. for Pb-207/Pb-206 to 231 m.y. for K/Ar. An age of 380 m.y. was used by Butler (1973) in his synthesis of regional metamorphism and deformation. Recent summaries by Butler and Fullagar (1982), K/Ar work by Kish (1982) and Ar-40/Ar-39 work by Sutter (1982) have shown that metamorphism in the Appalachians was a complex, multi-step process. However, in the Blue Ridge, current thinking on the age of the major (Taconic) period of deformation and metamorphism is that it took place at about 480 to 435 m.y. ago (Glover and others, 1983).

The timing of movement of the major thrust faults of the Blue Ridge is similarly complex. Several pre-metamorphic faults have been clearly established southwest of the study area as evidenced by annealed mylonites and a lack of offset of metamorphic isograds. Examples of two prominent faults of this type are the Greenbriar Fault of the Ocoee Series (Milton, 1983), and the Hayesville Fault (Hatcher and others, 1979, Eckert, 1984).

However, a syn-or-post-metamorphic age has been argued for the Fries Fault. This is based on the following arguements:

1. the Fries Fault cuts metamorphic isograds in some places and generally separates lower grade rocks on the northwest from higher grade rocks on the southeast (Rankin and others, 1972, and Espenshade and others, 1975),

2. K/Ar and Rb/Sr whole rock dates from mylonite in the Fries Fault zone in southern Montgomery and northern Floyd Counties, Virginia by Dietrich and others (1969) show 345 m.y. and 330 m.y. respectively, and

3. cataclasis was believed concurrent with regional metamorphism and folding in a study of rocks north of Grandfather Mountain, North Carolina and south of Roanoke, Virginia (Bartholomew and Lewis, 1977).

Both Rankin and others (1973) and Bartholomew and Lewis (1984) have interpreted the last Fries Fault movement to be both post-Taconic metamorphism and post-emplacement of the Spruce Pine Pegmatites, consistent with the 345 m.y. age.

Stratigraphy

The distribution of the various lithologies is shown on the geologic map (Plate I). Major thrust faults divide the study area into a series of thrust sheets which contain their own characteristic lithologies. From northwest to southeast, and from bottom to top, they are: the Stone Mountain Sheet containing the Unicoi Formation, the Bowers Ferry Sheet containing highly sheared metaconglomerates informally called the "Bowers Ferry Rocks", and the Fries Thrust Sheet containing the Cranberry Gneiss and the overlying Ashe Formation. In addition, a shear zone has been mapped within the Ashe Formation in the southern part of the study area, causing no obvious repetition of lithologic layering. In general, rocks dip to the southeast, with the oldest in a sheet rocks being found along the northwest boundary of the sheet, with the overall age of the rocks in a sheet found increasing toward the uppermost sheets. The following is a desciption of the major lithologies in order of decreasing age.

The Fries Thrust Sheet

Cranberry Gneiss

The Cranberry Gneiss was originally defined by Keith (1903) as the Cranberry Granite for the coarse plutonic rocks cropping out near Cranberry, North Carolina. Mapping by Rankin and others (1972) and Espenshade and others (1975) extended the "Cranberry Gneiss" into the study area as a thin sliver of outcrop area, less than one-half kilometer wide on the immediate southeast side of the Fries Fault. The Cranberry Gneiss was considered by them to be composed of approximately 1 billion year old rocks of the "Elk Park Plutonic Group" (Rankin and others, 1973) which comprise the sole of the Fries Thrust Sheet. Stose and Stose (1957), mapping only in Virginia, termed these rocks "granite mylonite" and "quartzite mylonite" of unknown Precambrian age. Careful review of these rocks during the present study, however, has redefined some of the "quartzite mylonite" as mylonitized gneisses of the Ashe Formation, thus causing a relocation of the Ashe - Cranberry contact as mapped by Stose and Stose. More recently, Bartholomew and Lewis (1984) differentiated between the true "Cranberry", an intrusive, generally coarse-grained felsic igneous rock, and the layered gneiss intimately associated with the Cranberry. The layered gneiss is apparently older than the granite and may represent the country rock into which the granite intruded. They defined this rock as the "Cranberry Mine-Layered Gneiss". Such heterogeneity in the "Cranberry" has been noted by many other workers (Eckelmann and Kulp, 1956, Bryant and Reed, 1970).

In the study area, the Cranberry Gneiss is entirely contained within the mylonite zone of the Fries Fault. In hand sample, it commonly is a coarse, generally planar augen gneiss. The augen are white to pink, up to 1 cm long, consist of plagioclase (albite) or K-feldspar (microcline), and have length to width ratios of 2 to 4:1 (figure 3a). Commonly, these feldspars show bent twin lamellae and are cracked, with the borders of grains showing recrystallization into the fine equant grains that make

up the mylonite matrix. Quartz is present both as matrix grains, and as highly strained lenses of up to several centimeters in length, with length to width ratios of typically 5:1 or more. The percentage of the mylonitic matrix versus augen is 20 to 80%. Mineralogically, the dominant minerals that are always present are: plagioclase (30-70%), quartz (20-35%), and muscovite (< 10%). K-feldspar, if present, is found only in the augen and usually makes up less than 5% of the rock. Biotite is locally present as fine to medium flakes that parallel the main mylonite foliation, with development limited to the most highly sheared and planar rocks found along the mapped Fries Fault trace. Manganiferous ilmenite, magnetite, and pyrite are common opaques along with accessory zircon and apatite. The rock frequently parts and weathers along paper-thin muscovite layers which may give the rock a superficially phyllitic appearance. The best outcrops are found along Va. Rt. 94 in the northern part of Fries, the west cliffs of the New River and along the railroad cuts on the west side of Chestnut Creek. The mylonite is a cliff-former that forms rapids in the New River and holds up Toby Knob.

Ashe Formation

The dominant formation in the study area is the Ashe Formation. In southwest Virginia, it forms a belt that trends N50°E and is approximately 20 km wide (Espenshade and others, 1975). No total stratigraphic thickness has been estimated because of the complexities of metamorphism and deformation. It contains many different lithologies, but is largely a metagraywacke-metapelite suite with varying amounts of amphibolite material. Ultramafic pods and pegmatites are found at some localities (Rankin and others, 1972, Espenshade and others, 1975), but these were not encountered in the study area. Marbles and calc-silicate are also rare, with carbonates occurring in only minor amounts at one locality southeast of the Fries Fault trace (location B2-1, Tso, 1987). Descriptions of the rocks common to the study area follow.

Muscovite-Biotite Gneiss: Muscovite-biotite gneiss is the dominant rock in the study area and makes up well over half the total stratigraphic package. It is equivalent to the "granofels" of Gair and Slack (1984) and is commonly a gray, medium-grained quartz-plagioclase (An_5-An_{13}) rock with 5 to 15% medium grained, evenly dispersed muscovite and biotite (figure 3b). The original sedimentary texture of these rocks is generally not preserved. However, the coarse sandy and arkosic nature of these rocks can be observed in the area just southeast of the Fries Fault where the metamorphic grade is lower as beds of 2-3 mm clasts of plagioclase and quartz are embedded in a finer quartz-mica matrix. In general, these clasts become less prominent toward the higher grade areas toward the southeast where biotite grows as prominent porphyroblastsorphyroblasts Other minerals that are usually present are: garnet, chlorite (normally late-growing), apatite, zircon, ilmenite and/or rutile. Overall, the rocks are slightly aluminous graywackes, with silica contents ranging from 67 to 77% and alumina contents of about 11 to 16% (Gair and Slack, 1984, Tso, 1987).

Pelitic Schists: The pelitic schists are ubiquitous throughout the area, but they are more prominent in the belt just southeast of the Gossan Lead trend along Iron Ridge, and in the staurolite-bearing belt of rocks that passes through the northern part of the city of Galax. In general, schists and gneisses are intimately interlayered on the one to tens of meter scale, parallel to the general foliation.

These rocks are predominantly muscovite (>45%) and quartz-bearing (10-30%). Minor plagioclase and biotite are present; Mn-bearing garnet is present throughout the Ashe except in the lower grade areas just southeast of the Fries Fault. Rocks that contain small percentages of graphite tend to have finer grain size in which case they are called "muscovite phyllite". Rocks with little or no graphite tend to be coarser, with porphyroblastic biotites becoming more prominent in the southeastern part of the area where they are called "muscovite-biotite schist" (figure 3c). Zircon and apatite are common accessories, along with late-growing chlorite, pyrrhotite, ilmenite and/or rutile. Commonly, pyrrhotite appears as a minor or accessory mineral, and where present in sufficient quantities, may cause the rock to weather to a distinctly orange-red soil.

There are several subtypes worthy of mention:

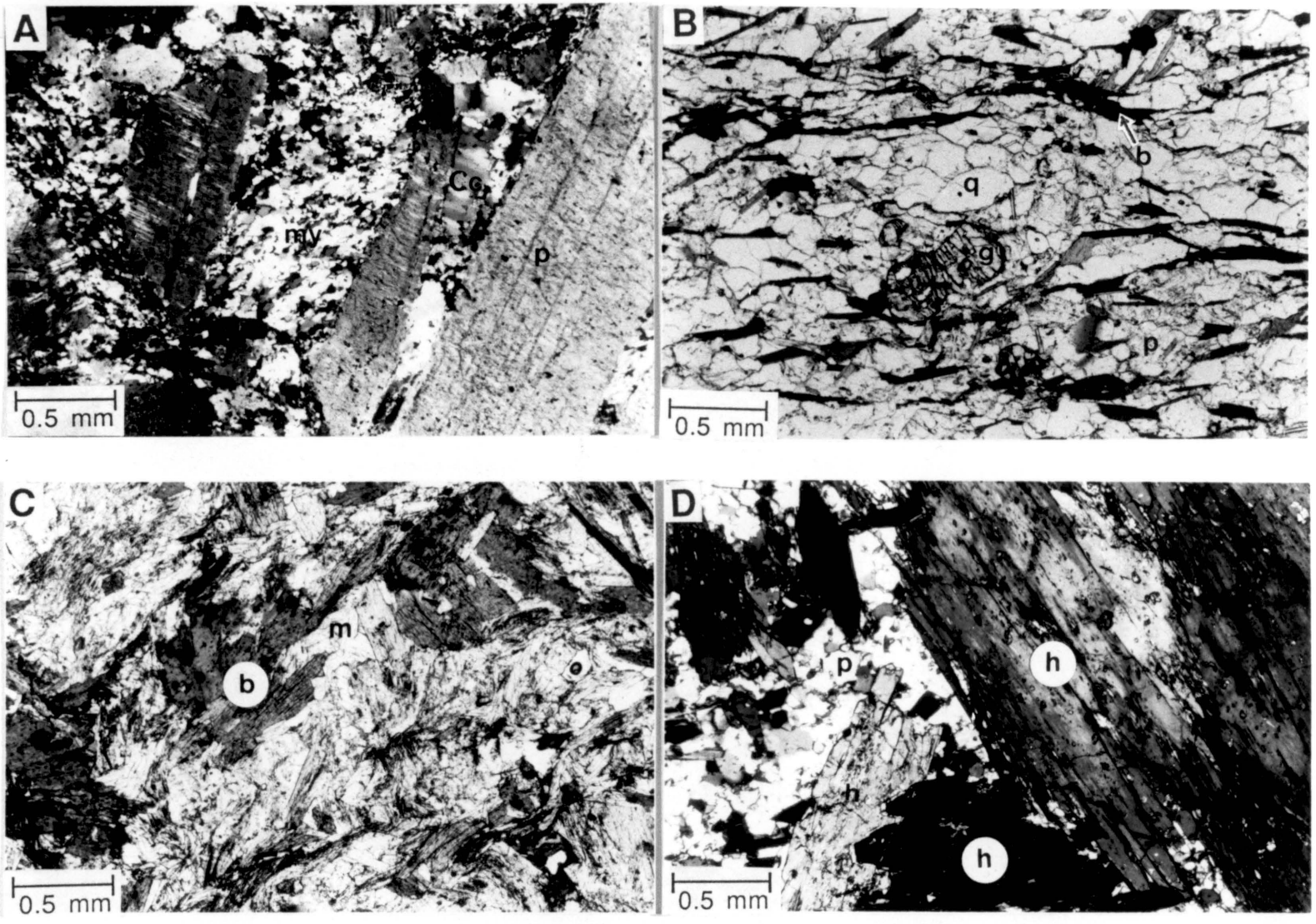
Garnet-Muscovite Schist: These are found in a belt just to the northwest of the Gossan Lead trend and contain easily visible 1-2 mm manganiferous garnet.

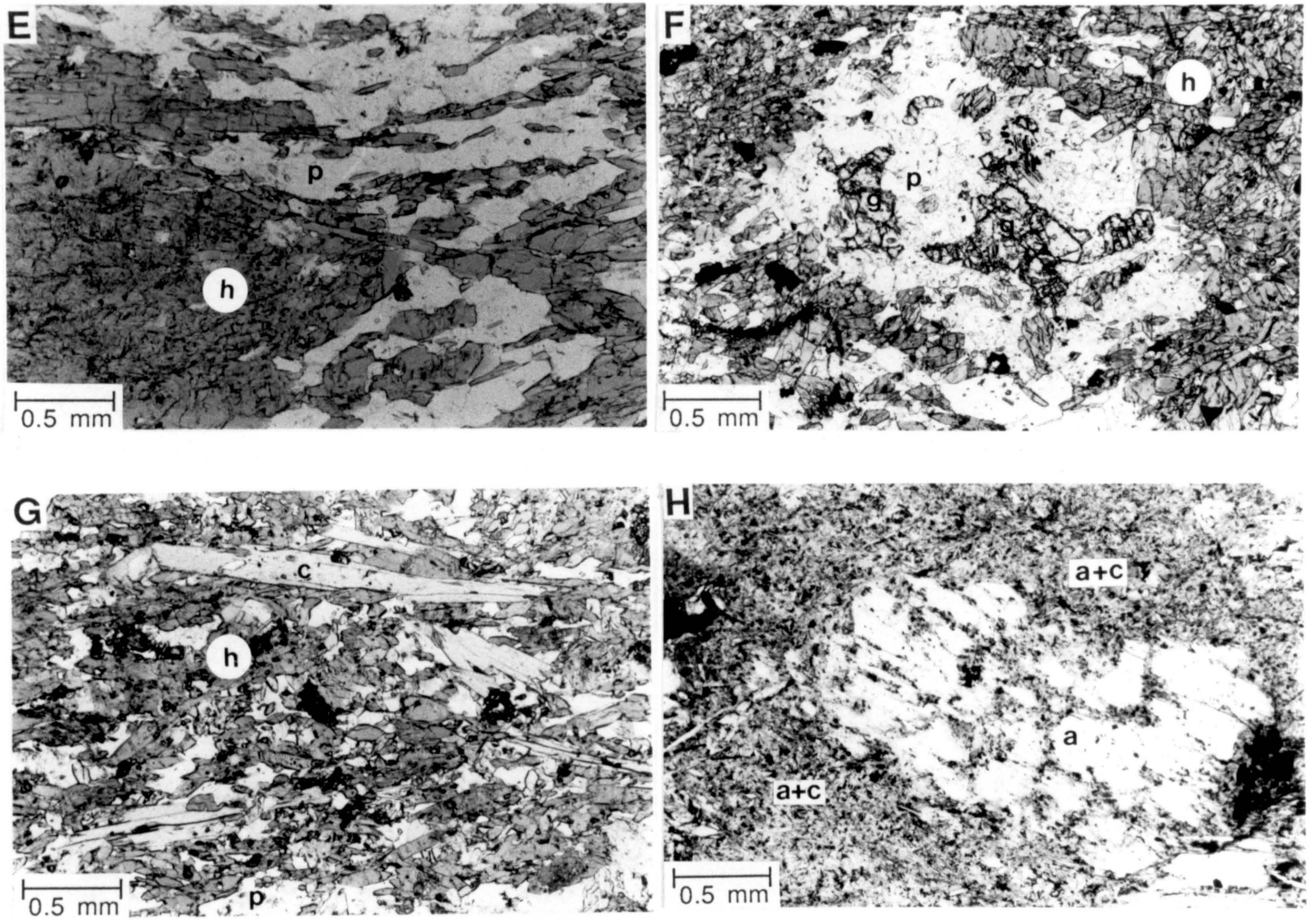
Chlorite Schist: This rock type is restricted in its occurrence to the immediate hanging wall of the Gossan Lead ore, to one or two cm-scale units within the ore body, and to several scattered outcrops the lie in a belt just southeast of the ore. Typically, it is a greenish-gray phyllite, with a notable "crinkle" lineation that is often the result of two intersecting foliations. Usually, it is nearly mono-mineralic with only minor amounts of biotite, quartz and ilmenite and occasional coarse grained manganiferous garnet porphyroblasts. Based on the similarity between the rare-earth element analyses of these schist and that of clastic sediments, Gair and Slack (1984) believed these rocks to represent clastic sediments that were altered by hydrothermal solutions after the deposition of the sulfides, or as a mixture of sediment and chemically precipitated material.

Staurolite-Muscovite-Biotite Schist: Staurolite-bearing schists are found in a belt that passes through the northern part of the city of Galax, and contain a complex assemblage of minerals that are not found elsewhere. These include: staurolite, muscovite-paragonite intergrowths and associated kyanite in quartz pods with additional garnet and chlorite showing textural with staurolite in some samples. These unusual rocks are discussed in more detail in Tso (1987). It should be noted that some spectacularly large staurolites of up to 10 cm in length can be found in Galax at some localities and are important to the deformational-metamorphic interpretation of the Blue Ridge.

Amphibolites: As seen on the geologic map (plate I), amphibolites are very common southeast of the Gossan Lead trend and are sparse northwest (stratigraphically below) the trend with the amphibolites being found in numerous layers trending to the northeast, parallel to the general strike of the foliation and to the gneiss-schist contacts. The thicknesses of the amphibolites vary from less than one meter to several tens of meters. Individual amphibolite units vary both in thickness and

Figure 3. Photomicrographs of the Cranberry and Ashe Formations: a) Cranberry Gneiss, sample A1-1A, crossed polars; note the cracked plagioclase with calcite filling and mylonite development; b) Ashe Formation gneiss, sample A4-6A, uncrossed polars; equigranular quartz-plagioclase rock with evenly dispersed biotite; c) Ashe Formation schist, sample B3-32A, uncrossed polars; muscovite rock with biotite porphyroblasts; d) Ashe Formation metagabbro, sample A3-93A, crossed polars; coarse, randomly oriented hornblende and finer plagioclase intergrowths; e) Ashe Formation, coarse-layered amphibolite, sample C3-117B, uncrossed polars; note stronger degree of parallelism of the hornblende; f) Ashe Formation, spotted amphibolite, sample C3-117A, uncrossed polars; rounded clot of plagioclase with garnet; g) Ashe Formation, medium-grained hornblende schist, sample A4-22A, uncrossed polars; finer grained hornblende with parallel chlorite defining the foliation; h) Ashe Formation, actinolite - chlorite schist, sample B4-100A, uncrossed polars; coarse, random relict actinolite in a fine actinolite - chlorite matrix. Abbreviations: a = actinolite, b = biotite, c = chlorite, Cc = calcite, g = garnet, gr = graphite, h = hornblende, K = K-feldspar, m = muscovite, my = mylonite matrix, p = plagioclase.


A
mV
Cc
p
0.5 mm
B
q
b
g
p
0.5 mm
C
m
b
o
0.5 mm
D
p
h
h
h
0.5 mm


E
p
h
0.5 mm
F
h
p
g
g
0.5 mm
G
c
h
0.5 mm
p
H
a+c
a
a+c
0.5 mm

lithology along strike, and frequently more than one textural type may be observed at a single outcrop. They tend to crop out in topographically low areas in streams or on steep hillsides, unless they are "metagabbros", which may hold up low ridges. In areas of sparse vegetation, the overlying soils are a distinct reddish color, a color which may be confused with that developing on sulfide-rich pelitic schists.

All amphibolites are dominated by hornblende and plagioclase (An_{18}-An_{35}) . Hornblende generally makes up 60% (maximum of 90%) of the rock while plagioclase generally makes up 30% (maximum of 80%), with quartz usually present in amounts less than 10%. Other common minerals are: clinozoisite, chlorite, sphene, ilmenite and/or rutile, and pyrrhotite. Biotite is rarely present and is ususally observed near contacts with metasediment. Garnet is also a rare accessory and primarily observed in the higher grade areas of the staurolite-bearing schists.

The amphibolites come in a variety of textural types which will be described below. It should be kept in mind that one lithologic type may grade into another in a continuous fashion. Therefore, the following descriptions should be considered to be "end-member" lithologies.

Metagabbro: The metagabbros are coarse, relatively non-foliated, and tend to be associated with the more massive amphibolite units. The hornblendes are commonly 1-2 cm long, random in orientation, with plagioclase filling the interstices between the hornblendes (figure 3d). Plagioclase is typically equant with a mosaic appearance. Chlorite content is typically less than 1%, but may rise to 4-5% with the grains being aligned parallel to foliation where most abundant. Thus, the chlorite content usually determines the degree of foliation exhibited by the rock.

Coarse-layered amphibolite: Coarse-layered amphibolite, a more foliated version of a metagabbro, is typified by hornblende stretched into black augen, with plagioclase occurring in light colored bands that parallel the dominant schistosity. In thin section, the coarse hornblendes are strictly anhedral and are rather randomly oriented. They are, however, overgrown with a new generation of finer, more needle-like amphibole which defines the schistosity and lies parallel to the foliation

of the surrounding rocks (figure 3e). Plagioclase is found in an equant, mosaic medium-grained texture.

Spotted amphibolite: These are medium-grained rocks that contain a well developed foliation that parallels the dominant schistosity. The "spots" are seen in hand specimen as 2-3 mm light gray to pink, elliptical to circular areas of polycrystalline plagioclase which stand out against the dark hornblende-rich matrix (figure 3f). However, specimens cut across the foliation reveal that the "spots" are actually pencil-like lenses of plagioclase. In garnet-bearing amphibolites, the "spots" may be composed of single grains of garnet.

Medium-grained hornblende schist: This rock type is one of the most common in the study area and can be found making up the stratigraphically thinner amphibolite layers and can be found along the edges of the metagabbro layers. This rock is typified be a predominance of needle-like hornblende that clearly overgrows the earlier, more random hornblende which appears only as relicts. In addition, chlorite lies parallel to the dominant amphibole foliation, thus making this rock appear quite schist-like in hand specimen (figure 3g). Usually, quartz is more common in this rock than in the metagabbros, commonly making up 10% of the mode.

Actinolite-chlorite schist: The actinolite-chlorite schist is a chemically and mineralogically distinct facie of amphibolite. It is typically bi-mineralic, with needle-like light green actinolite and chlorite (up to 30%) forming the dominant foliation (figure 3h). Plagioclase and quartz are rare, and a trace amount of talc was found in one specimen (C3-32B) in the hinge area of an F_3 kink fold. Davison (1973), mapping the Ashe Formation in Floyd County, Virginia, also noted chlorite-amphibole schists. However, unlike those at Galax, his contained two-amphiboles (actinolite and cummingtonite) and dolomite. Bulk chemical analyses presented by Davison are essentially similar to sample B4-9Z of the present study (appendix B) which shows that this unit is somewhat ultramafic with a silica content of 41.5% and an MgO content of 20.8%, a composition which Davison interpreted as being similar to that of a picritic basalt. Actinolite-chlorite schist was col-

lected from the present study area and analyzed for major and minor element chemistry by Slack and others (1985). Based on Mg, Ni, Co, and Cr data, they also interpreted these rocks as picritic basalts. In outcrop, the thicknesses of these units vary from about one meter to ten meters or more, and are always found with other amphibolites of varying textures nearby along strike, although within a single outcrop, no other rock type is observed. These units are mappable for short distances, follow the general strike of the other amphibolites, and may be found interlayered in a typical fashion with the surrounding schists and amphibolites.

Rocks of the Bowers Ferry Thrust Sheet

The rocks of the Bowers Ferry Block lie in a wedge-shaped area in the northeast section of the study area immediately south of the Bowers Ferry Fault as mapped by Stose and Stose (1957), and north of the Fries Fault (plate I). According to Stose and Stose, these rocks comprise the southwestern-most occurrence of a 1 km wide belt that extends along strike at least 26 km to the northeast where it runs to the edge of their map area approximately 2 km NNE of Sylvatus, Virginia. Stose and Stose (p. 95) believed these rocks to belong to the Unicoi Formation of lower Cambrian(?) age and described them as being mostly arkosic and conglomeratic with several basalt bodies, one of which was mapped at Stoneman's Hill in the northern part of the study area. Espenshade and others (1975), on the other hand, described this belt as belonging to the Ashe Formation, and traced these rocks to the Sylvatus area where, according to their map, they are faulted-out by the Fries Fault. They noted that the "Ashe" in this belt was conglomeratic with granule to pebble-sized detrital clasts.

In the study area, good exposures are seen along the railroad tracks along Chestnut Creek and along the cliffs on the east side of the New River where they are partially inaccessible. A fairly complete section may be viewed north of the study area starting at the railroad trestle over the New River across from Fries Junction in the Austinville Quadrangle, south along the tracks on the west side

of Chestnut Creek into the Galax Quadrangle to its contact with the Fries Fault. Overall, the rocks dip to the southeast, with cross bedding indicating that the rocks are right-side up.

The stratigraphically lower (northern) part of the sequence is dominated by arkosic conglomerates (clasts up to 2 cm) and arkosic sandstones, succeeded by the dominant rock type of somewhat mylonitized dark green arkosic sandstone and graywacke. Further southwest, these lower units are overlain by the mafic unit that crops out on the top of Stoneman's Hill. Between this unit and the Fries Fault, the dominant lithology is more conglomerate and green arkosic sandstone, with several prominent, well indurated quartzite layers, and some minor pelitic schists. At the very top of the exposed section, where it is cut off by the Fries Fault, is another mafic unit which crops out along the railroad tracks along Chestnut Creek. The total thickness of exposed stratigraphy between the east side of the New River near Fries Junction and the Fries Fault is estimated to be approximately 450 m.

In general, these rocks contain one foliation, which is parallel to to the primary sedimentary layering. As will be discussed later, thin section analysis indicates that the foliation is mylonite related which serves to stretch the clasts out so that the rock attains a banded appearance. The greatest development of this texture is found adjacent to the Fries Fault to the southeast, and the Bowers Ferry Fault to the northwest. The center of the sheet contains the least recrystallized rocks, especially along Chestnut Creek at the northern border of the Galax Quadrangle where arkosic gravel beds may be discerned, along with the faint remains of crossbedding.

The appearance of these rocks contrasts sharply with that of the Ashe Formation elsewhere in the study area. Although coarse conglomerates are present in the Ashe, their distribution is only local and they are not generally abundant. In addition, while muscovite schists are common everywhere within the Ashe Formation, they are present in only small amounts near the top of the Bowers Ferry sequence, indicating that the Ashe in the study area has a much stronger pelitic component than the Bowers Ferry rocks. Thus, the gross stratigaphic package bears a stronger resemblance to the Unicoi Formation than the Ashe Formation in the study area. In addtion, the Bowers Ferry

rocks do not resemble those from the type locality of the Ashe Formation in Ashe County, North Carolina (Rankin, 1970) which also has a much stronger pelitic component.

However, affinity with the Unicoi Formation is also not clear-cut. As described by Cooper (1961) and Stose and Stose (1957), the lower Cambrian Unicoi is a series conglomerates, arkoses and quartzites with minor shales with several prominent basalts in the middle part of the unit, some bearing amygdules. In the study area, the mafic units, though mylonitized, lack amygdules, and appear to have been originally coarse grained similar to the amphibolites of the Ashe Formation as evidenced by the persistence of coarse-grained plagioclase. Major element analysis of one sample (#A2-3X,Tso, 1987, appendix B) indicates that these rocks are somewhat lower in MgO content (3.6%) and CaO content (7.1%) that normal Ashe Formation amphibolites. This results, along with its relatively low metamorphic grade, in the unusual assemblage of albite + chlorite + biotite + stilpnomelane + epidote + ilmenite + sphene + calcite (secondary), without any amphibole.

It should be noted that confusion over the formation assignment also exists for rocks in a similar stratigraphic position in northern Floyd County, some 100 km to the northeast. There, Dietrich (1959) and Kaygi (1979) have mapped a belt of weakly metamorphosed conglomerates and other sedimentary rocks northwest of the Fries Fault as lower Cambrian "Chilhowee Group" sediments, while Espenshade and others mapped this as "Ashe". In the study area, it appears that these rocks have similarities to both formations. It is clear that the Bowers Ferry rocks and the rocks to the northeast merit further study.

The Stone Mountain Thrust Sheet

Unicoi Formation

Rocks in the northern-most belt of the study area are within the Unicoi Formation. The best outcrops are found along the railroad tracks on the west side of the New River and in the stream that runs east of Vaughn School. The bulk of the outcrops along the New River are a coarse green arkosic conglomerate, with clasts of feldspar, quartz and occasional pink quartzite lithic fragments which may attain a size of 2 cm. Numerous other lithologies crop out including white coarse quartz sandstones, dark green quartzites, and minor tan shales.

Structural Geology

Over most of the study area, the dominant structural element of the Ashe Formation is a pervasive and penetrative schistosity which strikes approximately N50°E, dips to the southeast at a variable angle, and consistently parallels the lithologic layering. This pattern is obvious from plate II, a map of structural data, in which strike and dip symbols serve to illustrate the monotony of the "structural grain". However, close inspection of rocks in the field and in thin section reveals that this schistosity overprints an earlier foliation, and that there is a general warping and local overturning of the foliation by later deformational events. Furthermore, these structures may be used, in a relative sense, as indicators of the timing of the thrust faulting. The following is a description of the structural elements.

Bedding - (S_0): Bedding is most obvious in the Unicoi Formation and the Bowers Ferry rocks where the metamorphic grade is relatively low and sedimentary structures such as crossbedding are preserved. In the Ashe Formation, metamorphism has obliterated most of the original sedimentary structures. However, sedimentary layering may be surmised from lithologic contacts between schists and gneisses, which represent shaley and sandy units, and from contacts between the metasediments and amphibolites which probably represent contacts with flows or shallow sills. Contacts between the metasediments and amphibolites in nearly all places are observed to be par-

allel to the "bedding" of the metasediments. In addition, the texture of the amphibolites may be at least partially inherited from the original igneous texture as evidenced by a distinctly non-foliated texture in the more massive metagabbros and in the reduction of grain size toward contacts with metasediments. Although the group of lithologies classified as the "Cranberry Gneiss" probably contains metasediments as well, the strong mylonitic overprinting observed in the study area has totally destroyed any bedding.

Early foliation parallel to layering - (S_1): This foliation is recognized only in the Ashe Formation and is defined as the penetrative schistosity that is crenulated by the later S_2 cleavage. In schists, it is observed as microscopic scale kink folded layers of muscovite, graphite, and occasionally, biotite (figure 4a). In gneisses, it is obvious as centimeter to meter scale isoclinally folded trains of muscovite and biotite in F_2 folds. However, where such folds are not found, it is difficult to distinguish the S_1 from the later S_2. The S_1 also is more difficult to recognize in amphibolites due to the non-foliated texture of the metagabbros and the lack of a well developed crenulation cleavage.

Crenulation cleavage and regional schistosity - (S_2, F_2): Evidence for a crenulation cleavage is quite pervasive, yet easily overlooked. As previously stated, S_1 foliation in muscovite schists are often overprinted by a second foliation that is penetrative and usually defines the weathering planes in outcrop. In outcrop, the S_2 is axial planar to centimeter to 1 meter scale tight to isoclinal folds (F_2, figure 4b) that rotate the S_1 so that limbs are parallel to subparallel to the S_2 , resulting in the transposition of the earlier foliation. Unless the S_1 and S_2 cross at a high angle, it is usually difficult to tell the two foliations apart. Thus, in outcrops where fold hinges are not observed, the dominant foliation is treated as an S_1/S_2 composite foliation. The folding also brings the S_1/S_2 into subparallelism with the sedimentary layering, and rarely does the dip of the foliation and the lithologic contacts deviate from each other by more than 5°. In thin section, however, the distinction between the S_1 and the S_2 can be observed as an overgrowth of coarser and parallel muscovites, biotites and ilmenites over the earlier kink-folded muscovites (figure 4a). In amphibolites, foliation is parallel to the surrounding S_2 of the metasediments and is defined by the parallel growth of chlorite and

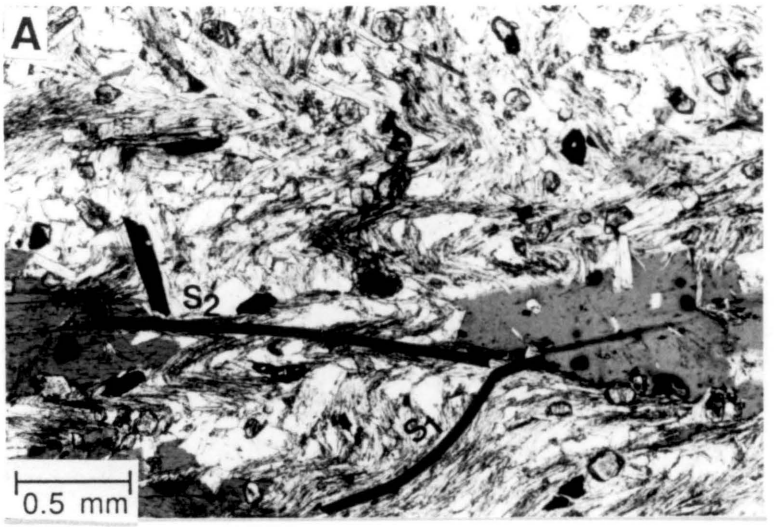
needles of hornblende or actinolite. In the metagabbros and coarse-layered amphibolites, older, more randomly oriented blocky hornblendes are usually overgrown by a new generation of finer, more needle-like grains which impart a weak foliation parallel to S_1/S_2 .

Lineations are also commonly observed, especially in the schists. They are usually observed in three styles: 1) as a fine "crinkle" lineation of mm-scale folds of muscovite plunging SE on foliation planes, 2) as a parallel alignment of porhyroblastic biotite in biotite-muscovite schists in the higher grade areas, and 3) as a fine "crinkle" lineation that results from the intersection of the S_1 and the S_2 . The first two types typically plunge down the dip of the foliation toward the southeast (L_2), while the third type trends toward the northeast (L_1 x L_2). In some rocks, types 1 and 3 may be observed together, crossing each other at approximately 90°.

Mylonite foliation - (S_m): Mylonite foliations are associated with the Fries Fault and to a lesser extent, the Bowers Ferry Fault. The most obvious manifestation of mylonitization is found in the Cranberry Gneiss which lies entirely within the Fries Fault shear zone. In the Fries area, the Fries Fault overrides relatively unmetamorphosed Unicoi. Samples taken from close to the Cranberry-Unicoi contact (A2-14C) show a highly planar fabric that strikes and dips N45°E, 36°SE, with a strong slickenside lineation (L_m) that trends approximately down the dip. As seen in thin section cut parallel to L_m (figure 5a), augens are composed of feldspars, while quartz is found in ribbons intimately intergrown with parallel muscovite and mylonite matrix composed of feldspar, quartz and muscovite. In this, the most intense of the mylonite fabrics, c-(cisaillement) and s-(schistose) surfaces as described by Berthe and others (1979) and Simpson and Schmid (1983) are parallel. Augens are symmetrical to asymmetrical (figure 5b) with the sense of asymmetry consistent with a movement from southeast to northwest. The planar banding of this rock (figure 5c), the quartz ribbons and feldspar augens are quite unlike the mylonitized sedimentary rocks in the study area which display some preservation of feldspar clasts.

The mylonitization is less well expressed in the overlying Ashe Formation. However, previous workers have noted the presence of phyllonites (Stose and Stose, 1957) or button phyllites and slip

Figure 4. **Photomicrograph and outcrop photo of structure:** a) S_1 and S_2, crenulation cleavage, sample A4-49B, uncrossed polars; b) contorted gneiss in graphitic phyllite displaying early early F_2 folds, location C3-8.


A
S2
S1
0.5 mm

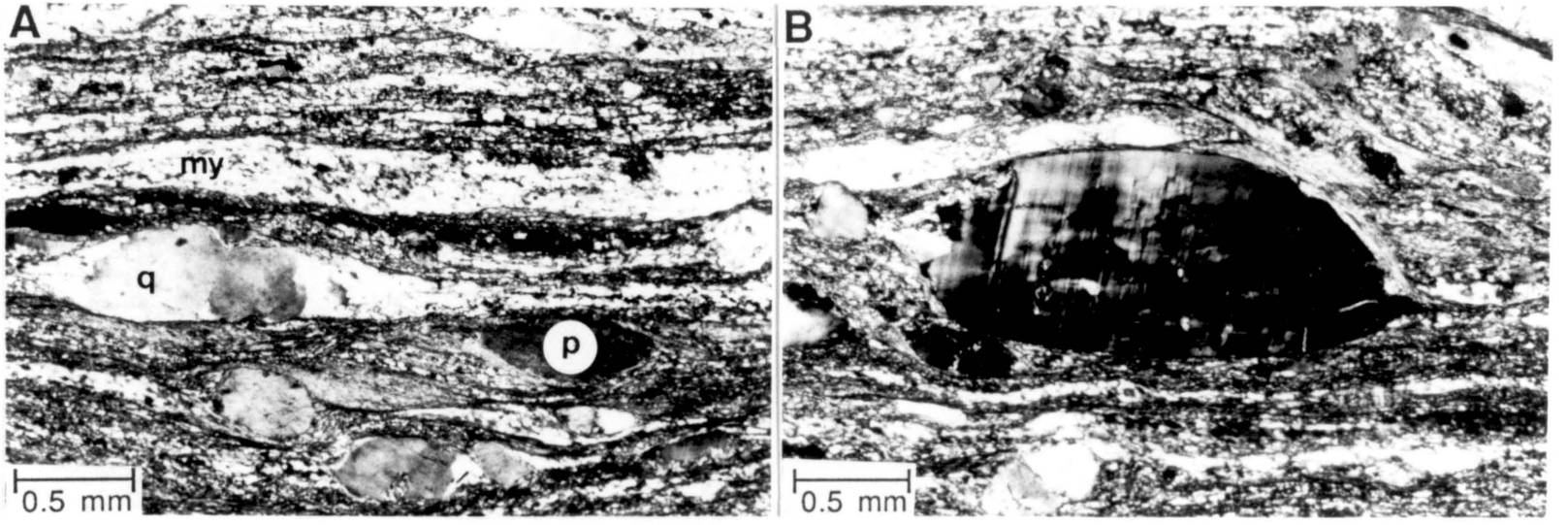

B

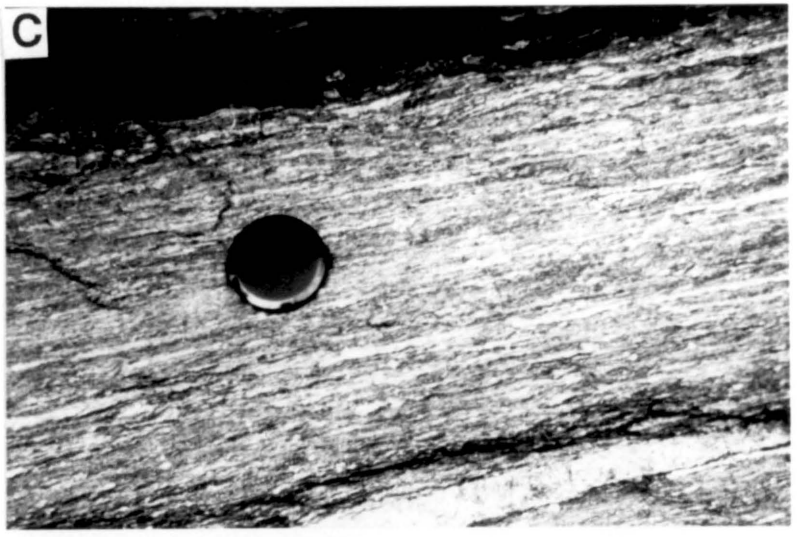
cleavages (Rankin, 1971). As seen in outcrop (figure 6a), the slip cleavage is a widely spaced (2-3 cm) cleavage which dips to the southeast. The "S_{slip}" can be found in the Ashe metagraywackes up to 1/2 km away to the southeast of the Ashe-Cranberry contact. In a thin section cut parallel to slickenside lineation (figure 6b), the slip cleavage is seen as thin zones of finer quartz, plagioclase and carbonate approximately 0.5 mm wide that cuts obliquely across the S_2 , at an angle of up to 55°. Commonly, the S_2 will curve toward the S_{slip} with the angle between the two cleavages approaching 0°. The sense of deflection of the S_2 gives a shear sense consistent with movement to the northwest, in agreement with evidence observed in the Cranberry Gneiss.

Somewhat similar structures in the Blue Ridge have been described by Boyer (1984) in the Grandfather Mountain Formation of North Carolina. He described discontinuous mica bands of less than 3 cm in length that represent small shear zones that have "horse-tail"-like folia that flare toward the shear zones in a manner that resembles the way the S_2 foliation curves toward the S_{slip} in the Ashe Formation. Boyer attributes his structures to a single phase of deformation, with the "horsetails" serving to transfer slip from one mica band to the next, similar to ramping during thrust faulting. The Ashe, however, is a bit more complex in that there is already a pre-existing cleavage - the S_2, which is in an orientation similar to the "horsetails". In addition, the attitude of the S_2 in the surrounding Ashe is parallel to the S_m of the mylonite zone in the nearby Cranberry Gneiss thus making distinctions between foliations difficult unless thin sections are examined. It is possible that a mechanism similar to that of the Grandfather Mountain Formation also existed within the Ashe Formation, with slip facilitated in the Ashe by the already existing foliation.

Further complications arise in the New River area in that the S_2 and S_{slip} are warped by the F_3 folds that are in the vicinity of the Fries Fault. This folding appears to be flexural-slip in style and thin mica-rich layers will often show cm-scale kink or box-type folds that are parasitic to the larger warps, especially if the more ductile mica layers are sandwiched between quartzo-feldspathic layers. The result is a kink-folded S_2 with the superficial appearance of an incipient S_{slip} that results when kinks of adjacent layers line up. However, in this case, the dip of the incipient cleavage is greater than that of the S_2, as opposed to less than the S_2 in the case of S_{slip}.

Figure 5. Photomicrographs and photograph of the Cranberry mylonite: a) Planar mylonite texture with quartz ribbon, plagioclase augen, and mylonite matrix; sample A2-14C, crossed polars; b) asymmetric plagioclase augen; sample A2-14C, crossed polars; c) outcrop photograph of planar Cranberry Gneiss, location A2-13. Abbreviations: my = quartz + plagioclase mylonite matrix, p = plagioclase, q = quartz.


A
my
q
p
0.5 mm
B
0.5 mm


C

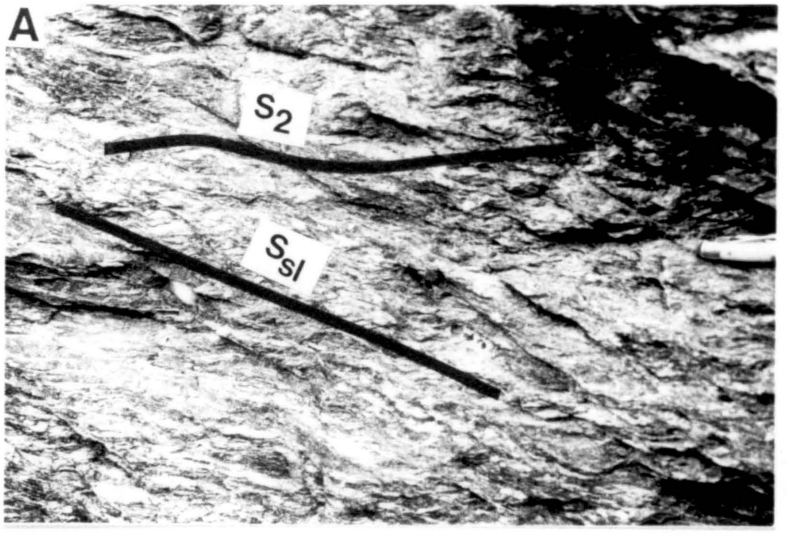
The rocks of the Bowers Ferry block also show extensive mylonitization with intensity generally increasing north to south towards the Fries Fault. When looking at a series of conglomerates collected from north to south along Chestnut Creek, one can document the overall increase in deformation and metamorphism. Looking at figure 7a from the Bowers Ferry sheet at the northern-most extremity in the study area, one can immediately observe the results of deformation as feldspar clasts are torn, broken, and filled with matrix. While quartz is commonly found stretched into ribbons, feldspars show less flattening, but more recrystallization around their rims. In addition, several 0.5 mm shear bands of fine grained recrystallized quartz and feldspar with carbonate stringers are visible in discontinuous zones parallel to the flattening direction. The carbonates are mostly calcite, but one specimen from close to the Fries Fault contained ankerite as observed in microprobe analysis. The micaceous matrix is composed of muscovite and chlorite, with biotite occurring in nearby samples as late-growing rosettes.

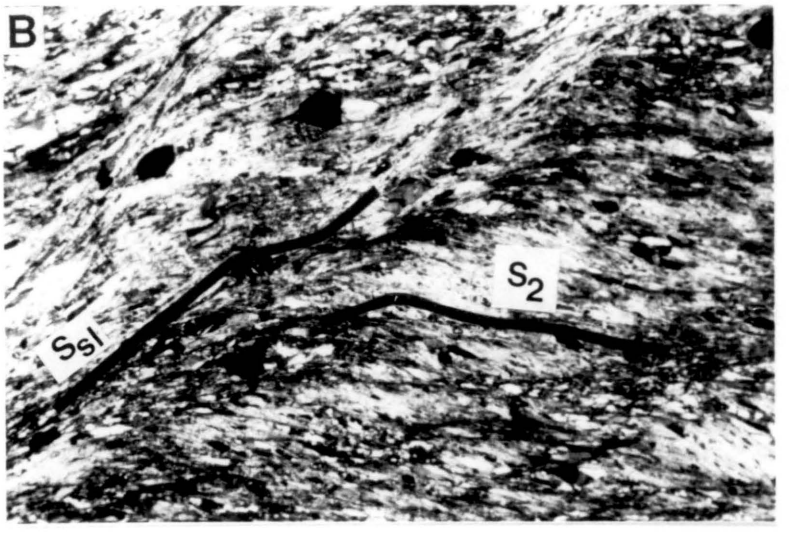
Figure 7b shows the results of increased recrystallization closer the Fries Fault. The main effects are an increased flattening of quartz, with feldspars holding their more equant shape, but at the same time showing more breakage, and an increased recrystallization to matrix. In figure 7c, from an outcrop at the Fries Fault, the amount of matrix increases, with the development of muscovite now defining the foliation. and grain growth from increased heating during or after faulting.

In the Unicoi Formation north of both the Fries and Bowers Ferry Faults, notable mylonitization is only observed within a few hundred meters of the faults. Mostly, feldpars may show some local recrystallization where broken. In the Fries area, where the Cranberry is thrust directly on the Unicoi, the sandstones and conglomerates have a notable powdery fault gouge texture, and a shale that crops out just north of the fault trace is transformed into a button phyllite.

Broad NE-trending folds - (F_3, S_3): All formations in the study area show the effects of broad, regional scale folding about NE-SW trending subhorizontal fold axes. The results of this folding come in different scales and styles. Usually, F_3 folds are noticeable as areas of oppositely dipping rocks as observed on the structural map (Plate II), or discerned indirectly from stereonets (figure

Figure 6. Photograph and photomicrograph of slip cleavage: a) Outcrop photograph of S_{slip} as cm-scale fracture spacing; location A2-12; b) photomicrograph of Ashe Formation slip cleavage; sample A2-12B, crossed polars.


A
S_2
S_{S1}


B
S_2
S_{S1}

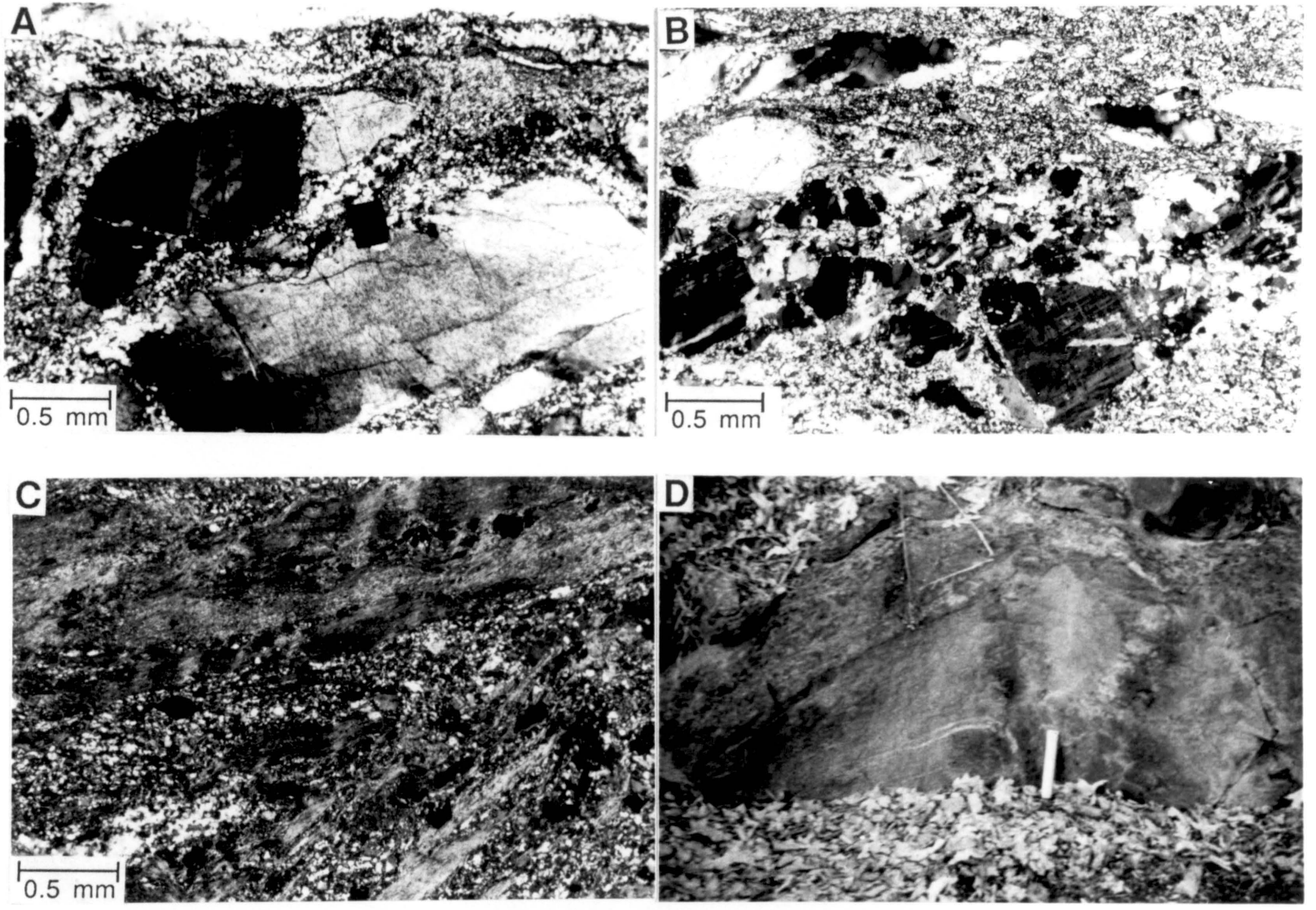
8). In order to better illustrate the development of F_3 folds, strike and dip readings in the study area were divided into a series of "zones" that are bordered by thrust faults, stratigraphic boundaries, and, for convenience sake, roads (figure 8a). These zones are: the Unicoi Formation, the Cranberry Gneiss, the Ashe Formation northwest of the Gossan Lead trend, the Ashe Formation southeast of the Gossan Lead and northwest of the Galax shear zone (with an eastern sector, and a western sector), and the Ashe Formation southeast of the Galax shear zone. As observed on the stereonets, the poles to S_2 and S_m cluster strongly (figures 8e-n), with the scatter attributable to the F_3 warping, causing the main variation in the dip, and with the F_4, causing the main variation in the strike.

The most obvious example of F_3 warping may be seen in the eastern sector of the Ashe Formation between the Gossan Lead and the Galax shear zone, where both stereonet and map patterns indicate a broad area of northwest-dipping rocks (figure 8l). A smaller area of northwest-diping rocks is found in the area just south of the Galax shear zone near Cliffview.

Centimeter scale kinking and crinkling are also common, as previously mentioned, in the Ashe Formation, paricularly where schistose units are caught between gneissic units in small versions of drag folds. In addition, cm-scale kink folds can be found in the actinolite-chlorite schists in the belt of rocks near Cliffview. In these rocks, S_2 chlorite and amphibole are clearly folded with NE-trending fold axes in areas of known macroscopic F_3 folds. Unfortunately, these rocks crop out only in small patches, but it is believed that they similarly represent small versions of F_3 folds.

S_3 foliations are only locally developed. One of these localities is in the Bumbarger Pit of the Gossan Lead on Iron Ridge, where the S_3 is axial planar to a mesoscopic F_3 fold and creates a 3 mm-spaced crenulation cleavage superimposed over the regional S_2 . F_3 folds are always asymmetrical in the study area, and are northwest verging. Overturning is generally not observed, but if so, as in the Cliffview area, the northwest limb is overturned. As far as can be determined, the folding has not produced any significant repetition of layering at least on the map scale.

Figure 7. Photomicrographs of Bowers Ferry rocks and F_4 fold: Development of mylonite in the Bowers Ferry rocks: a) broken plagioclase; sample A2-6B, crossed polars; b) additional deformation; sample A2-4A, crossed polars; c) muscovite development near Fries Fault; sample A2-3Z, crossed polars; d) F_4 fold in Ashe Formation, location C3-8. For further explanation, see text.


A
0.5 mm
B
0.5 mm
C
0.5 mm
D

The F_3 folds mapped in this study were also mapped on a more regional scale by Stose and Stose (1957). According to their maps, these folds are not only common in the Blue Ridge but are also found in the nearby Valley and Ridge as well. Indeed, the present study shows that even the mylonites of the Fries and Bowers Ferry faults are folded as well as the Unicoi and Bowers Ferry rocks.

SE-trending mesoscopic folds - (F_4, S_4): Throughout the Ashe Formation, a number of folds whose axes plunge 20° to 40° toward S20°E to S40°E were observed primarily in the mesoscopic scale (figure 7d). These folds are only locally developed, with a typically open, flexural-slip style. These structures cut the overall structural grain of the area, being nearly 90° from the regional schsitosity and warping. It should be noted that other workers (Rankin, 1971, Jones, 1976) have also found NW trending folds which they also considered to be late, post-thrusting structures. We therefore place these sets of structures last in the relative order of events and term them "F_4."

These folds have somewhat tighter interlimb angles than the F_3 , occasionally approaching 90°, resulting in more common occurrences of S_4 axial plane foliations. This is seen as a 2-3 mm spaced crenulation cleavage that overprints the S_2. In phyllitic rocks, the S_4 intersects with the S_2 to create a lineation in the form of mm-scale sets of "crinkle" folds on the more dominant S_2. In gneisses, parallel trains of biotites are seen bent into folds. In amphibolites, stretching of the plagioclases areas into lenses occurs at some of the fold hinges.

Other faulting events: Several other faults and shear zones have been recognized in local areas.

Shear zone north of Galax: A narrow belt of slickensided outcrops and float pieces was mapped in the area just north of the Galax City line. On the geologic map (plate I), at least two amphibolites are projected to be cut off at this zone with a 10° offset in the overall strike of the main foliation from one side of the zone to the other. On the basis of increased celadonite composition of muscovite and amphibole-plagioclase equilibria compared with rocks from outside the

Figure 8. Stereonets - poles to bedding and foliation: a) Location map of structural data zones; b) Unicoi Formation, zone A, open circle = bedding (S_0), n = 28; closed triangle = B_3 = 18°, N 44° E; open triangle = B_4 = 25°, S 40° E; c) Unicoi Formation, zone A, closed circle = mylonite foliation (S_m), n = 9; open triangle = B_4 = 30°, S 40° E; d) Bowers Ferry thrust sheet, zone B, open circle = bedding (S_0), n = 21; closed triangle = B_3 = 10°, N 70° E; open triangle = B_4 = 16°, S 26° E; e) Bowers Ferry thrust sheet, zone B, S_m, contours = 1, 5, 10, 15, 20, 30%, n = 56; closed triangle = B_3 = 14°, N 77° E; open triangle = B_4 = 31°, S 27° E; f) Cranberry Gneiss, zone C, closed square = mylonite foliation (S_m), n = 35, closed hexagon = mylonite lineation, n = 6, open triangle = B_4 = 27°, S 16° E; g) Ashe Formation, zone D, closed square = mylonite foliation (S_m), n = 9; open hexagon = crinkle lineation, n = 9; circled dots = slip cleavage, n = 5; open triangle = B_4 = 46°, S 47° E; h) Ashe Formation, zone D, S_2, contours = 1, 5, 10, 15%, n = 133; closed triangle = B_3 = 5°, N 43° E; i) Ashe Formation, zone E, S_2, contours = 1, 5, 10, 15, 20, 25%, n = 74; j) Ashe Formation, zone F, S_2, contours = 1, 5, 10, 15%, n = 209; k) Ashe Formation, zone G, S_2, contours = 1, 5, 10, 15, 20%, n = 72; l) Ashe Formation, zone H, S_2 , contours = 1, 5, 10%, n = 180; closed triangle = B_3 = 5°, S 35° W; m) Ashe Formation, zone I, closed circle = S_2, n = 46; open triangle = B_4 = 44°, S 13° E; n) Ashe Formation, zone J, S_2, contours = 1, 5, 10, 15, n = 86; closed triangle = B_3 = 6°, S 51° W; o) Ashe Formation, zones D-J, closed circle = S_1, n = 36; p) Ashe Formation, zones D-J, open circle = microfold and biotite lineation (L_2), n = 37; open triangle = S_{1x2} intersecting lineation (L_{1x2}), n = 8; closed square = F_2 fold axes, n = 19; q) Ashe Formation, zones D-J, closed triangle = F_3 mesoscopic fold axes, n = 8; open triangles = F_4 mesoscopic fold axes, n = 6.

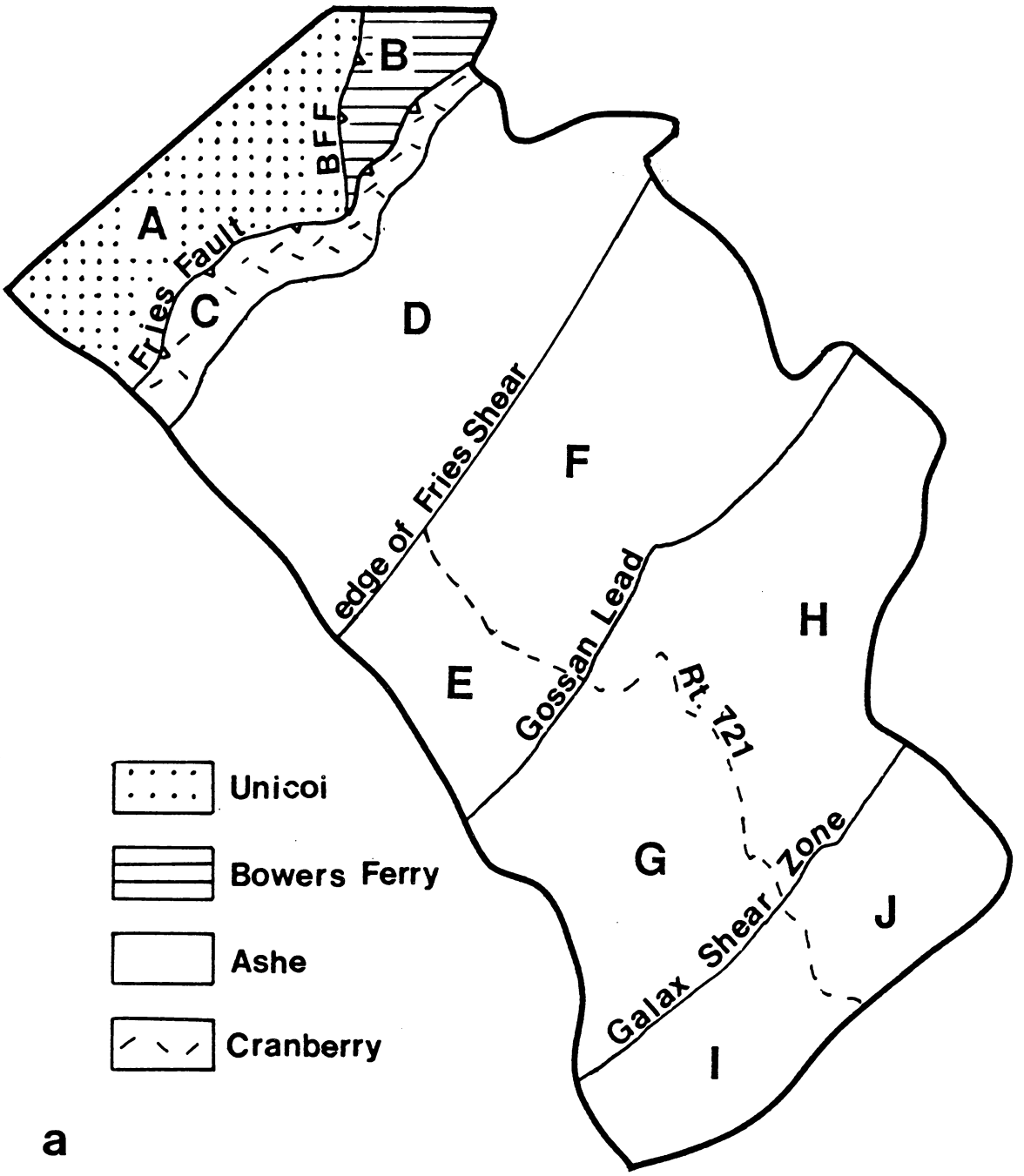


Figure 8 (continued)

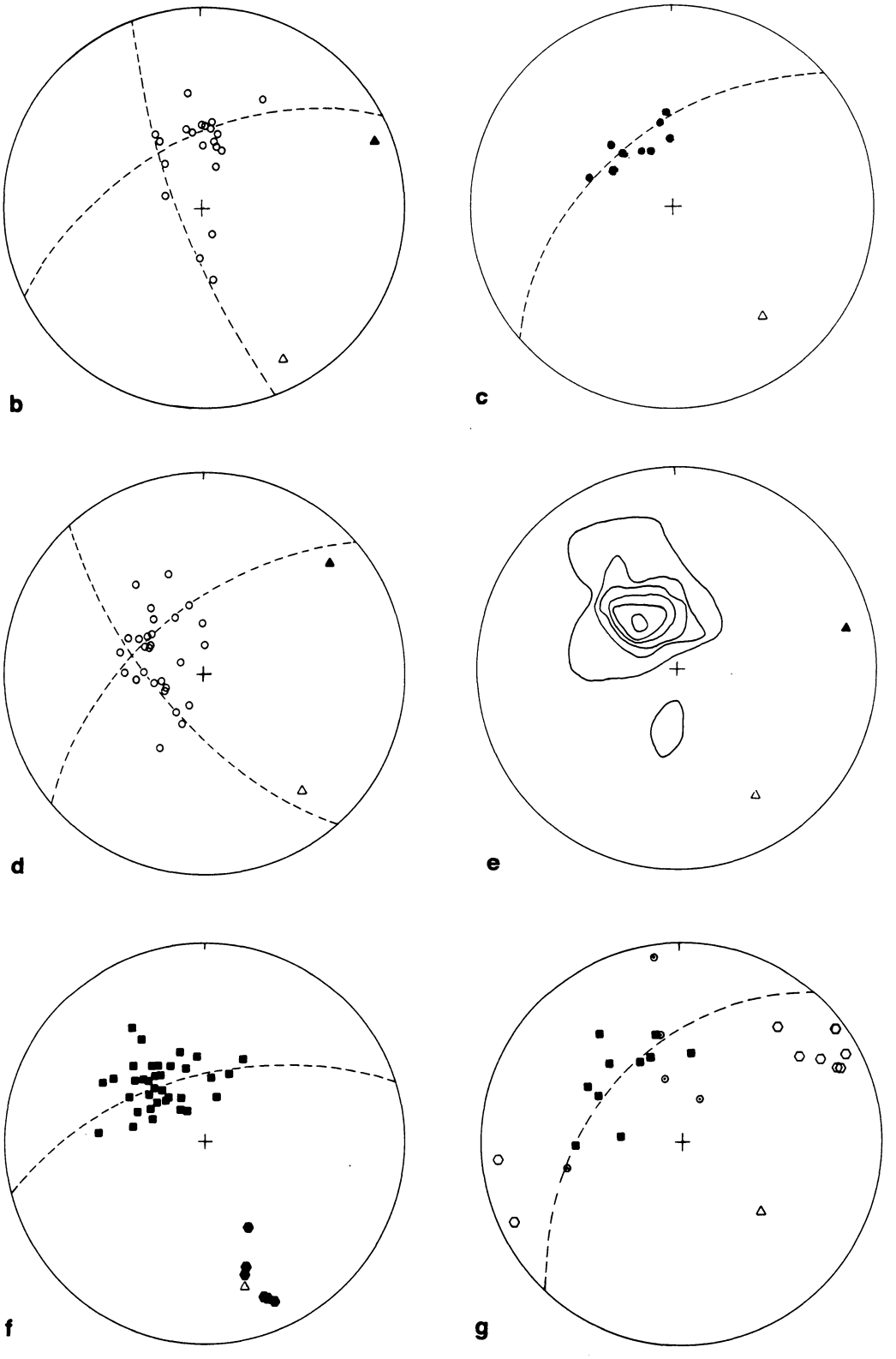


Figure 8 (continued)

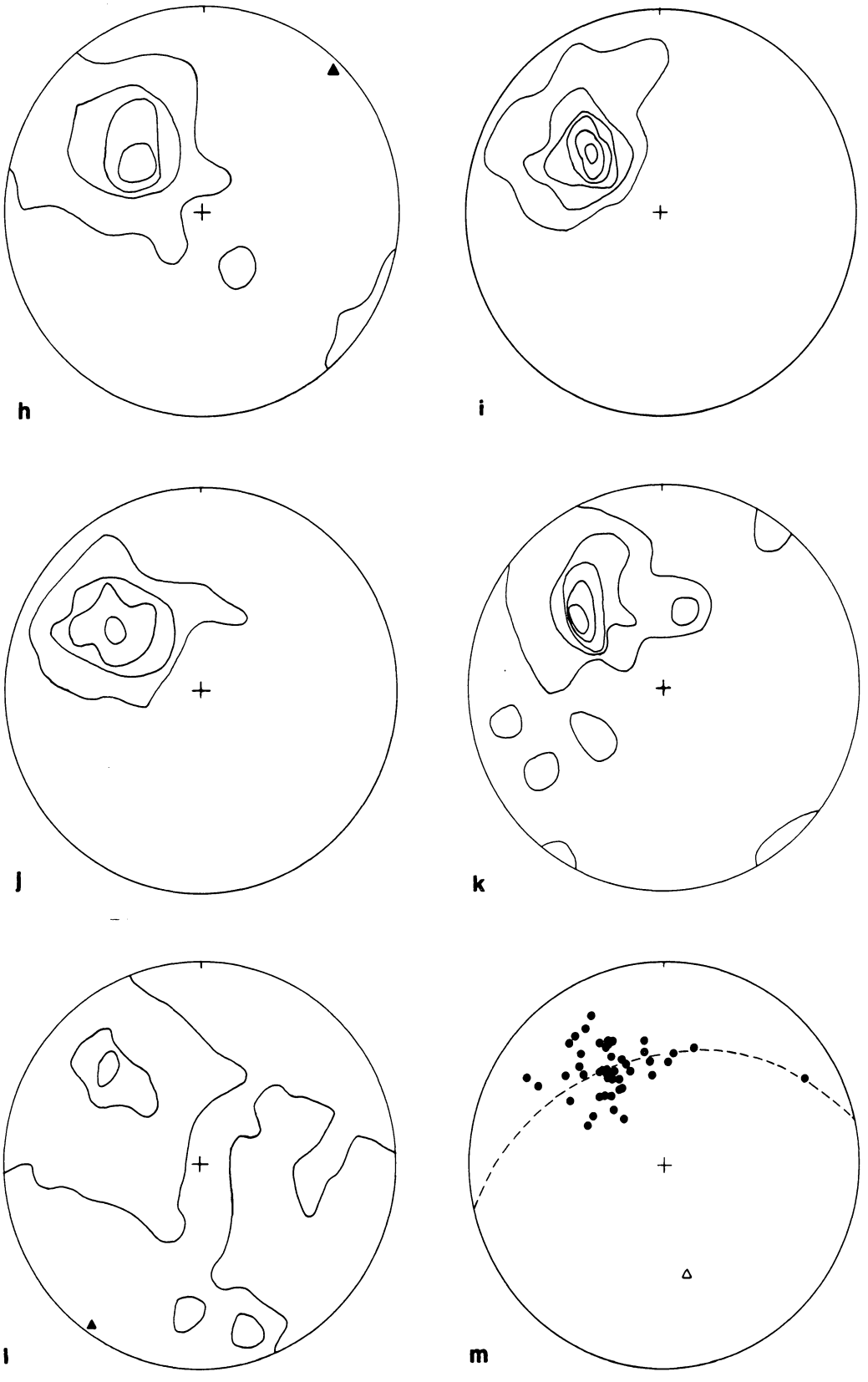


Figure 8 (continued)

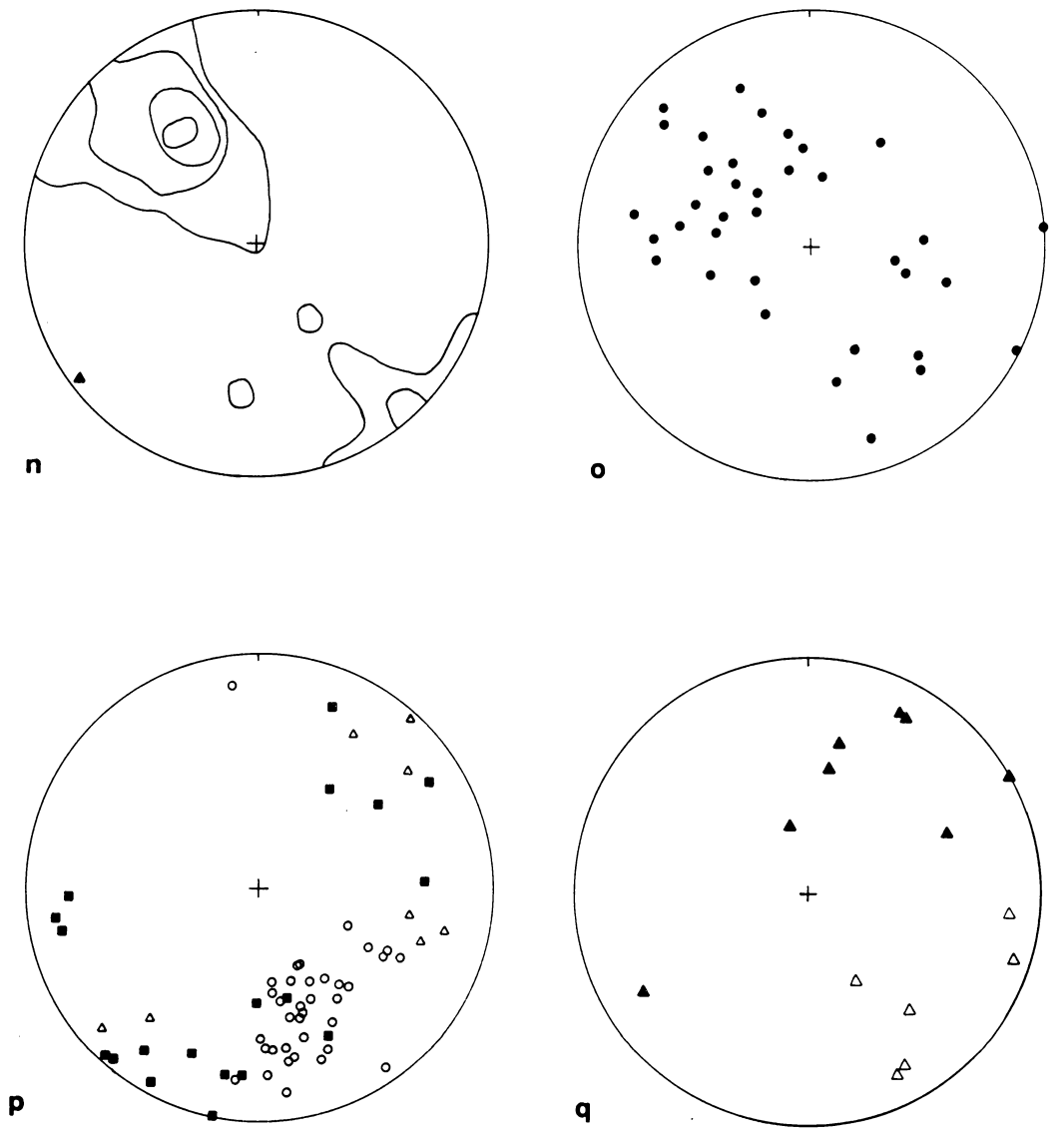


Figure 8 (continued)

shear zone, Tso (1987) interpreted the rocks to have equilibrated at temperatures somewhat lower than the surrounding area. Thus, these rocks represent a late, retrogressive shearing event.

High angle faults: Two normal-slip faults have been observed at the Bumbarger Pit (Gair and Slack, 1984, Tso, 1987), one striking approximately N60°E, the other N20°W. These faults are evident because of the unusual circumstance of having a fairly well defined stratigraphic boundary, the "hanging wall" of the Gossan Lead massive sulfide, exposed at a very large outcrop, an open pit mine. It is quite probable that such faults are much more common in the study area but have gone undetected. In any case, these faults do show some fault gouge, but no major ductile deformation, and it appears that they are rather late events.

Relationship of deformation to metamorphism

Detailed microprobe analysis of the rocks have been reported by Tso (1987) and temperatures, using the Ferry and Spear (1978) and Hodges and Spear (1982) geothermometers, are in the range 470 to 600 °C ± 60°C, increasing to the southeast, with pressures estimated to be between 4 and 7 kb by use of several geobarometers, including the one of Ghent and Stout (1981).

The above determinations represents near peak metamorphic conditions. However, textural evidence indicates that metamorphism rose and fell with the peak cresting sometime after D_2 but before D_m , with recrystallization occurring in an almost continuous, "moving picture" fashion spanning all folding and thrusting events (figure 9).

The S_1 foliation is defined by kink folded white micas, chlorite, graphite and biotite. As deformation proceded and metamorphic conditions rose, the F_2 crenulation and isoclinal folds were superposed over the S_1 with the result of the growth of coarser muscovite, biotite and ilmenite lining up

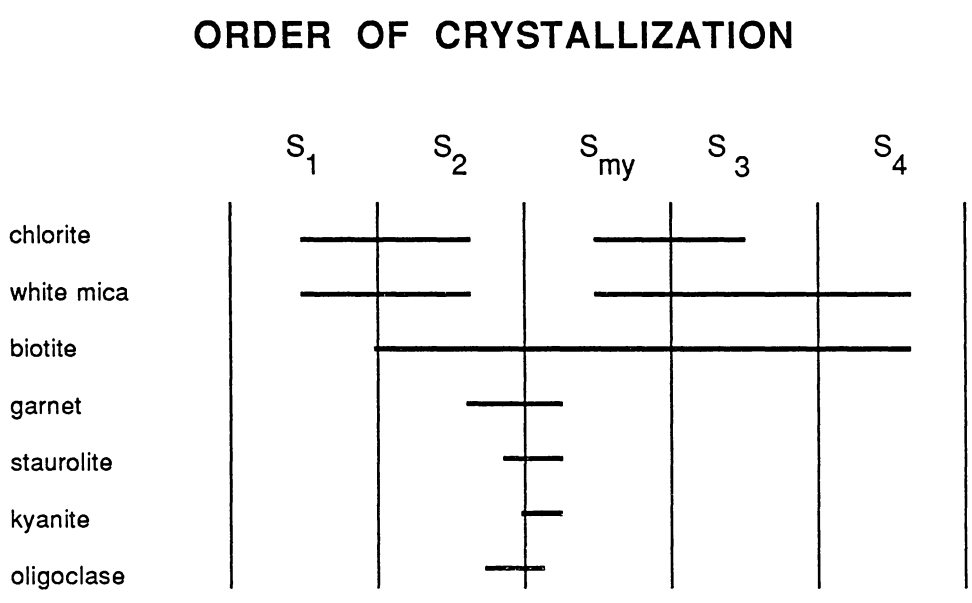


Figure 9. Chart of mineral growth in relation to deformational events

axial planar to F_2 folds. Garnet euhedra appear next, some showing flattening parallel to the S_2 , along with coarser, more random biotite that commonly overgrows garnet. In several samples, the biotite contains some kink folding, testifying to the overlap between this round of mineral growth and the D_2. Next, in the Galax area, staurolite appears in porphyroblasts up to 7-8 cm long. These spectacularly twinned crystals often show little effects of deformation, and in thin section, they clearly overgrow previously flattened quartz and garnet euhedra, with only a few showing S_2 related cracking and stretching. These unusual rocks also contain S_1 paragonite-muscovite intergrowths and S_2 and post-S_2 chlorite, discussed in more detail in Tso (1987). Thus, the metamorphic peak clearly post-dates the main regional schistosity.

These metamorphic index minerals were the basis of the metamorphic isograd maps of Espenshade and others (1975) and Rankin and others (1972), which clearly showed that the metamorphic isograds are offset by the Fries Fault. This is corroborated in the present study where both the Fries and Bowers Ferry Faults juxtaposes higher grade rocks onto lower grade rocks. Unfortunately, estimates of temperatures and pressures within the fault zones are difficult, as garnet is not found in the mylonite zone. The garnet-in isograd occurs in the Ashe Formation just at edge of the mylonite shear zone as seen by the first appearance of the "S_{slip}." Although this would suggest that perhaps mylonitization had a retrogressive effect on the Ashe Formation, and by extension, the Cranberry Gneiss, no evidence of retrogressive chlorite pseudomorphs after garnet was found in Ashe rocks closer to the fault. Thus, the assumption is made that garnet grade was never achieved there.

In the Ashe Formation, development of mylonite is locally confined to the quartz-feldspar-rich gneisses that border the Cranberry Gneiss. In addition, the presence of a slip cleavage indicates some shearing took place, probably related to Fries thrusting. However, unlike the Cranberry, the Ashe Formation lacks an overwhelmingly planar texture typical of extensive recrystallization. Indeed, as will be discussed in the next section, some samples taken close the the fault still contain feldspar clasts that are not strongly strained.

However, the thrusting did have a local prograde effect on the thrust slices underlying the Fries block. Growth of biotite and muscovite in mylonitic rocks of the Bowers Ferry Block, with chlorite and rare biotite in the Unicoi indicates that greenschist conditions were acheived during thrusting. In addition, biotite rosettes seen in Bowers Ferry rocks indicate some static heating after thrusting ceased, with metamorphic grade increasing up the stratigraphic section toward the thrust fault.

Closely associated with thrusting is the F_3 folding event, with only sparse recrystallization being evident. F_4 folds are similarly locally developed. However, recrystallization is evident in the hinge areas of the F_4 folds with a locally developed axial plane foliation.

The Ashe-Cranberry Contact

Nowhere in the study area is the Ashe-Cranberry contact exposed. However, along the west side of the New River, 3 km north of the town of Fries, the contact can be placed within a 5 meter span. All rocks there are extensively sheared, with the Ashe and Cranberry Formations dominated by S_m and S_{slip}. In order to determine both the lithology and the deformational style, a suite of thin sections was made from samples taken across this zone, starting with samples taken at the Fries Fault itself, where it thrusts the Cranberry Gneiss over the Unicoi Formation, through the Cranberry - Ashe contact (figure 10)

In figure 11a, a thin section from the Cranberry - Unicoi contact, the Cranberry Gneiss shows a highly planar fabric, with symmetrical quartz and feldspar augens, and with parallel c-s surfaces as defined by muscovite growth and the plagioclase-quartz mylonitic matrix. Figure 11b was taken from the Cranberry just below the contact with the Ashe. Note that the sample is still highly strained, yet considerably coarser overall. Augens are coarser intergrowths of feldspar and quartz that appear to predate the development of the mylonite fabric. Figure 11c, from lowest part of the Ashe just above the contact, shows extensive shearing, but also shows the survival of some of the original detrital clasts of quartz and plagioclase of up to 2 mm. In figure 11d, taken another 0.18 km further south, the Ashe Formation is more micaceous, with the obvious development of the S_{slip} , and with overall grain size being coarser due to a decrease in the amount of mylonitization.

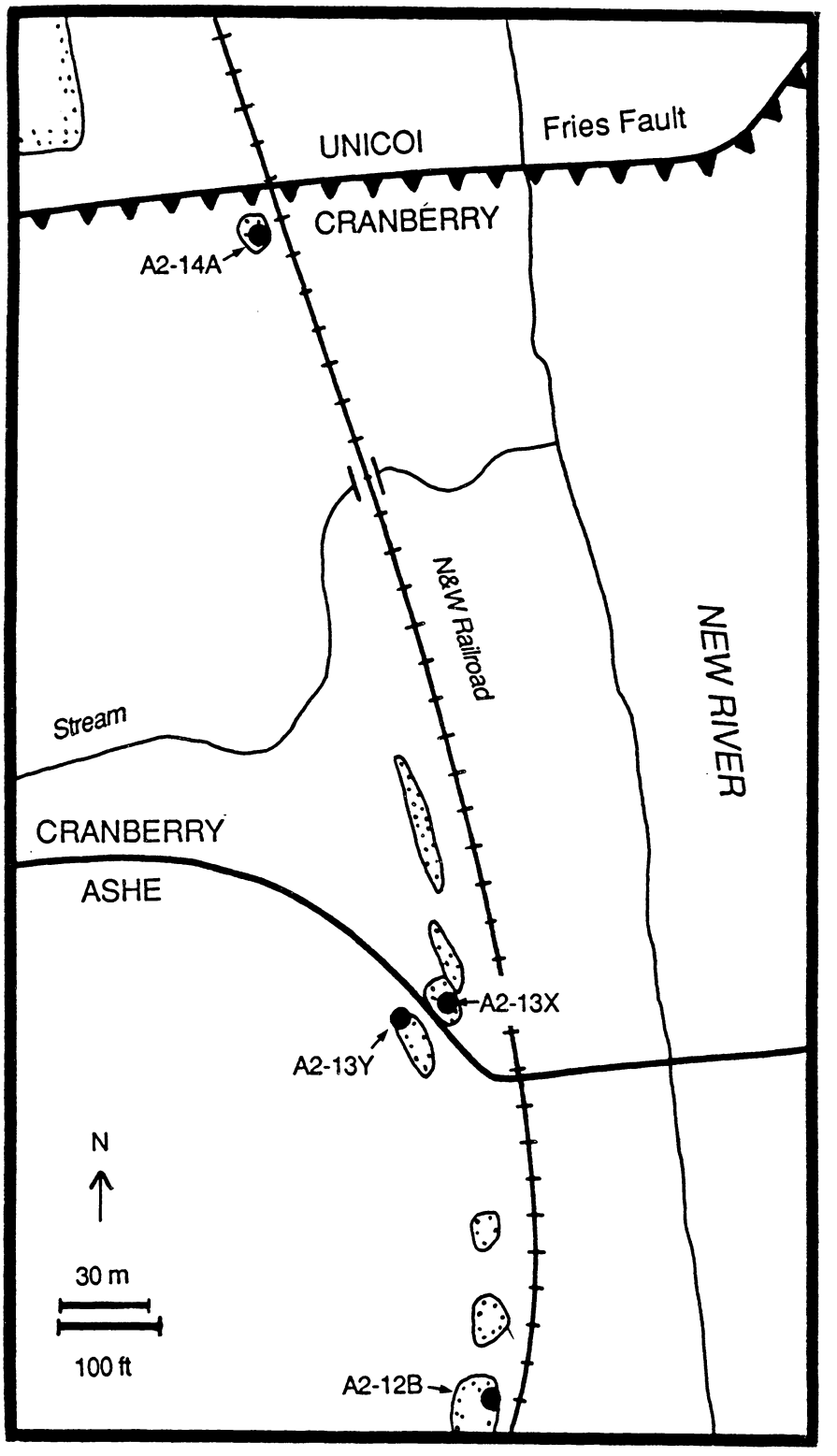


Figure 10. Sketch map of Cranberry-Ashe contact, west side of New River.

However, it is also evident that this sample also lacks the coarse clasts that were found in the rocks below.

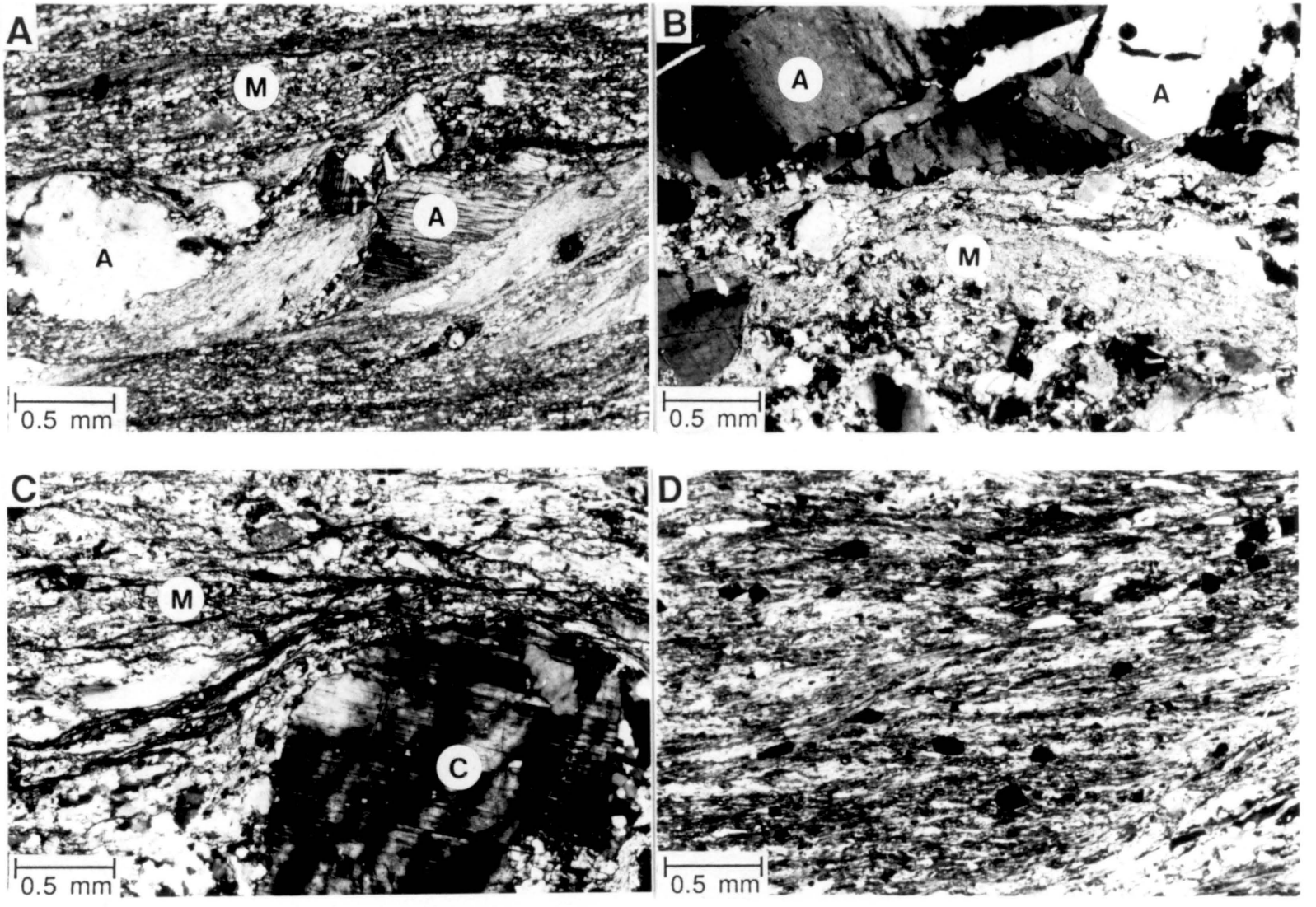
The Ashe section observed near Fries is considerably different, however, from the "basal conglomerate" near Crumpler, North Carolina that Rankin (1971) described as containing cobble-sized granitic and quartz clasts. Abbott and Raymond (1984), later revisited this locality and concluded that the rocks there were actually mylonitized Cranberry Gneiss with a texture similar to that of conglomerates. It is likewise observed that in the Fries area, ultra-mylonitized Cranberry can have a conglomeratic appearance caused by rounded augens set in a mylonitic matrix. However, in the Fries area, these "conglomeratic" rocks are not observed in the Ashe Formation, but in the Cranberry, where the shearing is the most intense, in particular adjacent to the Unicoi, not the Ashe.

As previously discussed, there has been considerable debate over the nature of the Ashe - Cranberry contact. Debate has centered on two principle theories: that the contact is a fault, and that the contact is a nonconformity. If the contact is a fault, one can also speculate as to whether or not the faulting occurred before, during or after the metamorphic peak.

The contact is a pre-peak metamorphic fault: This hypothesis implies that after faulting, regional metamorphism occurred, establishing the regional S_2 foliation, and possibly obliterating some of the mylonite or shearing texture that may have developed. Later, the Fries Fault mylonite texture was superposed on the contact, further destroying any early shearing texture. Although this hypothesis cannot be discounted entirely, neither is there much evidence to support it. Sampling of the Cranberry and Ashe shows that in rocks adjacent to the contact, pre-Fries rock textures may still be preserved as coarse feldspar-quartz augens or sedimentary clasts. Nowhere have textures been observed that might be interpreted as annealed mylonite or older fault breccia.

The contact is a post-peak metamorphic fault: This hypothesis is favored by Abbott and Raymond (1984) who cite the fact that in North Carolina, rocks of higher metamorphic grade are in contact

Figure 11. **Photomicrographs of the Cranberry-Ashe contact:** a)Cranberry Gneiss, sample A2-14C, crossed polars; b) Cranberry Gneiss, sample A2-13X, crossed polars; c) Ashe Formation, sample A2-13Y, crossed polars; d) Ashe Formation, sample A2-12B, crossed polars. Abbreviations: A = augen, C = clast, M = matrix. For further explanation, see text.


A
M
A
A
0.5 mm
B
A
A
M
0.5 mm
C
M
C
0.5 mm
D
0.5 mm

with rocks of lower metamorphic grade. Petrologic data collected in the present study, however, indicates that the metamorphic grade of the Ashe Formation in the immediate area of the contact is in the chlorite zone. Although rocks in the Cranberry Gneiss contain a different mineral assemblage (in particular, a lack of chlorite), the general lack of biotite and a similar celadonite content of the muscovite in the Cranberry and adjoining Ashe (Tso, 1987) indicates that metamorphic conditions were approximately the same on both sides of the contact. Thus, any offset of the metamorphic isograds along the contact is not strongly pronounced, or has been masked by Fries Fault mylonitization.

In addition, a syn- or post-metamorphic fault hypothesis is not supported by structural evidence, as previously discussed, which does not show a great increase in mylonite development in the Cranberry at the contact with the Ashe.

The contact is a nonconformity: As observed in the study area, the Ashe-Cranberry contact is parallel to the lithologic layering within the Ashe without any obvious truncation of beds. Although a coarse basal conglomerate such as described by Rankin (1971) has not been observed, the rocks at the contact do preserve a coarse-sandy texture of feldspar-rich rock.

Although the study area is small, careful sampling has not uncovered a widespread zone of mylonitization in the Ashe similar to that observed in the Cranberry. There does not appear to be a major offset of metamorphic isograds at the contact, and there is no evidence of any annealed mylonite textures. Local mylonitization and the development of slip cleavages may be simply explained as being part of the same shearing event that produced the mylonite associated with the Fries Fault. Although shearing undoubtably took place along the contact, the above criteria does not support the notion of the contact being a major thrust fault as envisioned by other workers. It should be pointed out that although evidence of a fault contact at Fries is apparently lacking, this does not preclude the possiblity of the contact being a fault at other locations. For example, faults within the Ashe are documented elsewhere within the study area, and also on the reconaissance

map of Espenshade and others (1975). However, in the study area, the hypothesis that the contact is a nonconformity offers the simplest explanation of the field data.

Comparison With Other Works

Detailed mapping and structural analysis of the Blue Ridge metamorphic complex of the type undertaken in this study is rare in Virginia. Mostly, studies have been concentrated in the Ducktown, Tennessee area, and in the Grandfather Mountain Window and Brevard Zone in the Carolinas. Studies that are directly comparable to this study are all fairly distant from the Galax area. Butler (1973) worked out the chronology of events near Spruce Pine, North Carolina, 130 km to the southwest, by combining the work of others with his own reconaissance. Jones (1976) carried out a detailed structural analysis and petrographic study of the Ashe Formation in the Jefferson Quadrangle, N.C., 50 km to the southwest. Rankin (1971), in his reconaissance mapping of the 1:250,000 scale Winston-Salem Quadrangle worked out a general structural chronology that applies to the present study area. Most recently, Bartholomew and others (1983), mapping parts of eight quadrangles between the Grandfather Mountain Window and the Mountain City Window, N.C., recognized 9 events, many of which can be related to the Galax area. A summary is given in table 1.

As can be seen from table 1, there is general agreement with the other studies. Due to extensive mylonitization, the Grenville metamorphism recognized by Jones and Bartholomew and others has not been observed near Fries. The major F_2 event of Butler and Rankin, which they have termed a retrogressive "Acadian" event, is seen mostly to the southwest in the Spruce Pine area but not in

Table 1. Structral data comparing other studies

Table of Comparison With Other Studies (Pt. 1)

This study	Butler (1973)	Jones (1976)	Rankin (1971)	Bartholomew and Lewis (1983)
				8. Iron Mountain thrusting.
S_4 : Local axial plane foliation: F_4 : Open to close, upright, SE-plunging, meso-micro.		S: $_4$ Local axial plane slip cleavage; F_4 : Open to tight, flexural, N25E to N25W, plunges south.	S_4 : Local axial plane slip cleavage; F_4 : S-plunging micro-macro.	7. E-W folds, NW-SE folds, broad doming.
				6. Stone Mountain faulting.
S_3 : Local axial plane foliation: F_3 : Open to close, upright, SE-plunging, meso-micro.	S_4 : Slip cleavage; F_4 : Close to gentle, NE-trending, meso-macro?, deforms pegmatites.			5. Crenulation cleavage, open-upright folds, warps Fries system mylonites.
S_{my} and S_{slip} : Fries, Bowers Ferry thrusting, c-s surfaces in Cranberry.			S_3 : Slip cleavage near thrust faults, large scale warping.	3. Fork Ridge-Linville Falls thrusting, greenschist metamorphism.
	S_2 : Axial plane foliation; F_2 : Open to tight isoclinal, upright, NE-trending, macro-meso., related to Spruce Pine pegmatites.	S_3 : Local slip cleavage; F_3 : tight, asymmetric, flexural, NE-trending, meso-micro.	S_2 : slip cleavage, axial planar foliation; F_2 : tight, overturned to NW, NE-trending meso-micro.	2. Tight to isoclinal, related to pegmatites, amphibolite metamorphism.

Table of Comparison With Other Studies (Pt. 2)

This study	Butler (1973)	Jones (1976)	Rankin (1971)	Bartholomew and Lewis (1983)
Metamorphic peak.	Metamorphic peak.	Metamorphic peak.	Metamorphic peak.	
S_2: Regional foliation, crenulation cleavage; F_2: Tight to isoclinal, NE-trending, micro-meso.	S_1: Axial plane foliation; F_1: Tight to isoclinal, meso-micro.	S_2: Dominant regional foliation; F_2: Isoclinal, NE-trending, meso-micro., formation of Blue Ridge Anticlinorium.	S_1: Pervasive schistosity in Ashe, parallel to compositional layering, slaty cleavage in Chilhowee; F_2: Isoclinal NE-trending, meso-micro. in Ashe; formation of Blue Ridge Anticlinorium.	1. Isoclinal folds, axial plane foliation with metamorphic peak.
S_1: Early foliation parallel to lithologic layering.				
S_0: Sedimentary layering in Ashe and Unicoi, lithologic contacts.	S_0: Primary layering.	Compositional layering.		S_0: Sedimentary layering, soft sediment deformation.
		S_1: Late Precambrian gneissic layering in Cranberry Gneiss.		Grenville metamorphism.

the study area. However, rocks in Galax do have an early (S_1) foliation, while rocks to the south do not, and that in general, the S_1 appears to be more prevalent to the northeast. For example, the author has observed that rocks in the Ashe Formation, 80 km to the northeast near Floyd, Va., show S_1 cut by a classic S_2 crenulation cleavage both of which predates garnet growth. Metamorphic grade there is distinctly lower than at Galax, and the S_1 , which is dominant at Floyd, is more openly folded and is less recrystallized by the S_2. Clearly, the Ashe Formation northeast of Galax is in need of additional study.

Finally, although rocks from the southwestern North Carolina-eastern Tennessee area are considerably distant from Galax, it is noteworthy that the latest compilation of events (Absher and McSween, 1985), reveals a general agreement with the rocks in the study area. Specifically, they cite two phases of isoclinal recumbant foldng, followed by a "Taconic" metamorphic peak, followed by additional phases of NE folding, ductile faulting, and finally, NW-trending folds.

Synthesis and Conclusions

Late Precambrian history

The eastern Blue Ridge has, since the work of Rankin (1975), been considered by most workers to be a late Proterozoic rift zone related to the opening of the Iapetus Ocean. Evidence for this is based along two principal lines of investigation: 1) regional stratigraphic studies coupled with geochronology of the igneous rocks presumably associated with rifting, and 2) major and trace element analysis of the now highly deformed and metamorphosed rocks that would suggest their protoliths.

A recent example of the first type of study is that of Wehr and Glover (1985), in which they interpreted the Blue Ridge as representing continental crust that was highly attenuated during rifting upon which metasediments and metavolcanics were deposited, especially in grabens. The Ashe/Lynchburg Formation was interpreted as representing sedimentation and volcanism in rapidly subsiding basins, with a likely sedimentation source to the east in the form of horst blocks, and with the main North American continent to the west.

The second approach is exemplified by Gair and Slack (1984). Although emphasizing the origin of the Gossan Lead sulfide body, they also did extensive sampling of the Ashe in the study area. Major element chemistry of the metasediments led them to conclude that the schists were originally aluminous shales, and the quartz-feldspar granofels were originally graywackes. They interpreted the amphibolites as being similar to tholeitic basalts, and their Ti-Zr-Y diagrams indicate that the amphibolites have an affinity with mid-ocean ridge basalts. A representative sampling of the major lithologies of the Ashe, Cranberry and Bowers Ferry rocks (Tso, 1987), using X-ray fluoresence analysis of the major elements, yielded good agreement with the Gair and Slack data.

In the Galax-Fries area, geologic mapping shows that the Ashe Formation is a thick metasedimentary package composed of alternating metagraywacke-pelitic schist, with numerous concordant mafic bodies, resting nonconformably on continental crust. Although not entirely analogous, a similar situation of a sediment-clogged, fault-bounded, deep water situation is in the Guaymas Basin in the Gulf of California (Lonsdale and Lawver, 1980). There, a thick sequence of turbidites cover an active spreading center, with igneous activity comprised of laccolith and sill-like intrusions with no observed surface lavas. The magmas intrude into the sediments, sometimes causing doming of the sediments above them. Hydrothermal venting similar to that observed above some of these intrusions (Lonsdale and others, 1980) may have contributed to the formation of the Gossan Lead (Gair and Slack, 1984, Tso, 1987). The contacts between the metasediments and the amphibolites are parallel to foliation and lithologic layering of the sediments while the thicker amphibolites invariably retain a coarse, phaneritic texture, with some minor recrystallization of the during Paleozoic deformation. In addition, a study by Ito and others (1983) shows that amphibolization can occur in situ where gabbroic intrusions are in contact with circulating seawater, especially near cracks, with little loss of original igneous texture, thus possibly accounting for for amphibolite with the "metagabbro" texture.

A schematic diagram of the late Precambrian sedimentary-igneous package is shown in figure 12. The Ashe Formation is envisioned as being deposited on continental or transitional crust, with the initial contact with the underlying rocks being a nonconformity, in agreement with Wehr and

Glover (1985). In the study area, the Ashe is observed to have a lower sandy and non-amphibolitic unit, and an upper, amphibolite-rich unit, with the Gossan Lead as being approximately on the border between the two units.

Paleozoic history

The Ashe Formation underwent two periods of penetrative (D_1, D_2) deformation, the second of which transposed the earlier foliation and formed mesoscopic and microscopic folds. This was followed by the metamorphic peak, isotopically dated at 435 to 480 m.y. ago, during which there was porhyroblast growth of garnet, staurolite and kyanite. However, the timing of the D_1 and D_2 is not precisely known. Rb/Sr work northeast of Galax, near Floyd, Va., by Fullagar and Dietrich (1976) points to an early age of 531 m.y. Glover and others (1983) used this data in their regional synthesis of the Appalachians and suggested that these rocks may have preserved an earler Cambrian isotopic event of dewatering or metamorphism, while in other areas, the Rb/Sr whole rock systems did not close until "Taconic", or locally, "Acadian" times. The observations seen in the Galax area are consistent with this interpretation, in that two pre-peak metamorphic events are also seen. However, it is quite likely that D_1, D_2, and the metamorphic peak are part of a continuum of events, loosely labeled as "Taconic" that spanned a considerable period of time between 480 to 435 m.y., which not only included uplift, deformation and early thrusting of the Blue Ridge, but also resulted in clastic sedimentation in the Valley and Ridge (Glover and others, 1983).

Thrusting in the Blue Ridge was apparently a complex, multi-step process. However, in the study area, the Fries Fault clearly offsets the metamorphic isograds and stacks the warmer Fries block over the cooler Bowers Ferry and Unicoi rocks. Faulting is envisioned as proceeding from east to west, with the Fries Fault first moving over the Bowers Ferry block, then with the Bowers Ferry Fault moving over the Unicoi. Thus, the Bowers Ferry block is interpreted as a fault-bounded "horse". The timing of the Fries Fault system movement is imprecisely known but, K/Ar and

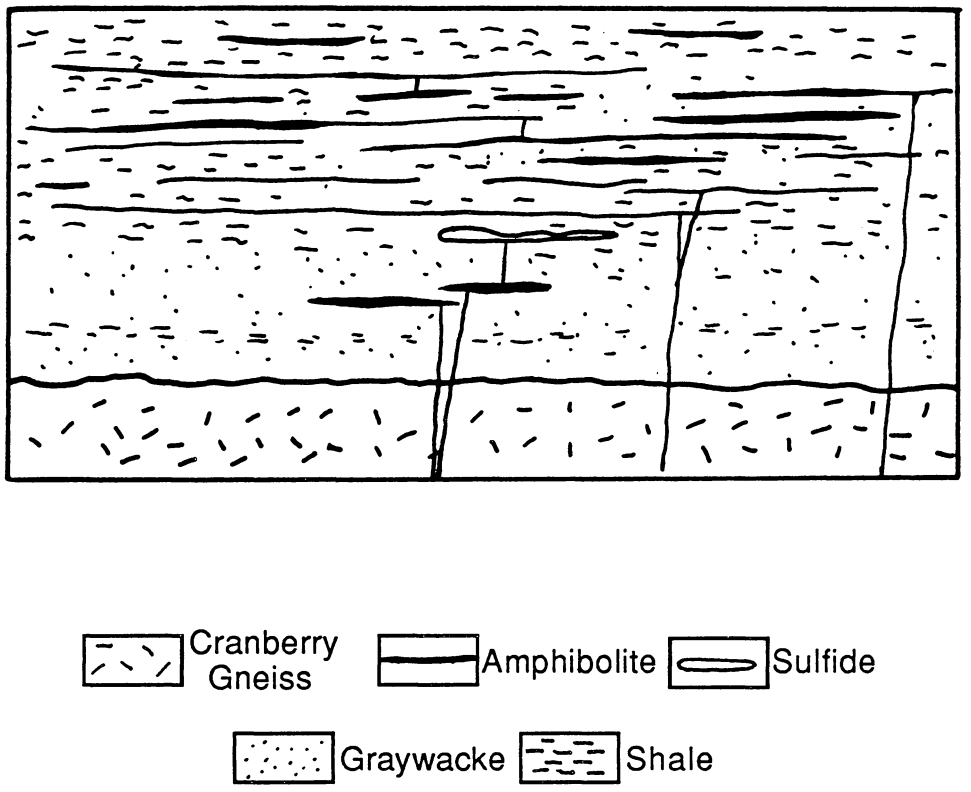


Figure 12. Schematic diagram showing depositional environment of the Ashe

Rb/Sr ages of Fries mylonites show ages of 345 and 330 m.y. respectively (Dietrich and others, 1969).

Closely related to thrusting is broad warping along NE-trending fold axes which accounts for micro-to-macroscopic folds, causing much of the variation in dip of the regional schistosity. This folding caused a local axial-plane foliation to form and created some local overturning. Finally, continued deformation during the waning stages of metamorphism produced in the Ashe a new generation of SE-dipping folds on the mesoscopic scale, causing some of the variation in the strike of the dominant schistosity, along with a locally developed axial plane foliation.

Sampling along the Ashe-Cranberry contact does not reveal strong evidence that the contact is a major fault in the sense that different mylonite textures are developed or that metamorphic isograds are offset. These observations place constraints on the various models of the development of the Blue Ridge.

Bibliography

Abbott, R.N. and Raymond, L.A., 1984, The Ashe metamorphic suite, northwest North Carolina; metamorphism and observations on geologic history: American Journal of Science, v.284, p. 350-375.

Absher, B.S. and McSween, H.Y. Jr., 1985, Granulites at Winding Stair Gap, North Carolina: The thermal axis of Paleozoic metamorphism in the southern Appalachians: Geological Society of America Bulletin, v. 96, p. 588-599.

Bartholomew, M.J. and Lewis, S.E., 1984, Evolution of Grenville massifs in the Blue Ridge geologic province, southern and central Appalachians: in Bartholomew, M.J., ed., The Grenville Event in the Appalachians and Related Topics: Geological Society of America, Special Paper 194, p. 229-254.

Bartholomew, M.J. and Lewis, S.E., 1977, Relationships of the Fries Thrust to the basement complex and Paleozoic deformation in the Blue Ridge of northwestern North Carolina and southwestern Virginia: Geological Society of America Abstracts with Programs, v. 9, p. 116-117.

Bartholomew, M.J., Lewis, S.E., Wilson, J.R. and Gryta, J.J., 1983, Deformational history of the region between the Grandfather Mountain and Mountain City Windows, North Carolina and Tennessee: in Geologic Investigations in the Blue Ridge of Northwestern North Carolina: Carolina Geological Society Fieldtrip Guidbook, 1983, p. 1-29.

Berthe, D., Choukroune, P. and Pegouzo, P., 1979, Orthogneiss, mylonite and non-coaxial deformation of granites: the example of the South Amorican Shear Zone: Journal of Structural Geology, v. 1, p. 31-42.

Boyer, S.E., 1984, Origin and significance of compsitional layering in Late Precambrian sediments, Blue Ridge Province, North Carolina, U.S.A.: Journal of Structural Geology, v. 6, p. 121-133.

Bryant, B.H. and Reed, J.C., 1970, Geology of the Grandfather Mountain Window and vicinity, North Carolina and Tennessee: U.S. Geological Survey Professional Paper 615, 190 p.

Butler, J.R., 1973, Paleozoic deformation and metamorphism in part of the Blue Ridge thrust sheet, North Carolina: American Journal of Science, v. 273-A, p. 72-88.

Butler, J.R., 1972, Age of Paleozoic regional metamorphism in the Carolinas, Georgia and Tennessee southern Appalachians: American Journal of Science, v. 272, p. 319-333.

Butler, J.R. and Fullagar, P.D., 1982, Timing of orogenic events in the Carolinas: Geological Society of America Abstracts with Programs, v. 14, p. 8.

Cooper, B.N., 1961, Grand Appalachian excursion: Geologic Guidebook no. 1, Virginia Polytechnic Institute Engineering Experimental Station Extension Series, 187 p.

Dallmeyer, R.D., 1975, Incremental 40-Ar/39-Ar ages of biotite and hornblende from retrograded basement gneisses of the southern Blue Ridge: Their bearing on the age of Paleozoic metamorphism: American Journal of Science, v. 275, p. 444-460.

Davison, W.D., Jr., 1973, Petrology of the Ashe Formation, Shortt's Knob Area, Floyd County, Virginia [M.S. thesis]: Virginia Polytechnic Institute and State University, Blacksburg, Virginia, 109 p.

Dietrich, R.V., 1959, Geology and mineral resources of Floyd County of the Blue Ridge upland, southwestern Virginia: Virginia Polytechnic Institute Bulletin, Engineering Experimental Station Series, no. 134.

Dietrich, R.V., Fullagar, P.D. and Bottino, M.L., 1969, K/Ar and Rb/Sr dating of tectonic events in the Appalachians of southwestern Virginia: Geological Society of America Bulletin, v. 80, p. 307-314.

Eckelmann, F.D. and Kulp, J.L., 1956, The sedimentary origin and stratigraphic equivalence of the so-called Cranberry and Henderson granites in western North Carolina: American Journal of Science, v. 254, p. 288-315.

Eckelmann, F.D. and Mose, D.G., 1981, Search for xenocrystic zircon in the latest Precambrian plutonic rocks of the Blue Ridge: Geological Society of America Abstracts with Programs, v. 13, p. 7.

Eckert, J.O. Jr., 1984, Stratigraphy, structure, and metamorphism along the Hayesville Fault west of Franklin, North Carolina: Geological Society of America Abstracts with Programs, v. 16, p. 135.

Espenshade, G.H., Rankin, D.W., Shaw, K.W. and Neuman, R.B., 1975, Geologic map of the east half of the Winston-Salem Quadrangle, North Carolina-Virginia: U.S. Geological Survey, Miscellaneous Investigations Series, Map I-709B.

Ferry, J.M. and Spear, F.S., 1978, Experimental calibration of the partitioning of Fe and Mg between biotite and garnet: Contributions to Mineralogy and Petrology, v. 66, p. 113-117.

Fullagar, P.D. and Dietrich, R.V., 1976, Rb-Sr isotopic study of the Lynchburg and probably correlative formations of the Blue Ridge and western Piedmont of Virginia and North Carolina: American Journal of Science, v. 276, 347-365.

Gair, J.E. and Slack, J.F., 1984, Deformation, geochemistry , and origin of massive sulfide deposits, Gossan Lead District, Virginia: Economic Geology, v. 79, p. 1483-1520.

Ghent, E.D. and Stout, M.Z., 1981, Geobarometry and geothermometry of plagioclase-biotite-garnet-muscovite assemblages: Contributions to Mineralogy and Petrology, v. 76, p. 92-97.

Glover, L.G. III, Spear, J.A., Russell, G.S. and Farrar, S.S., 1983, Ages of regional metamorphism and ductile deformation in the central and southern Appalachians: Lithos, v. 16, p. 223-245.

Hadley, J.B., 1970, The Ocoee Series and its possible correlatives: in Fisher, G.W., Pettijohn, F.J., Reed, J.C. and Weaver, K.N., eds., *Studies of Appalachian Geology: Central and Southern*: New York, Wiley-Interscience, p. 127-147.

Hatcher, R.D. Jr., 1978, Tectonics of the western Piedmont and Blue Ridge, southern Appalachians: Review and speculation: American Journal of Science, v. 278, p. 276-304.

Hatcher, R.D. Jr., Acker, L.L., Bryan, J.G. and Godfrey, S.C., 1979, The Hayesville thrust of the central Blue Ridge of North Carolina and nearby Georgia: A premetamorphic, polydeformed thrust and cryptic suture within the Blue Ridge thrust sheet: Geological Society of America Abstracts with Programs, v. 11, p. 181.

Hatcher, R.D. Jr., Butler, J.R., Fullagar, P.D., Secor, D.T. and Snoke, A.W., 1980, Geologic synthesis of the Tennessee-Carolinas- northeast Georgia southern Appalachians: in Wones, D.R., ed., Proceedings, The Caledonides in the U.S.A.: I.G.C.P. Project 27: Caledonide Orogen: Department of Geological Sciences, Virginia Polytechnic Institute and State University, Memoir no. 2.

Hodges, K.V. and Spear, F.S., 1982, Geothermometry, geobarometry and the Al_2SiO_5 triple point at Mt. Moosilauke, New Hampshire: American Mineralogist, v. 67, p. 1118-1134.

Ito, E. and Anderson, A.T., 1983, Submarine metamorphism of gabbros from the Mid-Cayman Rise: Petrographic and mineralogic constraints on hydrothermal processes at slow-spreading ridges: Contributions to Mineralogy and Petrology, v. 82, p. 371-388.

Jones, T.Z., 1976, Petrography, structure, and metamorphic history of the Warrensville and Jefferson Quadrangles, southern Blue Ridge, northwestern North Carolina [Ph.d. dissert.]: Miami University, Oxford, Ohio, 130 p.

Kaygi, P.B., 1979, The Fries Fault near Riner, Virginia: An example of a polydeformed, ductile deformation zone [M.S. thesis]: Virginia Polytechnic Institute and State University, Blacksburg, Va., 165 p.

Keith, A., 1903, Description of the Cranberry Quadrangle, North Carolina-Tennessee: U.S. Geological Survey Geologic Atlas, Folio 90.

Keith, A., 1904, Description of the Asheville Quadrangle, North Carolina-Tennessee: U.S. Geological Survey Geologic Atlas, Folio 116.

Keith, A., 1907, Description of the Roan Mountain Quadrangle, Tennessee-North Carolina: U.S. Geological Survey Geologic Atlas, Folio 147.

Kish, S.A., 1982, The application of potassium-argon dating of slates to the study of the metamorphic history of the southern Appalachian Piedmont and Blue Ridge: Geological Society of America Abstracts with Programs, v. 14, p. 31.

Lesure, F.G., 1968, Mica deposits of the Blue Ridge in North Carolina: U.S. Geological Survey Professional Paper 577, 124 p.

Lonsdale, P.F., Bischoff, J.L., Burns, V.M., Kastner, M. and Sweeney, R.E., 1980, A high-temperature hydrothermal deposit on the seabed at a Gulf of California spreading center: Earth and Planetary Science Letters, v. 49, p. 8-20.

Lonsdale, P. and Lawver, L.A., 1980, Immature plate boundary zones studied with a submersible in the Gulf of California: Geological Society of America Bulletin, Part I, v. 91, p. 555-569.

Milton, D.J., 1983, Garnet-biotite geothermometry confirms the premetamorphic age of the Greenbrier Fault, Great Smokey Mountains, North Carolina: Geological Society of America Abstracts with Programs, v. 15, p. 90.

Mose, D.G., Nagel, M.S. and Tunsoy, A., 1983, Progress on the chronology of latest Precambrian granitic plutons in the Blue Ridge: Geological Society of America Abstracts with Programs, v. 15. p. 91.

Odom, A.L. and Fullagar, P.D., 1982, The time of opening of the Iapetus Ocean: Age of the Crossnore plutonic-volcanic group, southern Appalachians: Geological Society of America Abstracts with Programs, v. 14, p. 69.

Odom, A.L. and Fullagar, P.D., 1971, A major discordancy between U-Pb zircon ages and Rb-Sr whole-rock ages of late Precambrian granites in the Blue Ridge province: Geological Society of America Abstracts with Programs, v. 3, p. 663.

Rankin, D.W., 1976, Appalachian salients and recesses: Late Precambrian continental breakup and the opening of the Iapetus Ocean: Journal of Geophysical Research, v. 81, p. 5605-5619.

Rankin, D.W., 1975, The continental margin of eastern North America in the southern Appalachians: The opening and closing of the proto-Atlantic ocean: American Journal of Science, v. 275-A, p. 298- 336.

Rankin, D.W., 1971, Geology of the Blue Ridge in southwestern Virginia and adjacent North Carolina: in Lowry, W.D., ed, Guidebook to Appalachian tectonics and sulfide mineralization of southwestern Virginia: Virginia Polytechnic Institute and State University, Department of Geological Sciences, Guidebook no. 5, p. 39-86.

Rankin, D.W., 1970, The Blue Ridge and the Reading Prong: stratigraphy and structure of Precambrian rocks in northwestern North Carolina: in Fisher, G.W., Pettijohn, F.J., Reed, J.C. and Weaver, K.N., eds., *Studies of Appalachian Geology, Central and Southern*: New York, Wiley-Interscience, p. 227-245.

Rankin, D.W., Espenshade, G.H. and Neuman, R.B., 1972, Geologic map of the west half of the Winston-Salem Quadrangle, North Carolina-Virginia-Tennessee: U.S. Geological Survey, Miscellaneous Investigations Series, Map I-709A.

Rankin, D.W., Espenshade, G.H., and Shaw, K.W., 1973, Stratigraphy and structure of the metamorphic belt in northwestern North Carolina and southwestern Virginia: a study from the Blue Ridge across the Brevard Fault Zones to the Sauratown Mountains Anticlinorium: American Journal of Science, v. 273-A, p. 1-40.

Rankin, D.W., Stern, T.W., Reed, J.C. and Newell, M.F., 1969, Zircon ages of the felsic volcanic rocks in the upper Precambrian of the Blue Ridge, Appalachian Mountains: Science, v. 166, p. 741-744.

Schwab, F.L., 1984, Late Precambrian rift-related sedimentation of the central and southern Appalachians: Geological Society of America Abstracts with Programs, v. 16, p. 193.

Simpson, C. and Schmid, S.M., 1983, An evaluation of criteria to deduce the sense of movement in sheared rocks: Geological Society of America Bulletin, v. 94, p. 1281-1288.

Slack, J.F., Gair, J.E., and Atelsek, P.J., 1985, Geochemistry of mafic rocks from part of the Ashe Formation, southwestern Virginia: Geological Society of America Abstracts with Programs, v. 17, p. 135.

Stose, A.J. and Stose, G.W., 1957, Geology and mineral resources of the Gossan Lead District and adjacent areas in Virginia: Virginia Division of Mineral Resources Bulletin 72, 233 p.

Sutter, J.F., 1982, Timing of metamorphism in the Appalachian Orogen based on 40-Ar/39-Ar dates of hornblende and biotite: Geological Society of America Abstracts with Programs, v. 14, p. 87.

Tso, J.L., 1987, Geology of the Ashe Formation Between Fries and Galax, Virginia [Ph.d. dissert.]: Virginia Polytechnic Institute and State University, Blacksburg, Va., 343 p.

Wehr, F., 1983, Geology of the Lynchburg Group in the Culpeper and Rockfish River areas, Virginia [Ph.d. dissert.]: Virginia Polytechnic Institute and State University, Blacksburg, Virginia, 245 p.

Wehr, F. and Glover, L. III, 1985, Stratigraphy and tectonics of the Virginia-North Carolina Blue Ridge: Evolution of a late Proterozoic-early Paleozoic hinge zone: Geological Society of America Bulletin, v. 96, p. 285-295.

Part II: Petrology of the Ashe Formation Between Fries and Galax, Virginia

Introduction

The Ashe Formation of southwest Virginia is considered to be one of the more important units in the southern Appalachian Blue Ridge. On the one hand, it represents a sequence of rift-related pelites, graywackes, mafic lavas, and massive sulfides that are associated with the opening of the Iapetus Ocean some 570-690 m.y. ago (Rankin, 1975, Odom and Fullagar, 1982). On the other hand, the Ashe Formation was extensively involved in the collisional tectonics of the Paleozoic, resulting in multiple stages of folding, faulting, and metamorphism (Rankin, 1971, Butler, 1973), with the time of metamorphism generally placed at 480-435 m.y. ago (Glover and others, 1983). As a result, the Ashe Formation has increasingly become the subject of a number of studies (for example, Jones, 1976, Abbott and Raymond, 1984, and Bartholmew and Lewis, 1984). As more data have accumulated, the structure and history of this unit are now understood to be far more complex than previously thought.

However, despite the increasing amount of information available, a number of key questions remain unanswered. In particular, there is considerable debate as to the nature of Ashe Formation's contact with the underlying Cranberry Gneiss, which represents approximately 1.1 b.y. old Precambrian basement (Bartholomew and Lewis, 1984). One school of thought believes this contact to be nonconformable (Rankin and others, 1973, Bartholomew and others, 1983), thus placing the Ashe Formation on continental crust, while other workers believe the contact to be a major

thrust fault (Hatcher, 1978, Abbott and Raymond, 1984), creating the possiblility that the Ashe was deposited on oceanic crust. In addition, reconaissance mapping on the 1:250,000 scale Winston-Salem Quadrangle (Rankin and others 1972, Espenshade and others, 1975) has indicated that the metamorphic grade of the Ashe Formation generally increases to the southeast from its northwestern edge. This is true especially in southwestern Virginia, where rocks range from chlorite-biotite grade near the town of Fries, upward to kyanite grade 10 km to the southeast, near the town of Galax. Complicating the geology, however, is the fact that these maps indicate that as the rocks dip uniformly to the southeast, the metamorphic grade apparently increases stratigraphically upward.

Unfortunately, more detailed mapping of the structure and stratigraphy of the Ashe Formation is rare, and the complex metamorphism and deformation has obliterated sedimentary structures, thus making facing criteria difficult to establish, and preventing the determination of a detailed internal stratigraphy. Much of the previous work on the Ashe has been done either in central Virginia, where these rocks are known as the Lynchburg Group (Wehr and Glover, 1985), or in North Carolina (Jones, 1976, Abbott and Raymond, 1984), thus creating a lack of detailed information in between these two areas, especially in southwest Virginia. In addition, there are few studies that relate the structure to the metamorphism, specifically employing chemical analyses to determine mineral equilibria.

This study focuses on the Blue Ridge in southwest Virginia between the towns of Galax and Fries (figure 13) in an 11 by 4 km area whose length is approximately perpendicular to the regional strike of the stratigraphy, dominant foliation, and metamorphic isograds. As shown on plate I, the area includes the portions of three thrust sheets: the Stone Mountain Thrust Sheet, the Bowers Ferry Thrust Sheet, and the Fries Thrust Sheet. In the northwest corner of the study area, the Stone Mountain Thrust Sheet contains the relatively unmetamorphosed rocks of the lower Cambrian Unicoi Formation of the Chilhowee Group. In the northeast part of the study area, the Bowers Ferry Fault thrusts the highly sheared sedimentary rocks of the Bowers Ferry Thrust Sheet of uncertain formational affinity over the Unicoi. Further southeast, the Fries Fault thrusts the

Cranberry Gneiss of the Fries Thrust Sheet over portions of both the Unicoi and the Bowers Ferry Rocks. The Ashe Formation, which comprises the bulk of the study area, rests on top of the Cranberry within the Fries Thrust Sheet. A regional map showing the thrust sheets is shown in figure 14.

The purpose of this study is to address the questions about the inversion of the isograds, and the nature of the Ashe-Cranberry contact by studying the relationship between the general geology of the area and the nature of the metamorphism. Specifically, by establishing the conditions of metamorphism, determinig the nature of the isograd reactions, and by observing metamorphic trends across the area, it is possible to place constraints on possible models that might explain the inversion of the isograds. In addition, the data collected in this study can be used to place constraints on the timing and nature of metamorphism of thrusting along the Fries Fault, and how this affects the rocks across the Ashe-Cranberry contact. The approach used in this study combines field, petrographic, structural and chemical approaches. A variety of different mineral equilibria were employed to determine metamorphic trends. In particular, garnet-biotite pairs combined with muscovite compositions and amphibole-plagioclase equilibria were used to determine general temperature trends across the area. Chemical zonation of garnet and amphibole proved valuable in determining the timing between metamorphism and various prograde and retrograde events deduced from the regional structure and rock texture.

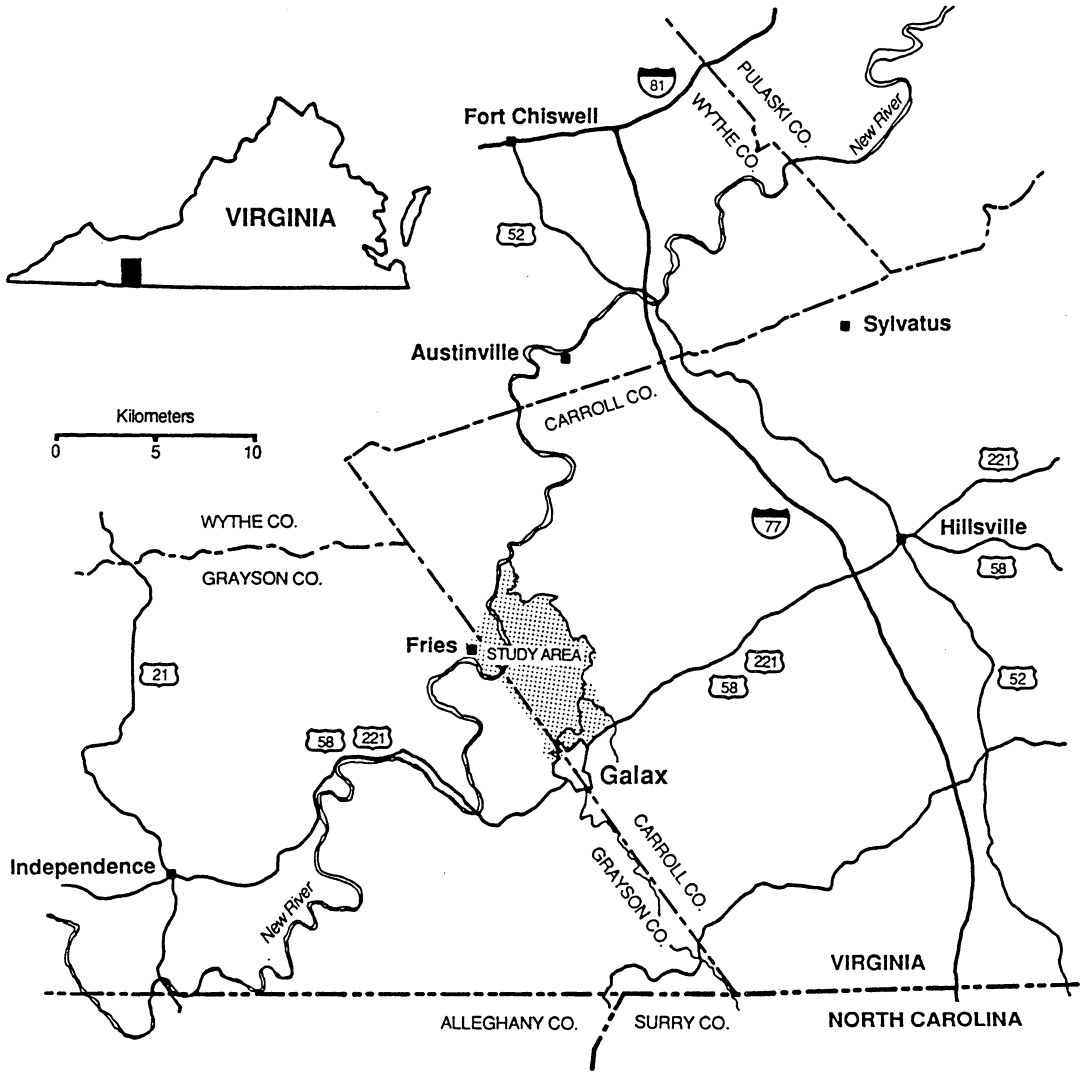


Figure 13. Location map

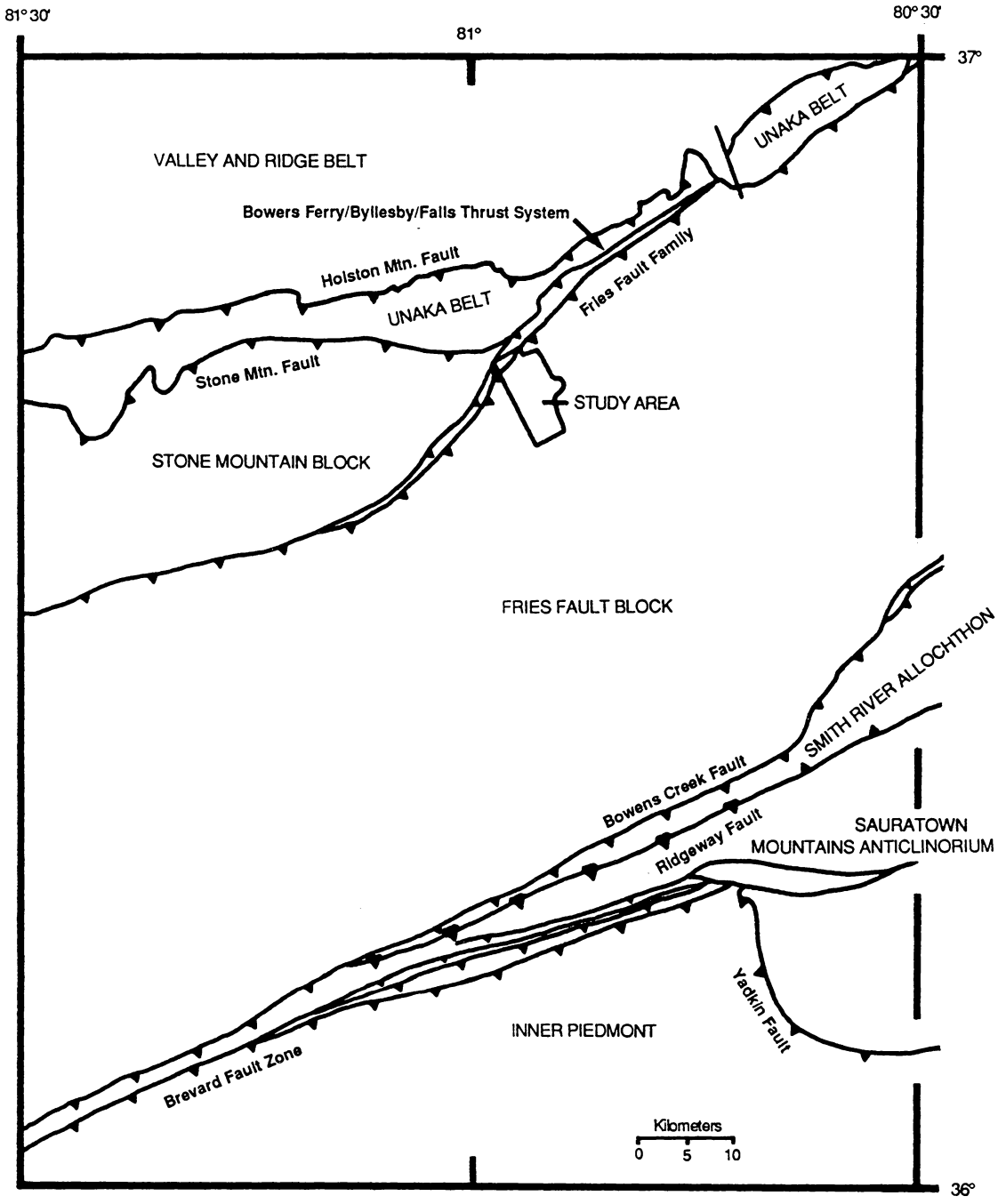


Figure 14. Tectonic map: Compiled from Rankin and others (1972) and Espenshade and others (1975).

Geologic Setting and Previous Works

The study area has been previously mapped in reconaissance fashion by three principle groups: 1) Stose and Stose (1957), mapped on the 1:62,500 scale from the Virginia - North Carolina border northward to the Sylvatus, Virginia area; 2) Espenshade and others (1975), along with Rankin and others (1972), mapped the 1:250,000 scale Winston-Salem quadrangle; and 3) Tso (1987) mapped the detailed structure and stratigraphy between Fries and Galax. The regional mapping by the Rankin and Espenshade group was summarized in Rankin and others (1973). On the Fries Thrust Sheet, the Ashe Formation rests on the Cranberry Gneiss, and is conformably overlain by the Alligator Back Formation, which consists a series of interlayered pelitic schists, gneisses and amphibolites of possibly late Precambrian to lower Paleozoic age.

A detailed geologic map of the study area is given in plate I. In general, the rocks strike monotonously to the northeast (approximately N51°E) and dip to the southeast. Lithologic contacts, metamorphic foliation, and various thrusts and shear zones are generally subparallel. The Ashe Formation, which dominates the study area, is predominantly composed of gneisses and schists, which are intimately interlayered on the meter scale, and by amphibolites, which are subparallel to the trends observed in the metasediments. In addition, a line of massive sulfide deposits known as the Gossan Lead are found within the Ashe that trend parallel to strike with the southwest end in the Galax area, extending to the Sylvatus area. Mapping during the present study un-

covered an additional shear zone within the Ashe Formation approximately 1 km north of the town of Galax, recognizable as a line of sheared gneisses, quartz vein material, and amphibolites.

As can be seen on plate I, one of the major features of the study area is the Fries Fault. The presence of the Fries Fault is of fundamental importance to the geology of the Blue Ridge. Over much of the Blue Ridge, the Fries Fault divides the province into two areas of distinctly different rocks. In general, rocks to the northwest of the fault contain much more continental basement material and shallow water late Precambrian rocks such as those of the partially glacial Mount Rogers Formation, (Rankin and others, 1973). Rocks southeast of the Fries Fault, as typified by the Ashe Formation, contrast with rocks of the northwest area by containing less continental basement, more deeper water sediments, more mafic igneous rocks, and occasional ophiolite bodies. This difference has prompted a number of workers to theorize about the significance of the Fries Fault. For example, Hatcher (1978) used the Fries Fault to divide the Blue Ridge into an eastern province and a western province, with the Fries Fault possibly serving as a major suture zone. Bartholomew and Lewis (1984), envisioned the Blue Ridge as being composed of "massifs" which contain areas of Precambrian basement overlain by various late Precambrian or Paleozoic cover rocks. According to their scheme, the Fries Fault separates the "Elk River Massif" to the southeast from the "Watauga Massif" to the northwest. Raymond (1987) divided the Blue Ridge into a number of "terranes" bounded by thrust faults, some of which are contained within the Ashe Formation itself. According to this plan, the Fries Fault represents the northwest boundary of the "Toe Terrane" which contains the Ashe, Alligator Back, and Tallulah Falls Formations, all containing pelitic, quartzo-feldspathic, and amphibolitic rocks. According to the metamorphic isograd map of Espenshade and others (1975), the Fries Fault offsets the metamorphic isograds, thus indicating that movement was after the metamorphic peak. Rb/Sr data from mylonites along the Fries Fault yield ages of 345 and 330 m.y. (Dietrich and others, 1969).

Another important feature is the Ashe-Cranberry contact, which parallels the Fries Fault approximately one-half kilometer to the southeast. The proximity of this contact to the Fries Fault has caused the contact to lie within the Fries Fault ductile deformation zone, thus obscuring the nature

of the contact. As the Fries Fault causes the offset of metamorphic isograds, the possibility exists that some retrogression of the metamorphic mineral assemblages occured along the fault. Because lower metamorphic grade rocks also occur along the fault, the question is raised as to whether or not thrusting caused widespread retrogression, thus causing the inversion of the isograds. The interpretation of the Ashe-Cranberry contact as a thrust fault adds to the complexity of the geology of the area, opening up the possibility of additional offset of the isograds, and the development of a second shearing texture for rocks along the contact.

A number of studies dealing with the metamorphic petrology of the Blue Ridge have been previously carried out. However, relatively few studies have been done on the Ashe Formation near the study area. Craig and others (1971) did preliminary microprobe work on amphibole, garnet, and biotite from the Gossan Lead massive sulfide zone and documented the fact that the silicates showed enrichment of Mg over Fe as a result of sulfide-silicate interaction. A more exhaustive study was done by Staten (1976) who carried out a microprobe study of drill core taken from the Betty Baker segment of the Gossan Lead near Sylvatus, Virginia, some 18 km along strike to the northeast of the present study area. The drill core contained both massive sulfide ore and adjacent silicate country rock. Staten studied the change in Fe/(Fe+Mg) of the ferromagnesian silicates along the drill core with respect to distance from the massive sulfide and found that within the ore zone, garnet, biotite, and chlorite all showed a marked decrease in Fe/(Fe+Mg). By using the garnet-biotite geothermometer of Thompson (1976b), he determined that the metamorphic temperature of both the ore and the wall rocks was 415-455 °C, implying that mineralization preceded metamorphism. Henry and others (1979), in a study of the ore mineralogy of the Gossan Lead, using samples from both the Betty Baker area and the study area, observed that the massive sulfide is composed of at least 90% pyrrhotite, with smaller amounts of sphalerite, chalcopyrite, and arsenopyrite. They found that the arsenopyrite geothermometer recorded a metamorphic temperature in excess of 400 °C, that the sphalerite - pyrite - pyrrhotite geobarometer indicated a pressure of 5.5 kb, and concluded that the ore bodies had formed as a result of syngenetic sulfide accumulation at a sea floor vent. Gair and Slack (1984) combined bulk chemistry of the Ashe Formation

with field observations in a study of the origin of the Gossan Lead ore. They concluded that the unusual rock types around the Gossan Lead were probably the result of the alteration of normal graywackes and shales during volcanic venting and that the ores themselves resulted from exhalative processes in a rift setting. Most recently, Tso (1987) combined detailed mapping with analysis of the structural geology of the study area, and determined that two periods of penetrative schistosity predated the metamorphic peak. The final movement of the Fries Fault followed the metamorphic peak, along with two periods of folding about NE and SE-trending axes. An important conclusion reached in that study was that the Ashe-Cranberry contact, although contained within the Fries Fault shear zone, contained no petrographic evidence of a post-metamorphic episode of shearing that could not be related to that of the Fries Fault, thus implying that the contact is not a major post-metamorphic fault.

Two other studies are worth mentioning, although they were undertaken in areas distant from the present study. Davison (1973), in a study of Ashe Formation rocks in Floyd County, Virginia, 53 km to the northeast, concluded from a dolomite - muscovite - plagioclase - biotite - quartz bearing assemblage that the temperature of metamorphism was no higher than approximately 560 °C in a Barrovian-style metamorphic terrane, a temperature that is consistent with those derived from this study. Abbott and Raymond (1984), on the other hand, looked at predominantly metabasic rocks in the Ashe Formation approximately 48 km to the southwest in North Carolina, and estimated from the sparse metapelitic units in the area that metamorphic temperatures were near 700 °C and that pressures were in excess of 7 kb. Clearly, these studies, as well as the metamorphic isograd maps of Rankin and others (1972) and Espenshade and others (1975), indicate that the metamorphic grade increases to the southwest of the study area.

Analytical Procedures

196 thin sections from 122 localities were analyzed with the petrographic microscope. 94 of the thin sections were polished and then analyzed under the electron microprobe using the automated ARL microprobe at Virginia Tech using the QALL analysis scheme (Solberg and Spear, 1982) incorporating the data reduction method of Bence and Albee (1968). In practice, 3 or 4 three mm diameter areas of interest were circled and probed for each thin section. Where possible, core and rim analyses were done to test for mineral heterogeneity. In general, sheet silicates and feldspars showed no significant variation in composition within a circled area whether or not they touched another iron-magnesium-manganese bearing phase. However, garnet and early-formed hornblende did show significant chemical variation from core to rim, especially if the garnet was greater than 0.25 mm in diameter and the hornblende was greater than 5 mm in length. In these cases, core and rim analyses were reported and rim analyses were used in geothermometry. See appendix A for details on the various recalculation methods of the raw probe data, and for tables of analyses.

In addition, 20 samples were analyzed for major element whole-rock chemistry using an X-ray fluoresence method of fused disks (Norrish and Chappel, 1967) on a Philips 1450 wavelength dispersive X-ray fluoresence spectrometer (appendix B).

Petrography

General Statement

The rocks of the study area have undergone multiple periods of deformation and metamorphism. The structural history of the study area has been studied by Tso (1987). Table 2 presents the tectonic history as deduced from petrographic and field observation. Each of the three thrust sheets has experienced its own unique geologic history. However, two overriding patterns have been observed. First, metamorphic grade, as determined by the presence of chlorite, biotite, garnet, and staurolite, generally increases to the southeast. Secondly, extensive mylonitization has accompanied the movement of both the Fries Fault and Bowers Ferry Fault, both of which appear to post-date the main regional metamorphic peak and caused some local recrystallization of the Ashe Formation.

Figures 15 and 16 show the sample localities and major and minor mineral assemblages for the metasediments and plutonic rocks and the mafic rocks respectively. Appendix C is a table of observed mineralogy and modal analyses for the analyzed samples. In order to facilitate comparisons of mineral chemistry across the study area, an arbitrary reference line (0 km) was drawn parallel to

Table 2. Table of structural history from Tso (1987)

SUMMARY OF STRUCTURAL TERMINOLOGY

S_0 - Unicoi Formation and Bowers Ferry Rocks: primary sedimentary layering
- Ashe Formation: primary lithologic layering, contacts between gneiss, schist, and amphibolite

S_1 - Early Penetrative Foliation: Ashe Formation - parallel alignment of muscovite, chlorite, biotite

S_2 - Dominant regional foliation: Ashe Formation - crenulation cleavage, transposition foliation, growth of muscovite, biotite, axial plane foliation of microscopic to mesoscopic isoclinal folds

S_{my} - Mylonite foliation: Cranberry Gneiss, Bowers Ferry Rocks, Ashe Formation - parallel alignment of quartz lenses, muscovite, biotite; stretching of feldspar augens, development of fine-grained plagioclase + quartz matrix; locally developed along Fries and Bowers Ferry Fault

S_{slip} - Slip cleavage: Ashe Formation -cm-scale, gently dipping fracture cleavage; locally developed near the Fries Fault

F_3 - Regional northeast-trending folds: broad gentle mesoscopic to macroscopic folds, causes variation in dip, with local NW-dipping rocks; warps Fries Fault mylonite

F_4 - Mesoscopic southeast-trending folds: Ashe Formation - locally developed gentle to open folds

strike (N51°E) along the northwest boundary of the study area. In the descriptions and figures that follow, distance from the reference line refers to the distance in kilometers as measured perpendicularly to the southeast on the map.

Unicoi Formation

The Unicoi consists of a relatively unmetamorphosed unit of interlayered arkosic conglomerate, white orthoquartzite and tan shale. A weak metamorphic overprint is evident only in the rocks in the vicinity of the Fries and Bowers Ferry Faults. There, fine chlorite becomes abundant as a matrix mineral in the arkosic conglomerates along with trace amounts of fine, interleaved green biotite (figure 17a). In addition, some feldspar clasts show evidence of shearing, as observed by cracking with secondary carbonate filling, and by recrystallization of the cracks into an incipient mylonite texture. Button phyllites are locally present adjacent to the Fries Fault trace.

Bowers Ferry Rocks

Rocks that lie in the wedge-shaped area bounded by the Bowers Ferry Fault to the northwest, and the Fries Fault to the southeast (plate I), have been included in the Unicoi Formation by Stose and Stose (1957), and in the Ashe Formation by Espenshade and others (1975). The relative merits of one formational affinity over the other has been discussed by Tso (1987). In this report, these rocks will be informally referred to as the "Bowers Ferry Rocks".

Overall, the Bowers Ferry consists of arkosic conglomerates and sandstones, quartzites, and minor pelitic units. However, they show a considerable amount of shearing and recrystallization, espe-

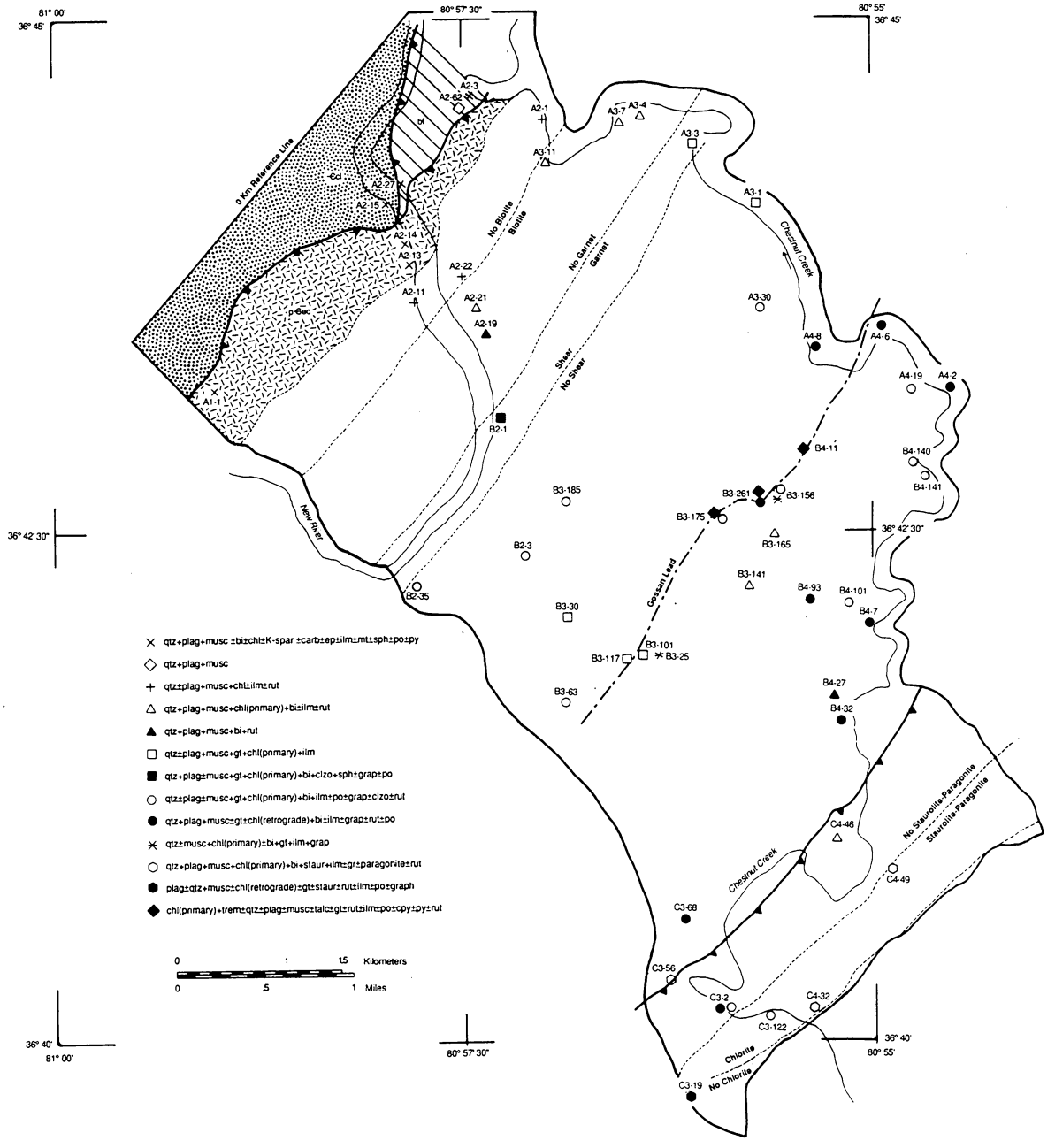


Figure 15. Plutonic and metasedimentary sample and assemblage map

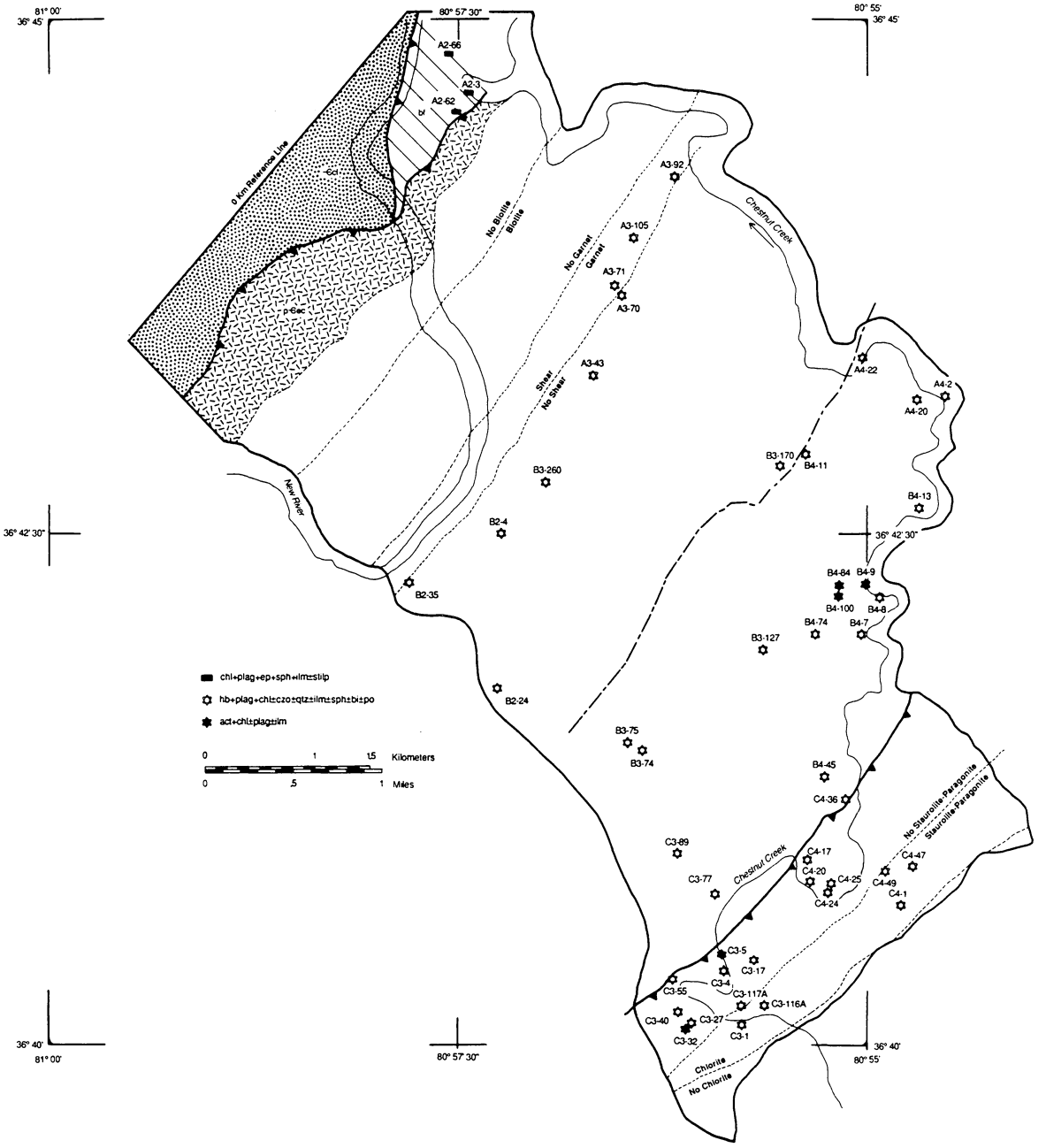


Figure 16. Mafic sample and assemblage map

cially in samples closer to the Fries Fault. The common assemblage is: albite + quartz + celadonitic muscovite ± chlorite ± green biotite ± rutile ± pyrite ± ilmenite ± magnetite ± secondary carbonate. Arkosic conglomerates retain their coarse grained sedimentary texture; in outcrop, a right-side up facing can still be determined from faint cross bedding. In addition, albite and quartz clasts are distinctly lense-shaped, with their long axes stretched subparallel with the mylonite foliation which roughly parallels the dominant S_2 schistosity of the region (figure 17b). In samples close to the Fries Fault, celadonitic muscovite becomes more prominent, forming in thin (0.2 mm) discontinuous bands of approximately 1 cm in length with minor interleaved chlorite. Quartz is mostly found in discrete ribbons of highly sheared grains up to 2 mm in length. Albite comprises most of the clast remnants, with the highly strained clasts showing abundant evidence of microfaulting, bent and distorted twinning and recrystallization of their tails to matrix. The matrix is primarily composed of fine intergrowths of quartz and albite, with muscovite becoming more common near the Fries Fault. Minor carbonate (calcite or ankerite) tends to be found in lenses or compositional bands, and as crack fillings in albite clasts. Biotite is rare in the Bowers Ferry rocks, and has only been observed in samples in the immediate vicinity of the Fries Fault. In one sample, biotite flakes were found in late-growing rosettes that clearly post-date the development of the mylonite texture.

A minor lithology is fine grained green mafic rock that is found at two localities in the Bowers Ferry Thrust Sheet. The texture appears to be that of a relict dolerite that contains albite + biotite + chlorite + stilpnomelane + epidote + ilmenite + quartz + pyrite.

Cranberry Gneiss

The Cranberry Gneiss is found exclusively within the Fries Fault deformation zone and shows an extensive development of mylonitic textures. Mylonite development ranges from nearly 90% fine

albite + quartz matrix along the fault trace where it overrides the Unicoi or Bowers Ferry rocks, to 50% near the contact with the Ashe Formation. Along the fault trace, the rock is overwhelmingly planar, with 5 mm-long eye-like porphyroclasts of strained albite (figure 17c). Quartz is found as planar ribbons that parallel foliation. Biotite and muscovite together make up between 5-10% of the rock, and are present as thin, discontinuous bands that parallel the foliation and wrap around the albite augens. Minor minerals include epidote + ilmentite ± sphene ± magnetite ± pyrite.

However, closer to the Ashe contact, the Cranberry is considerably coarser, with up to 0.5 cm-long augen commonly composed of K-feldspar-albite-quartz intergrowths that appear to preserve an earlier texture. In addition, biotite, which is present in the highly sheared rocks found along the fault trace, has not been observed in the less mylonitized rocks near the Ashe contact (figure 17d), implying that biotite grade conditions were generated locally along the fault trace as a result of the increased strain in these locations.

Ashe Formation

Metasediments

The Ashe Formation metasediments consist of two principal lithologies: metagraywacke or gneiss, and metapelite. Metagraywacke is generally recognizable in the lower grade areas near the Cranberry contact by its coarse sandy texture. Although primary sedimentary textures are difficult to recognize elsewhere in the Ashe, these rocks contain recognizable 1-2 mm clasts of plagioclase and K-feldspar embedded in a finer matrix of quartz, plagioclase, muscovite and chlorite. However, further to the southeast, where the metamorphic grade is higher, the clasts become more difficult

to recognize, and the rock is predominantly a monotonously uniform gneiss or "granofels" of quartz, plagioclase and less than 20% widely desseminated medium grained mica (figure 17e).

Pelitic rocks tend to show more lithologic variability than the gneisses. Commonly, they are found in two major lithologies: muscovite phyllite, and muscovite-biotite schist. The phyllite is commonly composed of up to 90% muscovite (figure 17f), with minor amounts of interleaved chlorite or biotite, and 0.2 mm wide lenses of quartz and plagioclase, with less than 2% very fine dusty grains of graphite which commonly outline the foliation. Garnet may be present in 1-2% 0.1 mm grains that are syn-to-post foliation. Schists, on the other hand, are coarser, lack graphite, and commonly contain porphyroblasts of biotite, with staurolite forming in higher grade areas (figures 17g and 17h). Other minor lithologies include: garnet-muscovite schist, chlorite-muscovite schist, and massive pyrrhotite ore. The mineral assemblage for the metasediments, in addition to quartz + plagioclase + muscovite, contain chlorite ± biotite, chlorite + biotite ± garnet, biotite + garnet + staurolite ± paragonite ± chlorite, and biotite + garnet + staurolite ± kyanite. Other minerals that are commonly present are: ilmenite, graphite, sphene, rutile, and pyrrhotite. Accesorry minerals are apatite, zircon, and tourmaline.

The following is a more detailed description of the mineral assemblages and how they relate to the structure as one procedes in the Ashe Formation from northwest to southeast. Discussion of the rocks in and around the Gossan Lead orebody will be presented in a different report.

Chlorite Zone

The chlorite zone extends from the Ashe - Cranberry contact to approximately 1.8 km to the southeast of the reference line (approximately 0.5 km southeast of the contact). Muscovite is the dominant foliation former, defining a planar schistosity that is the dominant S_1/S_2 foliation. In some cases, especially in phyllitic rocks, small 2-3 mm kink folds and fold closures on the cm scale may be observed in thin section, thus differentiating between the earlier S_1 and a later crenulation

cleavage, the S_2. Chlorite appears as minor amounts of fine (0.1-0.2 mm) pale green flakes that parallel the dominant foliation, and are intimately intergrown with the muscovite. The chlorite zone is entirely contained within the Fries Fault shear zone that extends into the Ashe to approximately 3.2 km from the reference line. In the Ashe Formation, evidence of shearing is observed as a "slip cleavage" or S_{slip} (the S_3 of Rankin, 1971), and as mm-scale kink folds as seen on mica surfaces. In thin section, the slip cleavages are observed as less than 1 mm wide bands of finely recrystallized quartz and plagioclase, that are distinctly finer and more equant than the coaser and more flattened grains found in the rest of the rock. The slip cleavage cross-cuts the previous S_2 at angles of up to 30°. In some of the quartz-rich rocks at the Ashe-Cranberry contact, some mylonitization parallel with that observed in the Cranberry is locally present.

Biotite Zone

At the biotite isograd, biotite is first confined to 2-3 mm wide bands of more biotite-rich mineralogy. In these rocks, the biotite is intimately intergrown with the muscovite and chlorite so that the biotite has the appearance of forming thin seams between the muscovite flakes. However, in samples further southeast, biotite becomes more evenly dispersed in the rock, and forms coarse clean porphyroblasts that clearly overgrow muscovite. While muscovite is commonly parallel to the S_1, and less commonly parallel to S_2, biotite shows the opposite tendency, and becomes the dominant S_2 -forming mineral. Chlorite forms parallel to both S_1 and S_2. The biotite zone is also included within the Fries Fault shear zone. However, slip cleavages are less common here. Instead mm to cm-scale kink folds that clearly deform the biotite are found in more micaceous-rich layers.

Garnet Zone

The garnet isograd (approximately 3.0 km from the reference line) was drawn on the basis of several widely spaced localities where the presence of garnet is either in trace amounts of widely

desseminated grains, or in rocks where the garnet appears locally abundant because of unusual lithology. In the first case (sample A3-1B, figure 17g), garnet is found in 0.5 mm equant grains with extremely fine dusty inclusions of undetermined composition . Chlorite is a common associate with garnet, growing in pressure shadows, and as partial inclusions. In the second case (sample B2-1Y), the rock contains nearly 8% garnet, one of the highest percentages of garnet in any rock in the study area. However, this rock has a more calcic bulk composition, as evidenced by the presence of nearly 4% carbonate, with additional sphene and clinozoisite. In rocks further southeast, garnet attains a common modal percentage of 2-3%, usually evenly dispersed in the samples, although in some samples, garnets appear to concentrate themselves in layers of higher abundance, which are interpreted as reflecting a relict original compositional layering. Generally, the garnets are subhedral, 0.5 mm in size, and post-date the S_2. Chlorite becomes less prominent to the southeast, and near Galax, (approximately 7 km southeast of the reference line) is less commonly observed as an early-formed mineral parallel to S_1. Instead, it appears as either an alteration product of biotite, or in late-growing rosettes that overgrow the main foliation. Biotite grows coarser, attaining sizes of 4-5 mm, and frequently forms late-growing, randomly oriented porphyroblasts.

Staurolite-Paragonite Zone

Staurolite occurs as very coarse 2-5 cm well-terminated crystals that are restricted to a well defined band of mica schists that pass through the town of Galax, 8.6 km southeast of the reference line. In thin section (figure 17h), the staurolites are generally unstrained or only slightly flattened parallel to S_2, contain numerous inclusions of quartz and garnet, and may attain modal percentages of 13%. Paragonite is intimately intergrown with muscovite and was identified during microprobe examination. Together with muscovite, the white micas define the kink-folded S_1 foliation, and less frequently, in coarser grains (0.5 cm) that parallel the dominant S_2 crenulation cleavage. Biotite is found in two habits: as 0.5 cm-long flakes parallel to S_2 , and as coarser 2 cm-random flakes that postdate the foliation. Garnet is more abundant in these rocks than in common schists, attaining

a modal percentage of over 5%, and is found as fine 0.1 mm equant grains that post-date the foliation. Chlorite is found in two habits: as 0.5 cm long flakes that parallel S_2 , and as random flakes that appear very late growing, overgrowing biotite and staurolite. In many cases, the chlorite appears as a retrograde product on biotite, nearly completely replacing biotite in a few locations. Thus, although the chlorite appears texturally primary, it can also be demonstrated that it mocks the S_2 habit of biotite. Although the presence of biotite + chlorite + biotite + staurolite indicates the presence of 4 AFM phases, it should be noted that chlorite and garnet are not observed touching. In addition, some samples in this zone do not contain primary chlorite, and thus, a "chlorite-out" isograd may be drawn just southeast of the "staurolite-in" isograd (figure 15). Plagioclase, in most cases, appears as 0.5 mm equant grains in lenses with quartz. However, in one specimen (C4-32A), it appears as 1-2 cm eye-like grains that are optically and chemically zoned (to be discussed below). These "eyes" often show evidence of internal strain, as observed by bent twin lamellae, and their edges are commonly wrapped by a thin envelope of white mica.

The unusual mineralogy of these rocks reflects the development of the structural fabric. White mica and plagioclase crystallized first during the development of S_1. White mica, joined by biotite and possibly chlorite define the S_2 crenulation cleavage. Garnet, then staurolite, along with biotite, partially crystallized during S_2-growth as well. However, as most grains of these minerals are unstrained, it appears that much of their growth took place after S_2. Chlorite flakes are found in textures associated with all the post-S_1 structures, although it may be a retrogression product in many cases.

Kyanite Zone

Although kyanite has been reported in Galax by Stose and Stose (1957), it unfortunately was not observd in place during the present study. However, it was observed outside the study area at location D2-1, approximately 5 km along strike southwest of Galax (figure 17i). There, kyanite can be found in very coarse blue blades (up to 8 cm long) that are primarily associated with lenses of

milky quartz. In the quartz lenses, kyanite can be found in the same rock as muscovite, biotite, garnet, staurolite, chlorite, and plagioclase. However, kyanite has certain textural preferences. Garnet has not been observed to be in textural equilibrium with kyanite. Instead, the modal amount of garnet is substantially reduced to less than 1% so that it is present only as inclusions in staurolite. Biotite is common as an inclusion in kyanite. However, it is commonly heavily chloritized where it is in contact with the exteriors of kyanite blades, although it can appear relatively unaltered away from kyanite. Chlorite is abundant as late-growing, fan-shaped bundles that are in contact with kyanite and staurolite. Although muscovite is common in these rocks and appears to be in textural equilibrium with all other minerals, microprobe analysis has failed to uncover any distinct flakes of paragonite, although the muscovites are paragonite-rich. Plagioclase does not appear in coarse "eyes". Instead, it forms in equant 0.3-1.0 mm grains in lenses with quartz.

However, kyanite is also observed in more conventional schists. These rocks rocks lack the retrogressive chlorite associated with the quartz veins, and the association kyanite + garnet, and kyanite + biotite are found.

Amphibolite

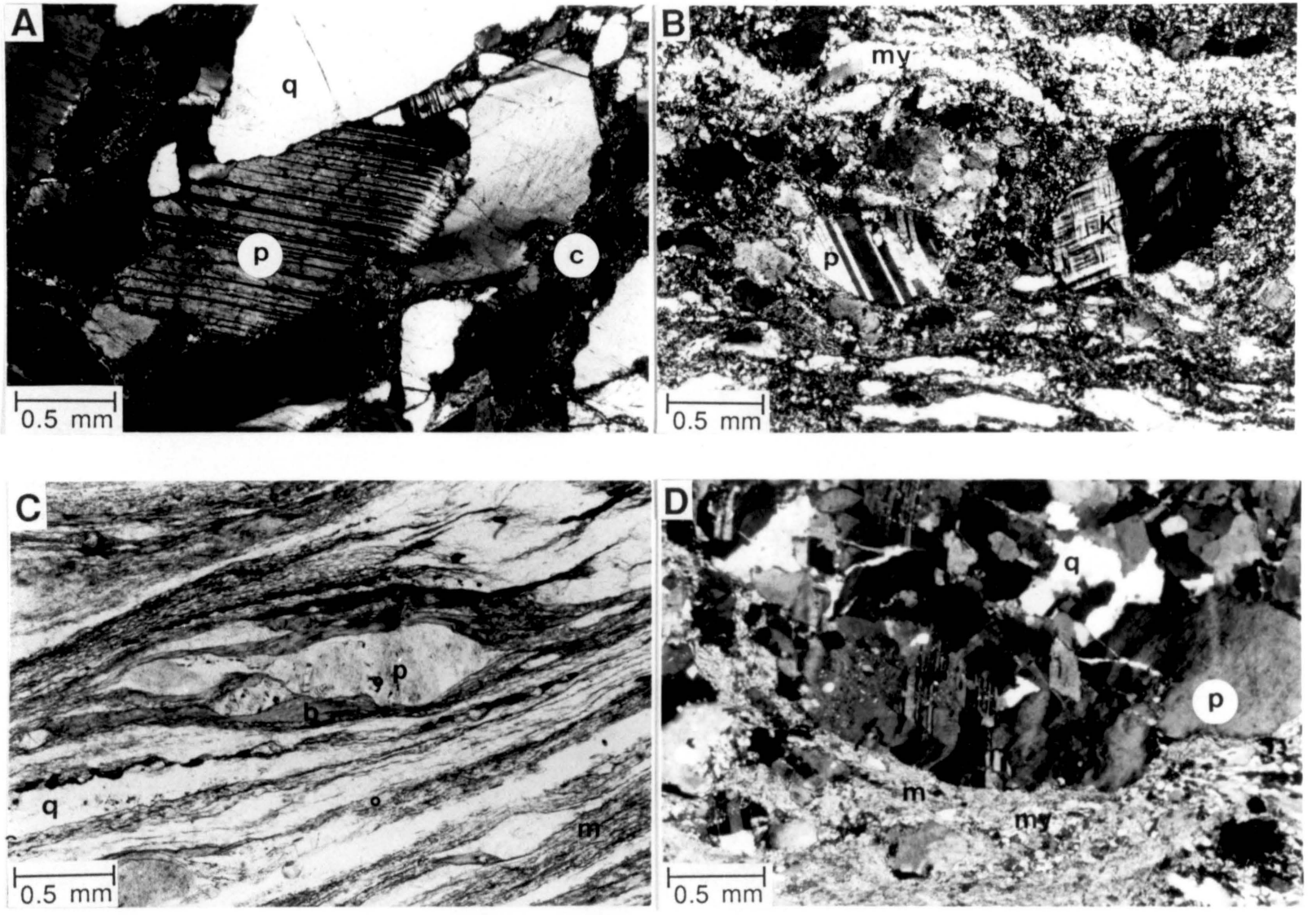
Amphibolite is found in a variety of textures and lithologies. The common assemblage is: hornblende + plagioclase + clinozoisite + chlorite + quartz + sphene + ilmenite ± garnet ± biotite, an assemblage that remains remarkably consistent throughout the study area. Only one other assemblage is found: actinolite + chlorite schist is a minor lithology and is distinctive in its abundance of chlorite and in its lack of plagioclase and quartz.

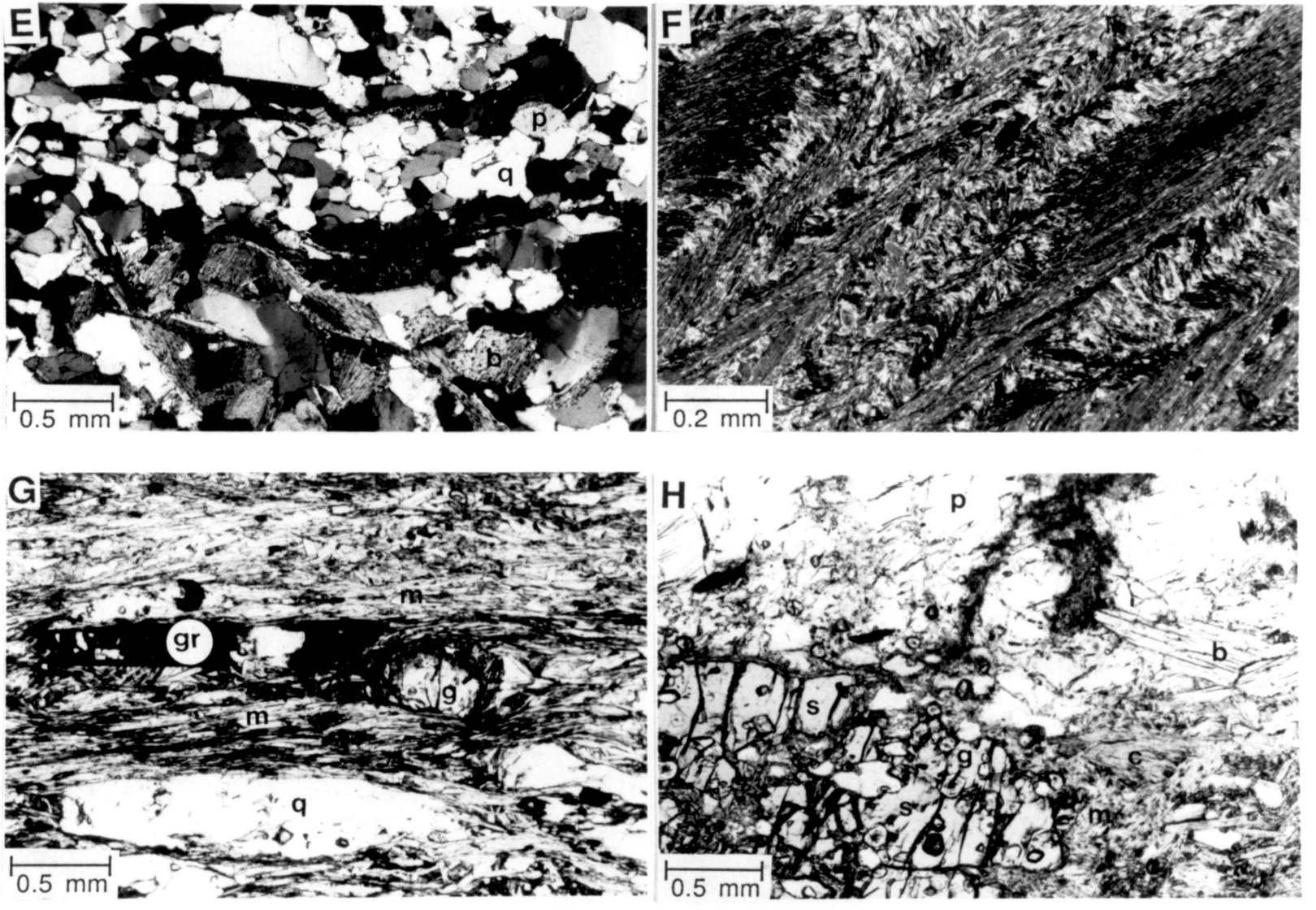
Despite the consistency of its mineralogy, amphibolite is found in a variety of textures that may be considered as variations between two "endmember" textures: metagabbro and medium-grained hornblende schist (Tso, 1987). Coarser grained rocks are termed "metagabbro", are distinctive in

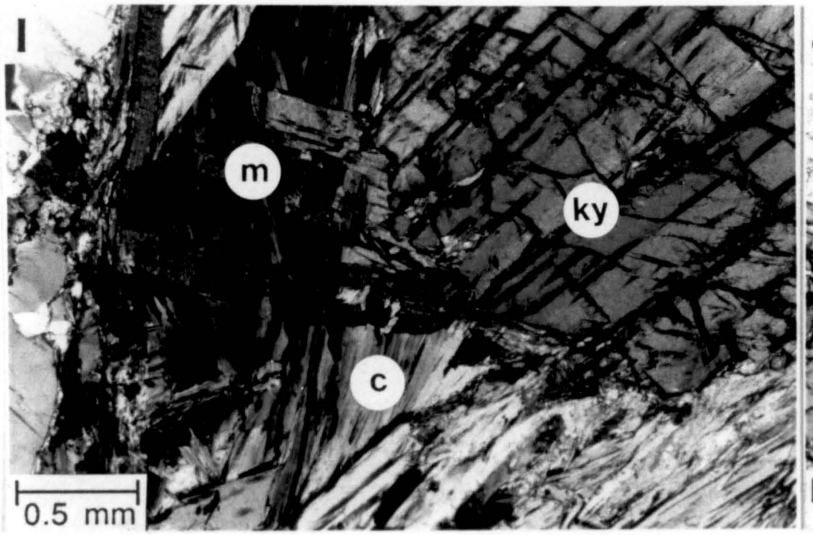
containing up to 5 mm-sized randomly oriented hornblende which apparently is relict of an original igneous texture, and show some optical and chemical zonation (figure 17j), to be discussed below. Plagioclase and quartz commonly form 0.1-0.2 mm equant grains in patches that are interstitial to the coarse hornblendes. Finer hornblendes are more needle-like and are dispersed throughout the plagioclase-quartz matrix. In an ideal "endmember" metagabbro, the finer hornblendes are randomly oriented.

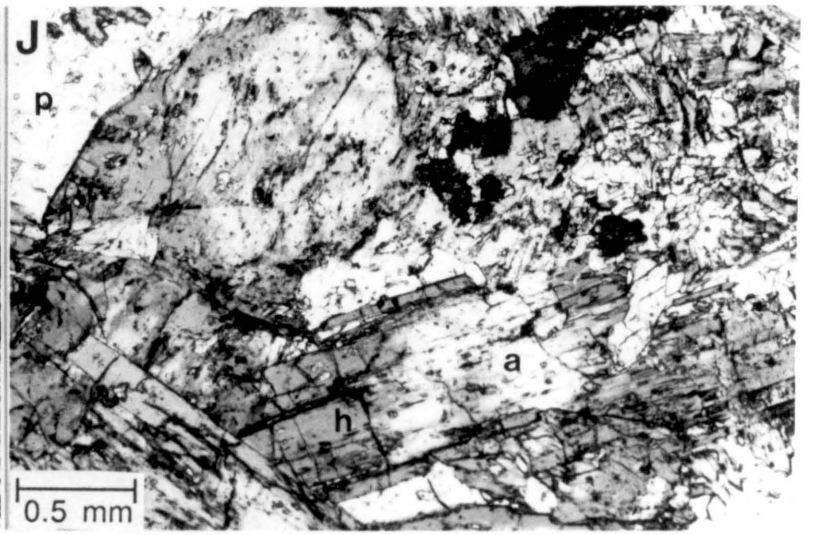
Medium grained amphibolite, on the other hand, lacks coarse hornblende, and contains needles of amphibole which lie in a well-defined foliation which is parallel to the dominant regional schistosity (S_2) as recognized in the surrounding metasediments (figure 17k). These hornblende needles have crystallized parallel to the dominant regional metamorphism and lack a consistently well defined chemical zonation pattern. Intermediate lithologies contain varying amounts of early-formed coarse amphibole, with finer, recrystallized needles of hornblende found on the rims of the early hornblende and in the plagioclase matrix.

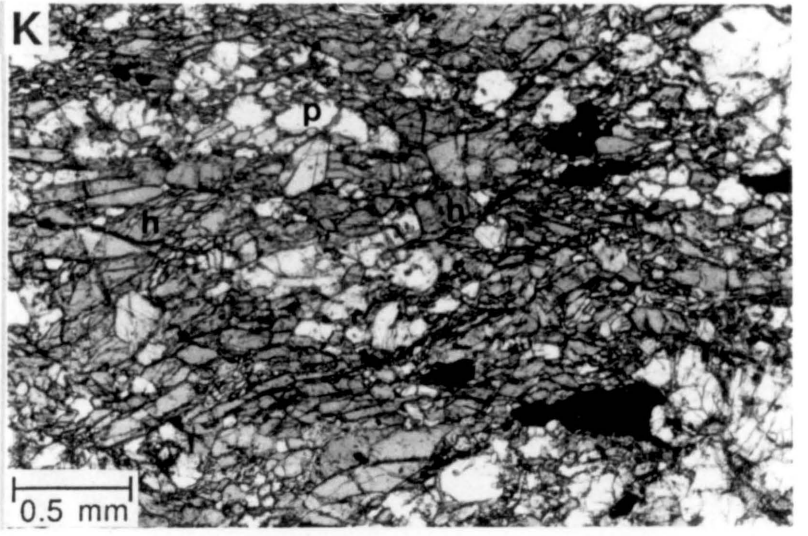
Figure 17. Photomicrographs of typical lithologies: a) Unicoi Formation, coarse arkosic conglomerate with chlorite matrix, sample A2-15A, crossed polars; b) Bowers Ferry rock, feldspar clasts in fine mylonitic matrix, sample A2-6B, crossed polars; c) Cranberry Gneiss, highly planar structure near fault trace, sample A2-14C, crossed polars; d) Cranberry Gneiss, quartz-feldspar augen, near Ashe contact, sample A2-13X, crossed polars; e) Ashe Formation, gneiss, with medium-grained interlocking quartz and plagioclase, and evenly dispersed biotite, sample B3-141A, crossed polars; f) Ashe Formation, muscovite phyllite, sample A2-1A, crossed polars; g) Ashe Formation, muscovite-graphite schist, with first occurrence of garnet, sample A3-1B, uncrossed polars; h) Ashe Formation, staurolite-muscovite-paragonite schist, with staurolite porphyroblast at edge of plagioclase "eye", sample C4-32A, uncrossed polars' i) Ashe Formation, kyanite-quartz rock, kyanite blade with muscovite and chlorite, sample D2-1D, crossed polars; j) Ashe Formation, metagabbro with coarse, randomly oriented hornblende, with pale actinolitic cores and dark hornblende rims, sample A3-43A, uncrossed polars; k) Ashe Formation, medium-grained hornblende schist, sample C4-24B, uncrossed polars. Abbreviations: a = actinolite, b = biotite, c = chlorite, g = garnet, gr = graphite, h = hornblende, K = K-feldspar, ky = kyanite, m = muscovite, my = mylonite matrix, p = plagioclase, q = quartz, s = staurolite.


A
q
p
c
0.5 mm
B
my
p
K
0.5 mm
C
p
b
q
m
0.5 mm
D
q
p
m
my
0.5 mm


E
p
q
b
0.5 mm
F
0.2 mm
G
m
gr
g
m
q
0.5 mm
H
p
b
s
g
c
s
m
0.5 mm


I
m
ky
c
0.5 mm


J
p
a
h
0.5 mm


K
p
h
h
0.5 mm

Mineral Chemistry

Metasedimentary and Plutonic Rocks

Muscovite and Paragonite

Muscovite varies in composition in two ways across the study area: in the amount of K versus Na, or paragonite content, and in the number of Si atoms per formula unit, or celadonite content (appendix A). Unicoi and Bowers Ferry rocks show considerable variation of Na/(Na + K) ranging from 0.01 to 0.10. However, the highly recrystallized rocks of the Cranberry Gneiss contain the lowest values of Na/(Na + K) in the area, in the range of 0.01 to 0.03. As one procedes toward higher grades, in the Ashe Formation, muscovite contains increasing amounts of Na (figure 18a), although there is some scatter of the data both within samples and between nearby localities. Values range from as low as 0.04 in the chlorite zone to 0.30 in the staurolite zone, just north of the Galax Shear Zone. It should be noted that in the staurolite zone, however, a two-white mica assemblage is observed (to be discussed below).

As seen on figure 18b, the number of Si atoms per formula unit (based on 11 oxygens) shows a weak, but discernable decrease toward higher grade areas, with a high of 3.3 atoms in the Fries Fault area, decreasing to 3.0 in the staurolite zone. In general, as Si and (Mg + Fe) content decreases, the Al content increases, which implies the substitution Al(VI),Al(IV) = (Mg,Fe),Si, or tschermak's substitution. In addition, Fe/(Fe + Mg) decreases from northwest to southeast, ranging from 0.70 in the ultramylonite zone of the Fries Fault, decreasing from 0.42 in the Ashe Formation in the chlorite zone to .24 in the staurolite zone.

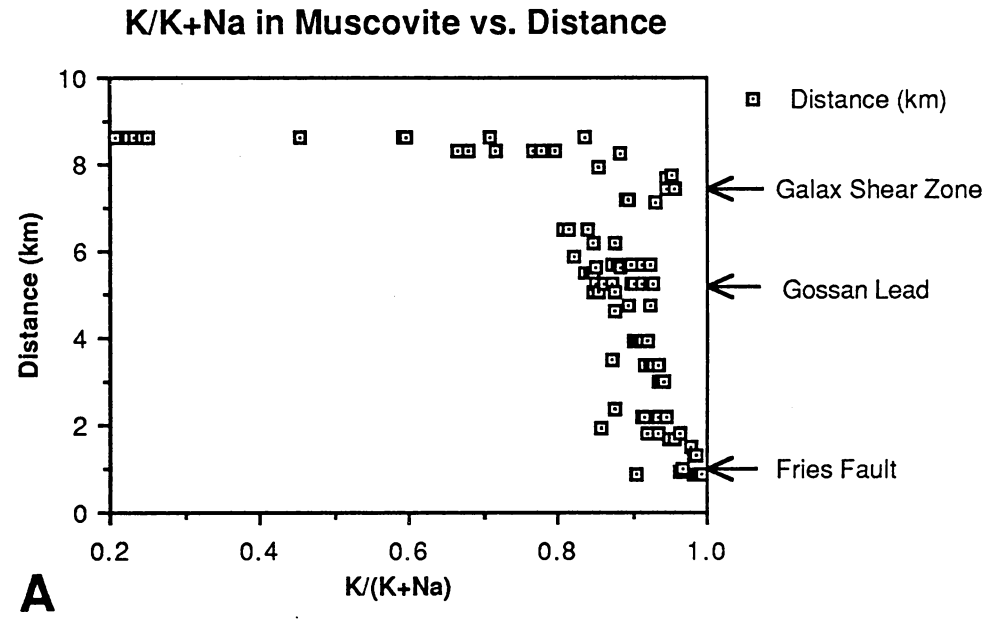
Chlorite

In order to facilitate chemical comparisons between different silicates, it is convenient to plot Fe/(Fe + Mg) vs. distance from the reference line (figure 19). This diagram plots coexisting chlorite, biotite, staurolite, and garnet (rim), with the rocks in the Gossan Lead sulfide zone omitted for simplicity. In general garnet > staurolite > biotite > chlorite.

Chlorite analyses plot within the compositional range of ripidolite. In general, Fe/(Fe + Mg) decreases toward the staurolite zone, no matter what textural habit the chlorite assumes. Higher values are associated with the Fries Fault area, where values are as high as 0.58, and decrease toward the staurolite zone where they are approximately 0.39. Additional weak, but discernable trends are: total Al(IV) + Al(VI) increases with a sympathetic decrease in Si + Mg + Fe toward the staurolite zone; and Mn content tends to decrease toward the staurolite zone (appendix A).

Biotite

Fe/(Fe + Mg) decreases in general toward the staurolite zone, with the mylonite zone containing the highest values in the study area of up to 0.65 (figure 19). Values within the Ashe Formation are



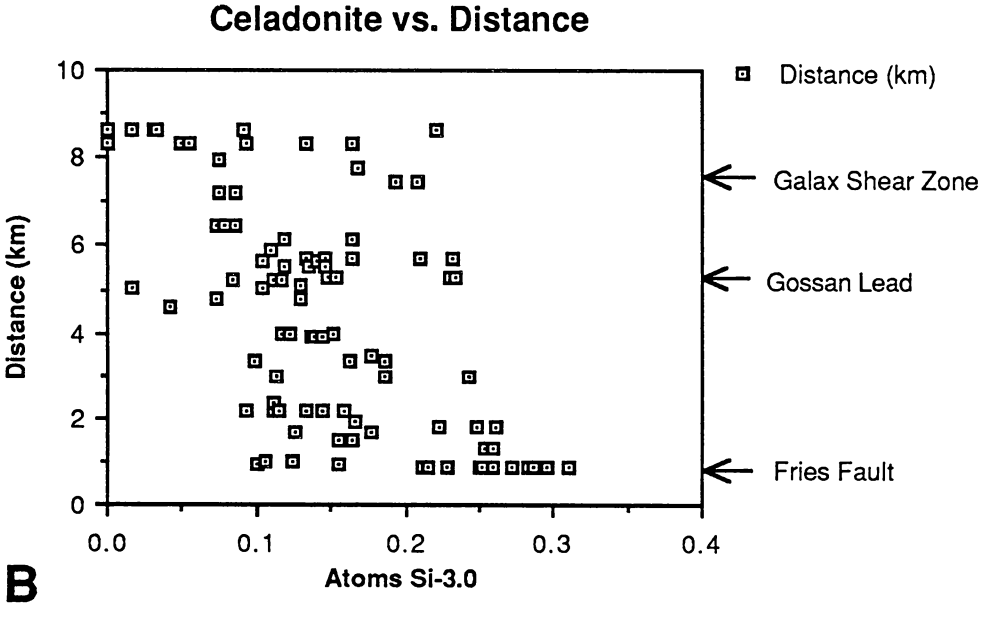


Figure 18. Muscovite compositions vs. distance: a) K/(K + Na) vs. distance, b) atoms of Si-3.0 vs. distance.

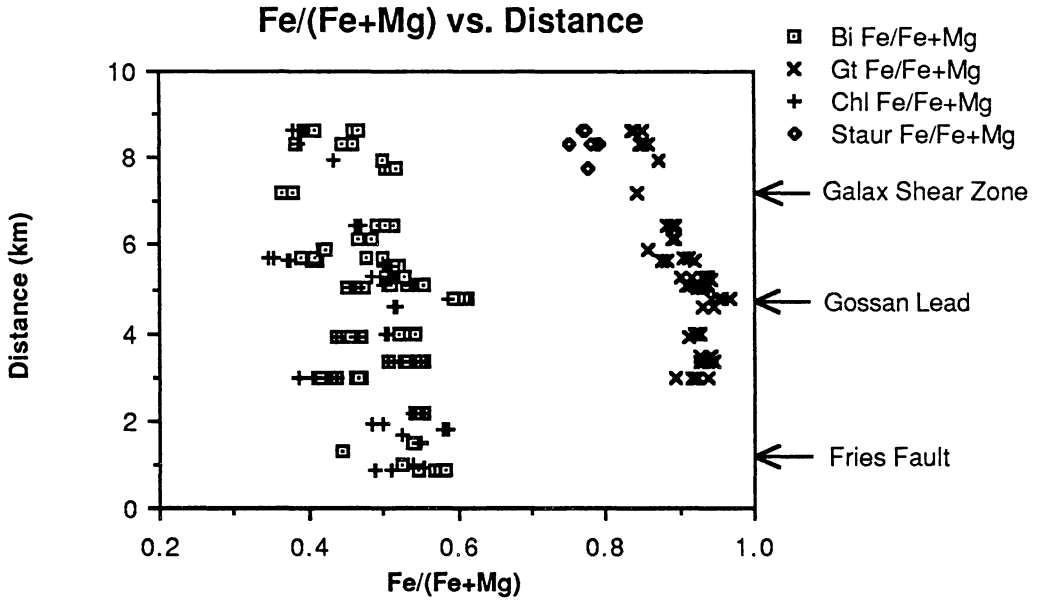


Figure 19. Fe/(Fe+Mg) vs. distance: Compositions of chlorite, biotite, staurolite, and garnet.

generally quite high in the in the biotite zone (0.55), and decrease to 0.41 in the staurolite zone. Significant trends were not observed in Al(VI) content, which ranged from 0.32 to 0.48 atoms per formula unit; in Ti content, which tended to fall between 0.07 to 0.13 atoms per formula unit; and in F content, which showed much scatter, but generally was near 0.08 atoms per formula unit.

Garnet

Garnets in the study area are essentially of almandine - grossular - spessartine composition. Near the garnet isograd, they show the greatest amount of chemical zoning along with the greatest enrichment of Mn and Ca. For example, at location B2-1, core analyses indicate as much as 30% spessartine component, and 31% grossular component, while rims show a distinct decrease in Mn (20%) while Ca holds approximately constant at 32% (table 3, appendix A). Mn content nearly always decreases from core to rim, while Ca usually decreases from core to rim with a less pronounced and consistent pattern. Fe/(Fe + Mg) content generally decrease toward the rim in most samples analyzed throughout the area. Notable exceptions occur where textural obervations indicate that some post-peak metamorphic fabric exists. Examples include the garnets at location B2-1 which is within the shear zone of the Fries Fault, and in the kyanite-bearing rocks of location D2-1, where late-growing retrogressive chlorite is abundant. In general, the degree of compositional zonation decreases with increasing metamorphic grade, so that at the staurolite zone, garnet compositions are essentially homogeneous within a grain. The following trends were observed across the area: 1) Fe/(Fe + Mg) decreases toward the staurolite zone from 0.94 in the northwest to 0.84 in the staurolite zone (figure 19). 2) There is considerable variation in Mn content, which apparently is due to slight differences in bulk composition (figure 20a). Analyses of Mn/(Mn + Ca + Mg + Fe) range from 0.20, along the garnet isograd to a low of 0.03 in the staurolite zone. These lower values, however, may be a function of the increase in modal amounts of garnet in this area. 3) Ca/(Ca + Mn + Mg + Fe) shows a systematic decrease with distance toward the

staurolite zone, with values as high as 0.32 at the garnet isograd, to values as low as 0.08 in the staurolite zone (figure 20b).

Plagioclase

Plagioclase grains show weak optical zonation that was usually not resolvable on the microprobe. However, a well defined An enrichment trend was observed over distance toward the staurolite zone (figure 21). In the Fries Fault area, plagioclase is albite, with compositions of An_{0-1}. At the garnet isograd, plagioclase composition ranges from An_{1-5} in some samples, but are as high as An_{18} in other samples, with no samples of intermediate composition observed. In general, a wide range of compositions can be observed nearly everywhere. However, the degree of range increases toward the southeast where the most calcic (An_{34}) compositions are found. At one locality (C4-32), plagioclase was observed in compositionally zoned, eye-like porphyroblasts with cores that were less calcic (An_{20}) than their rims (An_{29}). Or contents are uniformly less than 1% and do not show any correlation with metamorphic grade.

Staurolite

Staurolite, despite its coarse size, shows no siginificant zoning patterns. Fe/(Fe + Mg) ranges from 0.75 to 0.80, with the value decreasing to the southeast (figure 19).

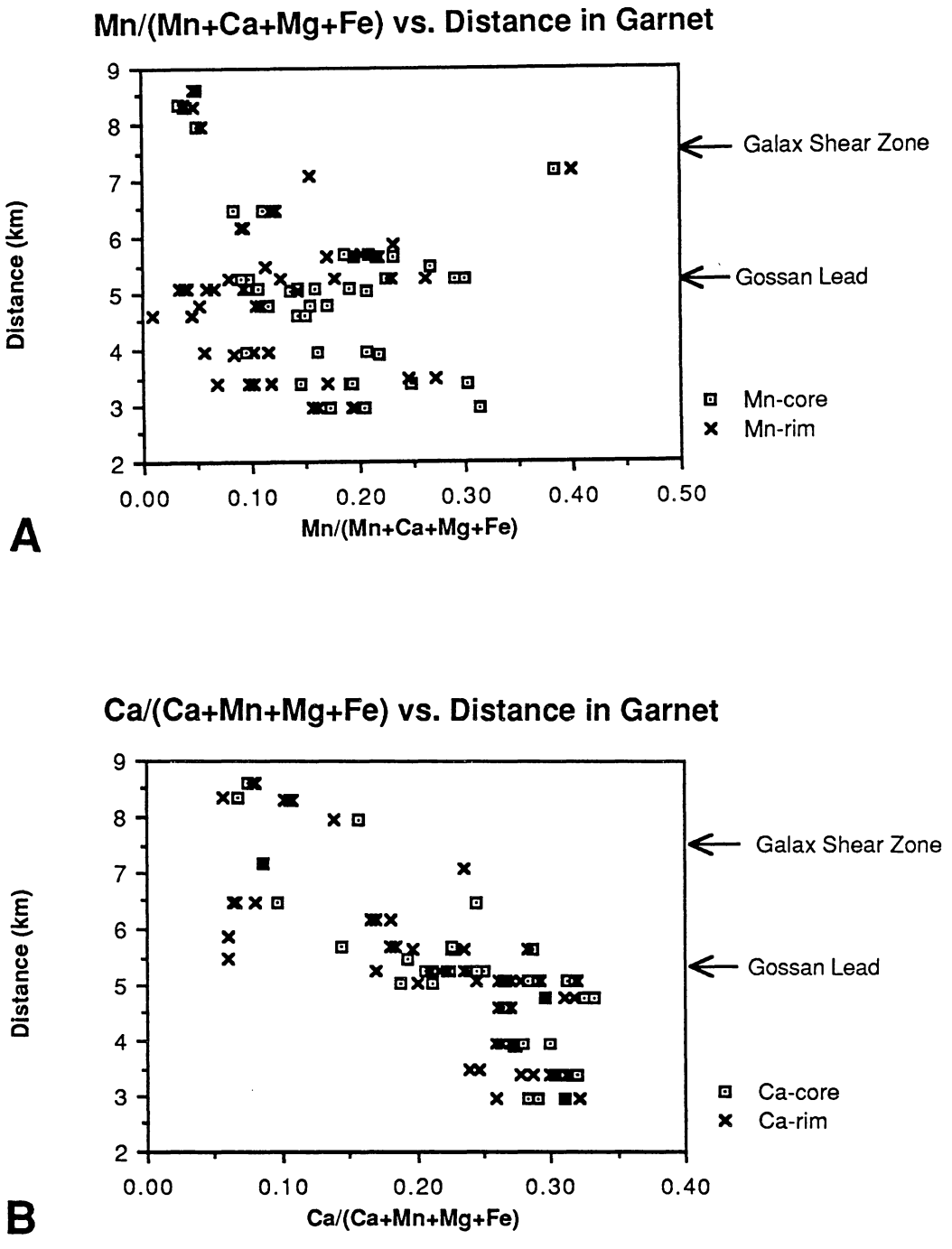


Figure 20. Ca and Mn content of garnet vs. distance: a) Mn/(Mn + Ca + Mg + Fe) in garnet vs. distance, b) Ca/(Ca + Mn + Mg + Fe) in garnet vs. distance.

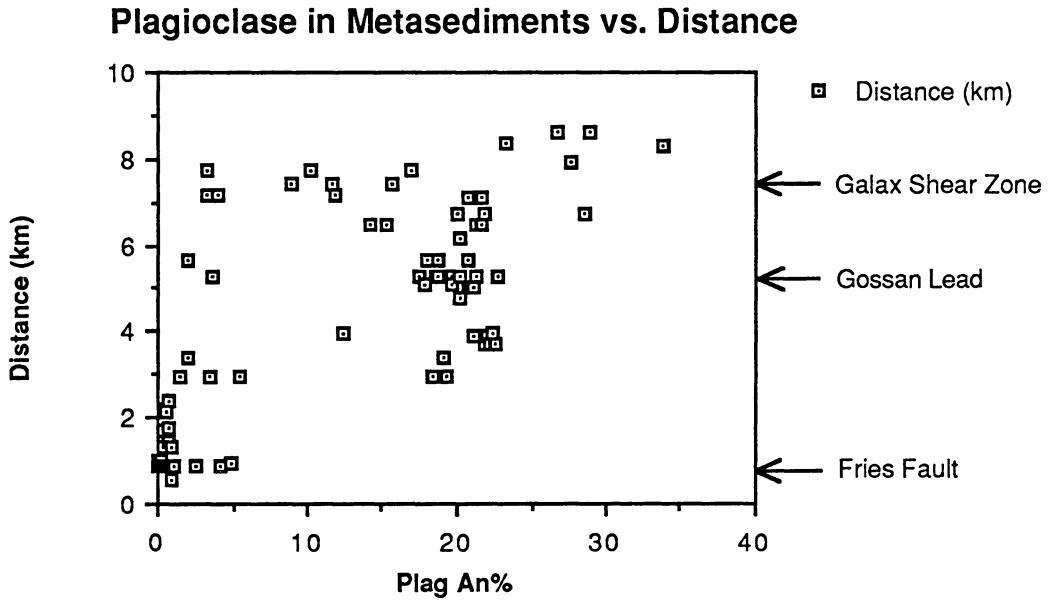


Figure 21. Plagioclase (An) composition vs. distance in metasediments

Amphibolites

Amphibole

Amphibole is found in a variety of compositions depending on rock type and metamorphic grade. Unfortunately, amphibole-bearing rocks are rare in the northwest part of the study area. Thus, well defined compositional trends are not present across the study area, as amphiboles are restricted to only the garnet and staurolite zones. However, a number of generalities may be noted. Many amphiboles show chemical zonation between core and rim and matrix. In amphibolites containing the common assemblage of amphibole + plagioclase + clinozoisite + chlorite + quartz + sphene + ilmenite, the coarser, early-formed amphiboles tend to have cores with higher Mg/(Mg + Fe), and lower Al/(Al + Si) and Na/(Na + Ca). The greatest degree of chemical zonation is found in the lower grade rocks near the garnet isograd. In the most extreme case (sample A3-43B, figures 17j, 22), pale green actinolitic cores are rimmed by darker green hornblende. However, toward the staurolite zone, the degree of zonation and range of compositions decrease, and the overall composition consistently falls into the range of hornblende to tschermakitic hornblende (figures 23a and 23b). Two exceptions have been observed: actinolites are found in amphibolites within the shear zone just north of Galax in rocks that contain annealed mylonitic textures (figure 23c); and in actinolite - chlorite schists, rocks that contain a more magnesium-rich bulk composition (appendix B) than other amphibolites. Other trends are: a sympathetic increase of Al(IV) with Al(VI) + Fe(3+) + Ti, which becomes better defined at higher grade, and a weakly defined increase in Na(A) + K(A) and Na(M4) toward the staurolite zone.

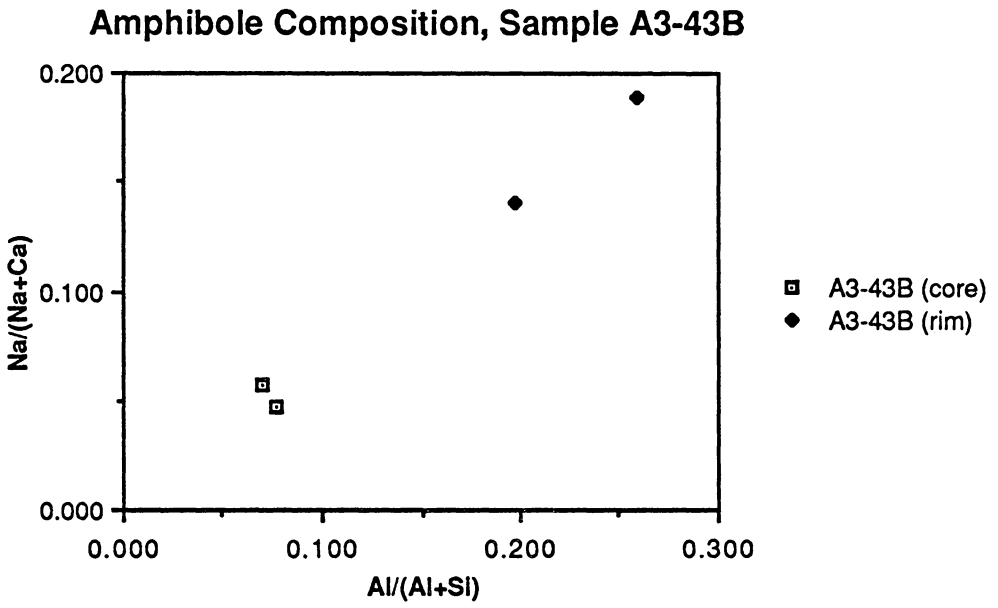
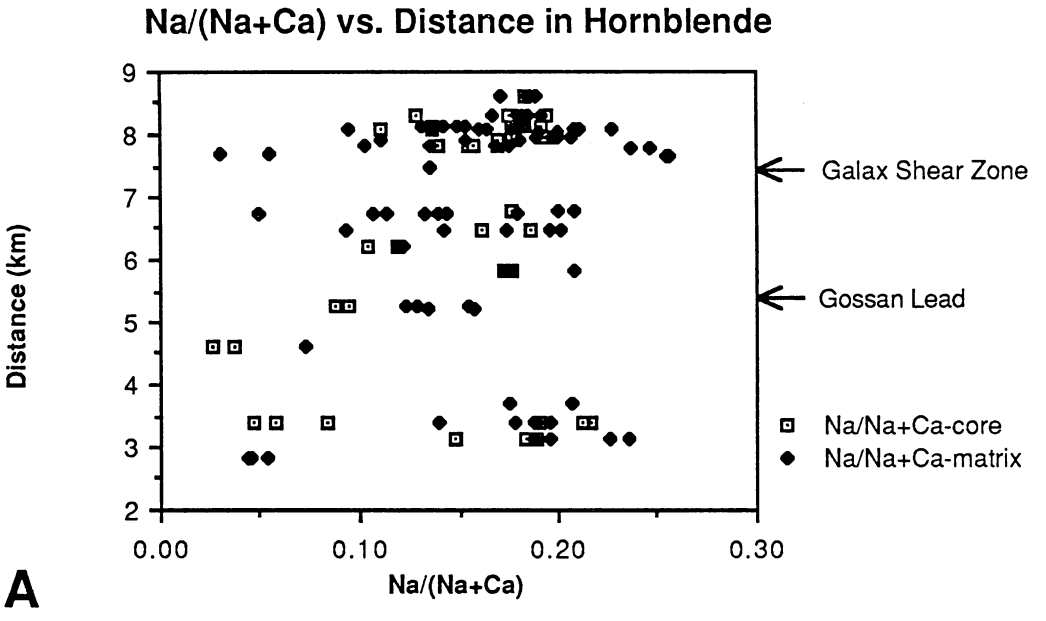


Figure 22. Na/(Na + Ca) vs Al/(Al + Si) in zoned amphibole, sample A3-43B



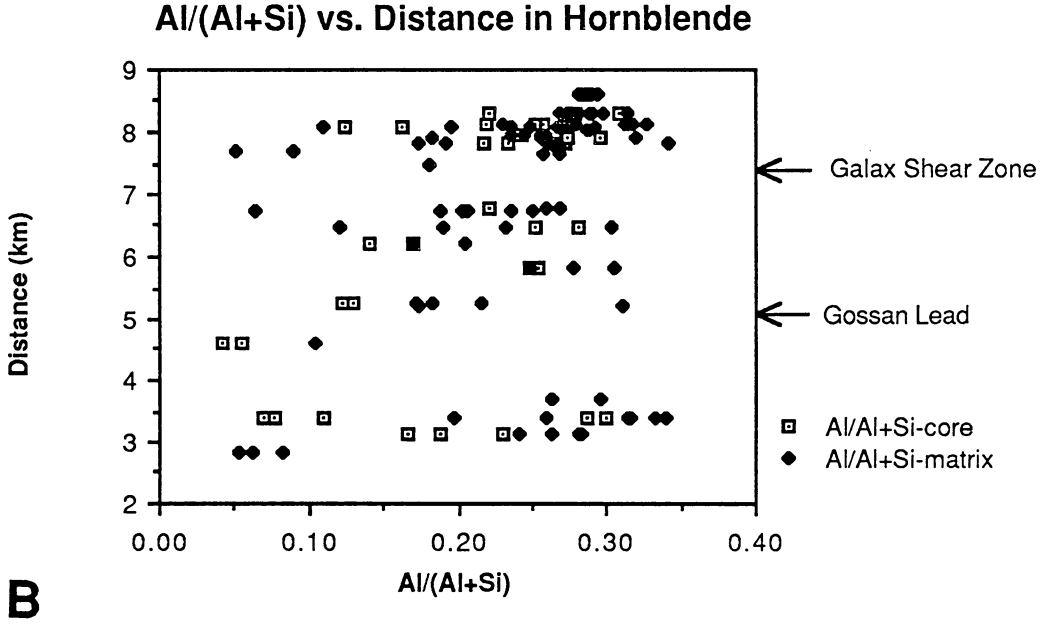


Figure 23. **Amphibole compositions vs. distance:** a) Na/(Na + Ca) vs. distance, b) Al/(Al + Si) vs distance, c) Fe/(Fe + Mg) vs. distance.

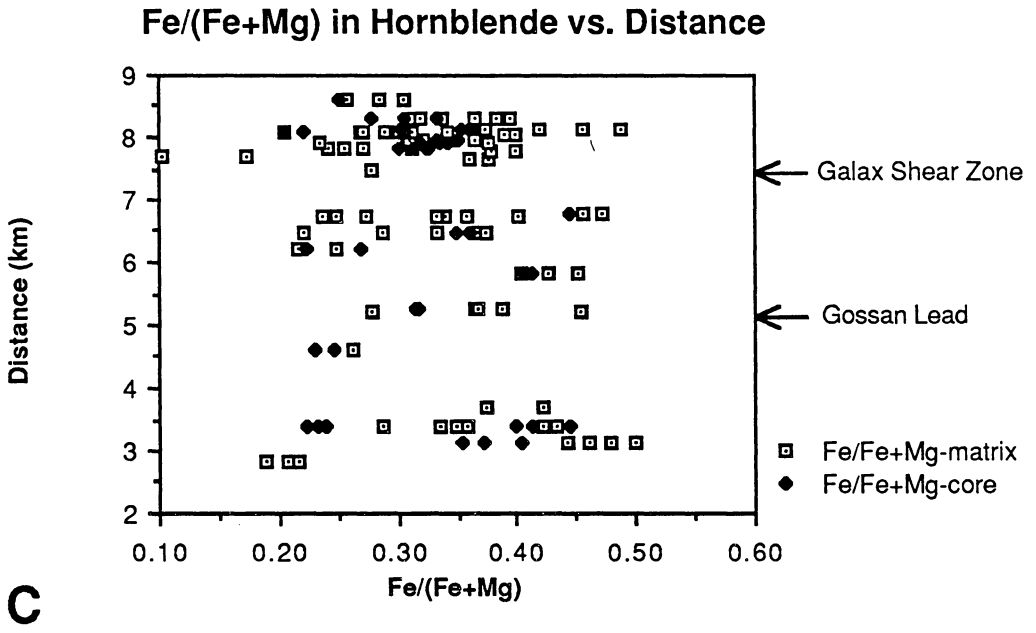


Figure 23 (continued)

Plagioclase

Plagioclase shows an increase in An content toward the staurolite zone. An content near the garnet isograd tends to be rather low, in the range of An_{2-8} (figure 24). However, at a distance of 3.7 km from the reference line (0.7 km southeast of the garnet isograd), the calcium content increases apparently abruptly to An_{22}, with An content steadily increasing to An_{46} toward the staurolite zone. An exception to this trend is found in the amphibolites of the Galax shear zone, where samples are generally less anorthitic, with An contents as low as An_{12}.

Chlorite

As a group, the chlorites are ripidolites, with Al(IV) in the range of 1.1 to 1.4 atoms per formula unit, and Al(VI) in the range of 1.25 to 1.55 atoms per formula unit. In general, the chlorites found in mafic rocks are slightly more magnesium-rich than those of the metasediments, with Fe/(Fe + Mg) values being as low as 0.24. Unlike the metasedimentary chlorite, these chlorites do not show discernable compositional trends with changing metamorphic grade.

Other Minerals

Clinozoisite is ubiquitous in amphibolites of the common assemblage. The primary variation is in the value of Fe(+3)/(Al(VI) + Fe(+3)) which varies from 0.09 to 0.26. However, no relationship between this variation and metamorphic grade was noted. Also, there were no observable trends in the Ti content nor in Mg + Fe(2+) substitution for Ca vs. distance in clinozoisite.

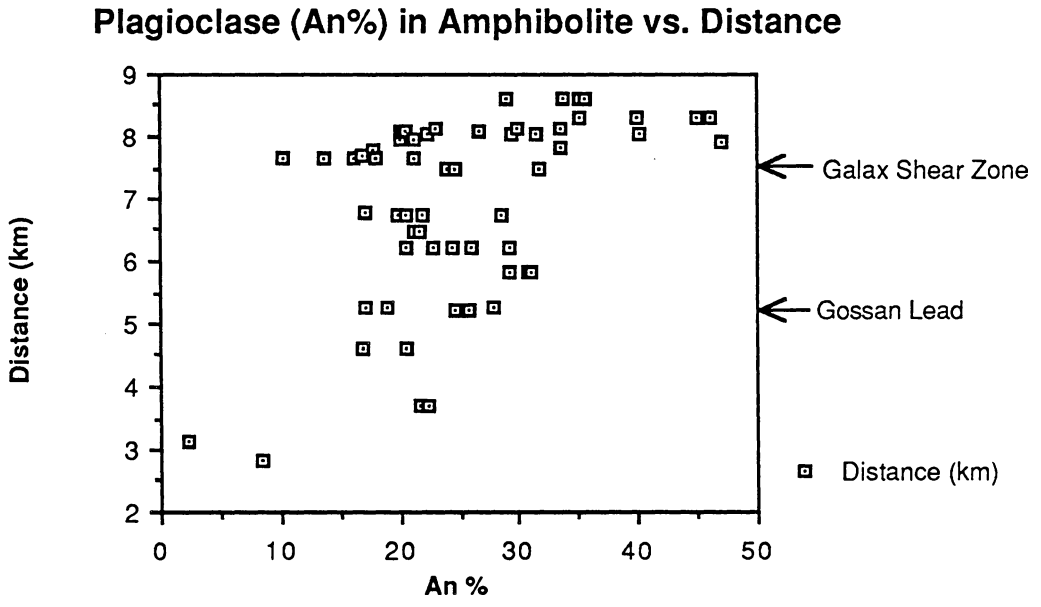


Figure 24. Plagioclase (An) composition vs. distance in amphibolite

Biotite was observed as a trace or minor mineral in a few amphibolites (analyzed in samples B2-4A, B4-7C, B3-13A, and C4-1C). There is no correlation between modal amounts of biotite and metamorphic grade, and the content of Fe/(Fe + Mg) is somewhat lower than those in metasediments, ranging from 0.32 to 0.40, with this value tending to decrease toward the staurolite zone (appendix A).

Garnet was analyzed in two samples. Sample B4-8B, within the garnet zone, 6.74 km from the reference line, is slightly more almandine-rich and less pyrope-rich than garnets in the surrounding metasediments (appendix A). These garnets, however, are quite Ca and Mn-rich, containing 31% grossular component and 11% spessartine component, similar to metasedimentary garnet, with Mn and Fe/(Fe + Mg) decreasing, and Ca increasing from core to rim. Sample C3-117A, from near the staurolite isograd, contains slightly more almandine, and less spessartine and grossular than in B4-8B, with similar zoning trends.

Discussion

Evolution of Mineral Assemblages

In order to observe the change in mineral chemistry of the continuous reactions observed in the Ashe Formation, mineral compositions of coexisting chlorite, biotite, garnet, and staurolite are plotted on the AFM diagrams of figure 25 in rocks with that contain muscovite and quartz. For convenience, the study area was divided into 4 parts: 1) rocks northwest of the garnet isograd which contain chlorite and biotite; 2) garnet zone rocks northwest of the Gossan Lead trend; 3) garnet zone rocks southeast of the Gossan Lead trend; and 4) staurolite zone rocks.

Biotite

The appearance of biotite in the Ashe Formation is not accompanied by the disappearance of another phase. However, as the modal abundance of biotite increases to the southeast, chlorite abundance decreases and the celadonite content of muscovite decreases. This suggests the following reaction:

chlorite + celadonitic muscovite = muscovite + biotite + quartz + H_2O, [1]

which is similar to the reaction suggested by Guidotti (1984).

Garnet

Garnet appears at approximately the southeast edge of the shear zone of the Fries Fault within the Ashe Formation. These first garnets are enriched in Ca and Mn, containing up to 30% grossular and 20% spessartine components. As has been reported by many workers, high Ca and Mn tend to stablize garnets at lower temperature ranges than the pure almandine end-member. Thus, although the petrogenetic grid of Koons and Thompson (1985) shows that the lower limit of pure almandine stabilitiy to be near 580 °C, the Ashe Formation supports garnet stability at near 480 °C.

As was true with biotite, the first appearance of garnet is not accompanied by the disappearance of another phase. However, rocks of the Ashe Formation below the garnet isograd tend to contain more primary chlorite (up to 9%) than rocks above the isograd. This decrease in chlorite appears to work in concert with the formation of biotite and with the sympathetic decrease in Fe/(Fe + Mg) in garnet, biotite, and chlorite. This causes a swing in the position of the biotite-garnet-chlorite tie lines toward more Mg-rich compositions, comparing figures 25a, 25b, and 25c. Thus typical pelitic bulk compositions (such as sample A2-1) tend to plot more in the three-phase biotite-garnet-chlorite field as temperatures increase to the southeast. Therefore, the general AFM reaction for garnet appearance is:

chlorite + muscovite + quartz = garnet + biotite + H_2O. [2]

(Thompson and Norton, 1968).

However, it appears that in the study area, in order to make the first occurrence of garnet, excess Mn and Ca must be available. In the first observed garnet locality, location B2-1, calcium is available as calcite and zoisite. This suggests the reaction:

2 zoisite + 5 calcite + 3 quartz = 3 grossular + 5 CO_2 + H_2O. [3]

This reaction, along with others in the system CaO - Al_2O_3 - H_2O - CO_2 has been compiled by Winkler (1979, p. 143) in T - X (CO_2) space. Keeping in mind that neither grossular nor zoisite are "pure" phases in these rocks, the above reaction is consistent with a temperature of 480 °C and a P_{fluid} of 4 kb estimated for the area, and indicates a mole fraction of X(CO_2) of 0.02. It should be noted that this occurrence of calcite is only one of three such occurrences known in the study area, making the above mineralogy exceedingly rare. Nevertheless, it can be demonstrated that in the first appearance of garnet, at least at this one locality, unusual mineralogy leading to garnets of 30% grossular component may be responsible for its first appearance.

The situation is less obvious for managanese, as the only other manganese-bearing phase in these rocks is ilmenite (up to 4 wt % MnO). Furthermore, there is no obvious relationship between Mn content of the garnet and that of the ilmenite. However, it seems apparent that the Ashe Formation metasediments are more Mn-rich than average pelitic rocks. For example, bulk rock chemical analyses of MnO in Ashe Formation pelites (appendix B) have a range of 0.06 - 0.28 weight percent, amounts that exceed nearly all of those tabulated by Shaw (1956) as representative of common pelites. It is evident that the actual garnet-producing reaction is the sum of equations [2], [3], and equations involving Mn component.

Staurolite

As previously mentioned, some rocks in the staurolite zone contain garnet, biotite and both primary and retrograde chlorite. Chlorite compositions in these rocks are among the most Mg-rich in the

Figure 25. AFM plots of mineral compositions: a) Rocks northwest of the garnet isograd, rectangle = bulk composition of sample A2-1Z, open circle = sample A3-4A, biotite zone; closed circle = sample A2-21A, biotite zone; closed triangle = sample A2-3HZ, Bowers Ferry rock; closed square = sample A2-13A, Cranberry Gneiss; b) garnet zone northwest of the Gossan Lead; c) garnet zone southeast of the Gossan Lead, rectangle = bulk composition of sample B4-16Z, d) staurolite zone, rectangle = bulk composition of sample C4-32B.

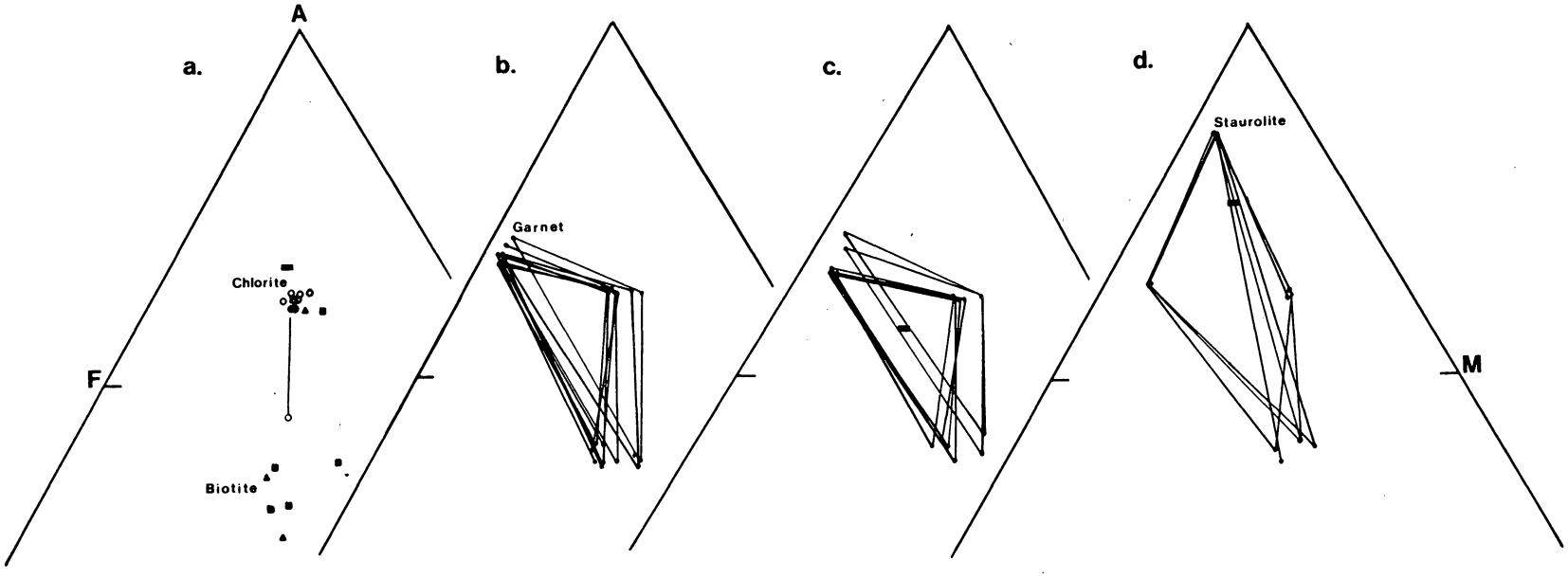


Figure 25 (continued)

study area, and have never been observed to be in contact with garnet. In addition, late-growing biotite porphyroblasts are a particularly common texture in these rocks. Other rocks lack primary chlorite altogether and contain the assemblage: garnet + biotite + staurolite. Thus, the garnet-chlorite tie line is replaced by the staurolite-biotite tie line in the reaction:

chlorite + garnet + muscovite = staurolite + biotite + H_2O. [4]

Kyanite

Kyanite at location D2-1 is found in two situations. In one case, it touches staurolite and biotite, with garnet also present in the rock, without primary chlorite. Thus, the chlorite-staurolite tie line is crossed by the kyanite-biotite tie line in the reaction:

staurolite + chlorite + muscovite = biotite + kyanite + H_2O. [5]

It should be noted that a decrease in water pressure would also cause this reaction to move to the right.

In the other case, kyanite is found in quartz vein material associated with late-growing chlorite and intergrown muscovite. These rocks are also depleted in garnet so that it is only present as staurolite inclusions. In addition, biotite shows extensive overgrowths of chlorite. Garnet rim-biotite temperatures in this rock show a wide variation in the range of 483 to 515 °C, with rim temperatures approximately 30° less than core temperatures. This suggests that chlorite is retrogressive in this instance, and that the reaction:

garnet + biotite + H_2O = chlorite + muscovite + quartz [6]

was a high-temperature, retrogressive reaction superimposed on an earlier kyanite + staurolite + biotite assemblage.

A summary of the AFM changes vs. metamorphic grade is plotted in figure 26. Here, the observed change in AFM topology and systematic increase in Mg/(Fe + Mg) is plotted as a function of increased metamorphic grade or distance from the reference line toward Galax.

Muscovite Compositional Changes With Metamorphic Grade

Muscovite is the most abundant sheet silicate in the study area. It is present in nearly all of the various lithologies except for the mafic rocks, and can be found in all of the shear zones. Unlike minerals such as staurolite and garnet, muscovite's presence in the field is not determined by discontinuous isograd reactions. Thus, muscovite provides the most continuous information across the field area.

Both celadonite and paragonite content of muscovites have been proposed as geothermometers. For example, Velde (1965) conducted experimental studies that clearly showed that celadonite decreases with increasing temperature and pressure. Eugster and others (1972) are among many workers who have dealt with the muscovite - paragonite solvus. These studies show that with increased temperature, a more sodic muscovite will co-exist with a more potassic paragonite. One way to illustrate white mica relationships in the system KNASH is to plot Al_2O_3 - $NaAlO_2$ - $KAlO_2$ (Guidotti and Sassi, 1976). A schematic diagram of this system is illustrated in figure 27. Three assemblages are relevant to this discussion: albite - K-feldspar - muscovite; albite - aluminosilicate - muscovite; and albite - muscovite. The first two assemblages are termed "limiting assemblages" in that because they contain three phases, the composition of muscovite is fixed at a given P, T and a(H_2O) regardless of bulk composition, whereas the two-phase albite-muscovite assemblage permits variations in mineral composition due to bulk compo-

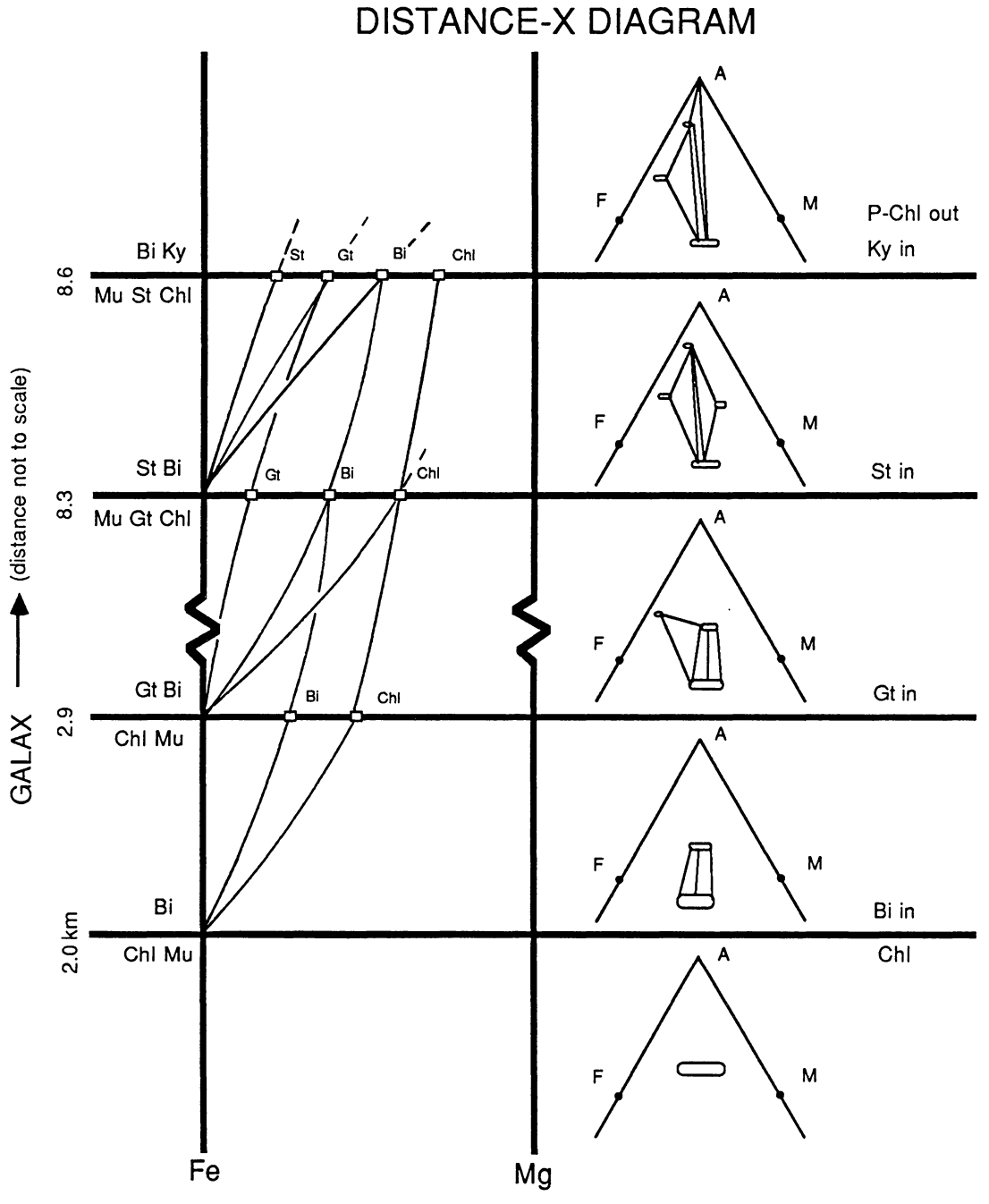


Figure 26. Distance vs. X diagram

sitional differences. Unfortunately, three-phase limiting assemblages are only found in a few localities within the study area: in the mylonite zone of the Cranberry Gneiss, which contain K-feldspar, albite, and celadonitic muscovite; in some staurolite-bearing rocks which contain Na-rich muscovite, oligoclase, and kyanite; and at locality C4-46, a rare metaconglomerate within the Ashe Formation that contains K-feldspar, albite and muscovite.

Over the bulk of the study area, the two-phase non-limiting assemblage of muscovite - plagioclase is common. However, the general increase in paragonite content and decrease in celadonite content indicates that much of the change in muscovite composition is due to a systematic relationship between the chemistry of the muscovite and the metamorphic grade which increases to the south-east. This causes the albite - muscovite tie lines of figure 27b to rotate toward more Na-rich muscovite compositions with increasing temperature.

The observations of this study are consistent with those of Guidotti and Sassi (1976) who reported Na/(Na + K) values of muscovites in aluminous schists in non-limiting assemblages. They similarly showed increasing Na/(Na + K) with increasing grade in specimens from N.W. Maine in rocks below their upper staurolite zone. Thus, it appears that despite variations imposed by bulk compositional differences, muscovite compositions can be used as qualitative geothemermometers with muscovite compositions approximating the position of the muscovite limb of the muscovite - paragonite solvus (Guidotti and Sassi, 1976).

A test of the consistency of the natural data from this study with the experimental muscovite-paragonite solvus of Chatterjee and Flux (1986) is given in figure 28. There, muscovite compositions from rocks where biotite-garnet temperatures (Hodges and Spear method) are known are plotted as a function of temperature. The natural data is generally consistent with the 6 kb solvus in that muscovite increase in Na content with increasing temperature, and the muscovite plots in the one-phase mica field. However, in sample C4-32, in the staurolite zone, a two-phase muscovite-paragonite assemblage is plotted. These compositions tend to plot within the two-phase field, with a scattering of the data. There are several possible reasons for this effect. Firstly, the

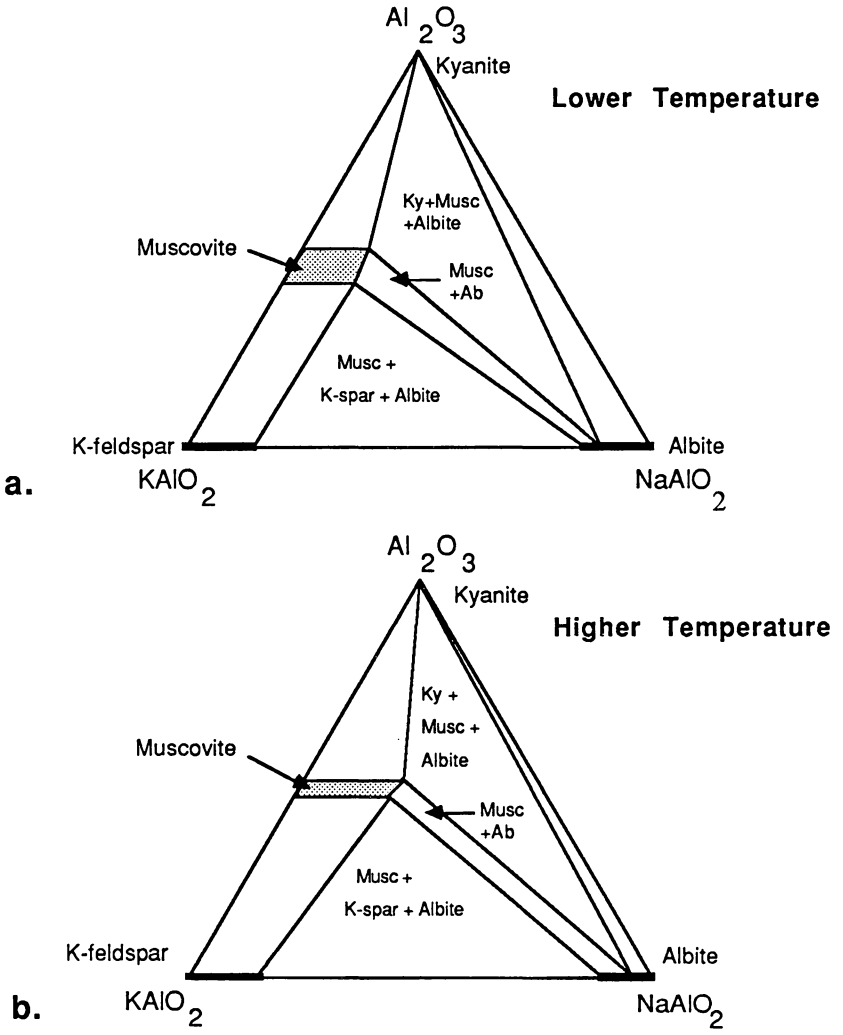


Figure 27. Na-Al-O system: a) Lower temperature, b) higher temperature.

compositions of the micas deviate somewhat off the ideal muscovite-paragonite join by containing small amounts of other elements such as Mg and Fe. Secondly, the white micas are found in finely intergrown lamellae that were not resolvable by the microprobe beam. This may account for the inconsistent scattering of the data.

From the previous discussion, the following inferences may be made about the muscovites in the study area. Firstly, the strongly mylonitized rocks of the Bowers Ferry Thrust Sheet and the Cranberry Gneiss contain rocks with generally higher celadonite and lower paragonite content. Part of this effect may be bulk compositional in nature; the Cranberry Gneiss samples have a lower bulk alumina content than the pelitic schists of the Ashe Formation (appendix B) and should coexist with muscovites with higher celadonite content. However, bulk chemical analyses of Bowers Ferry and Cranberry rocks are similar to metagraywackes and gneisses of the Ashe Formation in Al_2O_3 that contain muscovite compositions with less celadonite. Thus, it appears that the major factor that affects celadonite content is metamorphic grade, which in turn affects the position of the muscovite - plagioclase tie lines of figure 27. Secondly, the celadonite decrease and paragonite increase toward the staurolite zone are consistent with the increase in temperatures as reflected by the mineralogic assemblages and by the garnet-biotite data. An exception to this increase is found in the shear zone north of Galax. There, celadonite increases, while paragonite decreases. This, however, is consistent with the petrographic observation that these rocks have the texture of somewhat annealled mylonites. Thus, shearing may have taken place after the metamorphic peak, but while the rocks were still warm. Another exception to the pattern is seen in the staurolite-bearing rocks. Here, paragonite content increases sharply, while celadonite content is similar to that of neighboring rocks. As garnet-biotite geothermometry does not indicate an abrupt increase in temperature in the staurolite zone, a more plausible explanation as will be discussed below, is that bulk compositional differences have led to paragonite formation.

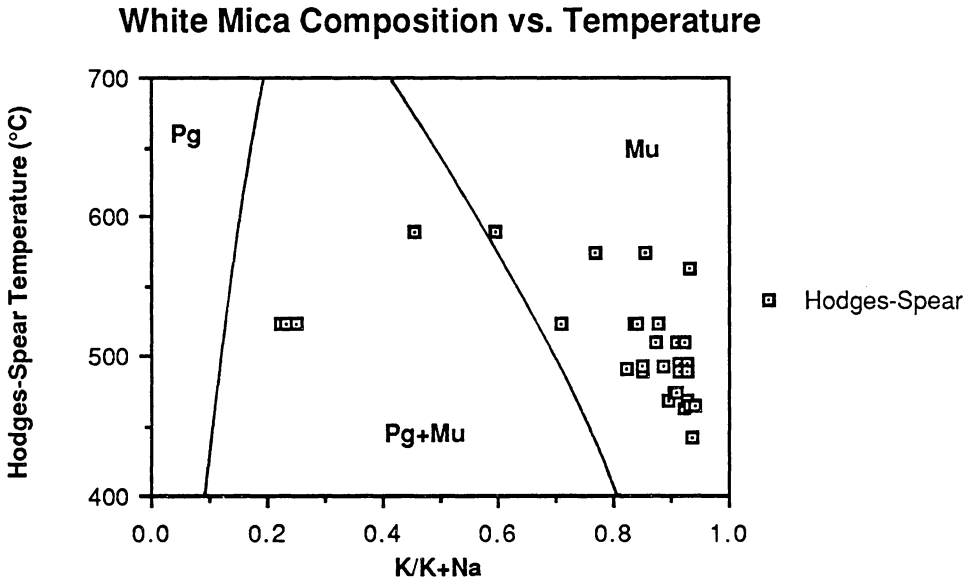


Figure 28. Muscovite-paragonite compositions vs. temperature: Solvii from Chatterjee and Flux (1986).

Paragonite

As previously discussed, "paragonite" as a component in muscovite is found everywhere in the study area, but shows a well defined increase to the southeast, towards the higher grades. However, it increases sharply once in the staurolite-bearing rocks, leading to the formation of paragonite as a second white mica forming fine intergrows with Na-rich muscovite, along with calcic plagioclase phenocrysts (An_{28}). This suggests the following reaction:

chlorite + albite (in plagioclase) + muscovite = paragonite + biotite + quartz + H_2O. [7]

As seen on figure 25d, the bulk chemical analysis of sample C3-32B which contains paragonite plots well above a line that would connect garnet and chlorite, a condition observed by Guidotti (1968) conducive to paragonite growth.

Paragonite can also be used to establish an upper limit to the metamorphic conditions. As has been documented by Hoffer (1978), and more recently by Mohr and Newton (1983) in the Blue Ridge of North Carolina, when paragonite + quartz breaks down, there is a simultaneous increase in the albite content of plagioclase. This is often manifested as albite-rich rims on the plagioclase porphyroblasts. This phenomenon, however, has not been observed in the study area, and plagioclase porphyroblasts, if anything, show **decreased** albite contents of rims, thus supporting reaction 7. However, the paragonite breakdown reaction has been experimentally calibrated by Chatterjee (1972):

paragonite + quartz = albite + kyanite + H_2O. [8]

At 5 kb, this reaction takes place at 570 - 625 °C, slightly higher than temperatures of the study area, and consistent with observations.

Garnet - Biotite Geothermometry

As previously stated, the garnet - biotite assemblage is common throughout much of the study area, and an attempt was made to determine temperatures using some of the various Fe-Mg exchange equilibria published in the literature, with particular attention paid to how they handled the problem of high amounts of Ca and Mn in garnet. Nearly all of the analyzed garnets, except for those in the staurolite zone, were above the value of (Ca + Mn)/(Ca + Mn + Fe + Mg) = 0.2 set by Ferry and Spear (1978) as the limit of allowable Ca + Mn for use of their garnet - biotite geothermometer. Thus, the various garnet - biotite geothermometers were put through a severe test, requiring them to handle garnets with a wide range of Ca + Mn. The tested geothermometers were: Goldman and Albee (1977), who related garnet - biotite compositions to oxygen isotope data and used statistical methods to account for Ca and Mn in their formulation; Ferry and Spear (1978), who experimentally determined the distribution constant using pure Fe-Mg garnets and biotites; Pigage and Greenwood (1982) who based their determination on thermodynamic mixing models in order to handle Ca and Mn; Hodges and Spear (1982) who adjusted the Ferry and Spear equation by using thermodynamic data combined with data from natural garnets to account for Ca and Mn; and Indares and Martignole (1985), who also adjusted the Ferry and Spear equation by using thermodynamic models to account for Ca and Mn in garnet, and also for Ti and Al(VI) in biotite.

All of these geothermometers are relatively insensitive to pressure. For example, it was estimated for the Ferry and Spear equation, that a pressure of 4.5 kb raised the derived temperature by approximately 8 °C over a temperature derived at 0 kb pressure. This is well within the errors of ± 50 °C posed by this calibration. Nevertheless, a minimum pressure could be estimated for kyanite - bearing rocks of location D2-1D by use of the aluminosilicate equilibria of Holdaway (1971). Temperatures derived by the various methods point to a temperature range of approximately 500 - 540 °C, which corresponds to a minimum pressure of about 4.5 kb. As will be shown,

this pressure is reasonable compared to results derived from other geobarometers. As a first approximation, a pressure of 4.5 kb was applied to the calculations used in the area. Errors in the determination of the Ferry and Spear (1978) temperatures, combined with an assumed error of ± 1 kb of pressure (to be discussed below) combine to create a temperature uncertainty of ± 60 °C. It should be noted that these estimates are also consistent with the experimental determination of the kyanite-sillimanite equilibria of Richardson and others (1968).

Results of representative calculations are presented in table 3. It is evident that there is considerable disagreement in two of the five methods, although the severity of the discrepancies are somewhat diminished in the staurolite zone, where the garnets have less Mn + Ca. A useful way to compare the effects of Ca and Mn is to plot temperature against X_{Mn+Ca} from different analyses from the same sample. This was done for sample A4-6A using the Hodges and Spear equation, a sample that lacks significant retrograde texture, and gives higher rim temperatures than core temperatures (figure 29). Thus, it can be assumed that the garnet-biotite pairs equilibrated at roughly the same temperature. As is obvious from comparing figures, the data scatter considerably more for the core-derived temperatures than for the rim-derived temperatures, with the core temperatures consistently lower than the rim temperatures. The lower core temperatures may be attributed to a number of factors such as: increasing temperature during garnet growth, increased Mn in the core thus decreasing the apparent "temperature" derived in the calculation of the temperature, disequilibrium between the core and the biotite outside of the garnet, and diffusion of elements into or out of the garnet. Because rim temperatures were generally higher and more consistent, the rims were used in temperature determinations. This is to be compared with the study of Indares and Martignole (1985) who used core temperatures because of persistent retrogression of their granulite facies rocks.

However, when comparing the rim temperatures of the different methods against each other, several factors become evident. Firstly, the Ferry and Spear equation, which does not take Ca and Mn into account, shows decreasing "temperature" with increasing Ca and Mn composition, even among different analyses within the same sample. As Ca content of garnet tends to decrease to the southeast, the inability of the Ferry and Spear method to account for excess Ca serves to amplify

Table 3. Representative results of biotite-garnet calculations

COMPARISON OF GARNET-BIOTITE TEMPERATURES

Core/Rim	Biotite	Garnet			Temperature °C				
	Fe/(Fe+Mg)	Fe/(Fe+Mg)	X(Mn)	X(Ca)	F-S	G-A	I-M	P-G	H-S
SAMPLE B2-1AB	**Distance=2.97 km**								
Core	0.47	0.93	0.21	0.31	326	457	480	540	425
Rim	0.47	0.94	0.20	0.31	315	446	468	528	417
SAMPLE A4-6A	**Distance=5.07 km**								
Core	0.53	0.95	0.19	0.31	318	431	463	524	416
Rim	0.53	0.92	0.04	0.29	422	494	509	589	522
SAMPLE A4-19A	**Distance=5.64 km**								
Core	0.41	0.89	0.23	0.23	393	525	533	599	470
Rim	0.41	0.87	0.20	0.20	420	531	535	606	490
SAMPLE C4-49B	**Distance=8.30 km**								
Core	0.45	0.86	0.04	0.11	503	501	500	584	543
Rim	0.45	0.86	0.05	0.10	501	499	499	581	540

F-S = Ferry and Spear (1978); G-A = Goldman and Albee (1977); I-M = Indares and Martingnole (1985);

P-G = Pigage and Greenwood (1982); H-S = Hodges and Spear (1982)

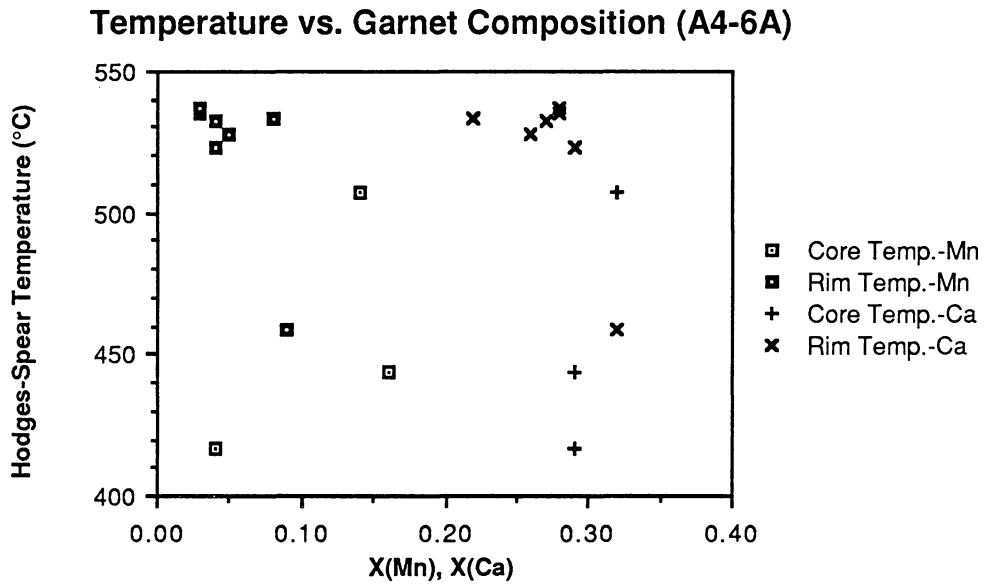


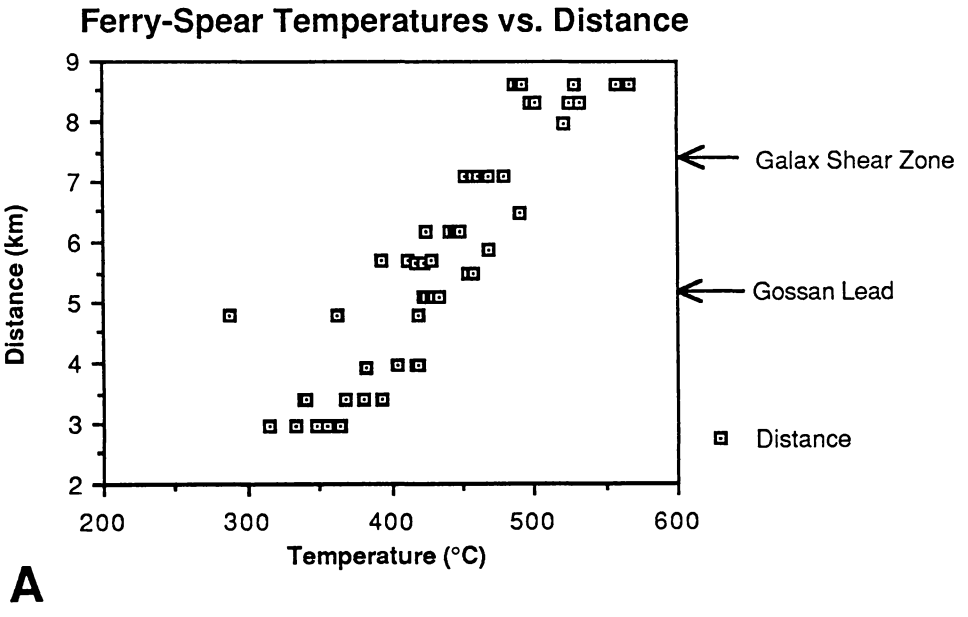
Figure 29. Temperature vs. X(Ca + Mn) in garnet, sample A4-6A

the trend toward higher temperatures to the southeast (figure 30a). On the other hand, the Pigage and Greenwood determinations are consistently 70 °C higher than the other methods. Such a discrepancy was also observed by St-Onge (1984) in his study of metapelites in the Wopmay Orogen in Canada, and by Gibson and Speer (1986) in their study of rocks from northern Alabama.

The Goldman-Albee, Indares-Martignole and Hodges-Spear methods, however, show more consistency despite variations in Ca and Mn. It is difficult to assess the accuracy of one of these methods over the others because the temperatures are not independently known. A plot of the Hodges and Spear temperatures versus distance from the reference line is given in figure 30b. As can be seen, temperatures steadily increase toward the staurolite zone, with temperatures at approximately 470 °C at the garnet isograd, and as high as approximately 600 °C in the staurolite zone.

Interpretation of the Amphibolites

Several authors have noted that hornblende compositions may be used, at least in a qualitative sense, as guides to temperature and pressure. For example, Brown (1977) noted that increased crossite (Na,M4) content of amphibole can be related to increased pressure. Hammarstrom and Zen (1985) have proposed a geobarometer based on the relationship between increased Al(IV) content and increased pressure in felsic plutonic rocks. Laird and Albee (1981) plotted total Na/Na + Ca against total Al/Al + Si for amphiboles that coexist with plagioclase, chlorite, quartz and epidote and showed that the slope of the resulting linear trend can be related in a qualitative sense to pressure. Since total amounts are used, this method also has the advantage of not depending upon site occupancy, values which depend upon the method of formula recalculation. In addition, they were able to note the relative temperature by the fact that higher temperature samples have higher values of Na/Na + Ca and Al/Al + Si. Unfortunately, there is considerable overlap



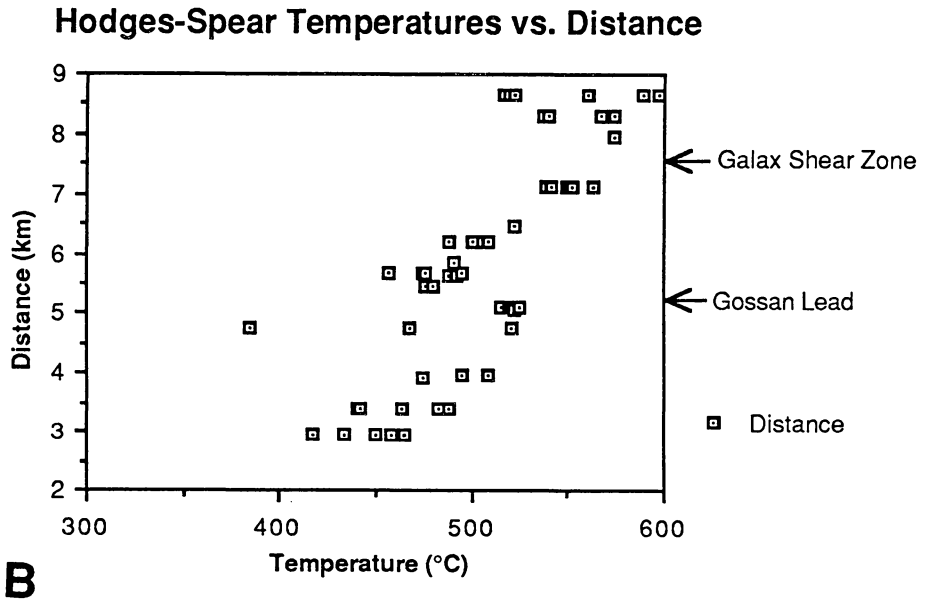


Figure 30. Garnet-biotite temperatures vs. distance: a) Ferry and Spear (1978) temperatures vs. distance b) Hodges and Spear (1982) temperatures vs. distance.

between their "low pressure", "medium pressure", and "high pressure" series. Data from this study plots well within their fields of overlap, thus limiting the usefulness of this technique.

However, if amphibole compositions are considered along with coexisting plagioclase, more detailed information can be obtained in terms of prograde and retrograde trends. Spear (1980), in a study of metamorphosed volcanic rocks from New Hampshire and Vermont, demonstrated the temperature dependence of the distribution between Na and Ca in the M4 site of amphibole and in plagioclase as reflected by its anorthite content. In general, taking into account possible compositional gaps such as the actinolite - hornblende gap, and the plagioclase peristerite gap, at relatively low temperature, a more sodic plagioclase coexists with a sodium-poor amphibole, whereas at higher temperature, the sodium content increases in amphibole but decreases in plagioclase. Variations in bulk composition will result, for example, in the coexistence of a less Na-rich plagioclase with a less Na-rich amphibole. Thus, at a higher temperature, it is possible for an actinolite to coexist with an unusually calcic plagioclase, as was observed in sample C3-32B of the staurolite zone. This effect may be illustrated as a series of tie lines connecting the Na(M4) content of amphibole with the anorthite content of plagioclase. These have been drawn (figure 31) for representative amphiboles of the study area, with the form of diagrams similar to that of Spear (1980) and the amphibole formulae recalculated according to the method of Spear for comparison purposes. In general, tie-lines rotate with increasing metamorphic grade consistent with the observations of Spear.

A comparison of amphibole core compositions as opposed to rim and matrix needle compositions similarly indictes a prograde trend. In sample A3-43B (figure 17j), core analyses plot in the range of 0.07 - 0.09 atoms of Na(M4), while rim and matrix analyses plot in the range of 0.09 to 1.55 atoms of Na(M4). These amphiboles are optically continuous, with no exsolution lamellae. In addition, no separate grains of low Na(M4) have been analyzed. No large compositional gaps that might represent immiscibility have been observed when all the samples are taken together. These observations are similar to those of Laird and Albee (1981) in amphiboles found in mafic schists

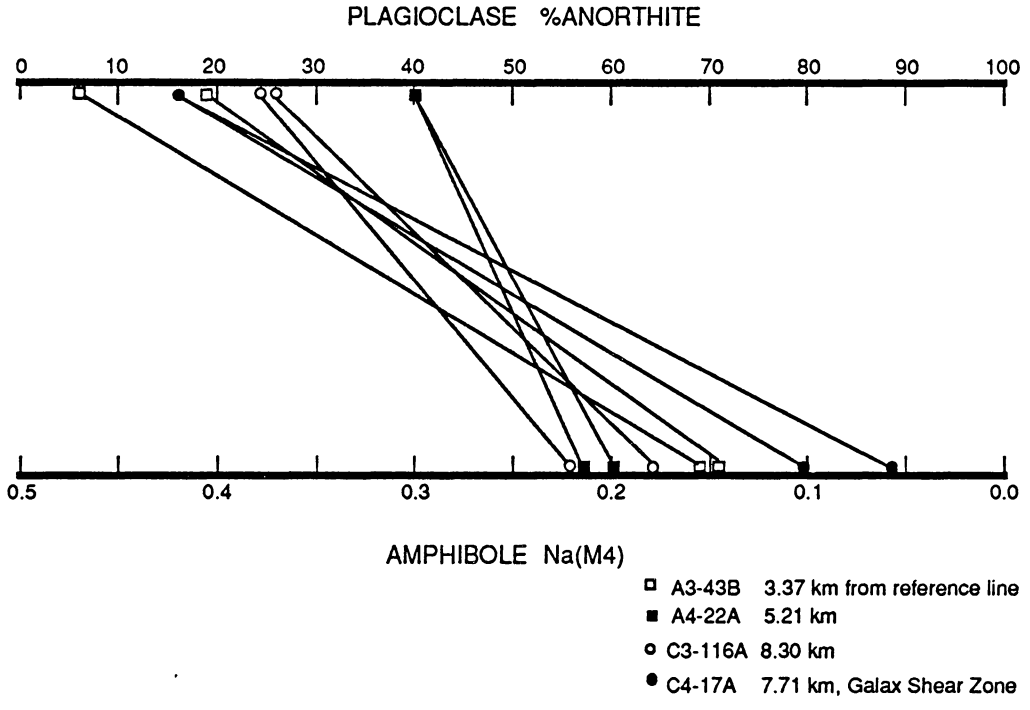


Figure 31. Amphibole-plagioclase tie lines (after Spear, 1980)

from Vermont. The preferred interpretation is that the amphibole zoning pattern represents prograde growth in a polymetamorphosed terrane.

An exception to the prograde trend is found in rocks from the Galax shear zone. Here, less Na-rich amphibole coexists with more Na-rich plagioclase, indicating possible retrogression, consistent with muscovite compositions in neighboring pelitic rocks.

The fact that the tie line position can be related to temperature implies that Na-Ca distribution can be used for quantitative determinations of temperature. A way of accomplishing this has been developed by Spear (1980) who plotted $\ln(X_{An}/X_{Ab})_{plag}$ vs. $\ln(Ca(M4)/Na(M4))_{amph}$ and noted where the plotted points fall with respect to isothermal contour lines. Figure 32 shows the data for coexisting amphiboles and plagioclases for the study area. The points are consistent with the temperatures derived from the garnet-biotite data from the metasediments. Rocks from the lower garnet zone (north of the Gossan Lead) plot on the low temperature side of the 490 °C contour line. Samples further to the southeast indicate higher temperatures, and mostly plot between the 490 and 530 °C contours, with generally higher temperatures in the staurolite zone.

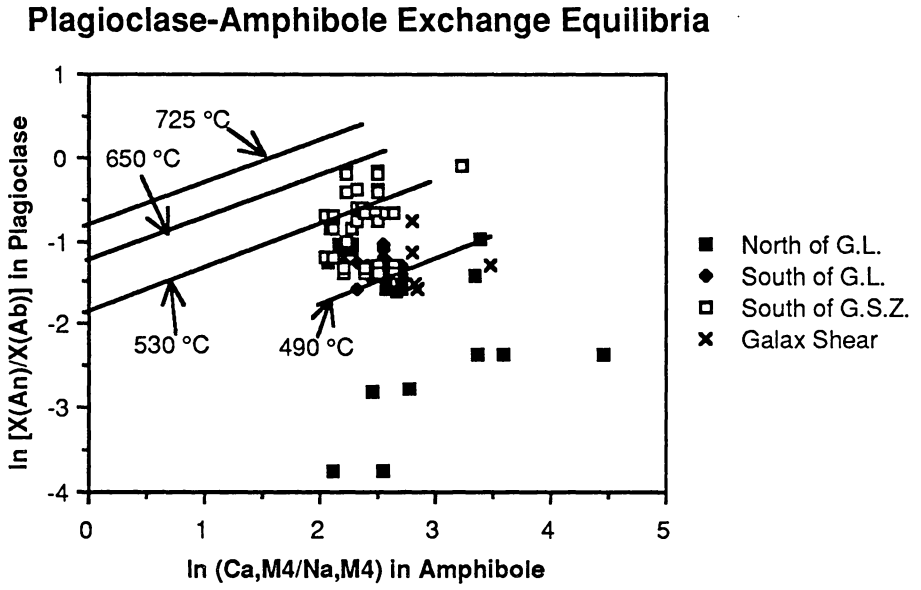


Figure 32. ln(X(An)/X(Ab)) in plagioclase vs. ln(Ca(M4)/Na(M4)) in amphibole: After Spear (1978)

Geobarometry

Pressures for the study area may be estimated by two geobarometers: 1) garnet - plagioclase - aluminosilicate - quartz equilibria (Ghent and others, 1979, and Newton and Haselton, 1981), and 2) garnet - biotite - muscovite - plagioclase equilibria (Ghent and Stout, 1981, and Hodges and Crowley, 1985). Due to the restricted occurrence of kyanite, the first method could only be applied to location D2-1, a locality previously mentioned as having experienced some local retrogression. As this method requires that temperature be independently determined, and that most biotite - garnet geothermometers require that pressure be independently determined, it is necessary to simultaneously solve both equations for P and T. Using the biotite-garnet equilibria of Ferry and Spear (1978) with the garnet - plagioclase - kyanite - quartz geobarometer of Ghent and others (1979) yields a pressure of 4.1 ± 1.0 kb at a temperature of 509 ± 60 °C., and 4.2 ± 1.0 kb and 498 ± 60 °C for Ferry and Spear (1978) and Newton and Haselton (1981).

The second method has more widespread applicability due to the more common occurrence of biotite - garnet - muscovite - plagioclase. However, it was found that caution was necessary when applying this method. In particular, outside of the staurolite zone, garnets contained high amounts of X_{Mn+Ca}. Results using temperatures derived either from the Ferry and Spear (1978) and the pressures of Ghent and Stout (1981) yielded pressures of 5.6 kb ± 1.0 kb. at 575±60 °C for sample C4-32A of the staurolite zone. Table 4 shows the results of the simultaneous solution the

Hodges and Spear (1982) geothermometer with the pressure calibration of Hodges and Crowley (1985). Pressures from samples C4-49B and C4-32B from the staurolite zone yield results that are consistent though slightly higher than the other methods. However, when these methods were applied to B2-1AB, at the garnet isograd, much higher pressures (9.8-11.6 kb) are recorded. Hodges and Crowley cautioned against the use of garnet with high Mn component, as their calibration is dependent on the particular solution model chosen. In addition, these high pressures are inconsistent with the pressure estimate of 5.5 kb for the Gossan Lead by Henry and others (1979) using the sphalerite - pyrhhotite - pyrite geobarometer. However, as has been noted by a number of workers (for example, Spear and Selverstone, 1983), plagioclase-garnet equilibria is strongly pressure dependent, with higher values of grossular associated with higher pressure, especially with a gentle or negative prograde P-T slope. Thus the garnets in the lower temperature rocks near the garnet isograd may have equilibrated at higher pressure than those in the staurolite zone. In addition, the observation that garnets, in general, have more calcic cores and less calcic rims indicates that pressures decreased while temperatures increased during prograde garnet growth. A P-T plot of the conditions in the study area is presented in figure 33.

Table 4. Pressure estimates

PRESSURE ESTIMATES

Sample	Dist.(km)	Bi. No.	Gt. No.	X_{Gr}	X_{Sp}	lnK	*T °C	†P(kb)
B2-1AB	2.97	21	17	.302	.144	-4.29	483±55	11.6 ±2.0
B2-1AB	2.97	27	26-core	.310	.206	-3.82	438±60	10.0 ±2.0
B2-1AB	2.97	27	28-rim	.321	.196	-3.93	430±57	9.8 ±1.5
A4-8A	4.77	20	52/53-c	.325	.155	0.23	511±60	8.3 ±1.6
A4-8A	4.77	20	54-rim	.295	.106	0.05	533±60	9.0±1.1
C4-49B	8.30	6/7	5/9-c	.106	.041	3.89	546±55	5.7±1.2
C4-49B	8.30	6/7	10-rim	.102	.047	4.01	541±55	5.5±1.1
C4-32B	8.63	7	8-core	.075	.050	3.37	596±55	7.1±1.3
C4-32B	8.63	14	9-rim	.079	.051	3.26	608±55	7.4±1.4

*Hodges and Spear (1982) temperatures
†Hodges and Crowley (1985) pressures

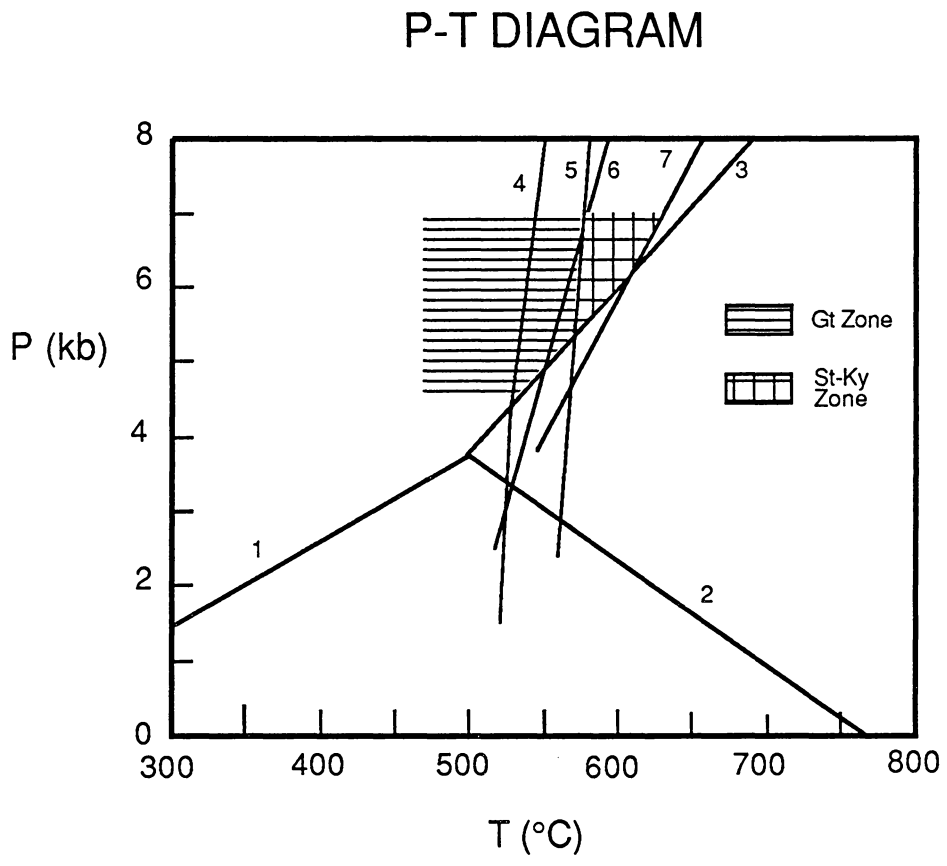


Figure 33. P-T diagram: Abbreviations - (1) kyanite-andalusite (Holdaway, 1971); (2) andalusite-sillimanite (Holdaway, 1971); (3) kyanite-sillimanite (Holdaway, 1971); (4) kyanite + chloritoid = staurolite + uqartz + vapor (Koons and Thompson, 1985); (5) garnet + chlorite = staurolite + biotite (Hess, 1969); (6) chlorite + muscovite = staurolite + biotite + quartz + vapor (Hoschek, 1969); paragonite + quartz = albite + kyanite + vapor (Chatterjee, 1972).

Regional Implications

From the preceding data, it is evident that the Ashe Formation presents problems typical of many metamorphic terranes: extensive solid solution of Ca and Mn in garnet, lack of determinative mineralogic assemblages, retrogression, and a complicated deformational history. Clearly, dealing with rocks of this complexity requires a previous knowledge of the structrual geology, and careful and detailed microprobe analysis is needed as the compositional changes that document the metamorphic history are quite subtle. In addition, multiple lines of investigation are necessary. This study looked carefully at garnet - biotite, muscovite, and amphibole - plagioclase equilibria. Each method is affected to various degrees by local retrogression and bulk compositional variation causing a scattering of the data, with the information derived being mostly qualitative in nature. However, when looking at the broad patterns across the study area, the methods converge at a common interpretation, and even the retrogressive trends can provide information on the post - peak - metamorphic history.

The weakly metamorphosed rocks of the Unicoi Formation, were studied in detail at only two locations and only muscovite data is available. The samples show a wide scattering of celadonite compositions, possibly indicating local effects of shearing due to the close proximity to the Fries Fault zone, although paragonite contents are consistent with a generally low crystallization temperature.

In the highly sheared rocks of the Bowers Ferry Thrust Sheet and the Cranberry Gneiss, muscovite compositons indicate, with their high celadonite and low paragonite contents, that they generally crystallized at a lower temperature than the overlying Ashe Formation. Textural observations of the mylonite indicate that the muscovites were crystallized during the mylonitization process, and that observations of rocks in the adjacent Ashe Formation that contain some mylonite texture, as well as the regional offset of the metamorphic isograds, indicate that mylonitization occurred after the main period of metamorphism. In the Ashe Formation, mylonitization is confined either to quartz-rich lithologies (locally developed along the Ashe-Cranberry contact), or in "slip cleavages" in pelitic rocks where the recrystallization appears confined to quartz-feldspar-rich bands. Muscovite compositions of Ashe rocks within the Fries Fault shear zone indicate the lowest temperatures observed in the Ashe Formation. The overall increase in temperature, destruction of primary structures, and recrystallization of the thrust sheets from northwest to southeast indicates a stacking of the thrust sheets so that "warmer" sheets are thrust over "cooler" sheets. These observations are consistent with isotopic data of Dietrich and others (1969) which places the time of mylonitization of the Fries Fault at 345 m.y., well after the generally accepted time of peak metamorphism of about 450 - 430 m.y. (Glover and others, 1983). The fact that muscovites with the lowest $K/(K + Na)$ are found only in the most highly mylonitized rocks indicates that substantial retrogression is confined only locally to the mylonite. However, the substantial overlap of the paragonite and celadonite compositions of muscovite between the mylonite and the adjacent Ashe indicates that metamorphic temperatures were probably very similar on both sides of the Ashe - Cranberry contact both before and during Fries faulting.

Increasing paragonite and decreasing celadonite contents of muscovite, garnet-biotite temperatures, and amphibole-plagioclase equilibria all indicate that metamorphic grade generally increases from the Fries area toward Galax. In addition, mineral zonation of garnet and amphibole indicates that mineral growth generally proceded in the prograde sense. An exception to the above occurs in the sheared rocks found north of Galax. There, muscovite compositions and amphibole-plagioclase equilibria indicate that recrystallization occurred after the metamorphic peak. Another exception

to the above is found in the kyanite-bearing rocks of location D2-1, which contain abundant late-growing chlorite, interpreted as a retrograde product. Garnet zoning and biotite-garnet temperatures indicate a lowering of temperatures during mineral growth at this locality. It should be noted that the general agreement of the different indicators of a rise in temperature toward the southeast supports the approximately 100 °C rise in temperature from the garnet isograd to the staurolite zone derived from garnet-biotite equilibria, despite the fact that such a rise is well within the estimated errors of ± 60 °C.

The detailed petrographic and petrochemical observations of this study, combined with the fact that the Ashe Formation dips nearly uniformly to the southeast, indicates that the metamorphic isograds increase structurally upward. Thus, the isograds are inverted. In addition, the isograds mapped during the present study, combined with the regional isograds mapped by Espenshade and others (1975), shows that the isograds generally follow the lithologic and structural grain of the Blue Ridge. The parallelism of the lithology, foliation, folding, thrust faulting, and metamorphism is perhaps the most dominant feature of the region.

Several hypotheses can now be advanced to explain this.

1. There was an intrusive heat source within the Ashe Formation overlying the study area. This possibility seems unlikely as there are no known igneous rocks in this part of the Blue Ridge that formed at the metamorphic peak 480-435 m.y. ago.

2. The metamorphic increase is caused by broad anticlinal folding, thus exposing warmer rocks along its axis. This possiblity is also considered unlikely as no folds have been observed at the scale required to make this possible. Although folds of the F_3 type have the correct orientation, they are not observed to be large enough to expose broad areas of oppositely dipping rocks or significant repetition of stratigraphy (Tso, 1987). In addition, the style of this folding appears to be rather gentle and not of the isoclinal nature that would give uniformly dipping rocks. It should be noted that relatively amphibolite-free rocks north of the Gossan Lead trend

are rather unique in the Ashe Formation sequence as observed on the regional maps of Stose and Stose (1957) and Espenshade and others (1975). On these maps, the Ashe Formation is shown to contain a significant amphibolite component nearly everywhere else higher in the stratigraphic sequence. As the overwhelming pattern observed in the Ashe Formation is that of monotonously SE-dipping rocks, it does not appear that major folding has repeated the stratigraphy.

3. Metamorphic isograds were inverted by post-metamorphic overturned folding. Again, no folds have been observed at the correct scale to make this possibility likely.

4. The dip of the isothermal/isobaric surfaces is to the northwest. This possibility requires that the isothermal surfaces are not parallel to the lithologic surfaces, thus creating the possibility that the lithologic surfaces were tilted prior to the main metamorphic and deformational events of the Paleozoic. Such a pre-metamorphic deformational event has not been identified in this part of the Appalachians. However, one test of this hypothesis would be to see if the various geobarometers indicate increasing pressure toward the southeast along with the increase in temperature, thus indicating a westward dipping isobaric/isothermal surface. Unfortunately, as previously discussed, the high amount of Ca + Mn in garnet, and the restricted occurrence of aluminosilicate, puts severe limitations on the application of a number of geobarometers. However, the general increase in Ca content of garnet toward the northwest and the general Ca-enrichment of garnet cores, shows that in a qualitative sense, pressure increases to the northwest in a prograde sense, thus giving a negative P-T slope. Thus, there is no evidence that supports this hypothesis.

5. The faulting associated with the Fries Fault caused major retrogression of a previously higher grade terrane. Although post-S_2 recrystallization due to mylonitization is an integral part of the structural fabric of the Fries Fault, the recrystallization is localized to the shear zone itself. Chemical zonation of garnet and amphibole, and the general lack of retrogressive textures such as pseudomorphs of garnet, indicate a general prograde sense over most of the study area.

Thus, for example, although the chlorite and biotite zones are largely within the area in which Fries Fault shearing structures such as slip cleavages can be identified, the petrographic observations indicate that the shear structures were superimposed on a prograde terrane.

A variation of this theme has been advanced by Abbott and Raymond (1984), who believe that the Ashe-Cranberry contact is a major post-metamorphic fault. They cite the fact that in North Carolina, the metamorphic grade of the rocks southeast of the contact is higher than the rocks northwest of the contact, thus raising the possiblity that retrogression along this contact could cause an apparent inversion of the isograds. In the study area, the metamorphic grade in the Ashe Formation immediately adjacent to the Cranberry-Ashe contact is in the chlorite zone. As previously discussed, the due to the relatively low grade of the Ashe in this area, primary sedimentary textures are unusually well preserved here, with retrogression textures limited to only certain quartzo-feldspathic rocks and slip cleavages. This leads to the conclusion that the Ashe probably never achieved conditions higher than metamorphic grade in this area.

Unfortunately, the Cranberry Gneiss shows more extensive recrystallization, thus obscuring the pre-mylonite mineralogy. However, some pre-mylonite textures may be observed in rocks away from the Fries Fault trace, and closer toward the Ashe-Cranberry contact. These rocks reveal no strong retrogressive textures such as porphyroblast psuedomorphs. In addition, muscovite conpositions are consistent with the generally low grade conditions in the neighboring Ashe. These observations are consistent with the general greenschist grade conditions observed elsewhere in the Cranberry (Rankin and others, 1972). Thus, if the Ashe-Cranberry contact is a fault, it would have thrusted chlorite grade rocks over other greenschist-grade rocks, and not caused an inversion of isograds. The possibility, however, that the contact represents a pre-metamorphic fault, and that the Ashe may indeed be upside-down as it rests on the fault remains open. However, no pre-metamorphic fault structures have been identified either, thus leaving no support for this possiblity. The simplest explanation is that the Ashe-

Cranberry contact is not a major fault, and that the two units were metamorphosed to greenschist grade together and later mylonitized together.

6. The inversion of the isograds was caused by Paleozoic overthrusting of warmer rocks over cooler rocks. As previously discussed, this possibility has been observed to some extent in the study area where the Cranberry Gneiss has been thrust over the Unicoi and Bowers Ferry Fault causing an increase in metamorphism and recrystallization upward toward the Fries Fault.

Inversion of metamorphic isograds by a thrusting or shearing mechanism has been observed at numerous localities throughout the world and is a topic of much recent discussion. Examples have been cited for both subduction-related terranes such as in Southern California (Graham and England, 1976), and for continental collisions such as in the Himalayas (Arita, 1983). In these examples, warmer rocks are moved over cooler rocks with the inversion of metamorphic isograds in the underlying rocks.

Two theoretical models are available. Oxburgh and Turcotte (1974), in a study of rocks in the eastern Alps, noted that immediately after thrusting, a "saw-tooth" shaped thermal profile is generated which then "relaxes" after thrusting to form a more normal thermal profile. Graham and England (1976), on the other hand, proposed a shear heating mechanism whereby temperature increases result from the conversion of mechanical energy to heat during thrusting. A detailed discussion of the merits of the shear heating model applied to various world-wide localities is given in Scholz (1980). The main drawback of the thermal relaxation model, unfortunately, is that the downward heat flux that produces the inverted metamorphic gradients operates only within the first million years after thrusting, due to the large heat flux from the upper plate toward the lower plate which "relaxes" the saw-toothed profile. This is not generally enough time to preserve the negative geothermal gradient by ordinary means such as by erosion of the overlying rocks. The shear heating model, on the other hand, produces a negative geothermal gradient that may last for 10 m.y. depending upon such factors as the thermal properties of the rocks and the rate of movement along

the fault. In addition, Graham and England claim that geologically reasonable erosion rates of 0.2 mm/year are rapid enough to preserve the inverted gradients.

Unfortunately, this mechanisim has not been well studied in the Appalachians. Most of the work on models involving shear heating have been applied to major thrust faults such as the Central Thrust Zone of the Himalayas. In the case of the study area, it is interesting to note that according to the regional isograds established by Espenshade and others (1975), the staurolite zone persists to approximately 8 km southeast of the study area where it decreases to garnet grade. This area is near the contact between the Ashe Formation and the overlying Alligator Back Formation. Along the contact in many places, small ultramafic ophiolite bodies have been mapped in a belt that trends along strike. Although Rankin and others (1973) describe the contact as nonconformable, they also hypothesize a tectonic emplacement of these bodies. Although some mapping and sampling of these ophiolite bodies have been carried out (for example, Scotford and Williams, 1983), detailed knowledge of the structural history of the rocks on each side of the contact is not known. As thrust faults and shear zones are known to parallel the regional strike and schistosity, this mechanism has the benefit of maintaining the parallelism of the lithology, structure, and metamorphism. In addition, the garnet compositions qualitatively indicate a negative P-T slope, which is consistent with the "clockwise" P-T loop observed in overthrust terranes (England and Richardson, 1977). It is clear, however, that further detailed petrologic and structural work needs to be done to evaluate this possibility.

Conclusions

1. Peak metamorphic temperatures within the study area, as measured by biotite-garnet equilibria range from about 470 °C near the garnet isograd to about 570 ± 60°C in Galax, with pressures of about 6 ± 1 kb.

2. The increase in metamorphic temperatures is also reflected in the the increase in paragonite and decrease in celadonite contents of muscovite toward the southeast. Muscovite compositions provided useful qualitative trends of temperature throughout the study area.

3. Amphibole compositions increase in Na(M4) relative to anorthite composition of plagioclase, which also indicates an increase in temperatures toward the southeast.

4. Local retrogression is found in a band of sheared gneisses and amphibolites just north of Galax, and in the formation of chlorite in kyanite-bearing rocks.

5. Mylonitization along the Fries Fault occurred later than the main period of metamorphism.

6. There is no difference in metamorphic grade between rocks on either side of the Cranberry-Ashe contact in the study area. The preferred interpretation is that the rocks of the Ashe

Formation in the study area were emplaced on the Cranberry Gneiss before regional metamorphism.

7. The metamorphic isograds increase structurally upward in the study area. Thus, the isograds are inverted.

8. The most consistent interpretation for the inversion of isograds is that of an overthrust mechanism.

Bibiliography

Abbott, R.N. and Raymond, L.A., 1984, The Ashe metamorphic suite, northwest North Carolina; metamorphism and observations on geologic history: American Journal of Science, v.284, p. 350-375.

Arita, K., 1983, Origin of the inverted metamorphism of the Lower Himalayas, Central Nepal: Tectonophysics, v. 95, 43-60.

Bartholomew, M.J. and Lewis, S.E., 1984, Evolution of Grenville massifs in the Blue Ridge geologic province, southern and central Appalachians: in Bartholomew, M.J., ed., The Grenville Event in the Appalachians and Related Topics: Geological Society of America, Special Paper 194, p. 229-254.

Bartholomew, M.J., Lewis, S.E., Wilson, J.R. and Gryta, J.J., 1983, Deformational history of the region between the Grandfather Mountain and Mountain City Windows, North Carolina and Tennessee: in Geologic Investigations in the Blue Ridge of Northwestern North Carolina: Carolina Geological Society Fieldtrip Guidebook, 1983, p. 1-29.

Bence, A.E. and Albee, A.L., 1968, Empirical correction factors for the electron microanalysis of silicates and oxides: Journal of Geology, v. 76, p. 382-403.

Brown, E.H., 1977, The crossite content of Ca-amphibole as a guide to pressure of metamorphism: Journal of Petrology, v. 18, p. 53-72.

Butler, J.R., 1973, Paleozoic deformation and metamorphism in part of the Blue Ridge thrust sheet, North Carolina: American Journal of Science, v. 273-A, p. 72-88.

Chatterjee, N.D., 1972, The upper stability limit of the assemblage paragonite + quartz and its natural occurrences: Contributions to Mineralogy and Petrology, v. 34, p.288-303.

Chatterjee, N.D. and Flux, S, 1986, Thermodynamic mixing properties of muscovite-paragonite crystalline solutions at high temperatures and pressures, and their geologic applications: Journal of Petrology, v. 27, p. 677-693.

Craig, J.R., Sears, C.E., Gilbert, M.C. and Hewitt, D.A., 1971, Sulfide mineralization, southwestern Virginia: B. Gossan Lead District: in Lowry, W.D., ed., Guidebook to Appalachian tectonics

and sulfide mineralization of southwestern Virginia: Virginia Polytechnic Institute and State University, Guidebook no. 5, p.25-38.

Davison, W.D., Jr., 1973, Petrology of the Ashe Formation, Shortt's Knob Area, Floyd County, Virginia [M.S. thesis]: Virginia Polytechnic Institute and State University, Blacksburg, Virginia, 109 p.

Dietrich, R.V., Fullagar, P.D. and Bottino, M.L., 1969, K/Ar and Rb/Sr dating of tectonic events in the Appalachians of southwestern Virginia: Geological Society of America Bulletin, v. 80, p. 307-314.

England, P.C. and Richardson, S.W., 1977, The influence of erosion upon the mineral facies of rocks from different metamorphic environments: Journal Geological Society of London, v. 134, p. 201-213.

Espenshade, G.H., Rankin, D.W., Shaw, K.W. and Neuman, R.B., 1975, Geologic map of the east half of the Winston-Salem Quadrangle, North Carolina-Virginia: U.S. Geological Survey, Miscellaneous Investigations Series, Map I-709B.

Eugster, H.P., Albee, A.L., Bence, A.E., Thompson, J.B., Jr. and Waldbaum, D.R., 1972, The two-phase region and excess mixing properties of paragonite - muscovite crystalline solutions: Jounal of Petrology, v. 13, p. 147-179.

Ferry, J.M. and Spear, F.S., 1978, Experimental calibration of the partitioning of Fe and Mg between biotite and garnet: Contributions to Mineralogy and Petrology, v. 66, p. 113-117.

Gair, J.E. and Slack, J.F., 1984, Deformation, geochemistry , and origin of massive sulfide deposits, Gossan Lead District, Virginia: Economic Geology, v. 79, p. 1483-1520.

Ghent, E.D., Robbins, D.B. and Stout, M.Z., 1979, Geothermometry, geobarometry, and fluid compositions of metamorphosed calc-silicates and pelites, Mica Creek, British Columbia: American Mineralogist, v. 64, p. 874-885.

Ghent, E.D. and Stout, M.Z., 1981, Geobarometry and geothermometry of plagioclase-biotite-garnet-muscovite assemblages: Contributions to Mineralogy and Petrology, v. 76, p. 92-97.

Gibson, R.G. and Speer, J.A., 1986, Contact aureoles as constraints on regional P-T trajectories: an example from the Northern Alabama Piedmont, USA: Journal of Metamorphic Geology, v. 4, p. 285-308.

Glover, L.G. III, Speer, J.A., Russell, G.S. and Farrar, S.S., 1983, Ages of regional metamorphism and ductile deformation in the central and southern Appalachians: Lithos, v. 16, p. 223-245.

Goldman, D.S. and Albee, A.L., 1977, Correlations of Mg/Fe partitioning between garnet and biotite with 18-O/16-O partitioning between quartz and magnetite: American Journal of Science, v. 277, p. 750-767.

Graham, C.M. and England, P.C., 1976, Thermal regimes and regional metamorphism in the vicinity of overthrust faults: an example of shear heating and inverted metamorphic zonation from southern California: Earth and Planetary Science Letters, v. 31, p. 142-152. of America, v. 13, p. 357-468.

Guidotti, C.V., 1984, Micas in metamorphic rocks: in Bailey, S.W., ed., *Micas*: Reviews in Mineralogy, Mineralogical Society of America, v. 13, p. 357-468.

Guidotti, C.V., 1968, On the relative scarcity of paragonite: American Mineralogist, v. 53, p. 963-974.

Guidotti, C.V. and Sassi, F.P., 1976, Muscovite as a petrogenetic indicator mineral in pelitic schists: Neues Jahrbuch fur Mineralogie Abhandlungen, v. 127, p. 97-142.

Hammarstrom, J.M. and Zen, E-an, 1985, An empirical equation for igneous calcic amphibole geobarometry: Geological Society of America Abstracts with Programs, v. 17, p. 602.

Hatcher, R.D. Jr., 1978, Tectonics of the western Piedmont and Blue Ridge, southern Appalachians: Review and speculation: American Journal of Science, v. 278, p. 276-304.

Henry, D.K., Craig, J.R. and Gilbert, M.C., 1979, Ore mineralogy of the Great Gossan Lead, Virginia: Economic Geology, v. 74, p. 645-656.

Hess, P., 1969, The metamorphic paragenesis of cordierite in pelitic rocks: Contributions to Mineralogy and Petrology, v. 24, p. 191-207.

Hodges, K.V. and Crowley, P.D., Error estimation and empirical geothermobarometry for pelitic systems: American Mineralogist, v. 70, p. 702-709.

Hodges, K.V. and Spear, F.S., 1982, Geothermometry, geobarometry and the Al_2SiO_5 triple point at Mt. Moosilauke, New Hampshire: American Mineralogist, v. 67, p. 1118-1134.

Hoffer, E., 1978, On the "late" formation of paragonite and its breakdown in pelitic rocks of the southern Damara Orogen (Namibia): Contributions to Mineralogy and Petrology, v. 67, 209-219.

Holdaway, M.J., 1971, Stability of andalusite and the aluminum silicate phase diagram: American Journal of Science, v. 271, p. 97-131.

Hoschek, G., 1969, The stability of staurolite and chloritoid and their significance in metamorphism of pelitic rocks: Contributions to Mineralogy and Petrology, v. 22, 208-232.

Hoschek, G., 1967, Untersuchungen zum stabilitatsbereich von chloritoid und staurolith: Contributions to Mineralogy and Petrology, v. 14, p. 123-162.

Indares, A. and Martignole, J., 1985, Biotite - garnet geothermometry in the granulite facies: the influence of Ti and Al in biotite: American Mineralogist, v. 70, p. 272-278.

Jones, T.Z., 1976, Petrography, structure, and metamorphic history of the Warrensville and Jefferson Quadrangles, southern Blue Ridge, northwestern North Carolina [Ph.d. dissert.]: Miami University, Oxford, Ohio, 130 p.

Koons, P.O. and Thompson, A.B., 1985, Non-mafic rocks in the greenschist, blueschist and eclogite facies: Chemical geology, v. 50, p. 3-30.

Laird, J. and Albee, A.L., 1981, Pressure, temperature, and time indicators in mafic schist: their application to reconstructing the polymetamorphic history of Vermont: American Journal of Science, v. 281, p. 127-175.

Mohr, D.W. and Newton, R.C., 1983, Kyanite - staurolite metamorphism in sulfidic schists of the Anakeesta Formation, Great Smokey Mountains, North Carolina: American Journal of Science, v. 283, p. 97-134.

Newton, R.C. and Haselton, H.T., 1981, Thermodynamics of the garnet-plagioclase-Al_2SiO_5-Quartz geobarometer: in Newton, R.C. and others, eds., *Thermodynamics of Minerals and Melts* New York, Springer-Verlag, p. 131-147.

Norrish, K. and Chappell, B.W., 1967, X-ray fluoresence spectrography: in Zussman, J., ed, *Physical Methods in Determinative Mineralogy*: New York, Academic Press, p. 161-214.

Odom A.L. and Fullagar, P.D., 1982, The time of opening of the Iapetus Ocean: Age of the Crossnore plutonic-volcanic group, southern Appalachians: Geological Society of America Abstracts with Programs, v. 14, p. 69.

Oxburgh, E.R. and Turcotte, D.L., 1974, Thermal gradients and regional metamorphism in overthrust terrains with special reference to the Eastern Alps: Schweizersche Mineralogische und Petrographische Mitteilungren, v. 54, p. 641-662.

Pigage, L.C. and Greenwood, H.J., 1982, Internally consistent estimates of pressure and temperature: the staurolite problem: American Journal of Science, v. 282, p. 943-969.

Rankin, D.W., 1976, Appalachian salients and recesses: Late Precambrian continental breakup and the opening of the Iapetus Ocean: Journal of Geophysical Research, v. 81, p. 5605-5619.

Rankin, D.W., 1975, The continental margin of eastern North America in the southern Appalachians: The opening and closing of the proto-Atlantic ocean: American Journal of Science, v. 275-A, p. 298- 336.

Rankin, D.W., 1971, Geology of the Blue Ridge in southwestern Virginia and adjacent North Carolina: in Lowry, W.D., ed., Guidebook to Appalachian tectonics and sulfide mineralization of southwestern Virginia: Virginia Polytechnic Institute and State University, Department of Geological Sciences, Guidebook n. 5, p. 29-86.

Rankin, D.W., Espenshade, G.H. and Neuman, R.B., 1972, Geologic map of the west half of the Winston-Salem Quadrangle, North Carolina-Virginia-Tennessee: U.S. Geological Survey, Miscellaneous Investigations Series, Map I-709A.

Rankin, D.W., Espenshade, G.H., and Shaw, K.W., 1973, Stratigraphy and structure of the metamorphic belt in northwestern North Carolina and southwestern Virginia: a study from the Blue Ridge across the Brevard Fault Zones to the Sauratown Mountains Anticlinorium: American Journal of Science, v. 273-A, p. 1-40.

Raymond, L.A., 1987, Terrane amalgamation in the Blue Ridge Belt, southern Appalachian orogen: Geological Society of America Abstracts with Programs, v. 19, p. 125.

Richardson, S.W., Bell, P.M., and Gilbert, M.C., 1968, Kyanite - Sillimanite Equilibrium Between 700° and 15007deg.C: American Journal of Science, v. 266, p. 513-541.

Scholz, C.H., 1980, Shear heating and the state of stress on faults: Journal of Geophysical Research, v. 85, p. 6174-6184.

Scotford, D.M. and Williams, J.R., 1983, Petrology and geochemistry of metamorphosed ultramafic bodies in a portion of the Blue Ridge of North Carolina and Virginia: American Mineralogist, v. 68, p. 78-94.

Shaw, D.M., 1956, Geochemistry of pelitic rocks. Part III: major elements and general geochemistry: Geological Society of America Bulletin, v. 67, p. 919-934.

Solberg, T.N. and Speer, J.A., 1982, QALL, a 16-element analytical scheme for efficient petrologic work on an automated ARL-SEMQ: Application to mica reference samples: in Heinrich, K.F.J., ed. ,*Microbeam Analysis*: San Francisco, San Franicsico Press, Inc., p. 422-426.

Spear, F.S., 1980, NaSi←→CaAl exchange equilibrium between plagioclase and amphibole: Contributions to Mineralogy and Petrolgy, v. 72, p. 33-41.

Spear, F.S. and Selverstone, J., 1983, Quantitative P-T paths from zoned minerals: Theory and tectonic applications: Contributions to Mineralogy and Petrology, v. 83, p. 348-357.

Staten, W.T., 1976, A chemical study of the silicate minerals of the Great Gossan Lead and surrounding rocks in southwestern Virginia [M.S. thesis]: Virginia Polytechnic Institute and State University, Blacksburg, Virginia, 110 p.

St-Onge, M.R., 1984, Geothermometry and geobarometry in pelitic rocks of north-central Wopmay Orogen (early Proterozoic), Northwest Territories, Canada: Geological Society of America Bulletin, v. 95, p. 196-208.

Stose, A.J. and Stose, G.W., 1957, Geology and mineral resources of the Gossan Lead District and adjacent areas in Virginia: Virginia Division of Mineral Resources Bulletin 72, 233 p.

Thompson, A.B., 1976a, Mineral reactions in pelitic rocks: I. Prediction of P-T-X(Fe,Mg) phase relations: American Journal of Science, v. 276, p. 401-424.

Thompson, A.B., 1976b, Mineral reactions in pelitic rocks: II. Calculation of some P-T-X (Fe-Mg) phase relations: American Journal of Science, v. 276, p. 425-454.

Thompson, J.B., Jr. and Norton, S.A., 1968, Paleozoic regional metamorphism in New England and adjacent areas: in Zen, E-an, ed, *Studies in Appalachian Geology: Northern and Maritime*: New York, Wiley-Interscience, p. 319-327.

Tso, J.L., 1987, Geology of the Ashe Formation between Fries and Galax, Virginia [Ph.d. dissert.]: Virginia Polytechnic Institute and State University, Blacksburg, Va., 343 p.

Velde, B., 1965, Phengite micas: Synthesis, stability and natural occurrence, American Journal of Science, v. 263, p. 886-913.

Wehr, F. and Glover, L. III, 1985, Stratigraphy and tectonics of the Virginia-North Carolina Blue Ridge: Evolution of a late Proterozoic-early Paleozoic hinge zone: Geological Society of America Bulletin, v. 96, p. 285-295.

Winkler, H.G.F., 1979, *Petrogenesis of Metamorphic Rocks*: New York, Springer-Verlag, 348 p.

Part III: Developmental History of the Gossan Lead Massive Sulfide

Introduction

Massive sulfide deposits of the southern Appalachian Blue Ridge have long been problematic in terms both of paragenesis and subsequent deformational history. The questions are exemplified by the Great Gossan Lead, located in southwest Virginia within the late Precambrian Ashe Formation. Theories as to its origin have followed two principle lines of thought: 1) that the ore material was introduced into its host rocks along a pre-existing fault plane (Ross, 1935 and Kinkel, 1967), and 2) that ore formation was syn-sedimentary and volcanogenically related and was later deformed, along with its wallrocks, during regional metamorphism.

Ascertaining the origin of the Gossan Lead, however, is complicated by its rather intense deformational history. The term "durchbewegung" has been used by Craig (1980) to describe its structure, as up to room sized inclusions of silicate are commonly scattered within a largely pyrrhotitic massive sulfide matrix that behaved rather plastically during deformation. A structural map (Plate III) of the largest of the open pits, the Bumbarger Pit near Galax, Virginia, shows numerous fold sets of various scales that trend primarily NE, although one set trends SE.

The purpose of this study has been to determine the relationship between the massive ore, its silicate inclusions, and the surrounding gneisses and schists of the Ashe Formation, with the primary goal being the development of a model of the ore's emplacement. This, however, requires

"seeing through" the metamorphism and deformation, a process in which the case study of the Gossan Lead provides general information on silicate behavior during regional metamorphism in a polydeformed terrane. At the Gossan Lead, it was found that metamorphism and deformation proceded in stages in which the different lithologies adopted unique styles depending upon such factors as mineralogy, thickness, and mechanical properties. It was then possible, once these structures were recognized, to reconstruct the original lithologic package contained within the ore.

Unfortunately, at present, the underground mine workings are inaccessible, and the open pit, not mined since 1935, has very little of the ore left in place. Fortunately, exposure of the contact between the ore and wallrock is excellent, especially at the hanging wall, and the ore itself can be studied to a limited extent on the walls of the pit and in the supporting pillars near the underground entrances.

Geologic Setting

The Gossan Lead is one of a number of massive sulfides found in the late Precambrian metasediments and amphiboles in the Blue Ridge which includes Ore Knob, North Carolina, and Ducktown, Tennessee (figure 34). All of these deposits are composed of a series of lense-like or pod-like bodies that have been complexly deformed and metamorphosed. All are primarily pyrrhotitic, with varying but minor amounts of pyrite, chalcopyrite, sphalerite, and galena.

The numerous sulfide deposits collectively known as the Gossan Lead extends approximately 28 km along strike from Galax, Virginia, its southwesternmost extremity, to near Sylvatus, Virginia to the northeast. It is entirely contained within the Ashe Formation (Espenshade and others, 1975), a package of metasediments and metavolcanics made of three principle constituents: 1) quartzo-feldspathic "gneisses" or "granofels" that are largely metamorphosed graywackes, sandstones and arkoses (Gair and Slack, 1984, Tso, 1987); 2) muscovite-biotite schists or muscovite phyllites that represent pelitic units and; 3) amphibolites that have been determined to be similar in composition to low Ti-tholeiitic basalts (Gair and Slack, 1984, Slack and others, 1985). Most of the Ashe is characterized by a dominant penetrative foliation that strikes approximately N50°E, and dips at variable angles to the southeast. Although the Ashe Formation in southwest Virginia has a map width of approximately 20 km, its true stratigraphic thickness is obscured by its polydeformed nature and the presence of thrust faulting within the Ashe (Espenshade and others, 1975).

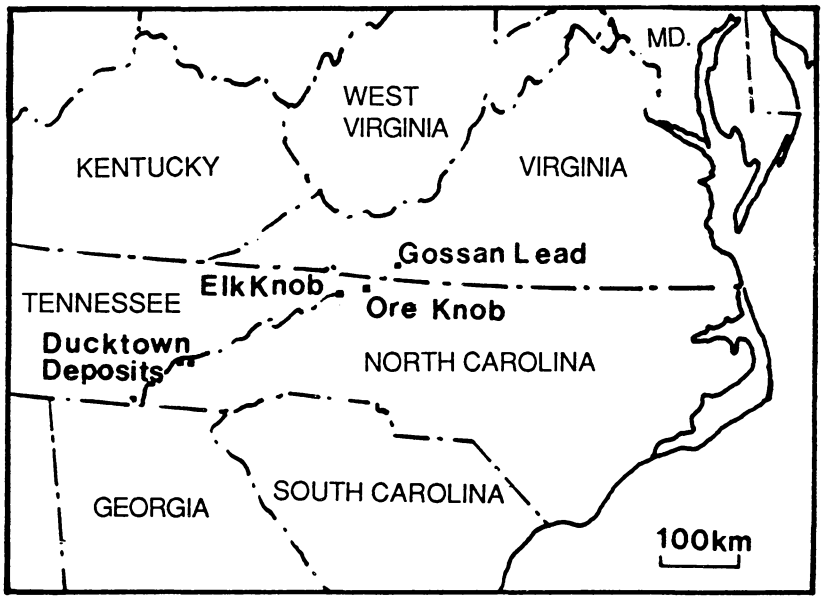


Figure 34. Map showing location of sulfide bodies in the Blue Ridge

Numerous models have been proposed for the depositional setting of the Ashe Formation and the correlative Lynchburg Group of central Virginia, ranging from deposition on continental or transitional crust (Rankin, 1975, Wehr and Glover, 1985) to deposition on oceanic crust (Hatcher, 1978, Abbott and Raymond, 1984). All of the recent models agree, however, that the Ashe Formation was deposited in a deep water rift setting associated with the opening of the Iapetus Ocean, some 570-690 m.y. ago (Odom and Fullagar, 1982). In the study area, the Ashe Formation rests upon the Cranberry Gneiss, a felsic-plutonic suite that represents approximately 1.1 b.y. continental basement (Bartholomew and Lewis, 1984), although the contact between the two formations has been interpreted either as a fault (Stose and Stose, 1957) or a nonconformity (Espenshade and others, 1975). Careful study of the contact near Fries, Virginia during an earlier phase of this study (Tso, 1987) has not revealed strong evidence that the contact is a major fault, although it is well tectonized as part of the Fries Fault ductile deformation zone that lies within one-half kilometer to the northwest. The Ashe Formation is overlain in southwest Virginia by the Alligator Back Formation of possible early Paleozoic age (Rankin and others, 1973). Rankin and others (1973) believe the contact to be that of a conformable sedimentary sequence, although the presence of a series of small, ophiolite-type ultramafic bodies (Espenshade and others, 1975) may indicate some thrusting along the contact.

Paleozoic metamorphism and thrust faulting is quite pervasive in the Blue Ridge, with the generally accepted age for the metamorphism being at approximately 480 - 435 m.y. (Glover and others, 1983), and the age of the thrusting of the Fries Fault, the major thrust near the Gossan Lead placed, on the basis of Rb-Sr data, at 330 to 345 m.y. (Dietrich and others, 1969). In addition, recent seismic studies of the Blue Ridge in Tennesee (Cook and others, 1979) have indicated that the southern Blue Ridge may be underlain by a master decollement zone along which thrusting may have moved at least 280 km to the northwest. If this is true, this would make the Gossan Lead not only entirely allochthonous, but raised to a considerably higher structural level.

Local Geology

Near Fries, Virginia, the Ashe Formation rests upon the highly mylonitized Cranberry Gneiss, a mostly planar plagioclase-quartz-muscovite-K-feldspar augen gneiss (plate I, from Tso, 1987). The mylonitization appears largely confined to the Cranberry Gneiss, with mylonite textures evident only in the quartzo-feldspathic units of the immediately overlying adjacent Ashe, and in local slip cleavages within the pelitic units, with no Fries Fault mylonite-related structures evident in the Gossan Lead orebody. The orientation of the mylonite follows that of the regional foliation within the Ashe.

The Ashe Formation is composed of predominantly parallel units that strike appoximately N50°E and dips at at variable angles to the southeast. For the purposes of this report, the Ashe will be divided into a "footwall", lower, or northwest part, and a "hanging wall", upper, or southeast part. The footwall rocks are composed of approximately 60% biotite - muscovite - plagioclase - quartz gneiss and 40% muscovite phyllite and muscovite - biotite ± chlorite ± garnet schist. The gneiss tends to be medium grained, weakly foliated, and occasionally shows some evidence of 3-4 mm clasts especially near its base near the Cranberry Gneiss contact. Commonly, it is a rather monotonous quartz-plagioclase dominated rock, with widely deseminated micas making up less than 10% of the volume. On the other hand, the schist varies a bit more in appearance and mineralogy. Near the base of the Ashe, it commonly appears as a fine-grained grained muscovite phyllite with

minor graphite. Higher up in the Ashe sequence, but below the ore, the phyllite becomes less common, and gives way to a coarse muscovite-biotite schist with some horizons containing 3-4 mm-sized manganiferous garnets. The gneisses and schists are found in beds ranging from centimenters to meters in thickness, with the contacts parallel to the regional schistosity.

The general pattern of the schists and gneisses continues in the Ashe Formation above the Gossan Lead horizon as well. However, there amphibolite becomes a prominent lithology, taking up 30% of the lithologic package, whereas below the ore horizon, the amphibolites are present only in volumetrically insignificant lense-like pods of limited areal extent. Above the Gossan Lead, the amphibolites are in conformable stratigraphic zones which may include some metasedimentary material, and which can commonly be traced for distances of 2 km or better along strike. Usually, the amphibolites are on the order of one meter to several tens of meters thick, and show sharp contacts with the surrounding schists and gneisses in such a way that they too are parallel to the regional schistosity and parallel with the gneiss-schist contacts. Despite a wide range of textural development (Tso, 1987), the amphibolites contain a fairly uniform mineralogy of hornblende + plagioclase ± chlorite ± clinozoisite ± ilmenite ± sphene.

Studies of the metamorphism of the Gossan Lead and surrounding area (Espenshade and others, 1975, Tso, 1987) has placed the metamorphism in a Barrovian sequence ranging from chlorite-biotite grade near the Fries Fault to staurolite-kyanite grade near Galax. Garnet-biotite temperatures (Tso, 1987) of the surrounding wall rocks are estimated to be approximately 500 °C ± 60°C with pressures at 6 ± 1 kb. Regionally, the metamorphic isograds roughly follow the dominant foliation (Espenshade and others, 1975), with the metamorphic grade increasing stratigraphically upward. In Galax, well developed euhedra of staurolite indicates a post-kinematic timing for the metamorphic peak with respect to the regional penetrative schistosity.

Previous Works

The Gossan Lead has been studied by numerous other writers. Some of the early works included the Gossan Lead as part of a larger study of Appalachian massive sulfides. Ross (1935), for example, concentrated on the Ducktown, Tennessee deposit, and Kinkel (1965) concentrated on the body at Ore Knob, North Carolina. Both discussed similarities between these deposits and others including the Gossan Lead. Stose and Stose (1957) were one of the first to take a detailed look at the regional geology around the Gossan Lead, and mapped the surrounding area on a 1:62,500 scale. Among the more recent studies, Staten (1976) used petrographic and microprobe techniques on drill core from the Betty Baker area, approximately 20 km to the northwest near Sylvatus, Virginia. He found that the Fe/(Fe + Mg) content of chlorite, biotite, and garnet decreases dramatically within the massive sulfide rocks as compared to the immediate country rock. He attributed this decrease to sulfidation reactions that took place during Paleozoic metamorphism, thus favoring a premetamorphic interpretation for the origin of the ore. Henry and others (1979) described the ore mineralogy in detail from the Betty Baker drill core and from grab samples from the Gossan Howard mine and the Bumbarger Pit, both near Galax. They found that the sulfide is composed of at least 90% massive hexagonal pyrrhotite with lesser amounts of sphalerite, galena, pyrite, and arsenopyrite. In addition, they were among the first to hypothesize a synsedimentary exhalitive volcanic setting for the origin of the ores. Craig (1980) studied ore-silicate interaction

textures from various Appalachian sulfides including the Gossan Lead, and described the structure of the Bumbarger Pit (or Iron Ridge) mine as the result of deformation during metamorphism. LeHuray (1982, 1984) studied lead and sulfur isotopes in the sulfide of numerous Appalachian deposits including the Gossan Lead and hypothesized that much of the sulfide material was derived from the metasedimentary wall rocks. Gair and Slack (1984) did a rather comprehensive structural and major and minor element geochemical study of the Bumbarger and Huey pits near Galax and of the surrounding rocks of the Ashe Formation. On the basis of bulk chemistry, they believed the Ashe Formation metasediments and amphibolites resulted from deposition in a rift setting, and that the Gossan Lead ore and its associated silicate inclusions and wall rocks originated during exhalitive processes. The present study overlaps somewhat with the Gair and Slack study in the study of the structure of the Bumbarger Pit. However, the present study places considerably more emphasis on the structural geology and Paleozoic deformation of the ore to derive a "moving picture" model of the development of the ore structure.

Description of the Gossan Lead at the Bumbarger Pit (Iron Ridge)

General Statement

The gross form of the ore, as seen both from the present study and from Gair and Slack (1984), shows that the body is lenticular and concordant with the surrounding lithology and foliation of the Ashe Formation. The hanging wall is composed of interbedded muscovite schist, phyllite and medium-grained biotite-muscovite gneiss that weathers to a powdery brown saprolite. The hanging wall contact is well exposed along the eastern and southern walls of the pit, especially underneath the overhangs behind the massive sulfide pillars, and is marked by the presence of a 1-2 cm powdery gray chloritic layer that weathers readily and falls to the floor below the overhangs as piles of fine gray dust. The orientation of the contact is parallel to the foliation of the wall rocks, striking approximately N45°E with a gently undulating dip to the southeast.

The rocks of the footwall of the mine pit consists of resistant biotite-quartz gneiss interlayered with < 1 m thick massive sulfide. The footwall, is not as well exposed as the hanging wall and must be

reconstructed from the structural data from the overlying ore. It is interpreted to be more complex than the hanging wall in that it shows a stronger degree of folding. Some of the later fold generations (the F_3 and F_4) are more obvious, and locally, the rocks dip vertically or are overturned. Precise data on the thickness and stratigraphy of the strata within the pit are lacking due to the fact that much of the massive ore has been mined out. However, from the remaining ore found on the mine pillars and walls, and the fact that the mine levels tend to follow the more sulfide-rich, inclusion-poor horizons, it was possible to establish an overall lithologic sequence.

It is difficult to determine the original dimensions of the body from just the exposures in the pit. Because the ore dips to the southeast, the southern and eastern walls lead to the extensive underground mine workings which are presently inaccessible. Kline and Ballard (1949), described the mining and drilling operations of the Gossan Lead and noted that one of the drill cores indicated a length of at least 1500 ft (457 m) down dip from the surface. At the Bumbarger Pit, the thickness of the massive ore is estimated to be approximately 30 ft (9 m), although thicknesses apparently pinch and swell (Kline and Ballard, 1949). We agree with the interpretation of Gair and Slack (1984) that there is a high angle fault cutting off part of the ore along the NW wall of the pit as evidenced by a narrow fault gouge. This then makes it necessary to extend the hanging wall above the topography in order to project the upper contact. The western end shows some thinning of the ore, and combined with the steep dip of the rocks, causes the width of the mine pit to narrow. The ore along line B-B′ is estimated to be 37 m thick.

Stratigraphy

A stratigraphic column (figure 35) has been constructed for the rocks that lie along the profile line B-B′ (figure 36) that identifies seven broad stratigraphic horizons labeled ″A″ through ″G″. Each

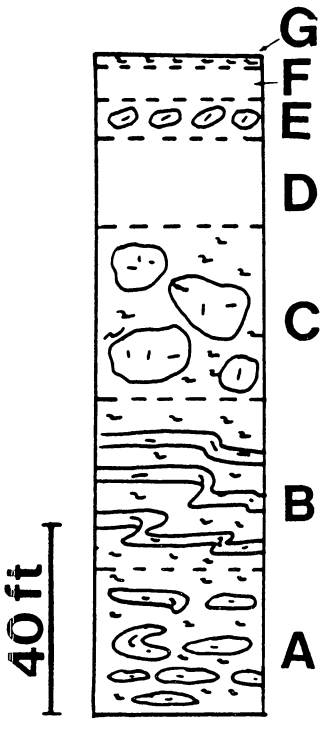
of the zones is distinctive in its combination of ore and silicate mineralogy and structure. Three main lithologic types have been recognized.

Foliated Ore (Zones A, B, C, G)

The foliated ore (figure 37a) is distinctive in containing greater than 40% silicate inclusions which range in size from less than 1 cm to 5 cm. The inclusions are charcterized by having abundant sheet silicates of biotite, chlorite and talc, including some quartz lenses and late-growing radiating bundles of actinolite. The inclusions define a foliation that is parallel to the dominant regional schistosity (the S_1/S_2) and appear as "shreds" of boudinaged isoclinal folds. This type of ore is the dominant type in zone G, just below the hanging wall. It is also a minor lithology in zones A, B, and C between inclusions of gneiss.

Massive Ore (Zones D and E)

This type of ore contains less than 40% silicate inclusions and tends to have a somewhat non-foliated look. However, close inspection invariably reveals abundant inclusions of biotite, chlorite, garnet and quartz in clots and stringers, occasionally up to 3 cm in size, but generally less than 1 cm across. In general, pyrrhotite is found in equant grains up to 3 mm in diameter, with grains frequently exhibiting 120° dihedral angles. Kink banding is occasionally observed in the pyrrhotite, demonstating some late, post-annealing deformation. In addition, chalcopyrite, being more ductile than the pyrrhotite, tends to be found in cracks and spaces between the silicate inclusions, in pressure shadows or as injected sulfides. This type of ore is the most heavily mined and is followed by the underground workings as observed by the arches and tunnels in figure 37b. Only the massive ore contained within the mine pillars remains of this lithology.



G — Foliated ore; cm-scale isoclinal folds

F — Massive ore

E — Gneissic ore; 1-2 meter rounded, rotated gneiss inclusions

D — Massive ore

C — Gneissic ore; >5 meter rounded gneissic inclusions; weakly foliated, interlayered foliated ore; lacks preservation of primary layering

B — Interlayered 1 meter thick gneissic ore and foliated ore; Gneissic ore contains 0.5 m tight to isoclinal folds

A — Interlayered gneissic ore and foliated ore; gneissic ore contains 1-3 m rotated, weakly foliated inclusions, truncated and rotated folds

Figure 35. Stratigraphic column of the ore horizons

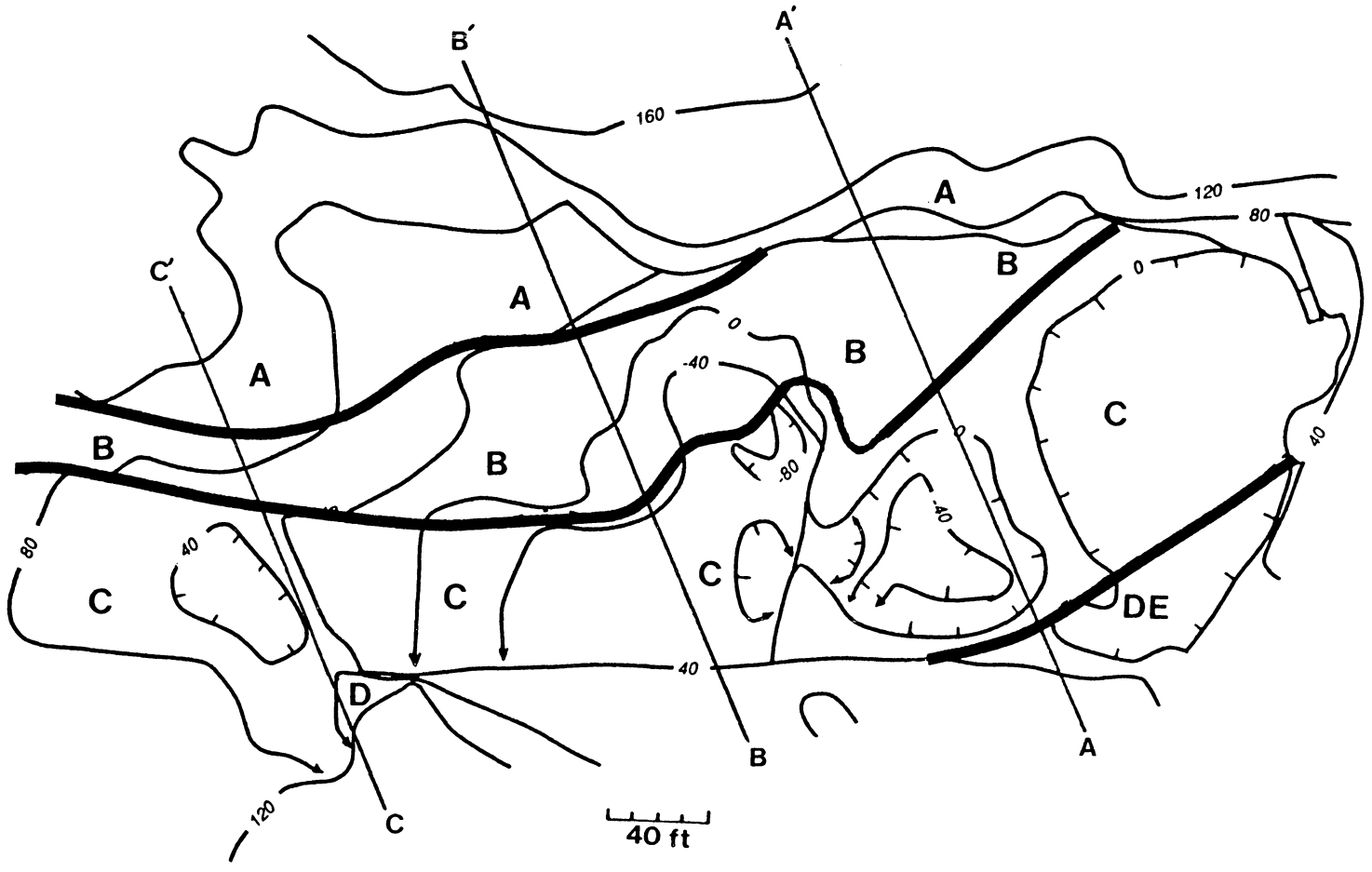


Figure 36. General map and cross sections of mine (A-A', B-B',C-C')

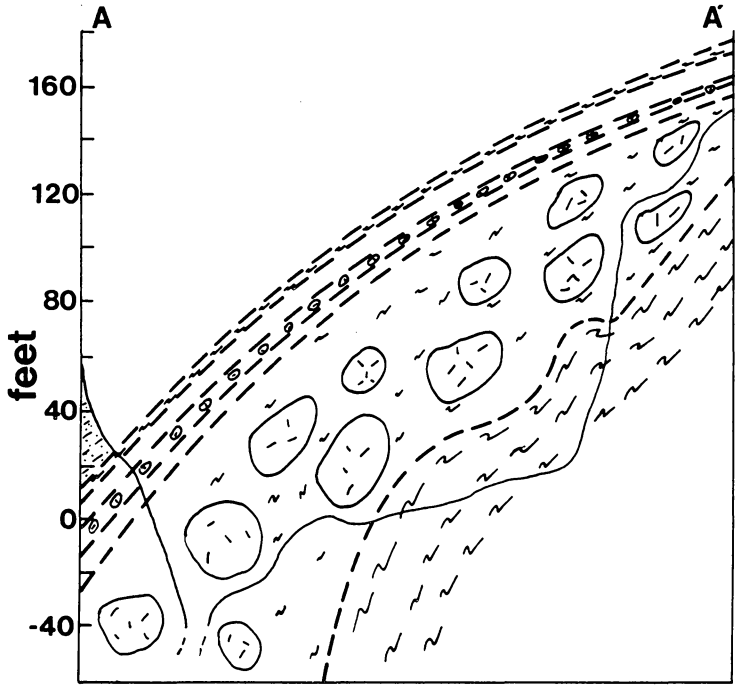


Figure 36 (continued)

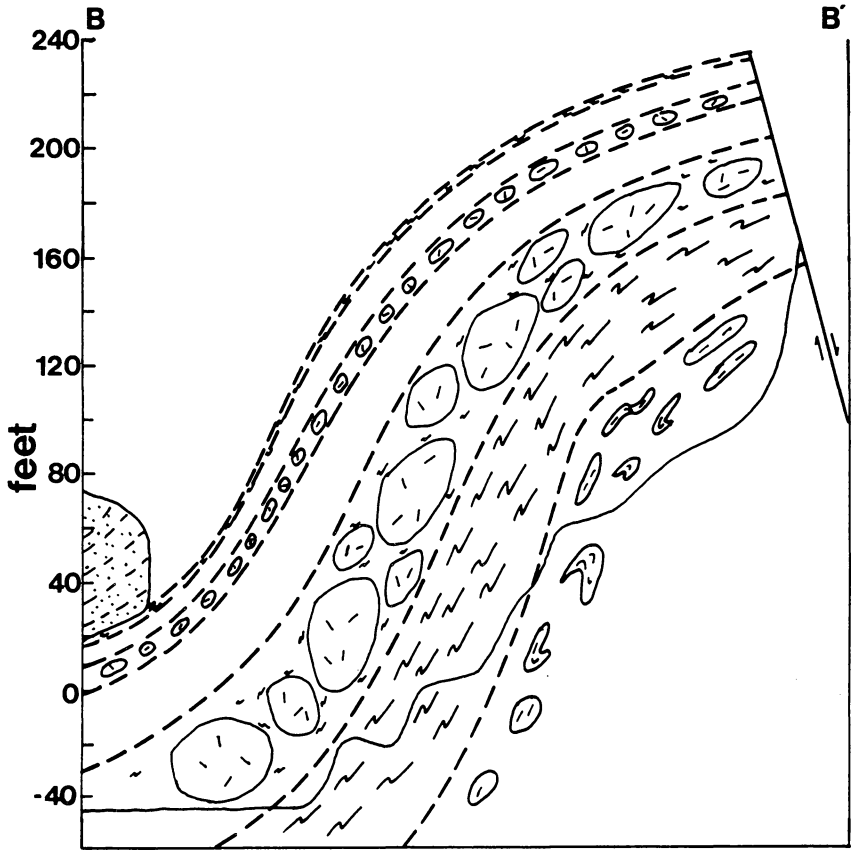


Figure 36 (continued)

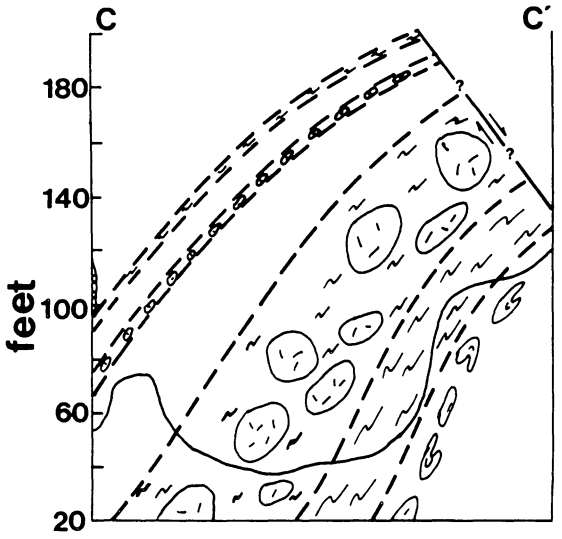


Figure 36 (continued)

Gneissic Ore (Zones A, B, C, and E)

This type of ore dominates the central thickness of the body and is characterized by 0.5 m to 4 m or larger sub-rounded blocks of gneiss (figure 37c). The blocks, as seen on the walls and arches of the mine are often randomly oriented with respect to the dominant foliation. Surrounding the blocks are 1 m or thinner envelopes of foliated ore which wrap around the gneissic inclusions. The inclusions themselves are, for the most part, composed of weakly foliated biotite quartzites and plagioclase-rich rocks with minor widely desseminated pyrrhotite. Despite the randomness of their orientations, most are elliptical to subrectangular in shape, and their foliations are invariably parallel to the long dimension of the blocks. As a result, the blocks have the appearance of having been rotated. This is especially true in zone E (figure 37d), where the blocks have kept their stratigraphic position, forming a layer of rotated blocks embedded in the pyrrhotitic matrix as if they were once a coherent layer with a continuously parallel foliation. In zone B, the gneisses are in layers that are somewhat thinner than in the other zones (less than 2 m). These rocks have not been detached into blocks, and as a result, the layers show interbedded gneisses and foliated ore. The greatest amount of rotation and detachment is in zone C, where the gneissic layers were apparently originally more massive and thicker bedded. It is more difficult in this zone to trace the original layering.

Figure 37. **Photomicrographs and outcrop photographs of stratigraphy:** a) Foliated ore showing isoclinally folded chlorite; b) view of line of arches. Zone F follows the line of arches from lower right to upper left; c) gneissic ore showing rounded gneiss inclusion; d) rotated blocks of zone E on pillar.

A
B
C
D

Structural Geology

General Statement

The structural elements of the surrounding Ashe Formation have been determined by Tso (1987). It was found that there is close agreement between the regional data and the structural data obtained at the Bumbarger Pit in terms of orientation, structural style and relative chronological order. Since the Bumbarger Pit is the best three dimensional outcrop of the Ashe Formation in the area, the various structural features are easier to observe in the mine than in other places. Table 5 summarizes the structural elements. The following text gives the detailed description.

Structural Elements

Original lithologic layering- S_0: The S_0 is defined as the lithologic contacts between the units within the Ashe wallrocks, such as between gneisses and schists, which represent the original layering be-

Table 5. Structural elements

SUMMARY OF STRUCTURAL TERMINOLOGY

S_0- Primary lithologic layering; contacts between schists, gneisses and amphibolites in the surrounding rocks, boundaries of ore inclusion zones in the ore body

S_1- Early penetrative foliation; parrallel alignment of muscovite, chlorite and biotite

F_2,S_2- Dominant regional penetrative foliation; crenulation cleavage, parallel growth of biotite and muscovite; 1-2 cm isoclinal folds (F_2) in foliated ore; 0.5 to 3 m tight to isoclinal folds in gneissic ore, transposes S_1

Metamorphic Peak- Porphyroblastic growth of garnet, actinolite and biotite

F_3,S_3- Gentle northeast-trending folds; mesoscopic to macroscopic scale, causes variation in dip, locally developed axial plane foliation; folds silicate inclusions

F_4,S_4- Close to gentle southeast-trending folds; mesoscopic scale, causes variation in strike, locally developed axial plane foliation; folds silicate inclusions

tween sediments of differing bulk compositions like graywackes and shales. Due to the mobilization of the ore sulfides during deformation, it is difficult in most cases to precisely define S_0 within the ore. However, the broad zones described previously are believed to represent packages of sediment deposited within the sulfide and thus to approximate original layering. The Paleozoic amphibolite grade metamorphism in the area has effectively removed nearly all of the primary bedding structures such as graded beds and cross beds. In addition, the ductile deformation of the pyrrhotite and inclusions has made it impossible to identify any soft sediment deformational structures.

Early foliation parallel to layering- D_1-S_1: Throughout the Gossan Lead area, rocks are characterized by a penetrative foliation that parallels the lithologic contacts. However, close inspection reveals that this foliation is a composite of a crenulation cleavage and centimeter to meter scale isoclinal folds that transposes an earlier foliation. In the schists of the surrounding Ashe Formation, the S_1 is defined as the early foliation cut by a crenulation cleavage (Tso, 1987). In the gneisses, usually only one foliation is observed. However, these early formed trains of biotite and muscovite are isoclinally folded so that isolated fold hinges may be observed by the high angle between the S_1 and the latter S_2 . In such a case, the foliation is treated as a composite S_1/S_2 . No folds of any scale have been associated with this deformation in the study area.

Penetrative foliation- D_3-F_3-S_3: The S_2 is the dominant planar and penetrative foliation that strikes generally northeast with a southeast dip. F_2 folds are identified on the microscopic and mesoscopic scales as either a crenulation cleavage superposed on the S_1 in schists, or as the axial plane foliation on cm scale isoclinal folds. In the foliated ore (figure 37a), micaceous inclusions are frequently observed as boudinaged folds, with thicker hinges and limbs that thin out to stringers of micas embedded in the sulfide host. Commonly, chlorite is isoclinally folded in these structures, with kink-folding becoming prominent near the hinges. The best examples of this texture is found just below the hanging wall on the eastern end of the Bumbarger Pit in zone H.

In the gneisses, however, the structural style of the S_2 is considerably different owing to the increased competency of these rocks compared to the schists and ore. In zone B, spectacular 5 cm trains of isoclinal folds can be observed (figure 38a). In general, the thicker the layering of the gneissic units, the larger the wavelength of the folds, and the less well defined the folds appear to be. In some cases, as in zone A, gneisses have been broken and rotated subsequent to their being folded (figure 38b).

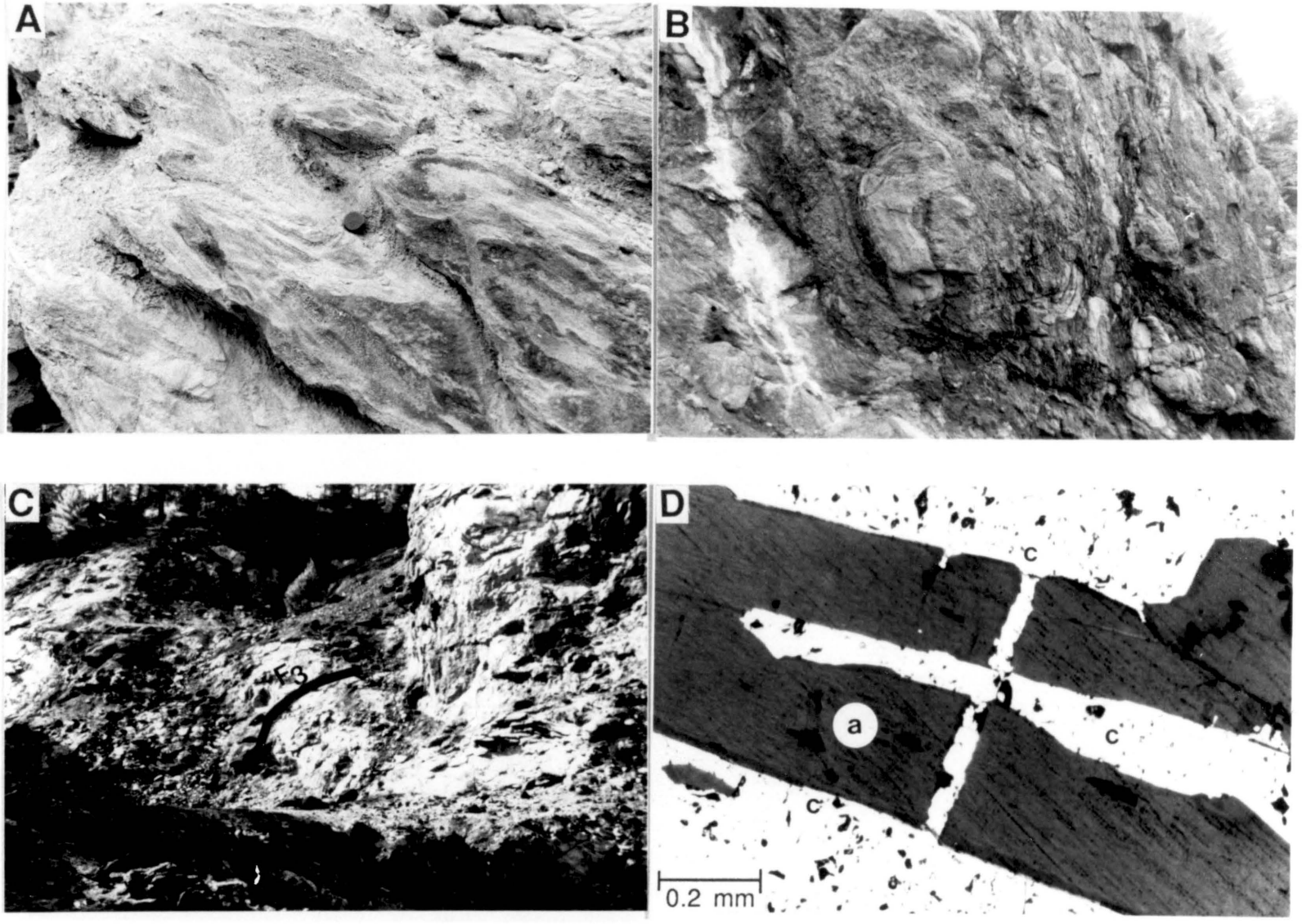
Mesoscopic folding about NE-trending axes- D_3-F_3-S_3: As observed especially on the footwall area on the northwest wall of the pit, the layers are mesoscopically folded about northeast trending axes (figure 38c). The folds are asymetrically folded with the longer and steeper limb being the southeast limb, with local overturning of that limb. Fold axes, where observed away from F_4 folds are subhorizontal and trend in the range of N50°E to N80°E as seen on stereonet (figure 39).

As seen on the schematic structural map of figure 40, the F_3 fold axes display an oscillating trend pattern. On the extreme western edge of the pit, the trend is nearly east-west, then moving east, the trend deflects to the northeast, then back to east-west, then finally deflects northeast again at the eastern end of the pit. This pattern is very similar to the strike and dip pattern of the regional schistosity in the surrounding Ashe (Tso, 1987).

As observed in both the surrounding area and the Bumbarger Pit, the F_3 broadly folds all previous D_1 and D_2 structures, with local northwest dips. In rare instances, where the F_3 folds are unusually tight, a local axial plane foliation (S_3) may be developed. The wavelength of the F_3 folds (20-30 m) are somewhat smaller than in the surrounding area, where folds may be of the macroscopic scale. Data from the surrounding area indicate that this fold generation is syn- or post-Fries thrusting, as the Fries Fault mylonites also show the effects of this deformation (Tso, 1987).

Mesoscopic folding about SE axes- D_4-F_4: As observed on the stereonets of figure 39, the S_2 is also folded about SE-plunging fold axes that trend in a well defined direction of S10°E to S30°E. These folds are generally open, although tighter hinged than the F_3, and are asymmetrical with the longer

Figure 38. Photographs of ore deformation: a) Tight to isoclinal folding in gneiss; b) broken fold as seen on northern wall of pit; c) F_3, NE-trending open fold; d) chalcopyrite fills crack of actinolite porphyroblast.


A
B
C
F3
D
c
a
c
c
0.2 mm

limb being the western limb. These folds are locally developed in the Ashe throughout the Galax-Fries area. However, the Bumbarger Pit affords better exposure, and locally, refolded gneissic inclusions of ore at F_4 hinges may be observed. Locally, some thickening of the ore has occurred in the hinges of these folds.

Late high angle faulting: Two late-forming high angle faults have been identified. The first is found along the northwest wall (plate III) which cuts off part of the ore and is represented by a white, powdery fault gouge. It is inferred that it is a normal-slip fault because hanging wall rocks are found immediately northwest of the fault trace. The second high angle fault is found crossing the hanging wall on the southern wall. It appears to be a normal-slip fault with a throw of approximately 3 m.

Timing of Metamorphism With Respect to Structure

The metamorphic peak was achieved after the development of the S_2 foliation. This is observed as the presence of 4-5 mm euhedra of spessartine-rich garnet that cuts across the dominant foliation, showing very little evidence of deformation. In addition, 7-8 cm diameter actinolite rosettes also grew after the main period of deformation had ceased, as evidenced by the fact that they are found with very little evidence of deformation in silicate inclusions that are otherwise isoclinally folded. However, some deformation did continue past the metamorphic peak as evidenced by the ductile flow of chalcopyrite into cracks of the actinolite rosettes (figure 38d). In addition, the kink-banding of pyrrhotite grains, the folding of gneissic inclusions about F_4 fold axes, and the local thickening of ore in F_4 hinges, indicate that the sulfides continued to strain during the later deformational events.

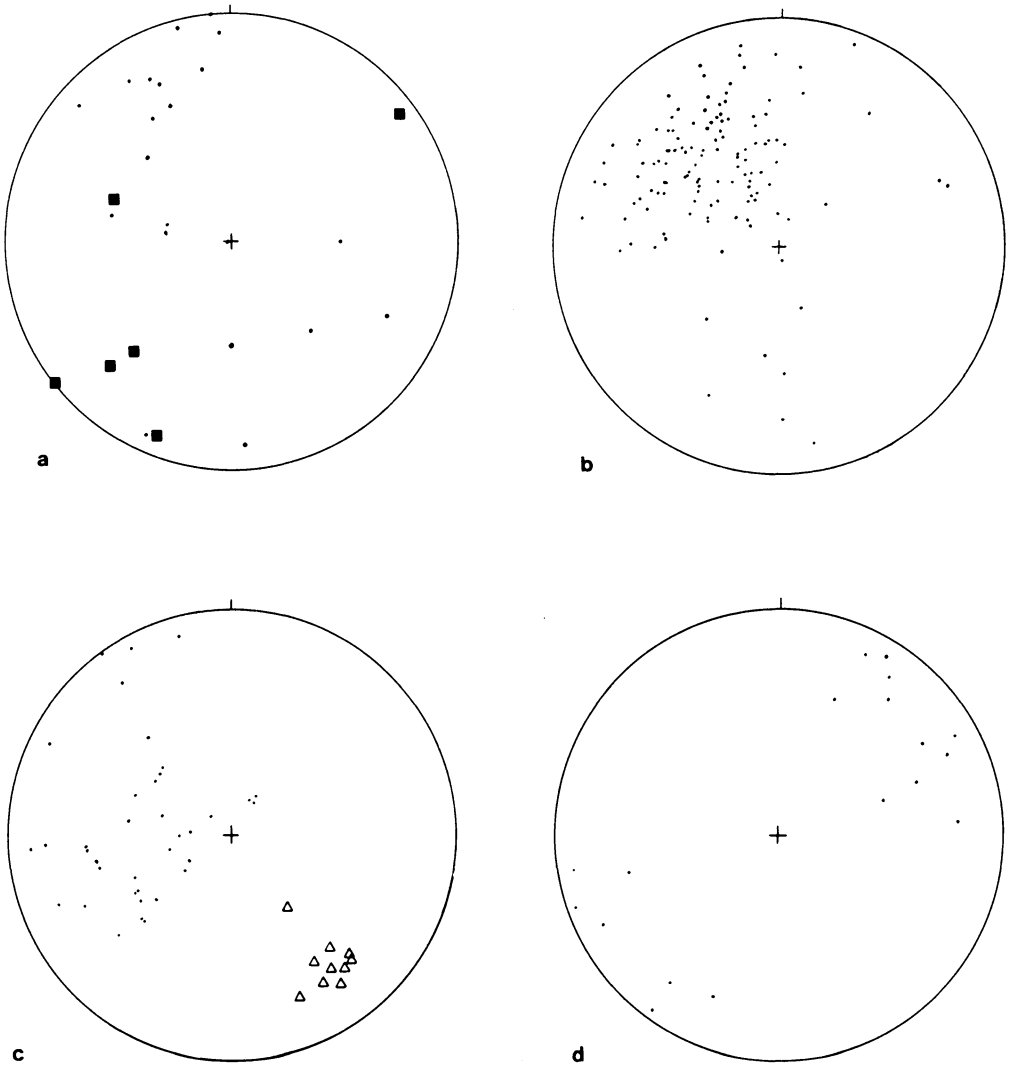


Figure 39. Series of stereonets: a) Dots = poles to S_1 foliation, n = 20; closed squares = F_2 fold axes, n = 6; b) dots = poles to S_2 foliation away from F_4 areas, n = 127; c) dots = poles to S_2 foliation in F_4 areas, n = 37; open triangles = F_4 fold axes, n = 10; d) dots = F_3 fold axes, n = 18.

Figure 40. Schematic structural map showing trends of F(3) and F(4) folds: Long arrows = F_3 fold axis trends; short arrows = F_4 fold axis trends; plunge angles given where data is available.

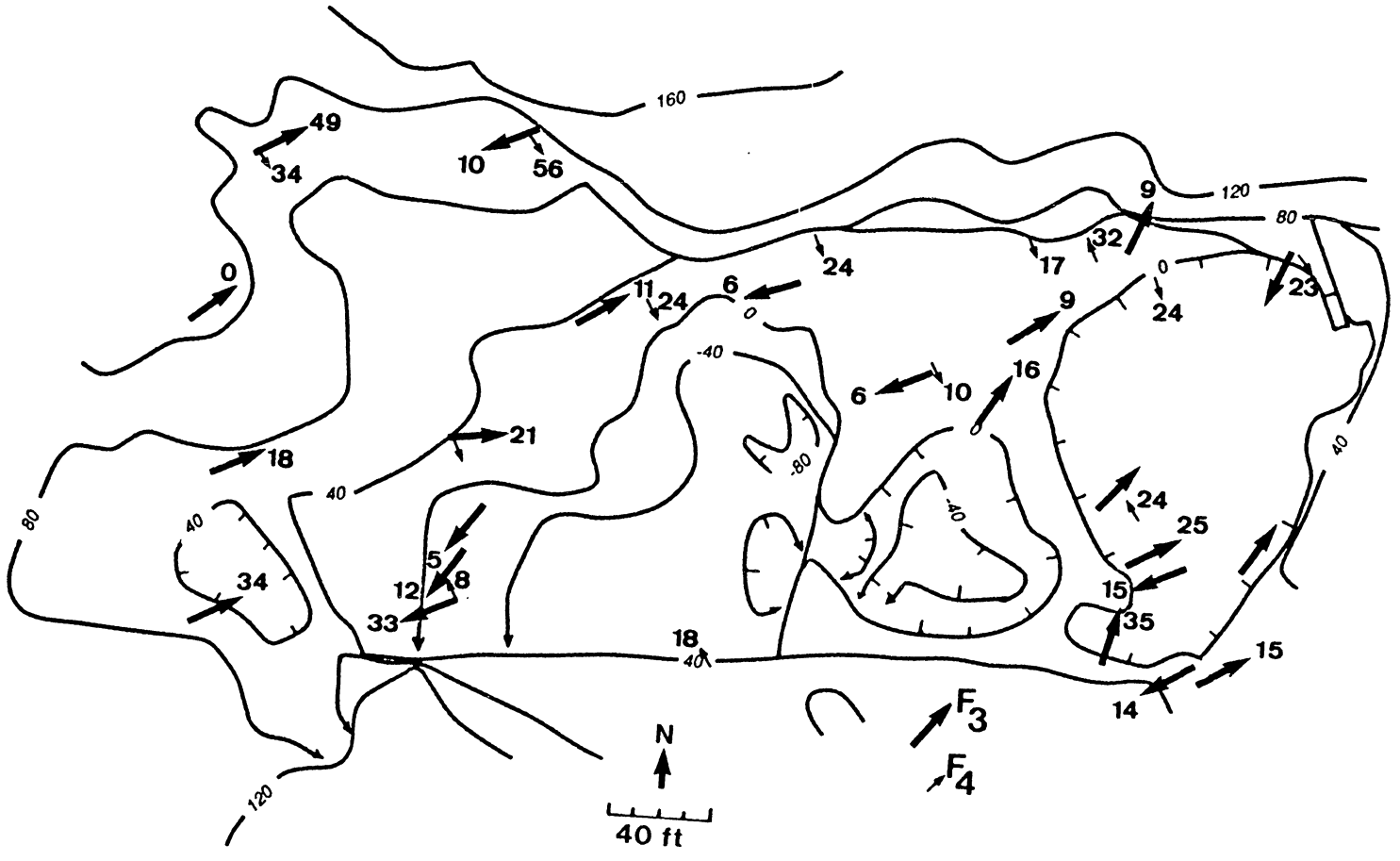


Figure 40 (continued)

As observed in the surrounding area (Tso, 1987), the metamorphic peak similarly followed the development of the dominant S_2 foliation as evidenced by the development of staurolite porphyroblasts in rocks in Galax. Regional mapping indicates that the Fries Fault offsets the metamorphic isograds (Espenshade and others, 1975), thrusting higher grade rocks over lower grade rocks. In addition, mylonites of the Fries Fault show folding related to the F_3 generation of folding. As a result, it is concluded that the metamorphic peak of the Gossan Lead occurred between D_2 and D_3.

Synthesis of the Development of the Gossan Lead Structure

Analysis of the Paleozoic structure of the Gossan Lead leads to the following model. The parallelism of the lithologic contacts within the Ashe Formation and with the hanging and footwall contacts of the ore indicate that the ore is generally stratabound (figure 41a). The broad lithologic zones within the ore body leads to the interpretation that this layering is primary to the ore deposition. During the early Paleozoic, the area underwent regional metamorphism so that a penetrative foliation was formed parallel to the lithologic contacts (figure 41b). As the metamorphic grade continued to increase, a second (D_2) style of deformation occurred (figure 41 c,d). This deformation was responsible for the creation of the ore textures as a variety of styles formed depending upon the rheological properties of the units. Inclusions of thin-banded schist (zones A, B, C, G) responded by isoclinally folding and having the folds boudinaged. Where gneissic layers are thinner and interbedded with ore (zone B), the layering remained intact, with mesoscopic scale isoclinal folds forming in trains. The development of the folds was followed by the breakage of some of the gneissic layers into segments, accompanied by rotation of the folds (zone A). This is evidenced by the rounding of the segments, the misorientation of the previously formed S_1/S_2 foliation with respect to the surrounding rocks, and the dismemberment of fold hinges. If the thickness of the gneiss was > 3 m, the layer tended not to fold. Instead it broke and rotated (zone C) to form rounded

inclusions that lack well defined foliations. The rotation of inclusions and the asymmetry of the folds indicates that the deformation was shear related, with a sense of movement consistent with that of the hanging wall moving to the NW. The metamorphic peak followed, resulting in the growth of garnet and actinolite porphyoblasts at approximately 480-435 m.y. ago (Glover and others, 1983). However, activation of the Fries Fault may have begun at this time or shortly thereafter, and the entire Gossan Lead was transported to the northwest. Following or during the latter stages of Fries faulting, the rocks of the Fries fault block were gently folded about subhorizontally trending mesoscopic to macroscopic fold axes that trend to the NE (figure 41e). This was followed by refolding about SE trending axes (figure 41f). The sulfide continued to be ductile during this stage, while silicates were more brittle. The ore was then crossed by two late developing faults, the largest of which cuts off part of the ore along the northwest part of the Bumbarger Pit.

Discussion of Structure

Studies relating the development and chronology of deformational events to mesoscopic ore textures are becoming more numerous in the literature. For example, Rui (1973), studied the ore structure in the mostlty pyritic Killingdal mine, Norway. He found that the ore is largely parallel to the schistosity of the wallrocks in manner similar to the Gossan Lead. There, "brecciated" textures are observed in the wallrocks due to the local mobilization of the massive ore. The structure of the ore at Killingdal is strongly influenced by the regional folding and is "synorogenic". Rui concluded that ore-forming fluids were introduced into the host rocks during deformation, and ore was deposited in favorable sites such as in fold hinges and thrust planes.

Remobilization of massive ore has also been reported at the Black Angel Mine, Greenland (Pedersen, 1980). Thrusting has locally caused rotation and rounding of earlier formed ore and marble to form a durchbewegung structure. Pedersen recognized an original banding that is pri-

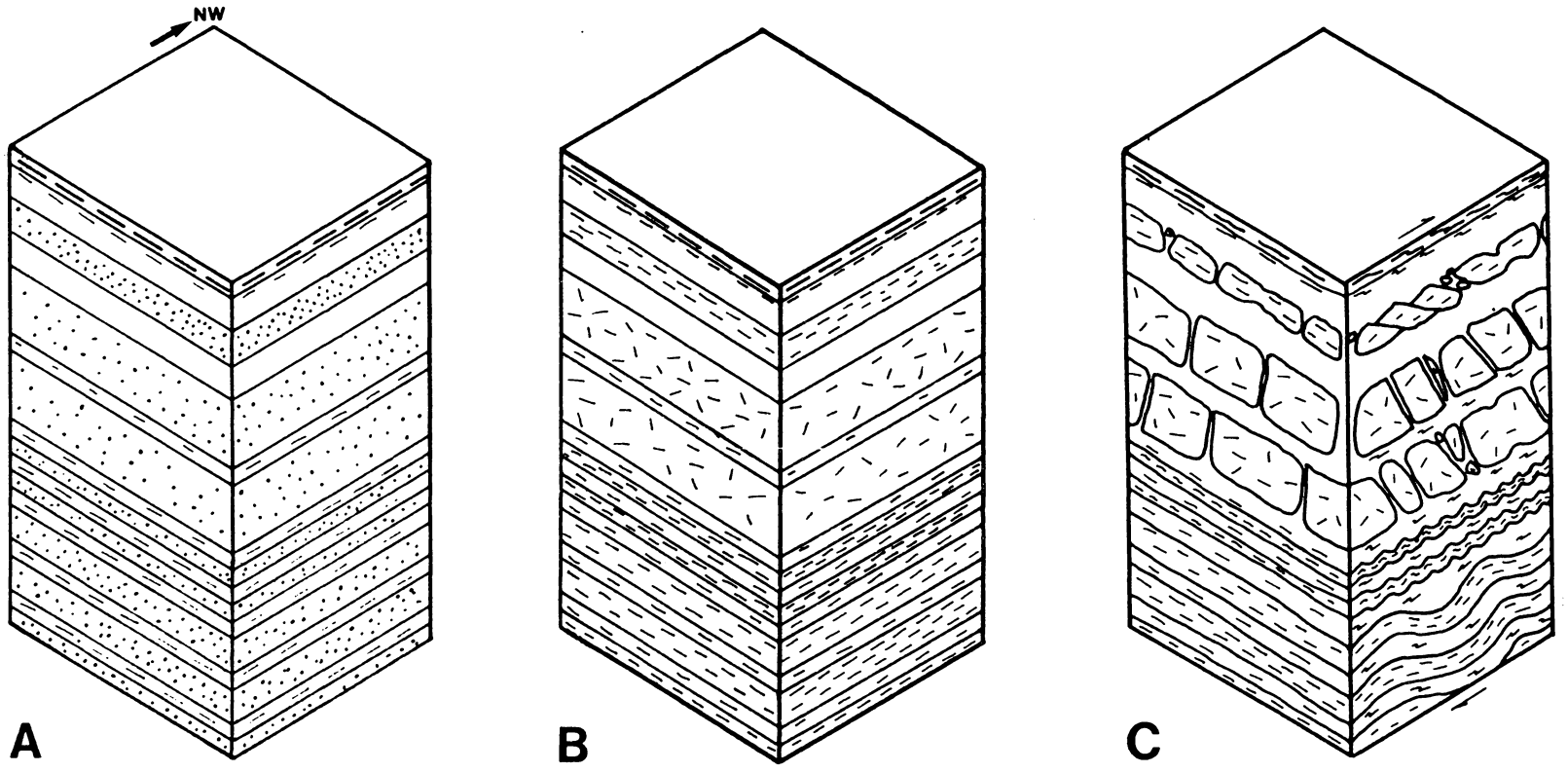


Figure 41 (continued)

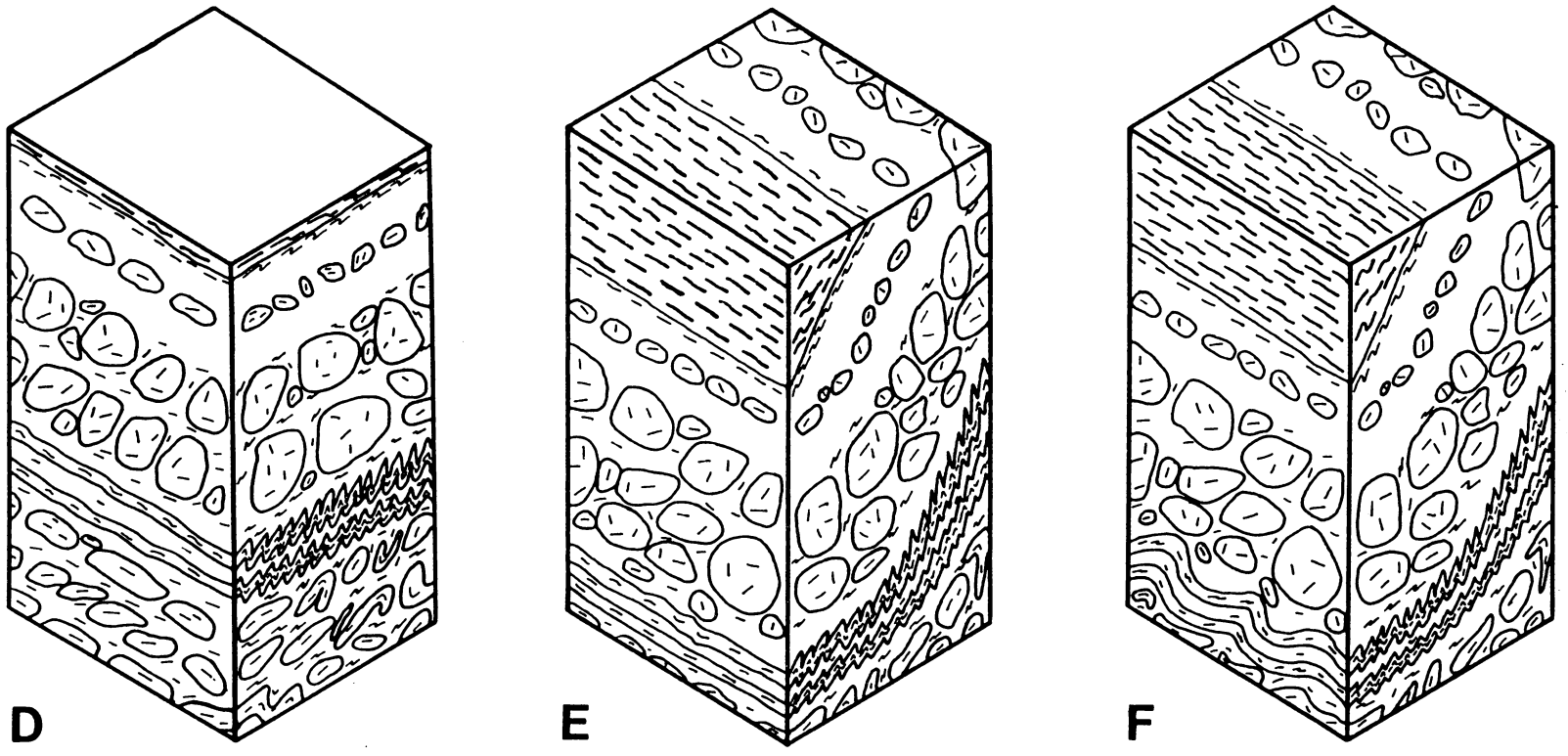


Figure 41 (continued)

mary, with the later destruction of this banding during shearing giving a "massive" texture consisting of "homogenized" sulfides and gangue. Later folding caused further remobilization of sulfides, brecciation of marbles, and extension fractures. He recognized an order of sulfide mobility of pyrite being the not as mobile, with chalcopyrite and galena being more mobile. During later folding, the more mobile sulfides flowed toward the hinge zones of the fold, thus accounting for the base metal distribution pattern observed in the mine.

At Mount Isa, Australia (Hewett and Solomon, 1964, McClay, 1979), despite relatively low metamorphic conditions of the lower greenschist facies, folding and rotation of beds is prevalent in these silver - lead - zinc ores. Different styles of folding have been recognized for different lithologies. For example, for folds of amplitudes of 1-100 cm, dolomitic siltstones in a galena matrix form simple buckle folds of single layers, with different thicknesses giving rise to different wavelengths of folds. On the other hand, laminated pyritic siltstones fold in multilayer packets, with a flexural-slip style, and with common saddle reef and faulted hinge structures (McClay, 1979). Apparently, galena layers also served as decollement surfaces allowing beds to slide over other beds. Breccia textures resulted from tectonic folding and rotation and not from sedimentary slumping.

Similarly, the ores of the southern Blue Ridge, such as the Gossan Lead and Ore Knob show the durchbewegung textures quite well. This is a result of two principle factors: 1) the complex polydeformational history that includes multi-phase folding and shearing with metamorphic conditions reaching amphibolite grade, and 2) the fact that these massive ores contain pyrrhotite as the dominant ore mineral.

Experimental deformation studies on sulfides (Clark and Kelly, 1973, Atkinson, 1974, Kelly and Clark, 1975) have shown that the strength of pyrrhotitic ore at the conditions of metamorphism experienced at the Gossan Lead (in excess of 450° and 4 kb) is below that of marble, as observed on plots of stress difference versus temperature (Clark and Kelly, 1973). In particular, deformational experiments at up to 2000 bars confining pressure show a strong drop in the strength of pyrrhotite between 200 °C and 300 °C, with the strength of pyrrhotite approaching that of galena.

Atkinson (1974) used polymineralic ore as starting material and was thus able to directly compare the behavior of pyrrhotite, chalcopyrite, and galena. His results showed a decrease in strength of all three minerals with increasing temperature, and an increase in strength with increasing confiniing pressure, although at temperatures above 200 °C, the pressure effect was not as strong. Experimentally, pyrrhotite was shown to be more ductile than galena, which was more ductile than chalcopyrite. The observed sequence at the Gossan Lead, however, is that chalcopyrite is more ductile than pyrrhotite, in accordance with what is generally observed in most field studies. Atkinson explains the discrepancy by noting that pyrrhotite behavior is more strain-rate dependent than other sulfides.

At the Gossan Lead, the silicate material can also be placed in order of ductility with respect to the sulfide. The thinly layered micaceous schists are the most ductile of the inclusions, though they are less ductile than sulfide. They are characterized by isoclinal folding on the centimeter scale, strong thickening of their hinges, and thinning and boudinage of their limbs. The gneisses are less ductile than the schists, and their behavior depends to a greater degree on their thicknesses. Where gneisses are less than 1 meter thick, trains of isoclinal folds are observed, although the folding seems confined to individual layers of gneiss. In layers between 1-3 meters in thickness, the gneisses are more likely to be folded and then broken and rotated. Fold style is observed as isolated parallel folds with little thickening of the hinges. Gneissic layers that are thicker show much less folding, and a poorly developed foliation. They tend to be segmented and rotated.

Models for Ore Emplacement and Deformation

Numerous models have been proposed for the ore emplacement of the Gossan Lead and simlar ore deposits of the southern Appalachian Blue Ridge. A major distinguishing feature that separates the various previously proposed models from one another is the relationship between the timing of the ore emplacement and the sedimentation and deformation of the surrounding rocks. The following discussion relates some of the previously proposed ideas about Blue Ridge sulfides to modern data in general and the Gossan Lead in particular.

Model 1: Ore emplacement is post-metamorphic and post-thrust faulting

There have been many versions of this idea, but the proposal by Ross (1935) is perhaps the most elaborate. His ideas were based primarily on the Ducktown, Tennessee deposit, but he extended his theory to the Gossan Lead as well. He envisioned a series of 5 stages that occurred sometime after the Cambrian and after the host sedimentary rocks were already metamorphosed. The first stage involved the injection of granitic igneous rocks such as aplites and pegmatites into the country rock producing a plagioclase-rich rock with few mafics and very little or no foliation. Secondly, quartz was introduced into fractures by fluids penetrating into cracks, with subsequent replacement of the country rock by the quartz resulting in a widening of the cracks. The third stage was a high

temperature silicate stage in which ferro-magnesian minerals such as amphibole, garnet and biotite grew replacing the quartz and aplite. Minerals such as chlorite and talc were said to be a secondary alteration of the biotite. The next stage involved carbonate replacement of the previously deposited minerals. Finally, sulfide mineralization replaced all previous rock types including the country rock, aplites and carbonates. Ross determined that the order of sulfide replacement was: pyrite followed by pyrrhotite, then sphalerite, then chalcopyrite, and finally galena. According to Ross, the aplites and pegmatites resulted from the differentiation of a parent magma of unknown whereabouts. The inclusion-rich texture of the ore was thought to be the result of some faulting prior to mineralization, causing an initial breccia texture, thus allowing the mineralizing fluids to enter the rock along fractures. This caused replacement, rounding of the inclusions by solution, and a "slumping together" of the silicate blocks to form the ore texture.

This hypothesis seems untenable in light of modern data. Ross' basic assumption is that the ores are post-metamorphic. The evidence that he cites for this is the relative lack of a crushing or shearing texture of the sulfides with "a complete absence of dynamic metamorphism". However, as described by many authors, a lack of apparent deformation and the presence of dihedral angles in sulfides such as pyrrhotite is excellent evidence of metamorphism. Sulfides readily anneal under such conditions, thus eliminating most, if not all, of the prior deformational textures, if any, that existed. In addition, late-forming deformation (D_3 and D_4) did occur, resulting in kink banding in some samples. As Kinkel (1967) pointed out at Ore Knob, North Carolina, the "aplites" and "pegmatites" are not really igneous in origin, but are alterations of the plagioclase-rich gneisses. Gair and Slack (1984) discuss the origin of this rock in some detail. On major element and rare earth element grounds, they noted that the plagioclase rocks could not be an igneous rock and that there is a strong affinity between this rock and the metasedimentary host rocks. They concluded that these rocks were sedimentary rocks that were altered in a convective hydrothermal cell on the sea floor. It should be noted that the surrounding sulfide may have had a "stress absorbing" effect that further prevented the formation of an obvious foliation (Vokes, 1969).

As far as the other "stages" of Ross' hypothesis is concerned, it should be noted that there are many sources of quartz for his second stage. Some could be deposited as part of the primary deposit, such as at Kuroko, Japan (Kalogeropoulos and Scott, 1983). The Ashe Formation also abounds with vein quartz, some of which is found in meter-wide veins that commonly cut across the main foliation at a steep angle. These veins freqently show a weak foliation themselves, and are often folded parallel to S_2 and would, if present in the ore, take part in all of the metamorphic and deformational events in the ore zone.

Unfortunately, carbonates are relatively rare at the Bumbarger Pit compared to Ducktown. Staten (1976) reported minor marbles in drill cores from the Betty Baker area, and some have been collected at the Gossan Howard mine (Craig and others, 1971). However, none have been observed by this author in place in the Bumbarger Pit, thus making the role of carbonate replacement difficult to evaluate.

Magee (1968) summarized the pre-1970 thinking on the Ducktown deposit. At this ore body, numerous limestone beds are found interlayered with the schists and gneisses and these were thought to be favorable horizons for hydrothermal replacement. According to Magee, thrust faulting and metamorphism took place in the early Paleozoic, causing brecciation, thus providing a structural control for later hydrothermal fluids. These fluids were thought to be associated with a Devonian deformational event, accompanied by amphibolite intrusions. The fluids then followed the shear zones and preferentially replaced the limestone units.

More recently, a variation on this theme was proposed by Fullagar and Bottino (1970) for Ore Knob and Ducktown. They studied Rb/Sr ratios of the wallrocks with respect to the ore zone and country rocks and concluded that the wallrocks' unusually high Rb/Sr ratio was the result of mineralization that took place approximately 400 m.y. ago which altered the isotopic composition of the wallrocks. The source of some of the ore minerals was thought to be from fluids that passed through the wallrocks.

One of the problems with hypotheses of this type is that they assume that metamorphism preceded mineralization. As originally observed by Staten (1976) in the Betty Baker area, and confirmed by Tso (1987) at the Bumbarger Pit, garnet-biotite temperatures indicate that metamorphism affected both the ore and the country rocks together. In addition, detailed sampling, probe analysis and mapping show that no offset of the biotite-garnet temperature has occurred along the ore zone that could be an indication of a post-metamorphic fault (Tso, 1987). Another problem with these theories is the lack of explanation of the bedded nature of the Gossan Lead ore. Although limestone replacement may explain this feature at Ducktown, the Gossan Lead is limestone poor and it is difficult to explain the layering of the ore on shear zone control alone. Finally, although amphibolites are present in the Gossan Lead area, they all show foliation to some degree. The foliation is invariably parallel to the regional schistosity, thus indicating that emplacement of the amphibolites was prior to regional metamorphism, not after.

Model 2: Ore emplacement is post-faulting and premetamorphic

This theory was proposed by Kinkel (1967) and takes into account the fact that the ore textures and unaligned silicates were recrystallized by a later metamorphic event. He thought that after an initial stage of metamorphism which caused the main foliation, faulting occurred and ore minerals were then introduced along the shear zones. Later faulting locally crumpled the ore, and then a second pulse of metamorphism allowed for the growth of the coarse amphibole rosettes.

Much of Kinkel's hypothesis depends upon radiometric ages from rocks at Ducktown and Ore Knob. K-Ar measurements from ore zone hornblendes and biotite give ages in the 1,120 m.y. (Ore Knob) and 1,200 to 1,045 m.y. (Ducktown) range. In contrast, ages of wallrock and ore at other ore bodies including the Gossan Lead give a range of 478 to 300 m.y. Kinkel believed that the older ages reflect Grenville metamorphism and that the younger ages represent Paleozoic regional thermal metamorphism. Although Kinkel assumed that the ore forming fluids (from an unspecified source)

were hydrothermal in origin and then were introduced into a shear zone, he did not rule out a primary depositional source of the sulfides.

Modern data, however, dispute the claim that the age of mineralization is older than 1 billion years. The generally accepted age of the enclosing metasediments of the Blue Ridge is in the 570 to 690 million year old range (Odom and Fullagar, 1982) and in light of the many age determinations done since Kinkel's paper, the old ages seem anomalous (Dallmeyer, 1975).

If one applies Kinkel's assumptions to the Gossan Lead, that the ore fluids penetrated into foliation planes that were parallel to a shear zone, but prior to the metamorphic peak, then it is necessary to place the time of mineralization as being later than D_1 and earlier than or concurrent with D_2. In this way, an initial (S_1) foliation can be formed, then broken and rotated during shearing during D_2, thus allowing channelways for the mineralizing fluids to enter. As a result, the Gossan Lead would then lie along a pre-peak metamorphic fault zone. This idea is difficult to test. Although it is obvious that some shearing took place in the ore zone, there is no obvious evidence for a shear zone along strike in the surrounding area. There is no evidence of any annealed mylonite, fault gouge, nor any obvious displacement or truncation of lithologic units, although poor outcrop exposure makes this assertion tentative.

Model 3: The ore is synsedimentary, but localized by later shearing

This is the hypothesis of Addy and Ypma (1977) proposed for Ducktown, Tennessee. They thought that through several possible mechanisms such as volcanic exhalations, later modified by groundwater, local beds of sulfide-rich material and disseminated sulfides were accumulated on the sea floor along with host sediments. Metamorphism, folding, and shearing in the Paleozoic created passageways for meteoric fluids. The fluids then remobilized the sulfides in the surrounding rocks and leached metals from minerals, thus adding more sulfides to the ore zone. They cited a depletion in the O-18/O-16 of the alteration zone as their principal line of evidence. Although similar isotopic

work has not been done at the Gossan Lead, the present work is consistent with the conclusions of Addy and Ypma. The structural analysis and petrographic study of the Bumbarger Pit show abundant evidence of local Paleozoic remobilization. However, it should be pointed out that while at Ducktown, the alteration halo that could have contributed metals to the ore may reach several hundreds of feet (Addy and Ypma, 1977), a study of drill core at the Betty Baker area of the Gossan Lead (Staten, 1976) showed a considerably smaller halo of only a few feet.

Model 4: Ore is synsedimentary

This hypothesis reflects the most recent work by several authors and incorporates submarine venting as a key component. The idea that submarine venting is possible is not new. For example, Gilmour and Still (1968) proposed that volcanic vents in a "eugeosynclinal trough" was a source of massive sulfides at Ducktown. A variation of this idea was proposed by Mauger (1972) based on sulfur isotope data at Ducktown. He thought that a submarine hot spring system similar to the Red Sea brine pools existed in which metals were extracted from the surrounding sediment by pore waters, and that these waters were expelled upwards during compaction of the thick sedimentary blanket.

Henry and others (1979) and Craig (1980) were among the first to connect the Gossan Lead deposits with submarine volcanic venting in a rift setting. A more elaborate model was proposed by LeHuray (1982, 1984) based on lead and sulfur isotopes studies primarily at Ducktown, with some sampling done at the Gossan Lead. She postulated a deep fault system in a rift environment that served as a conduit for a circulating hydrothermal cell. The heat source that drove the cell would be an amphibolite body intruded within the metasediments, with much of the lead derived from the surrounding sediments, and a lesser supply from the amphibolite itself. Gair and Slack (1984) also proposed a volcanic setting in a rift basin and were the first to make a comparison between the Gossan Lead and the Guaymas Basin in the Gulf of California. They envisioned a package of

sulfide ore, enclosing sediments, and associated alteration rocks that formed as a result of a convecting geothermal cell.

Discussion

The data generated in this study can be used to refine previous models of the emplacement of the Gossan Lead. It is evident from the present work and from previous studies, that the immediate wall rocks are overwhemingly metasedimentary. Modern tectonic models of the Ashe Formation (Rankin, 1976, Wehr and Glover, 1985) place the host Ashe/Lynchburg Formation as part of a rift system with horst blocks to the east and west, and the Ashe in a marginal rift that filled with turbidites and amphibolites. Wehr and Glover (1985) envision the Ashe/Lynchburg as deposited on the deep water side of a hinge zone on continental crust that opened during the late Precambrian that eventually led to the development of a passive continental margin. Recent geochemical work done on the amphibolites of the Ashe (Slack and others, 1985, Conte and Misra, 1986) suggests that they were intruded into a rifted margin floored by transitional continental-oceanic crust.

The present study reveals that the sulfides are found in a zone that is roughly parallel to the overall lithologic layering, including amphibolite - metasedimentary contacts. The position of the amphibolites with respect to the ore is critical in models of the depositional setting. The parallelism of the contacts and the coarseness of the grain size of some of the amphibolites indicate that many may have been intrusive sills. During the field mapping of the Ashe Formation surrounding the Gossan Lead (Tso, 1987), it was observed that coarse-grained amphibolite or "metagabbro" preserved a texture of relict coarse, randomly oriented hornblende that is apparently a reflection of an

original igneous texture which can be differentiated from the more recrystallized and foliated D_2 texture. The large majority of the amphibolites are found to the southeast of the sulfide trend and are thus in the hanging wall. These units are therefore not believed to play a direct role in the formation of the ore. However, a smaller number of amphibolites are found to the northwest or in the footwall. Although none of these lower units are as extensive as the ones higher in the sequence, some are locally quite massive. During the mapping of this study, several metagabbro units unmapped by previous workers were discovered. One sample (#A3-91A, Tso, 1987) contained hornblendes as long as 3 cm, which were the coarsest encountered in the study area. These underlying amphibolites are quite discontinuous, and there are gaps where no amphibolite underlies the sulfide trend. However, it is interesting to note, and perhaps coincidental, that the main areas of mineralization, the Bumbarger, Huey, and Gossan Howard mines, and the prospects west of Dixon Branch, all have amphibolite below them. A drawback in using these particular amphibolites as a source of heat and materials is that they lie 1 km or more stratigraphically below the sulfides, which is considerably deeper than that modeled for modern deposits such as at the Guaymas Basin. However, the true stratigraphic thickness of any part of the Ashe is always complicated by the transposition foliation associated with F_2 . Thus, the original stratigraphic separation may have been considerably different from the presently observed distance. Further study of the total strain of the Ashe Formation during Paleozoic deformation is needed.

During the mapping of the area surrounding the ore, a smaller amphibolite was found only a few hundered meters north of the Bumbarger Pit, and one float sample of amphibolite (#B3-170A) from a second location within 100 meters northwest of the Bumbarger Pit shows significant iron depletion of its hornblendes, and iron depletion and manganese enrichment of its garnets in a manner similar to the the iron depletion of gangue minerals noted by Staten (1976), and in microprobe analyses of inclusions from the Bumbarger Pit (Tso, 1987). This is the first sample collected that clearly shows that at least some amphibolite material is either within the ore or in the immediate wallrocks of the ore zone.

Gair and Slack (1984) reported finding samples of metagabbro in the dump piles of the Bumbarger Pit near the entrance to the pit. The present study has found that considerably more of this material can be found in the Gossan Howard dump and thus there is a suspicion that the few pieces at the Bumbarger Pit entrance may have been trucked in. Microprobe studies (Tso, 1987) show none of the expected iron depletion of the amphiboles and none of this material has been found in place.

The bedded nature of the ore indicates that sulfide deposition was concurrent with sedimentary deposition. In general, gneisses, which are relatively sulfide poor, interlayer with massive sulfide, which tend to have more micaceous inclusions. We envision a period of sulfide depostion in a thermal vent system, driven by amphibolitic sills. Hydrothermal activity was an apparently sporadic process, and times of activity were interrupted by times of quiescence and times of more rapid sedimentation that would deposit the internal packages of gneisses. Faults that would extend through the semiconsolidated sediment to the amphibolite would help to channel the hydrothermal fluids as they do in modern systems, although evidence for such faults have not apparently survived Paleozoic metamorphism. A schematic diagram showing the sedimentary-volcanic depositional setting is shown in figure 42. Subsequent to the main phase of mineralization, deposition of sediment continued. However, the increase in the amount of amphibolite in the hanging wall rocks indicate that igneous activity was considerably more intense in the time period following the main mineralization.

Modern mineralization in rift zones has recently been discovered in many different types of geological situations such as active midocean ridges like the East Pacific Rise (Goldfarb and others, 1983), and in island arc rifts such as Kuroko, Japan (Cathles and others, 1983). A modern setting analagous to the Gossan Lead that rests on continental or transitional crust is lacking. However, hydrothermal deposits in the Guaymas Basin in the Gulf of California is a close approximation (Lonsdale and others, 1980, Lonsdale and Lawver, 1980). Submersible dives in this area revealed hydrothermal pyrrhotite-talc rocks associated with hydrothermal vents in a fault-bounded trough choked with turbidites and diatomites. Although basaltic activity is common, no surface basalt flows were observed. Instead, the magmas preferred to form sill-like intrusions that formed

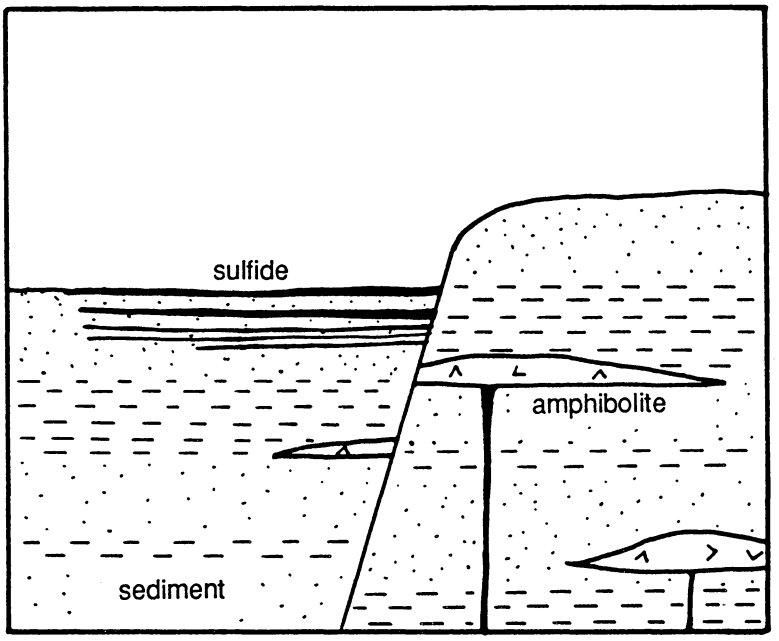


Figure 42. Schematic diagram showing sedimentary-volcanic setting

"bysmaliths" with the vents located over the intrusions on fault scarps and hill crests. Einsele and others (1980) calculated that the reduction in porosity of the contact area between a sill and its host sediments would expell a thickness of water on the same order of magnitude as the thickness of the sill itself, thus making it relatively easy for the intrusion to make room for itself. Due to the relative smallness of the amphibolites in the immediate ore zone area at the Gossan Lead, we agree with LeHuray (1984) that it appears that much of the ore material was probably derived from the sediments and not from the amphibolite. However, recent work at Ducktown by Abrams and others (1986) has shown that much of the rock formerly interpreted to be metasedimentary is actually metavolcanic. It is possible that similar work will turn up similar findings at the Gossan Lead.

Finally, it should be noted that there are few places in the world where a rifted contnental margin such as that represented in the Blue Ridge is preserved in a way that is easily accessible. Studies of modern analogues such as the Brazillian continental shelf (Ojeda, 1982) shows that deep water sedimentation in rifted marginal basins are often intruded by sill-like mafic bodies. Further study of these environments may uncover other Gossan Lead-type sulfide bodies.

Summary and Conclusions

The Gossan Lead is envisioned as having formed from a series of vents driven by amphibolite sills with simultaneous sedimentation in a rifted trough. This resulted in the interlayering of massive sulfide with sediment. Initially, the ore was stratabound with numerous arkosic sandstone, graywacke, and mud layers. Subsequent deformation caused the obscuring of the sediment-ore layering, although in a gross way, the layers survive as packages of ore with silicate inclusions.

During the Paleozoic, a series of deformational events occurred. The first formed a penetrative foliation parallel to lithologic layering. The second produced isoclinal folding of the earlier foliation in the more micaceous lithologies and in the thinner bedded gneisses, forming a transpostion foliation. Further shearing caused the rotation of some of the thicker bedded gneisses. Geologic mapping surrounding the ore zone, however, indicates that the shearing is apparently localized to the ore zone itself, and that the shearing reflects the relative ductility of the sulfide with respect to the metasediments. Following this phase of shearing, the metamorphic peak was reached, which is reflected as the growth of idioblastic garnets and amphiboles. The growth of metamorphic porphyroblasts cross-cuts the development of much of the ore's deformational structure, thus eliminating hypotheses that the ore was introduced along late post-metamorphic shear zones. Mapping by Espenshade and others (1975) and Tso (1987), which shows offsetting of the metamorphic isograds, demonstrates that the main shearing event in the region, the Fries Thrust

Fault, concluded after the metamorphic peak. Subsequent to the metamorphic peak, deformation continued in the form of two sets of larger, more open folding. One set produced NE-trending folds that affected not only the ore, but also rocks in the Fries Fault mylonite zone. The second set is comprised of SE-trending folds. The sulfide is believed to have been somewhat remobilized by both of these generations of folding, with pyrrhotite samples showing some deformation textures and ductile sulfides such as chalcopyrite filling cracks in late-growing amphiboles.

Bibiliography

Abbott, R.N. and Raymond, L.A., 1984, The Ashe metamorphic suite, northwest North Carolina; metamorphism and observations on geologic history: American Journal of Science, v.284, p. 350-375.

Abrams, C.E., McConnell, K.I. and Allard, G.O., 1986, Igneous rocks in the Ocoee Supergroup of Georgia and southernmost Tennessee: Geological Society of America Abstract With Programs, v. 18, p. 209.

Addy, S.K. and Ypma, P.J.M., 1977, Origin of massive sulfide deposits at Ducktown, Tennessee: An oxygen, carbon, and hydrogen isotope study: Economic Geology, v. 72, p. 1245-1268.

Atkinson, B.K. (1974) Experimental deformation of polycrystalline galena, chalcopyrite and pyrrhotite: Transactions the of Institution of Mining and Metallurgy, Section B, v. 83, p. B19-B28.

Bartholomew, M.J. and Lewis, S.E., 1984, Evolution of Grenville massifs in the Blue Ridge geologic province, southern and central Appalachians: in Bartholomew, M.J., ed., The Grenville Event in the Appalachians and Related Topics: Geological Society of America, Special Paper 194, p. 229-254.

Cathles, L.M., Guber, A.L., Lenagh, T.C. and Dudas, F.O., 1983, Kuroko-type massive sulfide deposits of Japan: Products of an aborted island-arc rift: in Ohmoto, H. and Skinner, B.J., eds., *The Kuroko and Related Volcanogenic Massive Sulfide Deposits*: Economic Geologic Monograph 5, p. 96-114.

Clark, B.R. and Kelly, W.C., 1973, Sulfide deformation studies: I. Experimental deformation of pyrrhotite and sphalerite to 2000 bars and 500° C: Economic Geology, v. 69, p. 332-352.

Conte, J.A. and Misra, K.C., 1986, Geochemistry of metabasites within the Ashe and Alligator Back Formations, North Carolina: Implications for late Precambrian tectonics of the Blue Ridge: Geological Society of America Abstracts With Programs, v. 18, p. 216.

Cook, F.A., Albaugh, D.S., Brown, L.D., Kaufman, S., Oliver, J.E. and Hatcher, R.D., Jr., 1979, Thin-skinned tectonics in the crystallime southern Appalachians; COCORP seismic-reflection profiling of the Blue Ridge and Piedmont: Geology, v. 7, p. 563-567.

Craig, J.R., 1980, Stratiform sulfide mineralization in the central U.S. Appalachians; Norges Geologisk Unersokelse; v. 360, p, 295-325.

Craig, J.R., Sears, C.E., Gilbert, M.C. and Hewitt, D.A., 1971, Sulfide mineralization, southwestern Virginia: B. Gossan Lead District: in Lowry, W.D., ed., Guidebook to Appalachian tectonics and sulfide mineralization of southwestern Virginia: Virginia Polytechnic Institute and State University, Guidebook, no. 5, p. 25-38.

Dallmeyer, R.D., 1975, 40-Ar/39-Ar incremental release ages of biotite from the Cherokee orebody, Ducktown, Tennessee: Their bearing on the age of sulfide mineralization: Economic Geology, v. 70, p. 341-345.

Dietrich, R.V., Fullagar, P.D., and Bottino, M.L., 1969, K/Ar and Rb/Sr dating of tectonic events in the Appalachians of southwestern Virginia: Geological Society of America Bulletin, v. 80, p. 307-314.

Einsele, G., Gieskes, J.M., Curray, J., Moore, D.M., Aguayo, E., Aubry, M., Fornari, D., Guerrero, J., Kastner, M., Kelts, K., Lyle, M., Matoba, Y., Molina-Cruz, A., Niemitz, J., Rueda, J., Saunders, A., Schrader, H., Simoneit, B. and Vacquier, V., 1980, Intrusion of basalt sills into highly porous sediments, and resulting hydrothermal activity: Nature, v. 283, p. 441-445.

Espenshade, G.H., Rankin, D.W., Shaw, K.W. and Neuman, R.B., 1975, Geologic map of the east half of the Winston-Salem Quadrangle, North Carolina-Virginia: U.S. Geological Survey, Miscellaneous Investigations Series, Map I-709B.

Fullagar, P.D. and Bottino, M.L., 1970, Sulfide mineralization and rubidium-strontium geochronology at Ore Knob, North Carolina, and Ducktown, Tennessee: Economic Geology, v. 65, p. 541-550.

Gair, J.E. and Slack, J.F., 1984, Deformation, geochemistry , and origin of massive sulfide deposits, Gossan Lead District, Virginia: Economic Geology, v. 79, p. 1483-1520.

Gilmour, P. and Still, A.R., 1968, The geology of the Iron King Mine: in Ridge, J.D., ed., *Ore Deposits of the United States, 1933-1967 (Graton-Sales vol.)*: New York, American Institute of Mining, Metallurgical, and Petrolium Engineers, v. II, p. 1238-1257.

Glover, L.G. III, Spear, J.A., Russell, G.S. and Farrar, S.S., 1983, Ages of regional metamorphism and ductile deformation in the central and southern Appalachians: Lithos, v. 16, p. 223-245.

Goldfarb, M.S., Converse, D.R., Holland, H.D. and Edmond, J.M., 1983, The genesis of hot spring deposits on the East Pacific Rise, 21° N: in Ohmoto, H. and Skinner, B.J., eds., *The Kuroko and Related Volcanogenic Massive Sulfide Deposits*: Economic Geology Monograph 5, 184-197.

Hatcher, R.D., 1978, Tectonics of the western Piedmont and Blue Ridge, southern Appalachians: Review and speculation: American Journal of Science, v. 278, p. 276-304.

Henry, D.K., Craig, J.R. and Gilbert, M.C., 1979, Ore mineralogy of the Great Gossan Lead, Virginia: Economic Geology, v. 74, p. 645-656.

Hewett, R.L. and Solomon, P.J., 1964, The role of mobilisation in silver - lead - zinc sulphide assemblages, with particular reference to Mount Isa, Australia: in Sundaram, R.K., ed., International Geological Congress, Report of the 22nd Session, India, 1964: Part V, Genetic Problems of Ores, p. 571-595.

Kalogeropoulos, S.I. and Scott, S.D., 1983, Mineralogy and geochemistry of tuffaceous exhalite (tetsusekiei) of the Fukazawa Mine, Hokuroku District, Japan: in Ohmoto, H. and Skinner, B.J., eds., *The Kuroko and Related Volcanogenic Massive Sulfide Deposits*: Economic Geology Monograph 5, p., 412-432.

Kelly, W.C. and Clark, B.R., 1975, Sulfide deformation studies: III. Experimental deformation of chalcopyrite to 2000 bars and 500° C: Economic Geology, v. 70, p. 431-453.

Kinkel, A.R., Jr., 1967, The Ore Knob Copper Deposit, North Carolina, and other massive sulfide deposits of the Appalachians: U.S. Geological Survey Professional Paper 558, 58 p.

Kline, M.H. and Ballard, T.J., 1949, Investigation of the Great Gossan Lead, Carroll County, Virginia: U.S. Bureau of Mines, Report of Investigations 4532, 39 p.

LeHuray, A.P., 1982, Lead isotopic patterns of galena in the Piedmont and Blue Ridge ore deposits, southern Appalachians: Economic Geology, v. 77, p. 335-351.

LeHuray, A.P., 1984, Lead and sulfure isotopes and a model for the origin of the Ducktown Deposit, Tennessee: Economic Geology, v. 79, p, 1561-1573.

Lonsdale, P.F., Bischoff, J.L., Burns, V.M., Kastner, M. and Sweeney, R.E., 1980, A high-temperature hydrothermal deposit on the seabed at a Gulf of California spreading center: Earth and Planetary Science Letters, v. 49, p. 8-20.

Lonsdale, P. and Lawver, L.A., 1980, Immature plate boundary zones studied with a submersible in the Gulf of California: Geological Society of America Bulletin, Part I, v. 91, p. 555-569.

Magee, M., 1968, Geology and ore deposits of the Ducktown District, Tennessee: in Ridge, J.D., ed., *Ore Deposits of the United States, 1933-1967 (Graton-Sales Vol.)*: New York, American Institute of Mining, Metallurgical, and Petroleum Engineers, v. I, p. 207-241.

Mauger, R.L., 1972, A sulfur isotope study of the Ducktown Tennessee district, U. S. A.: Economic Geology, v. 67, p. 497-510.

McClay, K.R., 1979, Folding in silver - lead - zinc orebodies, Mount Isa, Australia: Transactions of the Institution of Mining and Metallurgy, Section B, v. 88, p. B5-B14.

Odom, A.L. and Fullagar, P.D., 1982, The time of opening of the Iapetus Ocean: Age of the Crossnore plutonic-volcanic group, southern Appalachians: Geological Society of America Abstracts with Programs, v. 14, p. 69.

Ojeda, H.A.O., 1982, Structural framework, stratigraphy, and evolution of Brazilian marginal basins: American Association of Petroleum Geologists Bulletin, v. 66, p. 732-749.

Pedersen, F.D., 1980, Remobilization of the massive sulfide ore of the Black Angel Mine, central west Greenland: Economic Geology, v. 75, p. 1022-1041.

Rankin, D.W., 1976, Appalachian salients and recesses: Late Precambrian continental breakup and the opening of the Iapetus Ocean: Journal of Geophysical Research, v. 81, p. 5605-5619.

Rankin, D.W., 1975, The continental margin of eastern North America in the southern Appalachians: The opening and closing of the proto-Atlantic Ocean: American Journal of Science, v. 275-A, p. 298-336.

Rankin, D.W., 1970, The Blue Ridge and the Reading Prong: stratigraphy and structure of Precambrian rocks in northwestern North Carolina: in Fisher, G.W., Pettijohn, F.J., Reed,

J.C. and Weaver, K.N., eds., *Studies of Appalachian Geology, Central and Southern*: New York, Wiley-Interscience, p. 227-245.

Rankin, D.W., Espenshade, G.H., and Shaw, K.W., 1973, Stratigraphy and structure of the metamorphic belt in northwestern North Carolina and southwestern Virginia: a study from the Blue Ridge across the Brevard Fault Zones to the Sauratown Mountains Anticlinorium: American Journal of Science, v. 273-A, p. 1-40.

Rankin, D.W., Stern, T.W., Reed, J.C. and Newell, M.F., 1969, Zircon ages of the felsic volcanic rocks in the upper Precambrian of the Blue Ridge, Appalachian Mountains: Science, v. 166, p. 741-744.

Ross, C.S., 1935, Origin of the copper deposits of the Ducktown type in the southern Appalachian region: U.S. Geological Survey Professional Paper 179, 165 p.

Rui, I., 1973, Structural control and wallrock alteration at Killingdal Mine, central Norwegian Caledonides: Economic Geology, v. 68, p. 859-883.

Slack, J.F., Gair, J.E. and Atelsek, P.J., 1985, Geochemistry of mafic rocks from part of the Ashe Formation, southwestern Virginia: Geological Society of America Abstracts with Programs, v. 17, p. 135.

Staten, W.T., 1976, A chemical study of the silicate minerals of the Great Gossan Lead and surrounding rocks in southwestern Virginia [M.S. thesis]: Virginia Polytechnic Institute and State University, Blacksburg, Virginia, 110 p.

Stose, A.J. and Stose, G.W., 1957, Geology and mineral resources of the Gossan Lead District and adjacent areas in Virginia: Virginia Division of Mineral Resources Bulletin 72, 233 p.

Tso, J.L., 1987, Geology of the Ashe Formation Between Fries and Galax, Virginia [Ph.d. dissert.]: Virginia Polytechnic Institute and State University, Blacksburg, Va., 343 p.

Vokes, F.M., 1969, A review of the metamorphism of sulphide deposits: Earth Science Review, v. 5, p. 99-143.

Wehr, F. and Glover, L. III, 1985, Stratigraphy and tectonics of the Virginia-North Carolina Blue Ridge: Evolution of a late Proterozoic-early Paleozoic hinge zone: Geological Society of America Bulletin, v. 96, p. 285-295.

Appendix A. Microprobe Analyses

Samples were analyzed on the automated ARL microprobe at the Department of Geological Sciences at Virginia Tech, as described in the text of Part II. The recalculation schemes were as follows:

Amphibole: Amphibole formulae were recalculated following the crystal chemical criteria of Robinson and others (1982). Numerous alternative methods of recalculating formulae are available. However, it was found that recalculations based on 13 cations except Ca, Na and K, with 22 oxygens and (OH + F + Cl) = 2 for a total of 46 charges, and variable Fe + 3/Fe + 2 to balance charges consistently violated none of the crystal chemical limitations for hornblende. Actinolites, however, favored the method of 15 cations, except K, with variable Fe + 3/Fe + 2.

Biotite: Calculations were based on 22 charges, with all Fe assumed to be FeO. (OH + F + Cl) = 2.0.

Chlorite: Chlorite was recalculated on the basis of 10 cations, so that ideally, O = 10, and (OH + Cl + F) = 8. Fe + 3 was calculated using the formula: Fe + 3 = Al(IV)-Al(VI)-Cr-2Ti, following the method of Laird and Albee (1981). In some cases, all Fe calculated as Fe + 2, leading

to a deficiency in negative charges. To compensate, an appropriate amount of OH was converted to O.

Clinozoisite and epidote: Clinozoisite/epidote was normalized assuming 8 cations. The Y-site was first filled with Al(VI) and Ti, with the remainder being Fe + 3. Any excess Fe was assumed to be Fe + 2, and placed in the X-site.

Feldspar: Feldspar was calculated on the basis of 16 charges, with all Fe assumed to be Fe + 2.

Garnet: Calculations were based on 8 cations and distributed as follows: all Si was put in the Z-site; any deficiencies were filled by Al; remaining Al, Cr, and Ti were placed in the Y-site, any deficiencies were filled by Fe + 3; remaining cations were placed in the X-site, Fe assumed to be Fe + 2. Endmember percentages were calculated using the method of Rickwood (1968).

Muscovite and paragonite: White mica recalculation followed the method of Laird and Albee (1981). Normalization was based on 6 cations except Na, K, Ca and Ba. Fe + 2 = Si (in excess of 3.0) - (Mg + Mn-Ti), with the remaining Fe assumed to be Fe + 3.

Staurolite: Staurolite formulae are based on 48 oxygens, with all Fe as Fe + 2, and H = 3.06 following the suggestion of Holdaway and others (1986) for staurolite that coexists with biotite or garnet.

In the tables that follow, the following abbreviations give information about the samples: in the core/rim heading, C = core L = large, random grain, R = rim, N = needle, S = small matrix grain; in the analysis heading, A = amphibolite, BFF = Bowers Ferry Fault block, C = chlorite schist, G = gneiss, My = mylonite, O = Gossan Lead ore zone, QMIN = 9 element analysis that includes Si, Al, Ti, Fe, Mg, Mn, Na, K, and Ca, with the concentration of other elements assumed equal to zero; S = schist.

References

Holdaway, M.J., Dutrow, B.L., and Shore, P., 1986, A model for the crystal chemistry of staurolite: American Mineralogist, v. 71, p. 1142-1159.

Laird, J., and Albee, A.L., 1981, High pressure metamorphism in mafic schist from northern Vermont: American Journal of Science, v. 281, p. 97-126.

Rickwood, P.C., 1968, On recasting analyses of garnet into end-member molecules: Contributions to Mineralogy and Petrology, v. 18, p. 175-198.

Robinson, P.L., Schumacher, J.C., and Spear, F.S., 1982, Formulation of electron probe analyses: in Veblin, D.R. and Ribbe, P.H., eds, *Amphibles: Petrology and Experimental Phase Relations*: Reviews in Mineralogy, Mineralogical Society of America, vol. 9B, p. 6-9.

AMPHIBOLE

SAMPLE NO.	A3-43B	A3-43B	A3-43B	A3-43B	A3-43B	A3-71A	A3-71A	A3-71A	A3-71A	A3-71A
ANALYSIS	02A	03A	07A	15A	17A	04A	05A	15A	16A	17A
CORE/RIM	L	L	N	L	N			C	C	R
SIO2	53.56	53.85	45.01	51.41	47.96	44.70	42.91	45.81	48.54	43.98
AL2O3	3.38	3.82	13.33	5.40	9.98	12.02	14.35	11.59	8.20	13.29
FE2O3(C)	2.73	1.91	4.15	3.45	4.61	3.00	3.15	4.00	3.58	3.17
TIO2	0.30	0.17	0.34	0.17	0.33	0.40	0.41	0.33	0.28	0.40
CR2O3	0.03	0.09	0.15	0.02	0.05	0.05	0.03	0.54	0.06	0.00
MGO	16.72	16.82	10.91	15.54	13.03	9.88	8.67	10.49	12.40	9.24
FEO(C)	8.19	8.76	10.48	8.39	9.00	13.74	13.85	12.32	11.76	13.72
MNO	0.35	0.32	0.33	0.38	0.37	0.28	0.31	0.33	0.32	0.38
CAO	12.55	12.15	11.64	12.43	11.90	11.86	11.31	11.63	11.99	11.69
NA2O	0.42	0.33	1.50	0.63	1.07	1.52	1.92	1.50	1.15	1.58
K2O	0.06	0.07	0.33	0.11	0.26	0.35	0.46	0.36	0.19	0.42
F	0.07	0.03	0.04	0.04	0.03	0.01	0.06	0.05	0.05	0.03
CL	0.00	0.02	0.00	0.00	0.01	0.02	0.00	0.01	0.00	0.00
H2O(C)	2.09	2.11	2.04	2.08	2.08	2.02	1.98	2.03	2.04	2.02
SUM	100.42	100.43	100.23	100.03	100.67	99.84	99.39	100.99	100.54	99.90
SI(T)	7.57	7.60	6.54	7.34	6.87	6.61	6.39	6.66	7.03	6.50
AL(T)	0.43	0.40	1.46	0.66	1.13	1.39	1.61	1.34	0.97	1.50
FE+3(T)	0.00	0.00	0.00	0.00	0.00	0.00	0.00	0.00	0.00	0.00
AL(M1)	0.14	0.23	0.82	0.25	0.56	0.70	0.91	0.65	0.43	0.82
FE+3(M1)	0.29	0.20	0.45	0.37	0.50	0.33	0.35	0.44	0.39	0.35
TI(M1)	0.03	0.02	0.04	0.02	0.04	0.04	0.05	0.04	0.03	0.04
CR(M1)	0.00	0.01	0.02	0.00	0.01	0.01	0.00	0.06	0.01	0.00
MG(M1)	3.52	3.54	2.36	3.31	2.78	2.18	1.93	2.27	2.68	2.04
FE+2(M1)	0.97	1.00	1.27	1.00	1.08	1.70	1.72	1.50	1.43	1.70
MN(M1)	0.04	0.00	0.04	0.05	0.05	0.04	0.04	0.04	0.04	0.05
CA(M1)	0.00	0.00	0.00	0.00	0.00	0.00	0.00	0.00	0.00	0.00
MG(M4)	0.00	0.00	0.00	0.00	0.00	0.00	0.00	0.00	0.00	0.00
FE+2(M4)	0.00	0.04	0.00	0.00	0.00	0.00	0.00	0.00	0.00	0.00
MN(M4)	0.00	0.04	0.00	0.00	0.00	0.00	0.00	0.00	0.00	0.00
CA(M4)	1.90	1.84	1.81	1.90	1.83	1.88	1.80	1.81	1.86	1.85
NA(M4)	0.10	0.09	0.19	0.10	0.17	0.12	0.20	0.19	0.14	0.15
CA(A)	0.00	0.00	0.00	0.00	0.00	0.00	0.00	0.00	0.00	0.00
NA(A)	0.02	0.00	0.23	0.07	0.12	0.31	0.36	0.24	0.18	0.31
K(A)	0.01	0.01	0.06	0.02	0.05	0.07	0.09	0.07	0.04	0.08
F	0.03	0.01	0.02	0.02	0.01	0.00	0.03	0.02	0.02	0.01
CL	0.00	0.00	0.00	0.00	0.00	0.00	0.00	0.00	0.00	0.00
OH(C)	1.97	1.98	1.98	1.98	1.99	1.99	1.97	1.97	1.98	1.99
O	22.00	22.00	22.00	22.00	22.00	22.00	22.00	22.00	22.00	22.00
FE/FE+MG	0.26	0.26	0.42	0.29	0.36	0.48	0.52	0.46	0.40	0.50
A	11.73	11.51	33.26	16.97	27.57	29.56	34.33	30.12	22.96	32.15
C	26.08	25.20	22.02	25.23	23.08	22.86	21.57	22.51	23.88	22.30
F	62.20	63.29	44.72	57.80	49.35	47.58	44.10	47.37	53.15	45.55

AMPHIBOLE

SAMPLE NO.	A3-71A	A3-71A	A3-92A	A3-92A	A3-92A	A4-22A	A4-22A	B2-4A	B2-4A	B2-24A
ANALYSIS	18A	19A	03A	09A	10A	14A	18A	05M	16M	19A
CORE/RIM	R	S	R	N	N	S	S		N	C
SIO2	43.09	47.79	53.98	53.76	53.15	43.38	49.73	43.58	45.33	54.96
AL2O3	14.33	9.40	2.57	3.02	4.04	16.55	8.84	15.54	13.71	2.70
FE2O3(C)	2.23	3.97	4.28	3.51	3.66	2.47	4.41	3.97	4.40	1.66
TIO2	0.39	0.22	0.08	0.05	0.05	0.46	0.20	0.41	0.37	0.10
CR2O3	0.02	0.05	0.01	0.05	0.05	0.06	0.07	0.02	0.04	0.09
MGO	8.55	11.44	17.60	17.05	16.60	8.69	13.39	9.18	10.25	17.26
FEO(C)	14.93	11.64	7.08	7.68	7.83	12.58	8.93	11.51	10.60	8.85
MNO	0.33	0.38	0.23	0.28	0.33	0.30	0.27	0.37	0.33	0.32
CAO	11.69	11.20	12.52	12.55	12.28	11.64	11.56	11.16	11.16	12.60
NA2O	1.88	1.40	0.31	0.33	0.39	1.20	0.99	1.60	1.31	0.27
K2O	0.43	0.37	0.05	0.05	0.09	0.46	0.20	0.43	0.44	0.05
F	0.09	0.08	0.02	0.07	0.03	0.15	0.24	0.06	0.04	0.02
CL	0.00	0.02	0.00	0.00	0.00	0.00	0.00	0.00	0.00	0.00
H2O(C)	1.98	2.01	2.12	2.09	2.11	1.98	1.99	2.02	2.05	2.13
SUM	99.90	99.95	100.85	100.46	100.60	99.86	100.72	99.82	100.03	101.00
SI(T)	6.40	6.97	7.59	7.59	7.51	6.35	7.08	6.38	6.58	7.71
AL(T)	1.60	1.03	0.41	0.41	0.49	1.65	0.92	1.62	1.42	0.29
FE+3(T)	0.00	0.00	0.00	0.00	0.00	0.00	0.00	0.00	0.00	0.00
AL(M1)	0.91	0.58	0.02	0.10	0.18	1.20	0.56	1.06	0.93	0.15
FE+3(M1)	0.25	0.44	0.45	0.37	0.39	0.27	0.47	0.44	0.48	0.18
TI(M1)	0.04	0.02	0.01	0.01	0.01	0.05	0.02	0.05	0.04	0.01
CR(M1)	0.00	0.01	0.00	0.01	0.00	0.01	0.01	0.00	0.00	0.01
MG(M1)	1.90	2.49	3.69	3.59	3.49	1.90	2.84	2.00	2.22	3.61
FE+2(M1)	1.86	1.42	0.83	0.91	0.93	1.54	1.06	1.41	1.29	1.04
MN(M1)	0.04	0.05	0.00	0.02	0.00	0.04	0.03	0.05	0.04	0.01
CA(M1)	0.00	0.00	0.00	0.00	0.00	0.00	0.00	0.00	0.00	0.00
MG(M4)	0.00	0.00	0.00	0.00	0.00	0.00	0.00	0.00	0.00	0.00
FE+2(M4)	0.00	0.00	0.00	0.00	0.00	0.00	0.00	0.00	0.00	0.00
MN(M4)	0.00	0.00	0.03	0.01	0.04	0.00	0.00	0.00	0.00	0.03
CA(M4)	1.86	1.75	1.89	1.90	1.86	1.82	1.76	1.75	1.74	1.89
NA(M4)	0.14	0.25	0.09	0.09	0.11	0.18	0.24	0.25	0.26	0.07
CA(A)	0.00	0.00	0.00	0.00	0.00	0.00	0.00	0.00	0.00	0.00
NA(A)	0.40	0.14	0.00	0.00	0.00	0.17	0.04	0.20	0.11	0.00
K(A)	0.08	0.07	0.01	0.01	0.02	0.09	0.04	0.08	0.08	0.01
F	0.04	0.04	0.01	0.03	0.01	0.07	0.11	0.03	0.02	0.01
CL	0.00	0.00	0.00	0.00	0.00	0.00	0.00	0.00	0.00	0.00
OH(C)	1.96	1.96	1.99	1.97	1.99	1.93	1.89	1.97	1.98	1.99
O	22.00	22.00	22.00	22.00	22.00	22.00	22.00	22.00	22.00	22.00
FE/FE+MG	0.53	0.43	0.26	0.26	0.27	0.49	0.35	0.48	0.44	0.25
A	32.80	26.44	12.02	11.98	14.38	37.10	25.55	37.45	34.86	8.62
C	22.12	22.56	25.79	26.00	25.18	21.66	23.03	21.02	21.41	26.31
F	45.08	51.00	62.19	62.02	60.44	41.23	51.42	41.53	43.73	65.07

AMPHIBOLE

SAMPLE NO.	B2-24A	B2-24A	B2-35C	B2-35C	B2-35C	B2-35C	B2-35C	B2-35C	B2-35C	B3-75A
ANALYSIS	20A	21A	03A	04	05A	06A	07A	08A	15A	08A
CORE/RIM	C	R	C	C	R	R	N	N	C	C
SIO2	55.40	52.74	43.87	43.61	42.70	42.29	42.00	42.30	43.54	45.59
AL2O3	2.08	5.18	15.03	15.89	16.59	16.58	18.32	17.95	15.80	12.75
FE2O3(C)	0.50	2.52	5.05	6.01	4.55	5.29	8.01	8.50	2.71	2.39
TIO2	0.02	0.12	0.32	0.36	0.30	0.30	0.35	0.30	0.33	0.36
CR2O3	0.25	0.14	0.18	0.18	0.14	0.13	0.22	0.16	0.05	0.05
MGO	17.37	15.35	9.13	9.13	8.69	8.74	8.76	8.98	9.07	10.40
FEO(C)	9.76	9.50	11.09	10.52	11.47	11.00	8.04	7.68	12.73	12.72
MNO	0.31	0.24	0.36	0.31	0.33	0.34	0.30	0.39	0.26	0.26
CAO	12.47	12.36	10.84	10.97	11.43	11.34	10.80	10.73	11.65	11.89
NA2O	0.18	0.54	1.65	1.63	1.37	1.47	1.37	1.44	1.51	1.37
K2O	0.05	0.16	0.44	0.44	0.46	0.46	0.38	0.36	0.44	0.27
F	0.03	0.04	0.12	0.13	0.14	0.18	0.20	0.20	0.17	0.05
CL	0.00	0.00	0.00	0.00	0.00	0.00	0.00	0.00	0.00	0.00
H2O(C)	2.11	2.10	1.99	2.01	1.98	1.96	1.98	1.99	1.97	2.03
SUM	100.52	100.98	100.01	101.13	100.06	100.01	100.65	100.90	100.17	100.10
SI(T)	7.81	7.45	6.41	6.30	6.25	6.20	6.06	6.09	6.37	6.65
AL(T)	0.19	0.55	1.59	1.70	1.75	1.80	1.94	1.91	1.63	1.35
FE+3(T)	0.00	0.00	0.00	0.00	0.00	0.00	0.00	0.00	0.00	0.00
AL(M1)	0.15	0.32	1.00	1.01	1.11	1.07	1.18	1.13	1.09	0.85
FE+3(M1)	0.05	0.27	0.56	0.65	0.50	0.58	0.87	0.92	0.30	0.26
TI(M1)	0.00	0.01	0.04	0.04	0.03	0.03	0.04	0.03	0.04	0.04
CR(M1)	0.03	0.02	0.02	0.02	0.02	0.02	0.02	0.02	0.01	0.01
MG(M1)	3.65	3.23	1.99	1.97	1.90	1.91	1.88	1.93	1.98	2.26
FE+2(M1)	1.12	1.12	1.35	1.27	1.40	1.35	0.97	0.92	1.56	1.55
MN(M1)	0.00	0.03	0.04	0.04	0.04	0.04	0.04	0.05	0.03	0.03
CA(M1)	0.00	0.00	0.00	0.00	0.00	0.00	0.00	0.00	0.00	0.00
MG(M4)	0.00	0.00	0.00	0.00	0.00	0.00	0.00	0.00	0.00	0.00
FE+2(M4)	0.03	0.00	0.00	0.00	0.00	0.00	0.00	0.00	0.00	0.00
MN(M4)	0.04	0.00	0.00	0.00	0.00	0.00	0.00	0.00	0.00	0.00
CA(M4)	1.88	1.87	1.70	1.70	1.79	1.78	1.67	1.65	1.83	1.86
NA(M4)	0.05	0.13	0.30	0.30	0.21	0.22	0.33	0.35	0.17	0.14
CA(A)	0.00	0.00	0.00	0.00	0.00	0.00	0.00	0.00	0.00	0.00
NA(A)	0.00	0.02	0.16	0.16	0.18	0.20	0.05	0.06	0.25	0.25
K(A)	0.01	0.03	0.08	0.08	0.09	0.09	0.07	0.07	0.08	0.05
F	0.01	0.02	0.05	0.06	0.07	0.08	0.09	0.09	0.08	0.02
CL	0.00	0.00	0.00	0.00	0.00	0.00	0.00	0.00	0.00	0.00
OH(C)	1.99	1.98	1.94	1.94	1.93	1.91	1.91	1.91	1.92	1.98
O	22.00	22.00	22.00	22.00	22.00	22.00	22.00	22.00	22.00	22.00
FE/FE+MG	0.25	0.30	0.49	0.50	0.50	0.50	0.49	0.49	0.48	0.44
A	5.59	15.30	38.21	40.31	39.59	40.43	46.64	46.55	35.91	30.08
C	26.46	25.33	20.62	20.38	21.09	20.88	19.53	19.43	21.70	22.78
F	67.95	59.36	41.18	39.32	39.32	38.69	33.83	34.02	42.39	47.14

AMPHIBOLE

SAMPLE NO.	B3-75A	B3-75A	B3-75A	B3-75A	B3-127A	B3-127A	B3-127A	B3-127A	B3-170A	B3-170A
ANALYSIS	09A	06A	10A	17A	05A	07A	09A	11A	100	220
CORE/RIM	C	R	R	N	R	C	C	R	N	C
SIO2	45.55	45.67	44.27	42.38	50.04	48.91	50.89	48.91	52.16	54.50
AL2O3	13.20	12.81	14.50	15.74	8.72	10.01	7.09	10.67	6.90	4.60
FE2O3(C)	2.60	1.64	3.84	4.18	2.91	5.54	1.66	5.04	2.94	3.73
TIO2	0.40	0.38	0.40	0.43	0.31	0.23	0.51	0.29	0.16	0.11
CR2O3	0.04	0.01	0.02	0.05	0.02	0.12	0.08	0.12	0.00	0.13
MGO	10.51	10.30	9.98	8.56	14.57	13.79	14.88	14.04	18.93	20.83
FEO(C)	12.49	13.40	11.71	12.16	8.32	6.72	9.36	6.56	1.86	0.23
MNO	0.27	0.25	0.29	0.41	0.29	0.39	0.33	0.34	1.06	1.13
CAO	11.99	11.97	11.90	11.31	12.11	11.43	12.30	11.74	12.53	12.30
NA2O	1.42	1.42	1.38	1.65	0.91	0.98	0.79	0.90	0.83	0.52
K2O	0.28	0.28	0.28	0.30	0.25	0.31	0.22	0.29	0.13	0.08
F	0.04	0.05	0.05	0.04	0.07	0.07	0.01	0.01	0.20	0.23
CL	0.00	0.01	0.00	0.00	0.00	0.00	0.01	0.00	0.00	0.01
H2O(C)	2.05	2.03	2.04	2.01	2.08	2.08	2.10	2.12	2.06	2.07
SUM	100.82	100.20	100.63	99.19	100.57	100.53	100.24	101.02	99.66	100.36
SI(T)	6.60	6.66	6.43	6.28	7.10	6.94	7.25	6.89	7.27	7.48
AL(T)	1.40	1.34	1.57	1.72	0.90	1.06	0.75	1.11	0.73	0.52
FE+3(T)	0.00	0.00	0.00	0.00	0.00	0.00	0.00	0.00	0.00	0.00
AL(M1)	0.85	0.87	0.92	1.03	0.55	0.61	0.44	0.66	0.40	0.22
FE+3(M1)	0.28	0.18	0.42	0.47	0.31	0.59	0.18	0.54	0.31	0.39
TI(M1)	0.04	0.04	0.04	0.05	0.03	0.02	0.05	0.03	0.02	0.01
CR(M1)	0.00	0.00	0.00	0.01	0.00	0.01	0.01	0.01	0.00	0.01
MG(M1)	2.27	2.24	2.16	1.89	3.08	2.92	3.16	2.95	3.93	4.26
FE+2(M1)	1.51	1.64	1.42	1.51	0.99	0.80	1.12	0.77	0.22	0.03
MN(M1)	0.03	0.03	0.04	0.05	0.04	0.05	0.04	0.04	0.13	0.08
CA(M1)	0.00	0.00	0.00	0.00	0.00	0.00	0.00	0.00	0.00	0.00
MG(M4)	0.00	0.00	0.00	0.00	0.00	0.00	0.00	0.00	0.00	0.00
FE+2(M4)	0.00	0.00	0.00	0.00	0.00	0.00	0.00	0.00	0.00	0.00
MN(M4)	0.00	0.00	0.00	0.00	0.00	0.00	0.00	0.00	0.00	0.05
CA(M4)	1.86	1.87	1.85	1.80	1.84	1.74	1.88	1.77	1.87	1.81
NA(M4)	0.14	0.13	0.15	0.20	0.16	0.26	0.12	0.23	0.13	0.14
CA(A)	0.00	0.00	0.00	0.00	0.00	0.00	0.00	0.00	0.00	0.00
NA(A)	0.26	0.27	0.24	0.27	0.09	0.01	0.10	0.02	0.10	0.00
K(A)	0.05	0.05	0.05	0.06	0.04	0.05	0.04	0.05	0.02	0.01
F	0.02	0.02	0.02	0.02	0.03	0.03	0.00	0.00	0.09	0.10
CL	0.00	0.00	0.00	0.00	0.00	0.00	0.00	0.00	0.00	0.00
OH(C)	1.98	1.98	1.98	1.98	1.97	1.97	1.99	1.99	1.91	1.90
O	22.00	22.00	22.00	22.00	22.00	22.00	22.00	22.00	22.00	22.00
FE/FE+MG	0.44	0.45	0.46	0.51	0.30	0.32	0.29	0.31	0.12	0.09
A	30.89	29.21	34.67	38.00	22.93	29.17	18.10	29.41	18.99	15.35
C	22.66	22.93	22.11	21.22	23.86	22.38	24.82	22.61	24.66	24.57
F	46.45	47.86	43.22	40.78	53.21	48.45	57.08	47.98	56.35	60.08

AMPHIBOLE

SAMPLE NO.	B4-1D	B4-1D	B4-1E	B4-1E	B4-7C	B4-7C.	B4-7C	B4-7C	B4-7C	B4-7C
ANALYSIS	130	140	060	070	12A	33A	16A	25A	26A	40A
CORE/RIM			R	R	S	S	S			S
SIO2	55.09	56.64	56.66	57.13	47.87	45.49	46.13	47.25	47.52	54.11
AL2O3	3.04	2.77	1.79	1.26	9.42	12.84	12.12	10.15	10.30	3.11
FE2O3(C)	3.31	1.68	1.14	0.65	2.61	1.86	3.34	2.19	2.41	2.50
TIO2	0.09	0.04	0.09	0.07	0.29	0.35	0.32	0.45	0.43	0.15
CR2O3	0.00	0.00	0.08	0.05	0.13	0.12	0.09	0.13	0.09	0.09
MGO	20.91	21.56	21.46	21.37	12.73	10.75	11.44	12.44	12.48	16.38
FEO(C)	0.47	1.88	2.84	3.49	10.96	12.51	10.96	10.98	10.77	9.33
MNO	1.43	1.37	1.11	1.11	0.34	0.35	0.38	0.36	0.37	0.36
CAO	12.47	12.27	12.39	12.61	12.18	11.94	12.01	12.07	12.09	12.47
NA2O	0.48	0.35	0.25	0.20	1.10	1.44	1.11	1.12	1.02	0.36
K2O	0.05	0.05	0.04	0.05	0.31	0.54	0.50	0.41	0.41	0.13
F	0.31	0.33	0.21	0.23	0.06	0.10	0.18	0.08	0.11	0.05
CL	0.00	0.00	0.01	0.00	0.00	0.00	0.02	0.00	0.00	0.00
H2O(C)	2.02	2.04	2.07	2.06	2.04	2.01	1.98	2.02	2.02	2.10
SUM	99.54	100.84	100.04	100.18	100.01	100.24	100.51	99.63	99.97	101.13
SI(T)	7.63	7.73	7.81	7.88	6.94	6.63	6.68	6.88	6.88	7.63
AL(T)	0.37	0.27	0.19	0.12	1.06	1.37	1.32	1.13	1.12	0.37
FE+3(T)	0.00	0.00	0.00	0.00	0.00	0.00	0.00	0.00	0.00	0.00
AL(M1)	0.13	0.18	0.10	0.08	0.55	0.84	0.75	0.62	0.64	0.14
FE+3(M1)	0.35	0.17	0.12	0.07	0.28	0.20	0.36	0.24	0.26	0.26
TI(M1)	0.01	0.00	0.01	0.01	0.03	0.04	0.04	0.05	0.05	0.02
CR(M1)	0.00	0.00	0.01	0.01	0.02	0.01	0.01	0.02	0.01	0.01
MG(M1)	4.32	4.39	4.41	4.39	2.75	2.34	2.47	2.70	2.69	3.44
FE+2(M1)	0.05	0.21	0.33	0.40	1.33	1.53	1.33	1.34	1.30	1.10
MN(M1)	0.15	0.05	0.03	0.05	0.04	0.04	0.05	0.05	0.05	0.03
CA(M1)	0.00	0.00	0.00	0.00	0.00	0.00	0.00	0.00	0.00	0.00
MG(M4)	0.00	0.00	0.00	0.00	0.00	0.00	0.00	0.00	0.00	0.00
FE+2(M4)	0.00	0.00	0.00	0.00	0.00	0.00	0.00	0.00	0.00	0.00
MN(M4)	0.02	0.11	0.10	0.08	0.00	0.00	0.00	0.00	0.00	0.02
CA(M4)	1.85	1.80	1.83	1.86	1.89	1.86	1.86	1.88	1.88	1.88
NA(M4)	0.13	0.09	0.07	0.05	0.11	0.13	0.14	0.12	0.12	0.10
CA(A)	0.00	0.00	0.00	0.00	0.00	0.00	0.00	0.00	0.00	0.00
NA(A)	0.00	0.00	0.00	0.00	0.20	0.27	0.18	0.20	0.16	0.00
K(A)	0.01	0.01	0.01	0.01	0.06	0.10	0.09	0.08	0.07	0.02
F	0.14	0.14	0.09	0.10	0.03	0.05	0.08	0.04	0.05	0.02
CL	0.00	0.00	0.00	0.00	0.00	0.00	0.01	0.00	0.00	0.00
OH(C)	1.86	1.86	1.91	1.90	1.97	1.95	1.91	1.96	1.95	1.98
O	22.00	22.00	22.00	22.00	22.00	22.00	22.00	22.00	22.00	22.00
FE/FE+MG	0.08	0.08	0.09	0.10	0.37	0.43	0.41	0.37	0.37	0.28
A	11.64	8.62	5.75	3.85	23.95	29.46	29.89	24.95	25.45	10.78
C	25.60	25.02	25.77	26.38	23.93	22.79	22.88	23.70	23.63	25.99
F	62.77	66.36	68.48	69.77	52.12	47.74	47.23	51.36	50.92	63.23

AMPHIBOLE

SAMPLE NO.	B4-8B	B4-8B	B4-11A	B4-11A	B4-11A	B4-11A	B4-11A	B4-11J	B4-11J	B4-11J
ANALYSIS	20G	21G	06A	07A	10A	11A	22A	130	160	220
CORE/RIM	N	N	N	N	C	C	N	N	S	C
SIO2	48.19	48.28	48.31	48.84	50.88	50.58	46.78	56.33	56.00	53.10
AL2O3	10.60	10.62	9.22	8.63	6.06	6.41	10.94	1.44	3.25	4.84
FE2O3(C)	5.48	4.20	2.82	2.08	2.75	2.90	3.39	2.78	3.47	5.52
TIO2	0.27	0.22	0.34	0.17	0.29	0.32	0.42	0.07	0.02	0.18
CR2O3	0.02	0.03	0.02	0.00	0.22	0.32	0.05	0.00	0.01	0.03
MGO	13.69	13.19	12.10	12.34	13.76	13.61	11.13	21.98	22.13	19.98
FEO(C)	7.05	8.40	12.13	12.48	10.98	10.96	12.15	1.80	0.00	0.34
MNO	0.52	0.48	0.26	0.26	0.29	0.29	0.35	1.38	1.12	1.21
CAO	12.06	12.04	12.21	12.23	12.21	12.18	11.93	12.00	12.10	11.58
NA2O	0.80	0.86	0.95	1.00	0.65	0.70	1.20	0.22	0.53	0.80
K2O	0.31	0.25	0.20	0.21	0.10	0.11	0.25	0.03	0.06	0.44
F	0.11	0.05	0.09	0.07	0.06	0.03	0.00	0.27	0.29	0.32
CL	0.00	0.00	0.00	0.01	0.00	0.01	0.00	0.00	0.00	0.00
H2O(C)	2.07	2.08	2.03	2.03	2.06	2.07	2.07	2.05	2.07	2.01
SUM	101.11	100.68	100.65	100.31	100.29	100.46	100.67	100.25	100.94	100.21
SI(T)	6.83	6.88	6.98	7.07	7.31	7.27	6.78	7.76	7.61	7.36
AL(T)	1.17	1.12	1.02	0.93	0.69	0.73	1.22	0.24	0.39	0.64
FE+3(T)	0.00	0.00	0.00	0.00	0.00	0.00	0.00	0.01	0.00	0.00
AL(M1)	0.60	0.66	0.55	0.55	0.34	0.35	0.65	0.00	0.13	0.15
FE+3(M1)	0.58	0.45	0.31	0.23	0.30	0.31	0.37	0.28	0.35	0.58
TI(M1)	0.03	0.02	0.04	0.02	0.03	0.03	0.05	0.01	0.00	0.02
CR(M1)	0.00	0.00	0.00	0.00	0.02	0.04	0.01	0.00	0.00	0.00
MG(M1)	2.89	2.80	2.61	2.66	2.95	2.91	2.41	4.51	4.48	4.13
FE+2(M1)	0.83	1.00	1.47	1.51	1.32	1.32	1.47	0.20	0.00	0.04
MN(M1)	0.06	0.06	0.03	0.03	0.04	0.04	0.04	0.00	0.03	0.08
CA(M1)	0.00	0.00	0.00	0.00	0.00	0.00	0.00	0.00	0.00	0.00
MG(M4)	0.00	0.00	0.00	0.00	0.00	0.00	0.00	0.00	0.00	0.00
FE+2(M4)	0.00	0.00	0.00	0.00	0.00	0.00	0.00	0.01	0.00	0.00
MN(M4)	0.00	0.00	0.00	0.00	0.00	0.00	0.00	0.16	0.10	0.06
CA(M4)	1.83	1.84	1.89	1.90	1.88	1.87	1.85	1.77	1.76	1.72
NA(M4)	0.17	0.16	0.11	0.10	0.12	0.13	0.15	0.06	0.14	0.21
CA(A)	0.00	0.00	0.00	0.00	0.00	0.00	0.00	0.00	0.00	0.00
NA(A)	0.05	0.07	0.16	0.18	0.06	0.07	0.19	0.00	0.00	0.00
K(A)	0.05	0.05	0.04	0.04	0.02	0.02	0.05	0.00	0.01	0.08
F	0.05	0.02	0.04	0.03	0.03	0.01	0.00	0.12	0.12	0.14
CL	0.00	0.00	0.00	0.00	0.00	0.00	0.00	0.00	0.00	0.00
OH(C)	1.95	1.98	1.96	1.97	1.97	1.98	2.00	1.88	1.88	1.86
O	22.00	22.00	22.00	22.00	22.00	22.00	22.00	22.00	21.99	22.00
FE/FE+MG	0.33	0.34	0.40	0.39	0.35	0.36	0.43	0.10	0.07	0.13
A	29.52	28.15	23.83	21.78	17.64	18.55	27.94	7.29	12.07	18.48
C	22.95	23.17	24.02	24.31	25.04	24.87	23.12	24.68	24.30	23.26
F	47.53	48.68	52.14	53.91	57.32	56.58	48.94	68.03	63.63	58.26

AMPHIBOLE

SAMPLE NO.	B4-11KA	B4-11KA	B4-11KA	B4-11KA	B4-11KA	B4-13A	B4-13A	B4-13A	B4-13A	B4-13A
ANALYSIS	050	060	110	150	190	03A	04A	05A	06A	18A
CORE/RIM	C	R	N	C	R	C	C	R	R	N
SIO2	52.17	55.78	56.66	55.14	55.30	44.26	45.56	43.46	43.65	48.46
AL2O3	6.08	1.56	1.10	3.43	3.36	14.75	12.98	16.06	16.10	9.63
FE2O3(C)	5.47	2.54	1.63	3.99	2.96	3.43	3.10	4.55	4.06	3.13
TIO2	0.20	0.04	0.06	0.09	0.07	0.49	0.39	0.45	0.49	0.38
CR2O3	0.02	0.00	0.03	0.01	0.01	0.17	0.26	0.10	0.09	0.08
MGO	18.75	20.60	21.07	20.96	20.56	10.67	11.45	10.02	9.98	13.42
FEO(C)	1.19	3.76	4.29	1.25	2.45	10.44	10.51	9.90	10.37	9.31
MNO	0.88	0.98	1.20	0.98	0.90	0.32	0.35	0.44	0.33	0.35
CAO	12.09	12.13	12.10	12.14	12.41	11.72	11.99	11.45	11.44	11.98
NA2O	0.80	0.25	0.13	0.49	0.36	1.48	1.28	1.54	1.60	1.10
K2O	0.12	0.03	0.03	0.08	0.06	0.45	0.40	0.49	0.48	0.25
F	0.20	0.24	0.23	0.16	0.22	0.03	0.07	0.06	0.05	0.03
CL	0.00	0.00	0.00	0.01	0.00	0.00	0.00	0.00	0.00	0.00
H2O(C)	2.06	2.04	2.06	2.11	2.07	2.05	2.04	2.04	2.05	2.07
SUM	99.94	99.85	100.51	100.77	100.65	100.26	100.35	100.52	100.67	100.17
SI(T)	7.27	7.77	7.83	7.56	7.61	6.42	6.59	6.29	6.31	6.95
AL(T)	0.73	0.23	0.17	0.44	0.39	1.58	1.41	1.71	1.69	1.05
FE+3(T)	0.00	0.00	0.00	0.00	0.00	0.00	0.00	0.00	0.00	0.00
AL(M1)	0.27	0.02	0.01	0.12	0.15	0.94	0.81	1.03	1.05	0.58
FE+3(M1)	0.57	0.27	0.17	0.41	0.31	0.37	0.34	0.50	0.44	0.34
TI(M1)	0.02	0.00	0.01	0.01	0.01	0.05	0.04	0.05	0.05	0.04
CR(M1)	0.00	0.00	0.00	0.00	0.00	0.02	0.03	0.01	0.01	0.01
MG(M1)	3.89	4.28	4.34	4.29	4.22	2.31	2.47	2.16	2.15	2.87
FE+2(M1)	0.14	0.43	0.46	0.14	0.28	1.27	1.27	1.20	1.25	1.12
MN(M1)	0.10	0.00	0.00	0.03	0.03	0.04	0.04	0.05	0.04	0.04
CA(M1)	0.00	0.00	0.00	0.00	0.00	0.00	0.00	0.00	0.00	0.00
MG(M4)	0.00	0.00	0.00	0.00	0.00	0.00	0.00	0.00	0.00	0.00
FE+2(M4)	0.00	0.01	0.03	0.00	0.00	0.00	0.00	0.00	0.00	0.00
MN(M4)	0.00	0.12	0.14	0.09	0.07	0.00	0.00	0.00	0.00	0.00
CA(M4)	1.81	1.81	1.79	1.78	1.83	1.82	1.86	1.78	1.77	1.84
NA(M4)	0.19	0.07	0.04	0.13	0.10	0.18	0.14	0.22	0.23	0.16
CA(A)	0.00	0.00	0.00	0.00	0.00	0.00	0.00	0.00	0.00	0.00
NA(A)	0.02	0.00	0.00	0.00	0.00	0.24	0.22	0.21	0.22	0.15
K(A)	0.02	0.00	0.00	0.01	0.01	0.08	0.07	0.09	0.09	0.05
F	0.09	0.11	0.10	0.07	0.10	0.02	0.03	0.03	0.02	0.02
CL	0.00	0.00	0.00	0.00	0.00	0.00	0.00	0.00	0.00	0.00
OH(C)	1.91	1.90	1.90	1.93	1.90	1.98	1.97	1.97	1.98	1.98
O	22.00	22.00	22.00	22.00	22.00	22.00	22.00	22.00	22.00	22.00
FE/FE+MG	0.15	0.14	0.13	0.12	0.12	0.42	0.39	0.44	0.44	0.34
A	20.92	7.28	4.91	13.25	11.68	34.76	31.14	38.41	37.90	25.09
C	24.03	25.27	25.17	24.46	25.11	21.86	22.68	21.08	21.10	23.50
F	55.05	67.45	69.92	62.29	63.21	43.38	46.18	40.52	41.00	51.41

AMPHIBOLE

SAMPLE NO.	B4-13A	B4-13A	B4-100A	B4-100A	B4-100A	B4-100A	B4-100A	C3-4A	C3-4A	C3-4A
ANALYSIS	19A	20A	01A	04A	05A	07A	14A	01A	02A	07A
CORE/RIM	N	N	C	R	N	C	S	C	R	S
SIO2	51.73	46.64	56.80	56.20	55.63	56.64	56.39	46.71	45.38	49.24
AL2O3	5.96	11.94	0.26	0.19	0.72	0.23	0.24	12.10	13.52	9.88
FE2O3(C)	4.31	3.10	1.34	1.69	1.84	1.26	2.29	4.10	4.65	4.02
TIO2	0.10	0.37	0.00	0.02	0.01	0.05	0.03	0.52	0.52	0.27
CR2O3	0.07	0.11	0.10	0.07	0.04	0.10	0.04	0.40	0.38	0.00
MGO	15.69	12.06	20.18	20.07	19.64	20.08	20.06	12.19	11.54	13.56
FEO(C)	7.48	10.41	7.04	6.51	6.85	7.48	6.83	9.56	9.04	8.67
MNO	0.39	0.30	0.24	0.28	0.26	0.25	0.31	0.28	0.28	0.33
CAO	11.61	11.88	12.48	12.49	12.29	12.12	12.28	12.00	11.70	11.90
NA2O	0.65	1.39	0.05	0.06	0.07	0.06	0.08	1.22	1.31	1.03
K2O	0.16	0.42	0.10	0.10	0.10	0.10	0.10	0.25	0.27	0.21
F	0.04	0.01	0.02	0.08	0.05	0.03	0.03	0.03	0.00	0.12
CL	0.00	0.01	0.00	0.00	0.00	0.01	0.00	0.01	0.00	0.01
H2O(C)	2.10	2.08	2.15	2.10	2.11	2.13	2.14	2.09	2.09	2.06
SUM	100.29	100.69	100.74	99.81	99.57	100.52	100.80	101.45	100.68	101.24
SI(T)	7.33	6.71	7.90	7.89	7.84	7.90	7.86	6.66	6.52	6.97
AL(T)	0.67	1.29	0.04	0.03	0.12	0.04	0.04	1.34	1.48	1.03
FE+3(T)	0.00	0.00	0.06	0.08	0.04	0.06	0.10	0.00	0.00	0.00
AL(M1)	0.33	0.74	0.00	0.00	0.00	0.00	0.00	0.69	0.81	0.62
FE+3(M1)	0.46	0.34	0.08	0.10	0.15	0.07	0.14	0.44	0.50	0.43
TI(M1)	0.01	0.04	0.00	0.00	0.00	0.00	0.00	0.06	0.06	0.03
CR(M1)	0.01	0.01	0.01	0.01	0.00	0.01	0.00	0.05	0.04	0.00
MG(M1)	3.31	2.59	4.18	4.20	4.13	4.18	4.17	2.59	2.47	2.86
FE+2(M1)	0.88	1.25	0.72	0.69	0.71	0.73	0.69	1.14	1.09	1.03
MN(M1)	0.00	0.04	0.00	0.00	0.00	0.00	0.00	0.03	0.03	0.04
CA(M1)	0.00	0.00	0.00	0.00	0.00	0.00	0.00	0.00	0.00	0.00
MG(M4)	0.00	0.00	0.00	0.00	0.00	0.00	0.00	0.00	0.00	0.00
FE+2(M4)	0.01	0.00	0.10	0.07	0.09	0.14	0.11	0.00	0.00	0.00
MN(M4)	0.05	0.00	0.03	0.03	0.03	0.03	0.04	0.00	0.00	0.00
CA(M4)	1.76	1.83	1.86	1.88	1.85	1.81	1.83	1.83	1.80	1.80
NA(M4)	0.18	0.17	0.01	0.02	0.02	0.02	0.02	0.17	0.20	0.20
CA(A)	0.00	0.00	0.00	0.00	0.00	0.00	0.00	0.00	0.00	0.00
NA(A)	0.00	0.22	0.00	0.00	0.00	0.00	0.00	0.17	0.17	0.09
K(A)	0.03	0.08	0.02	0.02	0.02	0.02	0.02	0.05	0.05	0.04
F	0.02	0.01	0.01	0.04	0.02	0.01	0.01	0.01	0.00	0.05
CL	0.00	0.00	0.00	0.00	0.00	0.00	0.00	0.00	0.00	0.00
OH(C)	1.98	1.99	1.99	1.97	1.98	1.99	1.99	1.98	2.00	1.95
O	22.00	22.00	22.00	22.00	22.00	22.00	22.00	22.00	22.00	22.00
FE/FE+MG	0.29	0.38	0.19	0.18	0.19	0.19	0.20	0.38	0.39	0.34
A	19.50	29.25	2.59	2.96	4.41	2.41	3.93	30.63	34.10	26.59
C	23.62	22.70	26.29	26.52	26.01	25.66	25.77	22.71	22.01	23.11
F	56.88	48.05	71.13	70.52	69.59	71.93	70.30	46.65	43.88	50.29

AMPHIBOLE

SAMPLE NO.	C3-4A	C3-4A	C3-4A	C3-4A	C3-4A	C3-5A	C3-5A	C3-5A	C3-5A	C3-5A
ANALYSIS	08A	12A	13A	17A	21A	01A	02A	05A	11A	12A
CORE/RIM	N	C	C	N	C	C	C	R	C	R
SIO2	42.67	44.83	45.70	49.31	47.04	49.47	49.56	53.63	49.66	50.04
AL2O3	18.86	14.29	14.03	8.81	11.11	9.16	8.47	4.77	8.18	8.94
FE2O3(C)	8.12	5.00	5.06	4.94	3.72	2.88	3.83	2.49	4.19	4.51
TIO2	0.47	0.50	0.40	0.31	0.44	0.29	0.31	0.10	0.25	0.34
CR2O3	0.00	0.49	0.38	0.04	0.78	0.45	0.93	0.07	0.97	0.07
MGO	10.26	11.18	11.28	14.01	12.40	14.75	15.21	17.32	15.18	15.25
FEO(C)	5.92	9.33	9.36	7.65	9.30	7.70	6.55	7.98	6.49	6.23
MNO	0.36	0.31	0.27	0.27	0.26	0.22	0.20	0.27	0.19	0.24
CAO	11.21	11.86	11.86	11.88	11.86	11.90	11.85	10.97	11.71	11.73
NA2O	1.31	1.35	1.23	0.75	1.06	1.30	1.19	0.59	1.24	1.16
K2O	0.34	0.35	0.28	0.13	0.23	0.19	0.18	0.15	0.18	0.21
F	0.15	0.04	0.03	0.01	0.00	0.02	0.01	0.05	0.02	0.00
CL	0.02	0.00	0.00	0.02	0.00	0.02	0.00	0.00	0.00	0.00
H2O(C)	2.04	2.08	2.10	2.09	2.08	2.10	2.11	2.11	2.11	2.13
SUM	101.67	101.59	101.94	100.22	100.29	100.43	100.39	100.49	100.35	100.84
SI(T)	6.04	6.41	6.49	7.03	6.77	7.02	7.02	7.53	7.05	7.04
AL(T)	1.96	1.59	1.51	0.97	1.23	0.98	0.98	0.47	0.95	0.96
FE+3(T)	0.00	0.00	0.00	0.00	0.00	0.00	0.00	0.00	0.00	0.00
AL(M1)	1.18	0.82	0.84	0.51	0.65	0.55	0.44	0.31	0.41	0.52
FE+3(M1)	0.87	0.54	0.54	0.53	0.40	0.31	0.41	0.26	0.45	0.48
TI(M1)	0.05	0.05	0.04	0.03	0.05	0.03	0.03	0.01	0.03	0.04
CR(M1)	0.00	0.06	0.04	0.00	0.09	0.05	0.10	0.01	0.11	0.01
MG(M1)	2.16	2.38	2.39	2.98	2.66	3.12	3.21	3.62	3.21	3.20
FE+2(M1)	0.70	1.11	1.11	0.91	1.12	0.91	0.78	0.78	0.77	0.73
MN(M1)	0.04	0.04	0.03	0.03	0.03	0.03	0.02	0.00	0.02	0.03
CA(M1)	0.00	0.00	0.00	0.00	0.00	0.00	0.00	0.00	0.00	0.00
MG(M4)	0.00	0.00	0.00	0.00	0.00	0.00	0.00	0.00	0.00	0.00
FE+2(M4)	0.00	0.00	0.00	0.00	0.00	0.00	0.00	0.16	0.00	0.00
MN(M4)	0.00	0.00	0.00	0.00	0.00	0.00	0.00	0.03	0.00	0.00
CA(M4)	1.70	1.82	1.81	1.81	1.83	1.81	1.80	1.65	1.78	1.77
NA(M4)	0.30	0.18	0.19	0.19	0.17	0.19	0.20	0.16	0.22	0.23
CA(A)	0.00	0.00	0.00	0.00	0.00	0.00	0.00	0.00	0.00	0.00
NA(A)	0.06	0.19	0.14	0.02	0.12	0.17	0.13	0.00	0.12	0.08
K(A)	0.06	0.06	0.05	0.02	0.04	0.03	0.03	0.03	0.03	0.04
F	0.07	0.02	0.01	0.00	0.00	0.01	0.00	0.02	0.01	0.00
CL	0.01	0.00	0.00	0.00	0.00	0.00	0.00	0.00	0.00	0.00
OH(C)	1.93	1.98	1.99	1.99	2.00	1.98	2.00	1.98	1.99	2.00
O	22.00	22.00	22.00	22.00	22.00	22.00	22.00	22.00	22.00	22.00
FE/FE+MG	0.42	0.41	0.41	0.33	0.36	0.28	0.27	0.25	0.27	0.27
A	46.53	35.50	35.12	25.94	28.85	23.86	23.89	14.41	23.89	25.49
C	19.73	21.90	21.94	23.42	23.07	23.48	23.56	22.62	23.42	22.99
F	33.74	42.60	42.95	50.64	48.09	52.67	52.55	62.97	52.69	51.52

AMPHIBOLE

SAMPLE NO.	C3-5A	C3-5A	C3-17D	C3-17D	C3-17D	C3-17D	C3-17D	C3-17D	C3-17D	C3-27AA
ANALYSIS	13A	20A	04A	17A	18A	19A	21A	23A	24A	01A
CORE/RIM	N	N	S	L	N	N	C	N	N	C
SIO2	49.92	53.51	44.91	45.50	45.38	45.49	45.74	46.17	45.37	44.75
AL2O3	9.02	4.15	13.31	12.39	13.36	12.46	12.33	12.12	13.23	14.22
FE2O3(C)	3.90	2.47	3.65	3.34	5.56	3.98	3.97	4.49	5.10	3.22
TIO2	0.31	0.13	0.64	0.61	0.46	0.49	0.54	0.49	0.57	0.38
CR2O3	0.06	0.02	0.11	0.28	0.07	0.26	0.28	0.13	0.11	0.38
MGO	14.87	17.63	10.98	11.37	11.43	11.55	11.70	12.02	11.45	11.26
FEO(C)	7.00	6.40	10.92	10.70	9.15	10.45	10.06	9.36	9.39	10.25
MNO	0.21	0.17	0.31	0.27	0.29	0.34	0.31	0.31	0.30	0.24
CAO	11.77	12.10	11.78	11.83	11.52	11.88	11.76	11.66	11.49	12.15
NA2O	1.06	0.50	1.61	1.40	1.59	1.62	1.55	1.50	1.65	1.37
K2O	0.23	0.12	0.23	0.19	0.21	0.20	0.17	0.16	0.23	0.25
F	0.07	0.03	0.05	0.11	0.07	0.06	0.03	0.05	0.14	0.08
CL	0.00	0.00	0.01	0.01	0.00	0.02	0.01	0.00	0.01	0.00
H2O(C)	2.09	2.11	2.04	2.01	2.06	2.04	2.06	2.06	2.02	2.04
SUM	100.48	99.34	100.54	99.96	101.12	100.79	100.48	100.49	101.00	100.56
SI(T)	7.06	7.57	6.51	6.61	6.51	6.57	6.61	6.65	6.52	6.46
AL(T)	0.94	0.43	1.49	1.39	1.49	1.43	1.39	1.35	1.48	1.54
FE+3(T)	0.00	0.00	0.00	0.00	0.00	0.00	0.00	0.00	0.00	0.00
AL(M1)	0.56	0.26	0.78	0.74	0.76	0.69	0.71	0.70	0.76	0.88
FE+3(M1)	0.42	0.26	0.40	0.37	0.60	0.43	0.43	0.49	0.55	0.35
TI(M1)	0.03	0.01	0.07	0.07	0.05	0.05	0.06	0.05	0.06	0.04
CR(M1)	0.01	0.00	0.01	0.03	0.01	0.03	0.03	0.01	0.01	0.04
MG(M1)	3.13	3.72	2.37	2.47	2.44	2.49	2.52	2.58	2.45	2.42
FE+2(M1)	0.83	0.75	1.32	1.30	1.10	1.26	1.22	1.13	1.13	1.24
MN(M1)	0.02	0.00	0.04	0.03	0.04	0.04	0.04	0.04	0.04	0.03
CA(M1)	0.00	0.00	0.00	0.00	0.00	0.00	0.00	0.00	0.00	0.00
MG(M4)	0.00	0.00	0.00	0.00	0.00	0.00	0.00	0.00	0.00	0.00
FE+2(M4)	0.00	0.01	0.00	0.00	0.00	0.00	0.00	0.00	0.00	0.00
MN(M4)	0.00	0.02	0.00	0.00	0.00	0.00	0.00	0.00	0.00	0.00
CA(M4)	1.78	1.83	1.83	1.84	1.77	1.84	1.82	1.80	1.77	1.88
NA(M4)	0.22	0.14	0.17	0.16	0.23	0.16	0.18	0.20	0.23	0.12
CA(A)	0.00	0.00	0.00	0.00	0.00	0.00	0.00	0.00	0.00	0.00
NA(A)	0.07	0.00	0.28	0.24	0.21	0.29	0.25	0.22	0.23	0.26
K(A)	0.04	0.02	0.04	0.04	0.04	0.04	0.03	0.03	0.04	0.05
F	0.03	0.01	0.02	0.05	0.03	0.03	0.01	0.02	0.06	0.04
CL	0.00	0.00	0.00	0.00	0.00	0.00	0.00	0.00	0.00	0.00
OH(C)	1.97	1.99	1.97	1.95	1.97	1.97	1.98	1.98	1.94	1.96
O	22.00	22.00	22.00	22.00	22.00	22.00	22.00	22.00	22.00	22.00
FE/FE+MG	0.28	0.21	0.42	0.40	0.41	0.40	0.39	0.38	0.41	0.40
A	24.96	13.11	32.44	30.60	34.83	31.22	31.15	31.44	34.14	33.21
C	23.19	25.17	22.21	22.68	21.57	22.46	22.41	22.25	21.63	22.54
F	51.85	61.72	45.35	46.72	43.60	46.32	46.44	46.31	44.24	44.25

AMPHIBOLE

SAMPLE NO.	C3-27AA	C3-27AA	C3-27AA	C3-27AA	C3-27AA	C3-32B	C3-32B	C3-32B	C3-32B	C3-55AA
ANALYSIS	02A	03A	10A	04A	06A	06A	18A	19A	23A	04G
CORE/RIM	R	C		C	S	N	N	N	N	N
SIO2	46.00	43.23	49.38	44.86	42.88	56.19	55.99	56.15	51.59	48.60
AL2O3	13.43	15.40	9.36	14.30	17.08	1.52	1.20	1.38	6.25	9.13
FE2O3(C)	4.12	4.83	4.77	4.94	4.00	0.70	1.07	0.71	5.42	5.96
TIO2	0.33	0.51	0.38	0.54	0.44	0.04	0.06	0.06	0.25	0.43
CR2O3	0.13	0.24	0.04	0.33	0.13	0.13	0.15	0.21	0.29	0.02
MGO	12.05	10.70	14.41	11.24	9.81	19.83	19.92	19.77	17.32	13.19
FEO(C)	9.23	9.37	7.70	9.10	10.26	6.82	6.22	6.62	3.60	8.68
MNO	0.26	0.25	0.20	0.29	0.29	0.16	0.13	0.16	0.16	0.38
CAO	12.21	11.91	12.30	11.70	11.85	11.80	11.90	11.89	11.55	11.75
NA2O	1.22	1.40	0.86	1.41	1.44	0.28	0.31	0.32	1.09	1.02
K2O	0.17	0.30	0.14	0.30	0.36	0.04	0.04	0.05	0.07	0.29
F	0.08	0.12	0.08	0.04	0.02	0.00	0.06	0.04	0.08	0.05
CL	0.01	0.00	0.00	0.00	0.01	0.00	0.00	0.00	0.00	0.01
H2O(C)	2.06	2.01	2.09	2.07	2.06	2.14	2.11	2.12	2.10	2.08
SUM	101.27	100.21	101.69	101.10	100.62	99.65	99.14	99.46	99.74	101.56
SI(T)	6.56	6.27	6.95	6.43	6.20	7.86	7.87	7.87	7.26	6.91
AL(T)	1.44	1.73	1.05	1.57	1.80	0.14	0.13	0.13	0.74	1.09
FE+3(T)	0.00	0.00	0.00	0.00	0.00	0.00	0.00	0.00	0.00	0.00
AL(M1)	0.82	0.91	0.50	0.85	1.11	0.11	0.07	0.10	0.29	0.44
FE+3(M1)	0.44	0.53	0.50	0.53	0.44	0.07	0.11	0.07	0.57	0.64
TI(M1)	0.04	0.06	0.04	0.06	0.05	0.00	0.01	0.01	0.03	0.05
CR(M1)	0.02	0.03	0.00	0.04	0.01	0.01	0.02	0.02	0.03	0.00
MG(M1)	2.56	2.31	3.02	2.40	2.12	4.14	4.17	4.13	3.63	2.80
FE+2(M1)	1.10	1.14	0.91	1.09	1.24	0.66	0.62	0.67	0.42	1.03
MN(M1)	0.03	0.03	0.02	0.04	0.04	0.00	0.00	0.00	0.02	0.05
CA(M1)	0.00	0.00	0.00	0.00	0.00	0.00	0.00	0.00	0.00	0.00
MG(M4)	0.00	0.00	0.00	0.00	0.00	0.00	0.00	0.00	0.00	0.00
FE+2(M4)	0.00	0.00	0.00	0.00	0.00	0.14	0.11	0.11	0.00	0.00
MN(M4)	0.00	0.00	0.00	0.00	0.00	0.02	0.02	0.02	0.00	0.00
CA(M4)	1.86	1.85	1.85	1.80	1.84	1.77	1.79	1.79	1.74	1.79
NA(M4)	0.13	0.15	0.15	0.20	0.16	0.08	0.09	0.09	0.26	0.21
CA(A)	0.00	0.00	0.00	0.00	0.00	0.00	0.00	0.00	0.00	0.00
NA(A)	0.20	0.25	0.09	0.19	0.24	0.00	0.00	0.00	0.04	0.07
K(A)	0.03	0.06	0.02	0.05	0.07	0.01	0.01	0.01	0.01	0.05
F	0.04	0.05	0.04	0.02	0.01	0.00	0.03	0.02	0.04	0.02
CL	0.00	0.00	0.00	0.00	0.00	0.00	0.00	0.00	0.00	0.00
OH(C)	1.96	1.95	1.96	1.98	1.99	2.00	1.97	1.98	1.97	1.97
O	22.00	22.00	22.00	22.00	22.00	22.00	22.00	22.00	22.00	22.00
FE/FE+MG	0.38	0.42	0.32	0.40	0.44	0.17	0.17	0.17	0.21	0.37
A	32.69	37.20	26.17	35.64	39.02	4.60	4.44	4.32	21.68	27.67
C	22.59	21.80	23.57	21.72	21.41	25.10	25.51	25.45	23.44	22.87
F	44.73	41.00	50.26	42.64	39.57	70.30	70.05	70.23	54.89	49.47

AMPHIBOLE

SAMPLE NO.	C3-77A	C3-77A	C3-77A	C3116AA	C3116AA	C3116AA	C3116AA	C3116AA	C3116AA	C3116AA
ANALYSIS	08A	10A	13A	11A	13A	24A	31A	44A	45A	46A
CORE/RIM	N	C	R	S	S	R	L	N	L	C
SIO2	43.82	46.12	44.02	43.77	44.70	45.04	47.85	44.46	43.62	44.72
AL2O3	13.05	11.09	13.76	16.99	14.88	14.10	11.46	15.47	16.48	14.71
FE2O3(C)	3.13	2.20	4.54	3.72	4.19	3.17	3.35	3.47	3.57	2.77
TIO2	0.40	0.58	0.54	0.37	0.51	0.42	0.21	0.51	0.43	0.45
CR2O3	0.12	0.28	0.09	0.13	0.12	0.11	0.01	0.07	0.08	0.04
MGO	9.08	10.27	9.08	9.69	11.13	11.45	13.07	11.44	11.25	11.29
FEO(C)	14.16	14.36	13.27	10.52	8.90	9.31	8.69	8.85	8.53	9.72
MNO	0.33	0.24	0.33	0.21	0.37	0.28	0.23	0.26	0.27	0.32
CAO	11.66	12.00	11.50	11.59	11.68	11.73	12.05	11.86	11.84	11.86
NA2O	1.61	1.42	1.68	1.43	1.30	1.30	0.99	1.43	1.59	1.40
K2O	0.46	0.35	0.42	0.35	0.24	0.22	0.16	0.26	0.27	0.27
F	0.07	0.09	0.03	0.05	0.00	0.00	0.00	0.09	0.13	0.04
CL	0.00	0.02	0.00	0.00	0.01	0.00	0.01	0.00	0.00	0.00
H2O(C)	1.98	2.01	2.04	2.06	2.08	2.06	2.10	2.04	2.02	2.05
SUM	99.84	101.01	101.29	100.87	100.09	99.20	100.17	100.18	100.04	99.62
SI(T)	6.50	6.73	6.43	6.29	6.44	6.54	6.84	6.39	6.28	6.48
AL(T)	1.50	1.27	1.57	1.71	1.56	1.46	1.16	1.61	1.72	1.52
FE+3(T)	0.00	0.00	0.00	0.00	0.00	0.00	0.00	0.00	0.00	0.00
AL(M1)	0.79	0.64	0.80	1.17	0.97	0.95	0.77	1.01	1.08	0.99
FE+3(M1)	0.35	0.24	0.50	0.40	0.45	0.35	0.36	0.38	0.39	0.30
TI(M1)	0.05	0.06	0.06	0.04	0.06	0.05	0.02	0.06	0.05	0.05
CR(M1)	0.01	0.03	0.01	0.02	0.01	0.01	0.00	0.01	0.01	0.00
MG(M1)	2.01	2.24	1.98	2.08	2.39	2.48	2.78	2.45	2.42	2.44
FE+2(M1)	1.76	1.75	1.62	1.27	1.07	1.13	1.04	1.06	1.03	1.18
MN(M1)	0.04	0.03	0.04	0.03	0.05	0.03	0.03	0.03	0.03	0.04
CA(M1)	0.00	0.00	0.00	0.00	0.00	0.00	0.00	0.00	0.00	0.00
MG(M4)	0.00	0.00	0.00	0.00	0.00	0.00	0.00	0.00	0.00	0.00
FE+2(M4)	0.00	0.00	0.00	0.00	0.00	0.00	0.00	0.00	0.00	0.00
MN(M4)	0.00	0.00	0.00	0.00	0.00	0.00	0.00	0.00	0.00	0.00
CA(M4)	1.85	1.88	1.80	1.79	1.80	1.82	1.84	1.83	1.83	1.84
NA(M4)	0.15	0.12	0.20	0.21	0.20	0.18	0.16	0.17	0.17	0.16
CA(A)	0.00	0.00	0.00	0.00	0.00	0.00	0.00	0.00	0.00	0.00
NA(A)	0.32	0.28	0.27	0.19	0.17	0.19	0.12	0.23	0.27	0.24
K(A)	0.09	0.07	0.08	0.06	0.04	0.04	0.03	0.05	0.05	0.05
F	0.04	0.04	0.01	0.02	0.00	0.00	0.00	0.04	0.06	0.02
CL	0.00	0.00	0.00	0.00	0.00	0.00	0.00	0.00	0.00	0.00
OH(C)	1.96	1.95	1.99	1.98	2.00	2.00	2.00	1.96	1.94	1.98
O	22.00	22.00	22.00	22.00	22.00	22.00	22.00	22.00	22.00	22.00
FE/FE+MG	0.51	0.47	0.52	0.44	0.39	0.37	0.33	0.37	0.37	0.38
A	31.74	26.73	34.52	38.90	35.94	33.54	28.67	35.80	37.51	33.85
C	22.36	23.33	21.67	21.17	21.74	22.18	23.10	21.82	21.53	22.16
F	45.90	49.95	43.81	39.93	42.32	44.27	48.23	42.37	40.96	43.98

AMPHIBOLE

SAMPLE NO.	C3116AA	C3-117A	C3-117A	C3-117A	C3-117A	C3-117B	C3-117B	C3-117B	C3-117B	C3-117B
ANALYSIS	47A	09A	11A	39A	41A	14A	15A	16A	17A	18A
CORE/RIM	R	S	S	N	N	R	C	C	C	C
SIO2	45.23	43.08	43.52	43.10	43.34	47.08	46.01	45.99	47.96	45.59
AL2O3	14.50	16.57	16.92	17.80	17.06	11.91	13.56	13.13	11.47	13.61
FE2O3(C)	2.49	5.85	4.37	4.12	3.24	3.89	3.17	2.58	3.92	3.44
TIO2	0.50	0.57	0.55	0.34	0.45	0.79	0.40	0.58	0.23	0.61
CR2O3	0.09	0.00	0.03	0.00	0.03	0.08	0.52	0.50	0.16	0.33
MGO	11.43	8.59	8.25	7.59	7.89	12.07	11.04	11.08	12.30	11.06
FEO(C)	10.10	10.81	12.16	12.57	13.20	9.21	10.36	10.77	9.27	10.17
MNO	0.26	0.26	0.17	0.26	0.26	0.25	0.43	0.35	0.25	0.33
CAO	11.91	11.25	11.28	11.36	11.42	11.57	11.48	11.59	11.62	11.69
NA2O	1.49	1.03	1.09	1.00	1.15	0.96	1.51	1.38	1.02	1.21
K2O	0.26	0.50	0.58	0.48	0.54	0.28	0.33	0.29	0.24	0.32
F	0.05	0.12	0.11	0.18	0.14	0.09	0.06	0.06	0.08	0.06
CL	0.00	0.03	0.04	0.04	0.00	0.00	0.00	0.00	0.00	0.00
H2O(C)	2.06	2.00	2.01	1.97	1.99	2.05	2.06	2.05	2.06	2.05
SUM	100.34	100.61	101.02	100.72	100.66	100.19	100.89	100.32	100.55	100.45
SI(T)	6.51	6.26	6.30	6.26	6.31	6.76	6.60	6.64	6.85	6.57
AL(T)	1.49	1.74	1.70	1.74	1.69	1.24	1.40	1.36	1.15	1.43
FE+3(T)	0.00	0.00	0.00	0.00	0.00	0.00	0.00	0.00	0.00	0.00
AL(M1)	0.97	1.09	1.19	1.31	1.24	0.77	0.90	0.87	0.78	0.88
FE+3(M1)	0.27	0.64	0.48	0.45	0.36	0.42	0.34	0.28	0.42	0.37
TI(M1)	0.05	0.06	0.06	0.04	0.05	0.08	0.04	0.06	0.02	0.07
CR(M1)	0.01	0.00	0.00	0.00	0.00	0.01	0.06	0.06	0.02	0.04
MG(M1)	2.45	1.86	1.78	1.64	1.71	2.58	2.36	2.38	2.62	2.38
FE+2(M1)	1.22	1.31	1.47	1.53	1.61	1.10	1.24	1.30	1.11	1.23
MN(M1)	0.03	0.03	0.02	0.03	0.03	0.03	0.05	0.04	0.03	0.04
CA(M1)	0.00	0.00	0.00	0.00	0.00	0.00	0.00	0.00	0.00	0.00
MG(M4)	0.00	0.00	0.00	0.00	0.00	0.00	0.00	0.00	0.00	0.00
FE+2(M4)	0.00	0.00	0.00	0.00	0.00	0.00	0.00	0.00	0.00	0.00
MN(M4)	0.00	0.00	0.00	0.00	0.00	0.00	0.00	0.00	0.00	0.00
CA(M4)	1.84	1.75	1.75	1.77	1.78	1.78	1.77	1.79	1.78	1.80
NA(M4)	0.16	0.25	0.25	0.23	0.22	0.22	0.24	0.21	0.22	0.20
CA(A)	0.00	0.00	0.00	0.00	0.00	0.00	0.00	0.00	0.00	0.00
NA(A)	0.25	0.04	0.06	0.05	0.11	0.05	0.19	0.18	0.06	0.14
K(A)	0.05	0.09	0.11	0.09	0.10	0.05	0.06	0.05	0.04	0.06
F	0.02	0.05	0.05	0.08	0.07	0.04	0.03	0.03	0.03	0.03
CL	0.00	0.01	0.01	0.01	0.00	0.00	0.00	0.00	0.00	0.00
OH(C)	1.98	1.94	1.94	1.91	1.93	1.96	1.97	1.97	1.97	1.97
O	22.00	22.00	22.00	22.00	22.00	22.00	22.00	22.00	22.00	22.00
FE/FE+MG	0.38	0.51	0.52	0.55	0.53	0.37	0.40	0.40	0.37	0.40
A	33.02	41.23	40.09	41.30	39.01	30.70	32.72	31.29	29.83	33.02
C	22.22	20.77	20.87	20.87	21.18	22.43	21.90	22.31	22.54	22.19
F	44.76	38.00	39.04	37.83	39.82	46.88	45.38	46.40	47.63	44.78

AMPHIBOLE

SAMPLE NO.	C3-117B	C3-117B	C4-1C	C4-1C	C4-1C	C4-1C	C4-17A	C4-17A	C4-20B	C4-20B
ANALYSIS	21A	22A	03A	04A	06A	18A	03G	18G	07G	13G
CORE/RIM	N	N	N	C	R		N	R	S	R
SIO2	45.55	45.05	44.21	45.60	45.35	45.16	54.83	55.70	43.67	43.26
AL2O3	14.49	14.77	15.18	15.50	15.96	14.99	4.56	2.58	13.60	13.26
FE2O3(C)	3.40	2.97	3.83	5.33	5.17	3.94	0.65	1.68	4.83	5.60
TIO2	0.45	0.58	0.44	0.46	0.44	0.51	0.31	0.08	0.53	0.41
CR2O3	0.08	0.05	0.15	0.07	0.00	0.12	0.00	0.05	0.04	0.03
MGO	10.64	10.46	11.27	11.93	11.76	11.71	18.90	20.59	10.18	10.43
FEO(C)	10.63	10.75	8.46	6.72	6.85	8.04	6.64	3.89	11.75	11.06
MNO	0.25	0.34	0.39	0.38	0.41	0.29	0.39	0.34	0.31	0.22
CAO	11.49	11.53	11.54	11.33	11.48	11.48	11.58	12.61	11.50	11.55
NA2O	1.43	1.40	1.49	1.40	1.31	1.44	0.38	0.22	2.07	1.98
K2O	0.33	0.34	0.25	0.25	0.25	0.26	0.05	0.03	0.37	0.34
F	0.06	0.05	0.09	0.13	0.16	0.18	0.11	0.11	0.02	0.09
CL	0.01	0.01	0.00	0.00	0.00	0.00	0.02	0.00	0.01	0.00
H2O(C)	2.06	2.05	2.02	2.06	2.05	2.01	2.10	2.11	2.04	1.99
SUM	100.84	100.34	99.29	101.11	101.12	100.06	100.46	99.93	100.90	100.20
SI(T)	6.54	6.50	6.41	6.44	6.41	6.47	7.61	7.72	6.38	6.36
AL(T)	1.46	1.50	1.59	1.56	1.59	1.53	0.39	0.28	1.62	1.64
FE+3(T)	0.00	0.00	0.00	0.00	0.00	0.00	0.00	0.00	0.00	0.00
AL(M1)	0.99	1.02	1.01	1.02	1.07	1.01	0.35	0.14	0.72	0.66
FE+3(M1)	0.37	0.32	0.42	0.57	0.55	0.43	0.07	0.18	0.53	0.62
TI(M1)	0.05	0.06	0.05	0.05	0.05	0.05	0.03	0.01	0.06	0.05
CR(M1)	0.01	0.01	0.02	0.01	0.00	0.01	0.00	0.00	0.00	0.00
MG(M1)	2.28	2.25	2.44	2.51	2.48	2.50	3.91	4.25	2.22	2.29
FE+2(M1)	1.28	1.30	1.03	0.79	0.81	0.96	0.64	0.42	1.44	1.36
MN(M1)	0.03	0.04	0.05	0.05	0.05	0.04	0.00	0.00	0.04	0.03
CA(M1)	0.00	0.00	0.00	0.00	0.00	0.00	0.00	0.00	0.00	0.00
MG(M4)	0.00	0.00	0.00	0.00	0.00	0.00	0.00	0.00	0.00	0.00
FE+2(M4)	0.00	0.00	0.00	0.00	0.00	0.00	0.13	0.03	0.00	0.00
MN(M4)	0.00	0.00	0.00	0.00	0.00	0.00	0.05	0.04	0.00	0.00
CA(M4)	1.77	1.78	1.79	1.72	1.74	1.76	1.72	1.87	1.80	1.82
NA(M4)	0.23	0.22	0.21	0.29	0.26	0.24	0.10	0.06	0.20	0.18
CA(A)	0.00	0.00	0.00	0.00	0.00	0.00	0.00	0.00	0.00	0.00
NA(A)	0.17	0.18	0.21	0.10	0.10	0.16	0.00	0.00	0.39	0.38
K(A)	0.06	0.06	0.05	0.05	0.05	0.05	0.01	0.01	0.07	0.06
F	0.03	0.02	0.04	0.06	0.07	0.08	0.05	0.05	0.01	0.04
CL	0.00	0.00	0.00	0.00	0.00	0.00	0.00	0.00	0.00	0.00
OH(C)	1.97	1.98	1.96	1.94	1.93	1.92	1.95	1.95	1.99	1.95
O	22.00	22.00	22.00	22.00	22.00	22.00	22.00	22.00	22.00	22.00
FE/FE+MG	0.42	0.42	0.37	0.35	0.35	0.36	0.18	0.13	0.47	0.46
A	34.51	34.54	36.22	38.32	38.74	35.97	11.20	8.27	34.35	34.69
C	21.64	21.73	21.56	20.88	20.99	21.44	23.72	25.96	21.52	21.64
F	43.85	43.73	42.21	40.80	40.27	42.59	65.09	65.78	44.13	43.68

AMPHIBOLE

SAMPLE NO.	C4-24A	C4-24A	C4-24A	C4-24A	C4-24A	C4-24A	C4-24A	C4-24A	C4-24A	C4-25A
ANALYSIS	20A	27A	22A	23A	25A	24A	26A	34A	19A	12A
CORE/RIM	C	C	R	R	R	S	S	S	S	R
SIO2	49.92	51.61	52.28	47.06	48.06	44.95	46.11	44.04	46.12	43.62
AL2O3	8.24	6.16	5.43	12.33	9.95	13.85	12.96	15.42	12.96	14.97
FE2O3(C)	5.28	4.78	4.00	3.96	4.77	5.17	4.72	4.58	5.98	3.19
TIO2	0.49	0.32	0.18	0.45	0.53	0.62	0.63	0.32	0.36	0.55
CR2O3	0.12	0.13	0.06	0.12	0.07	0.05	0.07	0.04	0.02	0.03
MGO	14.53	15.54	16.14	12.31	13.19	11.59	11.76	10.63	11.80	9.95
FEO(C)	7.02	6.98	7.26	8.70	8.36	8.69	9.26	9.70	7.62	11.61
MNO	0.28	0.23	0.21	0.27	0.27	0.26	0.29	0.21	0.25	0.18
CAO	11.59	11.70	11.68	11.45	11.51	11.44	11.41	11.36	11.17	11.62
NA2O	1.02	0.81	0.68	1.36	1.25	1.69	1.66	1.85	1.18	1.60
K2O	0.10	0.07	0.08	0.16	0.15	0.21	0.20	0.33	0.17	0.36
F	0.06	0.03	0.05	0.06	0.10	0.08	0.08	0.03	0.04	0.06
CL	0.00	0.00	0.00	0.00	0.00	0.02	0.02	0.01	0.01	0.01
H2O(C)	2.09	2.11	2.09	2.07	2.04	2.04	2.05	2.06	2.06	2.02
SUM	100.71	100.44	100.13	100.28	100.21	100.61	101.17	100.56	99.73	99.75
SI(T)	7.07	7.30	7.40	6.73	6.89	6.46	6.59	6.36	6.64	6.39
AL(T)	0.93	0.70	0.60	1.27	1.11	1.54	1.41	1.64	1.36	1.61
FE+3(T)	0.00	0.00	0.00	0.00	0.00	0.00	0.00	0.00	0.00	0.00
AL(M1)	0.44	0.32	0.30	0.81	0.57	0.81	0.77	0.98	0.83	0.97
FE+3(M1)	0.56	0.51	0.43	0.43	0.51	0.56	0.51	0.50	0.65	0.35
TI(M1)	0.05	0.03	0.02	0.05	0.06	0.07	0.07	0.04	0.04	0.06
CR(M1)	0.01	0.01	0.01	0.01	0.01	0.01	0.01	0.00	0.00	0.00
MG(M1)	3.07	3.27	3.40	2.63	2.82	2.48	2.50	2.29	2.53	2.17
FE+2(M1)	0.83	0.82	0.84	1.04	1.00	1.05	1.11	1.17	0.92	1.42
MN(M1)	0.03	0.02	0.00	0.03	0.03	0.03	0.04	0.02	0.03	0.02
CA(M1)	0.00	0.00	0.00	0.00	0.00	0.00	0.00	0.00	0.00	0.00
MG(M4)	0.00	0.00	0.00	0.00	0.00	0.00	0.00	0.00	0.00	0.00
FE+2(M4)	0.00	0.00	0.02	0.00	0.00	0.00	0.00	0.00	0.00	0.00
MN(M4)	0.00	0.01	0.03	0.00	0.00	0.00	0.00	0.00	0.00	0.00
CA(M4)	1.76	1.77	1.77	1.76	1.77	1.76	1.75	1.76	1.72	1.82
NA(M4)	0.24	0.22	0.19	0.25	0.23	0.24	0.25	0.24	0.28	0.18
CA(A)	0.00	0.00	0.00	0.00	0.00	0.00	0.00	0.00	0.00	0.00
NA(A)	0.04	0.00	0.00	0.13	0.12	0.23	0.21	0.27	0.05	0.28
K(A)	0.02	0.01	0.01	0.03	0.03	0.04	0.04	0.06	0.03	0.07
F	0.02	0.01	0.02	0.03	0.05	0.04	0.04	0.01	0.02	0.03
CL	0.00	0.00	0.00	0.00	0.00	0.00	0.00	0.00	0.00	0.00
OH(C)	1.98	1.99	1.98	1.97	1.95	1.96	1.96	1.98	1.98	1.97
O	22.00	22.00	22.00	22.00	22.00	22.00	22.00	22.00	22.00	22.00
FE/FE+MG	0.31	0.29	0.27	0.36	0.35	0.39	0.39	0.42	0.38	0.45
A	25.41	20.64	18.01	31.48	28.10	35.32	33.28	37.33	35.36	35.04
C	23.05	23.84	23.96	22.05	22.61	21.41	21.61	21.01	21.41	21.77
F	51.54	55.52	58.03	46.47	49.29	43.26	45.11	41.66	43.23	43.18

AMPHIBOLE

SAMPLE NO.	C4-25A	C4-36A	C4-36A	C4-49A	C4-49A
ANALYSIS	13A	10A	25A	07A	22A
CORE/RIM	R	S	N	N	N
SIO2	43.61	43.70	44.01	43.70	43.95
AL2O3	14.89	13.57	13.00	15.72	15.17
FE2O3(C)	3.77	10.18	5.50	3.82	1.16
TIO2	0.48	0.33	0.43	0.44	0.57
CR2O3	0.03	0.04	0.09	0.03	0.09
MGO	10.05	10.13	10.44	10.27	10.35
FEO(C)	11.14	6.91	10.95	10.18	11.78
MNO	0.26	3.19	0.34	0.28	0.20
CAO	11.67	11.23	11.18	11.57	11.88
NA2O	1.51	2.14	2.11	1.52	1.44
K2O	0.37	0.40	0.37	0.39	0.45
F	0.05	0.34	0.19	0.05	0.07
CL	0.01	0.00	0.00	0.00	0.00
H2O(C)	2.03	1.94	1.96	2.04	2.01
SUM	99.85	103.97	100.47	99.99	99.09
SI(T)	6.38	6.23	6.44	6.35	6.44
AL(T)	1.62	1.77	1.56	1.65	1.56
FE+3(T)	0.00	0.00	0.00	0.00	0.00
AL(M1)	0.94	0.51	0.68	1.04	1.07
FE+3(M1)	0.42	1.09	0.61	0.42	0.13
TI(M1)	0.05	0.04	0.05	0.05	0.06
CR(M1)	0.00	0.00	0.01	0.00	0.01
MG(M1)	2.19	2.15	2.28	2.22	2.26
FE+2(M1)	1.36	0.82	1.34	1.24	1.44
MN(M1)	0.03	0.38	0.04	0.03	0.02
CA(M1)	0.00	0.00	0.00	0.00	0.00
MG(M4)	0.00	0.00	0.00	0.00	0.00
FE+2(M4)	0.00	0.00	0.00	0.00	0.00
MN(M4)	0.00	0.00	0.00	0.00	0.00
CA(M4)	1.83	1.72	1.75	1.80	1.87
NA(M4)	0.17	0.28	0.25	0.20	0.13
CA(A)	0.00	0.00	0.00	0.00	0.00
NA(A)	0.26	0.31	0.35	0.23	0.27
K(A)	0.07	0.07	0.07	0.07	0.08
F	0.02	0.15	0.09	0.02	0.03
CL	0.00	0.00	0.00	0.00	0.00
OH(C)	1.98	1.85	1.91	1.98	1.97
O	22.00	22.00	22.00	22.00	22.00
FE/FE+MG	0.45	0.47	0.46	0.43	0.41
A	35.51	39.91	34.47	36.99	32.94
C	21.78	20.31	21.23	21.43	22.35
F	42.71	39.78	44.30	41.59	44.71

BIOTITE

SAMPLE NO.	A1-1A	A1-1A	A1-1A	A1-1D	A1-1D	A2-3CA	A2-3CA	A2-3CA	A2-3D	A2-3D
ANALYSIS	11	14	15	07	08	07	08	23	11	13
CORE/RIM										
SIO2	36.97	36.88	36.96	38.33	38.51	35.53	35.60	35.46	36.78	35.31
AL2O3	14.96	15.13	15.48	15.45	15.38	15.11	15.41	14.22	15.60	16.54
MGO	9.77	9.46	9.28	10.51	10.35	6.35	6.30	5.57	8.50	7.55
FEO	22.95	22.83	22.62	20.37	20.26	26.48	26.46	23.40	23.22	23.34
MNO	0.48	0.46	0.51	0.40	0.45	0.19	0.22	0.18	0.21	0.19
TIO2	1.17	1.22	1.09	0.50	0.55	1.62	2.00	5.00	0.87	1.97
K2O	8.02	9.40	9.16	9.00	9.00	8.77	8.64	7.61	9.75	9.17
NA2O	0.06	0.03	0.08	0.08	0.02	0.03	0.07	0.03	0.06	0.07
CAO	0.32	0.16	0.30	0.10	0.10	0.44	0.69	3.79	0.09	0.23
BAO	0.14	0.13	0.18	0.13	0.09	0.29	0.42	0.35	0.13	1.77
F	0.10	0.10	0.17	0.15	0.09	0.27	0.25	0.24	0.15	0.12
CL	0.04	0.04	0.05	0.02	0.02	0.04	0.01	0.01	0.02	0.05
H2O(C)	3.81	3.82	3.79	3.84	3.87	3.63	3.69	3.72	3.77	3.76
SUM	98.74	99.60	99.59	98.83	98.65	98.63	99.66	99.48	99.08	100.00
SI	2.87	2.85	2.85	2.93	2.95	2.83	2.81	2.77	2.87	2.76
AL(IV)	1.13	1.15	1.15	1.07	1.05	1.17	1.19	1.23	1.13	1.24
AL(VI)	0.23	0.23	0.26	0.33	0.34	0.25	0.24	0.08	0.30	0.29
MG	1.13	1.09	1.07	1.20	1.18	0.75	0.74	0.65	0.99	0.88
FE	1.49	1.48	1.46	1.30	1.30	1.76	1.74	1.53	1.51	1.53
MN	0.03	0.03	0.03	0.03	0.03	0.01	0.02	0.01	0.01	0.01
TI	0.07	0.07	0.06	0.03	0.03	0.10	0.12	0.29	0.05	0.12
K	0.79	0.93	0.90	0.88	0.88	0.89	0.87	0.76	0.97	0.92
NA	0.01	0.00	0.01	0.01	0.00	0.00	0.01	0.00	0.01	0.01
CA	0.03	0.01	0.02	0.01	0.01	0.04	0.06	0.32	0.01	0.02
BA	0.00	0.00	0.01	0.00	0.00	0.01	0.01	0.01	0.00	0.05
F	0.02	0.02	0.04	0.04	0.02	0.07	0.06	0.06	0.04	0.03
CL	0.00	0.01	0.01	0.00	0.00	0.01	0.00	0.00	0.00	0.01
OH(C)	1.97	1.97	1.95	1.96	1.97	1.93	1.94	1.94	1.96	1.96
O	10.00	10.00	10.00	10.00	10.00	10.00	10.00	10.00	10.00	10.00
FE/FE+MG	0.57	0.57	0.58	0.52	0.52	0.70	0.70	0.70	0.61	0.63
A"	-0.24	-0.38	-0.35	-0.33	-0.34	-0.33	-0.31	-0.29	-0.42	-0.34
F"	0.70	0.79	0.78	0.69	0.70	0.93	0.92	0.90	0.86	0.85
M"	0.54	0.58	0.57	0.64	0.64	0.40	0.39	0.38	0.56	0.49

BIOTITE

SAMPLE NO.	A2-3HA	A2-3HA	A2-13A	A2-14AA	A2-66A	A2-66A	A2-66A	A3-4A	A4-2A	A4-2A
ANALYSIS	17	20	12	26	05	17	18	29	21	22
CORE/RIM										
SIO2	37.06	38.43	36.10	38.21	36.04	35.63	36.70	37.37	37.65	36.89
AL2O3	14.88	14.40	15.56	15.47	15.40	16.27	16.77	19.15	18.03	18.35
MGO	9.76	10.40	10.34	12.72	6.14	6.80	6.20	8.83	12.73	12.74
FEO	24.33	22.38	21.61	18.11	25.26	26.08	24.36	18.83	16.36	16.59
MNO	0.07	0.06	0.33	0.40	0.20	0.20	0.23	0.20	0.28	0.20
TIO2	1.31	0.70	1.19	0.67	1.78	1.70	1.54	1.95	1.47	1.54
K2O	8.38	9.90	9.32	8.14	8.68	9.03	8.87	6.64	8.55	7.72
NA2O	0.04	0.00	0.04	0.07	0.05	0.06	0.02	0.08	0.06	0.13
CAO	0.24	0.10	0.15	0.55	0.22	0.31	0.31	0.39	0.06	0.15
BAO	0.11	0.03	0.27	0.03	0.46	0.48	0.45	0.18	0.02	0.18
F	0.60	0.73	0.51	0.61	0.36	0.51	0.35	0.51	0.42	0.46
CL	0.02	0.01	0.08	0.08	0.01	0.03	0.03	0.01	0.00	0.01
H2O(C)	3.61	3.58	3.60	3.64	3.60	3.60	3.68	3.72	3.83	3.78
SUM	100.17	100.43	98.86	98.42	98.03	100.46	99.37	97.64	99.28	98.55
SI	2.85	2.93	2.81	2.90	2.86	2.78	2.86	2.83	2.80	2.76
AL(IV)	1.15	1.07	1.19	1.10	1.14	1.22	1.14	1.17	1.20	1.24
AL(VI)	0.20	0.23	0.23	0.28	0.31	0.27	0.39	0.53	0.38	0.38
MG	1.12	1.18	1.20	1.44	0.73	0.79	0.72	1.00	1.41	1.42
FE	1.56	1.43	1.40	1.15	1.68	1.70	1.59	1.19	1.02	1.04
MN	0.00	0.00	0.02	0.03	0.01	0.01	0.02	0.01	0.02	0.01
TI	0.08	0.04	0.07	0.04	0.11	0.10	0.09	0.11	0.08	0.09
K	0.82	0.96	0.92	0.79	0.88	0.90	0.88	0.64	0.81	0.74
NA	0.01	0.00	0.01	0.01	0.01	0.01	0.00	0.01	0.01	0.02
CA	0.02	0.01	0.01	0.05	0.02	0.03	0.03	0.03	0.00	0.01
BA	0.00	0.00	0.01	0.00	0.01	0.02	0.01	0.00	0.00	0.00
F	0.15	0.18	0.13	0.15	0.09	0.13	0.09	0.12	0.10	0.11
CL	0.00	0.00	0.01	0.01	0.00	0.00	0.00	0.00	0.00	0.00
OH(C)	1.85	1.82	1.86	1.84	1.91	1.87	1.91	1.88	1.90	1.89
O	10.00	10.00	10.00	10.00	10.00	10.00	10.00	10.00	10.00	10.00
FE/FE+MG	0.58	0.55	0.54	0.44	0.70	0.68	0.69	0.55	0.42	0.42
A"	-0.26	-0.44	-0.35	-0.23	-0.33	-0.32	-0.31	-0.05	-0.21	-0.14
F"	0.74	0.79	0.73	0.55	0.93	0.90	0.90	0.57	0.51	0.48
M"	0.53	0.65	0.62	0.69	0.40	0.42	0.41	0.48	0.70	0.66

BIOTITE

SAMPLE NO.	A4-6A	A4-6A	A4-8A	A4-8A	A4-8A	A4-8A	A4-19A	A4-19A	A4-19A	B2-1AB
ANALYSIS	16	33	20	46	64	67	08	09	16	21
CORE/RIM										
SIO2	36.51	36.07	35.90	36.60	35.65	35.20	37.97	37.91	37.79	37.30
AL2O3	18.11	17.74	18.30	17.40	17.76	18.21	18.65	18.96	18.26	17.67
MGO	9.76	10.40	7.90	8.02	8.06	8.13	12.61	12.50	12.47	11.33
FEO	19.80	19.38	22.43	22.34	21.59	21.40	15.25	15.50	15.66	17.32
MNO	0.24	0.12	0.27	0.21	0.15	0.17	0.26	0.19	0.26	0.36
TIO2	1.61	1.85	2.02	1.55	2.04	1.94	1.59	1.73	1.74	1.52
K2O	8.31	8.58	8.44	8.59	8.64	8.98	8.03	7.91	8.51	8.78
NA2O	0.14	0.11	0.19	0.07	0.09	0.22	0.13	0.20	0.12	0.06
CAO	0.24	0.02	0.29	0.22	0.23	0.22	0.29	0.31	0.07	0.12
BAO	0.21	0.33	0.29	0.31	0.25	0.24	0.07	0.13	0.13	0.31
F	0.32	0.35	0.37	0.25	0.33	0.29	0.37	0.43	0.32	0.16
CL	0.03	0.02	0.02	0.01	0.00	0.02	0.02	0.00	0.00	0.02
H2O(C)	3.78	3.75	3.74	3.78	3.71	3.72	3.87	3.87	3.89	3.89
SUM	98.91	98.57	100.00	99.24	98.38	98.62	98.96	99.46	99.09	98.77
SI	2.78	2.76	2.74	2.81	2.76	2.73	2.81	2.79	2.81	2.82
AL(IV)	1.22	1.24	1.26	1.19	1.24	1.27	1.19	1.21	1.19	1.18
AL(VI)	0.40	0.36	0.39	0.39	0.39	0.39	0.44	0.44	0.41	0.39
MG	1.11	1.19	0.90	0.92	0.93	0.94	1.39	1.37	1.38	1.27
FE	1.26	1.24	1.43	1.44	1.40	1.39	0.94	0.95	0.97	1.09
MN	0.02	0.01	0.02	0.01	0.01	0.01	0.02	0.01	0.02	0.02
TI	0.09	0.11	0.12	0.09	0.12	0.11	0.09	0.10	0.10	0.09
K	0.81	0.84	0.82	0.84	0.85	0.89	0.76	0.74	0.81	0.85
NA	0.02	0.02	0.03	0.01	0.01	0.03	0.02	0.03	0.02	0.01
CA	0.02	0.00	0.02	0.02	0.02	0.02	0.02	0.02	0.01	0.01
BA	0.01	0.01	0.01	0.01	0.01	0.01	0.00	0.00	0.00	0.01
F	0.08	0.08	0.09	0.06	0.08	0.07	0.09	0.10	0.07	0.04
CL	0.00	0.00	0.00	0.00	0.00	0.00	0.00	0.00	0.00	0.00
OH(C)	1.92	1.91	1.91	1.94	1.92	1.93	1.91	1.90	1.93	1.96
O	10.00	10.00	10.00	10.00	10.00	10.00	10.00	10.00	10.00	10.00
FE/FE+MG	0.53	0.51	0.61	0.61	0.60	0.60	0.40	0.41	0.41	0.46
A"	-0.20	-0.23	-0.21	-0.25	-0.25	-0.27	-0.16	-0.14	-0.21	-0.26
F"	0.64	0.63	0.75	0.76	0.75	0.76	0.47	0.47	0.50	0.58
M"	0.56	0.60	0.47	0.49	0.50	0.51	0.69	0.67	0.71	0.68

BIOTITE

SAMPLE NO.	B2-1AB	B2-1AB	B2-1B	B2-1B	B2-1B	B2-1Y	B2-1Y	B2-1Y	B2-1Y	B2-3A
ANALYSIS	23	27	01	02	17	16	22	23	36	14
CORE/RIM										
SIO2	37.16	37.18	37.29	37.63	37.95	36.98	37.23	37.56	36.80	36.62
AL2O3	18.23	18.10	18.16	17.88	17.64	18.03	18.62	18.58	17.60	17.77
MGO	11.30	11.45	11.75	11.92	12.13	12.62	12.75	12.80	12.38	9.29
FEO	17.91	17.93	17.23	17.01	17.26	16.05	16.28	16.34	17.18	19.71
MNO	0.32	0.34	0.26	0.27	0.19	0.29	0.26	0.20	0.34	0.28
TIO2	1.60	1.73	1.53	1.60	1.74	1.32	1.33	1.14	1.32	2.17
K2O	9.24	8.86	9.36	9.31	9.28	9.31	8.99	8.87	8.69	8.80
NA2O	0.03	0.09	0.11	0.09	0.17	0.10	0.13	0.07	0.17	0.10
CAO	0.05	0.13	0.07	0.05	0.03	0.12	0.23	0.27	0.28	0.14
BAO	0.24	0.33	0.23	0.11	0.26	0.27	0.44	0.39	0.33	0.17
F	0.19	0.14	0.21	0.18	0.17	0.23	0.25	0.24	0.21	0.27
CL	0.01	0.01	0.00	0.01	0.00	0.00	0.00	0.00	0.01	0.00
H2O(C)	3.92	3.94	3.92	3.94	3.97	3.89	3.93	3.94	3.88	3.81
SUM	100.12	100.20	100.04	99.93	100.72	99.10	100.32	100.29	99.08	99.01
SI	2.78	2.78	2.78	2.80	2.81	2.78	2.76	2.78	2.77	2.79
AL(IV)	1.22	1.22	1.22	1.20	1.19	1.22	1.24	1.22	1.23	1.21
AL(VI)	0.38	0.37	0.38	0.37	0.35	0.37	0.38	0.40	0.34	0.38
MG	1.26	1.27	1.31	1.32	1.34	1.41	1.41	1.41	1.39	1.06
FE	1.12	1.12	1.08	1.06	1.07	1.01	1.01	1.01	1.08	1.26
MN	0.02	0.02	0.02	0.02	0.01	0.02	0.02	0.01	0.02	0.02
TI	0.09	0.10	0.09	0.09	0.10	0.07	0.07	0.06	0.07	0.12
K	0.88	0.84	0.89	0.88	0.88	0.89	0.85	0.84	0.83	0.86
NA	0.00	0.01	0.02	0.01	0.02	0.01	0.02	0.01	0.02	0.01
CA	0.00	0.01	0.00	0.00	0.00	0.01	0.02	0.02	0.02	0.01
BA	0.01	0.01	0.01	0.00	0.01	0.01	0.01	0.01	0.01	0.00
F	0.04	0.03	0.05	0.04	0.04	0.05	0.06	0.05	0.05	0.06
CL	0.00	0.00	0.00	0.00	0.00	0.00	0.00	0.00	0.00	0.00
OH(C)	1.95	1.97	1.95	1.96	1.96	1.95	1.94	1.94	1.95	1.94
O	10.00	10.00	10.00	10.00	10.00	10.00	10.00	10.00	10.00	10.00
FE/FE+MG	0.47	0.47	0.45	0.44	0.44	0.42	0.42	0.42	0.44	0.54
A"	-0.28	-0.24	-0.29	-0.29	-0.29	-0.29	-0.24	-0.23	-0.24	-0.27
F"	0.60	0.58	0.58	0.57	0.57	0.54	0.52	0.51	0.54	0.69
M"	0.68	0.66	0.71	0.72	0.72	0.75	0.72	0.71	0.69	0.58

BIOTITE

SAMPLE NO.	B2-3A	B2-3A	B2-3A	B2-4A	B2-35A	B2-35A	B2-35A	B2-35A	B2-35B	B2-35B
ANALYSIS	15	26	34	13	08	09	26	35	04	05
CORE/RIM										
SIO2	37.10	36.05	39.98	38.64	36.20	36.36	37.00	36.15	36.14	36.25
AL2O3	18.08	17.72	18.78	18.14	18.06	17.79	17.71	17.24	18.35	18.18
MGO	9.50	9.72	8.67	12.28	9.28	9.29	9.80	9.36	9.92	9.91
FEO	18.95	19.37	16.90	14.18	20.63	20.67	19.93	20.38	20.03	20.22
MNO	0.20	0.20	0.20	0.12	0.37	0.37	0.34	0.33	0.39	0.33
TIO2	2.19	2.13	0.94	1.54	1.77	1.75	1.47	1.80	1.85	1.79
K2O	8.89	8.74	7.08	6.56	8.34	8.45	8.89	8.60	8.48	8.20
NA2O	0.09	0.14	1.48	0.15	0.10	0.06	0.11	0.07	0.05	0.07
CAO	0.08	0.15	0.55	0.67	0.23	0.18	0.08	0.07	0.32	0.38
BAO	0.24	0.23	0.17	0.14	0.07	0.11	0.10	0.07	0.10	0.06
F	0.25	0.31	0.38	0.26	0.39	0.34	0.32	0.29	0.41	0.35
CL	0.00	0.00	0.00	0.00	0.00	0.00	0.01	0.02	0.00	0.02
H2O(C)	3.85	3.76	3.86	3.89	3.74	3.76	3.80	3.74	3.76	3.78
SUM	99.31	98.38	98.83	96.46	99.03	99.00	99.41	97.99	99.63	99.41
SI	2.80	2.77	2.96	2.89	2.76	2.78	2.81	2.79	2.74	2.75
AL(IV)	1.20	1.23	1.04	1.11	1.24	1.22	1.19	1.21	1.26	1.25
AL(VI)	0.41	0.37	0.60	0.49	0.39	0.38	0.39	0.36	0.38	0.37
MG	1.07	1.11	0.96	1.37	1.06	1.06	1.11	1.08	1.12	1.12
FE	1.20	1.24	1.05	0.89	1.32	1.32	1.27	1.32	1.27	1.28
MN	0.01	0.01	0.01	0.01	0.02	0.02	0.02	0.02	0.02	0.02
TI	0.12	0.12	0.05	0.09	0.10	0.10	0.08	0.11	0.11	0.10
K	0.86	0.86	0.67	0.63	0.81	0.82	0.86	0.85	0.82	0.79
NA	0.01	0.02	0.21	0.02	0.02	0.01	0.02	0.01	0.01	0.01
CA	0.01	0.01	0.04	0.05	0.02	0.02	0.01	0.01	0.03	0.03
BA	0.01	0.01	0.00	0.00	0.00	0.00	0.00	0.00	0.00	0.00
F	0.06	0.08	0.09	0.06	0.10	0.08	0.08	0.07	0.10	0.08
CL	0.00	0.00	0.00	0.00	0.00	0.00	0.00	0.00	0.00	0.00
OH(C)	1.94	1.92	1.91	1.94	1.90	1.92	1.92	1.93	1.90	1.91
O	10.00	10.00	10.00	10.00	10.00	10.00	10.00	10.00	10.00	10.00
FE/FE+MG	0.53	0.53	0.52	0.39	0.56	0.56	0.53	0.55	0.53	0.53
A"	-0.27	-0.26	-0.10	-0.07	-0.21	-0.22	-0.27	-0.25	-0.21	-0.19
F"	0.67	0.66	0.57	0.42	0.67	0.68	0.68	0.69	0.64	0.63
M"	0.60	0.59	0.53	0.65	0.54	0.54	0.59	0.56	0.57	0.55

BIOTITE

SAMPLE NO.	B2-35B	B2-35B	B3-25B	B3-63A	B3-63A	B3-141A	B3-141A	B3-141A	B3156AA	B3156AA
ANALYSIS	09	18	10	10	12	04	12	17	14	15
CORE/RIM										
SIO2	36.02	36.43	35.20	36.20	36.96	37.52	37.17	37.82	37.13	36.52
AL2O3	17.97	18.47	19.48	18.70	19.11	17.82	17.81	18.64	18.08	18.03
MGO	9.94	10.47	10.06	9.15	9.07	13.45	13.08	12.45	10.20	10.16
FEO	20.19	19.10	19.39	19.89	20.06	15.41	15.71	15.36	19.35	19.18
MNO	0.28	0.31	0.15	0.13	0.10	0.26	0.26	0.32	0.19	0.18
TIO2	1.75	1.61	1.47	1.57	1.48	1.73	1.52	1.75	1.82	1.63
K2O	8.89	8.94	7.77	8.35	7.80	9.34	9.16	8.73	8.81	8.78
NA2O	0.12	0.07	0.27	0.14	0.11	0.22	0.25	0.11	0.12	0.22
CAO	0.20	0.16	0.25	0.08	0.13	0.12	0.13	0.17	0.07	0.08
BAO	0.10	0.18	0.18	0.21	0.14	0.12	0.17	0.10	0.06	0.10
F	0.32	0.35	0.76	0.65	0.54	0.27	0.28	0.25	0.32	0.32
CL	0.00	0.00	0.00	0.01	0.00	0.00	0.01	0.00	0.00	0.00
H2O(C)	3.79	3.81	3.56	3.61	3.71	3.92	3.88	3.94	3.84	3.79
SUM	99.43	99.75	98.24	98.41	98.97	100.07	99.30	99.51	99.85	98.86
SI	2.74	2.75	2.69	2.77	2.79	2.78	2.78	2.80	2.79	2.78
AL(IV)	1.26	1.25	1.31	1.23	1.21	1.22	1.22	1.20	1.21	1.22
AL(VI)	0.36	0.39	0.44	0.45	0.49	0.33	0.34	0.42	0.39	0.39
MG	1.13	1.18	1.15	1.04	1.02	1.48	1.46	1.37	1.14	1.15
FE	1.29	1.21	1.24	1.27	1.27	0.95	0.98	0.95	1.22	1.22
MN	0.02	0.02	0.01	0.01	0.01	0.02	0.02	0.02	0.01	0.01
TI	0.10	0.09	0.08	0.09	0.08	0.10	0.09	0.10	0.10	0.09
K	0.86	0.86	0.76	0.81	0.75	0.88	0.87	0.82	0.85	0.85
NA	0.02	0.01	0.04	0.02	0.02	0.03	0.04	0.02	0.02	0.03
CA	0.02	0.01	0.02	0.01	0.01	0.01	0.01	0.01	0.01	0.01
BA	0.00	0.00	0.00	0.01	0.00	0.00	0.00	0.00	0.00	0.00
F	0.08	0.08	0.18	0.16	0.13	0.06	0.06	0.06	0.07	0.08
CL	0.00	0.00	0.00	0.00	0.00	0.00	0.00	0.00	0.00	0.00
OH(C)	1.92	1.92	1.82	1.84	1.87	1.94	1.93	1.94	1.93	1.92
O	10.00	10.00	10.00	10.00	10.00	10.00	10.00	10.00	10.00	10.00
FE/FE+MG	0.53	0.51	0.52	0.55	0.55	0.39	0.40	0.41	0.52	0.51
A"	-0.25	-0.25	-0.12	-0.20	-0.14	-0.29	-0.27	-0.22	-0.25	-0.25
F"	0.67	0.63	0.58	0.66	0.63	0.50	0.51	0.50	0.64	0.64
M"	0.59	0.62	0.54	0.54	0.51	0.78	0.76	0.72	0.60	0.61

BIOTITE

SAMPLE NO.	B3156AA	B3156AA	B3156AA	B3-165A	B3-165A	B3-165A	B3-175A	B3-175A	B3-175A	B3-175A
ANALYSIS	26	28	29	02	13	17	02	35	36	46
CORE/RIM										
SIO2	36.55	36.48	36.61	36.09	36.33	36.88	36.46	36.29	36.40	37.04
AL2O3	18.34	18.02	18.17	17.65	17.94	17.70	17.57	18.30	18.08	17.67
MGO	10.25	9.88	10.32	10.11	10.41	10.36	11.25	11.42	11.35	12.04
FEO	18.93	19.76	18.69	19.71	19.24	19.55	18.12	17.54	17.47	17.66
MNO	0.24	0.15	0.20	0.16	0.14	0.16	0.30	0.24	0.26	0.29
TIO2	1.99	2.23	1.50	1.79	1.74	1.73	1.51	1.71	1.60	1.69
K2O	8.88	8.92	8.88	8.55	8.59	8.76	8.72	9.03	8.91	9.17
NA2O	0.16	0.14	0.18	0.10	0.15	0.10	0.20	0.24	0.19	0.19
CAO	0.08	0.04	0.04	0.15	0.17	0.06	0.03	0.02	0.02	0.04
BAO	0.13	0.12	0.06	0.10	0.15	0.18	0.33	0.31	0.41	0.20
F	0.40	0.26	0.36	0.63	0.71	0.67	0.62	0.61	0.47	0.80
CL	0.01	0.00	0.00	0.00	0.02	0.02	0.02	0.00	0.00	0.00
H2O(C)	3.78	3.84	3.77	3.61	3.60	3.64	3.64	3.68	3.73	3.63
SUM	99.59	99.73	98.63	98.40	98.89	99.53	98.51	99.15	98.71	100.08
SI	2.76	2.76	2.78	2.77	2.76	2.79	2.78	2.74	2.76	2.77
AL(IV)	1.24	1.24	1.22	1.23	1.24	1.21	1.22	1.26	1.24	1.23
AL(VI)	0.39	0.37	0.41	0.36	0.37	0.37	0.36	0.37	0.38	0.33
MG	1.15	1.11	1.17	1.15	1.18	1.17	1.28	1.29	1.28	1.34
FE	1.19	1.25	1.19	1.26	1.22	1.24	1.15	1.11	1.11	1.10
MN	0.02	0.01	0.01	0.01	0.01	0.01	0.02	0.02	0.02	0.02
TI	0.11	0.13	0.09	0.10	0.10	0.10	0.09	0.10	0.09	0.10
K	0.86	0.86	0.86	0.84	0.83	0.85	0.85	0.87	0.86	0.88
NA	0.02	0.02	0.03	0.02	0.02	0.02	0.03	0.04	0.03	0.03
CA	0.01	0.00	0.00	0.01	0.01	0.00	0.00	0.00	0.00	0.00
BA	0.00	0.00	0.00	0.00	0.00	0.00	0.01	0.01	0.01	0.01
F	0.10	0.06	0.09	0.15	0.17	0.16	0.15	0.15	0.11	0.19
CL	0.00	0.00	0.00	0.00	0.00	0.00	0.00	0.00	0.00	0.00
OH(C)	1.90	1.94	1.91	1.85	1.83	1.84	1.85	1.85	1.89	1.81
O	10.00	10.00	10.00	10.00	10.00	10.00	10.00	10.00	10.00	10.00
FE/FE+MG	0.51	0.53	0.50	0.52	0.51	0.51	0.48	0.46	0.46	0.45
A"	-0.25	-0.26	-0.25	-0.23	-0.23	-0.25	-0.25	-0.26	-0.25	-0.28
F"	0.63	0.67	0.63	0.64	0.63	0.64	0.59	0.58	0.58	0.58
M"	0.61	0.59	0.62	0.59	0.60	0.61	0.65	0.68	0.67	0.70

BIOTITE

SAMPLE NO.	B3-185A	B3-185A	B3-185A	B3-261A	B3-261A	B3-261A	B4-1D	B4-1D	B4-1D	B4-1D
ANALYSIS	11	12	23	21	22	29	07	08	09	18
CORE/RIM										
SIO2	37.22	38.07	37.35	39.60	39.05	38.81	39.92	40.37	40.55	40.46
AL2O3	18.46	18.99	17.75	17.66	17.85	17.94	14.80	16.46	16.72	15.34
MGO	11.52	11.39	11.44	17.40	17.27	17.09	18.98	20.59	20.22	19.63
FEO	17.12	15.72	18.26	9.88	9.70	9.74	8.49	6.53	6.40	8.53
MNO	0.23	0.25	0.25	0.63	0.58	0.64	0.62	0.60	0.66	0.69
TIO2	1.94	2.26	1.72	1.38	1.19	1.08	1.04	0.74	0.73	1.09
K2O	8.54	8.80	8.66	8.91	8.91	9.27	9.71	9.55	9.42	9.26
NA2O	0.12	0.12	0.04	0.11	0.15	0.14	0.18	0.20	0.23	0.19
CAO	0.08	0.05	0.06	0.06	0.03	0.05	0.04	0.05	0.06	0.02
BAO	0.13	0.20	0.12	0.04	0.07	0.03	0.13	0.14	0.12	0.15
F	0.42	0.27	0.31	0.65	0.62	0.50	0.81	0.69	0.87	0.67
CL	0.01	0.01	0.00	0.00	0.00	0.00	0.00	0.00	0.00	0.01
H2O(C)	3.82	3.94	3.85	3.86	3.84	3.89	3.70	3.87	3.79	3.85
SUM	99.44	99.96	99.68	99.91	99.01	98.97	98.09	99.49	99.40	99.60
SI	2.78	2.81	2.80	2.85	2.83	2.82	2.93	2.88	2.89	2.91
AL(IV)	1.22	1.19	1.20	1.15	1.17	1.18	1.07	1.12	1.11	1.09
AL(VI)	0.40	0.45	0.36	0.34	0.36	0.36	0.21	0.27	0.30	0.21
MG	1.28	1.25	1.28	1.86	1.87	1.85	2.07	2.19	2.15	2.11
FE	1.07	0.97	1.14	0.59	0.59	0.59	0.52	0.39	0.38	0.51
MN	0.01	0.02	0.02	0.04	0.04	0.04	0.04	0.04	0.04	0.04
TI	0.11	0.13	0.10	0.07	0.06	0.06	0.06	0.04	0.04	0.06
K	0.81	0.83	0.83	0.82	0.82	0.86	0.91	0.87	0.86	0.85
NA	0.02	0.02	0.01	0.02	0.02	0.02	0.03	0.03	0.03	0.03
CA	0.01	0.00	0.00	0.00	0.00	0.00	0.00	0.00	0.00	0.00
BA	0.00	0.01	0.00	0.00	0.00	0.00	0.00	0.00	0.00	0.00
F	0.10	0.06	0.07	0.15	0.14	0.11	0.19	0.16	0.20	0.15
CL	0.00	0.00	0.00	0.00	0.00	0.00	0.00	0.00	0.00	0.00
OH(C)	1.90	1.94	1.93	1.85	1.86	1.89	1.81	1.84	1.80	1.85
O	10.00	10.00	10.00	10.00	10.00	10.00	10.00	10.00	10.00	10.00
FE/FE+MG	0.45	0.44	0.47	0.24	0.24	0.24	0.20	0.15	0.15	0.20
A"	-0.21	-0.23	-0.23	-0.24	-0.24	-0.27	-0.39	-0.31	-0.30	-0.31
F"	0.55	0.54	0.58	0.30	0.30	0.31	0.28	0.20	0.20	0.26
M"	0.66	0.69	0.65	0.94	0.94	0.96	1.11	1.11	1.10	1.06

BIOTITE

SAMPLE NO.	B4-1D	B4-1D	B4-1D	B4-7C	B4-7C	B4-11J	B4-11J	B4-11K	B4-11K	B4-11K
ANALYSIS	24	25	29	13	30	03	04	38	39	55
CORE/RIM										
SIO2	39.36	40.16	40.49	37.68	38.09	40.76	41.54	39.25	39.13	38.24
AL2O3	15.23	15.59	16.28	17.30	17.49	14.89	14.34	16.89	16.69	17.91
MGO	19.36	19.34	19.35	12.69	12.56	20.82	20.85	16.66	16.68	16.29
FEO	8.59	8.71	7.27	16.40	15.91	7.89	7.85	11.24	11.23	11.32
MNO	0.75	0.87	0.62	0.26	0.21	0.42	0.48	0.43	0.46	0.40
TIO2	0.93	1.08	1.19	1.18	1.26	0.88	0.98	1.40	1.33	1.34
K2O	9.84	9.66	8.83	9.44	9.23	8.71	8.65	9.60	9.56	9.25
NA2O	0.14	0.09	0.30	0.08	0.12	0.20	0.16	0.20	0.19	0.20
CAO	0.04	0.04	0.19	0.05	0.04	0.14	0.09	0.04	0.03	0.05
BAO	0.15	0.24	0.10	0.19	0.30	0.07	0.19	0.21	0.27	0.23
F	0.65	0.83	0.70	0.15	0.21	0.83	1.00	0.62	0.56	0.55
CL	0.00	0.00	0.00	0.00	0.00	0.00	0.00	0.00	0.00	0.00
H2O(C)	3.79	3.77	3.84	3.93	3.92	3.78	3.72	3.83	3.85	3.84
SUM	98.55	100.02	98.86	99.29	99.26	99.03	99.42	100.12	99.75	99.39
SI	2.88	2.89	2.91	2.82	2.84	2.93	2.97	2.85	2.85	2.80
AL(IV)	1.12	1.11	1.09	1.18	1.16	1.07	1.03	1.15	1.15	1.20
AL(VI)	0.20	0.22	0.29	0.35	0.38	0.19	0.18	0.30	0.29	0.34
MG	2.11	2.08	2.07	1.42	1.40	2.23	2.22	1.80	1.81	1.77
FE	0.53	0.52	0.44	1.03	0.99	0.47	0.47	0.68	0.69	0.69
MN	0.05	0.05	0.04	0.02	0.01	0.03	0.03	0.03	0.03	0.02
TI	0.05	0.06	0.06	0.07	0.07	0.05	0.05	0.08	0.07	0.07
K	0.92	0.89	0.81	0.90	0.88	0.80	0.79	0.89	0.89	0.86
NA	0.02	0.01	0.04	0.01	0.02	0.03	0.02	0.03	0.03	0.03
CA	0.00	0.00	0.02	0.00	0.00	0.01	0.01	0.00	0.00	0.00
BA	0.00	0.01	0.00	0.01	0.01	0.00	0.00	0.01	0.01	0.01
F	0.15	0.19	0.16	0.04	0.05	0.19	0.23	0.14	0.13	0.13
CL	0.00	0.00	0.00	0.00	0.00	0.00	0.00	0.00	0.00	0.00
OH(C)	1.85	1.81	1.84	1.97	1.95	1.81	1.77	1.86	1.87	1.87
O	10.00	10.00	10.00	10.00	10.00	10.00	10.00	10.00	10.00	10.00
FE/FE+MG	0.20	0.20	0.17	0.42	0.42	0.18	0.17	0.27	0.27	0.28
A"	-0.38	-0.35	-0.26	-0.32	-0.30	-0.26	-0.27	-0.33	-0.33	-0.27
F"	0.27	0.27	0.22	0.55	0.54	0.22	0.22	0.36	0.36	0.36
M"	1.10	1.07	1.04	0.76	0.76	1.04	1.05	0.96	0.96	0.91

BIOTITE

SAMPLE NO.	B4-11K	B4-11K	B4-11KA	B4-11KA	B4-13A	B4-13A	B4-32A	B4-32A	B4-93A	B4-93A
ANALYSIS	50	76	03	04	08	09	56	57	QMIN1	QMIN2
CORE/RIM										
SIO2	39.05	38.20	40.37	39.99	37.29	37.92	36.60	37.16	37.44	36.99
AL2O3	17.71	17.46	14.22	14.40	17.72	17.60	17.90	17.68	18.38	18.47
MGO	16.48	16.11	19.58	19.58	13.27	13.13	9.60	9.08	11.17	11.11
FEO	11.39	11.81	9.57	9.75	15.03	15.48	19.47	19.13	18.70	18.57
MNO	0.44	0.43	0.29	0.33	0.21	0.24	0.29	0.25	0.16	0.19
TIO2	1.42	1.31	1.02	1.14	1.56	1.65	2.18	1.94	1.67	1.60
K2O	9.31	8.79	9.08	8.98	9.26	9.19	9.89	9.47	8.47	8.36
NA2O	0.21	0.14	0.15	0.16	0.12	0.11	0.13	0.06	0.25	0.22
CAO	0.04	0.17	0.12	0.15	0.18	0.11	0.10	0.15	0.14	0.12
BAO	0.11	0.18	0.11	0.08	0.24	0.21	0.16	0.16	0.00	0.00
F	0.64	0.54	0.84	0.88	0.14	0.08	0.25	0.19	0.00	0.00
CL	0.00	0.01	0.01	0.00	0.00	0.00	0.00	0.00	0.00	0.00
H2O(C)	3.85	3.82	3.72	3.69	3.94	4.01	3.85	3.85	4.04	4.01
SUM	100.37	98.74	98.71	98.75	98.90	99.70	100.32	99.04	100.41	99.63
SI	2.82	2.81	2.94	2.92	2.79	2.81	2.77	2.83	2.78	2.77
AL(IV)	1.18	1.19	1.06	1.08	1.21	1.19	1.23	1.17	1.22	1.23
AL(VI)	0.33	0.32	0.16	0.15	0.35	0.35	0.36	0.41	0.39	0.40
MG	1.77	1.77	2.13	2.13	1.48	1.45	1.08	1.03	1.24	1.24
FE	0.69	0.73	0.58	0.60	0.94	0.96	1.23	1.22	1.16	1.16
MN	0.03	0.03	0.02	0.02	0.01	0.02	0.02	0.02	0.01	0.01
TI	0.08	0.07	0.06	0.06	0.09	0.09	0.12	0.11	0.09	0.09
K	0.86	0.82	0.84	0.84	0.88	0.87	0.95	0.92	0.80	0.80
NA	0.03	0.02	0.02	0.02	0.02	0.02	0.02	0.01	0.04	0.03
CA	0.00	0.01	0.01	0.01	0.02	0.01	0.01	0.01	0.01	0.01
BA	0.00	0.00	0.00	0.00	0.01	0.01	0.00	0.00	0.00	0.00
F	0.15	0.13	0.19	0.20	0.03	0.02	0.06	0.05	0.00	0.00
CL	0.00	0.00	0.00	0.00	0.00	0.00	0.00	0.00	0.00	0.00
OH(C)	1.85	1.87	1.81	1.80	1.97	1.98	1.94	1.95	2.00	2.00
O	10.00	10.00	10.00	10.00	10.00	10.00	10.00	10.00	10.00	10.00
FE/FE+MG	0.28	0.29	0.21	0.22	0.39	0.40	0.53	0.54	0.48	0.48
A"	-0.28	-0.24	-0.32	-0.30	-0.29	-0.29	-0.38	-0.35	-0.20	-0.19
F"	0.36	0.36	0.28	0.29	0.50	0.51	0.73	0.73	0.58	0.57
M"	0.92	0.88	1.03	1.02	0.79	0.77	0.64	0.62	0.62	0.61

BIOTITE

SAMPLE NO.	B4-93A	B4-93A	B4-101A	B4-101A	B4-101A	B4-101A	B4-101A	B4-141A	B4-141A	C3-2B
ANALYSIS	22	23	49	34	51	20	55	04	15	18
CORE/RIM										
SIO2	36.51	36.78	36.83	36.42	35.92	35.87	36.64	36.37	36.18	35.85
AL2O3	18.58	18.21	18.36	19.17	18.92	19.45	18.84	17.95	17.97	17.69
MGO	11.31	11.46	10.37	10.28	9.81	9.82	10.24	11.16	10.42	11.02
FEO	17.66	17.87	17.81	18.64	18.61	18.61	18.64	18.27	18.50	19.73
MNO	0.11	0.13	0.16	0.19	0.23	0.17	0.24	0.21	0.27	0.08
TIO2	1.60	1.48	1.91	1.58	1.99	2.08	1.68	1.96	1.84	1.77
K2O	8.81	8.65	8.52	8.85	8.84	8.43	8.60	8.88	8.99	7.93
NA2O	0.11	0.09	0.26	0.23	0.13	0.09	0.20	0.17	0.15	0.12
CAO	0.10	0.12	0.24	0.05	0.19	0.19	0.12	0.18	0.09	0.09
BAO	0.10	0.11	0.09	0.60	0.13	0.17	0.15	0.21	0.14	0.07
F	0.25	0.30	0.37	0.28	0.29	0.30	0.35	0.40	0.31	0.58
CL	0.02	0.00	0.00	0.01	0.02	0.00	0.01	0.00	0.00	0.00
H2O(C)	3.85	3.83	3.79	3.85	3.80	3.82	3.81	3.78	3.78	3.65
SUM	98.91	98.92	98.55	100.02	98.74	98.88	99.36	99.40	98.52	98.35
SI	2.75	2.77	2.78	2.74	2.73	2.72	2.76	2.75	2.76	2.74
AL(IV)	1.25	1.23	1.22	1.26	1.27	1.28	1.24	1.25	1.24	1.26
AL(VI)	0.40	0.39	0.42	0.44	0.43	0.45	0.43	0.35	0.38	0.33
MG	1.27	1.29	1.17	1.15	1.11	1.11	1.15	1.26	1.19	1.26
FE	1.11	1.13	1.13	1.17	1.18	1.18	1.17	1.15	1.18	1.26
MN	0.01	0.01	0.01	0.01	0.02	0.01	0.02	0.01	0.02	0.01
TI	0.09	0.08	0.11	0.09	0.11	0.12	0.10	0.11	0.11	0.10
K	0.85	0.83	0.82	0.85	0.86	0.81	0.83	0.86	0.88	0.77
NA	0.02	0.01	0.04	0.03	0.02	0.01	0.03	0.02	0.02	0.02
CA	0.01	0.01	0.02	0.00	0.02	0.02	0.01	0.02	0.01	0.01
BA	0.00	0.00	0.00	0.02	0.00	0.00	0.00	0.01	0.00	0.00
F	0.06	0.07	0.09	0.07	0.07	0.07	0.08	0.10	0.07	0.14
CL	0.00	0.00	0.00	0.00	0.00	0.00	0.00	0.00	0.00	0.00
OH(C)	1.94	1.93	1.91	1.93	1.93	1.93	1.92	1.90	1.93	1.86
O	10.00	10.00	10.00	10.00	10.00	10.00	10.00	10.00	10.00	10.00
FE/FE+MG	0.47	0.47	0.49	0.50	0.51	0.51	0.50	0.48	0.50	0.50
A"	-0.23	-0.22	-0.22	-0.22	-0.24	-0.18	-0.21	-0.25	-0.27	-0.17
F"	0.57	0.57	0.60	0.62	0.64	0.61	0.61	0.60	0.63	0.59
M"	0.65	0.65	0.62	0.61	0.60	0.57	0.60	0.65	0.64	0.58

BIOTITE

SAMPLE NO.	C3-19B	C3-55A	C3-68A	C3-68A	C3-68A	C4-1C	C4-32A	C4-32A	C4-32A	C4-32B
ANALYSIS	21	21	03	06	15	15	07	14	35	10
CORE/RIM										
SIO2	37.82	36.54	37.45	37.22	37.36	38.51	36.04	35.01	36.08	36.79
AL2O3	19.41	18.19	18.12	18.76	18.74	17.57	18.51	19.80	18.51	18.80
MGO	13.48	11.67	13.35	13.76	13.75	15.17	11.60	11.73	11.30	13.14
FEO	14.83	16.94	14.44	14.09	13.97	12.77	17.45	18.27	17.63	15.80
MNO	0.02	0.29	0.48	0.43	0.40	0.16	0.14	0.12	0.10	0.05
TIO2	1.26	2.13	1.69	1.81	1.61	1.38	1.55	1.34	1.43	1.51
K2O	8.79	8.40	8.33	9.20	8.67	9.55	8.42	7.18	8.87	7.96
NA2O	0.49	0.09	0.16	0.15	0.16	0.14	0.29	0.24	0.25	0.35
CAO	0.04	0.13	0.27	0.08	0.16	0.06	0.03	0.22	0.05	0.02
BAO	0.10	0.30	0.18	0.09	0.10	0.09	0.11	0.13	0.06	0.13
F	0.37	0.10	0.28	0.23	0.21	0.33	0.51	0.56	0.50	0.31
CL	0.00	0.02	0.00	0.00	0.00	0.00	0.00	0.01	0.00	0.00
H2O(C)	3.93	3.93	3.90	3.96	3.95	3.93	3.71	3.68	3.71	3.87
SUM	100.39	98.67	98.53	99.69	99.00	99.51	98.14	98.04	98.28	98.59
SI	2.76	2.75	2.79	2.75	2.76	2.83	2.74	2.66	2.74	2.75
AL(IV)	1.24	1.25	1.21	1.25	1.24	1.17	1.26	1.34	1.26	1.25
AL(VI)	0.44	0.37	0.38	0.38	0.40	0.35	0.39	0.43	0.40	0.40
MG	1.47	1.31	1.48	1.51	1.52	1.66	1.31	1.33	1.28	1.46
FE	0.91	1.07	0.90	0.87	0.86	0.78	1.11	1.16	1.12	0.99
MN	0.00	0.02	0.03	0.03	0.02	0.01	0.01	0.01	0.01	0.00
TI	0.07	0.12	0.09	0.10	0.09	0.08	0.09	0.08	0.08	0.08
K	0.82	0.81	0.79	0.87	0.82	0.89	0.81	0.69	0.86	0.76
NA	0.07	0.01	0.02	0.02	0.02	0.02	0.04	0.04	0.04	0.05
CA	0.00	0.01	0.02	0.01	0.01	0.00	0.00	0.02	0.00	0.00
BA	0.00	0.01	0.00	0.00	0.00	0.00	0.00	0.00	0.00	0.00
F	0.09	0.02	0.06	0.05	0.05	0.08	0.12	0.13	0.12	0.07
CL	0.00	0.00	0.00	0.00	0.00	0.00	0.00	0.00	0.00	0.00
OH(C)	1.91	1.97	1.94	1.95	1.95	1.92	1.88	1.86	1.88	1.93
O	10.00	10.00	10.00	10.00	10.00	10.00	10.00	10.00	10.00	10.00
FE/FE+MG	0.38	0.45	0.38	0.37	0.36	0.32	0.46	0.47	0.47	0.40
A"	-0.20	-0.20	-0.20	-0.25	-0.21	-0.31	-0.19	-0.07	-0.24	-0.14
F"	0.46	0.54	0.45	0.46	0.44	0.42	0.55	0.50	0.58	0.46
M"	0.74	0.66	0.75	0.80	0.77	0.89	0.65	0.57	0.66	0.68

BIOTITE

SAMPLE NO.	C4-32B	C4-32B	C4-32B	C4-46A	C4-46A	C4-46A	C4-46A	C4-49B	C4-49B	C4-49B
ANALYSIS	12	34	35	10	11	30	31	06	07	32
CORE/RIM										
SIO2	37.03	37.43	37.27	36.63	36.99	37.40	36.67	37.40	37.16	36.52
AL2O3	19.42	19.40	19.33	16.70	16.90	17.92	17.20	18.33	18.54	18.39
MGO	12.75	12.53	12.60	10.20	10.20	10.00	10.20	11.79	11.76	11.71
FEO	15.53	15.39	15.46	19.63	18.50	18.63	19.55	17.42	17.23	17.75
MNO	0.05	0.05	0.06	0.24	0.21	0.18	0.23	0.08	0.05	0.10
TIO2	1.42	1.52	1.53	2.78	2.19	2.48	2.48	1.60	1.53	1.55
K2O	8.33	8.53	8.50	9.78	9.61	9.39	9.69	8.82	8.78	8.35
NA2O	0.50	0.48	0.52	0.08	0.08	0.05	0.11	0.25	0.28	0.22
CAO	0.02	0.03	0.03	0.06	0.08	0.08	0.07	0.03	0.04	0.08
BAO	0.11	0.08	0.09	0.14	0.13	0.05	0.09	0.11	0.05	0.10
F	0.36	0.25	0.30	0.28	0.37	0.31	0.37	0.37	0.36	0.47
CL	0.01	0.01	0.00	0.00	0.00	0.00	0.01	0.01	0.02	0.02
H2O(C)	3.87	3.94	3.91	3.83	3.76	3.86	3.79	3.85	3.84	3.75
SUM	99.25	99.55	99.48	100.24	98.87	100.22	100.31	99.91	99.47	98.81
SI	2.74	2.76	2.76	2.77	2.82	2.80	2.77	2.78	2.77	2.75
AL(IV)	1.26	1.24	1.24	1.23	1.18	1.20	1.23	1.22	1.23	1.25
AL(VI)	0.44	0.45	0.44	0.26	0.34	0.38	0.30	0.39	0.41	0.39
MG	1.41	1.38	1.39	1.15	1.16	1.12	1.15	1.31	1.31	1.32
FE	0.96	0.95	0.96	1.24	1.18	1.17	1.23	1.08	1.08	1.12
MN	0.00	0.00	0.00	0.02	0.01	0.01	0.01	0.00	0.00	0.01
TI	0.08	0.08	0.08	0.16	0.13	0.14	0.14	0.09	0.09	0.09
K	0.79	0.80	0.80	0.94	0.93	0.90	0.93	0.84	0.84	0.80
NA	0.07	0.07	0.07	0.01	0.01	0.01	0.02	0.04	0.04	0.03
CA	0.00	0.00	0.00	0.00	0.01	0.01	0.01	0.00	0.00	0.01
BA	0.00	0.00	0.00	0.00	0.00	0.00	0.00	0.00	0.00	0.00
F	0.08	0.06	0.07	0.07	0.09	0.07	0.09	0.09	0.08	0.11
CL	0.00	0.00	0.00	0.00	0.00	0.00	0.00	0.00	0.00	0.00
OH(C)	1.91	1.94	1.93	1.93	1.91	1.93	1.91	1.91	1.91	1.89
O	10.00	10.00	10.00	10.00	10.00	10.00	10.00	10.00	10.00	10.00
FE/FE+MG	0.41	0.41	0.41	0.52	0.50	0.51	0.52	0.45	0.45	0.46
A"	-0.16	-0.18	-0.18	-0.39	-0.38	-0.32	-0.36	-0.23	-0.23	-0.19
F"	0.47	0.48	0.48	0.72	0.70	0.68	0.71	0.56	0.55	0.55
M"	0.69	0.70	0.70	0.67	0.68	0.65	0.66	0.67	0.67	0.64

BIOTITE

SAMPLE NO.	C4-49B	D2-1CA	D2-1CA	D2-1CA	D2-1CA	D2-1CA	D2-1D	D2-1D	D2-1D	D2-1D
ANALYSIS	37	03	07	08	19	22	16	17	23	46
CORE/RIM										
SIO2	36.94	37.34	37.04	37.32	37.55	37.65	36.80	36.78	36.25	36.82
AL2O3	18.23	19.50	19.20	19.71	19.96	19.92	19.20	18.85	18.68	18.93
MGO	12.00	12.04	12.87	12.23	13.32	13.78	12.42	12.29	12.35	12.30
FEO	17.17	15.42	15.38	15.09	14.42	15.30	16.35	16.90	16.59	16.64
MNO	0.03	0.06	0.04	0.00	0.07	0.02	0.10	0.05	0.04	0.07
TIO2	1.46	2.36	1.59	2.37	1.56	1.56	1.61	1.85	1.80	1.44
K2O	8.87	8.76	8.56	8.71	8.56	7.76	8.39	8.26	8.73	8.93
NA2O	0.33	0.33	0.30	0.36	0.39	0.34	0.25	0.25	0.25	0.27
CAO	0.06	0.05	0.04	0.03	0.08	0.10	0.14	0.14	0.03	0.08
BAO	0.06	0.14	0.22	0.10	0.11	0.12	0.24	0.26	0.23	0.15
F	0.38	0.36	0.30	0.31	0.35	0.31	0.29	0.26	0.24	0.28
CL	0.02	0.00	0.00	0.00	0.00	0.00	0.02	0.00	0.00	0.01
H2O(C)	3.81	3.91	3.90	3.94	3.94	3.99	3.89	3.91	3.88	3.89
SUM	99.22	100.13	99.32	100.02	100.18	100.71	99.56	99.68	98.97	99.68
SI	2.77	2.74	2.75	2.74	2.74	2.73	2.73	2.73	2.72	2.74
AL(IV)	1.23	1.26	1.25	1.26	1.26	1.27	1.27	1.27	1.28	1.26
AL(VI)	0.38	0.44	0.42	0.44	0.46	0.43	0.42	0.39	0.38	0.40
MG	1.34	1.32	1.42	1.34	1.45	1.49	1.38	1.36	1.38	1.36
FE	1.08	0.95	0.95	0.93	0.88	0.93	1.02	1.05	1.04	1.04
MN	0.00	0.00	0.00	0.00	0.00	0.00	0.01	0.00	0.00	0.00
TI	0.08	0.13	0.09	0.13	0.09	0.08	0.09	0.10	0.10	0.08
K	0.85	0.82	0.81	0.81	0.80	0.72	0.80	0.78	0.84	0.85
NA	0.05	0.05	0.04	0.05	0.05	0.05	0.04	0.04	0.04	0.04
CA	0.00	0.00	0.00	0.00	0.01	0.01	0.01	0.01	0.00	0.01
BA	0.00	0.00	0.01	0.00	0.00	0.00	0.01	0.01	0.01	0.00
F	0.09	0.08	0.07	0.07	0.08	0.07	0.07	0.06	0.06	0.06
CL	0.00	0.00	0.00	0.00	0.00	0.00	0.00	0.00	0.00	0.00
OH(C)	1.91	1.92	1.93	1.93	1.92	1.93	1.93	1.94	1.94	1.93
O	10.00	10.00	10.00	10.00	10.00	10.00	10.00	10.00	10.00	10.00
FE/FE+MG	0.44	0.42	0.40	0.41	0.38	0.38	0.43	0.44	0.43	0.43
A"	-0.24	-0.21	-0.19	-0.20	-0.17	-0.10	-0.17	-0.17	-0.21	-0.23
F"	0.55	0.50	0.48	0.49	0.44	0.42	0.50	0.51	0.52	0.53
M"	0.69	0.70	0.71	0.71	0.73	0.68	0.67	0.66	0.69	0.70

CHLORITE

SAMPLE NO.	A2-3CA	A2-3CA	A2-3D	A2-3D	A2-3D	A2-3D	A2-3E	A2-3E	A2-11A	A2-13A
ANALYSIS	18A	19A	09A	10A	15A	16A	09BFF	10BFF	11S	05MY
CORE/RIM										
AVERAGE OF										
SIO2	25.05	25.33	26.52	27.18	24.89	25.66	26.56	25.90	24.63	25.72
AL2O3	19.63	19.51	18.76	21.37	21.27	20.66	19.18	19.68	22.79	19.22
TIO2	0.49	0.16	2.55	0.14	0.05	0.06	0.16	0.03	0.07	0.09
CR2O3	0.04	0.05	0.02	0.02	0.01	0.04	0.03	0.03	0.02	0.03
FE2O3(C)	0.00	0.00	0.00	0.00	0.00	0.00	0.27	0.15	0.00	0.00
FEO(C)	34.26	34.61	27.59	28.26	29.74	29.92	26.35	26.89	26.44	28.70
MGO	8.30	8.20	9.93	10.66	11.37	11.53	15.58	14.52	13.45	13.09
MNO	0.47	0.46	0.32	0.42	0.43	0.41	0.30	0.21	0.11	0.45
CAO	0.34	0.15	1.94	0.08	0.09	0.08	0.08	0.12	0.04	0.09
NA2O	0.04	0.01	0.02	0.02	0.00	0.00	0.01	0.05	0.00	0.01
K2O	0.31	0.34	0.94	1.00	0.04	0.03	0.02	0.02	0.03	0.04
F	0.05	0.04	0.05	0.06	0.05	0.07	0.16	0.16	0.16	0.08
CL	0.00	0.00	0.00	0.00	0.00	0.00	0.01	0.02	0.00	0.01
H2O(C)	10.75	10.71	10.39	10.70	10.90	10.86	11.34	11.17	11.02	11.03
SUM	99.71	99.56	99.01	99.87	98.84	99.31	100.00	98.87	98.70	98.52
SI	2.76	2.79	2.88	2.90	2.69	2.77	2.79	2.76	2.62	2.78
AL(IV)	1.24	1.21	1.12	1.10	1.31	1.23	1.21	1.24	1.38	1.22
AL(VI)	1.30	1.33	1.28	1.59	1.41	1.39	1.17	1.23	1.48	1.23
TI	0.04	0.01	0.21	0.01	0.00	0.00	0.01	0.00	0.01	0.01
CR	0.00	0.00	0.00	0.00	0.00	0.00	0.00	0.00	0.00	0.00
FE+3	0.00	0.00	0.00	0.00	0.00	0.00	0.02	0.01	0.00	0.00
FE+2	3.15	3.19	2.51	2.52	2.69	2.70	2.31	2.40	2.35	2.59
MG	1.36	1.35	1.61	1.69	1.84	1.85	2.44	2.31	2.14	2.11
MN	0.04	0.04	0.03	0.04	0.04	0.04	0.03	0.02	0.01	0.04
CA	0.04	0.02	0.23	0.01	0.01	0.01	0.01	0.01	0.00	0.01
NA	0.01	0.00	0.00	0.00	0.00	0.00	0.00	0.01	0.00	0.00
K	0.04	0.05	0.13	0.14	0.01	0.00	0.00	0.00	0.00	0.01
F	0.02	0.01	0.02	0.02	0.02	0.03	0.05	0.05	0.05	0.03
CL	0.00	0.00	0.00	0.00	0.00	0.00	0.00	0.00	0.00	0.00
OH(C)	7.89	7.88	7.53	7.61	7.87	7.81	7.95	7.94	7.83	7.95
O	10.09	10.11	10.45	10.37	10.11	10.17	10.00	10.00	10.11	10.02
FE/FE+MG	0.70	0.70	0.61	0.60	0.60	0.59	0.49	0.51	0.52	0.55
A	35.63	35.53	35.47	38.65	37.22	36.35	33.34	34.40	38.84	33.98
C	0.57	0.25	3.33	0.13	0.14	0.13	0.13	0.19	0.05	0.15
F	63.80	64.22	61.20	61.21	62.63	63.53	66.53	65.40	61.11	65.87
A"	0.21	0.21	0.20	0.21	0.23	0.22	0.20	0.21	0.24	0.20
F"	0.55	0.56	0.49	0.47	0.46	0.46	0.39	0.40	0.40	0.44
M"	0.24	0.24	0.31	0.32	0.31	0.32	0.41	0.39	0.36	0.36

CHLORITE

SAMPLE NO.	A2-15A	A2-15A	A2-21B	A2-22A	A2-27B	A2-27B	A3-4A	A3-4A	A3-11B	A3-11B
ANALYSIS	09U	10U	18SQM	05SQM	25U	26U	10S	27S	03G	23G
CORE/RIM										
AVERAGE OF										
SIO2	26.51	25.95	24.88	25.73	26.01	26.54	25.66	25.47	25.73	26.07
AL2O3	19.74	19.93	21.59	22.93	19.64	19.84	21.90	22.91	20.98	20.37
TIO2	0.06	0.04	0.12	0.11	0.03	0.09	0.10	0.13	0.15	0.11
CR2O3	0.01	0.04	0.00	0.00	0.00	0.07	0.01	0.05	0.03	0.03
FE2O3(C)	0.00	0.00	0.00	0.00	0.00	0.00	0.00	0.00	0.00	0.00
FEO(C)	28.83	29.06	27.15	24.65	28.16	28.41	27.05	27.28	28.87	29.21
MGO	13.85	13.18	12.96	14.67	13.49	13.55	12.85	12.29	11.44	11.89
MNO	0.27	0.30	0.31	0.26	0.22	0.23	0.26	0.29	0.24	0.26
CAO	0.06	0.07	0.02	0.03	0.04	0.04	0.04	0.11	0.08	0.08
NA2O	0.02	0.00	0.01	0.01	0.02	0.01	0.00	0.01	0.00	0.00
K2O	0.02	0.02	0.02	0.13	0.04	0.02	0.04	0.08	0.02	0.03
F	0.14	0.12	0.00	0.00	0.14	0.11	0.07	0.18	0.08	0.08
CL	0.00	0.00	0.00	0.00	0.01	0.00	0.01	0.00	0.00	0.01
H2O(C)	11.27	11.13	10.96	11.20	11.01	11.08	10.85	10.82	10.60	10.75
SUM	100.71	99.78	98.01	99.71	98.75	99.94	98.80	99.53	98.19	98.86
SI	2.79	2.77	2.68	2.69	2.79	2.81	2.74	2.70	2.79	2.81
AL(IV)	1.21	1.23	1.32	1.31	1.21	1.19	1.26	1.30	1.21	1.19
AL(VI)	1.24	1.27	1.43	1.51	1.28	1.30	1.50	1.57	1.48	1.40
TI	0.00	0.00	0.01	0.01	0.00	0.01	0.01	0.01	0.01	0.01
CR	0.00	0.00	0.00	0.00	0.00	0.01	0.00	0.00	0.00	0.00
FE+3	0.00	0.00	0.00	0.00	0.00	0.00	0.00	0.00	0.00	0.00
FE+2	2.54	2.59	2.45	2.15	2.53	2.52	2.42	2.42	2.62	2.64
MG	2.18	2.10	2.08	2.28	2.16	2.14	2.05	1.94	1.85	1.91
MN	0.02	0.03	0.03	0.02	0.02	0.02	0.02	0.03	0.02	0.02
CA	0.01	0.01	0.00	0.00	0.00	0.00	0.00	0.01	0.01	0.01
NA	0.00	0.00	0.00	0.00	0.00	0.00	0.00	0.00	0.00	0.00
K	0.00	0.00	0.00	0.02	0.00	0.00	0.01	0.01	0.00	0.00
F	0.05	0.04	0.00	0.00	0.05	0.04	0.02	0.06	0.03	0.03
CL	0.00	0.00	0.00	0.00	0.00	0.00	0.00	0.00	0.00	0.00
OH(C)	7.92	7.92	7.88	7.81	7.89	7.84	7.73	7.66	7.68	7.74
O	10.04	10.04	10.12	10.19	10.06	10.12	10.25	10.28	10.30	10.23
FE/FE+MG	0.54	0.55	0.54	0.49	0.54	0.54	0.54	0.56	0.59	0.58
A	34.06	34.67	37.56	38.75	34.52	34.61	38.04	39.42	37.34	36.12
C	0.09	0.11	0.02	0.04	0.07	0.05	0.07	0.17	0.14	0.13
F	65.85	65.23	62.41	61.21	65.41	65.34	61.90	60.41	62.53	63.76
A"	0.21	0.21	0.23	0.24	0.21	0.21	0.24	0.25	0.23	0.22
F"	0.43	0.44	0.42	0.37	0.43	0.43	0.41	0.42	0.45	0.45
M"	0.37	0.35	0.35	0.39	0.37	0.36	0.35	0.34	0.32	0.33

CHLORITE

SAMPLE NO.	A3-11B	A3-43B	A3-43B	A3-71A	A3-71A	A3-71A	A3-92A	A3-92A	A4-2A	A4-2A
ANALYSIS	24G	05A	16A	08A	09A	13A	07A	20A	03G	04G
CORE/RIM						A				
AVERAGE OF										
SIO2	25.73	26.68	26.78	26.53	26.22	25.82	26.49	26.65	25.70	25.55
AL2O3	20.39	21.77	20.87	20.94	21.77	23.01	21.89	22.23	22.10	22.35
TIO2	0.09	0.12	0.11	0.24	0.17	0.13	0.09	0.10	0.19	0.16
CR2O3	0.05	0.17	0.09	0.02	0.05	0.13	0.05	0.12	0.01	0.06
FE2O3(C)	0.00	0.00	0.00	0.00	0.00	0.00	0.00	0.00	0.00	0.00
FEO(C)	29.37	18.64	18.30	21.48	21.29	21.46	19.76	20.19	20.90	20.90
MGO	11.73	19.98	20.40	17.48	17.17	17.12	19.34	19.74	17.82	17.74
MNO	0.23	0.26	0.24	0.29	0.26	0.34	0.31	0.28	0.29	0.31
CAO	0.08	0.03	0.03	0.13	0.32	0.07	0.07	0.02	0.02	0.02
NA2O	0.00	0.00	0.01	0.00	0.00	0.00	0.00	0.00	0.00	0.00
K2O	0.02	0.01	0.00	0.03	0.03	0.01	0.05	0.01	0.01	0.00
F	0.09	0.06	0.03	0.15	0.13	0.17	0.04	0.05	0.09	0.12
CL	0.00	0.00	0.01	0.02	0.01	0.01	0.01	0.01	0.00	0.00
H2O(C)	10.74	11.64	11.63	11.21	11.23	11.33	11.69	11.91	11.39	11.39
SUM	98.47	99.33	98.50	98.43	98.60	99.52	99.77	101.27	98.49	98.55
SI	2.79	2.72	2.75	2.77	2.73	2.66	2.70	2.68	2.67	2.65
AL(IV)	1.21	1.28	1.25	1.23	1.27	1.34	1.30	1.32	1.33	1.35
AL(VI)	1.40	1.33	1.27	1.34	1.40	1.46	1.33	1.31	1.38	1.39
TI	0.01	0.01	0.01	0.02	0.01	0.01	0.01	0.01	0.02	0.01
CR	0.00	0.01	0.01	0.00	0.00	0.01	0.00	0.01	0.00	0.00
FE+3	0.00	0.00	0.00	0.00	0.00	0.00	0.00	0.00	0.00	0.00
FE+2	2.66	1.59	1.57	1.88	1.85	1.85	1.68	1.69	1.82	1.82
MG	1.90	3.03	3.12	2.72	2.66	2.63	2.94	2.95	2.76	2.75
MN	0.02	0.02	0.02	0.02	0.02	0.03	0.03	0.02	0.03	0.03
CA	0.01	0.00	0.00	0.02	0.04	0.01	0.01	0.00	0.00	0.00
NA	0.00	0.00	0.00	0.00	0.00	0.00	0.00	0.00	0.00	0.00
K	0.00	0.00	0.00	0.00	0.00	0.00	0.01	0.00	0.00	0.00
F	0.03	0.02	0.01	0.05	0.04	0.06	0.01	0.02	0.03	0.04
CL	0.00	0.00	0.00	0.00	0.00	0.00	0.00	0.00	0.00	0.00
OH(C)	7.77	7.90	7.95	7.80	7.80	7.79	7.95	7.98	7.89	7.89
O	10.20	10.08	10.04	10.15	10.16	10.15	10.04	10.01	10.08	10.07
FE/FE+MG	0.58	0.34	0.33	0.41	0.41	0.41	0.36	0.37	0.40	0.40
A	36.22	36.00	34.86	35.73	36.85	38.22	36.09	36.01	37.02	37.33
C	0.13	0.05	0.05	0.20	0.50	0.10	0.11	0.03	0.03	0.04
F	63.65	63.96	65.09	64.07	62.65	61.68	63.80	63.96	62.95	62.63
A"	0.22	0.22	0.21	0.22	0.23	0.24	0.22	0.22	0.23	0.23
F"	0.45	0.27	0.26	0.32	0.32	0.31	0.28	0.28	0.31	0.31
M"	0.32	0.51	0.52	0.46	0.46	0.45	0.50	0.50	0.47	0.46

CHLORITE

SAMPLE NO.	A4-6A	A4-6A	A4-7C	A4-7C	A4-8A	A4-8A	A4-8A	A4-19A	A4-19A	A4-19A
ANALYSIS	07G	08G	03C	05C	47G	48G	69G	04G	05G	17G
CORE/RIM										
AVERAGE OF										
SIO2	25.41	26.01	25.94	25.04	25.08	25.19	24.58	26.09	26.04	25.85
AL2O3	21.88	22.37	23.35	23.76	21.39	21.62	22.06	23.33	23.82	23.57
TIO2	0.10	0.11	0.10	0.05	0.12	0.07	0.20	0.14	0.11	0.10
CR2O3	0.07	0.08	0.04	0.00	0.05	0.05	0.06	0.01	0.05	0.03
FE2O3(C)	0.00	0.00	0.00	0.00	0.00	0.00	0.00	0.00	0.00	0.00
FEO(C)	25.40	24.83	23.42	23.14	29.06	28.98	28.83	19.53	19.59	19.57
MGO	14.24	13.85	15.88	15.46	11.52	11.59	11.62	18.41	18.57	18.31
MNO	0.23	0.23	0.26	0.25	0.27	0.24	0.32	0.46	0.37	0.37
CAO	0.07	0.07	0.02	0.02	0.12	0.12	0.09	0.08	0.09	0.03
NA2O	0.00	0.02	0.02	0.00	0.00	0.03	0.00	0.05	0.02	0.03
K2O	0.02	0.06	0.00	0.01	0.08	0.06	0.17	0.02	0.02	0.04
F	0.05	0.07	0.06	0.08	0.10	0.09	0.11	0.08	0.07	0.05
CL	0.01	0.01	0.00	0.00	0.00	0.01	0.00	0.02	0.02	0.02
H2O(C)	11.03	10.82	11.34	11.21	10.79	10.83	10.92	11.53	11.61	11.52
SUM	98.50	98.49	100.41	98.99	98.54	98.83	98.91	99.71	100.33	99.45
SI	2.70	2.76	2.67	2.61	2.72	2.72	2.65	2.66	2.64	2.64
AL(IV)	1.30	1.24	1.33	1.39	1.28	1.28	1.35	1.34	1.36	1.36
AL(VI)	1.44	1.55	1.51	1.54	1.44	1.46	1.45	1.46	1.48	1.48
TI	0.01	0.01	0.01	0.00	0.01	0.01	0.02	0.01	0.01	0.01
CR	0.01	0.01	0.00	0.00	0.00	0.00	0.00	0.00	0.00	0.00
FE+3	0.00	0.00	0.00	0.00	0.00	0.00	0.00	0.00	0.00	0.00
FE+2	2.26	2.20	2.02	2.02	2.63	2.61	2.60	1.66	1.66	1.67
MG	2.26	2.19	2.44	2.41	1.86	1.86	1.87	2.80	2.80	2.79
MN	0.02	0.02	0.02	0.02	0.02	0.02	0.03	0.04	0.03	0.03
CA	0.01	0.01	0.00	0.00	0.01	0.01	0.01	0.01	0.01	0.00
NA	0.00	0.00	0.00	0.00	0.00	0.01	0.00	0.01	0.00	0.01
K	0.00	0.01	0.00	0.00	0.01	0.01	0.02	0.00	0.00	0.00
F	0.02	0.02	0.02	0.03	0.03	0.03	0.04	0.02	0.02	0.02
CL	0.00	0.00	0.00	0.00	0.00	0.00	0.00	0.00	0.00	0.00
OH(C)	7.82	7.65	7.79	7.81	7.79	7.79	7.85	7.84	7.84	7.85
O	10.16	10.33	10.19	10.16	10.18	10.18	10.11	10.13	10.13	10.13
FE/FE+MG	0.50	0.50	0.45	0.46	0.59	0.58	0.58	0.37	0.37	0.38
A	37.62	38.75	38.75	39.65	37.60	37.85	38.35	38.32	38.70	38.70
C	0.12	0.11	0.04	0.02	0.20	0.19	0.14	0.12	0.13	0.05
F	62.26	61.15	61.21	60.32	62.21	61.96	61.51	61.55	61.17	61.26
A"	0.23	0.24	0.24	0.25	0.23	0.23	0.23	0.24	0.24	0.24
F"	0.38	0.38	0.34	0.34	0.45	0.45	0.45	0.28	0.28	0.29
M"	0.38	0.38	0.42	0.41	0.32	0.32	0.32	0.48	0.48	0.48

CHLORITE

SAMPLE NO.	A4-22A	A4-22A	B2-1AB	B2-1AB	B2-1B	B2-1B	B2-1Y	B2-1Y	B2-1Y	B2-3A
ANALYSIS	15A	16A	19G	24G	23G	24G	07G	08G	27G	20G
CORE/RIM			G							
AVERAGE OF										
SIO2	26.17	26.68	26.39	26.57	29.02	26.56	27.85	26.09	25.86	25.66
AL2O3	22.05	21.67	21.32	20.85	22.84	22.64	21.77	22.79	22.44	22.13
TIO2	0.07	0.06	0.04	0.03	0.05	0.09	0.29	0.12	0.16	0.00
CR2O3	0.08	0.06	0.04	0.02	0.05	0.04	0.03	0.02	0.06	0.02
FE2O3(C)	0.00	0.00	0.00	0.00	0.00	0.00	0.00	0.00	0.00	0.00
FEO(C)	22.07	19.85	22.12	22.96	19.92	21.32	19.63	20.16	20.55	25.24
MGO	16.83	18.80	16.76	16.67	16.57	17.73	17.43	18.11	17.07	13.97
MNO	0.27	0.22	0.56	0.56	0.41	0.35	0.38	0.43	0.50	0.29
CAO	0.04	0.03	0.05	0.06	0.19	0.05	0.07	0.06	0.09	0.07
NA2O	0.00	0.00	0.00	0.00	0.48	0.00	0.00	0.00	0.00	0.00
K2O	0.01	0.01	0.01	0.02	0.01	0.02	1.23	0.12	0.55	0.17
F	0.12	0.12	0.00	0.01	0.07	0.04	0.07	0.05	0.08	0.09
CL	0.01	0.01	0.00	0.00	0.00	0.01	0.00	0.00	0.00	0.01
H2O(C)	11.23	11.40	11.24	11.32	11.08	11.49	11.47	11.50	11.41	10.98
SUM	98.90	98.86	98.52	99.06	100.65	100.33	100.20	99.41	98.76	98.59
SI	2.72	2.75	2.76	2.77	2.94	2.71	2.84	2.68	2.69	2.72
AL(IV)	1.28	1.25	1.24	1.23	1.06	1.29	1.16	1.32	1.31	1.28
AL(VI)	1.43	1.37	1.39	1.34	1.66	1.43	1.45	1.43	1.43	1.49
TI	0.00	0.00	0.00	0.00	0.00	0.01	0.02	0.01	0.01	0.00
CR	0.01	0.00	0.00	0.00	0.00	0.00	0.00	0.00	0.00	0.00
FE+3	0.00	0.00	0.00	0.00	0.00	0.00	0.00	0.00	0.00	0.00
FE+2	1.92	1.71	1.94	2.00	1.69	1.82	1.67	1.73	1.78	2.24
MG	2.61	2.89	2.61	2.59	2.50	2.70	2.65	2.77	2.64	2.21
MN	0.02	0.02	0.05	0.05	0.04	0.03	0.03	0.04	0.04	0.03
CA	0.00	0.00	0.01	0.01	0.02	0.01	0.01	0.01	0.01	0.01
NA	0.00	0.00	0.00	0.00	0.10	0.00	0.00	0.00	0.00	0.00
K	0.00	0.00	0.00	0.00	0.00	0.00	0.16	0.02	0.07	0.02
F	0.04	0.04	0.00	0.00	0.02	0.01	0.02	0.02	0.02	0.03
CL	0.00	0.00	0.00	0.00	0.00	0.00	0.00	0.00	0.00	0.00
OH(C)	7.79	7.82	7.84	7.88	7.47	7.82	7.80	7.87	7.90	7.77
O	10.17	10.13	10.16	10.11	10.51	10.16	10.18	10.11	10.07	10.19
FE/FE+MG	0.42	0.37	0.43	0.44	0.40	0.40	0.39	0.38	0.40	0.50
A	37.23	36.28	36.34	35.53	39.10	37.43	37.48	37.76	38.00	38.17
C	0.06	0.05	0.08	0.10	0.30	0.08	0.11	0.09	0.14	0.11
F	62.71	63.67	63.59	64.38	60.60	62.49	62.41	62.15	61.86	61.72
A"	0.23	0.22	0.22	0.22	0.25	0.23	0.20	0.23	0.22	0.23
F"	0.33	0.29	0.33	0.34	0.30	0.31	0.31	0.30	0.31	0.39
M"	0.44	0.49	0.45	0.44	0.45	0.46	0.49	0.47	0.46	0.38

CHLORITE

SAMPLE NO.	B2-3A	B2-4A	B2-24A	B2-35A	B2-35A	B2-35A	B2-35C	B2-35C	B3-25B	B3-25B
ANALYSIS	21G	14A	10A	10G	11G	36G	11A	13A	03C	04C
CORE/RIM										
AVERAGE OF										
SIO2	25.49	26.14	27.54	25.31	25.89	25.57	23.77	25.56	24.21	24.46
AL2O3	22.16	21.71	21.97	21.21	21.66	21.83	28.80	23.11	23.41	23.16
TIO2	0.11	0.03	0.05	0.07	0.04	0.12	0.14	0.10	0.10	0.09
CR2O3	0.04	0.01	0.08	0.06	0.02	0.03	0.10	0.12	0.00	0.03
FE2O3(C)	0.00	0.00	0.00	0.00	0.00	0.00	0.00	0.00	0.00	0.00
FEO(C)	25.62	20.36	19.63	27.63	27.11	25.99	19.60	21.32	26.34	25.69
MGO	13.94	18.11	18.96	12.69	13.12	14.14	15.76	17.41	13.67	13.52
MNO	0.36	0.27	0.27	0.73	0.66	0.44	0.22	0.28	0.23	0.22
CAO	0.05	0.11	0.10	0.06	0.07	0.04	0.09	0.05	0.04	0.02
NA2O	0.00	0.04	0.00	0.01	0.04	0.00	0.00	0.00	0.00	0.01
K2O	0.11	0.01	0.01	0.02	0.03	0.04	0.02	0.01	0.02	0.01
F	0.07	0.12	0.00	0.09	0.09	0.05	0.16	0.19	0.14	0.10
CL	0.00	0.00	0.00	0.01	0.00	0.00	0.00	0.00	0.00	0.01
H2O(C)	11.05	11.35	11.49	10.95	11.03	11.14	11.20	11.40	11.20	10.99
SUM	98.97	98.21	100.09	98.81	99.73	99.36	99.79	99.48	99.30	98.26
SI	2.70	2.72	2.79	2.72	2.74	2.70	2.42	2.63	2.56	2.61
AL(IV)	1.30	1.28	1.21	1.28	1.26	1.30	1.58	1.37	1.44	1.39
AL(VI)	1.47	1.38	1.42	1.40	1.44	1.42	1.88	1.44	1.48	1.52
TI	0.01	0.00	0.00	0.01	0.00	0.01	0.01	0.01	0.01	0.01
CR	0.00	0.00	0.01	0.00	0.00	0.00	0.01	0.01	0.00	0.00
FE+3	0.00	0.00	0.00	0.00	0.00	0.00	0.00	0.00	0.00	0.00
FE+2	2.27	1.77	1.67	2.48	2.40	2.30	1.67	1.84	2.33	2.29
MG	2.20	2.81	2.87	2.03	2.07	2.23	2.40	2.68	2.15	2.15
MN	0.03	0.02	0.02	0.07	0.06	0.04	0.02	0.02	0.02	0.02
CA	0.01	0.01	0.01	0.01	0.01	0.00	0.01	0.00	0.00	0.00
NA	0.00	0.01	0.00	0.00	0.01	0.00	0.00	0.00	0.00	0.00
K	0.02	0.00	0.00	0.00	0.00	0.01	0.00	0.00	0.00	0.00
F	0.02	0.04	0.00	0.03	0.03	0.02	0.05	0.06	0.05	0.03
CL	0.00	0.00	0.00	0.00	0.00	0.00	0.00	0.00	0.00	0.00
OH(C)	7.81	7.87	7.77	7.84	7.79	7.85	7.62	7.84	7.90	7.82
O	10.17	10.09	10.23	10.13	10.18	10.13	10.33	10.10	10.05	10.15
FE/FE+MG	0.51	0.39	0.37	0.55	0.54	0.51	0.41	0.41	0.52	0.52
A	38.03	36.57	36.51	36.93	37.32	37.31	45.80	38.20	39.28	39.48
C	0.08	0.16	0.15	0.10	0.11	0.06	0.13	0.07	0.06	0.04
F	61.89	63.26	63.34	62.98	62.56	62.63	54.07	61.73	60.66	60.48
A"	0.23	0.23	0.22	0.23	0.23	0.23	0.30	0.24	0.25	0.25
F"	0.39	0.30	0.29	0.42	0.41	0.39	0.29	0.31	0.39	0.39
M"	0.38	0.48	0.49	0.35	0.36	0.38	0.41	0.45	0.36	0.37

CHLORITE

SAMPLE NO.	B3-25B	B3-30A	B3-63A	B3-63A	B3-127A	B3-127A	B3-141A	B3-141A	B3-156A	B3156AA
ANALYSIS	13C	04S	03G	18G	14A	15A	21G	23G	21C	38S
CORE/RIM										
AVERAGE OF										
SIO2	24.37	24.74	25.15	24.82	26.73	27.01	27.10	26.33	25.15	24.99
AL2O3	23.91	23.98	23.15	23.54	22.14	22.00	23.06	22.35	23.14	22.96
TIO2	0.06	0.11	0.05	0.06	0.11	0.12	0.12	0.12	0.05	0.08
CR2O3	0.03	0.04	0.03	0.04	0.04	0.14	0.02	0.04	0.04	0.06
FE2O3(C)	0.00	0.00	0.00	0.00	0.00	0.00	0.00	0.00	0.00	0.00
FEO(C)	25.76	25.89	25.53	26.50	17.21	17.37	18.59	18.46	25.98	24.80
MGO	13.54	13.55	14.05	12.89	20.48	20.36	19.05	19.60	13.81	14.16
MNO	0.28	0.10	0.12	0.23	0.30	0.26	0.50	0.43	0.31	0.26
CAO	0.07	0.03	0.05	0.07	0.05	0.06	0.04	0.02	0.04	0.08
NA2O	0.01	0.00	0.00	0.00	0.01	0.00	0.00	0.00	0.00	0.02
K2O	0.02	0.02	0.01	0.01	0.11	0.11	0.01	0.01	0.01	0.03
F	0.19	0.09	0.10	0.12	0.01	0.01	0.01	0.02	0.11	0.04
CL	0.01	0.00	0.00	0.01	0.00	0.00	0.00	0.00	0.00	0.00
H2O(C)	11.08	11.09	11.09	10.94	11.65	11.60	11.47	11.59	11.12	11.06
SUM	99.24	99.61	99.29	99.18	98.84	99.04	99.95	98.96	99.72	98.53
SI	2.57	2.60	2.65	2.63	2.72	2.74	2.74	2.69	2.64	2.65
AL(IV)	1.43	1.40	1.35	1.37	1.28	1.26	1.26	1.31	1.36	1.35
AL(VI)	1.55	1.57	1.52	1.57	1.37	1.38	1.49	1.38	1.51	1.51
TI	0.00	0.01	0.00	0.00	0.01	0.01	0.01	0.01	0.00	0.01
CR	0.00	0.00	0.00	0.00	0.00	0.01	0.00	0.00	0.00	0.00
FE+3	0.00	0.00	0.00	0.00	0.00	0.00	0.00	0.00	0.00	0.00
FE+2	2.27	2.28	2.25	2.35	1.46	1.48	1.57	1.58	2.28	2.20
MG	2.13	2.12	2.21	2.04	3.10	3.08	2.87	2.99	2.16	2.24
MN	0.02	0.01	0.01	0.02	0.02	0.02	0.04	0.04	0.03	0.02
CA	0.01	0.00	0.00	0.01	0.01	0.01	0.00	0.00	0.00	0.01
NA	0.00	0.00	0.00	0.00	0.00	0.00	0.00	0.00	0.00	0.00
K	0.00	0.00	0.00	0.00	0.01	0.01	0.00	0.00	0.00	0.00
F	0.06	0.03	0.03	0.04	0.00	0.00	0.00	0.01	0.04	0.01
CL	0.00	0.00	0.00	0.00	0.00	0.00	0.00	0.00	0.00	0.00
OH(C)	7.81	7.78	7.79	7.74	7.90	7.86	7.74	7.90	7.80	7.82
O	10.13	10.19	10.18	10.22	10.10	10.14	10.25	10.10	10.16	10.17
FE/FE+MG	0.52	0.52	0.50	0.54	0.32	0.32	0.35	0.35	0.51	0.50
A	40.14	40.24	39.13	39.99	36.59	36.47	37.97	36.90	39.02	39.10
C	0.10	0.05	0.07	0.11	0.08	0.09	0.06	0.03	0.06	0.13
F	59.76	59.71	60.80	59.90	63.34	63.44	61.98	63.07	60.92	60.77
A"	0.25	0.25	0.24	0.25	0.22	0.22	0.24	0.23	0.24	0.24
F"	0.39	0.39	0.38	0.40	0.25	0.25	0.27	0.27	0.39	0.38
M"	0.36	0.36	0.38	0.35	0.53	0.53	0.49	0.50	0.37	0.38

CHLORITE

SAMPLE NO.	B3-165A	B3-165A	B3-165A	B3-170A	B3-170A	B3-185A	B3-185A	B3261AB	B3261AB	B4-1D
ANALYSIS	14S	15S	18S	07A	08A	16G	27G	28S	30S	16G
CORE/RIM										
AVERAGE OF										
SIO2	25.08	25.02	25.69	27.48	27.57	26.74	26.56	28.03	27.15	28.74
AL2O3	21.96	22.27	21.77	22.63	22.49	20.98	22.36	22.10	22.90	21.39
TIO2	0.17	0.14	0.11	0.08	0.12	0.05	0.22	0.07	0.09	0.05
CR2O3	0.10	0.08	0.09	0.08	0.07	0.05	0.01	0.09	0.10	0.00
FE2O3(C)	0.00	0.00	0.00	0.00	0.00	0.00	0.00	0.00	0.00	0.00
FEO(C)	26.08	25.48	25.81	13.13	12.33	23.87	22.49	12.05	12.48	10.63
MGO	14.02	14.03	14.45	23.87	24.39	15.34	16.30	23.86	23.18	25.03
MNO	0.25	0.21	0.26	0.67	0.67	0.44	0.43	0.79	0.95	0.97
CAO	0.12	0.09	0.06	0.02	0.01	0.06	0.04	0.04	0.04	0.03
NA2O	0.03	0.04	0.00	0.00	0.00	0.01	0.02	0.02	0.00	0.02
K2O	0.12	0.13	0.12	0.01	0.01	0.02	0.08	0.28	0.11	0.01
F	0.10	0.10	0.08	0.05	0.09	0.08	0.08	0.13	0.10	0.13
CL	0.05	0.01	0.00	0.00	0.00	0.00	0.01	0.00	0.00	0.00
H2O(C)	11.17	11.10	11.20	12.05	12.03	10.98	11.22	11.88	11.80	11.79
SUM	99.19	98.69	99.63	100.06	99.74	98.59	99.78	99.28	98.85	98.74
SI	2.66	2.66	2.70	2.71	2.72	2.82	2.74	2.78	2.71	2.84
AL(IV)	1.34	1.34	1.30	1.29	1.28	1.18	1.26	1.22	1.29	1.16
AL(VI)	1.40	1.44	1.40	1.34	1.33	1.43	1.47	1.36	1.40	1.34
TI	0.01	0.01	0.01	0.01	0.01	0.00	0.02	0.00	0.01	0.00
CR	0.01	0.01	0.01	0.01	0.00	0.00	0.00	0.01	0.01	0.00
FE+3	0.00	0.00	0.00	0.00	0.00	0.00	0.00	0.00	0.00	0.00
FE+2	2.31	2.26	2.27	1.08	1.02	2.10	1.94	1.00	1.04	0.88
MG	2.21	2.22	2.27	3.51	3.58	2.41	2.51	3.52	3.45	3.69
MN	0.02	0.02	0.02	0.06	0.06	0.04	0.04	0.07	0.08	0.08
CA	0.01	0.01	0.01	0.00	0.00	0.01	0.00	0.00	0.00	0.00
NA	0.01	0.01	0.00	0.00	0.00	0.00	0.00	0.00	0.00	0.00
K	0.02	0.02	0.02	0.00	0.00	0.00	0.01	0.04	0.01	0.00
F	0.03	0.03	0.03	0.01	0.03	0.03	0.03	0.04	0.03	0.04
CL	0.01	0.00	0.00	0.00	0.00	0.00	0.00	0.00	0.00	0.00
OH(C)	7.89	7.86	7.86	7.92	7.90	7.72	7.74	7.85	7.85	7.78
O	10.07	10.10	10.11	10.06	10.07	10.25	10.23	10.11	10.12	10.18
FE/FE+MG	0.51	0.50	0.50	0.24	0.22	0.47	0.44	0.22	0.23	0.19
A	37.55	38.18	37.15	36.12	35.93	36.37	37.72	35.97	37.07	34.89
C	0.19	0.14	0.09	0.03	0.01	0.10	0.05	0.05	0.05	0.05
F	62.26	61.68	62.76	63.84	64.05	63.54	62.22	63.97	62.88	65.06
A"	0.23	0.23	0.23	0.22	0.22	0.22	0.23	0.21	0.23	0.21
F"	0.39	0.39	0.39	0.18	0.17	0.36	0.33	0.17	0.18	0.15
M"	0.38	0.38	0.39	0.59	0.61	0.42	0.43	0.61	0.59	0.63

CHLORITE

SAMPLE NO.	B4-1D	B4-1E	B4-1E	B4-7C	B4-7C	B4-7C	B4-7C	B4-11J	B4-11J	B4-11K
ANALYSIS	17G	09S	10S	02A	21A	22A	08A	07O	08O	16G
CORE/RIM										
AVERAGE OF										
SIO2	28.54	28.78	28.17	26.43	27.73	27.57	26.90	28.50	28.65	27.14
AL2O3	21.50	21.01	21.84	21.78	19.66	19.62	20.69	22.32	22.30	22.00
TIO2	0.06	0.04	0.04	0.04	0.03	0.01	0.04	0.07	0.07	0.13
CR2O3	0.02	0.06	0.07	0.04	0.05	0.07	0.00	0.01	0.00	0.07
FE2O3(C)	0.00	0.00	0.00	0.00	0.00	0.00	0.00	0.00	0.00	0.00
FEO(C)	10.65	9.96	10.08	21.33	22.74	22.89	24.22	9.68	9.45	14.46
MGO	25.19	26.45	26.04	17.56	16.91	16.74	15.71	26.69	26.86	22.95
MNO	0.95	0.54	0.57	0.43	0.38	0.33	0.34	0.67	0.58	0.61
CAO	0.03	0.01	0.00	0.03	0.05	0.07	0.05	0.02	0.02	0.06
NA2O	0.03	0.05	0.02	0.00	0.01	0.02	0.03	0.01	0.00	0.01
K2O	0.01	0.01	0.00	0.01	0.09	0.08	0.01	0.00	0.01	0.01
F	0.08	0.09	0.14	0.04	0.02	0.05	0.08	0.16	0.15	0.13
CL	0.00	0.01	0.00	0.00	0.00	0.01	0.00	0.00	0.00	0.00
H2O(C)	11.90	12.06	12.03	11.37	11.16	11.12	11.12	12.22	12.20	11.90
SUM	98.92	99.03	98.95	99.04	98.82	98.55	99.15	100.29	100.22	99.40
SI	2.82	2.82	2.77	2.74	2.90	2.89	2.82	2.76	2.77	2.71
AL(IV)	1.18	1.18	1.23	1.26	1.10	1.11	1.18	1.24	1.23	1.29
AL(VI)	1.32	1.25	1.30	1.39	1.32	1.32	1.38	1.30	1.31	1.30
TI	0.00	0.00	0.00	0.00	0.00	0.00	0.00	0.00	0.00	0.01
CR	0.00	0.00	0.00	0.00	0.00	0.00	0.00	0.00	0.00	0.00
FE+3	0.00	0.00	0.00	0.00	0.00	0.00	0.00	0.00	0.00	0.00
FE+2	0.88	0.82	0.83	1.85	1.99	2.01	2.12	0.78	0.76	1.21
MG	3.71	3.87	3.81	2.71	2.64	2.62	2.45	3.85	3.87	3.42
MN	0.08	0.05	0.05	0.04	0.03	0.03	0.03	0.05	0.05	0.05
CA	0.00	0.00	0.00	0.00	0.01	0.01	0.01	0.00	0.00	0.01
NA	0.01	0.01	0.00	0.00	0.00	0.00	0.01	0.00	0.00	0.00
K	0.00	0.00	0.00	0.00	0.01	0.01	0.00	0.00	0.00	0.00
F	0.02	0.03	0.04	0.01	0.01	0.02	0.03	0.05	0.05	0.04
CL	0.00	0.00	0.00	0.00	0.00	0.00	0.00	0.00	0.00	0.00
OH(C)	7.84	7.89	7.89	7.85	7.78	7.78	7.78	7.88	7.86	7.93
O	10.14	10.08	10.07	10.14	10.21	10.20	10.20	10.07	10.09	10.03
FE/FE+MG	0.19	0.17	0.18	0.40	0.43	0.43	0.46	0.17	0.17	0.26
A	34.89	33.93	35.03	36.63	34.18	34.22	35.65	35.18	35.17	35.61
C	0.04	0.01	0.00	0.05	0.08	0.11	0.08	0.03	0.03	0.08
F	65.07	66.06	64.97	63.32	65.73	65.68	64.27	64.79	64.80	64.31
A"	0.21	0.21	0.21	0.23	0.20	0.21	0.22	0.21	0.21	0.22
F"	0.15	0.14	0.14	0.31	0.34	0.35	0.36	0.13	0.13	0.20
M"	0.63	0.66	0.65	0.46	0.45	0.45	0.42	0.65	0.66	0.58

CHLORITE

SAMPLE NO.	B4-11K	B4-11K	B4-11K	B4-11K	B4-11KA	B4-11KA	B4-11KA	B4-11L	B4-11L	B4-13A
ANALYSIS	17G	47G	40G	41G	010	020	070	16S	15S	24A
CORE/RIM										
AVERAGE OF										
SIO2	27.18	26.67	27.47	26.96	27.74	27.72	28.16	25.43	25.44	28.45
AL2O3	22.32	23.30	21.59	21.62	21.52	21.63	21.22	22.86	22.71	18.58
TIO2	0.15	0.08	0.07	0.07	0.06	0.12	0.08	0.07	0.08	0.10
CR2O3	0.04	0.09	0.08	0.11	0.03	0.00	0.01	0.02	0.03	0.05
FE2O3(C)	0.00	0.00	0.00	0.50	0.00	0.00	0.00	0.00	0.00	0.00
FEO(C)	14.41	14.19	14.85	16.48	12.06	12.05	12.40	24.20	24.01	21.68
MGO	23.21	22.51	23.01	21.76	24.73	24.79	24.71	15.11	14.96	17.71
MNO	0.61	0.59	0.69	0.75	0.54	0.53	0.49	0.38	0.34	0.25
CAO	0.05	0.06	0.03	0.02	0.02	0.02	0.03	0.02	0.02	0.13
NA2O	0.01	0.01	0.01	0.02	0.00	0.02	0.00	0.04	0.00	0.05
K2O	0.01	0.01	0.01	0.01	0.01	0.01	0.01	0.05	0.05	0.26
F	0.11	0.10	0.15	0.12	0.10	0.13	0.21	0.08	0.05	0.05
CL	0.00	0.00	0.00	0.01	0.00	0.00	0.00	0.01	0.01	0.00
H2O(C)	12.02	11.87	11.94	11.92	11.96	11.98	11.89	11.25	11.12	11.18
SUM	100.09	99.45	99.83	100.31	98.74	98.94	99.14	99.48	98.78	98.46
SI	2.69	2.66	2.74	2.70	2.76	2.75	2.79	2.66	2.68	2.97
AL(IV)	1.31	1.34	1.26	1.30	1.24	1.25	1.21	1.34	1.32	1.03
AL(VI)	1.30	1.40	1.27	1.25	1.28	1.28	1.27	1.47	1.49	1.26
TI	0.01	0.01	0.00	0.00	0.00	0.01	0.01	0.01	0.01	0.01
CR	0.00	0.01	0.01	0.01	0.00	0.00	0.00	0.00	0.00	0.00
FE+3	0.00	0.00	0.00	0.04	0.00	0.00	0.00	0.00	0.00	0.00
FE+2	1.19	1.18	1.24	1.38	1.00	1.00	1.03	2.11	2.11	1.89
MG	3.43	3.35	3.42	3.25	3.66	3.66	3.65	2.35	2.35	2.76
MN	0.05	0.05	0.06	0.06	0.05	0.04	0.04	0.03	0.03	0.02
CA	0.01	0.01	0.00	0.00	0.00	0.00	0.00	0.00	0.00	0.01
NA	0.00	0.00	0.00	0.00	0.00	0.00	0.00	0.01	0.00	0.01
K	0.00	0.00	0.00	0.00	0.00	0.00	0.00	0.01	0.01	0.03
F	0.03	0.03	0.05	0.04	0.03	0.04	0.07	0.02	0.02	0.02
CL	0.00	0.00	0.00	0.00	0.00	0.00	0.00	0.00	0.00	0.00
OH(C)	7.95	7.90	7.93	7.96	7.93	7.92	7.86	7.84	7.81	7.78
O	10.02	10.07	10.02	10.00	10.04	10.04	10.07	10.13	10.18	10.20
FE/FE+MG	0.26	0.26	0.27	0.30	0.21	0.21	0.22	0.47	0.47	0.41
A	35.77	37.39	34.96	35.54	34.84	34.93	34.42	38.47	38.54	32.79
C	0.08	0.09	0.04	0.04	0.04	0.04	0.05	0.03	0.04	0.20
F	64.15	62.52	65.00	64.42	65.13	65.04	65.53	61.50	61.43	67.00
A"	0.22	0.23	0.21	0.21	0.21	0.21	0.21	0.24	0.24	0.19
F"	0.20	0.20	0.21	0.24	0.17	0.17	0.17	0.36	0.36	0.33
M"	0.58	0.57	0.58	0.55	0.62	0.62	0.62	0.40	0.40	0.48

CHLORITE

SAMPLE NO.	B4-13A	B4-93A	B4-93A	B4-93A	B4-100A	B4-100A	B4-101A	B4-101A	B4-101A	B4-101A
ANALYSIS	25A	17G	18G	20G	11A	12A	22G	54G	35G	56G
CORE/RIM										
AVERAGE OF										
SIO2	28.83	25.71	25.71	25.37	30.41	29.49	24.83	25.20	25.17	24.88
AL2O3	18.04	22.63	22.36	22.65	16.75	17.23	23.77	23.38	23.27	23.15
TIO2	0.44	0.13	0.19	0.11	0.05	0.02	0.12	0.10	0.09	0.13
CR2O3	0.09	0.04	0.06	0.00	0.30	0.32	0.01	0.05	0.02	0.03
FE2O3(C)	0.00	0.00	0.00	0.00	0.00	0.14	0.00	0.00	0.00	0.00
FEO(C)	21.45	22.54	23.02	23.29	15.30	14.84	23.72	23.70	23.60	23.57
MGO	18.01	15.76	16.15	15.65	23.30	24.54	14.88	15.37	15.06	15.22
MNO	0.25	0.18	0.18	0.19	0.18	0.14	0.26	0.21	0.30	0.24
CAO	0.44	0.04	0.04	0.05	0.72	0.05	0.04	0.03	0.03	0.06
NA2O	0.03	0.04	0.00	0.00	0.04	0.00	0.00	0.00	0.00	0.01
K2O	0.36	0.08	0.08	0.08	0.09	0.09	0.11	0.06	0.08	0.08
F	0.07	0.05	0.08	0.04	0.06	0.01	0.07	0.04	0.06	0.03
CL	0.00	0.00	0.00	0.00	0.00	0.00	0.00	0.00	0.00	0.01
H2O(C)	11.25	11.10	11.27	11.22	11.65	11.93	11.19	11.28	11.15	11.22
SUM	99.24	98.26	99.09	98.63	98.83	98.79	98.97	99.40	98.81	98.61
SI	2.99	2.70	2.68	2.66	3.07	2.97	2.60	2.63	2.64	2.62
AL(IV)	1.01	1.30	1.32	1.34	0.93	1.03	1.40	1.37	1.36	1.38
AL(VI)	1.19	1.50	1.43	1.47	1.06	1.01	1.54	1.50	1.52	1.49
TI	0.03	0.01	0.02	0.01	0.00	0.00	0.01	0.01	0.01	0.01
CR	0.01	0.00	0.00	0.00	0.02	0.02	0.00	0.00	0.00	0.00
FE+3	0.00	0.00	0.00	0.00	0.00	0.01	0.00	0.00	0.00	0.00
FE+2	1.86	1.98	2.01	2.05	1.29	1.25	2.08	2.07	2.07	2.07
MG	2.78	2.47	2.51	2.45	3.51	3.68	2.33	2.39	2.36	2.39
MN	0.02	0.02	0.02	0.02	0.02	0.01	0.02	0.02	0.03	0.02
CA	0.05	0.00	0.00	0.00	0.08	0.00	0.00	0.00	0.00	0.01
NA	0.01	0.01	0.00	0.00	0.01	0.00	0.00	0.00	0.00	0.00
K	0.05	0.01	0.01	0.01	0.01	0.01	0.02	0.01	0.01	0.01
F	0.02	0.02	0.03	0.01	0.02	0.00	0.02	0.01	0.02	0.01
CL	0.00	0.00	0.00	0.00	0.00	0.00	0.00	0.00	0.00	0.00
OH(C)	7.78	7.78	7.84	7.85	7.84	8.00	7.83	7.85	7.81	7.87
O	10.20	10.20	10.14	10.14	10.14	10.00	10.15	10.14	10.17	10.12
FE/FE+MG	0.40	0.44	0.44	0.45	0.27	0.25	0.47	0.46	0.47	0.46
A	31.87	38.54	37.71	38.29	28.95	29.34	39.85	39.09	39.24	39.00
C	0.70	0.06	0.06	0.07	1.13	0.07	0.05	0.04	0.05	0.10
F	67.43	61.40	62.23	61.63	69.92	70.59	60.09	60.87	60.72	60.90
A"	0.18	0.24	0.23	0.24	0.17	0.17	0.25	0.24	0.24	0.24
F"	0.33	0.34	0.34	0.35	0.22	0.21	0.36	0.35	0.35	0.35
M"	0.49	0.42	0.43	0.42	0.61	0.62	0.40	0.41	0.40	0.41

CHLORITE

SAMPLE NO.	C3-2B	C3-4A	C3-4A	C3-5A	C3-5A	C3-5A	C3-19BB	C3-19BB	C3-27AA	C3-32B
ANALYSIS	19G	14A	22A	10A	23A	24A	09S	10S	07A	04A
CORE/RIM										
AVERAGE OF										
SIO2	25.46	27.08	26.67	27.31	27.27	27.81	25.96	25.34	26.46	28.01
AL2O3	22.27	22.99	22.55	21.71	21.88	21.20	23.66	23.47	22.39	21.73
TIO2	0.12	0.05	0.09	0.12	0.06	0.09	0.13	0.42	0.19	0.04
CR2O3	0.01	0.05	0.02	0.11	0.10	0.08	0.00	0.00	0.17	0.43
FE2O3(C)	0.00	0.00	0.00	0.00	0.00	0.00	0.00	0.00	0.00	0.00
FEO(C)	22.66	18.95	18.85	14.70	15.30	15.83	20.10	20.28	19.00	14.09
MGO	16.65	20.22	19.40	22.85	22.00	21.80	17.37	17.56	19.91	22.88
MNO	0.09	0.19	0.29	0.10	0.13	0.13	0.04	0.04	0.24	0.09
CAO	0.05	0.05	0.06	0.02	0.04	0.02	0.03	0.03	0.10	0.05
NA2O	0.00	0.00	0.01	0.01	0.02	0.01	0.00	0.02	0.00	0.00
K2O	0.06	0.01	0.01	0.07	0.07	0.07	0.02	0.02	0.01	0.04
F	0.06	0.06	0.03	0.05	0.00	0.05	0.08	0.13	0.03	0.04
CL	0.01	0.00	0.01	0.00	0.01	0.00	0.00	0.02	0.01	0.00
H2O(C)	11.36	11.87	11.57	11.83	11.71	11.60	11.17	11.27	11.78	11.69
SUM	98.78	101.49	99.54	98.87	98.58	98.66	98.53	98.54	100.26	99.07
SI	2.66	2.69	2.71	2.74	2.75	2.81	2.68	2.62	2.67	2.80
AL(IV)	1.34	1.31	1.29	1.26	1.25	1.19	1.32	1.38	1.33	1.20
AL(VI)	1.40	1.39	1.41	1.31	1.36	1.34	1.57	1.49	1.34	1.36
TI	0.01	0.00	0.01	0.01	0.00	0.01	0.01	0.03	0.01	0.00
CR	0.00	0.00	0.00	0.01	0.01	0.01	0.00	0.00	0.01	0.03
FE+3	0.00	0.00	0.00	0.00	0.00	0.00	0.00	0.00	0.00	0.00
FE+2	1.98	1.58	1.60	1.23	1.29	1.34	1.74	1.76	1.60	1.18
MG	2.59	3.00	2.94	3.42	3.31	3.29	2.68	2.71	3.00	3.41
MN	0.01	0.02	0.02	0.01	0.01	0.01	0.00	0.00	0.02	0.01
CA	0.00	0.00	0.01	0.00	0.00	0.00	0.00	0.00	0.01	0.00
NA	0.00	0.00	0.00	0.00	0.00	0.00	0.00	0.00	0.00	0.00
K	0.01	0.00	0.00	0.01	0.01	0.01	0.00	0.00	0.00	0.00
F	0.02	0.02	0.01	0.02	0.00	0.02	0.03	0.04	0.01	0.01
CL	0.00	0.00	0.00	0.00	0.00	0.00	0.00	0.00	0.00	0.00
OH(C)	7.91	7.88	7.85	7.92	7.88	7.82	7.70	7.78	7.94	7.80
O	10.07	10.10	10.14	10.06	10.11	10.16	10.27	10.17	10.05	10.19
FE/FE+MG	0.43	0.35	0.35	0.26	0.28	0.29	0.39	0.39	0.35	0.26
A	37.41	36.97	37.13	35.51	36.05	35.27	39.47	39.04	36.52	35.75
C	0.07	0.07	0.10	0.03	0.06	0.03	0.05	0.05	0.14	0.07
F	62.51	62.96	62.77	64.45	63.89	64.70	60.48	60.92	63.34	64.18
A"	0.23	0.23	0.23	0.21	0.22	0.21	0.25	0.24	0.22	0.22
F"	0.33	0.27	0.27	0.21	0.22	0.23	0.30	0.30	0.27	0.20
M"	0.44	0.51	0.50	0.58	0.56	0.56	0.46	0.46	0.50	0.58

CHLORITE

SAMPLE NO.	C3-32B	C3116AA	C3-117A	C3-117A	C3-117B	C4-1CA	C4-1CA	C4-7B	C4-7B	C4-17A
ANALYSIS	05A	15A	34A	36A	07A	07A	16A	01G	03G	04G
CORE/RIM										
AVERAGE OF										
SIO2	27.76	26.64	26.88	26.73	27.23	27.08	26.96	26.17	27.01	28.34
AL2O3	21.99	23.03	22.11	21.64	21.23	23.34	22.62	21.99	21.93	22.16
TIO2	0.13	0.08	0.14	0.13	0.13	0.11	0.11	0.09	0.13	0.02
CR2O3	0.48	0.09	0.05	0.03	0.00	0.01	0.14	0.50	0.09	0.04
FE2O3(C)	0.00	0.00	0.00	0.00	0.00	0.00	0.00	0.00	0.00	0.00
FEO(C)	14.31	18.27	21.66	21.34	19.32	15.20	15.52	20.31	18.74	9.79
MGO	23.00	18.76	17.49	17.35	18.90	21.52	21.81	18.57	20.34	26.45
MNO	0.08	0.29	0.15	0.10	0.27	0.24	0.26	0.20	0.14	0.24
CAO	0.04	0.07	0.06	0.07	0.03	0.04	0.02	0.03	0.02	0.03
NA2O	0.01	0.00	0.02	0.07	0.03	0.00	0.00	0.00	0.00	0.03
K2O	0.02	0.01	0.02	0.04	0.01	0.01	0.01	0.01	0.01	0.01
F	0.00	0.02	0.08	0.11	0.08	0.12	0.05	0.04	0.04	0.05
CL	0.00	0.00	0.01	0.00	0.00	0.00	0.00	0.00	0.00	0.00
H2O(C)	11.83	11.29	11.36	11.23	11.30	11.59	11.74	11.55	11.76	12.13
SUM	99.65	98.54	100.01	98.81	98.51	99.21	99.21	99.46	100.20	99.27
SI	2.76	2.73	2.76	2.77	2.81	2.72	2.71	2.69	2.72	2.77
AL(IV)	1.24	1.27	1.24	1.23	1.19	1.28	1.29	1.31	1.28	1.23
AL(VI)	1.34	1.52	1.43	1.42	1.39	1.47	1.39	1.35	1.33	1.32
TI	0.01	0.01	0.01	0.01	0.01	0.01	0.01	0.01	0.01	0.00
CR	0.04	0.01	0.00	0.00	0.00	0.00	0.01	0.04	0.01	0.00
FE+3	0.00	0.00	0.00	0.00	0.00	0.00	0.00	0.00	0.00	0.00
FE+2	1.19	1.57	1.86	1.85	1.67	1.27	1.30	1.74	1.58	0.80
MG	3.41	2.87	2.67	2.68	2.90	3.22	3.27	2.84	3.06	3.85
MN	0.01	0.02	0.01	0.01	0.02	0.02	0.02	0.02	0.01	0.02
CA	0.00	0.01	0.01	0.01	0.00	0.00	0.00	0.00	0.00	0.00
NA	0.00	0.00	0.00	0.02	0.01	0.00	0.00	0.00	0.00	0.00
K	0.00	0.00	0.00	0.00	0.00	0.00	0.00	0.00	0.00	0.00
F	0.00	0.01	0.02	0.04	0.02	0.04	0.02	0.01	0.01	0.02
CL	0.00	0.00	0.00	0.00	0.00	0.00	0.00	0.00	0.00	0.00
OH(C)	7.85	7.73	7.77	7.77	7.77	7.76	7.87	7.90	7.91	7.90
O	10.15	10.27	10.20	10.19	10.20	10.21	10.12	10.08	10.08	10.08
FE/FE+MG	0.26	0.35	0.41	0.41	0.36	0.28	0.29	0.38	0.34	0.17
A	35.85	38.39	36.99	36.76	35.95	37.92	36.82	36.61	35.90	35.31
C	0.06	0.11	0.10	0.11	0.04	0.05	0.02	0.05	0.03	0.05
F	64.09	61.50	62.91	63.13	64.01	62.03	63.16	63.34	64.06	64.64
A"	0.22	0.24	0.23	0.23	0.22	0.24	0.23	0.22	0.22	0.21
F"	0.20	0.27	0.32	0.32	0.28	0.22	0.22	0.30	0.27	0.13
M"	0.58	0.49	0.46	0.46	0.50	0.55	0.55	0.48	0.51	0.65

CHLORITE

SAMPLE NO.	C4-17A	C4-24A	C4-24A	C4-32A	C4-32A	C4-32A	C4-32B	C4-32B	C4-32B	C4-32B
ANALYSIS	05G	28A	29A	30S	49S	50S	19S	20S	39S	40S
CORE/RIM										
AVERAGE OF										
SIO2	30.52	26.87	27.46	25.17	25.87	25.95	25.93	25.76	25.75	25.52
AL2O3	25.21	21.91	21.60	22.99	25.00	25.08	23.02	23.16	24.17	23.99
TIO2	0.08	0.18	0.22	0.13	0.15	0.07	0.14	0.10	0.09	0.12
CR2O3	0.03	0.05	0.07	0.06	0.04	0.04	0.03	0.07	0.05	0.07
FE2O3(C)	0.00	0.00	0.00	0.00	0.00	0.00	0.00	0.00	0.00	0.00
FEO(C)	9.07	18.89	18.64	20.00	19.73	19.71	20.00	20.03	19.94	20.00
MGO	22.96	19.77	19.33	18.39	17.16	17.32	17.74	17.76	17.77	17.77
MNO	0.26	0.18	0.21	0.11	0.11	0.07	0.08	0.09	0.08	0.07
CAO	0.09	0.06	0.07	0.02	0.07	0.07	0.04	0.04	0.02	0.02
NA2O	0.01	0.06	0.02	0.00	0.00	0.01	0.03	0.00	0.00	0.02
K2O	0.02	0.02	0.02	0.07	0.02	0.02	0.12	0.12	0.02	0.02
F	0.12	0.04	0.02	0.13	0.18	0.14	0.09	0.07	0.03	0.01
CL	0.04	0.00	0.00	0.00	0.00	0.02	0.02	0.02	0.00	0.01
H2O(C)	10.90	11.65	11.37	11.51	11.15	11.22	11.29	11.33	11.39	11.42
SUM	99.25	99.67	99.02	98.53	99.39	99.65	98.47	98.51	99.30	99.03
SI	2.98	2.73	2.81	2.60	2.65	2.65	2.68	2.66	2.64	2.62
AL(IV)	1.02	1.27	1.19	1.40	1.35	1.35	1.32	1.34	1.36	1.38
AL(VI)	1.88	1.35	1.41	1.40	1.66	1.66	1.49	1.49	1.56	1.53
TI	0.01	0.01	0.02	0.01	0.01	0.00	0.01	0.01	0.01	0.01
CR	0.00	0.00	0.00	0.00	0.00	0.00	0.00	0.00	0.00	0.00
FE+3	0.00	0.00	0.00	0.00	0.00	0.00	0.00	0.00	0.00	0.00
FE+2	0.74	1.60	1.59	1.73	1.69	1.68	1.73	1.73	1.71	1.72
MG	3.34	2.99	2.94	2.83	2.62	2.63	2.74	2.74	2.71	2.72
MN	0.02	0.02	0.02	0.01	0.01	0.01	0.01	0.01	0.01	0.01
CA	0.01	0.01	0.01	0.00	0.01	0.01	0.00	0.00	0.00	0.00
NA	0.00	0.01	0.00	0.00	0.00	0.00	0.00	0.00	0.00	0.00
K	0.00	0.00	0.00	0.01	0.00	0.00	0.02	0.02	0.00	0.00
F	0.04	0.01	0.01	0.04	0.06	0.05	0.03	0.02	0.01	0.00
CL	0.01	0.00	0.00	0.00	0.00	0.00	0.00	0.00	0.00	0.00
OH(C)	7.09	7.89	7.75	7.94	7.61	7.63	7.79	7.81	7.78	7.83
O	10.86	10.10	10.25	10.02	10.33	10.32	10.18	10.16	10.21	10.17
FE/FE+MG	0.18	0.35	0.35	0.38	0.39	0.39	0.39	0.39	0.39	0.39
A	41.36	36.21	36.31	37.98	41.10	41.06	38.53	38.65	39.71	39.49
C	0.13	0.09	0.11	0.04	0.10	0.10	0.06	0.06	0.03	0.04
F	58.51	63.70	63.58	61.99	58.80	58.84	61.41	61.29	60.26	60.47
A"	0.26	0.22	0.22	0.23	0.26	0.26	0.24	0.24	0.25	0.25
F"	0.13	0.27	0.27	0.29	0.29	0.29	0.30	0.30	0.29	0.29
M"	0.60	0.51	0.50	0.48	0.45	0.45	0.47	0.47	0.46	0.46

CHLORITE

SAMPLE NO.	C4-49A	C4-49A	C4-49B	D2-1CA	D2-1CA	D2-1CA	D2-1D	D2-1D
ANALYSIS	11A	12A	38S	15S	16S	17S	05S	06S
CORE/RIM								
AVERAGE OF								
SIO2	26.66	26.85	25.40	24.48	25.54	25.46	25.40	25.10
AL2O3	22.42	22.33	23.16	26.24	23.82	25.10	23.26	22.94
TIO2	0.17	0.15	0.13	0.19	0.07	0.15	0.11	0.14
CR2O3	0.07	0.04	0.04	0.01	0.00	0.04	0.02	0.03
FE2O3(C)	0.00	0.00	0.00	0.00	0.00	0.00	0.00	0.00
FEO(C)	18.47	18.43	20.23	18.92	19.43	19.04	21.84	21.54
MGO	19.75	19.81	17.93	17.96	18.64	18.46	17.69	17.53
MNO	0.22	0.26	0.07	0.10	0.01	0.06	0.08	0.08
CAO	0.08	0.08	0.02	0.07	0.03	0.07	0.02	0.03
NA2O	0.05	0.03	0.00	0.00	0.00	0.00	0.00	0.00
K2O	0.02	0.01	0.07	0.02	0.01	0.04	0.08	0.08
F	0.14	0.04	0.07	0.09	0.07	0.08	0.08	0.06
CL	0.00	0.00	0.01	0.01	0.01	0.01	0.00	0.00
H2O(C)	11.59	11.62	11.42	11.52	11.53	11.56	11.67	11.54
SUM	99.58	99.65	98.53	99.56	99.13	100.04	100.23	99.04
SI	2.70	2.72	2.63	2.49	2.61	2.58	2.60	2.60
AL(IV)	1.30	1.28	1.37	1.51	1.39	1.42	1.40	1.40
AL(VI)	1.39	1.39	1.45	1.64	1.48	1.57	1.40	1.40
TI	0.01	0.01	0.01	0.02	0.00	0.01	0.01	0.01
CR	0.00	0.00	0.00	0.00	0.00	0.00	0.00	0.00
FE+3	0.00	0.00	0.00	0.00	0.00	0.00	0.00	0.00
FE+2	1.57	1.56	1.75	1.61	1.66	1.61	1.87	1.86
MG	2.99	2.99	2.77	2.72	2.84	2.79	2.70	2.70
MN	0.02	0.02	0.01	0.01	0.00	0.00	0.01	0.01
CA	0.01	0.01	0.00	0.01	0.00	0.01	0.00	0.00
NA	0.01	0.01	0.00	0.00	0.00	0.00	0.00	0.00
K	0.00	0.00	0.01	0.00	0.00	0.00	0.01	0.01
F	0.04	0.01	0.02	0.03	0.02	0.03	0.02	0.02
CL	0.00	0.00	0.00	0.00	0.00	0.00	0.00	0.00
OH(C)	7.84	7.85	7.88	7.82	7.87	7.80	7.97	7.97
O	10.11	10.13	10.09	10.15	10.11	10.17	10.01	10.01
FE/FE+MG	0.34	0.34	0.39	0.37	0.37	0.37	0.41	0.41
A	36.91	36.77	38.43	41.98	38.91	40.44	37.99	37.93
C	0.12	0.12	0.04	0.10	0.05	0.10	0.03	0.05
F	62.96	63.11	61.53	57.92	61.04	59.46	61.97	62.03
A"	0.23	0.23	0.24	0.27	0.24	0.25	0.23	0.23
F"	0.27	0.26	0.30	0.27	0.28	0.27	0.31	0.31
M"	0.51	0.51	0.47	0.46	0.48	0.47	0.45	0.45

CLINOZOISITE AND EPIDOTE

SAMPLE NO.	A1-1A	A1-1A	A1-1D	A1-1D	A2-3CA	A2-3CA	A2-3CA	A2-3D	A2-3D	A2-3D
ANALYSIS	07MY	08MY	16MY	17MY	10A	11A	14A?	08A	28A	29A
CORE/RIM	C	R								
SIO2	37.94	37.59	37.97	37.74	38.30	38.65	38.45	38.31	38.07	37.76
AL2O3	21.80	22.04	23.44	23.62	24.05	24.16	24.07	27.22	26.48	26.15
TIO2	0.08	0.09	0.10	0.07	0.08	0.07	1.00	0.03	0.30	0.25
FE2O3(C)	15.60	15.11	13.23	12.84	12.84	13.04	11.73	9.01	9.93	10.52
FEO(C)	0.00	0.68	0.00	0.07	0.00	0.00	0.00	0.92	1.74	1.54
MGO	0.04	0.07	0.02	0.06	0.01	0.06	0.07	0.04	0.56	0.64
MNO	0.30	0.28	0.19	0.21	0.16	0.19	0.15	0.08	0.12	0.17
CAO	22.57	22.19	22.94	22.73	23.59	23.72	23.24	23.13	21.65	21.48
NA2O	0.04	0.03	0.01	0.02	0.02	0.00	0.03	0.02	0.00	0.00
K2O	0.03	0.02	0.10	0.10	0.08	0.08	0.14	0.02	0.05	0.13
F	0.03	0.01	0.00	0.00	0.01	0.02	0.04	0.03	0.05	0.07
H2O(C)	1.86	1.86	1.88	1.88	1.90	1.91	1.88	1.91	1.90	1.88
SUM	100.27	99.97	99.89	99.33	101.03	101.88	100.78	100.70	100.82	100.55
SI	3.04	3.01	3.02	3.02	3.02	3.02	3.04	2.98	2.97	2.95
AL(IV)	0.00	0.00	0.00	0.00	0.00	0.00	0.00	0.02	0.03	0.05
AL(VI)	2.06	2.08	2.20	2.22	2.23	2.23	2.24	2.47	2.40	2.37
TI	0.00	0.00	0.01	0.00	0.00	0.00	0.06	0.00	0.02	0.01
FE+3(VI)	0.94	0.91	0.79	0.77	0.76	0.77	0.70	0.53	0.58	0.62
FE+2(VIII)	0.00	0.05	0.00	0.00	0.00	0.00	0.00	0.06	0.11	0.10
MG	0.00	0.01	0.00	0.01	0.00	0.01	0.01	0.00	0.06	0.07
MN	0.02	0.02	0.01	0.01	0.01	0.01	0.01	0.00	0.01	0.01
CA	1.94	1.91	1.96	1.95	1.99	1.99	1.97	1.93	1.81	1.80
NA	0.00	0.00	0.00	0.00	0.00	0.00	0.00	0.00	0.00	0.00
K	0.00	0.00	0.01	0.01	0.01	0.01	0.01	0.00	0.00	0.01
F	0.01	0.00	0.00	0.00	0.00	0.00	0.01	0.01	0.01	0.02
OH(C)	0.99	1.00	1.00	1.00	1.00	1.00	0.99	0.99	0.99	0.98
O	12.04	12.01	12.03	12.01	12.05	12.06	12.10	11.99	11.99	11.98
FE/FE+MG	1.00	0.99	1.00	0.99	1.00	0.99	0.99	0.99	0.92	0.91
A	60.46	60.22	60.27	60.30	59.92	59.87	59.68	60.21	60.18	60.40
C	39.05	38.33	39.42	39.17	39.84	39.75	39.95	38.40	36.09	35.88
F	0.50	1.45	0.31	0.53	0.23	0.38	0.37	1.39	3.72	3.72

CLINOZOISITE AND EPIDOTE

SAMPLE NO.	A2-14AA	A2-66A	A3-43B	A3-43B	A3-71A	A3-71A	A3-92A	A4-22A	A4-22A	B2-1AB
ANALYSIS	30MY	03A	11A	12A	07A	23A	13A	08A	11A	08G
CORE/RIM										
SIO2	38.05	37.90	38.35	38.23	38.08	38.53	38.80	38.34	39.22	39.13
AL2O3	24.45	27.91	26.47	26.39	24.56	25.14	29.21	28.33	28.98	28.24
TIO2	0.10	0.11	0.05	0.07	0.10	0.17	0.07	0.08	0.13	0.15
FE2O3(C)	12.73	9.22	9.67	9.56	12.01	11.26	6.30	7.04	6.30	7.01
FEO(C)	1.16	0.57	0.00	0.00	0.00	0.00	0.18	0.00	0.00	0.24
MGO	0.03	0.04	0.05	0.06	0.05	0.03	0.07	0.03	0.04	0.04
MNO	0.23	0.11	0.12	0.22	0.07	0.12	0.14	0.08	0.23	0.17
CAO	22.64	23.60	24.19	24.06	23.59	23.49	23.93	24.03	24.06	23.22
NA2O	0.00	0.00	0.00	0.00	0.00	0.02	0.00	0.02	0.00	0.01
K2O	0.03	0.03	0.02	0.02	0.01	0.02	0.01	0.01	0.01	0.02
F	0.00	0.05	0.02	0.02	0.06	0.06	0.00	0.01	0.08	0.00
H2O(C)	1.91	1.92	1.91	1.90	1.87	1.88	1.95	1.92	1.91	1.93
SUM	101.34	101.42	100.84	100.50	100.37	100.69	100.65	99.88	100.92	100.17
SI	2.98	2.92	2.99	3.00	3.00	3.02	2.98	2.98	3.02	3.03
AL(IV)	0.02	0.08	0.01	0.00	0.00	0.00	0.02	0.02	0.00	0.00
AL(VI)	2.24	2.46	2.43	2.43	2.28	2.32	2.63	2.58	2.63	2.58
TI	0.01	0.01	0.00	0.00	0.01	0.01	0.00	0.00	0.01	0.01
FE+3(VI)	0.75	0.54	0.57	0.56	0.71	0.67	0.36	0.41	0.37	0.41
FE+2(VIII)	0.08	0.04	0.00	0.00	0.00	0.00	0.01	0.00	0.00	0.02
MG	0.00	0.00	0.00	0.01	0.01	0.00	0.01	0.00	0.00	0.00
MN	0.02	0.01	0.01	0.01	0.00	0.01	0.01	0.00	0.02	0.01
CA	1.90	1.95	2.02	2.02	1.99	1.98	1.97	2.00	1.98	1.93
NA	0.00	0.00	0.00	0.00	0.00	0.00	0.00	0.00	0.00	0.00
K	0.00	0.00	0.00	0.00	0.00	0.00	0.00	0.00	0.00	0.00
F	0.00	0.01	0.00	0.00	0.02	0.02	0.00	0.00	0.02	0.00
OH(C)	1.00	0.99	1.00	1.00	0.99	0.99	1.00	1.00	0.98	1.00
O	11.99	11.96	12.04	12.04	12.01	12.04	11.99	12.01	12.04	12.04
FE/FE+MG	1.00	0.99	0.99	0.99	0.99	1.00	0.98	0.99	0.99	0.99
A	60.12	60.60	59.59	59.52	59.91	60.08	60.10	59.95	59.92	60.39
C	37.99	38.45	40.14	40.07	39.87	39.69	39.33	39.89	39.70	38.97
F	1.89	0.95	0.27	0.42	0.22	0.23	0.56	0.17	0.38	0.64

CLINOZOISITE AND EPIDOTE

SAMPLE NO.	B2-1AB	B2-1B	B2-1Y	B2-1Y	B2-4A	B2-4A	B2-24A	B2-24A	B2-35C	B2-35C
ANALYSIS	10G	03G	01G	02G	08A	25A	08A	09A	10A	14A
CORE/RIM										
SIO2	39.10	38.32	38.50	38.27	38.96	39.41	39.57	39.86	38.84	38.01
AL2O3	28.27	28.91	30.80	30.57	27.85	29.85	29.56	29.18	30.71	29.14
TIO2	0.18	0.12	0.18	0.14	0.11	0.16	0.18	0.06	0.15	0.12
FE2O3(C)	7.01	5.86	4.79	5.25	7.80	5.28	5.73	6.52	4.74	7.44
FEO(C)	0.26	1.12	0.95	0.68	0.27	0.23	0.00	0.00	1.00	0.62
MGO	0.04	0.14	0.09	0.07	0.04	0.08	0.04	0.05	0.06	0.05
MNO	0.16	0.18	0.24	0.23	0.09	0.17	0.12	0.09	0.17	0.11
CAO	23.33	22.62	23.38	23.55	23.62	23.88	24.06	24.05	23.48	23.63
NA2O	0.00	0.03	0.00	0.00	0.00	0.00	0.00	0.01	0.00	0.00
K2O	0.02	0.02	0.01	0.02	0.01	0.01	0.01	0.01	0.01	0.02
F	0.03	0.05	0.02	0.04	0.00	0.01	0.00	0.00	0.00	0.05
H2O(C)	1.92	1.90	1.95	1.94	1.94	1.96	1.96	1.97	1.97	1.92
SUM	100.30	99.25	100.89	100.74	100.69	101.03	101.24	101.77	101.12	101.09
SI	3.03	2.99	2.94	2.93	3.01	3.01	3.02	3.04	2.96	2.92
AL(IV)	0.00	0.01	0.06	0.07	0.00	0.00	0.00	0.00	0.04	0.08
AL(VI)	2.58	2.65	2.71	2.69	2.54	2.69	2.66	2.62	2.72	2.56
TI	0.01	0.01	0.01	0.01	0.01	0.01	0.01	0.00	0.01	0.01
FE+3(VI)	0.41	0.34	0.28	0.30	0.45	0.30	0.33	0.37	0.27	0.43
FE+2(VIII)	0.02	0.07	0.06	0.04	0.02	0.02	0.00	0.00	0.06	0.04
MG	0.00	0.02	0.01	0.01	0.00	0.01	0.00	0.00	0.01	0.00
MN	0.01	0.01	0.02	0.02	0.01	0.01	0.01	0.01	0.01	0.01
CA	1.94	1.89	1.91	1.93	1.96	1.95	1.97	1.97	1.92	1.95
NA	0.00	0.00	0.00	0.00	0.00	0.00	0.00	0.00	0.00	0.00
K	0.00	0.00	0.00	0.00	0.00	0.00	0.00	0.00	0.00	0.00
F	0.01	0.01	0.01	0.01	0.00	0.00	0.00	0.00	0.00	0.01
OH(C)	0.99	0.99	0.99	0.99	1.00	1.00	1.00	1.00	1.00	0.99
O	12.03	11.99	11.98	11.97	12.02	12.01	12.03	12.06	11.98	11.96
FE/FE+MG	0.99	0.96	0.97	0.98	0.99	0.97	0.99	0.99	0.98	0.99
A	60.30	60.11	60.40	60.50	60.13	60.07	60.14	60.26	60.26	60.58
C	39.05	37.86	37.90	38.19	39.32	39.25	39.60	39.52	38.12	38.39
F	0.65	2.03	1.69	1.31	0.55	0.68	0.26	0.22	1.62	1.03

CLINOZOISITE AND EPIDOTE

SAMPLE NO.	B3-75A	B3-127A	B3-127A	B4-8B	B4-8B	B4-11A	B4-11A	B4-13A	B4-13A	B4-13A
ANALYSIS	14A	20A	21A	08G	22G	08A	17A	10A	11A	23A
CORE/RIM										
SIO2	37.95	38.82	38.62	39.20	38.93	39.14	38.87	39.02	38.72	39.02
AL2O3	27.80	29.21	29.26	27.92	29.42	27.79	27.89	28.44	28.38	29.03
TIO2	0.02	0.12	0.11	0.36	0.27	0.09	0.12	0.14	0.17	0.15
FE2O3(C)	9.38	5.91	6.29	6.87	5.53	8.35	8.12	6.91	6.81	5.98
FEO(C)	0.20	0.00	0.10	0.00	0.00	0.07	0.00	0.00	0.00	0.00
MGO	0.06	0.04	0.04	0.08	0.10	0.03	0.04	0.05	0.08	0.09
MNO	0.06	0.17	0.16	0.36	0.25	0.08	0.08	0.17	0.16	0.17
CAO	23.90	23.87	23.86	23.74	24.15	24.03	24.12	23.85	23.85	23.62
NA2O	0.00	0.01	0.00	0.03	0.01	0.05	0.00	0.01	0.00	0.01
K2O	0.02	0.10	0.11	0.00	0.01	0.02	0.02	0.07	0.07	0.07
F	0.07	0.00	0.00	0.00	0.00	0.02	0.00	0.02	0.00	0.03
H2O(C)	1.91	1.94	1.95	1.92	1.95	1.95	1.95	1.93	1.93	1.93
SUM	101.34	100.19	100.48	100.49	100.62	101.60	101.20	100.61	100.17	100.10
SI	2.93	2.99	2.97	3.07	3.00	3.00	2.99	3.01	3.00	3.02
AL(IV)	0.07	0.00	0.03	0.00	0.00	0.00	0.01	0.00	0.00	0.00
AL(VI)	2.45	2.65	2.63	2.57	2.66	2.51	2.52	2.59	2.59	2.64
TI	0.00	0.01	0.01	0.02	0.02	0.00	0.01	0.01	0.01	0.01
FE+3(VI)	0.55	0.34	0.37	0.40	0.32	0.48	0.47	0.40	0.40	0.35
FE+2(VIII)	0.01	0.00	0.01	0.00	0.00	0.00	0.00	0.00	0.00	0.00
MG	0.01	0.00	0.00	0.01	0.01	0.00	0.00	0.01	0.01	0.01
MN	0.00	0.01	0.01	0.02	0.02	0.00	0.00	0.01	0.01	0.01
CA	1.98	1.97	1.97	1.99	1.99	1.98	1.99	1.97	1.98	1.96
NA	0.00	0.00	0.00	0.00	0.00	0.01	0.00	0.00	0.00	0.00
K	0.00	0.01	0.01	0.00	0.00	0.00	0.00	0.01	0.01	0.01
F	0.02	0.00	0.00	0.00	0.00	0.00	0.00	0.01	0.00	0.01
OH(C)	0.98	1.00	1.00	1.00	1.00	1.00	1.00	0.99	1.00	0.99
O	11.96	12.00	11.98	12.17	12.03	12.00	12.00	12.03	12.01	12.02
FE/FE+MG	0.99	0.99	0.99	0.98	0.97	0.99	0.99	0.99	0.98	0.97
A	60.59	60.12	60.28	59.54	59.68	60.10	60.02	60.04	59.92	60.20
C	38.95	39.56	39.30	39.78	39.76	39.64	39.79	39.62	39.69	39.36
F	0.46	0.32	0.42	0.68	0.56	0.27	0.19	0.35	0.39	0.44

CLINOZOISITE AND EPIDOTE

SAMPLE NO.	C3-17D	C3-27AA	C3-55A	C3116AA	C3116AA	C3116AA	C3-117A	C4-20B	C4-20B	C4-20B
ANALYSIS	12A	08A	23G	16A	19A	41A	18A	05G	06G	14G
CORE/RIM										
SIO2	39.01	38.95	38.81	39.39	38.88	38.88	39.76	38.26	38.46	37.70
AL2O3	29.82	30.26	30.05	30.15	30.70	29.84	25.99	26.50	26.96	26.03
TIO2	0.22	0.25	0.15	0.08	0.08	0.19	0.16	0.12	0.13	0.08
FE2O3(C)	5.93	5.22	5.20	4.64	4.60	5.48	10.01	10.32	9.26	10.66
FEO(C)	0.73	0.01	0.00	0.59	0.88	0.13	0.00	0.30	0.63	0.34
MGO	0.08	0.09	0.11	0.00	0.00	0.07	0.08	0.08	0.06	0.07
MNO	0.09	0.17	0.18	0.13	0.13	0.24	0.12	0.20	0.13	0.17
CAO	23.72	24.21	24.13	23.46	23.64	23.95	23.14	23.53	23.36	23.27
NA2O	0.01	0.00	0.00	0.01	0.00	0.00	0.02	0.01	0.00	0.00
K2O	0.01	0.01	0.01	0.01	0.01	0.02	0.02	0.02	0.01	0.02
F	0.00	0.02	0.03	0.00	0.00	0.00	0.03	0.00	0.04	0.03
H2O(C)	1.97	1.96	1.94	1.95	1.96	1.96	1.90	1.93	1.91	1.90
SUM	101.59	101.14	100.62	100.42	100.88	100.76	101.21	101.27	100.95	100.26
SI	2.97	2.97	2.98	3.02	2.97	2.98	3.12	2.97	2.98	2.96
AL(IV)	0.03	0.03	0.02	0.00	0.03	0.02	0.00	0.03	0.02	0.04
AL(VI)	2.65	2.69	2.69	2.73	2.73	2.67	2.40	2.39	2.45	2.37
TI	0.01	0.01	0.01	0.00	0.00	0.01	0.01	0.01	0.01	0.00
FE+3(VI)	0.34	0.30	0.30	0.27	0.26	0.32	0.59	0.60	0.54	0.63
FE+2(VIII)	0.05	0.00	0.00	0.04	0.06	0.01	0.00	0.02	0.04	0.02
MG	0.01	0.01	0.01	0.00	0.00	0.01	0.01	0.01	0.01	0.01
MN	0.01	0.01	0.01	0.01	0.01	0.02	0.01	0.01	0.01	0.01
CA	1.94	1.98	1.98	1.93	1.93	1.97	1.94	1.96	1.94	1.96
NA	0.00	0.00	0.00	0.00	0.00	0.00	0.00	0.00	0.00	0.00
K	0.00	0.00	0.00	0.00	0.00	0.00	0.00	0.00	0.00	0.00
F	0.00	0.00	0.01	0.00	0.00	0.00	0.01	0.00	0.01	0.01
OH(C)	1.00	1.00	0.99	1.00	1.00	1.00	0.99	1.00	0.99	0.99
O	11.99	11.99	12.00	12.02	11.99	11.99	12.20	11.99	12.00	11.98
FE/FE+MG	0.98	0.97	0.96	1.00	1.00	0.98	0.98	0.99	0.99	0.99
A	60.16	60.15	60.05	60.26	60.23	60.11	60.40	60.23	60.07	60.31
C	38.61	39.40	39.47	38.81	38.48	39.25	39.24	38.94	38.80	38.86
F	1.22	0.45	0.48	0.93	1.30	0.64	0.36	0.82	1.13	0.83

CLINOZOISITE AND EPIDOTE

SAMPLE NO.	C4-25A	C4-25A	C4-36A	C4-36A	C4-49A	C4-49A	C4-49A
ANALYSIS	05A	15A	12A	24A	04A	05A	20A
CORE/RIM							
SIO2	39.00	38.88	38.34	38.61	39.11	39.27	38.85
AL2O3	27.94	28.15	25.48	24.96	30.11	30.13	30.43
TIO2	0.09	0.09	0.12	0.13	0.09	0.19	0.10
FE2O3(C)	7.52	7.26	10.73	11.49	5.14	5.20	4.59
FEO(C)	0.00	0.00	0.00	0.00	0.53	0.39	0.00
MGO	0.03	0.42	0.03	0.06	0.05	0.12	0.12
MNO	0.19	0.13	0.13	0.11	0.15	0.12	0.11
CAO	23.84	23.37	23.43	23.65	23.76	23.89	24.10
NA2O	0.04	0.03	0.01	0.02	0.03	0.02	0.01
K2O	0.08	0.14	0.07	0.07	0.02	0.03	0.02
F	0.02	0.02	0.04	0.03	0.00	0.03	0.02
H2O(C)	1.92	1.92	1.89	1.89	1.96	1.95	1.94
SUM	100.66	100.40	100.26	101.03	100.95	101.34	100.28
SI	3.03	3.01	3.01	3.03	2.99	2.99	2.98
AL(IV)	0.00	0.00	0.00	0.00	0.01	0.01	0.02
AL(VI)	2.56	2.57	2.36	2.31	2.70	2.69	2.73
TI	0.00	0.00	0.01	0.01	0.00	0.01	0.01
FE+3(VI)	0.44	0.42	0.63	0.68	0.30	0.30	0.26
FE+2(VIII)	0.00	0.00	0.00	0.00	0.03	0.02	0.00
MG	0.00	0.05	0.00	0.01	0.00	0.01	0.01
MN	0.01	0.01	0.01	0.01	0.01	0.01	0.01
CA	1.98	1.94	1.97	1.99	1.94	1.95	1.98
NA	0.01	0.00	0.00	0.00	0.00	0.00	0.00
K	0.01	0.01	0.01	0.01	0.00	0.00	0.00
F	0.00	0.01	0.01	0.01	0.00	0.01	0.00
OH(C)	1.00	0.99	0.99	0.99	1.00	0.99	1.00
O	12.06	12.04	12.02	12.09	11.99	12.00	11.99
FE/FE+MG	0.99	0.90	0.99	0.99	0.99	0.96	0.95
A	59.98	59.99	60.13	59.87	60.13	60.08	60.11
C	39.71	38.87	39.62	39.85	38.89	39.01	39.48
F	0.31	1.15	0.25	0.28	0.98	0.91	0.41

FELDSPAR

SAMPLE NO.	A1-1A	A1-1A	A1-1A	A1-1B	A1-1B	A1-1B	A1-1B	A1-1D	A2-3CA	A2-3D
ANALYSIS	02MY	03MY	20MY	01MY	07MY	17MY	18MY	23MY	01A	01A
CORE/RIM										
SIO2	68.05	69.07	68.60	64.38	63.70	64.27	68.79	68.14	69.01	66.75
AL2O3	19.35	19.16	19.23	18.30	18.27	18.48	19.43	19.76	19.72	19.72
FE2O3(C)	0.00	0.00	0.00	0.00	0.00	0.00	0.00	0.00	0.00	0.00
TIO2	0.00	0.01	0.02	0.01	0.07	0.04	0.03	0.02	0.02	0.04
K2O	0.14	0.08	0.20	16.25	16.31	16.03	0.06	0.45	0.12	0.07
NA2O	11.41	11.40	11.86	0.31	0.09	0.40	12.13	11.35	11.50	11.72
CAO	0.09	0.11	0.17	0.02	0.02	0.02	0.09	0.07	0.24	0.57
MGO	0.00	0.00	0.00	0.03	0.01	0.03	0.00	0.00	0.00	0.00
FEO(C)	0.05	0.00	0.00	0.03	0.04	0.06	0.01	0.20	0.01	0.35
MNO	0.00	0.00	0.01	0.04	0.03	0.00	0.03	0.00	0.00	0.01
BAO	0.00	0.02	0.00	0.75	0.97	1.04	0.04	0.00	0.05	0.02
SUM	99.09	99.84	100.09	100.12	99.52	100.37	100.59	100.00	100.68	99.25
SI	3.00	3.02	3.00	2.99	2.98	2.98	2.99	2.98	2.99	2.95
AL	1.01	0.99	0.99	1.00	1.01	1.01	1.00	1.02	1.01	1.03
FE+3	0.00	0.00	0.00	0.00	0.00	0.00	0.00	0.00	0.00	0.00
TI	0.00	0.00	0.00	0.00	0.00	0.00	0.00	0.00	0.00	0.00
K	0.01	0.00	0.01	0.96	0.98	0.95	0.00	0.02	0.01	0.00
NA	0.97	0.96	1.01	0.03	0.01	0.04	1.02	0.96	0.97	1.01
CA	0.00	0.00	0.01	0.00	0.00	0.00	0.00	0.00	0.01	0.03
MG	0.00	0.00	0.00	0.00	0.00	0.00	0.00	0.00	0.00	0.00
FE+2	0.00	0.00	0.00	0.00	0.00	0.00	0.00	0.01	0.00	0.01
MN	0.00	0.00	0.00	0.00	0.00	0.00	0.00	0.00	0.00	0.00
BA	0.00	0.00	0.00	0.01	0.02	0.02	0.00	0.00	0.00	0.00
%OR	0.80	0.44	1.11	97.13	99.07	96.23	0.31	2.56	0.69	0.38
%AB	98.76	99.05	98.13	2.78	0.86	3.69	99.30	97.09	98.19	97.02
%AN	0.44	0.51	0.76	0.10	0.08	0.09	0.39	0.35	1.12	2.61

FELDSPAR

SAMPLE NO.	A2-3D	A2-3E	A2-3E	A2-3HA	A2-11A	A2-13A	A2-14AA	A2-14AA	A2-15A	A2-15A
ANALYSIS	25A	06BF	08BF	01BF	04S	03MY	01MY	07MY	07U	08U
CORE/RIM										
SIO2	67.94	68.70	69.25	68.54	68.12	68.07	68.02	64.68	64.55	63.97
AL2O3	19.84	19.73	19.48	19.75	19.79	20.40	20.05	18.68	18.39	19.01
FE2O3(C)	0.00	0.00	0.00	0.00	0.00	0.00	0.00	0.00	0.00	0.00
TIO2	0.59	0.00	0.02	0.02	0.17	0.00	0.01	0.01	0.02	0.03
K2O	0.06	0.09	0.07	0.06	0.05	0.05	0.29	13.45	16.35	16.19
NA2O	11.44	11.57	11.61	11.45	11.39	11.40	11.37	2.49	0.26	0.27
CAO	0.90	0.21	0.15	0.21	0.09	0.16	0.19	0.06	0.03	0.03
MGO	0.01	0.01	0.00	0.00	0.00	0.00	0.00	0.00	0.03	0.03
FEO(C)	0.07	0.16	0.10	0.01	0.18	0.02	0.02	0.07	0.07	0.16
MNO	0.01	0.01	0.01	0.00	0.04	0.00	0.00	0.01	0.02	0.02
BAO	0.02	0.01	0.00	0.00	0.00	0.00	0.06	0.63	0.27	0.30
SUM	100.86	100.49	100.69	100.03	99.83	100.11	100.00	100.09	100.00	100.01
SI	2.95	2.99	3.00	2.99	2.98	2.97	2.97	2.98	2.99	2.97
AL	1.02	1.01	1.00	1.02	1.02	1.05	1.03	1.01	1.01	1.04
FE+3	0.00	0.00	0.00	0.00	0.00	0.00	0.00	0.00	0.00	0.00
TI	0.02	0.00	0.00	0.00	0.01	0.00	0.00	0.00	0.00	0.00
K	0.00	0.00	0.00	0.00	0.00	0.00	0.02	0.79	0.97	0.96
NA	0.96	0.98	0.98	0.97	0.97	0.96	0.96	0.22	0.02	0.02
CA	0.04	0.01	0.01	0.01	0.00	0.01	0.01	0.00	0.00	0.00
MG	0.00	0.00	0.00	0.00	0.00	0.00	0.00	0.00	0.00	0.00
FE+2	0.00	0.01	0.00	0.00	0.01	0.00	0.00	0.00	0.00	0.01
MN	0.00	0.00	0.00	0.00	0.00	0.00	0.00	0.00	0.00	0.00
BA	0.00	0.00	0.00	0.00	0.00	0.00	0.00	0.01	0.00	0.00
%OR	0.33	0.52	0.38	0.33	0.30	0.31	1.61	77.80	97.51	97.37
%AB	95.53	98.50	98.92	98.67	99.28	98.90	97.51	21.92	2.36	2.47
%AN	4.14	0.98	0.70	1.01	0.42	0.79	0.88	0.28	0.13	0.17

FELDSPAR

SAMPLE NO.	A2-15A	A2-19A	A2-19A	A2-21B	A2-21B	A2-27B	A2-27B	A2-66A	A3-4A	A3-11B
ANALYSIS	05U	16GQM	18GQM	04GQM	06GQM	01U	27U	21A	26S	15G
CORE/RIM										
SIO2	66.16	68.05	69.36	66.65	69.41	64.33	68.38	69.76	67.79	68.50
AL2O3	20.06	19.04	20.48	19.13	20.21	18.59	19.21	19.73	19.81	19.71
FE2O3(C)	0.00	0.00	0.00	0.00	0.00	0.00	0.00	0.00	0.00	0.00
TIO2	0.35	0.04	0.02	0.01	0.03	0.00	0.05	0.01	0.03	0.03
K2O	0.12	0.05	0.05	0.11	0.09	16.40	0.12	0.06	0.07	0.03
NA2O	11.11	11.42	11.79	11.33	11.64	0.21	11.73	11.86	11.52	11.87
CAO	1.05	0.15	0.16	0.11	0.08	0.04	0.02	0.20	0.09	0.14
MGO	0.19	0.00	0.00	0.00	0.00	0.03	0.01	0.00	0.00	0.00
FEO(C)	0.61	0.02	0.00	0.01	0.08	0.15	0.09	0.06	0.17	0.04
MNO	0.00	0.00	0.01	0.00	0.00	0.03	0.00	0.01	0.00	0.00
BAO	0.00	0.00	0.00	0.00	0.00	0.23	0.02	0.05	0.00	0.00
SUM	99.66	98.79	101.87	97.36	101.54	100.02	99.62	101.75	99.48	100.32
SI	2.92	3.01	2.97	2.99	2.98	2.98	3.00	3.00	2.98	2.98
AL	1.05	0.99	1.03	1.01	1.02	1.02	0.99	1.00	1.03	1.01
FE+3	0.00	0.00	0.00	0.00	0.00	0.00	0.00	0.00	0.00	0.00
TI	0.01	0.00	0.00	0.00	0.00	0.00	0.00	0.00	0.00	0.00
K	0.01	0.00	0.00	0.01	0.00	0.97	0.01	0.00	0.00	0.00
NA	0.95	0.98	0.98	0.99	0.97	0.02	1.00	0.99	0.98	1.00
CA	0.05	0.01	0.01	0.00	0.00	0.00	0.00	0.01	0.00	0.01
MG	0.01	0.00	0.00	0.00	0.00	0.00	0.00	0.00	0.00	0.00
FE+2	0.02	0.00	0.00	0.00	0.00	0.01	0.00	0.00	0.01	0.00
MN	0.00	0.00	0.00	0.00	0.00	0.00	0.00	0.00	0.00	0.00
BA	0.00	0.00	0.00	0.00	0.00	0.00	0.00	0.00	0.00	0.00
%OR	0.67	0.27	0.29	0.65	0.51	97.85	0.68	0.36	0.39	0.18
%AB	94.42	99.00	98.98	98.82	99.13	1.94	99.23	98.74	99.17	99.18
%AN	4.91	0.73	0.73	0.53	0.36	0.21	0.09	0.91	0.44	0.65

FELDSPAR

SAMPLE NO.	A3-43B	A3-43B	A3-71A	A3-92A	A4-2A	A4-6A	A4-6A	A4-8A	A4-19A	A4-19A
ANALYSIS	08A	09A	11A	05A	17G	12G	13G	61G	02G	10G
CORE/RIM										
SIO2	63.59	67.08	68.64	66.47	68.50	64.43	63.57	61.47	64.10	63.59
AL2O3	22.50	20.04	19.76	21.13	20.09	22.85	23.50	23.73	22.89	23.07
FE2O3(C)	0.00	0.00	0.00	0.00	0.00	0.00	0.00	0.00	0.00	0.00
TIO2	0.00	0.01	0.00	0.05	0.00	0.11	0.01	0.03	0.00	0.03
K2O	0.08	0.04	0.04	0.06	0.04	0.07	0.07	0.09	0.07	0.08
NA2O	9.20	10.93	11.97	10.26	11.30	9.65	9.18	9.47	9.43	9.13
CAO	4.00	1.22	0.52	1.74	0.63	3.82	4.10	4.34	3.97	4.34
MGO	0.01	0.00	0.00	0.00	0.00	0.00	0.01	0.00	0.00	0.00
FEO(C)	0.18	0.01	0.11	0.18	0.04	0.11	0.03	0.05	0.05	0.02
MNO	0.00	0.02	0.01	0.02	0.01	0.00	0.00	0.01	0.00	0.02
BAO	0.05	0.04	0.01	0.00	0.00	0.02	0.00	0.00	0.01	0.01
SUM	99.60	99.39	101.07	99.90	100.61	101.05	100.47	99.18	100.52	100.29
SI	2.82	2.95	2.98	2.92	2.98	2.82	2.79	2.75	2.81	2.80
AL	1.18	1.04	1.01	1.09	1.03	1.18	1.22	1.25	1.19	1.20
FE+3	0.00	0.00	0.00	0.00	0.00	0.00	0.00	0.00	0.00	0.00
TI	0.00	0.00	0.00	0.00	0.00	0.00	0.00	0.00	0.00	0.00
K	0.00	0.00	0.00	0.00	0.00	0.00	0.00	0.00	0.00	0.00
NA	0.79	0.93	1.01	0.87	0.95	0.82	0.78	0.82	0.80	0.78
CA	0.19	0.06	0.02	0.08	0.03	0.18	0.19	0.21	0.19	0.20
MG	0.00	0.00	0.00	0.00	0.00	0.00	0.00	0.00	0.00	0.00
FE+2	0.01	0.00	0.00	0.01	0.00	0.00	0.00	0.00	0.00	0.00
MN	0.00	0.00	0.00	0.00	0.00	0.00	0.00	0.00	0.00	0.00
BA	0.00	0.00	0.00	0.00	0.00	0.00	0.00	0.00	0.00	0.00
%OR	0.44	0.21	0.24	0.35	0.20	0.38	0.40	0.50	0.39	0.48
%AB	80.26	93.99	97.41	91.11	96.80	81.75	79.89	79.40	80.81	78.84
%AN	19.29	5.80	2.36	8.55	3.00	17.87	19.71	20.10	18.80	20.68

FELDSPAR

SAMPLE NO.	A4-22A	A4-22A	B2-1AB	B2-1AB	B2-1B	B2-1B	B2-1Y	B2-1Y	B2-3A	B2-3A
ANALYSIS	23A	25A	02G	14G	26G	27G	09G	10G	04G	09G
CORE/RIM										
SIO2	62.16	62.14	68.03	66.61	68.24	68.40	64.04	62.59	64.33	63.43
AL2O3	23.72	23.56	20.33	20.92	19.52	19.55	22.48	23.07	21.14	23.74
FE2O3(C)	0.00	0.00	0.00	0.00	0.00	0.00	0.00	0.00	0.00	0.00
TIO2	0.05	0.01	0.07	0.01	0.03	0.02	0.01	0.00	0.02	0.00
K2O	0.08	0.07	0.07	0.05	0.05	0.06	0.10	0.08	0.05	0.07
NA2O	8.55	8.89	10.80	10.54	11.41	12.03	9.41	9.40	10.31	8.98
CAO	5.40	5.32	0.70	1.09	0.31	0.31	3.88	4.06	2.64	4.73
MGO	0.00	0.00	0.00	0.00	0.00	0.02	0.00	0.02	0.00	0.00
FEO(C)	0.04	0.04	0.09	0.03	0.01	0.06	0.03	0.08	0.12	0.03
MNO	0.01	0.00	0.00	0.00	0.01	0.00	0.00	0.00	0.00	0.00
BAO	0.09	0.02	0.06	0.05	0.00	0.00	0.01	0.01	0.00	0.04
SUM	100.09	100.06	100.15	99.32	99.58	100.45	99.95	99.32	98.62	101.03
SI	2.76	2.76	2.97	2.93	2.99	2.98	2.83	2.79	2.88	2.78
AL	1.24	1.23	1.05	1.09	1.01	1.00	1.17	1.21	1.11	1.23
FE+3	0.00	0.00	0.00	0.00	0.00	0.00	0.00	0.00	0.00	0.00
TI	0.00	0.00	0.00	0.00	0.00	0.00	0.00	0.00	0.00	0.00
K	0.00	0.00	0.00	0.00	0.00	0.00	0.00	0.00	0.00	0.00
NA	0.74	0.76	0.91	0.90	0.97	1.02	0.81	0.81	0.89	0.76
CA	0.26	0.25	0.03	0.05	0.02	0.01	0.18	0.19	0.13	0.22
MG	0.00	0.00	0.00	0.00	0.00	0.00	0.00	0.00	0.00	0.00
FE+2	0.00	0.00	0.00	0.00	0.00	0.00	0.00	0.00	0.00	0.00
MN	0.00	0.00	0.00	0.00	0.00	0.00	0.00	0.00	0.00	0.00
BA	0.00	0.00	0.00	0.00	0.00	0.00	0.00	0.00	0.00	0.00
%OR	0.45	0.42	0.42	0.32	0.30	0.35	0.54	0.44	0.30	0.42
%AB	73.80	74.82	96.13	94.30	98.23	98.27	81.00	80.37	87.34	77.15
%AN	25.75	24.76	3.46	5.38	1.47	1.38	18.45	19.19	12.36	22.43

FELDSPAR

SAMPLE NO.	B2-4A	B2-4A	B2-4A	B2-24A	B2-24A	B2-35A	B2-35B	B3-75A	B3-75A	B3-75A
ANALYSIS	02A	03A	20A	03A	07A	03G	03S	01A	02A	18A
CORE/RIM										
SIO2	63.28	62.63	63.06	63.33	64.33	63.76	67.80	59.98	60.45	60.93
AL2O3	23.08	23.16	23.45	23.23	22.44	23.07	20.30	24.60	24.63	24.61
FE2O3(C)	0.00	0.00	0.00	0.00	0.00	0.00	0.00	0.00	0.00	0.00
TIO2	0.00	0.03	0.00	0.00	0.00	0.00	0.02	0.03	0.02	0.00
K2O	0.07	0.06	0.07	0.07	0.06	0.07	0.09	0.06	0.06	0.07
NA2O	8.74	8.72	8.63	8.98	9.52	8.92	11.19	7.95	7.84	8.22
CAO	4.41	4.59	4.50	4.22	3.49	3.81	0.40	6.42	6.42	6.20
MGO	0.01	0.00	0.00	0.00	0.01	0.00	0.00	0.01	0.02	0.02
FEO(C)	0.18	0.17	0.04	0.04	0.16	0.02	0.13	0.05	0.04	0.08
MNO	0.01	0.00	0.01	0.01	0.05	0.00	0.05	0.00	0.00	0.02
BAO	0.00	0.01	0.00	0.06	0.01	0.00	0.00	0.00	0.03	0.02
SUM	99.78	99.35	99.76	99.95	100.07	99.64	99.97	99.10	99.51	100.17
SI	2.80	2.79	2.79	2.80	2.84	2.82	2.96	2.69	2.70	2.71
AL	1.20	1.22	1.22	1.21	1.16	1.20	1.05	1.30	1.30	1.29
FE+3	0.00	0.00	0.00	0.00	0.00	0.00	0.00	0.00	0.00	0.00
TI	0.00	0.00	0.00	0.00	0.00	0.00	0.00	0.00	0.00	0.00
K	0.00	0.00	0.00	0.00	0.00	0.00	0.00	0.00	0.00	0.00
NA	0.75	0.75	0.74	0.77	0.81	0.76	0.95	0.69	0.68	0.71
CA	0.21	0.22	0.21	0.20	0.17	0.18	0.02	0.31	0.31	0.30
MG	0.00	0.00	0.00	0.00	0.00	0.00	0.00	0.00	0.00	0.00
FE+2	0.01	0.01	0.00	0.00	0.01	0.00	0.00	0.00	0.00	0.00
MN	0.00	0.00	0.00	0.00	0.00	0.00	0.00	0.00	0.00	0.00
BA	0.00	0.00	0.00	0.00	0.00	0.00	0.00	0.00	0.00	0.00
%OR	0.39	0.36	0.42	0.43	0.34	0.42	0.49	0.37	0.33	0.38
%AB	77.88	77.17	77.31	79.04	82.87	80.57	97.59	68.89	68.62	70.31
%AN	21.73	22.47	22.27	20.53	16.79	19.01	1.91	30.75	31.05	29.31

FELDSPAR

SAMPLE NO.	B3-127A	B3-127A	B3-127A	B3-127A	B3-127A	B3-127A	B3-141A	B3156AA	B3156AA	B3-170A
ANALYSIS	03A	04A	25A	26A	31A	30A	03G	01S	25S	03A
CORE/RIM										
SIO2	61.46	61.42	62.60	62.16	62.64	63.11	68.68	64.96	63.40	64.16
AL2O3	24.63	24.58	23.78	24.21	23.92	22.85	19.84	22.35	22.88	22.06
FE2O3(C)	0.00	0.00	0.00	0.00	0.00	0.00	0.00	0.00	0.00	0.00
TIO2	0.03	0.04	0.00	0.02	0.00	0.02	0.00	0.02	0.00	0.01
K2O	0.16	0.17	0.19	0.18	0.16	0.18	0.03	0.09	0.09	0.08
NA2O	7.91	7.79	8.63	8.45	8.70	9.03	11.43	8.84	8.93	8.85
CAO	5.96	5.93	4.71	5.45	5.16	4.27	0.41	3.72	3.68	3.73
MGO	0.00	0.01	0.01	0.01	0.00	0.01	0.00	0.00	0.00	0.00
FEO(C)	0.25	0.23	0.30	0.32	0.28	0.17	0.06	0.02	0.02	0.08
MNO	0.06	0.08	0.08	0.06	0.04	0.11	0.00	0.00	0.02	0.01
BAO	0.00	0.06	0.00	0.00	0.00	0.01	0.00	0.01	0.03	0.00
SUM	100.48	100.28	100.30	100.85	100.91	99.76	100.45	99.99	99.05	98.98
SI	2.72	2.72	2.77	2.74	2.76	2.80	2.99	2.85	2.82	2.85
AL	1.28	1.28	1.24	1.26	1.24	1.19	1.02	1.16	1.20	1.15
FE+3	0.00	0.00	0.00	0.00	0.00	0.00	0.00	0.00	0.00	0.00
TI	0.00	0.00	0.00	0.00	0.00	0.00	0.00	0.00	0.00	0.00
K	0.01	0.01	0.01	0.01	0.01	0.01	0.00	0.00	0.00	0.00
NA	0.68	0.67	0.74	0.72	0.74	0.78	0.96	0.75	0.77	0.76
CA	0.28	0.28	0.22	0.26	0.24	0.20	0.02	0.18	0.18	0.18
MG	0.00	0.00	0.00	0.00	0.00	0.00	0.00	0.00	0.00	0.00
FE+2	0.01	0.01	0.01	0.01	0.01	0.01	0.00	0.00	0.00	0.00
MN	0.00	0.00	0.00	0.00	0.00	0.00	0.00	0.00	0.00	0.00
BA	0.00	0.00	0.00	0.00	0.00	0.00	0.00	0.00	0.00	0.00
%OR	0.94	0.98	1.07	1.00	0.93	1.03	0.18	0.54	0.51	0.46
%AB	69.95	69.71	76.01	72.98	74.60	78.49	97.90	80.72	81.02	80.73
%AN	29.12	29.32	22.92	26.01	24.48	20.48	1.93	18.75	18.46	18.81

FELDSPAR

SAMPLE NO.	B3-170A	B3-175A	B3-175A	B3-175A	B3-185A	B3-184A	B3261AB	B3261AB	B4-1D	B4-7C
ANALYSIS	12A	17S	20S	44S	34G	35G	07S	20S	20G	09A
CORE/RIM										
SIO2	62.39	62.42	62.41	63.18	62.83	63.02	63.38	63.45	67.79	61.22
AL2O3	23.94	23.37	23.49	22.53	23.14	22.77	22.49	22.71	19.58	24.01
FE2O3(C)	0.00	0.00	0.00	0.00	0.00	0.00	0.00	0.00	0.00	0.00
TIO2	0.06	0.04	0.01	0.00	0.02	0.00	0.04	0.00	0.02	0.00
K2O	0.08	0.18	0.19	0.18	0.09	0.08	0.19	0.18	0.06	0.09
NA2O	8.38	8.78	9.03	9.10	9.05	9.23	9.05	9.12	11.07	8.08
CAO	5.64	4.30	4.37	4.34	4.65	4.49	4.22	4.07	0.75	5.91
MGO	0.01	0.00	0.00	0.00	0.00	0.00	0.01	0.00	0.00	0.00
FEO(C)	0.15	0.20	0.22	0.18	0.08	0.08	0.27	0.22	0.06	0.09
MNO	0.02	0.05	0.04	0.06	0.00	0.00	0.05	0.05	0.01	0.06
BAO	0.02	0.23	0.00	0.00	0.01	0.00	0.04	0.00	0.00	0.00
SUM	100.69	99.57	99.76	99.57	99.87	99.69	99.74	99.80	99.34	99.45
SI	2.75	2.78	2.77	2.81	2.78	2.80	2.81	2.81	2.98	2.73
AL	1.24	1.23	1.23	1.18	1.21	1.19	1.18	1.19	1.02	1.26
FE+3	0.00	0.00	0.00	0.00	0.00	0.00	0.00	0.00	0.00	0.00
TI	0.00	0.00	0.00	0.00	0.00	0.00	0.00	0.00	0.00	0.00
K	0.00	0.01	0.01	0.01	0.00	0.00	0.01	0.01	0.00	0.00
NA	0.72	0.76	0.78	0.78	0.78	0.80	0.78	0.78	0.94	0.70
CA	0.27	0.20	0.21	0.21	0.22	0.21	0.20	0.19	0.04	0.28
MG	0.00	0.00	0.00	0.00	0.00	0.00	0.00	0.00	0.00	0.00
FE+2	0.01	0.01	0.01	0.01	0.00	0.00	0.01	0.01	0.00	0.00
MN	0.00	0.00	0.00	0.00	0.00	0.00	0.00	0.00	0.00	0.00
BA	0.00	0.00	0.00	0.00	0.00	0.00	0.00	0.00	0.00	0.00
%OR	0.46	1.04	1.06	1.02	0.51	0.46	1.08	1.03	0.34	0.52
%AB	72.56	77.88	78.08	78.33	77.49	78.45	78.66	79.39	96.07	70.86
%AN	26.98	21.08	20.86	20.64	21.99	21.09	20.26	19.58	3.60	28.62

FELDSPAR

SAMPLE NO.	B4-7C	B4-7C	B4-8B	B4-8B	B4-11A	B4-11A	B4-11A	B4-11K	B4-11K	B4-11L
ANALYSIS	27A	28A	24A	28A	05A	09A	18A	21O	51O	21S
CORE/RIM										
SIO2	63.12	63.10	63.22	62.93	63.93	64.73	61.18	63.21	63.52	64.18
AL2O3	23.06	23.65	22.59	22.96	22.76	22.34	23.98	23.10	23.24	22.05
FE2O3(C)	0.00	0.00	0.00	0.00	0.00	0.00	0.00	0.00	0.00	0.00
TIO2	0.06	0.00	0.01	0.01	0.00	0.11	0.04	0.03	0.00	0.06
K2O	0.14	0.15	0.08	0.08	0.07	0.07	0.06	0.09	0.09	0.07
NA2O	9.09	9.25	9.35	9.12	9.56	9.68	8.46	8.75	9.14	9.70
CAO	4.65	4.22	4.23	4.29	4.08	3.64	5.94	4.71	4.48	3.73
MGO	0.00	0.01	0.00	0.00	0.01	0.01	0.01	0.00	0.02	0.00
FEO(C)	0.07	0.05	0.03	0.00	0.06	0.05	0.13	0.13	0.02	0.03
MNO	0.00	0.00	0.00	0.00	0.00	0.01	0.00	0.00	0.00	0.00
BAO	0.02	0.00	0.01	0.02	0.05	0.02	0.05	0.00	0.03	0.01
SUM	100.23	100.45	99.52	99.41	100.54	100.67	99.84	100.03	100.53	99.84
SI	2.79	2.78	2.81	2.80	2.81	2.84	2.73	2.79	2.79	2.84
AL	1.20	1.23	1.18	1.20	1.18	1.15	1.26	1.20	1.20	1.15
FE+3	0.00	0.00	0.00	0.00	0.00	0.00	0.00	0.00	0.00	0.00
TI	0.00	0.00	0.00	0.00	0.00	0.00	0.00	0.00	0.00	0.00
K	0.01	0.01	0.00	0.00	0.00	0.00	0.00	0.00	0.00	0.00
NA	0.78	0.79	0.81	0.79	0.81	0.82	0.73	0.75	0.78	0.83
CA	0.22	0.20	0.20	0.20	0.19	0.17	0.28	0.22	0.21	0.18
MG	0.00	0.00	0.00	0.00	0.00	0.00	0.00	0.00	0.00	0.00
FE+2	0.00	0.00	0.00	0.00	0.00	0.00	0.00	0.00	0.00	0.00
MN	0.00	0.00	0.00	0.00	0.00	0.00	0.00	0.00	0.00	0.00
BA	0.00	0.00	0.00	0.00	0.00	0.00	0.00	0.00	0.00	0.00
%OR	0.81	0.86	0.45	0.43	0.40	0.41	0.35	0.50	0.50	0.42
%AB	77.34	79.19	79.66	79.03	80.58	82.47	71.81	76.68	78.29	82.13
%AN	21.85	19.95	19.89	20.53	19.02	17.12	27.84	22.82	21.22	17.45

FELDSPAR

SAMPLE NO.	B4-11L	B4-13A	B4-13A	B4-32A	B4-32A	B4-93A	B4-101A	B4-101A	B4-101A	B4-141A
ANALYSIS	22S	01A	16A	53S	54S	31G	04G	05G	33G	02S
CORE/RIM										
SIO2	64.06	62.91	62.45	62.70	63.05	64.08	64.42	64.20	64.68	63.07
AL2O3	21.94	22.86	22.85	22.95	23.43	22.98	22.51	21.99	22.26	22.61
FE2O3(C)	0.00	0.00	0.00	0.00	0.00	0.00	0.00	0.00	0.00	0.00
TIO2	0.00	0.01	0.02	0.05	0.04	0.00	0.00	0.00	0.00	0.03
K2O	0.08	0.16	0.14	0.16	0.16	0.07	0.14	0.11	0.12	0.17
NA2O	9.59	8.76	8.88	9.13	9.04	9.34	9.89	9.90	9.82	9.32
CAO	3.69	4.43	4.38	4.36	4.59	4.28	3.28	2.98	2.97	3.73
MGO	0.00	0.00	0.00	0.00	0.00	0.01	0.00	0.00	0.00	0.00
FEO(C)	0.02	0.17	0.16	0.24	0.21	0.03	0.20	0.21	0.17	0.29
MNO	0.01	0.00	0.05	0.04	0.09	0.00	0.03	0.06	0.02	0.02
BAO	0.00	0.00	0.04	0.00	0.00	0.02	0.10	0.00	0.00	0.00
SUM	99.39	99.30	98.97	99.63	100.60	100.80	100.57	99.44	100.03	99.25
SI	2.84	2.80	2.79	2.79	2.78	2.81	2.83	2.85	2.85	2.81
AL	1.15	1.20	1.20	1.20	1.22	1.19	1.17	1.15	1.16	1.19
FE+3	0.00	0.00	0.00	0.00	0.00	0.00	0.00	0.00	0.00	0.00
TI	0.00	0.00	0.00	0.00	0.00	0.00	0.00	0.00	0.00	0.00
K	0.00	0.01	0.01	0.01	0.01	0.00	0.01	0.01	0.01	0.01
NA	0.82	0.76	0.77	0.79	0.77	0.79	0.84	0.85	0.84	0.81
CA	0.18	0.21	0.21	0.21	0.22	0.20	0.15	0.14	0.14	0.18
MG	0.00	0.00	0.00	0.00	0.00	0.00	0.00	0.00	0.00	0.00
FE+2	0.00	0.01	0.01	0.01	0.01	0.00	0.01	0.01	0.01	0.01
MN	0.00	0.00	0.00	0.00	0.00	0.00	0.00	0.00	0.00	0.00
BA	0.00	0.00	0.00	0.00	0.00	0.00	0.00	0.00	0.00	0.00
%OR	0.43	0.95	0.83	0.89	0.91	0.38	0.80	0.64	0.67	0.95
%AB	82.09	77.43	77.94	78.42	77.39	79.51	83.85	85.21	85.12	81.14
%AN	17.47	21.62	21.23	20.70	21.70	20.12	15.35	14.15	14.21	17.91

FELDSPAR

SAMPLE NO.	C3-2B	C3-4A	C3-17D	C3-17D	C3-19BB	C3-27AA	C3-55AA	C3-55AA	C3-55AA	C3-55AA
ANALYSIS	24G	05A	15A	16A	31S	13A	02A	20A	08A	09A
CORE/RIM										
SIO2	61.57	60.54	62.46	63.25	62.90	56.27	61.43	59.83	62.16	61.72
AL2O3	23.91	24.87	23.34	23.45	22.93	27.94	25.46	25.64	24.00	24.24
FE2O3(C)	0.00	0.00	0.00	0.00	0.00	0.00	0.00	0.00	0.00	0.00
TIO2	0.01	0.02	0.07	0.02	0.04	0.04	0.00	0.00	0.01	0.01
K2O	0.05	0.06	0.06	0.05	0.07	0.04	0.09	0.08	0.06	0.08
NA2O	8.42	7.30	8.97	9.42	8.68	6.09	8.67	7.81	8.58	8.68
CAO	5.83	6.68	4.41	4.32	4.80	9.85	4.99	6.64	5.11	5.26
MGO	0.00	0.00	0.00	0.01	0.01	0.02	0.02	0.01	0.02	0.02
FEO(C)	0.04	0.13	0.04	0.06	0.02	0.03	0.04	0.05	0.02	0.07
MNO	0.04	0.02	0.00	0.02	0.03	0.00	0.01	0.00	0.00	0.02
BAO	0.00	0.11	0.00	0.07	0.02	0.06	0.00	0.02	0.04	0.00
SUM	99.88	99.72	99.34	100.66	99.49	100.35	100.69	100.08	100.00	100.11
SI	2.74	2.70	2.78	2.78	2.80	2.52	2.70	2.66	2.75	2.73
AL	1.25	1.31	1.22	1.22	1.20	1.48	1.32	1.35	1.25	1.27
FE+3	0.00	0.00	0.00	0.00	0.00	0.00	0.00	0.00	0.00	0.00
TI	0.00	0.00	0.00	0.00	0.00	0.00	0.00	0.00	0.00	0.00
K	0.00	0.00	0.00	0.00	0.00	0.00	0.00	0.00	0.00	0.00
NA	0.73	0.63	0.77	0.80	0.75	0.53	0.74	0.67	0.74	0.75
CA	0.28	0.32	0.21	0.20	0.23	0.47	0.24	0.32	0.24	0.25
MG	0.00	0.00	0.00	0.00	0.00	0.00	0.00	0.00	0.00	0.00
FE+2	0.00	0.00	0.00	0.00	0.00	0.00	0.00	0.00	0.00	0.00
MN	0.00	0.00	0.00	0.00	0.00	0.00	0.00	0.00	0.00	0.00
BA	0.00	0.00	0.00	0.00	0.00	0.00	0.00	0.00	0.00	0.00
%OR	0.29	0.36	0.32	0.26	0.39	0.21	0.50	0.44	0.35	0.46
%AB	72.09	66.18	78.39	79.59	76.30	52.70	75.50	67.75	74.97	74.56
%AN	27.61	33.46	21.28	20.15	23.31	47.09	24.00	31.81	24.68	24.98

FELDSPAR

SAMPLE NO.	C3-56A	C3-56A	C3-56A	C3-68AA	C3-68AA	C3-68AA	C3-77A	C3116AA	C3116AA	C3116AA
ANALYSIS	02G	12G	16G	07G	08G	12G	06A	04A	33A	36A
CORE/RIM										
SIO2	64.29	65.44	65.30	68.05	67.87	64.49	63.39	57.07	58.15	56.70
AL2O3	22.07	21.74	20.92	20.14	20.20	20.98	22.21	27.16	25.99	26.75
FE2O3(C)	0.00	0.00	0.00	0.00	0.00	0.00	0.00	0.00	0.00	0.00
TIO2	0.00	0.00	0.03	0.00	0.00	0.01	0.01	0.00	0.03	0.03
K2O	0.15	0.11	0.10	0.04	0.04	0.09	0.07	0.05	0.05	0.04
NA2O	9.83	10.17	10.79	11.17	11.34	10.28	9.86	6.17	6.80	6.03
CAO	3.34	2.43	1.91	0.86	0.70	2.49	3.73	9.16	8.25	9.39
MGO	0.00	0.00	0.00	0.00	0.00	0.02	0.01	0.00	0.02	0.04
FEO(C)	0.02	0.01	0.00	0.01	0.00	0.02	0.14	0.05	0.02	0.08
MNO	0.00	0.00	0.00	0.02	0.00	0.00	0.01	0.00	0.01	0.00
BAO	0.00	0.24	0.00	0.00	0.00	0.00	0.13	0.00	0.00	0.01
SUM	99.70	100.14	99.06	100.30	100.15	98.38	99.55	99.67	99.32	99.07
SI	2.84	2.88	2.90	2.97	2.96	2.89	2.82	2.56	2.62	2.57
AL	1.15	1.13	1.10	1.03	1.04	1.11	1.16	1.44	1.38	1.43
FE+3	0.00	0.00	0.00	0.00	0.00	0.00	0.00	0.00	0.00	0.00
TI	0.00	0.00	0.00	0.00	0.00	0.00	0.00	0.00	0.00	0.00
K	0.01	0.01	0.01	0.00	0.00	0.00	0.00	0.00	0.00	0.00
NA	0.84	0.87	0.93	0.94	0.96	0.89	0.85	0.54	0.59	0.53
CA	0.16	0.12	0.09	0.04	0.03	0.12	0.18	0.44	0.40	0.45
MG	0.00	0.00	0.00	0.00	0.00	0.00	0.00	0.00	0.00	0.00
FE+2	0.00	0.00	0.00	0.00	0.00	0.00	0.00	0.00	0.00	0.00
MN	0.00	0.00	0.00	0.00	0.00	0.00	0.00	0.00	0.00	0.00
BA	0.00	0.00	0.00	0.00	0.00	0.00	0.00	0.00	0.00	0.00
%OR	0.82	0.61	0.55	0.21	0.23	0.52	0.39	0.30	0.30	0.25
%AB	83.51	87.79	90.57	95.71	96.47	87.71	82.40	54.76	59.70	53.63
%AN	15.67	11.60	8.88	4.08	3.30	11.77	17.21	44.93	40.00	46.12

FELDSPAR

SAMPLE NO.	C3-117A	C3-117A	C3-117B	C4-1C	C4-1C	C4-1C	C4-1C	C4-7B	C4-17A	C4-20B
ANALYSIS	Q1A	Q2A	11A	02A	05A	13A	14A	07CS	16A	16A
CORE/RIM										
SIO2	59.40	63.23	62.24	61.26	60.65	59.84	61.46	66.64	65.15	63.74
AL2O3	25.40	23.36	24.61	25.08	25.82	25.17	23.81	20.96	22.62	22.60
FE2O3(C)	0.00	0.00	0.00	0.00	0.00	0.00	0.00	0.00	0.00	0.00
TIO2	0.04	0.03	0.01	0.00	0.00	0.06	0.00	0.03	0.00	0.04
K2O	0.06	0.07	0.05	0.06	0.06	0.07	0.08	0.05	0.07	0.06
NA2O	7.61	8.83	7.43	7.10	6.86	6.97	8.01	10.68	8.69	10.06
CAO	6.98	4.78	5.79	6.63	6.78	7.04	5.98	1.93	3.23	3.94
MGO	0.00	0.01	0.03	0.00	0.01	0.00	0.00	0.00	0.00	0.02
FEO(C)	0.10	0.07	0.03	0.03	0.13	0.02	0.01	0.05	0.03	0.05
MNO	0.00	0.01	0.00	0.02	0.00	0.01	0.04	0.00	0.03	0.00
BAO	0.00	0.00	0.00	0.06	0.04	0.04	0.03	0.01	0.03	0.00
SUM	99.59	100.40	100.19	100.25	100.35	99.23	99.41	100.34	99.85	100.53
SI	2.66	2.78	2.74	2.71	2.68	2.68	2.74	2.91	2.86	2.81
AL	1.34	1.21	1.28	1.31	1.35	1.33	1.25	1.08	1.17	1.17
FE+3	0.00	0.00	0.00	0.00	0.00	0.00	0.00	0.00	0.00	0.00
TI	0.00	0.00	0.00	0.00	0.00	0.00	0.00	0.00	0.00	0.00
K	0.00	0.00	0.00	0.00	0.00	0.00	0.00	0.00	0.00	0.00
NA	0.66	0.75	0.63	0.61	0.59	0.61	0.69	0.91	0.74	0.86
CA	0.33	0.23	0.27	0.31	0.32	0.34	0.29	0.09	0.15	0.19
MG	0.00	0.00	0.00	0.00	0.00	0.00	0.00	0.00	0.00	0.00
FE+2	0.00	0.00	0.00	0.00	0.00	0.00	0.00	0.00	0.00	0.00
MN	0.00	0.00	0.00	0.00	0.00	0.00	0.00	0.00	0.00	0.00
BA	0.00	0.00	0.00	0.00	0.00	0.00	0.00	0.00	0.00	0.00
%OR	0.32	0.39	0.32	0.39	0.38	0.42	0.46	0.25	0.43	0.35
%AB	66.17	76.66	69.67	65.73	64.42	63.92	70.47	90.70	82.62	81.91
%AN	33.51	22.95	30.01	33.89	35.20	35.66	29.07	9.05	16.95	17.74

FELDSPAR

SAMPLE NO.	C4-24A	C4-24A	C4-24A	C4-24A	C4-25A	C4-25A	C4-25A	C4-25A	C4-32A	C4-32A
ANALYSIS	30A	31A	35A	41A	02A	03A	20A	21A	23S	44S
CORE/RIM									C	C
SIO2	63.52	63.68	61.95	63.21	59.42	58.51	63.28	60.71	63.05	63.18
AL2O3	22.90	22.99	23.93	23.10	25.02	26.28	23.28	24.36	23.05	23.20
FE2O3(C)	0.00	0.00	0.00	0.00	0.00	0.00	0.00	0.00	0.00	0.00
TIO2	0.06	0.06	0.03	0.00	0.03	0.07	0.00	0.01	0.02	0.02
K2O	0.06	0.06	0.06	0.06	0.12	0.11	0.12	0.13	0.16	0.10
NA2O	9.40	9.30	8.40	9.30	7.84	6.79	8.97	8.00	8.97	9.35
CAO	4.29	4.40	5.59	4.31	6.58	8.37	4.74	6.12	4.23	4.30
MGO	0.01	0.00	0.00	0.00	0.00	0.00	0.00	0.02	0.01	0.00
FEO(C)	0.04	0.08	0.05	0.03	0.05	0.04	0.02	0.07	0.00	0.00
MNO	0.00	0.02	0.02	0.00	0.00	0.00	0.00	0.00	0.00	0.00
BAO	0.04	0.05	0.05	0.03	0.02	0.00	0.03	0.02	0.02	0.01
SUM	100.33	100.64	100.08	100.04	99.08	100.17	100.45	99.43	99.50	100.15
SI	2.80	2.80	2.75	2.79	2.67	2.61	2.79	2.71	2.80	2.79
AL	1.19	1.19	1.25	1.20	1.33	1.38	1.21	1.28	1.21	1.21
FE+3	0.00	0.00	0.00	0.00	0.00	0.00	0.00	0.00	0.00	0.00
TI	0.00	0.00	0.00	0.00	0.00	0.00	0.00	0.00	0.00	0.00
K	0.00	0.00	0.00	0.00	0.01	0.01	0.01	0.01	0.01	0.00
NA	0.80	0.79	0.72	0.80	0.68	0.59	0.77	0.69	0.77	0.80
CA	0.20	0.21	0.27	0.20	0.32	0.40	0.22	0.29	0.20	0.20
MG	0.00	0.00	0.00	0.00	0.00	0.00	0.00	0.00	0.00	0.00
FE+2	0.00	0.00	0.00	0.00	0.00	0.00	0.00	0.00	0.00	0.00
MN	0.00	0.00	0.00	0.00	0.00	0.00	0.00	0.00	0.00	0.00
BA	0.00	0.00	0.00	0.00	0.00	0.00	0.00	0.00	0.00	0.00
%OR	0.35	0.35	0.32	0.34	0.67	0.63	0.69	0.75	0.90	0.54
%AB	79.57	79.00	72.86	79.33	67.85	59.12	76.87	69.78	78.62	79.31
%AN	20.08	20.65	26.82	20.34	31.48	40.25	22.44	29.47	20.48	20.15

FELDSPAR

SAMPLE NO.	C4-32A	C4-32A	C4-36A	C4-36A	C4-36A	C4-36A	C4-36A	C4-46A	C4-46A	C4-46A
ANALYSIS	25S	43S	01A	03A	04A	05A	16A	09G	35G	08G
CORE/RIM	R	R								
SIO2	61.14	61.34	64.07	65.41	64.40	65.23	62.78	64.26	64.49	67.95
AL2O3	23.90	24.42	22.40	21.72	22.52	21.96	23.45	18.91	18.95	20.29
FE2O3(C)	0.00	0.00	0.00	0.00	0.00	0.00	0.00	0.00	0.00	0.00
TIO2	0.04	0.00	0.00	0.00	0.00	0.03	0.04	0.04	0.00	0.00
K2O	0.12	0.07	0.12	0.11	0.13	0.13	0.13	14.86	15.13	0.10
NA2O	8.33	8.23	9.37	10.62	9.77	9.98	9.09	1.03	0.80	11.53
CAO	5.56	6.12	3.74	2.20	3.45	2.88	4.45	0.07	0.03	0.70
MGO	0.00	0.00	0.00	0.00	0.00	0.00	0.01	0.02	0.02	0.00
FEO(C)	0.00	0.03	0.00	0.00	0.00	0.00	0.02	0.01	0.02	0.00
MNO	0.01	0.03	0.00	0.00	0.02	0.00	0.00	0.00	0.00	0.00
BAO	0.00	0.05	0.07	0.01	0.00	0.00	0.00	1.57	1.23	0.00
SUM	99.09	100.30	99.77	100.09	100.30	100.20	99.95	100.77	100.67	100.57
SI	2.74	2.72	2.83	2.88	2.83	2.86	2.78	2.97	2.97	2.96
AL	1.26	1.28	1.17	1.13	1.17	1.14	1.22	1.03	1.03	1.04
FE+3	0.00	0.00	0.00	0.00	0.00	0.00	0.00	0.00	0.00	0.00
TI	0.00	0.00	0.00	0.00	0.00	0.00	0.00	0.00	0.00	0.00
K	0.01	0.00	0.01	0.01	0.01	0.01	0.01	0.88	0.89	0.00
NA	0.72	0.71	0.80	0.90	0.83	0.85	0.78	0.09	0.07	0.97
CA	0.27	0.29	0.18	0.10	0.16	0.13	0.21	0.00	0.00	0.03
MG	0.00	0.00	0.00	0.00	0.00	0.00	0.00	0.00	0.00	0.00
FE+2	0.00	0.00	0.00	0.00	0.00	0.00	0.00	0.00	0.00	0.00
MN	0.00	0.00	0.00	0.00	0.00	0.00	0.00	0.00	0.00	0.00
BA	0.00	0.00	0.00	0.00	0.00	0.00	0.00	0.03	0.02	0.00
%OR	0.69	0.42	0.67	0.63	0.71	0.73	0.74	90.11	92.41	0.52
%AB	72.57	70.59	81.37	89.15	83.07	85.64	78.11	9.54	7.43	96.24
%AN	26.75	28.99	17.96	10.23	16.22	13.63	21.15	0.35	0.16	3.24

FELDSPAR

SAMPLE NO.	C4-46A	C4-49A	C4-49B	D2-1CA	D2-1CA	D2-1D	D2-1D
ANALYSIS	22G	02A	02S	13S	15S	04S	30S
CORE/RIM							
SIO2	65.90	59.43	60.38	60.55	62.24	60.64	60.22
AL2O3	21.62	25.46	25.20	24.16	24.11	24.94	24.67
FE2O3(C)	0.00	0.00	0.00	0.00	0.00	0.00	0.00
TIO2	0.03	0.00	0.02	0.01	0.03	0.04	0.04
K2O	0.15	0.10	0.11	0.05	0.05	0.13	0.13
NA2O	10.66	7.53	7.55	8.52	8.77	7.86	8.09
CAO	2.21	7.48	7.06	5.83	5.56	6.48	6.47
MGO	0.00	0.03	0.02	0.05	0.01	0.03	0.00
FEO(C)	0.03	0.10	0.04	0.09	0.05	0.06	0.00
MNO	0.02	0.00	0.00	0.01	0.02	0.05	0.01
BAO	0.03	0.04	0.06	0.00	0.00	0.05	0.00
SUM	100.64	100.17	100.43	99.26	100.84	100.28	99.61
SI	2.88	2.65	2.68	2.71	2.74	2.69	2.69
AL	1.11	1.34	1.32	1.28	1.25	1.31	1.30
FE+3	0.00	0.00	0.00	0.00	0.00	0.00	0.00
TI	0.00	0.00	0.00	0.00	0.00	0.00	0.00
K	0.01	0.01	0.01	0.00	0.00	0.01	0.01
NA	0.90	0.65	0.65	0.74	0.75	0.68	0.70
CA	0.10	0.36	0.34	0.28	0.26	0.31	0.31
MG	0.00	0.00	0.00	0.00	0.00	0.00	0.00
FE+2	0.00	0.00	0.00	0.00	0.00	0.00	0.00
MN	0.00	0.00	0.00	0.00	0.00	0.00	0.00
BA	0.00	0.00	0.00	0.00	0.00	0.00	0.00
%OR	0.85	0.57	0.65	0.28	0.28	0.71	0.70
%AB	88.97	64.19	65.49	72.37	73.85	68.22	68.87
%AN	10.18	35.24	33.86	27.35	25.86	31.07	30.43

GARNET

SAMPLE NO.	A3-1B	A3-1B	A3-1B	A4-2A	A4-6A	A4-6A	A4-6A	A4-6A	A4-6A	A4-6A
ANALYSIS	02S	03S	09S	20G	04G	20G	21G	18G	17G	24G
CORE/RIM				R	R	R	R	C	R	C
SIO2	37.21	37.43	38.08	37.36	38.27	37.57	37.61	38.45	38.87	38.03
AL2O3	20.59	20.48	20.82	21.57	20.69	21.76	21.47	20.52	21.33	21.18
CR2O3	0.00	0.00	0.00	0.06	0.08	0.07	0.04	0.08	0.06	0.08
TIO2	0.22	0.23	0.24	0.07	0.16	0.08	0.05	0.25	0.15	0.22
FE2O3(C)	1.08	0.71	0.55	0.17	0.68	0.00	0.07	0.96	0.24	0.27
MGO	0.74	0.70	0.95	2.59	1.48	1.52	1.55	0.63	1.39	1.03
FEO(C)	19.71	19.59	20.91	27.21	27.35	28.42	28.40	20.45	27.35	22.51
MNO	12.25	12.07	10.93	10.45	1.43	1.69	1.50	8.52	1.76	6.47
CAO	8.75	8.68	8.44	2.13	9.94	9.67	9.72	10.96	10.22	11.35
NA2O	0.04	0.05	0.05	0.01	0.00	0.00	0.02	0.00	0.06	0.02
K2O	0.03	0.03	0.02	0.03	0.02	0.02	0.03	0.02	0.04	0.02
SUM	100.64	99.96	100.99	101.66	100.10	100.80	100.47	100.83	101.45	101.17
SI	2.98	3.01	3.03	2.96	3.05	2.97	2.98	3.06	3.05	3.00
AL(IV)	0.02	0.00	0.00	0.04	0.00	0.03	0.02	0.00	0.00	0.00
AL(VI)	1.92	1.94	1.95	1.98	1.94	2.00	1.99	1.92	1.97	1.97
CR	0.00	0.00	0.00	0.00	0.00	0.00	0.00	0.00	0.00	0.00
TI	0.01	0.01	0.01	0.00	0.01	0.00	0.00	0.02	0.01	0.01
FE+3	0.06	0.04	0.03	0.01	0.04	0.00	0.00	0.06	0.01	0.02
MG	0.09	0.08	0.11	0.31	0.18	0.18	0.18	0.07	0.16	0.12
FE+2	1.32	1.32	1.39	1.81	1.82	1.88	1.88	1.36	1.80	1.48
MN	0.83	0.82	0.74	0.70	0.10	0.11	0.10	0.57	0.12	0.43
CA	0.75	0.75	0.72	0.18	0.85	0.82	0.83	0.93	0.86	0.96
NA	0.01	0.01	0.01	0.00	0.00	0.00	0.00	0.00	0.01	0.00
K	0.00	0.00	0.00	0.00	0.00	0.00	0.00	0.00	0.00	0.00
O	11.99	12.02	12.03	11.98	12.06	11.99	11.99	12.06	12.05	12.00
%PYR	2.98	2.84	3.81	10.34	5.99	6.02	6.13	2.52	5.53	4.05
%ALM	43.92	44.33	47.00	59.87	61.90	62.59	62.80	46.22	61.17	49.35
%SPS	27.90	27.65	24.88	23.70	3.27	3.81	3.39	19.50	3.99	14.49
%UVA	0.00	0.00	0.00	0.20	0.24	0.22	0.14	0.24	0.18	0.24
%GRS	21.92	23.01	22.63	5.37	26.51	27.37	27.33	28.58	28.41	31.08
%ANR	3.28	2.16	1.68	0.52	2.09	0.00	0.22	2.93	0.71	0.80
FE/FE+MG	0.94	0.94	0.93	0.86	0.91	0.91	0.91	0.95	0.92	0.93
A	40.17	40.02	40.15	40.37	40.26	40.40	40.19	40.24	40.38	39.85
C	15.02	15.10	14.55	3.60	17.23	16.33	16.50	18.98	17.47	19.24
F	44.80	44.88	45.31	56.03	42.51	43.26	43.31	40.78	42.16	40.91
A"	0.40	0.40	0.39	0.32	0.32	0.33	0.32	0.39	0.33	0.38
F"	0.57	0.56	0.57	0.58	0.62	0.61	0.62	0.58	0.61	0.58
M"	0.04	0.04	0.05	0.10	0.06	0.06	0.06	0.03	0.05	0.05

GARNET

SAMPLE NO.	A4-6A	A4-6A	A4-6A	A4-6A	A4-8A	A4-8A	A4-8A	A4-8A	A4-8A	A4-8A
ANALYSIS	25G	29G	38G	37G	07G	09G	52G	53G	54G	27G
CORE/RIM	R	R	C	R	C	R	C	C	R	C
SIO2	38.37	37.78	39.07	37.96	37.49	37.60	37.50	37.28	36.83	37.33
AL2O3	21.95	22.01	21.24	21.62	20.96	21.50	22.27	22.01	21.95	21.37
CR2O3	0.06	0.04	0.10	0.05	0.05	0.06	0.03	0.02	0.07	0.03
TIO2	0.10	0.05	0.12	0.13	0.11	0.07	0.26	0.21	0.18	0.21
FE2O3(C)	0.00	0.00	0.31	0.03	0.11	0.00	0.00	0.00	0.00	0.00
MGO	1.49	1.61	0.88	0.98	0.59	0.69	0.71	0.67	0.89	0.24
FEO(C)	28.06	28.18	22.80	25.01	25.04	26.92	22.16	22.02	25.21	21.33
MNO	2.40	3.46	7.04	4.17	5.14	2.33	6.98	6.78	4.68	8.21
CAO	9.26	7.81	10.12	11.39	10.26	10.70	11.47	11.32	10.28	11.38
NA2O	0.01	0.04	0.01	0.01	0.02	0.00	0.02	0.00	0.04	0.01
K2O	0.04	0.04	0.01	0.02	0.02	0.03	0.02	0.02	0.04	0.02
SUM	101.75	101.03	101.69	101.39	99.79	99.91	101.44	100.33	100.17	100.12
SI	3.01	2.99	3.07	2.98	3.01	3.01	2.95	2.96	2.93	2.98
AL(IV)	0.00	0.01	0.00	0.02	0.00	0.00	0.05	0.04	0.07	0.02
AL(VI)	2.03	2.04	1.97	1.99	1.98	2.03	2.01	2.02	1.99	2.00
CR	0.00	0.00	0.01	0.00	0.00	0.00	0.00	0.00	0.00	0.00
TI	0.01	0.00	0.01	0.01	0.01	0.00	0.02	0.01	0.01	0.01
FE+3	0.00	0.00	0.02	0.00	0.01	0.00	0.00	0.00	0.00	0.00
MG	0.17	0.19	0.10	0.12	0.07	0.08	0.08	0.08	0.11	0.03
FE+2	1.84	1.86	1.50	1.64	1.68	1.80	1.46	1.46	1.68	1.43
MN	0.16	0.23	0.47	0.28	0.35	0.16	0.46	0.46	0.32	0.56
CA	0.78	0.66	0.85	0.96	0.88	0.92	0.96	0.96	0.88	0.98
NA	0.00	0.01	0.00	0.00	0.00	0.00	0.00	0.00	0.01	0.00
K	0.00	0.00	0.00	0.00	0.00	0.00	0.00	0.00	0.00	0.00
O	12.03	12.01	12.07	11.99	12.01	12.02	11.99	12.00	11.97	12.00
%PYR	5.91	6.44	3.53	3.86	2.38	2.79	2.83	2.66	3.60	0.94
%ALM	62.33	63.24	51.27	54.70	56.35	60.86	48.63	49.38	55.70	47.77
%SPS	5.40	7.87	16.04	9.31	11.70	5.34	15.77	15.41	10.77	18.63
%UVA	0.19	0.14	0.31	0.16	0.17	0.20	0.10	0.08	0.24	0.11
%GRS	26.16	22.31	27.92	31.89	29.06	30.81	32.67	32.46	29.68	32.56
%ANR	0.00	0.00	0.93	0.08	0.34	0.00	0.00	0.00	0.00	0.00
FE/FE+MG	0.91	0.91	0.94	0.94	0.96	0.96	0.95	0.95	0.94	0.98
A	40.73	41.04	40.46	40.09	40.01	40.66	40.98	41.03	40.88	40.28
C	15.62	13.24	17.36	19.18	17.74	18.40	19.19	19.19	17.42	19.50
F	43.65	45.72	42.18	40.73	42.25	40.94	39.83	39.78	41.70	40.22
A"	0.33	0.33	0.38	0.36	0.36	0.35	0.40	0.40	0.37	0.41
F"	0.61	0.61	0.58	0.60	0.61	0.62	0.57	0.57	0.60	0.58
M"	0.06	0.06	0.04	0.04	0.03	0.03	0.03	0.03	0.04	0.01

GARNET

SAMPLE NO.	A4-8A	A4-8A	A4-8A	A4-19A	A4-19A	A4-19A	A4-19A	A4-19A	A4-19A	A4-19A
ANALYSIS	55G	26G	56G	29S	26S	24S	23S	21S	22S	19S
CORE/RIM	C	R	R	C	R	C	R	C	C	R
SIO2	37.44	37.71	37.51	37.69	38.04	37.89	37.46	37.77	37.25	37.75
AL2O3	22.07	21.68	22.31	22.06	22.13	22.21	22.15	22.19	21.99	22.40
CR2O3	0.04	0.07	0.08	0.04	0.07	0.05	0.10	0.06	0.06	0.10
TIO2	0.25	0.16	0.15	0.13	0.17	0.17	0.13	0.17	0.25	0.14
FE2O3(C)	0.00	0.00	0.00	0.00	0.00	0.00	0.00	0.00	0.00	0.00
MGO	0.48	0.45	0.69	1.01	1.00	1.64	1.72	1.56	1.45	1.86
FEO(C)	21.73	24.93	24.10	20.21	20.23	22.62	23.19	21.52	20.99	23.42
MNO	7.00	4.80	4.87	9.48	9.67	8.58	7.49	9.88	10.40	8.70
CAO	11.80	10.94	11.13	9.94	9.87	7.94	8.12	7.57	7.98	6.85
NA2O	0.01	0.00	0.03	0.02	0.02	0.05	0.03	0.07	0.07	0.03
K2O	0.03	0.03	0.04	0.03	0.03	0.02	0.03	0.04	0.03	0.03
SUM	100.84	100.79	100.90	100.60	101.24	101.18	100.40	100.82	100.47	101.28
SI	2.96	2.99	2.96	2.99	3.00	2.99	2.97	2.99	2.96	2.98
AL(IV)	0.04	0.01	0.04	0.01	0.00	0.01	0.03	0.01	0.04	0.02
AL(VI)	2.02	2.02	2.04	2.05	2.05	2.05	2.04	2.06	2.02	2.06
CR	0.00	0.00	0.00	0.00	0.00	0.00	0.01	0.00	0.00	0.01
TI	0.02	0.01	0.01	0.01	0.01	0.01	0.01	0.01	0.02	0.01
FE+3	0.00	0.00	0.00	0.00	0.00	0.00	0.00	0.00	0.00	0.00
MG	0.06	0.05	0.08	0.12	0.12	0.19	0.20	0.19	0.17	0.22
FE+2	1.44	1.65	1.59	1.34	1.33	1.49	1.54	1.42	1.40	1.54
MN	0.47	0.32	0.33	0.64	0.64	0.57	0.50	0.66	0.70	0.58
CA	1.00	0.93	0.94	0.84	0.83	0.67	0.69	0.64	0.68	0.58
NA	0.00	0.00	0.00	0.00	0.00	0.01	0.00	0.01	0.01	0.00
K	0.00	0.00	0.00	0.00	0.00	0.00	0.00	0.00	0.00	0.00
O	12.00	12.02	12.01	12.02	12.03	12.03	12.02	12.03	12.00	12.02
%PYR	1.91	1.82	2.77	4.04	4.02	6.57	6.93	6.34	5.82	7.49
%ALM	48.50	55.87	54.14	45.58	45.50	50.94	52.41	48.90	47.35	52.84
%SPS	15.84	10.90	11.07	21.66	22.03	19.57	17.15	22.73	23.76	19.88
%UVA	0.13	0.23	0.25	0.12	0.24	0.17	0.31	0.18	0.20	0.31
%GRS	33.62	31.19	31.77	28.60	28.21	22.75	23.19	21.86	22.87	19.49
%ANR	0.00	0.00	0.00	0.00	0.00	0.00	0.00	0.00	0.00	0.00
FE/FE+MG	0.96	0.97	0.95	0.92	0.92	0.89	0.88	0.88	0.89	0.88
A	40.98	40.65	41.39	41.22	41.22	41.34	41.36	41.55	41.14	41.59
C	19.91	18.65	18.77	16.88	16.72	13.44	13.78	12.88	13.58	11.56
F	39.10	40.70	39.84	41.90	42.06	45.21	44.86	45.57	45.28	46.85
A"	0.41	0.37	0.38	0.41	0.41	0.38	0.37	0.39	0.40	0.37
F"	0.57	0.61	0.59	0.54	0.54	0.55	0.56	0.54	0.54	0.55
M"	0.02	0.02	0.03	0.05	0.05	0.07	0.07	0.07	0.07	0.08

GARNET

SAMPLE NO.	A4-19A	B2-1AB	B2-1AB	B2-1AB	B2-1AB	B2-1AB	B2-1Y	B2-1Y	B2-1Y	B2-1Y
ANALYSIS	20S	15G	16G	17G	26G	28G	30S	29S	42S	43S
CORE/RIM	R				C	R	C	R	C	R
SIO2	37.52	38.90	38.42	38.15	38.78	39.13	37.32	37.66	37.26	37.65
AL2O3	22.38	21.58	21.66	21.87	21.75	21.59	22.89	23.21	22.96	22.78
CR2O3	0.08	0.06	0.05	0.06	0.02	0.08	0.05	0.05	0.03	0.04
TIO2	0.15	0.12	0.07	0.12	0.17	0.20	0.20	0.15	0.14	0.11
FE2O3(C)	0.00	0.07	0.00	0.00	0.00	0.00	0.00	0.00	0.00	0.00
MGO	1.88	1.03	1.00	1.15	0.82	0.77	0.90	0.96	1.20	1.56
FEO(C)	23.22	21.29	21.58	22.71	20.49	20.46	16.51	20.65	22.31	23.29
MNO	8.42	8.01	6.97	6.37	9.21	8.73	13.78	8.62	7.81	6.99
CAO	6.79	11.04	10.96	10.55	10.97	11.32	9.86	10.98	10.40	9.05
NA2O	0.05	0.00	0.03	0.03	0.03	0.02	0.00	0.00	0.00	0.00
K2O	0.03	0.02	0.03	0.02	0.02	0.02	0.03	0.03	0.02	0.03
SUM	100.53	102.13	100.76	101.04	102.24	102.33	101.53	102.32	102.13	101.50
SI	2.98	3.04	3.03	3.01	3.02	3.05	2.93	2.93	2.90	2.95
AL(IV)	0.02	0.00	0.00	0.00	0.00	0.00	0.07	0.07	0.10	0.05
AL(VI)	2.07	1.98	2.02	2.03	2.00	1.98	2.05	2.05	2.01	2.06
CR	0.00	0.00	0.00	0.00	0.00	0.00	0.00	0.00	0.00	0.00
TI	0.01	0.01	0.00	0.01	0.01	0.01	0.01	0.01	0.01	0.01
FE+3	0.00	0.00	0.00	0.00	0.00	0.00	0.00	0.00	0.00	0.00
MG	0.22	0.12	0.12	0.13	0.10	0.09	0.11	0.11	0.14	0.18
FE+2	1.54	1.39	1.43	1.50	1.34	1.33	1.08	1.34	1.45	1.53
MN	0.57	0.53	0.47	0.43	0.61	0.58	0.92	0.57	0.52	0.46
CA	0.58	0.92	0.93	0.89	0.92	0.95	0.83	0.91	0.87	0.76
NA	0.01	0.00	0.00	0.00	0.00	0.00	0.00	0.00	0.00	0.00
K	0.00	0.00	0.00	0.00	0.00	0.00	0.00	0.00	0.00	0.00
O	12.03	12.04	12.04	12.03	12.03	12.05	12.00	12.00	11.97	12.01
%PYR	7.66	4.05	4.00	4.58	3.21	3.03	3.59	3.81	4.81	6.22
%ALM	53.01	46.91	48.54	50.78	45.21	45.28	36.84	45.55	47.53	52.05
%SPS	19.48	17.88	15.88	14.42	20.58	19.58	31.27	19.40	17.76	15.81
%UVA	0.26	0.20	0.18	0.19	0.06	0.25	0.15	0.15	0.08	0.12
%GRS	19.58	30.76	31.41	30.04	30.94	31.84	28.16	31.08	29.82	25.79
%ANR	0.00	0.20	0.00	0.00	0.00	0.02	0.00	0.00	0.00	0.00
FE/FE+MG	0.87	0.92	0.92	0.92	0.93	0.94	0.91	0.92	0.91	0.89
A	41.86	40.17	40.71	40.80	40.35	40.25	41.92	42.00	41.46	41.77
C	11.54	18.64	18.73	17.89	18.49	19.19	16.42	18.06	17.07	15.09
F	46.60	41.19	40.57	41.31	41.15	40.56	41.66	39.94	41.48	43.14
A"	0.37	0.39	0.39	0.38	0.41	0.41	0.47	0.42	0.40	0.38
F"	0.55	0.56	0.56	0.57	0.55	0.55	0.48	0.53	0.55	0.55
M"	0.08	0.05	0.05	0.05	0.04	0.04	0.05	0.04	0.05	0.07

GARNET

SAMPLE NO.	B2-3A	B2-3A	B2-3A	B2-3A	B2-3A	B2-3A	B2-3A	B2-35A	B2-35A	B2-35A
ANALYSIS	10G	11G	13G	24G	25G	32G	33G	04G	16G	15G
CORE/RIM	C	C	R	C	R	C	R	C	C	R
SIO2	38.12	38.06	38.55	38.49	38.51	37.83	38.02	37.98	38.15	38.28
AL2O3	21.35	21.35	21.18	21.83	22.10	21.23	21.54	21.37	21.39	21.39
CR2O3	0.05	0.08	0.03	0.03	0.04	0.04	0.04	0.06	0.00	0.00
TIO2	0.19	0.19	0.05	0.16	0.06	0.18	0.10	0.10	0.11	0.16
FE2O3(C)	0.00	0.00	0.15	0.00	0.00	0.04	0.00	0.00	0.00	0.06
MGO	1.02	1.03	1.18	0.97	1.40	0.60	1.15	0.79	0.75	0.85
FEO(C)	23.57	23.41	24.87	26.23	27.84	21.25	26.00	23.39	23.27	25.41
MNO	6.90	7.37	5.02	4.25	2.47	9.22	4.52	6.60	6.46	4.61
CAO	9.54	9.42	8.85	9.80	9.15	10.56	9.44	10.71	10.71	10.62
NA2O	0.07	0.02	0.27	0.01	0.03	0.01	0.02	0.02	0.03	0.00
K2O	0.02	0.02	0.04	0.02	0.04	0.02	0.03	0.02	0.02	0.03
SUM	100.84	100.96	100.20	101.79	101.64	100.97	100.85	101.05	100.90	101.42
SI	3.02	3.02	3.07	3.02	3.02	3.00	3.01	3.00	3.02	3.02
AL(IV)	0.00	0.00	0.00	0.00	0.00	0.00	0.00	0.00	0.00	0.00
AL(VI)	1.99	1.99	1.99	2.02	2.04	1.98	2.01	1.99	1.99	1.99
CR	0.00	0.00	0.00	0.00	0.00	0.00	0.00	0.00	0.00	0.00
TI	0.01	0.01	0.00	0.01	0.00	0.01	0.01	0.01	0.01	0.01
FE+3	0.00	0.00	0.01	0.00	0.00	0.00	0.00	0.00	0.00	0.00
MG	0.12	0.12	0.14	0.11	0.16	0.07	0.14	0.09	0.09	0.10
FE+2	1.56	1.55	1.65	1.72	1.83	1.41	1.72	1.55	1.54	1.68
MN	0.46	0.49	0.34	0.28	0.16	0.62	0.30	0.44	0.43	0.31
CA	0.81	0.80	0.75	0.82	0.77	0.90	0.80	0.91	0.91	0.90
NA	0.01	0.00	0.04	0.00	0.00	0.00	0.00	0.00	0.00	0.00
K	0.00	0.00	0.00	0.00	0.00	0.00	0.00	0.00	0.00	0.00
O	12.02	12.02	12.05	12.04	12.04	12.00	12.02	12.01	12.02	12.02
%PYR	4.10	4.12	4.85	3.87	5.59	2.36	4.59	3.11	3.00	3.37
%ALM	52.84	52.27	57.32	58.52	62.49	46.81	58.14	51.75	51.85	56.21
%SPS	15.67	16.66	11.73	9.60	5.61	20.76	10.23	14.79	14.58	10.33
%UVA	0.16	0.25	0.10	0.10	0.14	0.13	0.14	0.20	0.00	0.00
%GRS	27.23	26.70	25.56	27.90	26.16	29.82	26.90	30.15	30.58	29.91
%ANR	0.00	0.00	0.46	0.00	0.00	0.11	0.00	0.00	0.00	0.18
FE/FE+MG	0.93	0.93	0.92	0.94	0.92	0.95	0.93	0.94	0.94	0.94
A	40.27	40.19	40.86	40.70	41.15	39.87	40.44	39.99	40.17	40.05
C	16.36	16.12	15.44	16.61	15.48	18.01	16.10	18.21	18.29	18.04
F	43.36	43.69	43.70	42.70	43.38	42.13	43.46	41.80	41.54	41.91
A"	0.37	0.37	0.35	0.35	0.34	0.40	0.35	0.38	0.38	0.36
F"	0.58	0.58	0.60	0.61	0.61	0.57	0.60	0.59	0.59	0.61
M"	0.05	0.05	0.05	0.04	0.05	0.03	0.05	0.04	0.03	0.04

GARNET

SAMPLE NO.	B2-35A	B2-35A	B2-35A	B2-35A	B2-35B	B2-35B	B2-35B	B2-35B	B3-25B	B3-25B
ANALYSIS	14G	13G	17G	20G	11S	12S	16S	17S	16C	17C
CORE/RIM	C	R	C	R	C	R	C	R	C	C
SIO2	38.38	38.68	38.26	38.07	37.38	37.46	37.33	37.83	37.26	37.02
AL2O3	21.34	21.61	21.42	22.00	23.11	23.19	23.12	23.07	22.90	22.44
CR2O3	0.07	0.07	0.01	0.04	0.08	0.05	0.03	0.09	0.04	0.06
TIO2	0.20	0.07	0.12	0.09	0.19	0.15	0.12	0.15	0.18	0.13
FE2O3(C)	0.13	0.00	0.00	0.00	0.00	0.00	0.00	0.00	0.00	0.00
MGO	0.58	0.96	0.44	1.19	0.45	0.74	0.58	1.06	0.98	0.98
FEO(C)	21.58	25.35	18.58	27.14	17.12	21.97	21.37	24.84	21.90	22.00
MNO	8.56	4.45	11.12	2.98	13.52	7.63	8.60	5.24	11.54	11.77
CAO	10.96	10.71	11.26	9.71	10.79	10.97	10.91	10.01	6.63	6.57
NA2O	0.03	0.01	0.00	0.00	0.01	0.02	0.00	0.03	0.06	0.10
K2O	0.02	0.02	0.02	0.02	0.02	0.04	0.03	0.04	0.03	0.02
SUM	101.86	101.91	101.24	101.24	102.68	102.22	102.10	102.35	101.51	101.08
SI	3.02	3.03	3.02	3.00	2.91	2.92	2.91	2.94	2.94	2.94
AL(IV)	0.00	0.00	0.00	0.00	0.09	0.08	0.08	0.06	0.05	0.06
AL(VI)	1.98	1.99	1.99	2.04	2.02	2.05	2.04	2.06	2.08	2.04
CR	0.00	0.00	0.00	0.00	0.00	0.00	0.00	0.00	0.00	0.00
TI	0.01	0.00	0.01	0.00	0.01	0.01	0.01	0.01	0.01	0.01
FE+3	0.01	0.00	0.00	0.00	0.00	0.00	0.00	0.00	0.00	0.00
MG	0.07	0.11	0.05	0.14	0.05	0.08	0.07	0.12	0.12	0.12
FE+2	1.42	1.66	1.23	1.79	1.11	1.43	1.40	1.62	1.45	1.46
MN	0.57	0.30	0.74	0.20	0.89	0.50	0.57	0.35	0.77	0.79
CA	0.92	0.90	0.95	0.82	0.90	0.92	0.91	0.83	0.56	0.56
NA	0.00	0.00	0.00	0.00	0.00	0.00	0.00	0.00	0.01	0.02
K	0.00	0.00	0.00	0.00	0.00	0.00	0.00	0.00	0.00	0.00
O	12.02	12.03	12.02	12.03	11.98	11.99	11.98	12.01	12.02	11.99
%PYR	2.30	3.77	1.76	4.76	1.78	2.93	2.34	4.23	3.99	3.95
%ALM	47.60	55.99	41.23	60.67	36.67	48.46	46.83	55.35	49.96	49.90
%SPS	19.13	9.95	25.00	6.75	30.63	17.25	19.52	11.82	26.67	27.04
%UVA	0.22	0.21	0.04	0.12	0.26	0.17	0.10	0.28	0.12	0.20
%GRS	30.34	30.09	31.98	27.69	30.66	31.20	31.21	28.31	19.26	18.91
%ANR	0.40	0.00	0.00	0.00	0.00	0.00	0.00	0.00	0.00	0.00
FE/FE+MG	0.95	0.94	0.96	0.93	0.96	0.94	0.95	0.93	0.93	0.93
A	39.98	40.21	40.12	40.94	41.76	42.04	41.94	42.01	42.41	41.77
C	18.58	18.11	19.17	16.43	17.72	18.07	17.99	16.58	11.16	11.13
F	41.43	41.68	40.71	42.63	40.52	39.88	40.07	41.41	46.43	47.10
A"	0.40	0.36	0.44	0.35	0.48	0.41	0.42	0.38	0.40	0.40
F"	0.57	0.60	0.54	0.61	0.50	0.56	0.55	0.58	0.55	0.56
M"	0.03	0.04	0.02	0.05	0.02	0.03	0.03	0.04	0.04	0.04

GARNET

SAMPLE NO.	B3-25B	B3-25B	B3-30A	B3-30A	B3-30A	B3-63A	B3-63A	B3-63A	B3-63A	B3-63A
ANALYSIS	14C	15C	07S	09S	17S	06G	07G	04G	05G	08G
CORE/RIM	R	R	C	R	R	C	C	R	R	
SIO2	36.82	37.14	38.22	36.82	37.53	38.11	37.89	38.34	38.43	37.98
AL2O3	22.64	22.84	22.34	22.59	23.18	21.45	21.70	21.71	21.51	21.42
CR2O3	0.04	0.01	0.02	0.05	0.04	0.06	0.06	0.04	0.02	0.05
TIO2	0.00	0.05	0.21	0.17	0.16	0.25	0.21	0.12	0.08	0.22
FE2O3(C)	0.00	0.00	0.00	0.00	0.00	0.00	0.00	0.00	0.00	0.00
MGO	2.02	1.96	0.61	0.92	1.26	0.85	0.83	1.07	1.10	1.38
FEO(C)	32.90	32.66	25.19	29.23	30.40	26.30	26.40	29.38	29.70	29.19
MNO	4.81	5.19	6.28	2.07	0.42	4.17	4.36	1.62	1.75	1.52
CAO	2.01	2.15	9.24	9.49	9.15	10.12	9.76	9.49	9.21	9.20
NA2O	0.02	0.03	0.06	0.05	0.00	0.00	0.01	0.00	0.00	0.05
K2O	0.03	0.02	0.02	0.02	0.03	0.02	0.03	0.02	0.02	0.02
SUM	101.30	102.05	102.19	101.40	102.17	101.32	101.26	101.79	101.81	101.04
SI	2.94	2.94	2.99	2.90	2.93	3.01	2.99	3.01	3.02	3.00
AL(IV)	0.06	0.06	0.00	0.10	0.07	0.00	0.00	0.00	0.00	0.00
AL(VI)	2.06	2.07	2.06	2.00	2.06	2.00	2.02	2.01	1.99	2.00
CR	0.00	0.00	0.00	0.00	0.00	0.00	0.00	0.00	0.00	0.00
TI	0.00	0.00	0.01	0.01	0.01	0.02	0.01	0.01	0.00	0.01
FE+3	0.00	0.00	0.00	0.00	0.00	0.00	0.00	0.00	0.00	0.00
MG	0.24	0.23	0.07	0.11	0.15	0.10	0.10	0.13	0.13	0.16
FE+2	2.19	2.16	1.65	1.93	1.98	1.74	1.74	1.93	1.95	1.93
MN	0.32	0.35	0.42	0.14	0.03	0.28	0.29	0.11	0.12	0.10
CA	0.17	0.18	0.78	0.80	0.76	0.86	0.83	0.80	0.78	0.78
NA	0.00	0.00	0.01	0.01	0.00	0.00	0.00	0.00	0.00	0.01
K	0.00	0.00	0.00	0.00	0.00	0.00	0.00	0.00	0.00	0.00
O	12.00	12.00	12.03	11.96	12.01	12.02	12.02	12.03	12.02	12.01
%PYR	8.19	7.93	2.45	3.73	5.01	3.36	3.31	4.24	4.32	5.48
%ALM	74.85	73.94	56.64	63.87	67.87	58.45	58.92	65.16	65.68	64.90
%SPS	11.09	11.90	14.29	4.77	0.95	9.38	9.85	3.64	3.91	3.42
%UVA	0.13	0.04	0.08	0.14	0.14	0.19	0.20	0.13	0.05	0.17
%GRS	5.74	6.20	26.53	27.48	26.03	28.61	27.71	26.82	26.03	26.02
%ANR	0.00	0.00	0.00	0.00	0.00	0.00	0.00	0.00	0.01	0.00
FE/FE+MG	0.90	0.90	0.96	0.95	0.93	0.95	0.95	0.94	0.94	0.92
A	42.06	42.15	41.45	41.36	42.17	40.18	40.56	40.42	40.14	40.16
C	3.40	3.61	15.58	15.80	15.13	17.23	16.59	16.06	15.62	15.68
F	54.54	54.24	42.97	42.84	42.69	42.58	42.85	43.52	44.24	44.17
A"	0.30	0.31	0.37	0.34	0.33	0.35	0.35	0.33	0.32	0.32
F"	0.63	0.63	0.60	0.63	0.62	0.61	0.61	0.63	0.63	0.63
M"	0.07	0.07	0.03	0.04	0.05	0.04	0.03	0.04	0.04	0.05

GARNET

SAMPLE NO.	B3-63A	B3-63A	B3-63A	B3-117B	B3-117B	B3-117B	B3-156A	B3-156A	B3-156A	B3-156A
ANALYSIS	09G	15G	17G	QMIN	10S	14S	01C	03C	05C	06C
CORE/RIM		C	R	C	C	R	C	C	C	R
SIO2	38.06	38.45	38.06	36.96	36.94	36.88	37.82	37.79	37.74	37.83
AL2O3	21.25	21.31	22.02	20.90	20.12	20.73	21.23	20.92	21.32	21.38
CR2O3	0.06	0.04	0.07	0.00	0.11	0.09	0.05	0.10	0.08	0.05
TIO2	0.09	0.21	0.14	0.30	0.14	0.17	0.18	0.19	0.23	0.15
FE2O3(C)	0.16	0.05	0.00	1.32	1.26	0.92	0.00	0.14	0.00	0.00
MGO	1.42	0.81	1.12	0.47	0.53	0.84	0.78	0.79	0.75	0.79
FEO(C)	29.24	26.70	28.13	19.20	18.90	24.15	20.17	20.08	20.19	21.32
MNO	1.55	4.75	2.63	13.47	13.71	7.94	12.36	12.77	12.82	12.04
CAO	9.18	9.33	9.46	8.54	7.99	8.29	7.73	7.75	7.83	7.30
NA2O	0.01	0.00	0.04	0.09	0.04	0.02	0.01	0.02	0.04	0.04
K2O	0.03	0.02	0.02	0.16	0.18	0.18	0.02	0.02	0.02	0.02
SUM	101.05	101.66	101.67	101.40	99.93	100.22	100.34	100.57	101.02	100.92
SI	3.01	3.03	2.99	2.94	2.99	2.97	3.03	3.02	3.01	3.02
AL(IV)	0.00	0.00	0.01	0.06	0.01	0.04	0.00	0.00	0.00	0.00
AL(VI)	1.98	1.98	2.03	1.90	1.91	1.93	2.01	1.97	2.00	2.01
CR	0.00	0.00	0.00	0.00	0.01	0.01	0.00	0.01	0.00	0.00
TI	0.00	0.01	0.01	0.02	0.01	0.01	0.01	0.01	0.01	0.01
FE+3	0.01	0.00	0.00	0.08	0.08	0.06	0.00	0.01	0.00	0.00
MG	0.17	0.10	0.13	0.05	0.06	0.10	0.09	0.09	0.09	0.09
FE+2	1.94	1.76	1.85	1.28	1.28	1.62	1.35	1.34	1.35	1.42
MN	0.10	0.32	0.18	0.91	0.94	0.54	0.84	0.87	0.87	0.81
CA	0.78	0.79	0.80	0.73	0.69	0.71	0.66	0.67	0.67	0.62
NA	0.00	0.00	0.00	0.01	0.01	0.00	0.00	0.00	0.01	0.01
K	0.00	0.00	0.00	0.02	0.02	0.02	0.00	0.00	0.00	0.00
O	12.01	12.04	12.02	11.97	11.99	11.98	12.04	12.03	12.02	12.03
%PYR	5.62	3.20	4.45	1.88	2.16	3.40	3.15	3.18	2.99	3.17
%ALM	64.82	59.46	62.63	42.48	42.99	54.29	45.87	45.27	45.33	48.16
%SPS	3.47	10.72	5.93	30.87	31.57	18.23	28.46	29.16	29.16	27.54
%UVA	0.19	0.13	0.21	0.00	0.36	0.28	0.15	0.33	0.25	0.17
%GRS	25.40	26.36	26.78	20.72	19.04	20.99	22.37	21.64	22.26	20.95
%ANR	0.49	0.13	0.00	4.05	3.88	2.81	0.00	0.42	0.00	0.00
FE/FE+MG	0.92	0.95	0.93	0.96	0.95	0.94	0.94	0.94	0.94	0.94
A	40.02	40.11	40.87	40.72	40.15	40.41	40.48	40.03	40.29	40.50
C	15.65	15.95	15.96	14.54	13.93	14.28	13.41	13.43	13.45	12.57
F	44.34	43.94	43.17	44.74	45.93	45.31	46.11	46.54	46.27	46.93
A"	0.32	0.35	0.34	0.40	0.40	0.35	0.41	0.40	0.41	0.40
F"	0.63	0.62	0.62	0.57	0.58	0.61	0.55	0.56	0.55	0.56
M"	0.05	0.03	0.04	0.02	0.03	0.04	0.04	0.04	0.04	0.04

GARNET

SAMPLE NO.	B3-156A	B3-156A	B3-156A	B3156AA	B3156AA	B3156AA	B3156AA	B3156AA	B3156AA	B3-170A
ANALYSIS	08C	28C	30C	03S	09S	12S	16S	37S	36S	17A
CORE/RIM	R	C	R	C	C	R	R	C	R	R
SIO2	37.65	38.36	38.39	37.92	38.21	38.36	38.34	38.11	37.52	38.28
AL2O3	21.27	21.68	21.58	21.74	22.23	21.55	21.39	21.39	21.49	22.89
CR2O3	0.08	0.07	0.02	0.03	0.04	0.02	0.04	0.04	0.04	0.08
TIO2	0.15	0.16	0.16	0.20	0.11	0.14	0.09	0.15	0.17	0.08
FE2O3(C)	0.00	0.00	0.00	0.00	0.00	0.00	0.02	0.00	0.00	0.00
MGO	0.85	0.82	0.98	0.55	1.48	1.49	1.49	1.21	1.72	2.56
FEO(C)	21.98	20.96	22.85	22.27	28.25	28.65	28.94	27.53	28.61	10.16
MNO	11.12	13.29	10.08	9.84	4.32	3.12	3.90	4.07	5.63	20.38
CAO	7.34	7.31	7.55	8.65	7.38	8.33	7.29	8.53	5.94	8.31
NA2O	0.05	0.04	0.04	0.00	0.05	0.03	0.01	0.03	0.03	0.02
K2O	0.02	0.02	0.02	0.02	0.03	0.03	0.05	0.02	0.06	0.03
SUM	100.50	102.71	101.66	101.22	102.09	101.72	101.56	101.07	101.21	102.79
SI	3.01	3.01	3.03	3.01	2.99	3.02	3.03	3.02	2.98	2.95
AL(IV)	0.00	0.00	0.00	0.00	0.00	0.00	0.00	0.00	0.02	0.05
AL(VI)	2.01	2.00	2.01	2.03	2.05	2.00	1.99	2.00	1.99	2.02
CR	0.00	0.00	0.00	0.00	0.00	0.00	0.00	0.00	0.00	0.00
TI	0.01	0.01	0.01	0.01	0.01	0.01	0.00	0.01	0.01	0.00
FE+3	0.00	0.00	0.00	0.00	0.00	0.00	0.00	0.00	0.00	0.00
MG	0.10	0.10	0.12	0.06	0.17	0.17	0.18	0.14	0.20	0.29
FE+2	1.47	1.37	1.51	1.48	1.85	1.89	1.91	1.82	1.90	0.65
MN	0.75	0.88	0.68	0.66	0.29	0.21	0.26	0.27	0.38	1.33
CA	0.63	0.61	0.64	0.74	0.62	0.70	0.62	0.72	0.50	0.69
NA	0.01	0.01	0.01	0.00	0.01	0.00	0.00	0.00	0.00	0.00
K	0.00	0.00	0.00	0.00	0.00	0.00	0.00	0.00	0.01	0.00
O	12.02	12.02	12.04	12.04	12.02	12.02	12.03	12.02	11.99	11.99
%PYR	3.45	3.25	3.92	2.21	5.89	5.88	5.90	4.82	6.83	9.98
%ALM	49.77	46.32	51.38	50.28	63.19	63.48	64.47	61.54	63.50	21.69
%SPS	25.49	29.74	22.96	22.49	9.78	7.00	8.81	9.20	12.70	45.08
%UVA	0.24	0.22	0.06	0.09	0.13	0.07	0.13	0.11	0.12	0.25
%GRS	21.04	20.48	21.68	24.93	21.01	23.58	20.63	24.32	16.85	23.00
%ANR	0.00	0.00	0.00	0.00	0.00	0.00	0.06	0.00	0.00	0.00
FE/FE+MG	0.94	0.94	0.93	0.96	0.92	0.92	0.92	0.93	0.90	0.69
A	40.44	40.30	40.61	40.88	41.20	40.22	40.19	40.25	40.24	41.22
C	12.68	12.35	12.91	14.79	12.43	14.14	12.45	14.60	10.11	13.60
F	46.88	47.35	46.48	44.33	46.37	45.64	47.36	45.15	49.65	45.18
A"	0.39	0.40	0.38	0.40	0.34	0.33	0.32	0.34	0.32	0.52
F"	0.57	0.56	0.57	0.58	0.61	0.62	0.62	0.62	0.61	0.33
M"	0.04	0.04	0.04	0.02	0.06	0.06	0.06	0.05	0.07	0.15

GARNET

SAMPLE NO.	B3-170A	B3-170A	B3-175A	B3-175A	B3-175A	B3-175A	B3-175A	B3-175A	B3-185A	B3-185A
ANALYSIS	18A	25A	49S	10S	50S	51S	52S	53S	20G	21G
CORE/RIM	R	C	C	R	R	C	C	C	C	R
SIO2	38.10	38.40	36.77	37.45	37.36	37.52	37.32	37.26	38.49	38.55
AL2O3	22.97	23.10	21.89	21.62	21.61	22.09	21.90	21.86	21.15	21.31
CR2O3	0.07	0.05	0.10	0.10	0.08	0.09	0.08	0.07	0.04	0.02
TIO2	0.12	0.13	0.18	0.17	0.10	0.17	0.12	0.04	0.24	0.06
FE2O3(C)	0.00	0.00	0.00	0.00	0.00	0.00	0.00	0.00	0.46	0.45
MGO	2.31	2.41	0.84	1.12	1.21	0.99	1.08	1.92	1.12	1.42
FEO(C)	10.95	9.09	24.10	27.50	26.55	27.07	27.23	28.16	20.70	26.46
MNO	19.60	20.03	9.04	6.23	6.32	5.74	5.69	6.55	9.94	3.82
CAO	8.38	9.07	7.24	6.73	7.07	7.39	7.38	4.66	9.79	9.72
NA2O	0.05	0.03	0.00	0.02	0.02	0.04	0.01	0.05	0.02	0.02
K2O	0.02	0.02	0.11	0.12	0.10	0.10	0.10	0.11	0.02	0.04
SUM	102.59	102.33	100.27	101.04	100.43	101.20	100.91	100.68	101.96	101.87
SI	2.94	2.96	2.95	2.98	2.99	2.98	2.97	2.97	3.02	3.02
AL(IV)	0.06	0.04	0.05	0.02	0.01	0.02	0.03	0.03	0.00	0.00
AL(VI)	2.03	2.06	2.02	2.01	2.02	2.04	2.02	2.03	1.96	1.97
CR	0.00	0.00	0.01	0.01	0.00	0.01	0.00	0.00	0.00	0.00
TI	0.01	0.01	0.01	0.01	0.01	0.01	0.01	0.00	0.01	0.00
FE+3	0.00	0.00	0.00	0.00	0.00	0.00	0.00	0.00	0.03	0.03
MG	0.27	0.28	0.10	0.13	0.14	0.12	0.13	0.23	0.13	0.17
FE+2	0.71	0.59	1.62	1.83	1.77	1.80	1.81	1.88	1.36	1.73
MN	1.28	1.31	0.61	0.42	0.43	0.39	0.38	0.44	0.66	0.25
CA	0.69	0.75	0.62	0.57	0.61	0.63	0.63	0.40	0.82	0.82
NA	0.01	0.00	0.00	0.00	0.00	0.00	0.00	0.01	0.00	0.00
K	0.00	0.00	0.01	0.01	0.01	0.01	0.01	0.01	0.00	0.00
O	11.99	12.02	11.99	12.00	12.01	12.01	12.00	11.99	12.03	12.02
%PYR	9.05	9.47	3.40	4.48	4.88	4.00	4.34	7.74	4.40	5.59
%ALM	23.81	20.06	54.67	61.91	60.12	61.35	61.38	63.73	45.70	58.38
%SPS	43.58	44.80	20.82	14.21	14.49	13.19	12.98	15.01	22.22	8.54
%UVA	0.23	0.15	0.32	0.30	0.27	0.30	0.27	0.23	0.13	0.07
%GRS	23.34	25.52	20.79	19.10	20.24	21.17	21.03	13.30	26.18	26.09
%ANR	0.00	0.00	0.00	0.00	0.00	0.00	0.00	0.00	1.38	1.33
FE/FE+MG	0.73	0.68	0.94	0.93	0.93	0.94	0.93	0.89	0.91	0.91
A	41.48	41.82	41.21	40.68	40.81	41.36	41.02	41.08	40.01	40.18
C	13.76	14.94	12.40	11.51	12.14	12.59	12.56	7.97	16.61	16.45
F	44.76	43.25	46.40	47.81	47.05	46.05	46.42	50.95	43.38	43.37
A"	0.52	0.55	0.37	0.34	0.34	0.35	0.34	0.32	0.39	0.34
F"	0.35	0.31	0.59	0.62	0.61	0.61	0.61	0.60	0.56	0.61
M"	0.13	0.14	0.04	0.05	0.05	0.04	0.04	0.07	0.05	0.06

GARNET

SAMPLE NO.	B3-261A	B3-261A	B3-261A	B3-261A	B3-261A	B3-261A	B3-261A	B3-261A	B4-1D	B4-1D
ANALYSIS	09S	10S	11S	12S	25S	26S	23S	24S	04G	05G
CORE/RIM	C	C	R	R	C	C	R	R	C	R
SIO2	37.07	37.31	37.50	37.01	38.09	38.13	38.12	38.10	37.71	37.75
AL2O3	22.08	22.24	22.29	22.29	21.43	21.43	21.32	21.11	22.05	22.41
CR2O3	0.05	0.09	0.11	0.11	0.11	0.09	0.15	0.09	0.01	0.10
TIO2	0.17	0.16	0.11	0.13	0.24	0.10	0.14	0.50	0.18	0.20
FE2O3(C)	0.00	0.00	0.00	0.00	0.03	0.33	0.23	0.17	0.00	0.00
MGO	1.65	1.63	1.88	1.88	1.90	1.92	1.83	1.76	1.65	1.77
FEO(C)	17.28	17.24	17.79	17.74	17.96	17.76	18.16	18.36	9.76	10.40
MNO	15.40	15.40	13.71	14.35	14.72	14.95	14.40	13.92	23.66	22.85
CAO	7.09	7.10	7.30	7.33	7.07	7.10	7.31	7.52	6.73	6.86
NA2O	0.05	0.04	0.03	0.04	0.07	0.06	0.03	0.07	0.00	0.04
K2O	0.14	0.14	0.15	0.14	0.13	0.12	0.14	0.13	0.02	0.02
SUM	100.99	101.36	100.87	101.02	101.74	102.00	101.82	101.75	101.78	102.41
SI	2.93	2.94	2.96	2.92	2.99	2.99	2.99	3.00	2.97	2.94
AL(IV)	0.07	0.06	0.04	0.08	0.01	0.01	0.00	0.00	0.04	0.05
AL(VI)	1.99	2.01	2.04	1.99	1.98	1.97	1.97	1.95	2.01	2.01
CR	0.00	0.01	0.01	0.01	0.01	0.01	0.01	0.00	0.00	0.01
TI	0.01	0.01	0.01	0.01	0.01	0.01	0.01	0.03	0.01	0.01
FE+3	0.00	0.00	0.00	0.00	0.00	0.02	0.01	0.01	0.00	0.00
MG	0.19	0.19	0.22	0.22	0.22	0.22	0.21	0.21	0.19	0.21
FE+2	1.14	1.14	1.18	1.17	1.18	1.16	1.19	1.21	0.64	0.68
MN	1.03	1.03	0.92	0.96	0.98	0.99	0.96	0.93	1.58	1.51
CA	0.60	0.60	0.62	0.62	0.60	0.60	0.62	0.63	0.57	0.57
NA	0.01	0.01	0.00	0.01	0.01	0.01	0.00	0.01	0.00	0.01
K	0.01	0.01	0.02	0.01	0.01	0.01	0.01	0.01	0.00	0.00
O	11.96	11.98	12.00	11.96	11.99	11.99	11.99	12.00	12.00	11.99
%PYR	6.64	6.51	7.55	7.59	7.48	7.52	7.20	6.98	6.53	7.00
%ALM	37.67	38.10	40.08	38.34	39.64	39.11	40.01	40.27	21.21	22.26
%SPS	35.19	34.98	31.29	32.84	32.89	33.35	32.14	31.34	53.15	51.27
%UVA	0.16	0.30	0.36	0.34	0.33	0.28	0.46	0.28	0.04	0.31
%GRS	20.34	20.11	20.73	20.89	19.56	18.77	19.53	20.61	19.07	19.15
%ANR	0.00	0.00	0.00	0.00	0.09	0.97	0.67	0.52	0.00	0.00
FE/FE+MG	0.85	0.86	0.84	0.84	0.84	0.84	0.85	0.86	0.77	0.77
A	40.93	41.14	41.45	41.10	40.02	40.16	40.00	39.80	40.70	40.98
C	11.95	11.95	12.35	12.29	11.99	11.98	12.39	12.82	11.29	11.40
F	47.12	46.92	46.20	46.61	47.99	47.86	47.61	47.38	48.02	47.62
A"	0.43	0.43	0.42	0.42	0.41	0.41	0.40	0.40	0.55	0.54
F"	0.49	0.49	0.49	0.49	0.50	0.50	0.50	0.51	0.35	0.36
M"	0.08	0.08	0.09	0.09	0.09	0.09	0.09	0.09	0.10	0.11

GARNET

SAMPLE NO.	B4-1D	B4-1D	B4-1D	B4-8B	B4-8B	B4-11K	B4-11K	B4-11K	B4-11K	B4-11K
ANALYSIS	23G	22G	30G	12A	15A	490	340	350	370	610
CORE/RIM	C	R		C	R	C	C	R	R	C
SIO2	38.04	37.86	38.36	37.38	37.95	37.63	38.61	37.91	37.52	37.43
AL2O3	22.38	22.23	22.52	21.01	20.71	22.65	20.94	20.89	20.83	22.57
CR2O3	0.01	0.04	0.04	0.07	0.05	0.03	0.03	0.06	0.11	0.05
TIO2	0.20	0.13	0.39	0.02	0.05	0.19	0.11	0.11	0.12	0.16
FE2O3(C)	0.00	0.00	0.00	0.89	0.93	0.00	1.01	0.98	1.06	0.00
MGO	1.74	2.01	1.68	1.38	1.47	1.62	1.65	2.27	2.22	1.49
FEO(C)	9.81	11.47	9.71	21.78	21.64	19.50	20.19	15.46	15.59	22.08
MNO	23.43	22.26	22.79	8.82	5.09	10.55	11.10	14.61	14.40	9.47
CAO	7.19	6.06	7.11	9.26	12.04	9.64	8.61	8.62	8.61	8.76
NA2O	0.05	0.10	0.03	0.00	0.01	0.05	0.02	0.02	0.00	0.03
K2O	0.02	0.02	0.02	0.05	0.04	0.02	0.03	0.06	0.04	0.02
SUM	102.86	102.19	102.65	100.67	99.97	101.86	102.29	101.00	100.51	102.08
SI	2.95	2.96	2.98	2.97	3.01	2.93	3.02	2.99	2.98	2.93
AL(IV)	0.05	0.04	0.02	0.03	0.00	0.07	0.00	0.01	0.02	0.07
AL(VI)	2.00	2.01	2.05	1.94	1.94	2.02	1.93	1.93	1.92	2.00
CR	0.00	0.00	0.00	0.00	0.00	0.00	0.00	0.00	0.01	0.00
TI	0.01	0.01	0.02	0.00	0.00	0.01	0.01	0.01	0.01	0.01
FE+3	0.00	0.00	0.00	0.05	0.06	0.00	0.06	0.06	0.06	0.00
MG	0.20	0.23	0.19	0.16	0.17	0.19	0.19	0.27	0.26	0.17
FE+2	0.64	0.75	0.63	1.45	1.44	1.27	1.32	1.02	1.03	1.44
MN	1.54	1.47	1.50	0.59	0.34	0.70	0.74	0.98	0.97	0.63
CA	0.60	0.51	0.59	0.79	1.02	0.81	0.72	0.73	0.73	0.73
NA	0.01	0.02	0.00	0.00	0.00	0.01	0.00	0.00	0.00	0.00
K	0.00	0.00	0.00	0.00	0.00	0.00	0.00	0.01	0.00	0.00
O	11.98	11.98	12.04	11.98	12.01	11.98	12.02	11.99	11.99	11.97
%PYR	6.81	7.92	6.67	5.50	5.85	6.41	6.49	8.91	8.82	5.95
%ALM	20.78	25.13	21.63	47.97	48.25	42.40	44.46	34.07	34.08	47.54
%SPS	52.17	49.81	51.41	19.99	11.50	23.74	24.76	32.65	32.52	21.43
%UVA	0.02	0.11	0.12	0.22	0.14	0.10	0.10	0.19	0.33	0.17
%GRS	20.22	17.03	20.18	23.64	31.46	27.35	21.20	21.25	21.05	24.90
%ANR	0.00	0.00	0.00	2.68	2.80	0.00	2.99	2.92	3.20	0.00
FE/FE+MG	0.76	0.76	0.76	0.90	0.89	0.87	0.88	0.80	0.81	0.89
A	40.76	40.85	41.41	40.31	40.10	41.27	40.12	40.07	40.16	41.11
C	11.90	10.12	11.89	15.72	20.61	15.97	14.55	14.60	14.61	14.51
F	47.35	49.03	46.70	43.97	39.30	42.76	45.34	45.33	45.23	44.38
A"	0.55	0.51	0.56	0.37	0.37	0.42	0.38	0.42	0.42	0.39
F"	0.34	0.37	0.34	0.57	0.57	0.51	0.55	0.47	0.47	0.54
M"	0.11	0.12	0.11	0.06	0.07	0.07	0.08	0.12	0.11	0.07

GARNET

SAMPLE NO.	B4-11K	B4-11K	B4-11L	B4-11L	B4-11L	B4-32A	B4-32A	B4-32A	B4-93A	B4-93A
ANALYSIS	740	750	02S	04S	05S	60S	62S	63S	28GQM	29GQM
CORE/RIM	C	R	C	R	R					
SIO2	37.63	37.85	37.16	36.96	37.54	37.28	37.55	37.52	37.97	37.01
AL2O3	22.43	22.80	21.22	21.19	21.53	21.94	22.34	22.13	20.38	20.33
CR2O3	0.05	0.05	0.04	0.06	0.03	0.09	0.05	0.09	0.00	0.00
TIO2	0.30	0.13	0.11	0.13	0.11	0.20	0.25	0.24	0.13	0.13
FE2O3(C)	0.00	0.00	0.00	0.20	0.00	0.00	0.00	0.00	1.31	1.21
MGO	1.30	1.86	0.48	1.34	1.41	1.34	1.44	1.48	2.06	1.99
FEO(C)	21.98	20.94	17.52	26.07	26.76	23.36	24.66	24.45	29.08	29.14
MNO	8.97	8.89	15.50	6.52	5.84	7.03	6.55	6.72	4.05	4.11
CAO	9.04	9.61	8.15	7.40	7.37	8.28	8.04	7.94	6.03	5.86
NA2O	0.02	0.02	0.02	0.02	0.03	0.01	0.02	0.01	0.01	0.02
K2O	0.03	0.04	0.02	0.04	0.04	0.13	0.11	0.11	0.03	0.03
SUM	101.75	102.20	100.23	99.94	100.65	99.65	101.00	100.70	101.05	99.84
SI	2.95	2.94	2.98	2.97	2.99	2.99	2.97	2.98	3.02	2.99
AL(IV)	0.05	0.06	0.02	0.03	0.01	0.01	0.03	0.02	0.00	0.01
AL(VI)	2.02	2.02	1.99	1.98	2.01	2.06	2.05	2.04	1.91	1.92
CR	0.00	0.00	0.00	0.00	0.00	0.01	0.00	0.01	0.00	0.00
TI	0.02	0.01	0.01	0.01	0.01	0.01	0.02	0.01	0.01	0.01
FE+3	0.00	0.00	0.00	0.01	0.00	0.00	0.00	0.00	0.08	0.07
MG	0.15	0.22	0.06	0.16	0.17	0.16	0.17	0.18	0.24	0.24
FE+2	1.44	1.36	1.18	1.75	1.78	1.56	1.63	1.62	1.94	1.97
MN	0.60	0.58	1.06	0.44	0.39	0.48	0.44	0.45	0.27	0.28
CA	0.76	0.80	0.70	0.64	0.63	0.71	0.68	0.68	0.51	0.51
NA	0.00	0.00	0.00	0.00	0.00	0.00	0.00	0.00	0.00	0.00
K	0.00	0.00	0.00	0.00	0.00	0.01	0.01	0.01	0.00	0.00
O	12.00	11.99	11.99	11.98	12.00	12.03	12.02	12.02	12.03	11.99
%PYR	5.17	7.34	1.93	5.40	5.63	5.48	5.79	6.01	8.23	8.03
%ALM	48.88	45.55	39.25	58.19	59.96	53.74	55.87	55.46	65.23	65.59
%SPS	20.20	19.90	35.33	14.95	13.26	16.38	15.02	15.44	9.21	9.40
%UVA	0.17	0.16	0.14	0.19	0.10	0.30	0.16	0.29	0.00	0.00
%GRS	25.59	27.04	23.35	20.64	21.06	24.10	23.16	22.80	13.36	13.28
%ANR	0.00	0.00	0.00	0.62	0.00	0.00	0.00	0.00	3.98	3.69
FE/FE+MG	0.90	0.86	0.95	0.92	0.91	0.91	0.91	0.90	0.89	0.89
A	41.28	41.35	40.18	40.28	40.48	41.57	41.63	41.44	40.15	40.13
C	15.13	15.84	14.03	12.71	12.59	14.26	13.61	13.52	10.38	10.14
F	43.60	42.81	45.79	47.01	46.93	44.17	44.76	45.04	49.48	49.74
A"	0.39	0.40	0.35	0.34	0.34	0.37	0.36	0.36	0.30	0.30
F"	0.55	0.52	0.53	0.60	0.60	0.57	0.58	0.58	0.63	0.63
M"	0.06	0.08	0.03	0.05	0.06	0.06	0.06	0.06	0.08	0.07

GARNET

SAMPLE NO.	B4-93A	B4-93A	B4-101A	B4-101A	B4-101A	B4-101A	B4-101A	B4-101A	B4-101A	B4-101A
ANALYSIS	11G	GQMIN	07G	37G	41G	10G	38G	40G	23G	26G
CORE/RIM	R		C	C	C	R	R	R	R	R
SIO2	37.69	37.87	37.31	37.22	37.46	36.32	37.19	36.70	37.18	37.10
AL2O3	20.71	19.99	22.23	22.03	22.51	22.94	22.45	22.36	22.79	22.43
CR2O3	0.05	0.00	0.08	0.07	0.08	0.07	0.10	0.07	0.06	0.07
TIO2	0.10	0.18	0.06	0.04	0.20	0.06	0.03	0.04	0.02	0.05
FE2O3(C)	1.50	1.49	0.00	0.00	0.00	0.00	0.00	0.00	0.00	0.00
MGO	2.06	1.93	2.11	2.19	2.38	2.20	2.32	2.27	2.15	2.17
FEO(C)	29.43	27.88	30.17	29.58	31.05	31.38	31.20	30.97	31.93	31.76
MNO	4.22	4.19	4.77	4.75	5.02	5.19	5.01	5.15	5.54	5.20
CAO	6.14	6.31	3.49	3.72	2.63	1.90	2.49	2.22	2.26	2.14
NA2O	0.03	0.03	0.00	0.00	0.06	0.01	0.03	0.02	0.00	0.02
K2O	0.09	0.03	0.10	0.09	0.08	0.11	0.10	0.10	0.08	0.08
SUM	102.01	99.91	100.33	99.68	101.48	100.17	100.91	99.90	102.01	101.01
SI	2.98	3.05	2.99	3.00	2.97	2.92	2.96	2.96	2.94	2.96
AL(IV)	0.02	0.00	0.01	0.00	0.03	0.08	0.04	0.04	0.06	0.04
AL(VI)	1.90	1.90	2.09	2.09	2.07	2.09	2.07	2.08	2.06	2.07
CR	0.00	0.00	0.00	0.00	0.00	0.00	0.01	0.00	0.00	0.00
TI	0.01	0.01	0.00	0.00	0.01	0.00	0.00	0.00	0.00	0.00
FE+3	0.09	0.09	0.00	0.00	0.00	0.00	0.00	0.00	0.00	0.00
MG	0.24	0.23	0.25	0.26	0.28	0.26	0.27	0.27	0.25	0.26
FE+2	1.94	1.88	2.02	1.99	2.06	2.11	2.08	2.09	2.11	2.12
MN	0.28	0.29	0.32	0.32	0.34	0.35	0.34	0.35	0.37	0.35
CA	0.52	0.55	0.30	0.32	0.22	0.16	0.21	0.19	0.19	0.18
NA	0.00	0.00	0.00	0.00	0.01	0.00	0.00	0.00	0.00	0.00
K	0.01	0.00	0.01	0.01	0.01	0.01	0.01	0.01	0.01	0.01
O	11.98	12.05	12.04	12.04	12.02	12.00	12.02	12.02	12.00	12.02
%PYR	8.17	7.87	8.71	9.05	9.70	9.11	9.47	9.39	8.66	8.85
%ALM	64.90	63.88	69.76	68.72	70.97	73.00	71.56	71.89	72.12	72.80
%SPS	9.48	9.72	11.18	11.17	11.63	12.22	11.64	12.11	12.68	12.06
%UVA	0.16	0.00	0.26	0.23	0.26	0.22	0.32	0.22	0.19	0.22
%GRS	12.79	13.91	10.10	10.83	7.44	5.44	7.00	6.39	6.35	6.06
%ANR	4.50	4.61	0.00	0.00	0.00	0.00	0.00	0.00	0.00	0.00
FE/FE+MG	0.89	0.89	0.89	0.88	0.88	0.89	0.88	0.88	0.89	0.89
A	40.29	40.34	42.01	41.90	42.04	42.93	42.06	42.25	42.05	42.01
C	10.38	11.05	6.00	6.43	4.46	3.24	4.24	3.82	3.79	3.64
F	49.33	48.60	51.99	51.67	53.50	53.84	53.70	53.94	54.16	54.35
A"	0.30	0.30	0.31	0.31	0.31	0.31	0.31	0.31	0.31	0.31
F"	0.63	0.63	0.61	0.61	0.61	0.61	0.61	0.61	0.62	0.62
M"	0.07	0.07	0.08	0.08	0.08	0.08	0.08	0.08	0.07	0.07

GARNET

SAMPLE NO.	B4-101A	B4-101A	B4-101A	B4-101A	B4-101A	B4-141A	B4-141A	B4-141A	B4-141A	C3-2B
ANALYSIS	27G	28G	46G	29G	47G	12S	13S	16S	17S	15G
CORE/RIM	C	C	C	R	R	C	R	C	R	C
SIO2	37.66	37.42	37.05	36.81	36.84	37.11	37.68	37.34	37.51	37.98
AL2O3	22.26	22.15	21.77	22.17	21.66	20.96	21.03	21.19	21.61	21.33
CR2O3	0.05	0.07	0.12	0.10	0.07	0.07	0.12	0.07	0.11	0.05
TIO2	0.15	0.16	0.23	0.02	0.08	0.07	0.12	0.15	0.08	0.10
FE2O3(C)	0.00	0.00	0.00	0.00	0.00	0.09	0.03	0.54	0.00	0.60
MGO	0.94	0.91	1.09	2.09	2.24	1.81	1.34	1.45	1.46	2.71
FEO(C)	27.92	27.67	27.38	31.08	30.44	25.27	24.53	23.51	24.71	31.14
MNO	4.00	3.79	3.33	5.11	5.03	9.18	9.26	8.44	8.96	2.34
CAO	8.45	8.35	8.36	2.63	2.77	5.01	6.26	8.00	6.45	5.68
NA2O	0.03	0.01	0.07	0.02	0.02	0.04	0.05	0.01	0.04	0.02
K2O	0.02	0.02	0.08	0.09	0.08	0.11	0.13	0.13	0.13	0.02
SUM	101.48	100.55	99.48	100.12	99.23	99.70	100.55	100.82	101.05	101.98
SI	2.97	2.98	2.98	2.96	2.99	2.99	3.02	2.97	2.98	2.98
AL(IV)	0.03	0.02	0.02	0.04	0.01	0.01	0.00	0.03	0.02	0.02
AL(VI)	2.05	2.06	2.04	2.06	2.06	1.99	1.98	1.95	2.00	1.95
CR	0.00	0.00	0.01	0.01	0.00	0.00	0.01	0.00	0.01	0.00
TI	0.01	0.01	0.01	0.00	0.00	0.00	0.01	0.01	0.00	0.01
FE+3	0.00	0.00	0.00	0.00	0.00	0.00	0.00	0.03	0.00	0.04
MG	0.11	0.11	0.13	0.25	0.27	0.22	0.16	0.17	0.17	0.32
FE+2	1.84	1.84	1.84	2.09	2.06	1.70	1.64	1.56	1.64	2.05
MN	0.27	0.26	0.23	0.35	0.35	0.63	0.63	0.57	0.60	0.16
CA	0.71	0.71	0.72	0.23	0.24	0.43	0.54	0.68	0.55	0.48
NA	0.00	0.00	0.01	0.00	0.00	0.01	0.01	0.00	0.01	0.00
K	0.00	0.00	0.01	0.01	0.01	0.01	0.01	0.01	0.01	0.00
O	12.02	12.03	12.02	12.01	12.02	11.99	12.01	11.98	11.99	11.99
%PYR	3.79	3.70	4.47	8.61	9.28	7.29	5.39	5.81	5.83	10.63
%ALM	62.77	63.14	63.09	71.67	70.65	57.17	55.36	52.10	55.35	68.13
%SPS	9.11	8.75	7.77	11.94	11.83	21.03	21.17	19.14	20.32	5.23
%UVA	0.15	0.22	0.40	0.31	0.23	0.21	0.39	0.22	0.33	0.15
%GRS	24.18	24.19	24.26	7.47	8.01	14.03	17.60	21.11	18.17	14.07
%ANR	0.00	0.00	0.00	0.00	0.00	0.26	0.10	1.62	0.00	1.79
FE/FE+MG	0.94	0.94	0.93	0.89	0.88	0.89	0.91	0.90	0.90	0.87
A	41.35	41.60	41.42	41.87	41.47	40.11	40.10	40.34	40.56	40.15
C	14.27	14.26	14.45	4.52	4.82	8.69	10.83	13.62	11.00	9.54
F	44.38	44.15	44.13	53.60	53.70	51.20	49.06	46.05	48.45	50.31
A"	0.35	0.35	0.34	0.31	0.31	0.34	0.35	0.36	0.35	0.29
F"	0.62	0.62	0.62	0.62	0.62	0.59	0.59	0.58	0.58	0.62
M"	0.04	0.04	0.04	0.07	0.08	0.07	0.06	0.06	0.06	0.09

GARNET

SAMPLE NO.	C3-2B	C3-19B	C3-19B	C3-68A	C3-68A	C3-117A	C3-117A	C3-117A	C3-117A	C3-117A
ANALYSIS	16G	07S	08S	16G	18G	30A	32A	44A	50A	72A
CORE/RIM	R	C	R	C	R	C	C	R		C
SIO2	38.13	37.93	37.86	37.68	37.58	38.48	38.32	38.67	39.08	40.04
AL2O3	21.76	22.73	22.50	22.71	22.75	21.14	21.05	21.03	20.18	19.98
CR2O3	0.06	0.03	0.06	0.06	0.04	0.02	0.13	0.06	0.06	0.07
TIO2	0.09	0.09	0.06	0.12	0.07	0.31	0.28	0.23	0.17	0.30
FE2O3(C)	0.25	0.00	0.00	0.00	0.00	0.81	0.56	0.91	1.93	2.38
MGO	2.70	3.82	3.25	2.41	2.01	1.11	1.19	1.75	1.99	1.58
FEO(C)	32.17	33.73	35.03	19.50	19.09	24.34	24.32	25.79	24.00	22.95
MNO	2.49	1.54	1.70	16.91	17.40	6.07	6.01	2.80	2.85	4.79
CAO	5.01	2.38	1.97	2.96	2.92	10.57	10.12	10.96	10.82	10.37
NA2O	0.00	0.00	0.01	0.02	0.02	0.02	0.11	0.04	0.04	0.04
K2O	0.03	0.03	0.03	0.03	0.04	0.02	0.02	0.02	0.02	0.02
SUM	102.69	102.27	102.47	102.41	101.91	102.90	102.12	102.26	101.12	102.50
SI	2.98	2.96	2.96	2.95	2.97	2.99	3.00	3.01	3.08	3.13
AL(IV)	0.02	0.04	0.04	0.05	0.04	0.01	0.00	0.00	0.00	0.00
AL(VI)	1.98	2.05	2.04	2.05	2.08	1.93	1.94	1.93	1.87	1.84
CR	0.00	0.00	0.00	0.00	0.00	0.00	0.01	0.00	0.00	0.00
TI	0.00	0.00	0.00	0.01	0.00	0.02	0.02	0.01	0.01	0.02
FE+3	0.02	0.00	0.00	0.00	0.00	0.05	0.03	0.05	0.11	0.14
MG	0.31	0.44	0.38	0.28	0.24	0.13	0.14	0.20	0.23	0.18
FE+2	2.10	2.20	2.29	1.28	1.26	1.58	1.59	1.68	1.58	1.50
MN	0.17	0.10	0.11	1.12	1.16	0.40	0.40	0.18	0.19	0.32
CA	0.42	0.20	0.17	0.25	0.25	0.88	0.85	0.91	0.91	0.87
NA	0.00	0.00	0.00	0.00	0.00	0.00	0.02	0.01	0.01	0.00
K	0.00	0.00	0.00	0.00	0.00	0.00	0.00	0.00	0.00	0.00
O	11.99	12.01	12.01	12.01	12.02	12.00	12.00	12.01	12.08	12.13
%PYR	10.56	15.07	12.85	9.61	8.14	4.33	4.66	6.82	8.02	6.43
%ALM	69.84	74.72	77.73	43.61	43.35	52.68	53.38	56.32	54.18	52.27
%SPS	5.54	3.46	3.82	38.30	40.01	13.42	13.41	6.19	6.51	11.04
%UVA	0.19	0.09	0.19	0.20	0.13	0.05	0.41	0.19	0.19	0.21
%GRS	13.14	6.66	5.41	8.27	8.37	27.12	26.49	27.80	25.22	22.73
%ANR	0.74	0.00	0.00	0.00	0.00	2.40	1.65	2.69	5.88	7.31
FE/FE+MG	0.87	0.83	0.86	0.82	0.84	0.93	0.92	0.89	0.88	0.90
A	40.21	41.51	41.30	41.71	42.13	39.88	39.86	39.95	40.52	40.83
C	8.35	3.95	3.29	4.94	4.92	17.70	17.14	18.42	18.61	17.90
F	51.44	54.54	55.41	53.36	52.95	42.42	42.99	41.63	40.87	41.27
A"	0.29	0.28	0.28	0.40	0.41	0.35	0.35	0.33	0.33	0.33
F"	0.62	0.60	0.62	0.49	0.49	0.60	0.60	0.60	0.59	0.60
M"	0.09	0.12	0.10	0.11	0.09	0.05	0.05	0.07	0.08	0.07

GARNET

SAMPLE NO.	C3-117A	C4-32A	C4-32A	C4-32A	C4-32A	C4-32B	C4-49B	C4-49B	C4-49B	C4-49B
ANALYSIS	71A	15S	34S	08S	09S	37S	05S	09S	10S	35S
CORE/RIM	R			C	R		C	C	R	
SIO2	39.74	37.62	37.48	37.33	36.76	37.55	38.18	38.27	38.78	37.99
AL2O3	19.98	21.40	22.55	20.68	20.56	22.17	21.09	20.93	20.83	21.48
CR2O3	0.13	0.07	0.05	0.06	0.05	0.07	0.02	0.04	0.04	0.04
TIO2	0.25	0.03	0.16	0.18	0.04	0.00	0.07	0.07	0.07	0.05
FE2O3(C)	2.37	0.67	0.00	1.33	1.71	0.00	0.62	0.65	0.91	0.00
MGO	1.52	3.34	3.55	3.77	3.71	3.53	3.23	3.07	3.07	3.32
FEO(C)	22.97	33.28	32.91	32.46	31.92	32.22	32.74	32.54	31.73	32.44
MNO	3.86	2.41	1.97	2.30	2.35	2.19	1.85	1.79	2.06	1.81
CAO	11.33	2.87	2.78	2.71	2.85	2.73	3.78	3.75	3.57	3.79
NA2O	0.12	0.00	0.04	0.00	0.01	0.05	0.02	0.00	0.01	0.03
K2O	0.02	0.10	0.03	0.09	0.11	0.04	0.11	0.11	0.36	0.09
SUM	102.29	101.79	101.51	100.90	100.07	100.57	101.72	101.22	101.41	101.04
SI	3.10	2.97	2.95	2.97	2.95	2.98	3.01	3.03	3.06	3.00
AL(IV)	0.00	0.03	0.05	0.03	0.05	0.02	0.00	0.00	0.00	0.00
AL(VI)	1.84	1.95	2.03	1.91	1.89	2.05	1.96	1.95	1.94	2.00
CR	0.01	0.00	0.00	0.00	0.00	0.00	0.00	0.00	0.00	0.00
TI	0.02	0.00	0.01	0.01	0.00	0.00	0.00	0.00	0.00	0.00
FE+3	0.14	0.04	0.00	0.08	0.10	0.00	0.04	0.04	0.05	0.00
MG	0.18	0.39	0.42	0.45	0.44	0.42	0.38	0.36	0.36	0.39
FE+2	1.50	2.19	2.16	2.16	2.14	2.14	2.16	2.16	2.10	2.15
MN	0.25	0.16	0.13	0.15	0.16	0.15	0.12	0.12	0.14	0.12
CA	0.95	0.24	0.23	0.23	0.24	0.23	0.32	0.32	0.30	0.32
NA	0.02	0.00	0.00	0.00	0.00	0.01	0.00	0.00	0.00	0.00
K	0.00	0.01	0.00	0.01	0.01	0.00	0.01	0.01	0.04	0.01
O	12.10	11.98	12.00	11.98	11.97	12.01	12.00	12.03	12.05	12.00
%PYR	6.15	13.22	14.13	15.04	15.03	14.24	12.74	12.26	12.47	13.13
%ALM	52.08	73.17	73.47	71.96	71.27	72.83	72.40	72.93	72.35	72.02
%SPS	8.85	5.43	4.45	5.22	5.40	5.02	4.15	4.06	4.75	4.08
%UVA	0.42	0.21	0.17	0.19	0.18	0.24	0.08	0.12	0.12	0.13
%GRS	25.24	5.96	7.78	3.57	2.85	7.67	8.78	8.66	7.51	10.64
%ANR	7.25	2.01	0.00	4.02	5.26	0.00	1.86	1.98	2.80	0.00
FE/FE+MG	0.90	0.85	0.84	0.83	0.83	0.84	0.85	0.86	0.86	0.85
A	40.72	40.41	41.50	40.28	40.66	41.39	40.10	40.27	40.76	40.19
C	19.51	4.84	4.65	4.61	4.86	4.64	6.42	6.43	6.18	6.44
F	39.77	54.75	53.85	55.11	54.49	53.98	53.48	53.30	53.06	53.37
A"	0.34	0.27	0.29	0.26	0.26	0.29	0.27	0.27	0.27	0.28
F"	0.60	0.62	0.60	0.62	0.62	0.60	0.62	0.62	0.63	0.61
M"	0.06	0.11	0.12	0.12	0.12	0.12	0.11	0.10	0.11	0.11

GARNET

SAMPLE NO.	C4-49B	D2-1CA	D2-1CA	D2-1D	D2-1D	D2-1D	D2-1D	D2-1D
ANALYSIS	36S	01S	02S	20S	21S	49S	22S	48S
CORE/RIM		C	R	C	C	C	R	R
SIO2	37.41	37.58	38.07	37.77	37.10	36.60	37.05	37.19
AL2O3	21.47	22.09	23.06	20.98	20.72	21.80	20.42	22.38
CR2O3	0.04	0.02	0.06	0.06	0.10	0.06	0.05	0.05
TIO2	0.04	0.02	0.09	0.10	0.07	0.10	0.05	0.09
FE2O3(C)	0.00	0.11	0.00	1.10	1.28	0.00	1.10	0.00
MGO	3.23	3.97	3.68	3.67	3.58	3.39	3.00	3.30
FEO(C)	32.34	33.39	33.74	33.58	33.14	33.29	33.78	33.82
MNO	1.64	1.65	1.42	1.55	1.56	1.54	1.75	1.50
CAO	3.77	2.76	2.84	2.85	2.82	2.96	2.68	2.65
NA2O	0.01	0.00	0.00	0.01	0.02	0.00	0.00	0.01
K2O	0.09	0.03	0.04	0.09	0.09	0.02	0.11	0.03
SUM	100.03	101.61	103.00	101.76	100.48	99.77	100.00	101.02
SI	2.99	2.95	2.95	2.98	2.96	2.93	2.99	2.94
AL(IV)	0.01	0.05	0.05	0.02	0.04	0.07	0.01	0.06
AL(VI)	2.01	1.99	2.05	1.93	1.91	1.99	1.93	2.03
CR	0.00	0.00	0.00	0.00	0.01	0.00	0.00	0.00
TI	0.00	0.00	0.00	0.01	0.00	0.01	0.00	0.01
FE+3	0.00	0.01	0.00	0.06	0.08	0.00	0.07	0.00
MG	0.38	0.46	0.42	0.43	0.43	0.40	0.36	0.39
FE+2	2.16	2.19	2.18	2.21	2.21	2.23	2.28	2.24
MN	0.11	0.11	0.09	0.10	0.11	0.10	0.12	0.10
CA	0.32	0.23	0.24	0.24	0.24	0.25	0.23	0.23
NA	0.00	0.00	0.00	0.00	0.00	0.00	0.00	0.00
K	0.01	0.00	0.00	0.01	0.01	0.00	0.01	0.00
O	11.99	11.97	12.00	11.99	11.98	11.97	11.99	11.99
%PYR	12.90	15.76	14.44	14.50	14.39	13.81	12.08	13.22
%ALM	72.54	72.65	74.37	73.93	73.90	73.96	76.18	75.74
%SPS	3.73	3.73	3.17	3.47	3.57	3.56	4.00	3.41
%UVA	0.12	0.05	0.18	0.19	0.32	0.21	0.17	0.17
%GRS	10.70	7.49	7.83	4.62	3.93	8.47	4.20	7.46
%ANR	0.00	0.32	0.00	3.28	3.88	0.00	3.37	0.00
FE/FE+MG	0.85	0.82	0.84	0.84	0.84	0.85	0.87	0.85
A	40.44	40.60	41.73	40.25	40.42	40.75	40.17	41.42
C	6.45	4.60	4.67	4.82	4.81	5.03	4.63	4.45
F	53.12	54.80	53.60	54.93	54.77	54.22	55.20	54.12
A"	0.28	0.28	0.29	0.26	0.26	0.28	0.26	0.28
F"	0.61	0.60	0.60	0.62	0.62	0.61	0.64	0.61
M"	0.11	0.13	0.12	0.12	0.12	0.11	0.10	0.11

MUSCOVITE AND PARAGONITE

SAMPLE NO.	A1-1A	A1-1A	A1-1A	A1-1B	A1-1B	A1-1B	A1-1B	A1-1B	A2-3E	A2-3E
ANALYSIS	04MY	06MY	17MY	05MY	06MY	16MY	20MY	21MY	16BF	17BF
CORE/RIM										
SIO2	46.24	46.99	47.80	46.94	46.25	45.22	46.30	45.35	47.41	47.75
AL2O3	25.75	26.98	26.41	27.04	26.21	26.01	26.95	26.71	26.55	27.15
TIO2	0.33	0.47	0.25	0.38	0.50	0.45	0.11	0.67	0.32	0.25
FE2O3(C)	9.13	7.64	7.18	9.39	10.03	10.81	8.97	10.38	6.71	6.90
FEO(C)	0.00	0.00	0.00	0.00	0.00	0.00	0.00	0.00	0.00	0.00
MGO	3.57	2.92	2.91	2.09	2.34	2.38	2.13	2.26	2.58	2.54
MNO	0.15	0.12	0.14	0.05	0.04	0.05	0.03	0.04	0.05	0.04
K2O	10.66	10.88	11.25	10.83	10.60	10.24	10.64	9.68	10.21	10.10
NA2O	0.13	0.10	0.08	0.12	0.10	0.11	0.11	0.07	0.11	0.08
CAO	0.06	0.07	0.04	0.02	0.04	0.05	0.04	0.05	0.03	0.02
BAO	0.91	0.94	0.70	0.58	0.75	0.54	0.75	0.42	1.00	1.07
F	0.02	0.03	0.03	0.07	0.08	0.05	0.05	0.08	0.19	0.13
CL	0.00	0.02	0.00	0.01	0.00	0.00	0.00	0.00	0.01	0.01
H2O(C)	4.45	4.45	4.43	4.43	4.39	4.37	4.38	4.39	4.30	4.38
SUM	101.38	101.59	101.21	101.91	101.29	100.25	100.41	100.09	99.37	100.37
SI	3.11	3.16	3.22	3.15	3.13	3.09	3.15	3.07	3.24	3.22
AL(IV)	0.89	0.84	0.78	0.85	0.87	0.91	0.85	0.93	0.76	0.78
AL(VI)	1.15	1.29	1.32	1.29	1.22	1.18	1.32	1.21	1.37	1.38
TI	0.02	0.02	0.01	0.02	0.03	0.02	0.01	0.03	0.02	0.01
FE+3	0.46	0.39	0.36	0.48	0.51	0.56	0.46	0.53	0.35	0.35
FE+2	0.00	0.00	0.00	0.00	0.00	0.00	0.00	0.00	0.00	0.00
MG	0.36	0.29	0.29	0.21	0.24	0.24	0.22	0.23	0.26	0.26
MN	0.01	0.01	0.01	0.00	0.00	0.00	0.00	0.00	0.00	0.00
K	0.92	0.93	0.97	0.93	0.92	0.89	0.92	0.84	0.89	0.87
NA	0.02	0.01	0.01	0.02	0.01	0.01	0.01	0.01	0.02	0.01
CA	0.00	0.00	0.00	0.00	0.00	0.00	0.00	0.00	0.00	0.00
BA	0.02	0.02	0.02	0.02	0.02	0.01	0.02	0.01	0.03	0.03
F	0.00	0.01	0.01	0.02	0.02	0.01	0.01	0.02	0.04	0.03
CL	0.00	0.00	0.00	0.00	0.00	0.00	0.00	0.00	0.00	0.00
OH(C)	2.00	1.99	1.99	1.98	1.98	1.99	1.99	1.98	1.96	1.97
O	9.88	9.94	9.98	9.97	9.95	9.90	9.96	9.88	9.98	9.96
FE/FE+MG	0.56	0.57	0.55	0.69	0.68	0.70	0.68	0.70	0.57	0.58
%MS	98.25	98.61	98.92	98.29	98.64	98.42	98.49	98.88	98.33	98.75
%PA	1.75	1.39	1.08	1.71	1.36	1.58	1.51	1.12	1.67	1.25

MUSCOVITE AND PARAGONITE

SAMPLE NO.	A2-3F	A2-3F	A2-3F	A2-3F	A2-3HA	A2-3HA	A2-11A	A2-11A	A2-13A	A2-13A
ANALYSIS	01BF	03BF	09BF	10BF	09BF	11BF	09S	10S	13MY	14MY
CORE/RIM										
SIO2	47.74	47.94	47.63	47.58	48.12	46.32	46.02	46.71	45.00	45.57
AL2O3	28.38	28.20	27.56	28.38	26.51	27.69	32.41	31.43	27.98	28.23
TIO2	0.28	0.28	0.34	0.37	0.22	0.36	0.50	0.56	0.62	0.60
FE2O3(C)	5.35	5.29	5.35	5.29	6.13	7.22	2.66	2.69	7.29	6.98
FEO(C)	0.00	0.00	0.00	0.00	0.74	0.00	0.00	0.00	0.00	0.00
MGO	2.73	2.74	2.83	2.73	2.36	2.35	1.82	1.87	2.41	2.41
MNO	0.02	0.04	0.03	0.04	0.01	0.00	0.00	0.00	0.05	0.06
K2O	10.73	11.12	10.95	10.33	10.19	10.80	10.37	10.47	10.62	10.86
NA2O	0.12	0.08	0.12	0.12	0.71	0.11	0.37	0.31	0.15	0.17
CAO	0.07	0.05	0.04	0.06	0.05	0.03	0.05	0.02	0.08	0.06
BAO	0.67	0.64	0.57	0.66	1.06	1.40	0.23	0.17	0.93	1.04
F	0.27	0.22	0.22	0.34	0.14	0.09	0.23	0.18	0.18	0.10
CL	0.00	0.00	0.00	0.00	0.02	0.00	0.00	0.00	0.00	0.00
H2O(C)	4.35	4.37	4.32	4.31	4.34	4.36	4.36	4.36	4.29	4.36
SUM	100.59	100.88	99.87	100.07	100.53	100.71	98.90	98.71	99.54	100.39
SI	3.20	3.21	3.22	3.19	3.27	3.15	3.09	3.15	3.08	3.10
AL(IV)	0.80	0.79	0.78	0.81	0.73	0.85	0.91	0.85	0.92	0.90
AL(VI)	1.44	1.44	1.42	1.44	1.39	1.37	1.66	1.65	1.34	1.36
TI	0.01	0.01	0.02	0.02	0.01	0.02	0.02	0.03	0.03	0.03
FE+3	0.27	0.27	0.27	0.27	0.31	0.37	0.13	0.14	0.38	0.36
FE+2	0.00	0.00	0.00	0.00	0.04	0.00	0.00	0.00	0.00	0.00
MG	0.27	0.27	0.29	0.27	0.24	0.24	0.18	0.19	0.25	0.24
MN	0.00	0.00	0.00	0.00	0.00	0.00	0.00	0.00	0.00	0.00
K	0.92	0.95	0.94	0.88	0.88	0.94	0.89	0.90	0.93	0.94
NA	0.02	0.01	0.02	0.02	0.09	0.01	0.05	0.04	0.02	0.02
CA	0.00	0.00	0.00	0.00	0.00	0.00	0.00	0.00	0.01	0.00
BA	0.02	0.02	0.02	0.02	0.03	0.04	0.01	0.00	0.02	0.03
F	0.06	0.05	0.05	0.07	0.03	0.02	0.05	0.04	0.04	0.02
CL	0.00	0.00	0.00	0.00	0.00	0.00	0.00	0.00	0.00	0.00
OH(C)	1.94	1.95	1.95	1.93	1.97	1.98	1.95	1.96	1.96	1.98
O	9.96	9.98	9.98	9.94	10.02	9.98	9.94	9.97	9.94	9.96
FE/FE+MG	0.50	0.49	0.49	0.49	0.60	0.61	0.43	0.42	0.60	0.59
%MS	98.35	98.90	98.39	98.25	90.43	98.49	94.92	95.72	97.84	97.69
%PA	1.65	1.10	1.61	1.75	9.57	1.51	5.08	4.28	2.16	2.31

MUSCOVITE AND PARAGONITE

SAMPLE NO.	A2-14AA	A2-15A	A2-15A	A2-19A	A2-21B	A2-21B	A2-22A	A2-27B	A2-27B	A2-27B
ANALYSIS	20MY	03U	04U	13GQM	07GQM	10GQM	02SQM	23U	31U	32U
CORE/RIM										
SIO2	48.04	45.98	45.68	46.56	47.11	45.64	47.86	48.82	48.00	47.47
AL2O3	28.37	31.99	34.23	34.36	34.59	33.83	34.76	25.83	36.00	36.37
TIO2	0.10	0.19	0.17	1.08	0.41	0.88	0.25	0.20	0.06	0.06
FE2O3(C)	5.31	3.33	2.20	0.00	2.48	1.60	0.00	6.71	0.31	0.00
FEO(C)	0.00	1.04	0.75	1.21	0.00	0.52	0.85	0.00	1.29	1.29
MGO	3.07	0.74	0.41	0.73	1.39	0.87	0.94	3.84	0.46	0.28
MNO	0.05	0.01	0.04	0.02	0.04	0.01	0.02	0.05	0.03	0.00
K2O	10.59	10.58	10.56	9.48	9.45	9.89	8.86	9.72	10.88	10.94
NA2O	0.12	0.25	0.25	0.87	0.59	0.59	0.96	0.07	0.23	0.24
CAO	0.34	0.04	0.04	0.09	0.05	0.03	0.02	0.09	0.03	0.03
BAO	0.37	0.04	0.11	0.00	0.00	0.00	0.00	0.12	0.15	0.15
F	0.14	0.10	0.09	0.00	0.00	0.00	0.00	0.28	0.12	0.08
CL	0.01	0.07	0.03	0.00	0.00	0.00	0.00	0.00	0.00	0.00
H2O(C)	4.44	4.35	4.40	4.50	4.60	4.45	4.56	4.38	4.56	4.55
SUM	100.89	98.64	98.90	98.89	100.70	98.31	99.09	99.99	102.09	101.44
SI	3.20	3.12	3.08	3.10	3.07	3.07	3.15	3.25	3.11	3.10
AL(IV)	0.80	0.88	0.92	0.90	0.93	0.93	0.85	0.75	0.89	0.90
AL(VI)	1.42	1.69	1.79	1.81	1.72	1.76	1.85	1.27	1.86	1.90
TI	0.00	0.01	0.01	0.05	0.02	0.04	0.01	0.01	0.00	0.00
FE+3	0.27	0.17	0.11	0.00	0.12	0.08	0.00	0.34	0.02	0.00
FE+2	0.00	0.06	0.04	0.07	0.00	0.03	0.05	0.00	0.07	0.07
MG	0.31	0.07	0.04	0.07	0.13	0.09	0.09	0.38	0.05	0.03
MN	0.00	0.00	0.00	0.00	0.00	0.00	0.00	0.00	0.00	0.00
K	0.90	0.92	0.91	0.81	0.79	0.85	0.74	0.82	0.90	0.91
NA	0.02	0.03	0.03	0.11	0.07	0.08	0.12	0.01	0.03	0.03
CA	0.02	0.00	0.00	0.01	0.00	0.00	0.00	0.01	0.00	0.00
BA	0.01	0.00	0.00	0.00	0.00	0.00	0.00	0.00	0.00	0.00
F	0.03	0.02	0.02	0.00	0.00	0.00	0.00	0.06	0.02	0.02
CL	0.00	0.01	0.00	0.00	0.00	0.00	0.00	0.00	0.00	0.00
OH(C)	1.97	1.97	1.98	2.00	2.00	2.00	2.00	1.94	1.98	1.98
O	9.94	9.98	9.98	9.97	9.91	9.97	9.94	9.86	9.97	9.98
FE/FE+MG	0.47	0.75	0.79	0.48	0.47	0.56	0.34	0.47	0.65	0.72
%MS	98.35	96.59	96.52	87.76	91.38	91.63	85.80	98.90	96.87	96.75
%PA	1.65	3.41	3.48	12.24	8.63	8.37	14.20	1.10	3.13	3.25

MUSCOVITE AND PARAGONITE

SAMPLE NO.	A3-1B	A3-4A	A3-4A	A3-4A	A3-4A	A3-11B	A3-11B	A4-2A	A4-6A	A4-8A
ANALYSIS	06SQM	11S	12S	24S	25S	06G	13G	14G	32G	63G
CORE/RIM										
SIO2	46.95	47.17	47.23	46.91	46.16	47.97	47.87	46.43	46.55	45.48
AL2O3	33.01	33.27	32.97	33.12	33.16	31.17	29.60	34.54	33.82	34.36
TIO2	0.43	0.42	0.45	0.50	0.46	0.29	1.34	0.58	0.50	0.41
FE2O3(C)	0.48	2.54	2.55	2.73	2.89	1.61	0.67	1.35	1.18	2.29
FEO(C)	1.09	0.00	0.00	0.00	0.00	1.02	2.16	0.05	0.36	0.00
MGO	1.17	1.53	1.48	1.62	1.52	1.72	1.80	1.11	1.18	1.08
MNO	0.01	0.03	0.06	0.00	0.00	0.00	0.01	0.02	0.00	0.03
K2O	8.99	9.99	9.96	10.26	10.04	9.22	9.48	8.41	9.22	9.48
NA2O	0.85	0.48	0.47	0.38	0.38	0.44	0.24	1.19	0.86	0.73
CAO	0.04	0.02	0.02	0.05	0.06	0.03	0.01	0.05	0.03	0.06
BAO	0.00	0.32	0.20	0.18	0.30	0.09	0.29	0.34	0.79	0.74
F	0.00	0.12	0.13	0.15	0.18	0.16	0.10	0.13	0.12	0.07
CL	0.00	0.00	0.02	0.02	0.02	0.00	0.00	0.00	0.01	0.00
H2O(C)	4.46	4.49	4.46	4.46	4.41	4.40	4.39	4.45	4.43	4.44
SUM	97.48	100.32	99.94	100.31	99.48	98.05	97.90	98.60	98.98	99.15
SI	3.16	3.11	3.13	3.10	3.08	3.21	3.24	3.09	3.11	3.04
AL(IV)	0.84	0.89	0.87	0.90	0.92	0.79	0.76	0.92	0.89	0.96
AL(VI)	1.77	1.70	1.70	1.68	1.68	1.68	1.59	1.79	1.78	1.75
TI	0.02	0.02	0.02	0.02	0.02	0.01	0.07	0.03	0.02	0.02
FE+3	0.02	0.13	0.13	0.14	0.14	0.08	0.03	0.07	0.06	0.12
FE+2	0.06	0.00	0.00	0.00	0.00	0.06	0.12	0.00	0.02	0.00
MG	0.12	0.15	0.15	0.16	0.15	0.17	0.18	0.11	0.12	0.11
MN	0.00	0.00	0.00	0.00	0.00	0.00	0.00	0.00	0.00	0.00
K	0.77	0.84	0.84	0.86	0.85	0.79	0.82	0.71	0.79	0.81
NA	0.11	0.06	0.06	0.05	0.05	0.06	0.03	0.15	0.11	0.09
CA	0.00	0.00	0.00	0.00	0.00	0.00	0.00	0.00	0.00	0.00
BA	0.00	0.01	0.00	0.00	0.01	0.00	0.01	0.01	0.02	0.02
F	0.00	0.02	0.03	0.03	0.04	0.03	0.02	0.03	0.02	0.02
CL	0.00	0.00	0.00	0.00	0.00	0.00	0.00	0.00	0.00	0.00
OH(C)	2.00	1.98	1.97	1.97	1.96	1.97	1.98	1.97	1.98	1.98
O	9.94	9.95	9.96	9.95	9.94	9.93	9.93	9.95	9.97	9.95
FE/FE+MG	0.42	0.45	0.47	0.46	0.49	0.45	0.46	0.39	0.40	0.52
%MS	87.43	93.18	93.35	94.65	94.59	93.25	96.24	82.25	87.64	89.59
%PA	12.57	6.82	6.65	5.35	5.41	6.75	3.77	17.75	12.36	10.41

MUSCOVITE AND PARAGONITE

SAMPLE NO.	A4-8A	A4-19A	A4-19A	B2-1AB	B2-1AB	B2-1AB	B2-3A	B2-3A	B2-3A	B2-35A
ANALYSIS	65G	06G	07G	03G	04G	07G	17G	19G	38G	30G
CORE/RIM										
SIO2	46.62	46.90	47.55	46.98	48.53	46.35	46.88	47.00	46.32	47.43
AL2O3	33.01	34.82	34.03	31.47	31.12	33.19	34.01	33.31	33.90	33.29
TIO2	0.47	0.48	0.49	0.44	0.34	0.61	0.60	0.61	0.49	0.35
FE2O3(C)	2.54	0.72	1.11	2.28	1.62	1.99	1.61	1.52	1.26	1.31
FEO(C)	0.00	0.41	0.20	0.00	0.53	0.00	0.39	0.52	0.47	0.59
MGO	1.57	1.04	1.43	1.94	2.12	1.70	1.10	1.26	1.01	1.33
MNO	0.03	0.00	0.04	0.04	0.04	0.08	0.05	0.05	0.03	0.01
K2O	10.16	10.05	10.04	9.99	10.06	9.93	9.77	9.36	9.90	10.31
NA2O	0.55	1.16	0.86	0.40	0.43	0.46	0.63	0.53	0.68	0.63
CAO	0.07	0.04	0.06	0.02	0.03	0.03	0.02	0.02	0.03	0.01
BAO	0.54	0.23	0.18	1.19	0.84	1.43	0.58	0.72	0.67	0.20
F	0.15	0.07	0.06	0.05	0.00	0.06	0.09	0.07	0.05	0.01
CL	0.00	0.00	0.01	0.00	0.00	0.00	0.00	0.00	0.00	0.00
H2O(C)	4.43	4.50	4.53	4.43	4.51	4.47	4.49	4.47	4.45	4.51
SUM	100.08	100.39	100.54	99.23	100.17	100.27	100.18	99.41	99.24	99.97
SI	3.10	3.10	3.13	3.16	3.22	3.09	3.10	3.13	3.10	3.15
AL(IV)	0.90	0.90	0.87	0.83	0.78	0.91	0.90	0.87	0.90	0.85
AL(VI)	1.69	1.81	1.77	1.66	1.66	1.70	1.76	1.74	1.78	1.75
TI	0.02	0.02	0.02	0.02	0.02	0.03	0.03	0.03	0.02	0.02
FE+3	0.13	0.04	0.05	0.12	0.08	0.10	0.08	0.08	0.06	0.06
FE+2	0.00	0.02	0.01	0.00	0.03	0.00	0.02	0.03	0.03	0.03
MG	0.16	0.10	0.14	0.19	0.21	0.17	0.11	0.13	0.10	0.13
MN	0.00	0.00	0.00	0.00	0.00	0.00	0.00	0.00	0.00	0.00
K	0.86	0.85	0.84	0.86	0.85	0.84	0.82	0.79	0.85	0.87
NA	0.07	0.15	0.11	0.05	0.05	0.06	0.08	0.07	0.09	0.08
CA	0.00	0.00	0.00	0.00	0.00	0.00	0.00	0.00	0.00	0.00
BA	0.01	0.01	0.00	0.03	0.02	0.04	0.02	0.02	0.02	0.00
F	0.03	0.01	0.01	0.01	0.00	0.01	0.02	0.02	0.01	0.00
CL	0.00	0.00	0.00	0.00	0.00	0.00	0.00	0.00	0.00	0.00
OH(C)	1.97	1.99	1.99	1.99	2.00	1.99	1.98	1.98	1.99	2.00
O	9.97	10.01	9.98	9.98	9.98	9.96	9.97	9.95	9.99	9.98
FE/FE+MG	0.45	0.36	0.32	0.37	0.34	0.37	0.48	0.46	0.47	0.43
%MS	92.46	85.05	88.49	94.28	93.91	93.43	91.14	92.13	90.60	91.50
%PA	7.54	14.95	11.51	5.72	6.09	6.57	8.86	7.87	9.40	8.50

MUSCOVITE AND PARAGONITE

SAMPLE NO.	B2-35A	B2-35B	B2-35B	B3-30A	B3-30A	B3-117B	B3-117B	B3-117B	B3-141A	B3-141A
ANALYSIS	32G	08G	21G	02S	03G	15S	16S	17S	08G	09G
CORE/RIM										
SIO2	47.47	46.74	46.01	46.05	44.99	45.88	45.98	46.23	47.57	46.62
AL2O3	32.37	34.36	33.86	35.85	34.93	34.61	33.25	34.09	30.15	31.76
TIO2	0.47	0.52	0.57	0.28	0.47	0.30	0.30	0.37	0.69	0.52
FE2O3(C)	1.22	2.15	2.75	2.34	5.04	2.31	2.63	1.95	2.14	2.97
FEO(C)	0.80	0.00	0.00	0.00	0.00	0.00	0.00	0.27	0.75	0.00
MGO	1.49	1.46	1.52	1.20	0.91	0.81	1.37	0.92	2.01	1.63
MNO	0.03	0.00	0.06	0.00	0.00	0.10	0.07	0.04	0.04	0.04
K2O	10.35	10.29	10.38	9.47	8.87	9.51	9.01	9.37	9.77	9.66
NA2O	0.52	0.47	0.57	0.87	0.88	1.00	1.05	0.91	0.75	0.88
CAO	0.01	0.06	0.07	0.06	0.06	0.04	0.09	0.04	0.05	0.04
BAO	0.15	0.23	0.23	0.22	0.20	0.40	0.43	0.42	0.38	0.38
F	0.05	0.11	0.00	0.18	0.14	0.11	0.11	0.06	0.02	0.04
CL	0.01	0.00	0.00	0.00	0.00	0.00	0.00	0.00	0.00	0.00
H2O(C)	4.46	4.52	4.53	4.52	4.51	4.44	4.42	4.46	4.43	4.43
SUM	99.38	100.87	100.55	100.98	100.95	99.46	98.66	99.08	98.73	98.97
SI	3.17	3.07	3.04	3.00	2.94	3.06	3.08	3.09	3.21	3.14
AL(IV)	0.83	0.93	0.96	1.00	1.06	0.94	0.92	0.91	0.79	0.86
AL(VI)	1.72	1.73	1.68	1.75	1.64	1.78	1.71	1.77	1.61	1.66
TI	0.02	0.03	0.03	0.01	0.02	0.02	0.02	0.02	0.04	0.03
FE+3	0.06	0.11	0.14	0.12	0.25	0.12	0.13	0.10	0.11	0.15
FE+2	0.05	0.00	0.00	0.00	0.00	0.00	0.00	0.02	0.04	0.00
MG	0.15	0.14	0.15	0.12	0.09	0.08	0.14	0.09	0.20	0.16
MN	0.00	0.00	0.00	0.00	0.00	0.01	0.00	0.00	0.00	0.00
K	0.88	0.86	0.88	0.79	0.74	0.81	0.77	0.80	0.84	0.83
NA	0.07	0.06	0.07	0.11	0.11	0.13	0.14	0.12	0.10	0.12
CA	0.00	0.00	0.00	0.00	0.00	0.00	0.01	0.00	0.00	0.00
BA	0.00	0.01	0.01	0.01	0.00	0.01	0.01	0.01	0.01	0.01
F	0.01	0.02	0.00	0.04	0.03	0.02	0.02	0.01	0.00	0.01
CL	0.00	0.00	0.00	0.00	0.00	0.00	0.00	0.00	0.00	0.00
OH(C)	1.99	1.98	2.00	1.96	1.97	1.98	1.98	1.99	1.99	1.99
O	9.98	9.95	9.94	9.91	9.88	9.98	9.95	9.97	9.98	9.98
FE/FE+MG	0.42	0.43	0.48	0.50	0.74	0.59	0.49	0.55	0.43	0.48
%MS	92.86	93.55	92.33	87.75	86.85	86.19	84.99	87.19	89.51	87.85
%PA	7.14	6.45	7.67	12.25	13.15	13.81	15.01	12.81	10.49	12.15

MUSCOVITE AND PARAGONITE

SAMPLE NO.	B3-141A	B3-141A	B3-156A	B3-156A	B3156AA	B3156AA	B3-165A	B3-165A	B3-165A	B3-175A
ANALYSIS	11G	14G	14C	15C	07S	08S	07S	09S	19S	37S
CORE/RIM										
SIO2	46.37	46.18	46.75	47.06	47.80	48.45	46.90	46.26	47.44	46.40
AL2O3	32.38	32.48	33.35	33.46	30.47	31.57	33.64	34.05	34.27	34.52
TIO2	0.51	0.56	0.37	0.41	0.39	0.29	0.40	0.32	0.35	0.39
FE2O3(C)	2.62	2.88	1.32	1.22	3.30	1.69	0.94	1.52	1.24	1.73
FEO(C)	0.23	0.00	0.39	0.48	0.00	0.75	0.87	0.20	0.63	0.03
MGO	1.34	1.40	1.27	1.29	2.24	1.85	1.02	1.02	1.04	0.99
MNO	0.02	0.05	0.04	0.02	0.03	0.02	0.03	0.06	0.06	0.08
K2O	9.49	9.72	9.65	9.68	9.33	9.80	9.07	9.14	9.51	9.33
NA2O	0.93	0.73	0.71	0.72	0.60	0.70	1.09	1.10	1.22	1.06
CAO	0.04	0.07	0.02	0.02	0.06	0.03	0.09	0.08	0.05	0.01
BAO	0.41	0.55	0.60	0.39	0.27	0.39	0.36	0.35	0.34	0.42
F	0.00	0.02	0.20	0.11	0.06	0.08	0.19	0.07	0.10	0.08
CL	0.00	0.00	0.00	0.00	0.00	0.00	0.00	0.00	0.00	0.00
H2O(C)	4.45	4.45	4.38	4.45	4.46	4.49	4.40	4.44	4.51	4.47
SUM	98.79	99.07	98.97	99.25	98.99	100.05	98.92	98.57	100.72	99.48
SI	3.12	3.11	3.13	3.14	3.19	3.21	3.13	3.10	3.12	3.09
AL(IV)	0.88	0.89	0.87	0.87	0.81	0.79	0.87	0.90	0.88	0.92
AL(VI)	1.69	1.68	1.76	1.76	1.59	1.68	1.78	1.79	1.78	1.79
TI	0.03	0.03	0.02	0.02	0.02	0.01	0.02	0.02	0.02	0.02
FE+3	0.13	0.15	0.07	0.06	0.17	0.08	0.05	0.08	0.06	0.09
FE+2	0.01	0.00	0.02	0.03	0.00	0.04	0.05	0.01	0.04	0.00
MG	0.13	0.14	0.13	0.13	0.22	0.18	0.10	0.10	0.10	0.10
MN	0.00	0.00	0.00	0.00	0.00	0.00	0.00	0.00	0.00	0.00
K	0.81	0.83	0.82	0.82	0.80	0.83	0.77	0.78	0.80	0.79
NA	0.12	0.10	0.09	0.09	0.08	0.09	0.14	0.14	0.16	0.14
CA	0.00	0.00	0.00	0.00	0.00	0.00	0.01	0.01	0.00	0.00
BA	0.01	0.01	0.02	0.01	0.01	0.01	0.01	0.01	0.01	0.01
F	0.00	0.00	0.04	0.02	0.01	0.02	0.04	0.01	0.02	0.02
CL	0.00	0.00	0.00	0.00	0.00	0.00	0.00	0.00	0.00	0.00
OH(C)	2.00	2.00	1.96	1.98	1.99	1.98	1.96	1.99	1.98	1.98
O	9.98	9.98	9.98	9.97	9.94	9.97	9.97	9.98	9.99	9.98
FE/FE+MG	0.52	0.51	0.41	0.41	0.43	0.41	0.49	0.46	0.49	0.47
%MS	87.09	89.79	89.91	89.89	91.07	90.19	84.59	84.47	83.65	85.27
%PA	12.91	10.21	10.08	10.11	8.93	9.81	15.41	15.53	16.35	14.73

MUSCOVITE AND PARAGONITE

SAMPLE NO.	B3-175A	B3-185A	B3-185A	B3-185A	B3261AB	B3261AB	B4-11K	B4-11K	B4-11L	B4-32A
ANALYSIS	39S	24G	25G	30G	15S	31S	78G	79G	12S	55S
CORE/RIM										
SIO2	44.17	46.89	47.00	47.23	47.82	48.07	48.71	48.16	46.89	46.61
AL2O3	33.28	33.57	33.65	33.81	31.96	32.25	31.74	32.48	34.61	32.09
TIO2	0.38	0.61	0.56	0.37	0.46	0.45	0.36	0.41	0.43	0.65
FE2O3(C)	4.51	1.54	1.73	1.77	1.16	0.86	1.19	1.19	0.76	3.30
FEO(C)	0.00	0.21	0.02	0.02	0.03	0.19	0.00	0.00	0.68	0.00
MGO	2.10	1.35	1.40	1.39	2.08	2.05	2.37	2.21	0.93	1.67
MNO	0.10	0.03	0.05	0.03	0.11	0.05	0.04	0.00	0.00	0.08
K2O	8.68	9.60	9.74	9.74	10.19	10.41	9.88	9.75	8.98	10.30
NA2O	1.03	0.68	0.64	0.70	0.54	0.56	0.73	0.74	1.06	0.51
CAO	0.02	0.03	0.07	0.02	0.05	0.02	0.02	0.04	0.02	0.14
BAO	0.48	0.26	0.28	0.26	0.24	0.17	0.35	0.65	0.24	0.27
F	0.11	0.07	0.04	0.09	0.11	0.07	0.14	0.12	0.11	0.07
CL	0.00	0.00	0.00	0.00	0.00	0.00	0.00	0.00	0.00	0.00
H2O(C)	4.46	4.48	4.51	4.49	4.44	4.48	4.48	4.49	4.47	4.46
SUM	99.27	99.28	99.66	99.88	99.12	99.59	99.95	100.18	99.14	100.13
SI	2.94	3.12	3.11	3.12	3.19	3.19	3.22	3.18	3.11	3.11
AL(IV)	1.06	0.88	0.88	0.88	0.81	0.81	0.78	0.82	0.89	0.89
AL(VI)	1.54	1.75	1.74	1.75	1.70	1.72	1.69	1.70	1.81	1.63
TI	0.02	0.03	0.03	0.02	0.02	0.02	0.02	0.02	0.02	0.03
FE+3	0.23	0.08	0.09	0.09	0.06	0.04	0.06	0.06	0.04	0.17
FE+2	0.00	0.01	0.00	0.00	0.00	0.01	0.00	0.00	0.04	0.00
MG	0.21	0.13	0.14	0.14	0.21	0.20	0.23	0.22	0.09	0.17
MN	0.01	0.00	0.00	0.00	0.01	0.00	0.00	0.00	0.00	0.00
K	0.74	0.81	0.82	0.82	0.87	0.88	0.83	0.82	0.76	0.88
NA	0.13	0.09	0.08	0.09	0.07	0.07	0.09	0.10	0.14	0.06
CA	0.00	0.00	0.00	0.00	0.00	0.00	0.00	0.00	0.00	0.01
BA	0.01	0.01	0.01	0.01	0.01	0.00	0.01	0.02	0.01	0.01
F	0.02	0.02	0.01	0.02	0.02	0.01	0.03	0.02	0.02	0.02
CL	0.00	0.00	0.00	0.00	0.00	0.00	0.00	0.00	0.00	0.00
OH(C)	1.98	1.98	1.99	1.98	1.98	1.99	1.97	1.98	1.98	1.98
O	9.82	9.96	9.97	9.96	9.98	9.98	9.97	9.97	9.96	9.97
FE/FE+MG	0.52	0.40	0.39	0.39	0.23	0.21	0.20	0.21	0.45	0.50
%MS	84.65	90.34	90.93	90.10	92.58	92.46	89.90	89.63	84.78	93.05
%PA	15.35	9.66	9.07	9.90	7.42	7.54	10.10	10.37	15.22	6.95

MUSCOVITE AND PARAGONITE

SAMPLE NO.	B4-93A	B4-93A	B4-101A	B4-101A	B4-101A	B4-141A	B4-141A	C3-2B	C3-19BB	C3-19BB
ANALYSIS	16G	24G	14G	15G	57G	20S	21S	04G	14S	15S
CORE/RIM										
SIO2	46.89	46.29	46.10	45.95	46.66	47.77	47.53	46.35	46.14	46.31
AL2O3	33.21	33.95	35.39	34.94	35.37	31.80	31.35	35.48	37.02	37.01
TIO2	0.39	0.51	0.35	0.35	0.29	0.47	0.55	0.51	0.33	0.38
FE2O3(C)	0.13	0.66	1.77	1.69	1.56	1.09	1.46	1.61	0.61	0.44
FEO(C)	1.21	0.83	0.00	0.00	0.04	0.81	0.76	0.00	0.04	0.23
MGO	1.09	0.91	0.81	0.83	0.85	1.71	1.73	0.88	0.49	0.46
MNO	0.02	0.00	0.06	0.07	0.05	0.05	0.09	0.01	0.01	0.00
K2O	9.62	9.56	8.99	9.03	9.73	10.00	10.17	9.40	7.27	7.28
NA2O	0.90	1.13	1.40	1.35	1.22	0.63	0.54	1.04	2.39	2.26
CAO	0.02	0.07	0.03	0.02	0.06	0.04	0.04	0.04	0.03	0.04
BAO	0.21	0.31	0.00	0.79	0.31	0.31	0.19	0.20	0.13	0.17
F	0.04	0.02	0.04	0.00	0.02	0.04	0.11	0.09	0.07	0.06
CL	0.00	0.00	0.00	0.00	0.00	0.00	0.00	0.00	0.00	0.01
H2O(C)	4.43	4.45	4.51	4.49	4.54	4.46	4.41	4.51	4.52	4.53
SUM	98.16	98.69	99.43	99.51	100.70	99.17	98.90	100.08	99.02	99.16
SI	3.16	3.11	3.05	3.06	3.07	3.19	3.19	3.05	3.03	3.04
AL(IV)	0.84	0.89	0.95	0.94	0.93	0.81	0.81	0.95	0.97	0.96
AL(VI)	1.80	1.80	1.81	1.81	1.82	1.70	1.68	1.81	1.90	1.90
TI	0.02	0.03	0.02	0.02	0.01	0.02	0.03	0.03	0.02	0.02
FE+3	0.01	0.03	0.09	0.08	0.08	0.05	0.07	0.08	0.03	0.02
FE+2	0.07	0.05	0.00	0.00	0.00	0.05	0.04	0.00	0.00	0.01
MG	0.11	0.09	0.08	0.08	0.08	0.17	0.17	0.09	0.05	0.05
MN	0.00	0.00	0.00	0.00	0.00	0.00	0.00	0.00	0.00	0.00
K	0.83	0.82	0.76	0.77	0.82	0.85	0.87	0.79	0.61	0.61
NA	0.12	0.15	0.18	0.18	0.15	0.08	0.07	0.13	0.31	0.29
CA	0.00	0.00	0.00	0.00	0.00	0.00	0.00	0.00	0.00	0.00
BA	0.01	0.01	0.00	0.02	0.01	0.01	0.00	0.00	0.00	0.00
F	0.01	0.00	0.01	0.00	0.00	0.01	0.02	0.02	0.02	0.01
CL	0.00	0.00	0.00	0.00	0.00	0.00	0.00	0.00	0.00	0.00
OH(C)	1.99	1.99	1.99	2.00	1.99	1.99	1.98	1.98	1.98	1.98
O	9.98	10.00	9.96	9.99	10.00	9.98	9.98	9.97	9.96	9.96
FE/FE+MG	0.41	0.47	0.52	0.51	0.49	0.37	0.40	0.48	0.40	0.43
%MS	87.52	84.82	80.90	81.44	84.05	91.21	92.52	85.62	66.70	67.93
%PA	12.48	15.18	19.10	18.56	15.95	8.79	7.48	14.38	33.30	32.07

MUSCOVITE AND PARAGONITE

SAMPLE NO.	C3-19BB	C3-19BB	C3-19BB	C3-56A	C3-56A	C3-68AA	C3-68AA	C4-7B	C4-17A	C4-32A
ANALYSIS	16S	20S	43S	05G	21G	13G	14G	04A	12G	37S
CORE/RIM										
SIO2	46.54	45.35	48.18	48.20	47.95	46.49	46.35	47.07	48.59	45.22
AL2O3	35.66	37.17	34.51	31.68	30.54	34.76	34.79	34.75	32.27	37.90
TIO2	0.23	0.21	0.40	1.26	1.25	0.79	0.87	0.06	0.09	0.29
FE2O3(C)	0.78	1.87	0.00	1.29	1.37	1.32	1.31	1.56	1.35	0.66
FEO(C)	0.12	0.00	0.82	0.13	0.00	0.00	0.00	0.05	0.00	0.00
MGO	0.82	1.08	1.28	2.35	2.67	1.39	1.36	1.09	2.44	0.40
MNO	0.04	0.00	0.00	0.01	0.02	0.02	0.01	0.00	0.03	0.02
K2O	7.89	7.14	8.48	10.67	10.80	9.60	9.78	9.60	10.68	4.91
NA2O	2.06	2.37	1.42	0.32	0.40	0.75	0.80	0.85	0.40	3.88
CAO	0.03	0.04	0.02	0.05	0.02	0.03	0.04	0.02	0.01	0.35
BAO	0.17	0.16	0.21	0.04	0.80	0.44	0.48	0.04	0.10	0.10
F	0.04	0.09	0.11	0.01	0.08	0.04	0.06	0.05	0.04	0.21
CL	0.00	0.00	0.00	0.00	0.00	0.00	0.00	0.00	0.00	0.00
H2O(C)	4.51	4.57	4.53	4.55	4.46	4.53	4.52	4.52	4.55	4.46
SUM	98.88	100.04	99.93	100.54	100.33	100.16	100.34	99.63	100.53	98.32
SI	3.08	2.95	3.15	3.18	3.20	3.06	3.06	3.11	3.19	2.97
AL(IV)	0.92	1.05	0.85	0.82	0.80	0.94	0.94	0.89	0.81	1.03
AL(VI)	1.86	1.79	1.81	1.64	1.60	1.76	1.76	1.81	1.69	1.91
TI	0.01	0.01	0.02	0.06	0.06	0.04	0.04	0.00	0.00	0.01
FE+3	0.04	0.09	0.00	0.06	0.07	0.06	0.06	0.08	0.07	0.03
FE+2	0.01	0.00	0.05	0.01	0.00	0.00	0.00	0.00	0.00	0.00
MG	0.08	0.11	0.13	0.23	0.27	0.14	0.13	0.11	0.24	0.04
MN	0.00	0.00	0.00	0.00	0.00	0.00	0.00	0.00	0.00	0.00
K	0.67	0.59	0.71	0.90	0.92	0.81	0.82	0.81	0.89	0.41
NA	0.26	0.30	0.18	0.04	0.05	0.10	0.10	0.11	0.05	0.50
CA	0.00	0.00	0.00	0.00	0.00	0.00	0.00	0.00	0.00	0.02
BA	0.00	0.00	0.01	0.00	0.02	0.01	0.01	0.00	0.00	0.00
F	0.01	0.02	0.02	0.00	0.02	0.01	0.01	0.01	0.01	0.04
CL	0.00	0.00	0.00	0.00	0.00	0.00	0.00	0.00	0.00	0.00
OH(C)	1.99	1.98	1.98	2.00	1.98	1.99	1.99	1.99	1.99	1.96
O	9.97	9.88	9.95	9.97	10.01	9.94	9.96	9.96	9.95	9.95
FE/FE+MG	0.36	0.46	0.26	0.24	0.21	0.32	0.33	0.43	0.22	0.45
%MS	71.62	66.45	79.73	95.64	94.60	89.36	89.00	88.18	94.63	45.40
%PA	28.38	33.55	20.27	4.36	5.40	10.64	11.00	11.82	5.37	54.60

MUSCOVITE AND PARAGONITE

SAMPLE NO.	C4-32A	C4-32A	C4-32A	C4-32A	C4-32B	C4-32B	C4-32B	C4-32B	C4-32B	C4-46A
ANALYSIS	38S	46S	47S	48S	29S	30S	41S	43S	45S	33G
CORE/RIM										
SIO2	45.64	46.06	45.84	46.15	45.88	45.90	48.97	46.31	43.92	47.13
AL2O3	36.77	37.89	40.05	40.27	37.36	35.13	32.88	39.33	37.75	31.30
TIO2	0.26	0.31	0.19	0.12	0.23	0.37	0.39	0.11	0.21	1.19
FE2O3(C)	0.89	0.56	0.35	0.35	0.13	0.09	0.00	0.39	3.19	2.59
FEO(C)	0.00	0.00	0.00	0.00	0.24	0.61	0.99	0.00	0.00	0.31
MGO	0.73	0.47	0.22	0.15	0.29	0.71	1.71	0.24	0.97	1.85
MNO	0.00	0.02	0.01	0.01	0.01	0.00	0.00	0.04	0.01	0.05
K2O	6.45	6.55	2.67	2.18	2.76	7.88	9.27	2.41	2.28	10.58
NA2O	2.86	2.95	5.45	5.54	5.37	2.12	1.19	5.28	5.21	0.35
CAO	0.24	0.14	0.48	0.50	0.51	0.03	0.05	0.60	0.56	0.06
BAO	0.13	0.08	0.05	0.05	0.07	0.22	0.17	0.02	0.07	0.25
F	0.18	0.11	0.11	0.10	0.00	0.04	0.10	0.05	0.05	0.09
CL	0.00	0.00	0.00	0.00	0.00	0.00	0.01	0.00	0.02	0.00
H2O(C)	4.46	4.55	4.63	4.66	4.54	4.44	4.52	4.64	4.59	4.45
SUM	98.55	99.64	100.01	100.05	97.38	97.53	100.18	99.39	98.81	100.17
SI	3.01	3.00	2.93	2.94	3.03	3.09	3.22	2.97	2.85	3.14
AL(IV)	0.99	1.00	1.07	1.06	0.97	0.91	0.79	1.03	1.15	0.86
AL(VI)	1.87	1.91	1.95	1.96	1.94	1.87	1.76	1.95	1.74	1.61
TI	0.01	0.02	0.01	0.01	0.01	0.02	0.02	0.00	0.01	0.06
FE+3	0.04	0.03	0.02	0.02	0.01	0.00	0.00	0.02	0.16	0.13
FE+2	0.00	0.00	0.00	0.00	0.01	0.03	0.05	0.00	0.00	0.02
MG	0.07	0.05	0.02	0.01	0.03	0.07	0.17	0.02	0.09	0.18
MN	0.00	0.00	0.00	0.00	0.00	0.00	0.00	0.00	0.00	0.00
K	0.54	0.54	0.22	0.18	0.23	0.68	0.78	0.20	0.19	0.90
NA	0.37	0.37	0.68	0.68	0.69	0.28	0.15	0.66	0.65	0.05
CA	0.02	0.01	0.03	0.03	0.04	0.00	0.00	0.04	0.04	0.00
BA	0.00	0.00	0.00	0.00	0.00	0.01	0.00	0.00	0.00	0.01
F	0.04	0.02	0.02	0.02	0.00	0.01	0.02	0.01	0.01	0.02
CL	0.00	0.00	0.00	0.00	0.00	0.00	0.00	0.00	0.00	0.00
OH(C)	1.96	1.98	1.98	1.98	2.00	1.99	1.98	1.99	1.99	1.98
O	9.95	9.95	9.94	9.93	10.00	9.98	9.98	9.95	9.85	9.98
FE/FE+MG	0.38	0.37	0.45	0.54	0.41	0.35	0.24	0.45	0.62	0.44
%MS	59.72	59.38	24.33	20.59	25.24	70.95	83.65	23.12	22.36	95.19
%PA	40.28	40.62	75.67	79.41	74.76	29.05	16.35	76.88	77.64	4.81

MUSCOVITE AND PARAGONITE

SAMPLE NO.	C4-49B	C4-49B	D2-1CA	D2-1D	D2-1D	D2-1D	D2-1D
ANALYSIS	30S	40S	09S	07S	08S	43S	44S
CORE/RIM							
SIO2	47.20	46.35	46.57	45.79	45.80	45.32	45.54
AL2O3	34.82	35.32	35.39	34.42	35.35	36.38	36.38
TIO2	0.51	0.43	0.36	0.85	0.46	0.34	0.25
FE2O3(C)	0.00	0.10	0.36	0.03	0.19	0.94	0.94
FEO(C)	0.77	0.83	0.46	1.12	0.76	0.00	0.00
MGO	0.68	0.65	0.82	0.67	0.53	0.53	0.56
MNO	0.00	0.00	0.00	0.00	0.02	0.02	0.00
K2O	8.63	8.83	8.58	8.70	8.38	8.91	8.80
NA2O	1.72	1.64	1.73	1.53	1.80	1.92	1.84
CAO	0.03	0.02	0.02	0.05	0.05	0.06	0.05
BAO	0.15	0.15	0.19	0.50	0.46	0.34	0.28
F	0.07	0.10	0.02	0.10	0.03	0.00	0.00
CL	0.00	0.00	0.00	0.00	0.01	0.00	0.00
H2O(C)	4.48	4.45	4.51	4.40	4.45	4.49	4.50
SUM	99.04	98.84	99.02	98.12	98.27	99.24	99.16
SI	3.14	3.09	3.09	3.09	3.07	3.02	3.03
AL(IV)	0.86	0.91	0.91	0.91	0.93	0.98	0.97
AL(VI)	1.86	1.86	1.86	1.82	1.87	1.88	1.89
TI	0.03	0.02	0.02	0.04	0.02	0.02	0.01
FE+3	0.00	0.00	0.02	0.00	0.01	0.05	0.05
FE+2	0.04	0.05	0.03	0.06	0.04	0.00	0.00
MG	0.07	0.06	0.08	0.07	0.05	0.05	0.05
MN	0.00	0.00	0.00	0.00	0.00	0.00	0.00
K	0.73	0.75	0.73	0.75	0.72	0.76	0.75
NA	0.22	0.21	0.22	0.20	0.23	0.25	0.24
CA	0.00	0.00	0.00	0.00	0.00	0.00	0.00
BA	0.00	0.00	0.00	0.01	0.01	0.01	0.01
F	0.02	0.02	0.00	0.02	0.01	0.00	0.00
CL	0.00	0.00	0.00	0.00	0.00	0.00	0.00
OH(C)	1.98	1.98	1.99	1.98	1.99	2.00	2.00
O	10.01	9.99	9.98	9.99	9.99	10.01	10.00
FE/FE+MG	0.39	0.44	0.35	0.49	0.49	0.47	0.46
%MS	76.73	77.96	76.56	78.89	75.44	75.37	75.93
%PA	23.27	22.04	23.44	21.11	24.56	24.63	24.07

STAUROLITE

SAMPLE NO.	C3-19BB	C3-19BB	C3-19BB	C3-19BB	C3-19BB	C3-19BB	C4-32A	C4-32B	C4-32B	C4-49B
ANALYSIS	01S	02S	03S	04S	24S	40S	53S	31S	33S	QMIN1S
CORE/RIM	C	C	C	R		R	R	R	R	
SIO2	27.72	28.07	27.60	27.99	28.28	28.13	27.68	28.18	28.22	28.78
AL2O3	55.78	55.72	54.99	56.14	55.70	55.59	55.48	55.69	55.72	55.38
TIO2	0.61	0.65	0.56	0.59	0.56	0.59	0.56	0.72	0.63	0.52
CR2O3	0.02	0.01	0.01	0.04	0.05	0.05	0.02	0.03	0.01	0.00
FEO	13.58	13.59	13.63	13.39	13.17	13.38	13.14	12.99	13.05	13.28
MGO	2.13	2.16	2.08	2.11	2.44	2.14	1.85	2.18	2.14	2.13
MNO	0.10	0.10	0.10	0.10	0.08	0.07	0.23	0.14	0.11	0.18
NA2O	0.01	0.00	0.01	0.02	0.00	0.00	0.04	0.00	0.02	0.05
K2O	0.02	0.01	0.01	0.01	0.01	0.01	0.01	0.01	0.01	0.01
CAO	0.02	0.02	0.02	0.02	0.01	0.02	0.01	0.01	0.02	0.01
F	0.03	0.07	0.00	0.04	0.02	0.01	0.03	0.02	0.00	0.00
H2O(C)	1.66	1.65	1.66	1.66	1.67	1.67	1.65	1.67	1.68	1.69
SUM	100.01	100.42	98.99	100.46	100.32	99.98	99.05	99.97	99.90	100.34
SI	7.59	7.66	7.64	7.62	7.70	7.69	7.64	7.69	7.71	7.83
AL	18.01	17.91	17.94	18.02	17.88	17.91	18.05	17.92	17.94	17.76
TI	0.13	0.13	0.12	0.12	0.11	0.12	0.12	0.15	0.13	0.11
CR	0.00	0.00	0.00	0.01	0.01	0.01	0.00	0.01	0.00	0.00
FE	3.11	3.10	3.16	3.05	3.00	3.06	3.03	2.97	2.98	3.02
MG	0.87	0.88	0.86	0.86	0.99	0.87	0.76	0.89	0.87	0.86
MN	0.02	0.02	0.02	0.02	0.02	0.02	0.05	0.03	0.02	0.04
NA	0.01	0.00	0.00	0.01	0.00	0.00	0.02	0.00	0.01	0.03
K	0.00	0.00	0.00	0.00	0.00	0.00	0.00	0.00	0.00	0.00
CA	0.01	0.01	0.00	0.01	0.00	0.01	0.00	0.00	0.00	0.00
F	0.03	0.06	0.00	0.04	0.02	0.01	0.03	0.02	0.00	0.00
H	3.03	3.00	3.06	3.02	3.04	3.05	3.03	3.04	3.06	3.06
O	47.99	47.97	48.00	47.98	47.99	48.00	47.99	47.99	48.00	48.00
FE/FE+MG	0.78	0.78	0.79	0.78	0.75	0.78	0.80	0.77	0.77	0.78
A	0.69	0.69	0.69	0.70	0.69	0.69	0.70	0.70	0.70	0.69
F	0.24	0.24	0.24	0.24	0.23	0.24	0.24	0.23	0.23	0.24
M	0.07	0.07	0.07	0.07	0.08	0.07	0.06	0.07	0.07	0.07

STAUROLITE

SAMPLE NO.	C4-49B	C4-49B	D2-1CA	D2-1CA	D2-1CA	D2-1D	D2-1D
ANALYSIS	QMIN2S	26S	10S	11S	12S	51S	52S
CORE/RIM			C	R	R		
SIO2	28.82	28.83	27.94	28.57	28.34	27.88	27.89
AL2O3	54.78	53.68	54.90	55.98	55.57	54.30	55.13
TIO2	0.52	0.67	0.60	0.58	0.61	0.70	0.56
CR2O3	0.00	0.01	0.03	0.03	0.02	0.00	0.04
FEO	13.07	13.09	12.83	13.34	13.13	13.38	13.22
MGO	1.96	1.94	2.27	2.45	2.50	2.00	2.07
MNO	0.20	0.12	0.09	0.11	0.10	0.10	0.09
NA2O	0.03	0.07	0.03	0.00	0.06	0.00	0.03
K2O	0.00	0.07	0.01	0.01	0.01	0.01	0.01
CAO	0.00	0.01	0.02	0.02	0.07	0.03	0.01
F	0.00	0.06	0.02	0.00	0.01	0.03	0.05
H2O(C)	1.67	1.63	1.65	1.70	1.68	1.64	1.64
SUM	99.38	98.56	98.72	101.06	100.35	98.42	99.11
SI	7.91	7.99	7.72	7.72	7.71	7.75	7.70
AL	17.72	17.54	17.88	17.83	17.82	17.80	17.93
TI	0.11	0.14	0.13	0.12	0.13	0.15	0.12
CR	0.00	0.00	0.01	0.01	0.00	0.00	0.01
FE	3.00	3.03	2.97	3.02	2.99	3.11	3.05
MG	0.80	0.80	0.94	0.99	1.01	0.83	0.85
MN	0.05	0.03	0.02	0.02	0.02	0.02	0.02
NA	0.01	0.04	0.02	0.00	0.03	0.00	0.02
K	0.00	0.02	0.00	0.00	0.00	0.00	0.00
CA	0.00	0.00	0.01	0.00	0.02	0.01	0.00
F	0.00	0.05	0.01	0.00	0.01	0.02	0.04
H	3.06	3.01	3.05	3.06	3.05	3.04	3.02
O	48.00	47.97	47.99	48.00	48.00	47.99	47.98
FE/FE+MG	0.79	0.79	0.76	0.75	0.75	0.79	0.78
A	0.70	0.69	0.70	0.69	0.69	0.69	0.70
F	0.24	0.24	0.23	0.23	0.23	0.24	0.24
M	0.06	0.06	0.07	0.08	0.08	0.06	0.07

Appendix B. X-Ray Fluorescence Analyses

Major element, bulk chemical analyses were performed using the methods outlined in Norrish and Chappell (1967) using a fused disk method for all elements except sodium, which used a pressed pellet method. Samples were analyzed on a Philips 1450 X-ray fluorescence spectrometer with a chrome tube, flow proportional detector, and using K-alpha lines. Standards used were U.S. Geological Survey Standards PCC, AGV, BCR, G2, and GSP.

Reference

Norrish, K and Chappell, B.W., 1967, X-ray fluorescence spectrography: in Zussman, J., ed., *Physical Methods in Determinative Mineralogy*: New York, Academic Press, p. 161-214.

XRF DATA, MAJOR ELEMENT ANALYSES, METASEDIMENTS

Sample	A2-3Y	A2-4A	A4-6Z	B4-7Z	B4-11O	D4-1Z	A2-1Z	C4-32B
SiO_2	75.83	75.92	72.52	70.39	71.14	77.27	54.46	47.63
TiO_2	0.15	0.49	0.84	0.88	0.88	0.65	0.99	1.09
Al_2O_3	13.42	9.84	12.94	13.51	10.55	11.17	24.58	29.77
Fe_2O_3	1.46	2.48	3.68	3.70	5.73	2.44	6.72	7.34
MnO	0.02	0.04	0.08	0.07	0.28	0.04	0.06	0.18
MgO	0.30	0.77	1.25	1.96	4.52	0.32	2.90	2.44
CaO	0.07	1.76	2.37	1.44	0.43	0.49	0.15	1.38
Na_2O	4.68	1.43	3.74	3.06	0.31	3.06	1.37	2.99
K_2O	2.85	3.77	1.26	2.36	1.55	3.22	4.22	3.24
P_2O_5	0.04	0.07	0.18	0.21	0.20	0.16	0.24	0.20
Loss	1.37	2.59	0.69	1.34	2.90	1.07	5.19	2.74
Sum	100.19	99.17	99.55	98.92	98.50	99.90	100.87	98.99

A2-3Y Quartz mylonite, Ashe Formation
A2-4A Quartz mylonite, Bowers Ferry Block
A4-6Z Quartz-plagioclase-biotite-muscovite gneiss, Ashe Formation
B4-7Z Biotite-quartz-plagioclase gneiss, Ashe Formation
B4-11O Chlorite-biotite-quartz gneiss, Bumbarger Pit, Gossan Lead, Ashe Formation
D4-1Z Biotite-muscovite gneiss, Ashe Formation
A2-1Z Graphite-muscovite-quartz phyllite, Ashe Formation
C4-32B Biotite-paragonite-muscovite-staurolite-garnet-quartz-plagioclase schist, Ashe Formation

XRF DATA, MAJOR ELEMENT ANALYSES, MAFIC ROCKS

Sample	A2-3X	A4-3ZA	B3-74Z	B3-162Z	B4-9Z	B4-13Z	B4-16X	B4-16Y
SiO_2	44.13	50.54	48.74	48.11	41.50	49.46	47.23	50.90
TiO_2	3.27	1.32	1.32	1.13	1.46	2.13	1.50	0.26
Al_2O_3	16.07	15.83	15.56	13.54	9.03	14.02	16.41	13.92
Fe_2O_3	13.45	9.30	10.92	10.07	14.63	10.35	9.69	10.18
MnO	0.18	0.16	0.17	0.21	0.24	0.17	0.18	0.15
MgO	3.57	7.51	6.47	10.08	20.77	6.77	9.33	8.53
CaO	7.14	11.13	12.82	13.18	6.85	9.74	8.72	11.03
Na_2O	2.37	2.46	1.16	1.01	0.0	1.33	2.02	0.46
K_2O	0.98	0.15	0.11	0.04	0.0	1.13	0.55	0.29
P_2O_5	0.81	0.0	0.0	0.13	0.16	0.22	0.14	0.08
Loss	5.55	1.33	1.46	1.38	5.83	3.03	2.01	2.13
Sum	97.47	99.73	98.54	99.07	100.46	98.35	97.84	97.97

Sample	C3-117Y	C3-117Z
SiO_2	47.80	47.65
TiO_2	2.08	3.16
Al_2O_3	15.77	15.13
Fe_2O_3	10.08	13.51
MnO	0.20	0.24
MgO	8.58	5.86
CaO	9.84	9.61
Na_2O	2.11	1.22
K_2O	0.21	0.30
P_2O_5	0.21	0.36
Loss	1.18	0.75
Sum	98.78	97.78

A2-3X Mylonitized biotite-chlorite-plagioclase amphibolite with minor carbonates, Bowers Ferry Block
A4-3ZA Coarse hornblende-plagioclase amphibolite, Ashe Formation
B4-74Z Coarse hornblende-plagioclase amphibolite, Ashe Formation
B3-162Z Coarse hornblende-plagioclase-clinozoisite amphibolite, Ashe Formation
B4-9Z Pale green amphibole-chlorite schist, Ashe Formation
B4-13Z Medium grained hornblende-plagioclase biotite-chlorite amphibolite, Ashe Formation
B4-16X Coarse hornblende-plagioclase amphibolite, Ashe Formation
B4-16Y Medium grained hornblende-plagioclase amphibolite, Ashe Formation
C3-117Y Coare hornblende-plagioclase amphibolite, Ashe Formation
C3-117Z Medium grained hornblende-plagioclase-garnet amphibolite, Ashe Formation

Appendix C. Thin Section Mineralogy

MODAL % OF REPRESENTATIVE SAMPLES

ASHE METASEDIMENTS (500 pts)

Sample	A4-6A	B2-35C	B3-175A	B4-7B	C4-32B	D2-1D
Quartz	45.2	27.4	4.0	33.8	23.8	2.2
Plagioclase	32.6	19.6	0.8	44.8	6.4	23.2
Muscovite	0.4	21.6	77.2	5.6	32.6*	13.0
Biotite	19.8	18.8	3.2	11.4	16.0	4.0
Chlorite	0.8	8.0	9.6	3.4	2.0	10.4
Garnet	0.8	0.4	2.0	tr	5.2	0.4
Staurolite	-	-	-	-	13.4	24.0
Kyanite	-	-	-	-	-	20.4
Zircon	tr	0.8	0.2	-	tr	-
Apatite	tr	tr	0.4	0.2	tr	tr
Rutile	-	-	0.4	0.2	0.3	-
Ilmenite	0.4	1.2	0.2	-	0.3	2.4
Clinozoisite	-	1.2	-	-	-	-
Pyrrhotite	-	1.2	2.2	0.6	-	tr

*-includes paragonite+muscovite

A4-6A Medium grained biotite gneiss
B2-35B Pale green chlorite-muscovite-biotite phyllite
B3-175A Biotite-muscovite-garnet schist from the Gossan Howard Mine dump
B4-7B Medium grained biotite-quartz gneiss
C4-32B Staurolite-muscovite schist
D2-1D Kyanite-chlorite-plagioclase rock associated with quartz vein material

MODAL % OF REPRESENTATIVE SAMPLES

ASHE AMPHIBOLITES (500 pts)

SAMPLE	A3-43B	A4-22A	B2-35C	B3-127A	B3-170A	B4-9B	C3-117A	C3-117B
Plagioclase	11.2	5.0	-	25.4	50.4	-	9.6	27.8
Amphibole	62.6	65.6	60.2	59.0	40.8	69.8	65.2	67.6
Clinozoisite	0.8	2.2	15.2	1.2	-	-	0.2	0.4
Sphene	3.0	3.2	3.6	3.2	2.2	-	-	2.0
Ilmenite	-	-	-	-	-	1.0	2.4	-
Pyrrhotite	0.4	tr	-	tr	5.6	-	-	-
Chlorite	19.4	7.6	7.4	11.2	tr	29.2	0.2	1.0
Quartz	2.6	16.4	13.0	-	-	-	19.8	1.0
Biotite	-	-	-	-	-	-	-	-
Apatite	tr	-	-	-	-	-	tr	tr
Zircon	-	-	0.6	-	-	-	-	tr
Rutile	-	-	-	tr	-	-	tr	tr
Chalcopyrite	-	-	-	-	tr	-	-	0.2
Garnet	-	-	-	-	-	-	2.6	-

A3-43B Coarse-layered amphibolite
A4-22A Medium-grained hornblende schist
B2-35C Medium-grained hornblende schist
B3-127A Coarse-grained metagabbro
B3-170A Actinolite-plagioclase rock from Gossan Lead sulfide zone
B4-9B Actinolite-chlorite schist
C3-117A Spotted amphibolite
C3-117B Coarse-layered amphibolite

UNICOI FORMATION

SAMPLE	A2-15A	A2-15B	A2-27B
Quartz	+	+	+
Plagioclase	+	+	+
Muscovite	+	m	tr
Biotite	-	-	m
Chlorite	m	+	m
K-feldspar	m	+	m
Carbonate	tr	-	m
Pyrite	tr	-	-
Rutile	m	m	tr
Tourmaline	-	-	tr
Apatite	tr	-	-
Zircon	tr	tr	-

Abbreviations: + = >10%, m = >1%, <10%, tr = < 1%, p = primary, r = retrograde

BOWERS FERRY THRUST SHEET

SAMPLE	A2-3E	A2-3F	A2-3HA	A2-4A	A2-6B	A2-54A	A2-62B
Quartz	+	+	+	+	+	+	+
Plagioclase	+	+	+	+	+	+	+
Muscovite	m	m	+	m	m	+	+
Biotite	-	-	tr	-	-	-	-
Chlorite	tr	-	-	-	-	m	-
K-feldspar	-	-	-	-	tr	-	-
Carbonate	m	-	+	m	-	-	-
Pyrite	-	tr	m	-	-	tr	tr
Pyrrhotite	-	-	-	tr	-	tr	-
Rutile	tr	tr	m	tr	tr	tr	m
Ilmenite	-	-	tr	tr	-	-	-
Apatite	-	tr	tr	-	tr	-	-
Zircon	-	-	tr	tr	tr	tr	tr

CRANBERRY GNEISS

SAMPLE	A1-1A	A1-1B	A1-1D	A2-3A	A2-3B	A2-3Z	A2-13A
Quartz	+	+	+	+	+	+	+
Plagioclase	+	+	+	+	+	+	+
Muscovite	m	+	+	+	m	m	m
Biotite	tr	-	tr	-	-	-	tr
Chlorite	-	-	-	-	-	-	tr
K-feldspar	-	tr	-	tr	m	-	-
Epidote	tr	-	tr	-	-	-	-
Sphene	-	-	tr	-	-	tr	tr
Carbontate	tr	-	-	-	-	m	-
Pyrite	tr	-	-	-	-	-	-
Pyrrhotite	-	tr	-	-	-	-	-
Rutile	-	-	-	tr	tr	tr	-
Magnetite	-	-	tr	tr	tr	tr	tr
Ilmenite	-	-	m	-	-	-	tr
Tourmaline	-	-	tr	-	-	-	-
Apatite	tr	-	tr	-	tr	tr	tr
Zircon	tr	tr	tr	tr	tr	tr	tr

CRANBERRY GNEISS

SAMPLE	A2-14A	A2-25B
Quartz	+	+
Plagioclase	+	+
Muscovite	-	m
Biotite	tr	tr
Chlorite	tr	-
K-feldspar	m	m
Epidote	m	-
Sphene	tr	-
Carbonate	tr	-
Pyrite	-	-
Pyrrhotite	-	-
Rutile	-	tr
Magnetite	tr	-
Ilmenite	tr	-
Tourmaline	-	-
Apatite	-	-
Zircon	tr	tr

ASHE FORMATION METASEDIMENTS

SAMPLE	A2-1A	A2-11A	A2-19A	A2-21B	A2-22A	A3-1B	A3-3A
Quartz	tr	+	+	+	m	+	+
Plagioclase	m	m	+	+	-	m	+
Muscovite	+	+	m	+	+	+	+
Chlorite	m(p)	tr(p)	-	tr(p)	+	tr(p,r)	m(p)
Biotite	-	-	+	+	-	-	tr
Garnet	-	-	-	-	-	tr	tr
Staurolite	-	-	-	-	-	-	-
Paragonite	-	-	-	-	-	-	-
Kyanite	-	-	-	-	-	-	-
Clinozoisite	-	-	-	-	-	-	-
Carbonate	-	-	-	-	-	-	-
K-feldspar	-	-	-	-	-	-	-
Graphite	tr	-	-	-	m	tr	tr
Ilmenite	m	m	-	-	-	m	tr
Rutile	-	-	tr	-	tr	-	tr
Sphene	-	-	-	-	-	-	-
Magnetite	-	-	-	-	-	-	-
Pyrrhotite	-	-	-	-	-	-	-
Tourmaline	tr	tr	-	-	-	-	-
Apatite	-	tr	-	-	-	tr	-
Zircon	tr	tr	tr	-	tr	tr	-

ASHE FORMATION METASEDIMENTS

SAMPLE	A3-4A	A3-7A	A3-11A	A3-11B	A3-30A	A4-2A	A4-6A
Quartz	+	+	+	+	+	+	+
Plagioclase	+	+	m	+	m	+	+
Muscovite	+	+	+	m	+	m	tr
Chlorite	tr(p,r)	m(p)	tr(p)	tr(p,r)	m(p,r)	tr(r)	tr(p,r)
Biotite	tr	tr	-	tr	m	m	+
Garnet	-	-	-	-	m	tr	tr
Staurolite	-	-	-	-	-	-	-
Paragonite	-	-	-	-	-	-	-
Kyanite	-	-	-	-	-	-	-
Clinozoisite	-	-	-	-	-	-	-
Carbonate	-	-	-	-	-	-	-
K-feldspar	-	-	-	-	-	-	-
Graphite	-	tr	tr	-	tr	-	-
Ilmenite	tr	tr	m	tr	m	tr	tr
Rutile	-	-	-	tr	-	tr	-
Sphene	-	-	-	-	-	tr	tr
Magnetite	-	-	-	tr	-	-	-
Pyrrhotite	-	-	-	-	tr	-	-
Tourmaline	tr	-	tr	-	-	-	-
Apatite	tr	tr	-	tr	tr	tr	tr
Zircon	tr	-	-	-	-	-	tr

ASHE FORMATION METASEDIMENTS

SAMPLE	A4-8A	A4-19A	B2-1A	B2-1B	B2-1Y	B2-3A	B2-35A
Quartz	+	+	+	+	+	+	+
Plagioclase	+	+	+	+	+	+	+
Muscovite	m	+	+	-	tr	m	m
Chlorite	tr(r)	tr(p,r)	tr(p)	m(p)	tr(p)	tr(p)	tr(p)
Biotite	m	m	+	m	m	+	m
Garnet	m	tr	m	-	m	m	tr
Staurolite	-	-	-	-	-	-	-
Paragonite	-	-	-	-	-	-	-
Kyanite	-	-	-	-	-	-	-
Clinozoisite	-	-	m	tr	m	tr(al)	-
Carbonate	-	-	-	m	tr	-	-
K-feldspar	-	-	-	-	-	-	-
Graphite	-	tr	tr	-	-	-	tr
Ilmenite	m	-	-	-	-	-	tr
Rutile	-	m	-	-	-	-	-
Sphene	-	-	tr	tr	m	-	-
Magnetite	-	-	-	-	-	-	-
Pyrrhotite	-	-	tr	m	tr	-	tr
Tourmaline	-	tr	-	-	-	-	-
Apatite	tr	tr	tr	tr	tr	tr	tr
Zircon	tr	tr	tr	tr	tr	-	tr

ASHE FORMATION METASEDIMENTS

SAMPLE	B2-35B	B3-9A	B3-25B	B3-30A	B3-63A	B3-101A	B3-117A
Quartz	+	-	m	tr	+	+	m
Plagioclase	+	-	-	-	-	-	-
Muscovite	+	+	-	+	tr	tr	m
Chlorite	m(p)	-	+(p)	m(p)	+(p)	+(p)	+(p)
Biotite	+	-	tr	-	tr	-	-
Garnet	tr	-	m	m	+	m	+
Staurolite	-	-	-	-	-	-	-
Paragonite	-	-	-	-	-	-	-
Kyanite	-	-	-	-	-	-	-
Clinozoisite	tr	-	-	-	-	-	-
Carbonate	-	-	-	-	-	-	-
K-feldspar	-	-	-	-	-	-	-
Graphite	-	m	tr	-	-	tr	-
Ilmenite	m	-	m	m	m	tr	m
Rutile	-	-	-	-	-	-	-
Sphene	-	-	-	-	-	-	-
Magnetite	-	-	-	-	-	-	-
Pyrrhotite	-	-	-	-	-	-	-
Tourmaline	-	-	-	-	-	-	-
Apatite	tr	-	tr	-	-	-	-
Zircon	tr	-	tr	-	tr	tr	-

ASHE FORMATION METASEDIMENTS

SAMPLE	B3-117B	B3-141A	B3-156A	B3-156AA	B3-165A	B3-185A	B4-7B
Quartz	m	+	+	+	+	+	+
Plagioclase	-	+	-	+	-	+	+
Muscovite	+	m	tr	+	+	m	m
Chlorite	tr(p)	tr(p)	+(p)	m(p)	+(p)	tr(p,r)	m(r)
Biotite	m	m	-	+	+	+	+
Garnet	m	-	m	m	-	m	tr
Staurolite	-	-	-	-	-	-	-
Paragonite	-	-	-	-	-	-	-
Kyanite	-	-	-	-	-	-	-
Clinozoisite	-	tr	-	-	-	-	-
Carbonate	-	-	-	-	-	-	-
K-feldspar	-	-	-	-	-	-	-
Graphite	-	-	-	tr	-	tr	-
Ilmenite	tr	-	tr	tr	m	m	-
Rutile	-	tr	tr	-	-	-	tr
Sphene	-	-	-	tr	-	-	-
Magnetite	-	-	-	-	-	-	-
Pyrrhotite	-	-	-	m	-	tr	tr
Tourmaline	-	-	-	-	-	tr	-
Apatite	-	tr	-	tr	tr	tr	-
Zircon	-	tr	tr	tr	tr	tr	-

ASHE FORMATION METASEDIMENTS

SAMPLE	B4-27B	B4-32B	B4-93A	B4-101A	B4-140A	B4-141A	C3-2B
Quartz	+	+	+	m	+	+	+
Plagioclase	+	+	+	+	m	+	+
Muscovite	+	+	+	m	+	+	m
Chlorite	-	-	tr(r)	m(p)	m(p)	tr(p,r)	tr(p)
Biotite	+	+	m	+	tr	m	m
Garnet	-	tr	m	tr	m	tr	tr
Staurolite	-	-	-	-	-	-	-
Paragonite	-	-	-	-	-	-	-
Kyanite	-	-	-	-	-	-	-
Clinozoisite	-	-	-	-	-	-	-
Carbonate	-	-	-	-	-	-	-
K-feldspar	-	-	-	-	-	-	-
Graphite	tr	tr	-	-	tr	tr	tr
Ilmenite	tr	tr	tr	tr	tr	tr	tr
Rutile	-	-	-	-	-	-	-
Sphene	-	-	-	-	-	-	-
Magnetite	-	-	-	-	-	-	-
Pyrrhotite	-	-	-	-	-	m	tr
Tourmaline	-	-	-	-	-	-	-
Apatite	-	-	tr	tr	-	-	tr
Zircon	tr	tr	tr	tr	-	-	tr

ASHE FORMATION METASEDIMENTS

SAMPLE	C3-2G	C3-19B	C3-56A	C3-68A	C3-78A	C3-122A	C4-32A
Quartz	+	+	+	+	+	+	m
Plagioclase	+	m	+	+	-	+	+
Muscovite	+	+	m	m	+	-	+
Chlorite	tr(r)	tr(r)	-	tr(r)	-	m(p)	m(p,r)
Biotite	+	m	tr	m	tr	tr	m
Garnet	-	+	-	tr	tr	tr	m
Staurolite	-	m	-	-	-	-	+
Paragonite	-	-	-	-	-	-	m
Kyanite	-	-	-	-	-	-	-
Clinozoisite	-	-	-	-	-	-	-
Carbonate	-	-	-	-	-	-	-
K-feldspar	-	-	-	-	-	-	-
Graphite	tr	-	-	-	-	-	-
Ilmenite	tr	tr	-	-	-	m	tr
Rutile	-	-	tr	tr	-	-	tr
Sphene	-	-	-	-	-	-	-
Magnetite	-	-	-	-	-	-	-
Pyrrhotite	-	tr	-	-	-	-	-
Tourmaline	-	-	-	-	-	-	-
Apatite	tr	tr	-	tr	-	tr	tr
Zircon	tr	tr	-	tr	-	tr	-

ASHE FORMATION METASEDIMENTS

SAMPLE	C4-32B	C4-46A	C4-49B	D2-1CA	D2-1D
Quartz	+	+	+	m	m
Plagioclase	m	+	+	+	+
Muscovite	+	m	+	+	+
Chlorite	m(p,r)	-	+(p,r)	tr(r)	+(r)
Biotite	+	m	m	m	m
Garnet	m	-	m	m	tr
Staurolite	+	-	m	+	+
Paragonite	+	-	-	-	-
Kyanite	-	-	-	-	+
Clinozoisite	-	-	-	-	-
Carbonate	-	-	-	-	-
K-feldspar	-	m	-	-	-
Graphite	-	-	tr	-	-
Ilmenite	tr	-	m	tr	m
Rutile	tr	m	-	-	-
Sphene	-	-	-	-	-
Magnetite	-	-	-	-	-
Pyrrhotite	-	-	m	-	-
Tourmaline	-	-	tr	tr	-
Apatite	tr	tr	-	tr	tr
Zircon	tr	tr	tr	tr	tr

MAFIC ROCKS

SAMPLE	A2-3C	A2-3D	A2-62A	A2-66A	A3-43B	A3-70A	A3-71A
Plagioclase	+	+	+	+	+	+	+
Amphibole	-	-	+	-	+	+	+
Clinozoisite	m(ep)	tr(ep)	m	m(ep)	tr	m	m(ep)
Sphene	tr	m	-	m	-	-	m
Ilmenite	tr	tr	-	tr	m	m	tr
Pyrrhotite	-	-	-	-	tr	-	-
Stilpnomelane	m	tr	-	m	-	-	-
White Mica	-	-	-	tr(r)	-	-	-
K-feldspar	-	-	-	-	-	-	-
Hematite	-	-	tr(r)	-	-	-	-
Garnet	-	-	-	-	-	-	-
Rutile	-	-	m	-	-	-	-
Carbonate	m	m	-	-	-	-	-
Chlorite	m	+	tr	-	+	tr	m
Quartz	tr	m	-	-	m	-	m
Biotite	+	tr	-	m	-	-	-
Apatite	tr	tr	-	-	tr	tr	-
Pyrite	tr	tr	-	-	-	-	-
Magnetite	-	-	-	-	-	-	-
Zircon	-	-	-	-	-	-	-

MAFIC ROCKS

SAMPLE	A3-92A	A3-71A	A3-92A	A3-105A	A4-2A	A4-20A	A4-22A
Plagioclase	+	+	+	+	+	+	m
Amphibole	+	+	+	+	+	+	+
Clinozoisite	m	m(ep)	+	m	m	-	tr
Sphene	-	m	tr	tr	m	-	m
Ilmenite	m	tr	-	tr	-	tr	-
Pyrrhotite	-	-	-	m	tr	tr	tr
Stilpnomelane	-	-	-	-	-	-	-
White Mica	-	-	-	-	-	-	-
K-feldspar	-	-	-	-	-	-	-
Hematite	-	-	-	-	-	tr(r)	-
Garnet	-	-	-	-	-	-	-
Rutile	-	-	-	tr	tr	tr	-
Carbonate	-	-	-	-	-	-	-
Chlorite	tr	m	+	m	tr	+	+
Quartz	-	m	m	+	-	tr	+
Biotite	-	-	-	-	-	tr	-
Apatite	tr	-	-	-	-	-	-
Pyrite	-	-	-	-	-	-	-
Magnetite	-	-	-	-	-	-	-
Zircon	-	-	-	-	-	-	-

MAFIC ROCKS

SAMPLE	B2-4A	B2-24A	B2-35C	B3-74A	B3-75A	B3-127A	B3-170A
Plagioclase	+	+	-	+	+	+	+
Amphibole	+	+	+	+	+	+	+
Clinozoisite	m	+	+	+	m	m	-
Sphene	m	-	m	m	m	m	m
Ilmenite	-	-	-	-	-	-	-
Pyrrhotite	tr	-	-	-	-	tr	m
Stilpnomelane	-	-	-	-	-	-	-
White Mica	-	-	-	-	-	-	-
K-feldspar	-	-	-	-	-	-	-
Hematite	-	-	-	-	tr(r)	-	tr(r)
Garnet	-	-	-	-	-	-	tr
Rutile	-	-	-	-	-	tr	-
Carbonate	-	-	-	-	-	-	-
Chlorite	tr	m	m	tr	-	+	tr
Quartz	+	-	+	m	m	-	-
Biotite	tr	-	-	-	-	-	-
Apatite	-	-	-	-	-	-	-
Pyrite(cpy)	-	-	-	-	-	-	tr(cpy)
Magnetite	-	-	-	-	-	-	-
Zircon	-	-	tr	-	tr	-	-

MAFIC ROCKS

SAMPLE	B3-260A	B4-7C	B4-8B	B4-9B	B4-11A	B4-13A	B4-45A
Plagioclase	m	+	+	-	+	+	+
Amphibole	+	+	+	+	+	+	+
Clinozoisite	m	m	m	-	+	tr	m
Sphene	m	tr	tr	-	tr	tr	m
Ilmenite	-	-	-	tr	-	tr	-
Pyrrhotite	tr	tr	-	-	-	tr	tr
Stilpnomelane	-	-	-	-	-	-	-
White Mica	-	tr(r)	-	-	-	-	-
K-feldspar	-	tr	-	-	-	-	-
Hematite	tr(r)	-	-	-	-	-	tr(r)
Garnet	-	-	tr	-	-	-	-
Rutile	-	tr	-	-	tr	tr	-
Carbonate	-	-	-	-	-	-	-
Chlorite	tr	+	-	+	-	tr	tr
Quartz	m	-	+	-	-	tr	-
Biotite	tr	tr	-	-	-	m	-
Apatite	-	-	-	-	-	tr	-
Pyrite(cpy)	-	tr(cpy)	tr	-	-	-	-
Magnetite	-	-	-	-	-	-	-
Zircon	-	-	-	-	-	-	-

MAFIC ROCKS

SAMPLE	B4-74A	B4-84A	B4-100A	C3-1E	C3-4A	C3-5A	C3-17B
Plagioclase	+	tr	-	m	+	-	+
Amphibole	+	+	+	+	+	+	+
Clinozoisite	m	-	-	tr	-	-	tr
Sphene	-	-	-	m	tr	tr	tr
Ilmenite	-	m	m	-	m	-	m
Pyrrhotite	tr	tr	-	tr	tr	-	-
Stilpnomelane	-	-	-	-	-	-	-
White Mica	-	-	-	-	-	-	-
K-feldspar	-	-	-	-	-	-	-
Hematite	-	tr(r)	-	tr(r)	-	-	-
Garnet	-	-	-	-	-	-	-
Rutile	-	-	-	tr	tr	tr	-
Carbonate	-	-	-	-	-	-	-
Chlorite	-	+	+	m	tr	+	-
Quartz	m	-	-	+	-	-	m
Biotite	-	-	-	-	-	-	-
Apatite	-	-	-	-	-	-	-
Pyrite	-	-	-	-	-	-	-
Magnetite	-	-	-	-	-	-	-
Zircon	-	-	-	-	-	-	tr

MAFIC ROCKS

SAMPLE	C3-27A	C3-32B	C3-40A	C3-55A	C3-77A	C3-89B	C3-116A
Plagioclase	m	-	+	+	+	+	m
Amphibole	+	+	+	m	+	+	+
Clinozoisite	tr	-	tr	tr	-	m	tr
Sphene	tr	-	m	m	tr	tr	tr
Ilmenite	-	-	-	tr	tr	-	-
Pyrrhotite	-	-	-	-	-	-	-
Stilpnomelane	-	-	-	-	-	-	-
White Mica	-	-	-	-	-	-	-
K-feldspar	-	-	-	-	-	-	-
Hematite	-	-	-	-	-	-	-
Garnet	-	-	-	-	-	-	-
Rutile	tr	tr	-	-	-	-	tr
Carbonate	-	-	-	-	-	-	-
Chlorite	tr	+	-	-	tr	tr	tr
Quartz	m	tr	tr	-	tr	-	+
Biotite	-	-	-	-	-	m	-
Apatite	tr	-	-	-	tr	-	tr
Pyrite	-	-	-	-	-	-	-
Magnetite	-	-	-	-	-	-	-
Zircon	-	-	-	tr	-	-	-
Talc	-	tr	-	-	-	-	-

MAFIC ROCKS

SAMPLE	C3-117A	C3-117B	C4-1C	C4-17A	C4-20B	C4-24A	C4-24B
Plagioclase	m	+	+	+	m	+	+
Amphibole	+	+	+	m	+	+	+
Clinozoisite	tr	tr	tr	-	m(ep)	-	-
Sphene	-	m	tr	-	-	-	-
Ilmenite	m	-	-	-	tr	m	m
Pyrrhotite	-	-	-	-	-	-	-
Stilpnomelane	-	-	-	-	-	-	-
White Mica	-	-	-	tr	-	-	-
K-feldspar	-	-	-	-	-	-	-
Hematite	-	-	-	-	tr(r)	-	-
Garnet	m	-	-	-	-	-	-
Rutile	-	tr	tr	tr	tr	tr	-
Carbonate	-	-	-	-	-	-	-
Chlorite	tr	m	tr	tr	-	tr	tr
Quartz	+	m	m	+	+	tr	tr
Biotite	-	-	tr	-	-	-	-
Apatite	tr	tr	tr	tr	tr	-	-
Pyrite(cpy)	-	tr(cpy)	-	-	-	-	-
Magnetite	-	-	-	-	-	-	-
Zircon	-	tr	tr	-	-	-	-

MAFIC ROCKS

SAMPLE	C4-25A	C4-36A	C4-47A	C4-49A
Plagioclase	+	+	+	+
Amphibole	+	+	+	+
Clinozoisite	tr	m	tr	m
Sphene	m	tr	m	m
Ilmenite	tr	m	m	-
Pyrrhotite	-	-	tr	tr
Stilpnomelane	-	-	-	-
White Mica	-	-	-	-
K-feldspar	-	-	-	-
Hematite	tr(r)	-	tr(r)	tr(r)
Garnet	-	-	-	-
Rutile	-	tr	tr	tr
Carbonate	-	-	-	-
Chlorite	tr	tr	tr	tr
Quartz	tr	m	-	tr
Biotite	-	-	-	-
Apatite	-	tr	-	-
Pyrite	-	-	-	-
Magnetite	-	-	-	-
Zircon	-	-	-	-

ORE ZONE ROCKS

SAMPLE	A4-7C	B4-1D	B4-11E	B4-11J	B4-11K	B4-11KA	B4-11L
Quartz	+	-	-	-	+	m	m
Plagioclase	-	tr	tr	-	+	-	m
Muscovite	-	-	-	-	-	-	+
Biotite	tr	+	-	m	+	m	m
Chlorite	+	+	+	m	tr	m	m
Garnet	-	+	-	-	-	-	-
Zircon	tr	tr	tr	-	tr	-	tr
Apatite	tr	tr	m	tr	tr	tr	tr
Hematite	-	tr(r)	-	m(r)	-	m(r)	-
Rutile	-	m	tr	tr	tr	tr	-
Ilmenite	tr	-	-	-	-	-	tr
Pyrrhotite	-	-	-	+	m	+	m
Graphite	-	-	-	-	-	-	tr
Tourmaline	-	-	-	-	-	-	-
Talc	-	-	-	m	-	m	-
Sphene	-	tr	-	-	-	-	-
Spahlerite	-	-	-	tr	tr	tr	-
Chalcopyrite	-	-	-	m	-	m	-
Amphibole	-	tr	m	m	-	+	-

Appendix D. Biotite-Garnet Geothermometry

The table below lists temperatures derived from four of the biotite-garnet geothermometers used in this study. X(Fe) Biotite = Fe/(Fe+Mg), X(Fe) Gt.= Fe/(Fe+Mg), X(Mn) Gt.= Mn/(Mn+Ca+Mg+Fe), and X(Ca) Gt.= Ca/(Ca+Mn+Mg+Fe). Note that the Hodges and Spear (1982) method defines X(Fe) Gt. as Fe/(Fe+Mn+Ca+Mg) (not listed here). The methods listed in this table are: Ferry and Spear (1978), Goldman and Albee (1977), Indares and Martignole (1985), and Hodges and Spear (1982). All temperatures are in °C. Distance represents the number of kilometers southeast from the reference line as described in Part II. See the discussion and bibliography in Part II for further details.

Sample	Biotite Sample	Garnet Sample	X(Fe) Biotite	X(Fe) Gt.	X(Mn) Gt.	X(Ca) Gt.	Ferry-Spear	Goldman-Albee	Indares-Mart.	Hodges-Spear	Dist. (km)
A4-2A	22	20G	.42	.86	.23	.06	467.96	511.76	549.32	490.66	5.87
A4-6A	16	17G	.53	.92	.04	.29	422.01	494.43	508.50	522.79	5.07
A4-8A	20	54G	.61	.94	.11	.29	419.07	482.59	529.95	520.60	4.77
A4-8A	64	26G	.60	.97	.11	.31	288.25	370.12	385.66	384.57	4.77
A4-8A	64	56G	.60	.95	.11	.32	362.63	442.78	433.70	467.74	4.77
A4-19A	16	19S	.41	.88	.20	.20	417.89	529.41	532.93	487.54	5.64
A4-19A	16	20S	.41	.87	.19	.20	422.41	533.76	536.50	492.51	5.64
B2-1AB	21	15G	.46	.92	.18	.31	356.05	490.65	507.37	457.85	2.97
B2-1AB	21	16G	.46	.92	.16	.32	347.38	477.15	489.99	449.87	2.97
B2-1AB	21	17G	.46	.92	.14	.30	364.93	487.51	498.80	464.72	2.97
B2-1AB	27	28G	.47	.94	.20	.32	315.96	446.88	467.79	417.10	2.97
B2-1Y	36	29S	.44	.92	.19	.31	333.27	468.49	495.54	433.14	2.97
B2-3A	14	13G	.54	.92	.12	.26	418.40	489.27	513.43	508.76	3.96
B2-3A	15	13G	.54	.92	.12	.26	404.90	484.38	494.36	494.40	3.96
B2-3A	26	25G	.53	.92	.06	.26	417.57	475.99	487.67	508.83	3.96
B2-35A	09	13G	.56	.94	.10	.30	381.52	464.65	494.52	482.88	3.38
B2-35A	26	20G	.53	.93	.07	.28	393.60	466.26	487.03	488.10	3.38
B2-35B	04	12S	.53	.94	.17	.31	339.40	446.93	480.11	439.96	3.38
B2-35B	05	12S	.53	.94	.17	.31	341.17	448.09	483.80	441.90	3.38
B2-35B	18	17S	.51	.93	.12	.29	368.04	463.31	482.63	463.06	3.38
B3-25B	10	14C	.52	.90	.11	.06	457.90	448.28	467.40	479.89	5.47
B3-25B	10	15C	.52	.90	.12	.06	453.12	447.97	468.57	476.34	5.47
B3-63A	10	08G	.55	.92	.03	.26	424.50	482.54	489.41	515.79	5.10
B3-63A	12	08G	.55	.92	.03	.26	428.67	490.43	493.08	520.22	5.10
B3-63A	10	09G	.55	.92	.03	.26	429.67	486.59	494.19	520.56	5.10
B3-63A	12	09G	.55	.92	.03	.26	433.90	494.61	497.91	525.05	5.10
B3-185A	23	21G	.47	.91	.08	.27	382.08	469.78	478.50	473.96	3.92
B4-32A	56	60S	.53	.91	.16	.24	452.32	530.50	568.49	539.25	7.10
B4-32A	57	60S	.54	.91	.16	.24	461.75	546.99	577.57	549.18	7.10
B4-32A	56	62S	.53	.91	.15	.23	457.37	525.54	561.79	541.02	7.10
B4-32A	57	62S	.54	.91	.15	.23	466.93	541.72	570.84	551.06	7.10
B4-32A	56	63S	.53	.90	.15	.23	469.10	537.70	576.10	552.50	7.10
B4-32A	57	63S	.54	.90	.15	.23	478.97	554.64	585.49	562.85	7.10

Sample	Biotite Sample	Garnet Sample	X(Fe) Biotite	X(Fe) Gt.	X(Mn) Gt.	X(Ca) Gt.	Ferry-Spear	Goldman-Albee	Indares-Mart.	Hodges-Spear	Dist. (km)
B4-93A	QMIN1	28GQ	.48	.89	.09	.17	447.92	486.93	502.09	509.05	6.18
B4-93A	QMIN2	28GQ	.48	.89	.09	.17	447.33	487.74	502.36	508.44	6.18
B4-93A	QMIN2	29GQ	.48	.89	.09	.17	440.72	480.57	494.49	500.32	6.18
B4-93A	QMIN1	29GQ	.48	.89	.09	.17	441.30	479.78	494.21	500.93	6.18
B4-93A	QMIN1	11G	.48	.89	.09	.17	445.12	484.87	500.07	506.08	6.18
B4-93A	QMIN2	11G	.48	.89	.09	.17	444.53	485.67	500.35	505.47	6.18
B4-93A	22	GQMN	.47	.89	.09	.18	424.94	479.50	484.49	488.84	6.18
B4-93A	23	GQMN	.47	.89	.09	.18	424.94	478.19	488.84	488.82	6.18
B4-101A	55	47G	.51	.88	.12	.08	490.57	489.41	510.42	521.90	6.48
B4-141A	04	13S	.48	.91	.21	.18	393.98	468.23	503.20	456.73	5.69
B4-141A	15	13S	.49	.91	.21	.18	411.21	483.80	522.16	474.79	5.69
B4-141A	04	17S	.48	.90	.20	.19	410.96	485.08	521.17	476.00	5.69
B4-141A	15	17S	.48	.90	.20	.19	429.09	501.77	521.17	494.99	5.69
C3-2B	18	16G	.50	.87	.05	.14	521.00	511.49	550.83	573.90	7.95
C4-32A	35	15S	.47	.85	.05	.08	529.65	510.65	522.50	560.79	8.63
C4-32A	14	34S	.47	.84	.04	.08	557.99	532.92	552.37	589.27	8.63
C4-32A	14	09S	.47	.84	.05	.08	566.69	542.11	564.87	597.90	8.63
C4-32B	10	37S	.40	.84	.05	.08	486.23	493.30	479.30	516.22	8.63
C4-32B	12	37S	.41	.84	.05	.08	489.85	501.77	475.36	519.90	8.63
C4-32B	34	37S	.41	.84	.05	.08	492.02	504.44	475.36	522.11	8.63
C4-32B	35	37S	.41	.84	.05	.08	491.76	502.64	476.00	521.85	8.63
C4-49B	06	10S	.45	.86	.05	.10	500.82	499.35	499.38	539.70	8.30
C4-49B	07	10S	.45	.86	.05	.10	498.53	500.20	497.39	537.36	8.30
C4-49B	32	35S	.46	.85	.04	.11	532.49	523.52	534.42	574.08	8.30
C4-49B	32	36S	.46	.85	.04	.11	525.08	516.49	525.34	566.67	8.30

The vita has been removed from the scanned document

GEOLOGY OF THE ASHE FORMATION, SOUTHWEST VIRGINIA BLUE RIDGE BETWEEN FRIES AND GALAX, VIRGINIA

Jonathan L. Tso
Department of Geological Sciences
Virginia Tech
Blacksburg, Virginia

1987

Plate I

81° 00'
80° 53' 30"
36° 45'
36° 39'

0 1 1.5 Kilometers
0 .5 1 Miles

EXPLANATION

CAMBRIAN

ϵcl — Chilhowee Group, Unicoi Formation:
Green chloritic arkosic conglomerate, white quartz sandstone, with minor interbedded tan to green shale, local dark green quartzite and muscovite-chlorite-bearing button phyllite near thrust faults.

CAMBRIAN OR LATE PRECAMBRIAN

bf — Rocks of the Bowers Ferry Thrust Sheet:
Highly sheared arkosic conglomerate, indurated pale green quartzite, arkosic sandstone, minor pelitic schists.
bfa: locally occurring metabasalts containing chlorite+albite+biotite.

Rocks of the Ashe Formation

LATE PRECAMBRIAN

s — Interbedded gneiss and pelitic schists:
Medium grained gray muscovite+biotite+quartz+plagioclase ±chlorite ±garnet gneiss, locally conglomeratic with 2-3 mm feldspar clasts; gray muscovite-graphitic phyllite; medium to coarse grained garnet +muscovite+biotite schist; minor garnet-chlorite schist; local staurolite+ garnet+biotite+muscovite+paragonite schist; minor interbedded metabasic rocks; locally developed quartz mylonite near thrust faults.

a — Metabasic rocks:
Coarse, weakly foliated honblende-plagioclase metagabbro; coarse foliated hornblende-plagioclase amphibolite; medium grained hornblende-plagioclase schist; minor chlorite-actinolite schist; minor interlayered metasedimentary gneiss and schist.

Gt — Coarse garnet-muscovite schist:
contains1-2 mm manganiferous garnet porphyroblasts.

o — Gossan Lead Massive Sulfide:
Massive pyrrhotite+minor sphalerite+chalcopyrite+galena with abundant silicate inclusionsof biotite gneiss and muscovite schist; local coarse blades of actinolite and euhedral spessartine-rich garnet.

PRECAMBRIAN

p-ϵec — Cranberry Gneiss:
Sheared mylonite and ultramylonite; albite-K-feldspar augen gneiss with thin ribbon quartz, muscovite±biotite layers, fine quartz+albite matrix.
p-ϵeca: locally occurring metabasic sills containing predominantly albite+chlorite.

STRUCTURAL DATA

- Strike and dip of bedding (S_0)
- Strike and dip of penetrative foliation (S_1)
- Strike and dip of dominant regional penetrative foliation (S_2)
- Strike and dip of mylonite foliation (S_{my})
- Strike and dip of locally developed axial plane cleavage (S_3)
- Plunge and trend of microscopic kink banding and biotite lineation (L_2)
- Plunge and trend of S_1 x S_2 intersection lineation (L_{1x2})
- Plunge and trend of micro-to mesoscopic folds of S_1 (F_2)
- Plunge and trend of mylonite lineation and slickensides (L_{my})
- Plunge and trend of mesoscopic folds (F_3)
- Plunge and trend of mesoscopic folds (F_4)

CONTACTS

- Contact exposed or constrained to within 10 m
- Location of contact aproximate

FAULTS

- Location of fault exposed or constrained to within 10 m
- Location of fault approximate

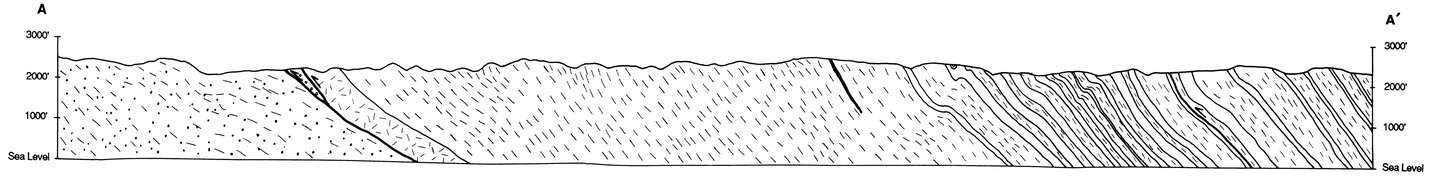
CROSS SECTION SYMBOLS

- Unicoi Formation
- Rocks of the Bowers Ferry Thrust Sheet
- Ashe Formation: metasediments
- Ashe Formation: amphibolite
- Ashe Formation: massive sulfide ore
- Cranberry Gneiss

VIRGINIA

MN 4°

GALAX, VIRGINIA
7 1/2' QUADRANGLE



STRUCTURAL GEOLOGY OF THE ASHE FORMATION, SOUTHWEST VIRGINIA BLUE RIDGE BETWEEN FRIES AND GALAX, VIRGINIA

Jonathan L. Tso
Department of Geological Sciences
Virginia Tech
Blacksburg, Virginia

1987

Plate II

81° 00'
80° 53' 30"
36° 45'
36° 39'

0 1 1.5 Kilometers
0 .5 1 Miles

EXPLANATION

CAMBRIAN

Ꞓcl — Chilhowee Group, Unicoi Formation:
Green chloritic arkosic conglomerate, white quartz sandstone, with minor interbedded tan to green shale, local dark green quartzite and muscovite-chlorite-bearing button phyllite near thrust faults.

CAMBRIAN OR LATE PRECAMBRIAN

bf — Rocks of the Bowers Ferry Thrust Sheet:
Highly sheared arkosic conglomerate, indurated pale green quartzite, arkosic sandstone, minor pelitic schists.
bfa: locally occurring metabasalts containing chlorite+albite+biotite.

Rocks of the Ashe Formation

LATE PRECAMBRIAN

s — Interbedded gneiss and pelitic schists:
Medium grained gray muscovite+biotite+quartz+plagioclase ±chlorite ±garnet gneiss, locally conglomeratic with 2-3 mm feldspar clasts; gray muscovite-graphitic phyllite; medium to coarse grained garnet +muscovite+biotite schist; minor garnet-chlorite schist; local staurolite+ garnet+biotite+muscovite+paragonite schist; minor interbedded metabasic rocks; locally developed quartz mylonite near thrust faults.

a — Metabasic rocks:
Coarse, weakly foliated honblende-plagioclase metagabbro; coarse foliated hornblende-plagioclase amphibolite; medium grained hornblende-plagioclase schist; minor chlorite-actinolite schist; minor interlayered metasedimentary gneiss and schist.

Gt — Coarse garnet-muscovite schist:
containsl-2 mm manganiferous garnet porphyroblasts.

o — Gossan Lead Massive Sulfide:
Massive pyrrhotite+minor sphalerite+chalcopyrite+galena with abundant silicate inclusionsof biotite gneiss and muscovite schist; local coarse blades of actinolite and euhedral spessartine-rich garnet.

PRECAMBRIAN

p-Ꞓec — Cranberry Gneiss:
Sheared mylonite and ultramylonite; albite-K-feldspar augen gneiss with thin ribbon quartz, muscovite±biotite layers, fine quartz+albite matrix.
p-Ꞓeca: locally occurring metabasic sills containing predominantly albite+chlorite.

STRUCTURAL DATA

- Strike and dip of bedding (S_0)
- Strike and dip of penetrative foliation (S_1)
- Strike and dip of dominant regional penetrative foliation (S_2)
- Strike and dip of mylonite foliation (S_{my})
- Strike and dip of locally developed axial plane cleavage (S_3)
- Plunge and trend of microscopic kink banding and biotite lineation (L_2)
- Plunge and trend of $S_1 \times S_2$ intersection lineation (L_{1x2})
- Plunge and trend of micro-to mesoscopic folds of S_1 (F_2)
- Plunge and trend of mylonite lineation and slickensides (L_{my})
- Plunge and trend of mesoscopic folds (F_3)
- Plunge and trend of mesoscopic folds (F_4)

CONTACTS

- Contact exposed or constrained to within 10 m
- Location of contact aproximate

FAULTS

- Location of fault exposed or constrained to within 10 m
- Location of fault approximate

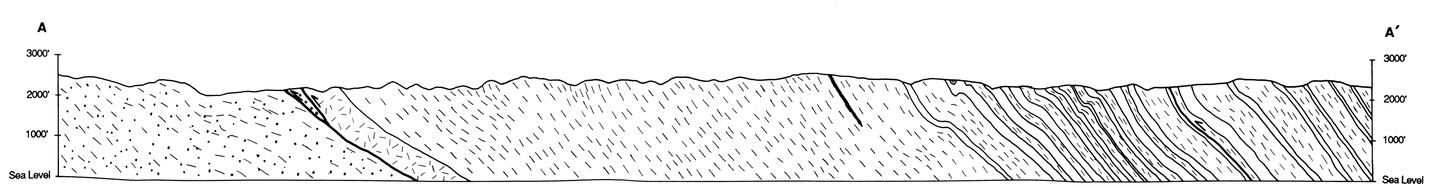
CROSS SECTION SYMBOLS

- Unicoi Formation
- Rocks of the Bowers Ferry Thrust Sheet
- Ashe Formation: metasediments
- Ashe Formation: amphibolite
- Ashe Formation: massive sulfide ore
- Cranberry Gneiss

VIRGINIA

MN 4°

GALAX, VIRGINIA
7 1/2 QUADRANGLE



STRUCTURAL GEOLOGY OF THE BUMBARGER MINE, GOSSAN LEAD MASSIVE SULFIDE GALAX, VIRGINIA

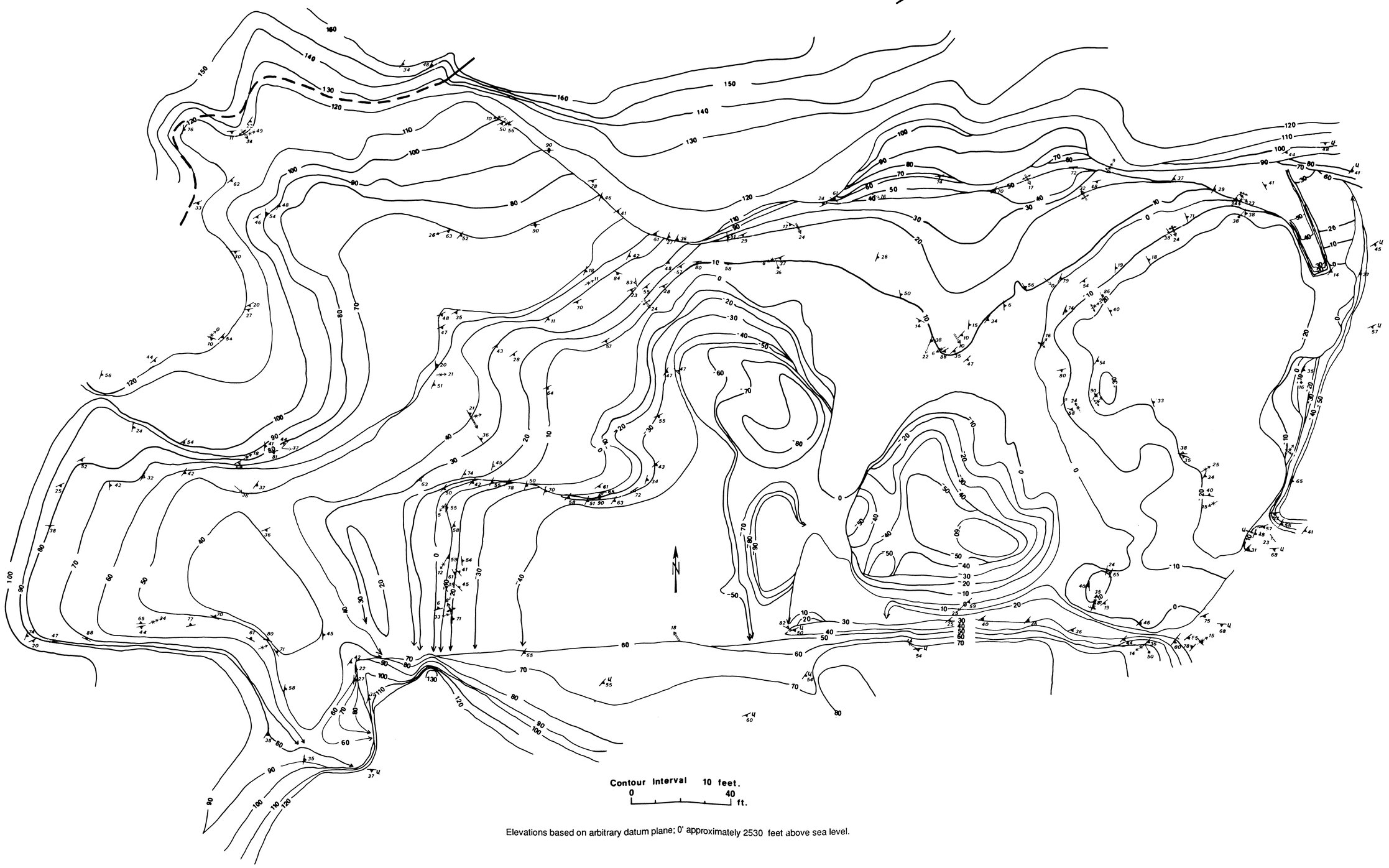
Jonathan L. Tso
Department of Geological Sciences
Virginia Tech
Blacksburg, Virginia

1987

Plate III

STRUCTURAL DATA

- Strike and dip of lithologic layering (S_0)
- Strike and dip of penetrative foliation (S_1)
- Strike and dip of dominant regional penetrative foliation (S_2)
- Strike and dip of locally developed axial plane cleavage (S_3)
- Strike and dip of locally developed axial plane cleavage (S_4)
- Plunge and trend of microscopic kink banding and biotite lineation (L_2)
- Plunge and trend of S_1 x S_2 intersection lineation (L_{1x2})
- Plunge and trend of micro-to mesoscopic folds of S_1 (F_2)
- Plunge and trend of mesoscopic folds (F_3)
- Plunge and trend of mesoscopic folds (F_4)
- u Reading measured underneath overhang
- Fault (Dashed where approximate)



Elevations based on arbitrary datum plane; 0' approximately 2530 feet above sea level.